ROSS LARGE

Studies of VHMS-related alteration: geochemical and mineralogical vectors to ore

Hole	WT0025	WT0025	WT0025
From (m)	3.4	46.2	79.8
To (m)	3.7	46.6	80.1
SiO2 (%)	69.81	69.56	51.71
TiO2 (%)	0.39	0.24	0.60
Al2O3 (%)	12.16	12.39	16.40
Fe2O3 (%)	6.26	6.96	10.21
MnO (%)	0.12	0.26	0.31
MgO (%)	2.63	0.33	2.88
CaO (%)	1.44	0.14	3.68
Na2O (%)	0.79	0.21	0.11
K2O (%)	2.23	3.62	3.98
P2O5 (%)	0.09	0.04	0.15
CuO (%)	0.00	0.00	0.00
BaO (%)	0.02	0.06	0.19
LOI (%)	4.22	5.27	8.98
Sum (%)	100.16	99.58	99.20
S (%)	<0.01	<0.01	0.01
C (%)	0.520	1.080	1.650
Ag (ppm)	0.2	0.1	0.1
As (ppm)	2	4	5
Ba (ppm)	397	494	1978
Bi (ppm)	<2	<2	<2
Cd (ppm)	0.4	0.4	0.5
Ce (ppm)	84	106	61
Cr (ppm)	70	110	43
Cs (ppm)	2.24	3.03	2.09
Cu (ppm)	13	20	37
La (ppm)	41	49	30
Mo (ppm)	0.8	0.9	1.0
Nb (ppm)	10	15	8
Nd (ppm)	37	49	29
Ni (ppm)	7	5	11
Pb (ppm)	101	7	13
Rb (ppm)	69	118	128
Sb (ppm)	0.7	1.8	2.8
Sc (ppm)	12	8	19
Se (ppm)	<0.5	<0.5	<0.5
Sr (ppm)	47	24	53
Th (ppm)	14	20	9
Tl (ppm)	<0.5	0.7	0.7
U (ppm)	3.02	4.71	2.81
V (ppm)	39	4	195
Y (ppm)	29	43	27
Zn (ppm)	165	67	213
Zr (ppm)	213	267	148

AMIRA/ARC project P439

Report 5
October 1997

Centre for Ore Deposit and Exploration Studies
University of Tasmania

CODES SRC

Studies of VHMS-related alteration: geochemical and mineralogical vectors to ore

Hole	WT0025	WT0025	WT0025
From (m)	3.4	46.2	79.8
To (m)	3.7	46.6	80.1
SiO2 (%)	69.81	69.56	51.71
TiO2 (%)	0.39	0.24	0.60
Al2O3 (%)	12.16	12.39	16.40
Fe2O3 (%)	6.26	6.96	10.21
MnO (%)	0.12	0.26	0.31
MgO (%)	2.63	0.83	2.88
CaO (%)	1.44	0.14	3.68
Na2O (%)	0.79	0.21	0.11
K2O (%)	2.23	3.62	3.98
P2O5 (%)	0.09	0.04	0.15
CuO (%)	0.00	0.00	0.00
BaO (%)	0.02	0.06	0.19
LOI (%)	4.22	5.27	8.98
Sum (%)	100.16	99.58	99.20
S (%)	<0.01	<0.01	0.01
C (%)	0.520	1.080	1.650
Ag (ppm)	0.2	0.1	0.1
As (ppm)	2	4	5
Ba (ppm)	397	494	1978
Bi (ppm)	<2	<2	<2
Cd (ppm)	0.4	0.4	0.5
Ce (ppm)	84	106	61
Cr (ppm)	70	110	43
Cs (ppm)	2.24	3.03	2.09
Cu (ppm)	13	20	37
La (ppm)	41	49	30
Mo (ppm)	0.8	0.9	1.0
Nb (ppm)	10	15	8
Nd (ppm)	37	49	29
Ni (ppm)	7	5	11
Pb (ppm)	101	7	13
Rb (ppm)	69	118	128
Sb (ppm)	0.7	1.8	2.8
Sc (ppm)	12	8	19
Se (ppm)	<0.5	<0.5	<0.5
Sr (ppm)	47	24	53
Th (ppm)	14	20	9
Tl (ppm)	<0.5	0.7	0.7
U (ppm)	3.02	4.71	2.81
V (ppm)	39	4	195
Y (ppm)	29	43	27
Zn (ppm)	165	67	213
Zr (ppm)	213	267	148

AMIRA/ARC project P439

Report 5
October 1997

Centre for Ore Deposit and Exploration Studies
University of Tasmania

CODES SRC

Centre for Ore Deposit and Exploration Studies,
Geology Department,
University of Tasmania,
GPO Box 252-79,
Hobart, Tasmania,
Australia

http://www.geol.utas.edu.au/codes

another Pongratz & Hlaing Production 1997

Contents

Aims and framework of the project

Introduction

Volcanic-hosted massive sulphide deposits (VHMS) provide a significant contribution to the total zinc, copper, lead, silver and gold production in Australia and continue to be a major target for most base metal explorers. However, due to the geological complexity of ancient submarine volcanic terrains, new VHMS deposits are becoming extremely difficult to discover, especially deposits that are buried more than a few tens of metres below the surface. To complement the conventional multidisciplinary approach utilising geology, geophysics and geochemistry, a new attack to the problem is developed here which involves the integration of volcanic facies analysis with alteration geochemical and mineral chemical studies to develop a set of vectors to guide explorers toward ore-grade mineralisation. The research concentrates on three productive submarine volcanic belts in Australia: the Mount Read Volcanics (MRV) in western Tasmania, the Mount Windsor Volcanics (MWV) in northern Queensland, and the Archean Murchison volcanic province in western Australia.

Project objectives

1. To characterise the mineralogy and geochemistry for the various styles of hydrothermal alteration throughout the Mount Read Volcanics (MRV) and the Mount Windsor Volcanics (MWV). This will be based on mapping supported by whole-rock and trace element geochemistry, mineral chemistry, REE and stable isotope geochemistry.
2. To determine the relationship between geochemical alteration patterns and sub-volcanic intrusions that are coeval with VHMS formation.
3. To undertake case studies of alteration halos related to specific VHMS deposits with particular emphasis on hangingwall alteration, and the relationship between alteration patterns and volcanic facies.
4. To develop a set of vectors towards ore, based on the regional studies and ore deposit specific studies, that can be applied in the exploration for VHMS deposits in submarine volcanic sequences throughout Australia. The vector matrix will include whole-rock, trace element, mineral chemistry, REE, isotope and volcanic facies factors.

Research framework

The emphasis in this project involves a multidisciplinary approach utilising studies in volcanic facies analysis, volcanic petrology and geochemistry, with alteration and mineralisation to develop models for the nature, style and extent of alteration throughout submarine volcanic environments hosting VHMS deposits. The basis of this approach is outlined in the diagram below.

The combination of data and interpretation from these three subdisciplines will be used in the development of vectors to ore.

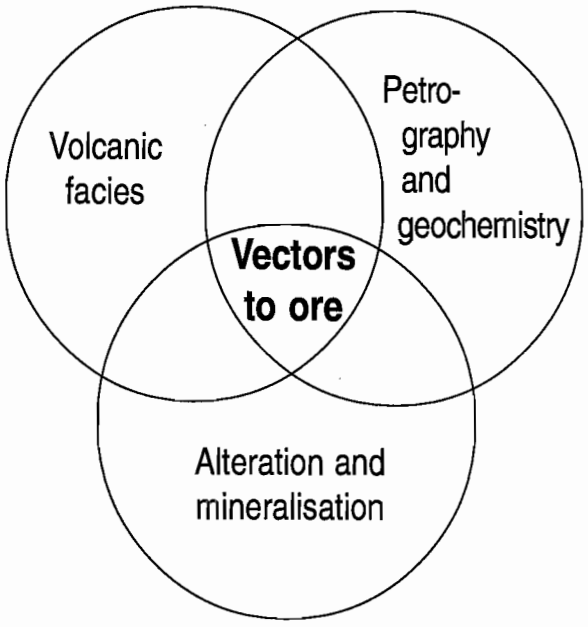

This Report

This fifth report on the project presents results of research in the 5-month period between May and October 1997.

The content reflects the multi-disciplinary approach to studying VHMS related alteration systems with major contributions on the factors which control "background" diagenetic alteration, the discrimination between diagenetic and ore related hydrothermal alteration, and specific alteration studies on a diverse range of deposits in Tasmania and North Queensland.

- David Huston presents geochemical data from the Western Tharsis disseminated pyrite-chalcopyrite deposit suggesting that Ba and Mn could be weathering resistant pathfinder elements to detect the outer alteration zones, K_2O depletion could indicate close proximity to ore, and As,Bi and Se could be useful vectors to ore lenses within the barren pyritic envelope.

- Tim Callaghan and Jason Beckton report on their new research into the Mt Julia and Henty gold deposits which are associated with extensive, stratabound, rather VHMS-like alteration zones adjacent to a major fault. However, some aspects of alteration, such as extreme silicification, mobility of Al_2O_3 and apparent overprinting of earlier pervasive carbonate and albite alteration, show these to be distinct from other deposits in the Mt Read Volcanics.

- Preliminary trace element results from the White Spur step out traverses indicate a coincident anomaly in Ag, As, Sb, Cd, Mo and Tl in altered and weakly mineralised volcaniclastic breccia at the base of the White Spur Formation, a few hundred metres north of drill hole MR1.

- In her report on background alteration in the Mt Black Volcanics, east of Rosebery, Cathryn Gifkins highlights the influence of volcanic facies and primary composition on diagenetic alteration, and shows how a complex pile of variably permeable and glassy felsic volcanics has been modified to a diverse and patchy arrangement of alteration types.

- Rod Allen texturally pursues diagenetic alteration into the confusion of the Rosebery-Hercules ore forming system and emerges with a convincing alteration sequence comprising: early diagenetic low temperature smectite + silica → early VHMS hydrothermal CO_3 → hydrothermal sericite + chlorite = diagenetic zeolite → advanced diagenetic feldspar + quartz.
  It has implications for large porosity and density changes during diagenesis and for regional scale exploration targeting.

- Initial interpretation, by Ross Large and Mike Blake, of microprobe and spectrographic data on mineral chemistry of Rosebery carbonates and muscovite, shows potential for these techniques in alteration mapping and exploration vectors.

- The latest appraisal results from Hellyer, by Bruce Gemmell and others, indicates that the PIMA portable infrared spectrometer also has applications in mapping of alteration intensity, particularly in recognition of Fe-Mg rich muscovites in alteration zones proximal to ore.

- Cliff Stanley presents the Pearce Element Ratio approach to interpretation of the Hellyer alteration system.

- Mark Doyle discusses the latest geochemical data from the alteration zones surrounding the syn-volcanic, sub-seafloor replacement Cu-Au deposits at Highway-Reward.

- Wally Herrmann presents for discussion, a draft outline of the format for the P439 final report.

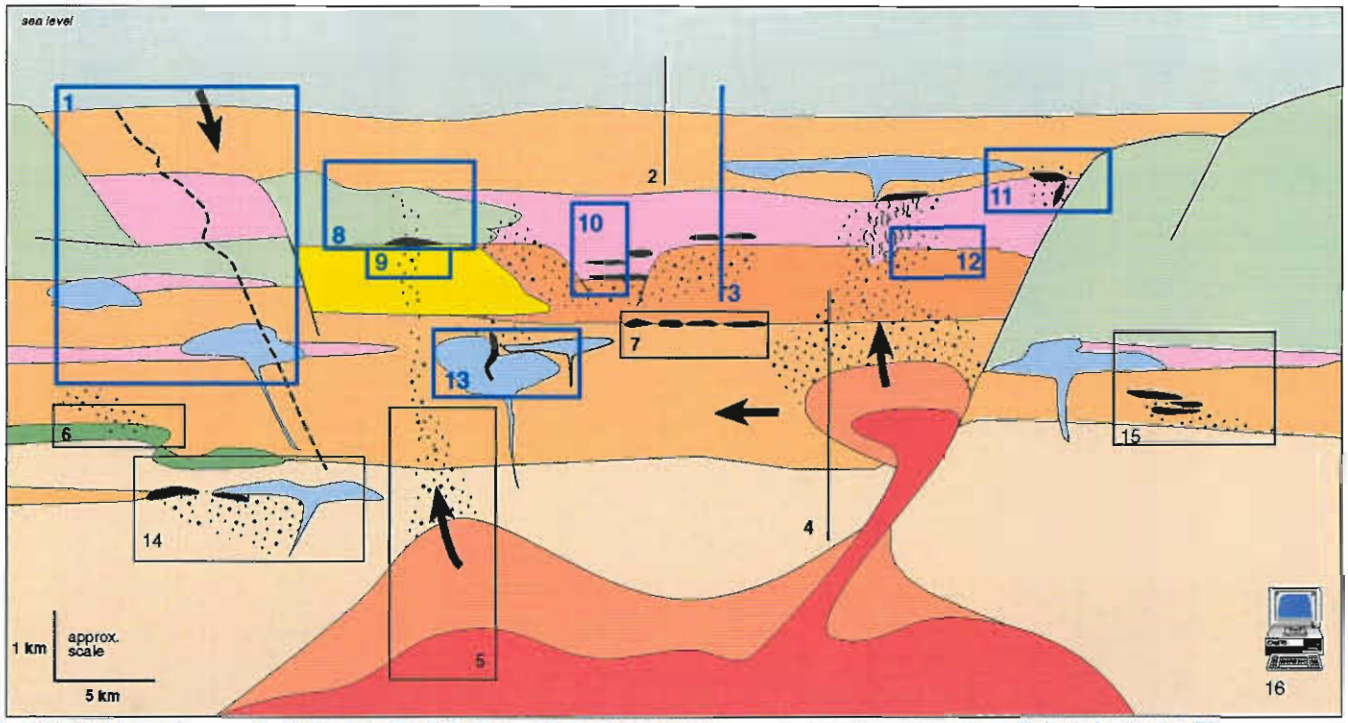

1. **Background diagenetic alteration and volcanic facies: JMcP, AJS, RLA, GD**
6. Barren pyritic alteration, Gydgie: AJS, GD
14. Thalanga alteration and facies: HP, JMcP, JBG
8. **Hellyer hangingwall alteration: RF, JBG**
9. **Hellyer footwall: CS, JBG**
5. Syn-volcanic granite-related alteration: BW, RRL, DC, RLA
10. **Rosebery carbonate alteration: RLA, RRL**
13. **Highway–Reward Cu–Au system: MD, JMcP, RRL**
7. Exhalite chemistry and textures: GD, MD, AJS
2. Mt Black traverse: KG, AJS, JMcP, RLA
3. **Hercules–Mt Read traverseL RLA, JMcP, RRL**
4. Red Hills–Selina traverse: AJS, JMcP, RLA
11. **Henty Au alteration: TC, JS**
12. **Mt Lyell alteration system: DLH**
15. Gossan Hill system: RS, JBG
16. Chemical modelling of fluid–rock interaction in alteration systems: DC

Figure 1 AMIRA Project P439 — Schematic working model of the relationship of project areas and topics (activity in this report shown in **bold**)

Summaries

Geochemical variations in the alteration zone surrounding the Western Tharsis deposit and their utility in exploration

David L. Huston

The Western Tharsis orebody is surrounded by a "barren" pyritic halo that extends 100–200 m stratigraphically above and below the ore zone. Although this halo extends laterally along the same stratagraphic position to the south, it probably closes off to the north. The ore zone is characterised by an assemblage of As, Bi, Cu, Mo, Ni, S and Se; with the exception of Mo, these elements are also enriched, but at a much lower level, in the pyrite halo.

Pronounced depletion anomalies of K_2O, Cs and MgO occur in 20–30 m wide stratiform zones that flank the orebody on both sides. The depletion of these elements suggests that these zones are characterised by advanced argillic alteration assemblages in contrast to the quartz-sericite±chlorite assemblages that predominate in the ore zone and the barren pyrite halo.

The barren pyrite halo is surrounded by a peripheral carbonate halo that is characterised by abundant siderite. This zone contains highly anomalous C, CaO and MnO, and weakly anomalous Zn and Tl. Zinc and Tl anomalism is most pronounced in the upper 100–150 m of the stratagraphically lower halo. In the stratagraphically upper halo, Zn and Tl anomalism is characterised by erratichigh values.

Barium anomalism, although mainly restricted to the pyrite halo, extends into the stratigraphically lower carbonate halo by up to 100 m. A Na_2O depletion anomaly extends from 150 m below the orebody and to the Owen contact in the hanging wall.

Preliminary investigations on the geology and geochemistry of Mt Julia Prospect

Tim Callaghan

The Mt Julia Prospect contains similar Au rich mineralisation as the Henty Gold Mine located 1.3 km to the north. The Mt Julia prospect does not contain the same bonanza grades as the Henty Gold Mine. The mineralisation is hosted in intensely silica-sericite-sulphide altered dacitic volcaniclastics at the base of the Lynchford Member. The South Henty Fault strongly controls the mineralisation and acted as the fluid conduit for mineralising fluids.

Alteration associated with the deposit is distinctly assymetric and can be broadly categorised into footwall alteration, alteration associated with the main mineralised zone or A-Zone alteration and hangingwall alteration. Footwall alteration is comprised of sericite-pyrite-carbonate alteration and is possibly hosted in the CVC. A-Zone alteration is comprised of silica-carbonate-sulphide (MQ), silica-sericite±carbonate±sulphide (MV), sericite-pyrite-silica (MZ), massive pyrite and /or galena-sphalerite (MS and MP) and massive carbonates. Intense albite-silica, albite-silica-chlorite and massive carbonates typify hangingwall alteration.

Immobile element geochemistry clearly defines the lithostratigraphic units hosting mineralisation and the other alteration styles. Some mobility of 'immobile' elements is observed, particularly within the most intensely altered MQ alteration where leaching of Al, Sc, V, Y, Nb and enrichment of Th has occurred. Immobile element geochemistry also indicates that much of the carbonate alteration has formed from intense carbonate addition to Lynchford Member volcaniclastics. From current studies it appears that the carbonates and albite alteration pre-exist the later silica-sericite-sulphide-Au event.

Strong K enrichment and Na depletion has occurred in the footwall and A-Zone rocks while strong Na enrichment is a feature of the hangingwall rocks reflecting the albitic alteration of the hangingwall and sericite alteration of the footwall rocks.

Henty Gold Mine — The Zone 96 orebody, geological and geochemical characteristics

Jason Beckton

The Henty Gold Mine is a high grade, low tonnage deposit (Zone 96 — 526,000t @ 26.2 g/t Au). Annual gold production is estimated to average 90,000 ounces over a 4.5 year mine life. Gold and subordinate basemetals occur within a quartz-sericite-sulphide alteration package within the lower Tyndall Group. The Tyndall Group volcaniclastics and epiclastics have not been previously known to host economic mineralisation within the Mount Read Volcanic Belt.

The Zone 96 orebody has extreme variation in both thickness and grade. Massive Quartz (MQ) alteration hosts the bulk of gold within the alteration package. Research has focused on the timing of formation and geometry of the MQ as well as controls on distribution of gold within the MQ. Zone 96 has been previously described as a gold-rich Cambrian VHMS deposit. Devonian deformation is interpreted to have remobilised gold within the alteration package and resulted in high grade pods. Structural relationships suggest transposed folding of the orebody.

The Darwin Granite–Slate Spur area: Preliminary geochemistry and a discussion of granite-related alteration

Bill Wyman

This paper clarifies the classification of the Darwin granite using both geochemistry and modal mineralogy. The paper documents the island arc setting of the granite and compares it to the Elliott Bay granite to the south and to the Murchison granite to the north. The Darwin granite most nearly follows the calc-alkaline granodiorite series of (Lameyre and Bowden, 1982), and fits most criteria for the magnetite series of (Ishihara, 1981). Effects of hydrothermal alteration are pointed out as they clearly render classification schemes that rely on major element variations, such as the I-S scheme of Chappell and White (1974), virtually useless.

Hydrothermal alteration assemblages, in the Jukes–Darwin field, resemble alteration assemblages found in other intrusion-related related hydrothermal systems throughout the world. These hydrothermal alteration assemblages share many similarities with porphyry Cu-Au alteration and mineralisation assemblages (e.g. Cooke et al, 1996; Sillitoe, 1993), and may be considered a submarine analogue to porphyry-style mineralisation. Alteration assemblages near the Darwin granite are dominated by K-feldspar, chlorite, silica and sericite in various combinations and intensities. Accessory minerals include pyrite, magnetite, tourmaline, barite and chalcopyrite. Alteration assemblages appear to be most intense and widespread above the granite, and appear to drop off rapidly along the sides. Mineralisation and alteration appear to be related to the late stage intrusion of the white equigranular granite and the porphyritic white granite phase. Magnetite and tourmaline veining also appears to be related to this phase of granitic intrusion.

Background alteration in the Mount Black Volcanics: textures, mineralogy and geochemistry

Cathryn Gifkins

All units of the Mount Black and Sterling Valley Volcanics have been variably modified by the combined effects of different alteration styles. The most common alteration assemblages within the volcanics are, silicification, feldspar ± quartz, sericite, sericite-chlorite ± carbonate ± quartz, carbonate, chlorite, chlorite-epidote ± carbonate and sphene. The wide distribution of many of these alteration styles and the remote location from known mineralisation suggests that these alteration assemblages are the product of regional processes rather than focussed hydrothermal events associated with mineralisation.

Background or regional style alteration is not a blanket style alteration. Instead regional processes produce a complex pattern of overlapping alteration styles and intensities. The distribution of alteration styles and their intensities is partly controlled by the geochemical signature and the permeability of the rocks. Mafic volcanic units tend to undergo alteration to more mafic assemblages which include chlorite and epidote while more felsic units are altered dominantly by sericite, feldspar and to a lesser extent chlorite. Ultimately the permeability is related to both the texture and the chemical stability of a rock. In a pile of glassy volcanic rocks the texture and hence porosity can vary considerably over a short distance due to both the primary volcanic textures and the post-depositional modification of these textures.

The complex and discontinuous nature of an originally glassy silicic volcanic pile like the Mount Black Volcanics has resulted in the patchy distribution of the different regional alteration facies. An individual unit with a constant primary geochemical signature may have vastly different primary volcanic, devitrification and hydration textures. Post-depositional alteration may highlight these textural differences. For example fracture controlled polyphase feldspar-quartz and chlorite-sericite alteration occurs in the dense perlitic core of a rhyolite flow. In the flow-banded margin of the flow individual bands are dominated by feldspar-quartz or sericite-chlorite alteration. In deposits where the margins are highly vesicular or pumiceous the sericite-chlorite altered bands have undergone subsequent compaction. The associated rhyolitic hyaloclastite at the flanks and top of the flow are much more strongly altered. Feldspar-quartz, sericite-chlorite, chlorite and carbonate assemblages are all commonly present. The patchy distribution of these alteration phases may result in an apparently polymictic volcaniclastic breccia.

Rosebery alteration study and regional alteration studies in the Mount Read Volcanics: The record of diagenetic alteration in the strongly deformed, felsic volcaniclastic succession enclosing the Rosebery and Hercules massive sulphide deposits

Rodney L. Allen

summary not supplied

Carbonate and muscovite mineral chemistry, Rosebery VHMS deposit

Ross Large, Rod Allen and Michael Blake

Microprobe analyses on samples from DDH 120R at the Rosebery north-end show a systematic variation in the chemistry of muscovites and carbonates relative to volcanic stratigraphy and ore position. These preliminary results indicate the potential to use both muscovite chemistry and carbonate chemistry as vectors to ore.

Comparison of data from PIMA, FTIR and microprobe analyses indicate a good correlation between muscovite spectra and muscovite chemistry. The FTIR is shown to provide accurate information on the substitution of Fe and Mg into the octahedral Al site of muscovite.

PIMA-II spectral analysis of hydrothermal alteration associated with the Hellyer VHMS deposit: new results

K. Yang, J.F. Huntington, J.B. Gemmell and R. Fulton

Further results of the spectral study of the altered volcanic samples from the Hellyer Zn-Pb deposit are presented in this report. The data show that the hydrothermal alteration system at Hellyer can be spectrally characterised using the PIMA-II portable infrared spectrometer.

Compositional variation of muscovite has been identified spectrally in this study. For muscovite at Hellyer, wavelength of the Al-OH absorption was found to vary between 2190 to 2225 nm, corresponding approximately to Al(vi)# at 0.95-0.65. The long Al-OH wavelengths (> 2216 nm) are characteristic of the muscovite in the most intensely altered rocks. In terms of rock types, the ore-hosting volcaniclastic rocks (i.e. HVS) tend to have the longest Al-OH (2216-2225 nm), the footwall andesites (i.e. FPS) show the medium Al-OH wavelengths (2210-2220 nm), and the hangingwall basalts (PLS) display the shortest Al-OH (2190-2216 nm).

Observed in several drill-holes, the mineralised volcanics (with high Pb, Zn and Cu contents) are characterised by muscovite with relatively longer Al-OH wavelengths, whereas the surrounding altered, but unmineralised, rocks show shorter Al-OH wavelengths. This finding suggests that in exploration the Al-OH wavelength could be used as a parameter for assessing alteration intensity and potential mineralisation.

Chlorite also shows a wide range of cation composition. Based on the observed Fe-OH wavelength range (2250-2264 nm), the Mg# value for chlorite in the altered volcanics is estimated at 0.7-0.2. The composition variation, however, does not appear to be related to the alteration intensity or mineralisation.

In two drill-holes from the northern part of the alteration system, an K-feldspar (Ba-bearing) enriched interval has been found in the altered footwall. The textures indicate the K-feldspar as hydrothermal in origin, but whether or not it represents an in situ hydrothermal alteration event needs to be further clarified.

In the unaltered volcanic rocks, the metamorphic effects are spectrally shown as either zoisite or prehnite-dominated assemblages. These metamorphic signatures were found only in the uppermost part of the hangingwall basalt.

Preliminary geochemical data from the Dobson Creek–White Spur traverses

Wally Herrmann, Rod Allen and Jocelyn McPhie

summary not supplied

Alteration geochemistry of the sub-seafloor replacement style Highway–Reward deposit, Mount Windsor Subprovince

Mark Doyle

Geochemical studies of hydrothermal and diagenetic alteration associated with the Cu-Au-rich Highway-Reward massive sulfide deposit in the Cambro-Ordovician, Mount Windsor Subprovince are discussed. Alteration in the footwall and hanging wall is similar and characterised by patterns of depletion (Na_2O, CaO, MgO) and enrichment (K_2O, Rb/Sr) which provide vectors to ore. Rb/Sr ratios are generally higher in the hanging wall alteration halo than the footwall and may discriminate the ore position. Sills and cryptodomes in the host succession to mineralisation range in composition from high-silica dacite to rhyolite and are similar to comparable facies in the remainder of the Trooper Creek Formation. The results of this analysis have application to other sub-seafloor replacement type VHMS deposits hosted by syn-sedimentary intrusion-dominated volcanic centres.

Geochemical variations in the alteration zone surrounding the Western Tharsis deposit and their utility in exploration

by David L. Huston
Australian Geological Survey Organisation, Canberra, ACT

Summary

The Western Tharsis orebody is surrounded by a "barren" pyritic halo that extends 100–200 m stratigraphically above and below the ore zone. Although this halo extends laterally along the same stratagraphic position to the south, it probably closes off to the north. The ore zone is characterised by an assemblage of As, Bi, Cu, Mo, Ni, S and Se; with the exception of Mo, these elements are also enriched, but at a much lower level, in the pyrite halo.

Pronounced depletion anomalies of K_2O, Cs and MgO occur in 20–30 m wide stratiform zones that flank the orebody on both sides. The depletion of these elements suggests that these zones are characterised by advanced argillic alteration assemblages in contrast to the quartz-sericite±chlorite assemblages that predominate in the ore zone and the barren pyrite halo.

The barren pyrite halo is surrounded by a peripheral carbonate halo that is characterised by abundant siderite. This zone contains highly anomalous C, CaO and MnO, and weakly anomalous Zn and Tl. Zinc and Tl anomalism is most pronounced in the upper 100–150 m of the stratagraphically lower halo. In the stratagraphically upper halo, Zn and Tl anomalism is characterised by erratichigh values.

Barium anomalism, although mainly restricted to the pyrite halo, extends into the stratigraphically lower carbonate halo by up to 100 m. A Na_2O depletion anomaly extends from 150 m below the orebody and to the Owen contact in the hanging wall.

Introduction

The geological setting of copper-gold deposits in the Mt Lyell mineral field differs substantially to other Cambrian volcanic-related ore deposits in western Tasmania. Rather than massive to semi-massive Zn-Pb-rich ores, most deposits in the Mt Lyell district are characterised by low grade, disseminated ores.

Copper-rich stratiform massive sulphide lenses, such as The Blow and South Lyell, constituted only a small portion of the original resource at Mt Lyell. Rather, most of the original resource, and the present ore reserve, was contained within broadly strataform orebodies, such as Prince Lyell, that are characterised by disseminated pyrite and chalcopyrite. The Western Tharsis orebody is the only known undeveloped orebody of this type in the Mt Lyell district.

A program of core logging and geochemical sampling has been undertaken at the Western Tharsis deposit to document the zonation of alteration assemblages and ore-related metals and to compare these distributions with those of "typical" VHMS deposits from the Mt Read volcanic belt. Huston (1997) presented preliminary descriptions of the distribution of rock types, alteration assemblages and iron minerals based on core logging. This report presents the results of whole rock geochemical analyses of samples collected during core logging.

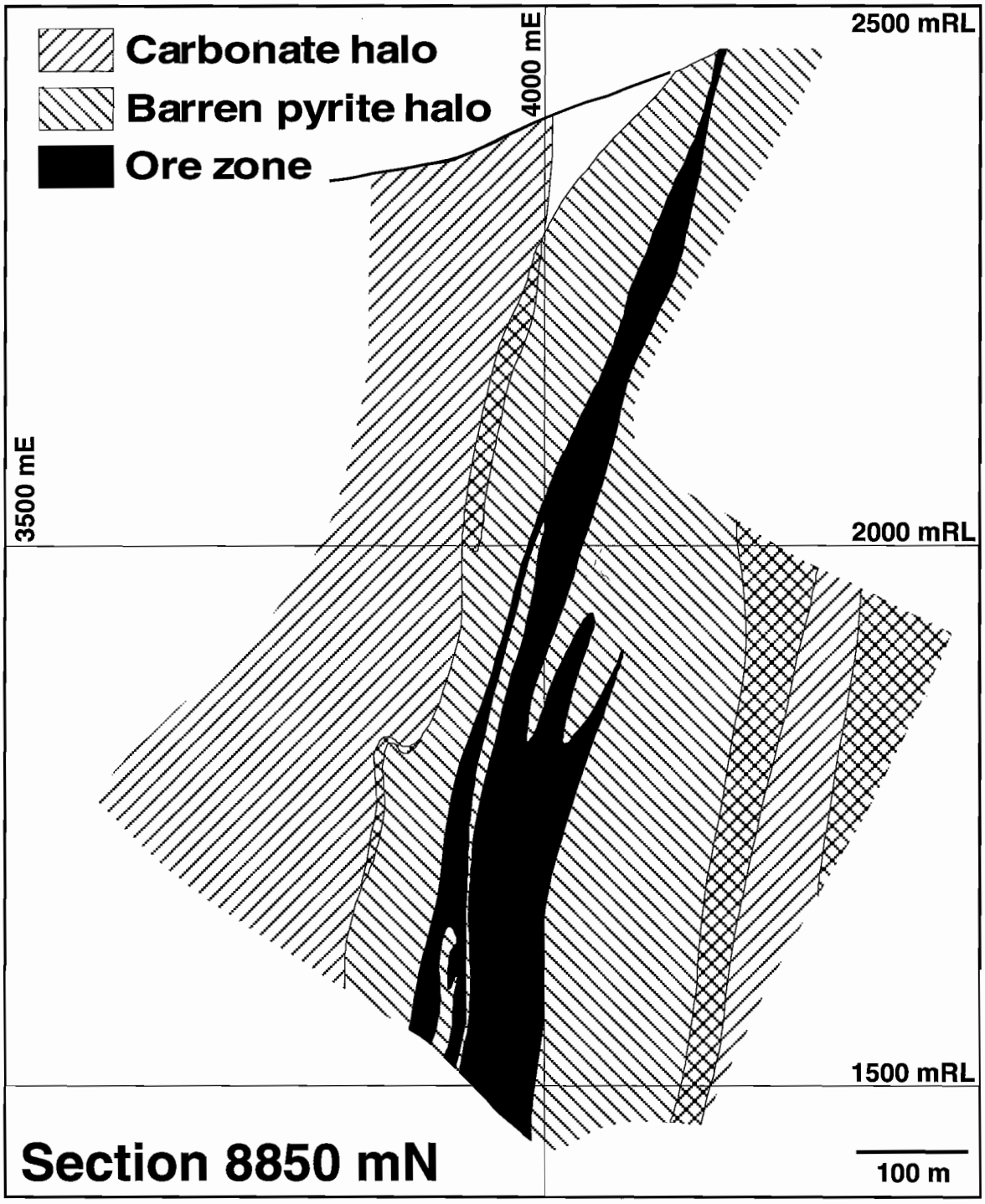

Figure 1 The distribution of pyrite and siderite on section 8850 mN, Western Tharsis deposit.

Distribution of rock types, alteration assemblages and iron minerals

Huston (1997) interpreted that the ore lens at Western Tharsis was hosted by a 200–300 m thick unit of felsic volcaniclastic rocks flanked on both sides by coherent and clastic "mafic" volcanic rocks. The felsic volcaniclastic rocks are generally characterised by quartz-sericite-bearing alteration assemblages that locally contain chlorite, whereas the "mafic" rocks are characterised by alteration assemblages containing abundant chlorite but lacking quartz. Of particular relevance to the following discussion is the distribution of pyrite and carbonate (Fig. 1).

A characteristic of the Western Tharsis ore system is the systematic distribution of iron minerals about the orebody. The orebody (approximated using a 0.5% Cu cutoff) is surrounded by a "barren" halo zone that extends 100 m to the west into the stratigraphic footwall and 150–200 m into the stratigraphic hanging wall (Fig. 1). This barren pyrite halo, which contains 1–20% pyrite, is surrounded and partly overlapped by an outer "carbonate" halo which contains 1–20% siderite. The distribution of pathfinder elements at Western Tharsis is closely related to these halos, as discussed below.

Analytical techniques

A total of 215 samples from Western Tharsis were analyzed at the University of Tasmania using XRF analysis (major elements, S, As, Ba, Bi, Ce, Cr, Cu, La, Nb, Nd, Ni, Pb, Rb, Sc, Sr, Th, V, Y, Zn and Zr) and at Analabs in Perth using ICP-MS analysis (Ag, As, Bi, Cd, Cs, Mo, Sb, Th, Tl and V), LECO titration analysis (C) and hydride generation AAS analysis (Se). With the exception of a few partial analyses, the analytical data is complete; the results are tabulated in Appendix 1. Although Co analyses were included in the original research proposal, the samples were pulverised in a tungsten carbide ring mill, which led to contamination that invalidated the Co results.

Both XRF and ICP-MS data exist for As, Bi and Th, which allows comparison of these two methods. The results for As and Bi were found to be similar. Owing to better detection limits, the Analabs ICP-MS data for these two elements were used in contouring cross sections. However, the Analabs data for Th differed substantially from the University of Tasmania data. For the Analabs data, two sets of sequential samples are characterised by a Th spike of up to 100 ppm, which decayed over three to four samples to the "typical" value of 10–20 ppm. Owing to this problem, the XRF Th data were used in calculating Th/U ratios. Examination of standard and repeat ICP-MS analyses indicates that, in addition to Th, problems exist in the analytical data for Cd and Mo. The distribution of Cd was not determined as it behaves very similar to Zn in ore forming enrironments. However, the distribution of Mo was determined using the ICP-MS data. Although the general results for Mo presented below are probably correct, the details of the relationships to other elements must be considered suspect.

Results

To establish stratigraphic zonation in ore-related metals, samples were collected from a suite of drill holes along section 8850 mN, which cuts through the centre of the Western Tharsis deposit. Analytical data for MgO, Na_2O, K_2O, C, S, Cu, Zn, As, Ba, Bi, Cs, Mo, Sb, Se, Tl, Th/U and S/Se were contoured by hand on this section. However, owing to budget constraints, only five of these sections (Cu, Zn, K_2O, Ba and As) have been captured into ARCINFO and MAPINFO (Figs. 2 to 6). Additional sections may be captured at a later date.

To establish lateral zonation in ore-related metals, samples were also collected from holes WT0037 (Fig. 7) and WT0048 (Fig. 8), which are located 100–150 m south and north of the orebody. Hole WT0037 is located on section 8600 mN, within a moderately mineralised interval between the Royal Tharsis and Western Tharsis deposits. Hole WT0048 is located on section 9100 mN, along the weakly mineralised northern perimeter to the Western Tharsis deposit. No known deposit occurs at the same stratagraphic position north of Western Tharsis.

Based on these contoured sections and inter-element correlations (see below), the elements of interest can be subdivided into three major groups (Table 1): (1) elements (C, MnO, CaO, Zn and Tl) that are enriched in the carbonate halo but depleted in the barren pyrite halo; (2) elements (K_2O and Cs) that are characterised uniform values except for extreme

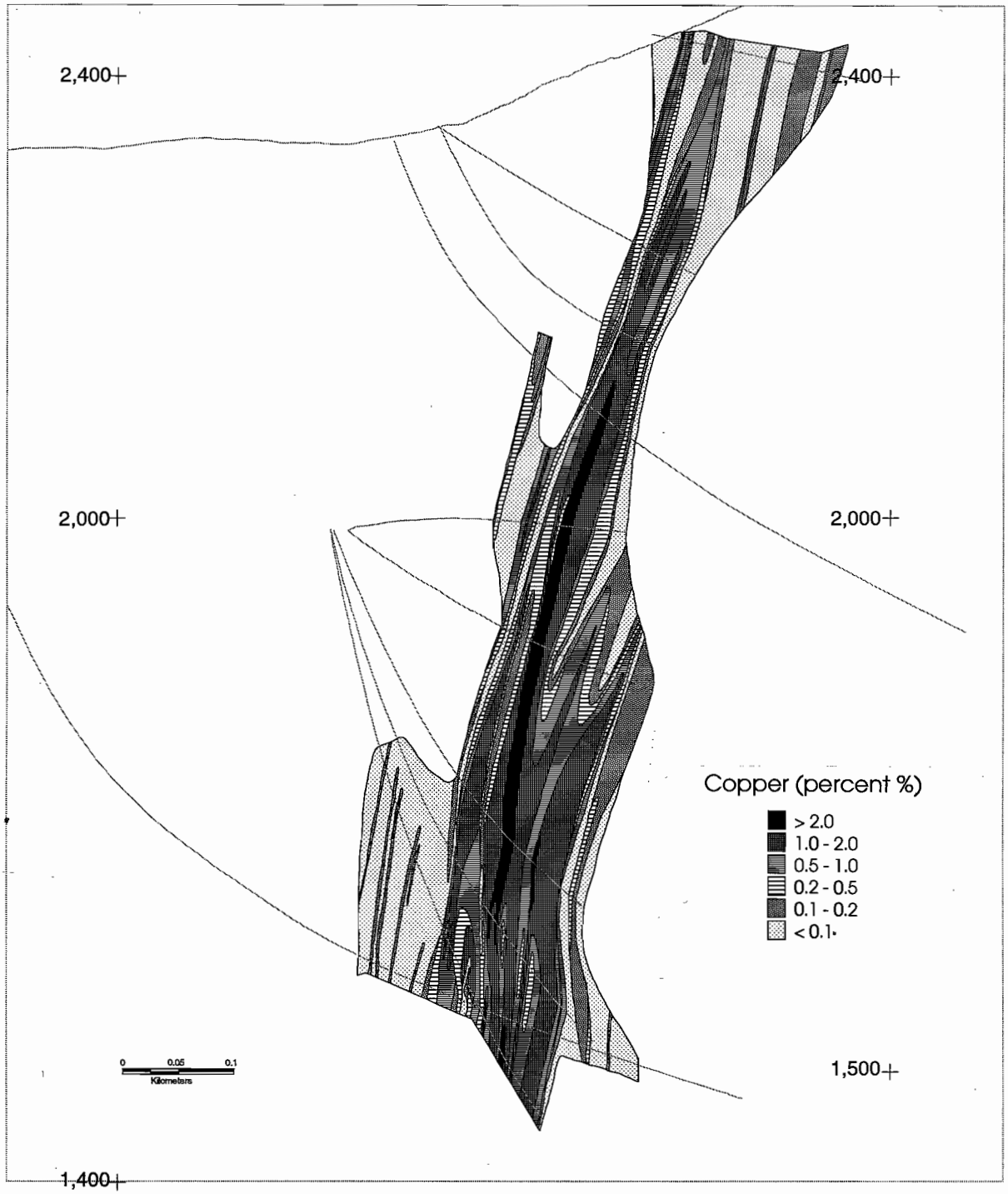

Figure 2 . The distribution of Cu on section 8850 mN, Western Tharsis deposit.

Figure 3 The distribution of As on section 8850 mN, Western Tharsis deposit.

Figure 4 The distribution of K_2O on section 8850 mN, Western Tharsis deposit.

Figure 5 The distribution of Zn on section 8850 mN, Western Tharsis deposit.

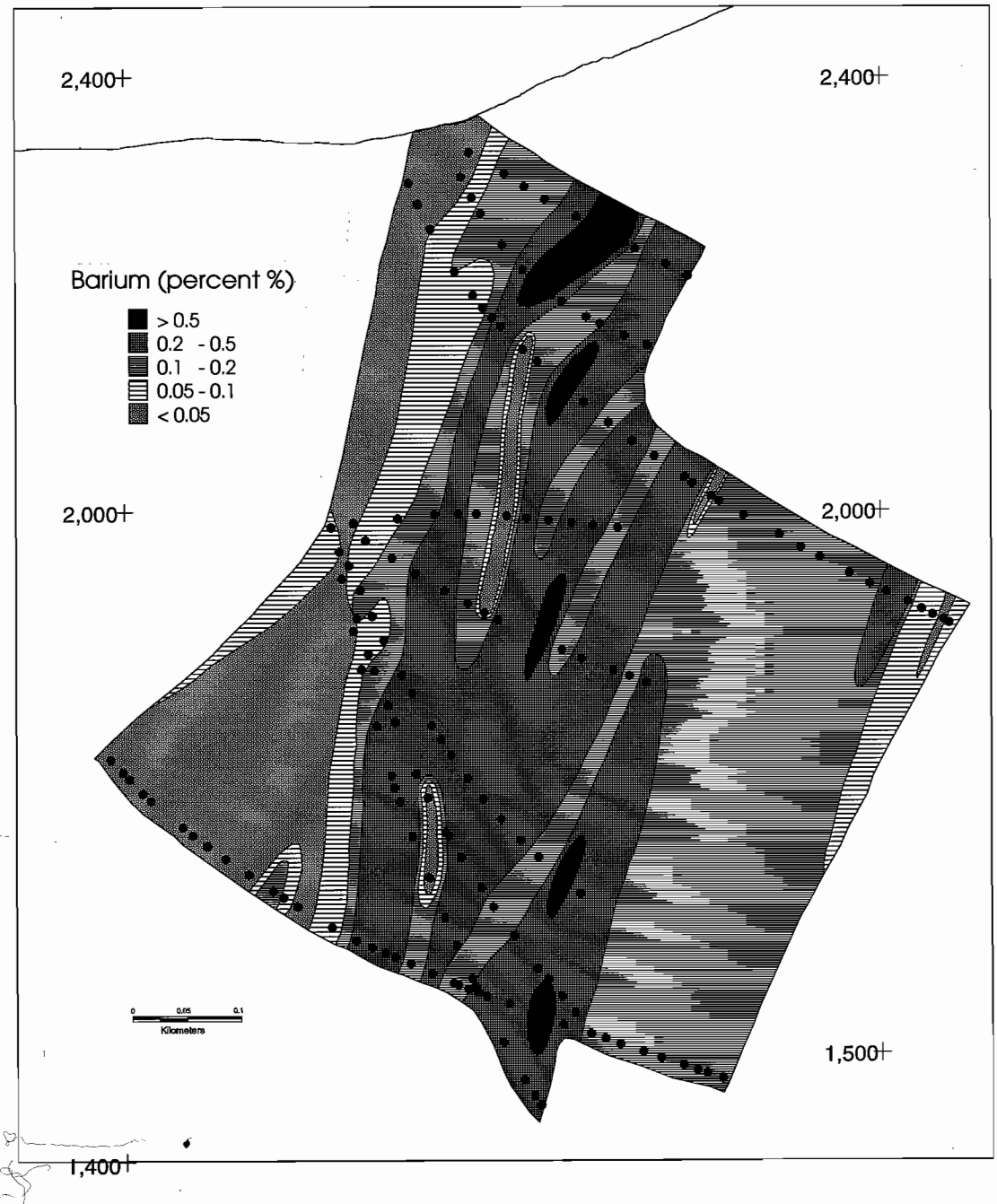

Figure 6 The distribution of Ba on section 8850 mN, Western Tharsis deposit.

depletion anomalies along the flank of the ore lens in the barren pyrite halo; and (3) elements (As, Bi, Cu, Mo, Ni, S and Se) that are strongly enriched in the ore zone, enriched in the barren pyrite halo, but depleted in the carbonate halo. Barium, MgO, Na_2O and Sb do not fit into these groupings.

Group 1: Elements enriched in the ore zone and barren pyrite halo

On section 8850 mN, the ore zone is surounded by a barren pyritic halo that extends 100 m into the stratigraphic footwall and up to 300 m into the hanging wall (Fig. 1). This halo is also developed in marginal hole WT0037, which contains a ~50 m zone of elevated Cu grades (to 1.2%; generally 0.2–0.6%; Fig. 7). In contrast, the pyritic halo is only weakly developed in hole WT0048, which is virtually barren of significant Cu grades, except for a ~30 m low grade (0.05–0.5% Cu) intersection at the base of the hole (Fig. 8).

Figure 2 illustrates the distribution of Cu on section 8850 mN as established using routine company analytical data on the holes logged in this study. Using a cutoff of 0.5%, the orebody, which is restricted to a thick rhyolitic volcaniclastic unit, thickens from a width of less than 2 m near the surface to ~110 m at the extent of drilling. Comparison of Figure 3 with Figure 2 illustrates the close correlation of As to the ore zone, and comparison of Figure 3 with Figure 1 illustrates that As enrichment extends into the barren pyrite zone, but not into the outer carbonate zone (Table 1).

Figure 9 illustrates that Mo, Ni and S correlate with Cu and form part of the ore metal assemblage. Although the correlation between Bi and Cu is not great (Fig. 9a), the contoured section (not shown) indicates Bi enrichment in the ore zone and, to a lesser extent, in the pyrite halo. Of these four elements, contouring along section 8850 mN (not shown) indicates that Mo enrichment is mainly restricted to the ore zone, but that anomalous Bi values extend well into barren pyrite zone (Table 1). Although Zn is enriched within the ore zone (Fig. 5), it has poor correlation with Cu (Fig. 9e) as Zn is also enriched in the carbonate halo (see below). The distribution of Se generally follows that of the S, but the highest values seem to be displaced to the hanging wall of the ore lens (Table 1). The significance of this relationships and S/Se ratios will be addressed in a future report.

Group 2: K_2O and Cs

The distribution of K_2O (Fig. 4) is characterised by zones of extreme depletion (0.06–0.9%) in narrow (20–30 m) zones that flank to orebodies both in the footwall and the hanging wall. Elsewhere in section 8850 mN, the abundance of K_2O is typically 2–4%. A similar zone of K_2O depletion occurs stratigraphically below the mineralised intersection in hole WT0037 (Fig. 7). Although extreme K_2O depletion zones are not recognised in hole WT0048 (Fig. 8), K_2O values in the weakly Cu-mineralised zone are significantly lower than the surrounding rocks (Fig. 8).

The combination of extreme K_2O and MgO (see below) depletion with "normal" Al_2O_3 abundances (7–18%; mainly 10–13%) suggests that these zones probably contain significant quantities of aluminosilicate minerals. Examination of thin sections suggests the presence of pyrophyllite and kaolinite in these zones, but this must be confirmed by XRD and PIMA analysis as pyrophyllite, in particular, can be very difficult to distinguish from sericite in thin section.

Group 3: Elements enriched in the outer carbonate halo

As described by Huston (1997), the barren pyrite zone is surrounded by a halo of abundant siderite (Fig. 1). This zone occurs 100–300 m from the ore zone, both in the footwall and the hanging wall. The extensive development of siderite in hole WT0048 (Fig. 8) suggests that the carbonate halo closes off the pyrite halo to the north.

In addition to high order C anomalism (>0.5%; not shown), contouring of section 8850 mN indicates that the carbonate halo is characterised by low level Zn (100–1000 ppm; Fig. 5) and Tl (0.5–1.2 ppm; not shown) anomalism. Zinc and Tl anomalism is restricted to the upper 100–150 m of the stratigraphically lower carboante halo. In the upper carbonate halo, Zn and Tl anomalism is erratic, but with higher values. Hole WT0048, to the north of the Western Tharsis deposit, is characterised by C, Zn and Tl anomalism throughout its entire length (Fig. 8). In contrast, C, Tl and weak Zn (approaching 100 ppm) anomalism is restricted to the upper 80 m of

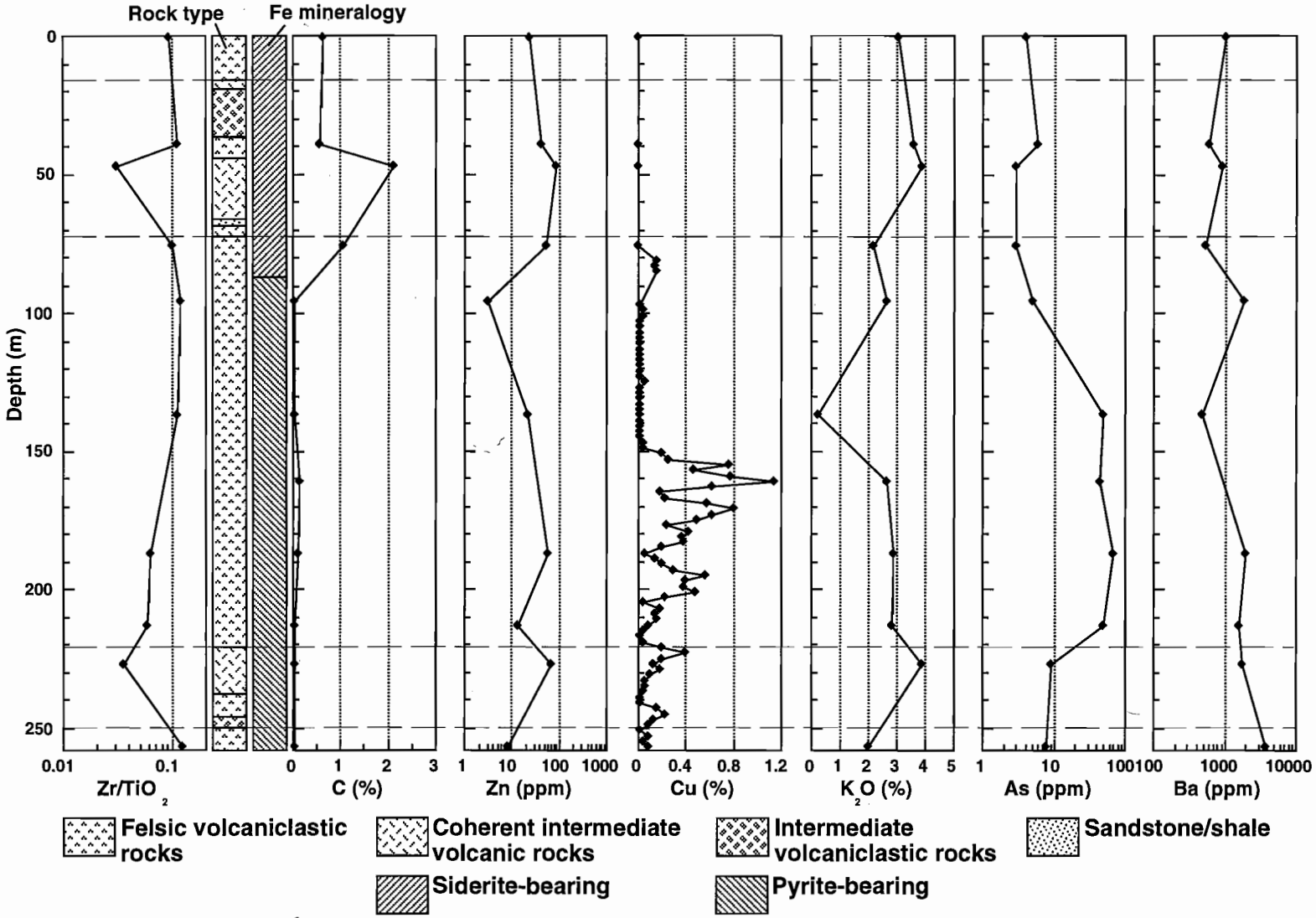

Figure 7 Variations in lithology, Fe mineralogy, Zr/TiO_2, C, Zn, Cu, K_2O, As and Ba as a function of depth in hole WT0037, Western Tharsis deposit.

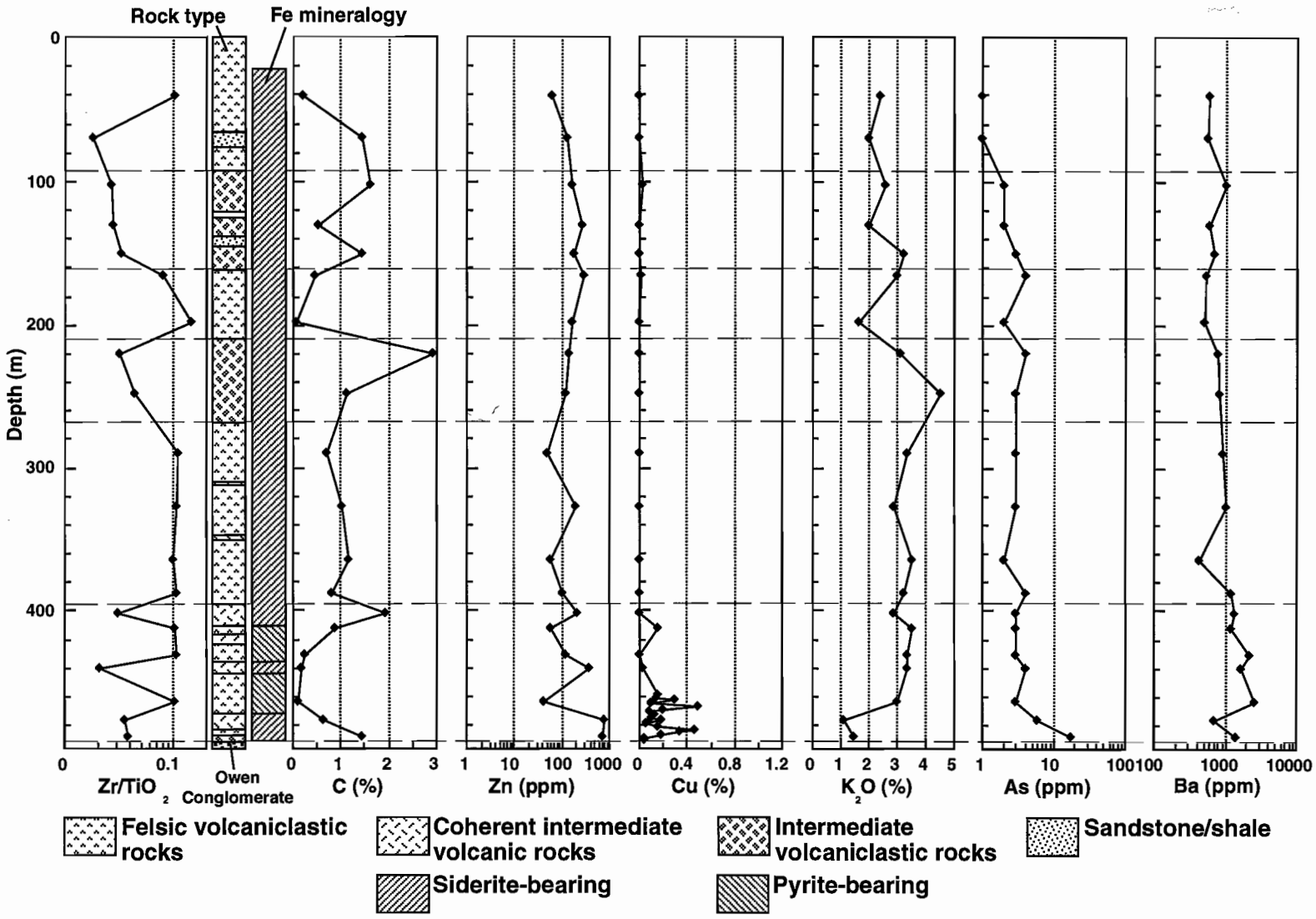

Figure 8 Variations in lithology, Fe mineralogy, Zr/TiO_2, C, Zn, Cu, K_2O, As and Ba as a function of depth in hole WT0048, Western Tharsis deposit.

Table 1 The distribution of selected elements with potential exploration utility at the Western Tharsis deposit, Mt Lyell, Tasmania.

As, Bi, Mo and S

These four elements are characterised by extreme enrichments in the ore zone flanked by less extreme enrichments in the barren pyrite zone and background values in the carbonate zone. In the case of Mo, enrichment in the barren pyrite zone is very limited, and Bi and S enrichments in the hanging wall are very erratic. Arsenic has the "smoothest" distribution. The following summarises the abundances of these elements:

	Ore zone	Barren pyrite zone		Carbonate zone
		Footwall	Hanging wall	
As (ppm)	10-100	5-20	5-10	<5
Bi (ppm)	0.5-1.3	0.5-2	0.5-6	<0.5
Mo (ppm)	20-800	1-10	<5	<1
S (%)	2-20	1-10	1-10	<1

Se

Selenium has a broadly similar distribution to the suite As-Bi-Mo-S. Although enriched in the ore zone (2-10 ppm), the highest values (5-50 ppm) occur marginal to the orebody, particularly in the hanging wall. Values in the hanging wall are highly erratic, although they drop off ~50 m from the Owen contact.

K_2O and Cs

K_2O and Cs are generally characterised by relatively uniform values (2-4% and 1.5-3 ppm, respectively) throughout, except in 20-30 m wide, stratiform zones that occur 20-70 m both above and below the margins of the ore zone. These zones are characterised by extreme depletion (0.06-0.9% and 0.1-0.9 ppm, respectively).

C, Zn

Carbon(ate)-rich (>0.5% C) zones occur within the peripheral carbonate zone that starts 50-250 m from the ore lens margin both in the footwall and in the hanging wall. Within the barren pyrite zone, C values are <0.1%, although slightly higher values (0.2-0.5%) occur locally in the ore zone. In several drill holes, C values increase gradually in the footwall carbonate zone (from 0.5 to 2%) and then dramatically decrease when the pyrite zone is reached. Zinc has a similar distribution, with low order anomalism (100-300 ppm) along the upper margin of the lower carbonate zone. In the upper carbonate zone, Zn anomalism is erratic but with higher maximum values (to 1200 ppm). In the barren pyrite zone Zn values are typically 5-50 ppm, but in the ore zone, Zn values are up to 50 ppm.

Tl

Thallium is characterised by anomalous values (0.5-1.2 ppm) in the peripheral carbonate zones and a depleted zone (<0.5 ppm) in the barren pyrite and ore zones. Although the anomaly in the hanging wall carbonate zone extends to the Owen contact, the anomaly only occurs in the upper 100-150 m of the footwall carbonate zone.

Sb

Antimony does not display a consistent distribution pattern, with most values between 0.5 and 2 ppm. There is an anomalous zone (2-3 ppm) in the upper 100 m of the footwall carbonate zone.

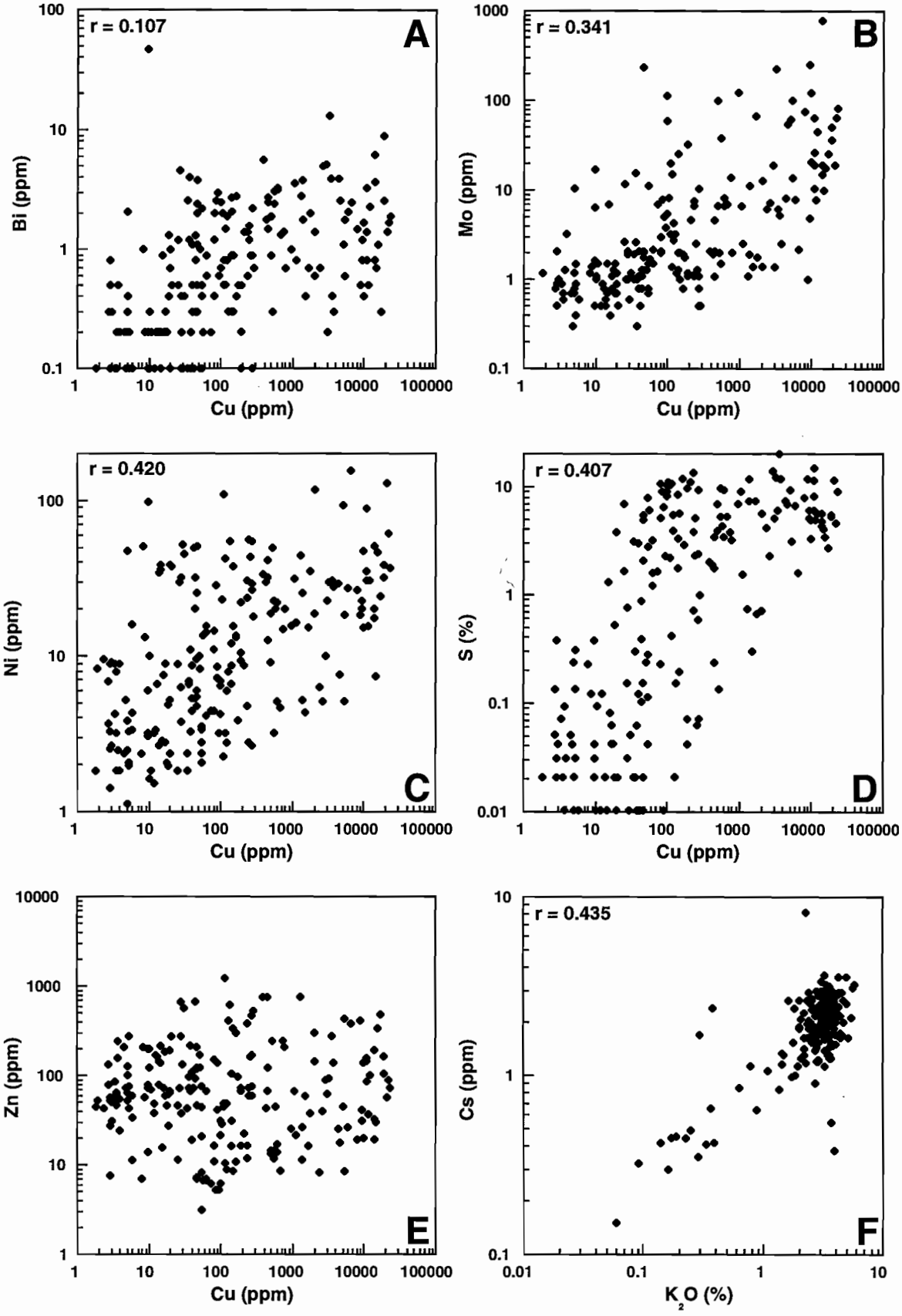

Figure 9 Scattergrams showing relationships between the following element pairs: (a) Cu-Bi, (b) Cu-Mo, (c) Cu-Ni, (d) Cu-S, (e) Cu-Zn, and (f) K_2O-Cs.

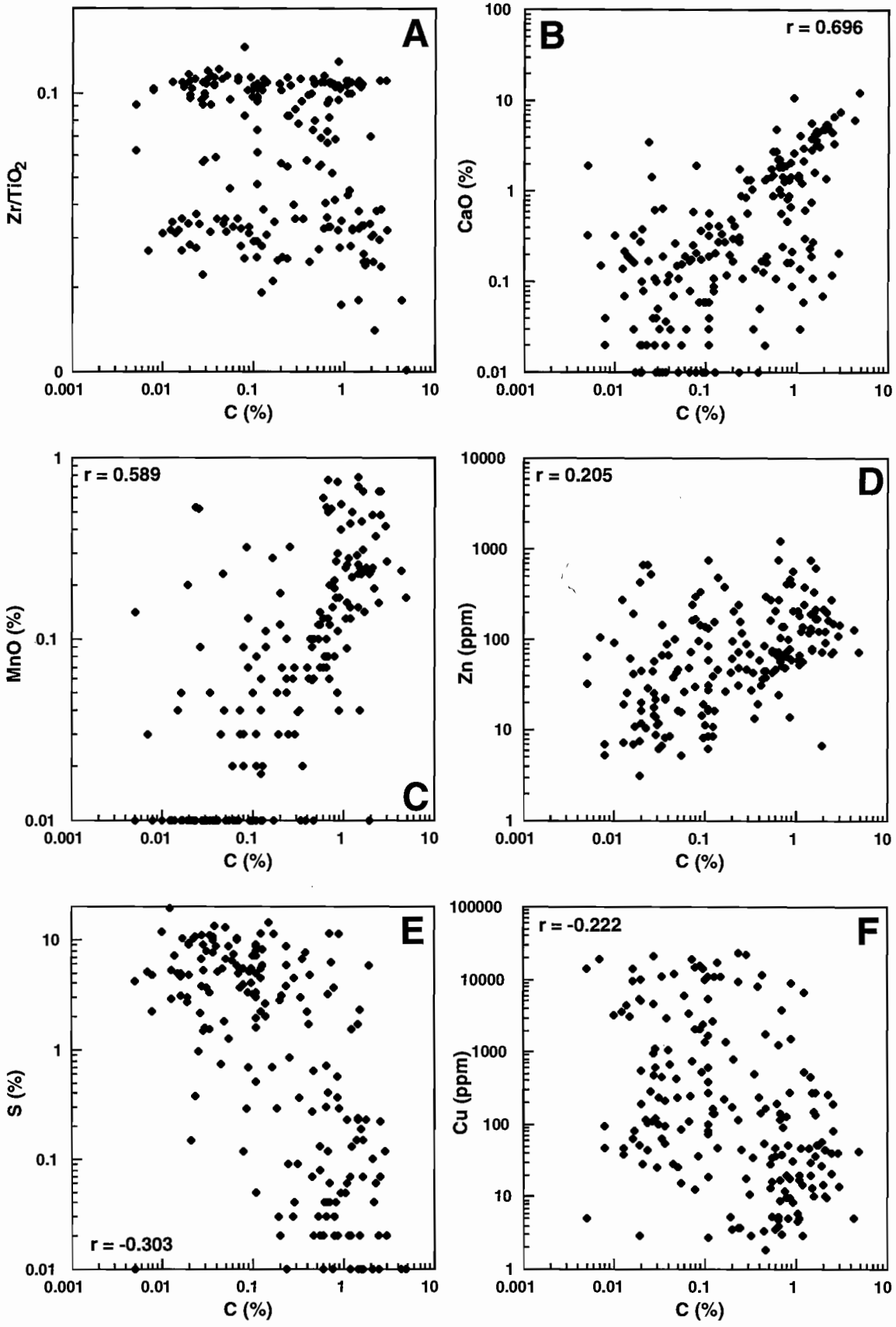

Figure 10 Scattergrams showing relationships between the following element pairs: (a) C-TiO_2, (b) C-CaO, (c) C-MnO, (d) C-Zn, (e) C-S, and (f) C-Se.

hole WT0037 (Fig. 7), which corresponds to the lower carbonate halo on section 8850 mnN.

To test if the carbonate halo is lithologically controlled, the Zr/TiO_2 ratio is plotted against C in Figure 10a. This diagram confirms the bimodal character of the Mt Lyell host volcanics (c.f. Manning, 1990; Raymond, 1992): the data clusters at Zr/TiO_2 ratios of 0.10–0.11 and 0.02–0.04. The higher Zr/TiO_2 ratios imply a rhyolitic composition for the felsic suite, whereas the lower ratios imply an andesitic to dacitic composition for the intermediate suite (c.f. Winchester and Floyd, 1977). This diagram also shows that the carbonate halo is not lithologically controlled as both the rhyolitic suite and the intermediate suites have large variations in C content.

Figure 10b and 10c show that CaO and MnO are strongly correlated with C, which is consistent with the substitution of these elements in carbonate minerals such as siderite. Figure 10d confirms the association of C and Zn; the element assemblage that characterises the carbonate halo is C-Ca-Mn-Zn-Tl. Figures 10e and 10f show that C is negatively correlated with Cu and S, confirming that these two elements are depleted in the carbonate halo.

Other elements

Anomalous Ba values of between 0.2 and 1.0% are centered on the orebody (Fig. 6). However, unlike the other elements enriched in the pyrite halo, anomalous Ba values extend into the lower carbonate halo, although not into the upper carbonate halo. In hole WT0037, Ba values generally increase down hole through the Cu-enriched zone, which is characterised by Ba values above 1000 ppm. In hole WT0048, anomalous Ba values (>1000 ppm) occur in the basal 100 m of the hole, and overlap the weakly Cu-mineralised zone.

The distribution of MgO is characterised by zones of extreme depletion that correspond to the K_2O-Cs depletion anomalies. Elsewhere the distribution is not uniform: high MgO values occur in a quartz-chlorite-sericite alteration zone within the ore zone and with intermediate volcanic rocks that flank the host rhyolitic package.

A Na_2O depletion anomaly extends 150 m into the stratigraphic footwall and up to the Owen contact in the hanging wall (not shown). This anomaly is present also in holes WT0037 and WT0048 (not shown). No consistent pattern was recognised for Sb.

Implications for exploration

These results define several relationships in the geochemical data that can be used as vectors in exploration. In addition to Cu, As, Bi, Mo, Ni, S and Se are potentially useful as vectors in the proximity of ore lenses. Barium anomalies appear to persist further from the orebody, and C, Zn, Tl, MnO and CaO form distinct anomalies on the stratagraphic and lateral peripheries of the Western Tharsis system. Extreme K_2O and Cs depletion anomalies indicate close proximity to the ore lens at Western Tharsis. These patterns probably also apply to other Prince Lyell-type orebodies in the Mt Lyell field. However, these patterns were developed using fresh, unweathered rock from drill core, and may not be directly transferable to the surficial environment.

The design of surficial geochemical surveys at Mt Lyell using the above relationships must take into account elemental behaviour in the weathering profile. Elements that are least mobile in the weathering environments are potentially the best guides. Using this criteria, the best elements for surficial geochemical surveys include Mn (to define the peripheral carbonate halo), Ba (to define broad zones of alteration centred on orebodies), Cu, As (to navigate within the "barren" pyrite halo), and K_2O (to define depletion anomalies immediately adjacent to orebodies). In addition, Na_2O should also be analysed to establish regions through which high temperature hydrothermal fluids have passed.

Comparison with other volcanogenic deposits in the Mt Read volcanic belt

One of the main scientific purposes of this study is to compare geochemical dispersion about disseminated Cu-only deposits, as represented by the Western Tharsis deposits, with geochemical dispersion about more typical massive Zn-Pb±Cu deposits.

In the mid 1970s, Smith (1975) and Fitzgerald (1974) studied the dispersion of selected elements about the Rosebery and Hercules deposits. Smith

and Huston (1992) combined these results with studies of trace elements in the ores to summarise the dispersion of trace elements in the Rosebery-Hercules mineral system. They found Tl and Hg to have the largest dispersion from the ore zones. Anomalous Tl values (1–30 ppm) occur 50 m statigraphically above the Rosebery ore position and at least 2 km along strike. Mercury has a broadly similar distribution, although it is not well quantified. Huston and Smith (1992) suggested that Bi, Cu, As, Cd, Zn, Pb, Sb, Au, Ag and Ba had limited dispersion outside of the ore lens at Rosebery.

Studies by Large (1996) and Large and Allen (1997) have confirmed the Tl halo at Hercules and Rosebery. At Rosebery, the Tl anomaly extends at least 100 m into the footwall and 200 m into the hanging wall. Antimony anomalism has a similar distribution, and erratic As anomalism is also present outside of the ore zone. Hence, Tl, As and Sb are characterised by extensive dispersion outside of the immediate ore zone, whereas Bi, Cd, Ba and the ore elements are only enriched in the ore zones.

The dispersion of elements about Western Tharsis has some similarities to the dispersion about Rosebery and Hercules. Thallium is enriched in a peripheral halo in all deposits, but at Western Tharsis the level of anomalism (0.5–1.2 ppm Tl) is much lower than at either Rosebery or Hercules (1–30 ppm Tl). In addition, other elements in the peripheral assemblage differ: the peripheral zone at Western Tharsis lacks As anomalism but is characterised by C, Ca, Mn and low level Zn anomalism. The K_2O and Cs depletion anomalies that flank the ore zone at Western Tharsis are not present at either Rosebery or Hercules.

Future directions

Although most of the analytical data were available for this report, a the distribution of a number of elements has not been determined, and variations in inter-element ratios (e.g. Th/U and S/Se) have not yet been evaluated as exploration guides. Interpretation of these data will be the major direction of future research in this project. A second direction will be more specialised studies, including isotope, PIMA, and mineral chemistry (electron and proton microprobe) studies to evaluate the efficacy of these techniques in exploration. A third possible direction is to evaluate the effect of weathering on elemental dispersion by analysing surface samples for the suite Mn, Ba, Cu, As, K_2O and Na_2O, as discussed above. The extent to which the latter two research directions are pursued depends, to a large degree, on the availablity of funds.

Acknowledgments

Nilar Hliang and Phil Robinson are thanked for their efforts to analyse the samples, and Mike Blake and Joe Stolz are thanked for their assistance at various stages of the project. Copper Mines of Tasmania provided access to drill core and logistical support in Queenstown. Paul Harbon, Peter Benjamin, Will Godsell, Geoff Iliff and Jeremy Lawrence are thanked for their assistance and discussion at the mine site.

References

Fitzgerald, F.G., 1974. The Primrose Pyroclastics in the Hercules–White Spur area, western Tasmania [Unpublished B.Sc. thesis]. University of Tasmania, 188 pp.

Huston, D.L., 1997. Research program and preliminary results of alteration studies at the Western Tharsis deposit, Mt Lyell field. AMIRA-ARC Project P439, Report 4.

Large, R.R., 1996. The Hercules–Mt Read traverse: relationships between volcanic mineralogy, alteration and geochemistry. AMIRA-ARC Project P439, Report 3: 153–234.

Large, R.R. and Allen, R., 1997. Preliminary report on the Rosebery lithochemical halo study. AMIRA-ARC Project P439, Report 4: 259–330.

Manning, C.G., 1990, The geology and mineralisation of the Western Tharsis copper deposit, Mt Lyell, Tasmania [Unpublished B.Sc. thesis]. University of Tasmania, 98 pp.

Raymond, O.L., 1992. Geology and mineralisation of the southern Prince Lyell deeps, Queenstown, Tasmania [Unpublished M.Sc. thesis]. University of Tasmania, 161 pp.

Smith, R.N., 1975. Precious and volatile metal distributions in the ores and host rocks of the Rosebery sulfide deposit [Unpublished M.Sc. thesis]. University of Melbourne, 171 pp.

Smith, R.N. and Huston, D.L., 1992. Distribution and association of selected trace elements at the Rosebery deposit, Tasmania. Econ. Geol. 87: 706–719.

Winchester, J.A. and Floyd, P.A., 1977, Geochemical discrimination of different magma series and their differentiation products using immobile elements. Chem. Geol. 20: 325–344.

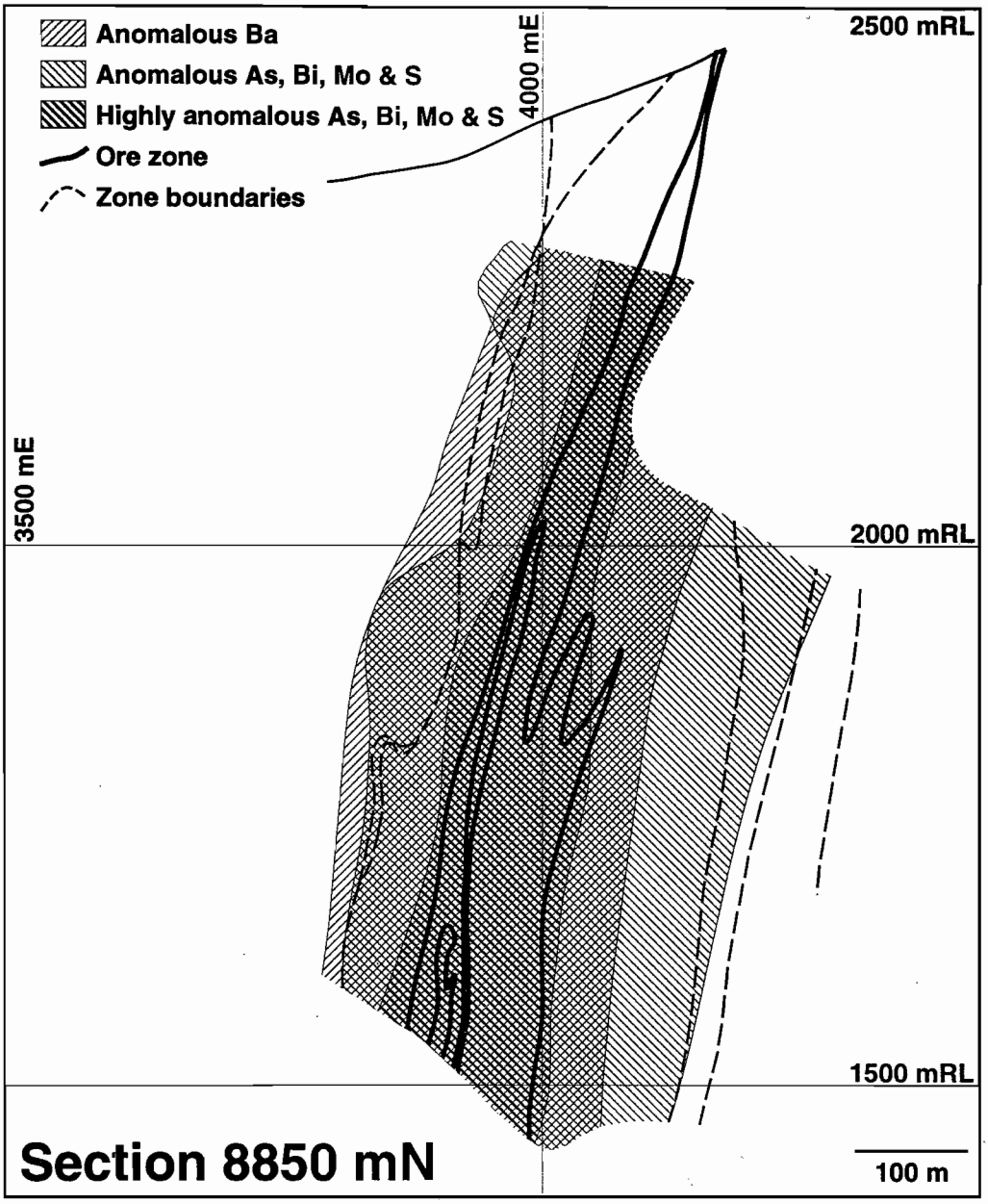

Figure 11 Schematic cross section showing the distribution of Ba, As, Bi, Mo and S anomalies relative to the orebody at Western Tharsis. The representation of the distribution of As, Bi, Mo and S is based on the actual distribution of As on section 8850 mN. The representation of the distribution of Ba is based on the actual distribution of Ba on section 8850 mN.

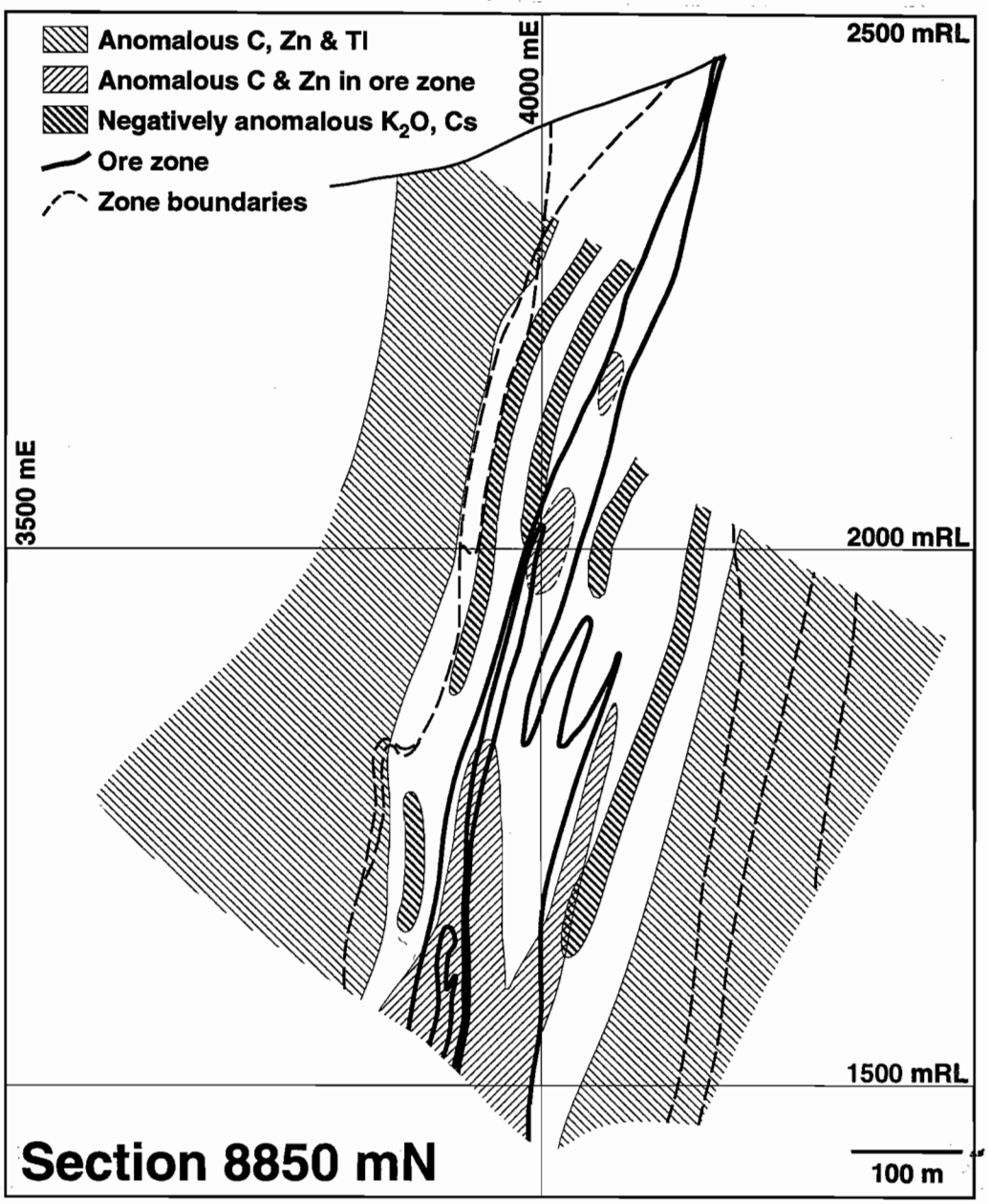

Figure 12. Schematic cross section showing the distribution of C, Zn, Tl, K_2O and Cs anomalies relative to the orebody at Western Tharsis. The representation of the distribution of C, Zn and Tl is based on the actual distribution of Zn on section 8850 mN. The representation of the distribution of K_2O and Cs is based on the actual distribution of K_2O on section 8850 mN.

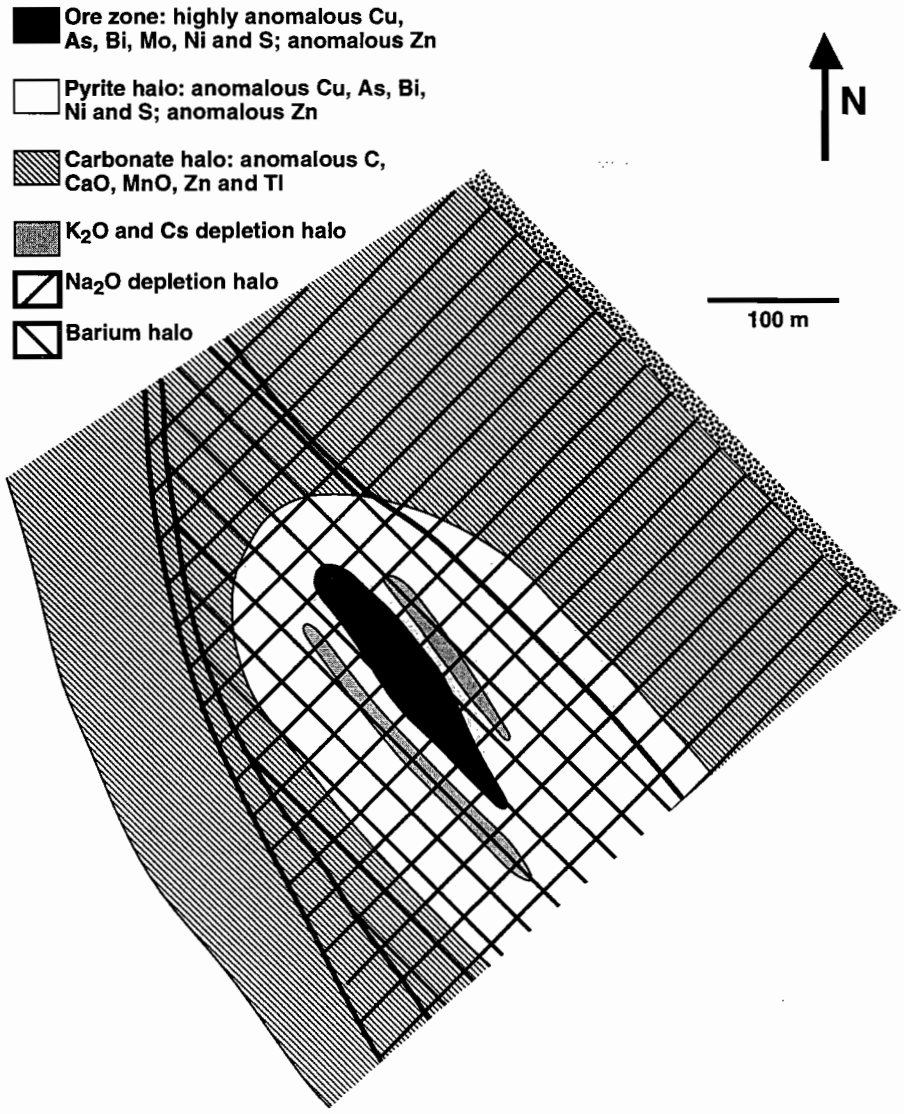

Figure 13. Schematic plan showing the distribution of dispersion halos at Western Tharsis.

Appendix: Analytical results

Hole	WT0025	WT0025	WT0025	WT0025	WT0025	WT0025	WT0025	WT0025	WT0025	WT0025	WT0025	WT0037	WT0037	WT0037	WT0037	WT0037
From (m)	3.4	46.2	79.8	103.1	118.7	146.7	166.2	186.0	209.1	229.2	252.4	0.2	39.3	47.2	75.7	95.3
To (m)	3.7	46.6	80.1	103.4	119.0	147.3	166.8	186.4	209.6	229.7	253.0	0.6	39.7	47.6	76.1	95.8
SiO2 (%)	69.81	69.56	51.71	52.51	71.69	73.44	67.75	62.52	57.81	71.25	66.36	72.58	75.24	53.48	67.84	75.72
TiO2 (%)	0.39	0.24	0.60	0.63	0.21	0.19	0.22	0.27	0.32	0.22	0.19	0.29	0.23	0.42	0.20	0.24
Al2O3 (%)	12.16	12.39	16.40	17.31	10.93	10.64	11.55	7.14	11.82	9.61	10.72	13.49	12.10	14.76	10.24	13.15
Fe2O3 (%)	6.26	6.96	10.21	10.00	8.00	8.48	9.35	17.69	13.76	8.56	12.43	2.00	3.08	7.92	11.74	3.59
MnO (%)	0.12	0.26	0.31	0.48	0.01	<0.01	<0.01	<0.01	0.10	0.01	<0.01	0.08	0.14	0.25	0.16	<0.01
MgO (%)	2.63	0.83	2.88	2.78	0.38	0.06	0.48	0.06	1.34	0.30	0.06	1.12	0.87	2.76	1.54	0.16
CaO (%)	1.44	0.14	3.68	1.39	<0.01	<0.01	0.02	0.10	0.31	0.11	0.08	1.86	0.90	5.37	0.03	<0.01
Na2O (%)	0.79	0.21	0.11	0.14	0.06	0.04	0.05	0.05	1.02	0.08	<0.05	1.29	0.16	0.26	0.12	0.34
K2O (%)	2.23	3.62	3.98	4.80	3.16	0.25	3.38	0.89	2.92	2.56	0.19	3.04	3.57	3.87	2.19	2.63
P2O5 (%)	0.09	0.04	0.15	0.17	0.04	0.04	0.06	0.21	0.39	0.17	0.21	0.05	0.04	0.21	0.02	0.03
CuO (%)	0.00	0.00	0.00	0.00	0.06	0.00	0.59	0.36	2.94	0.13	0.01	0.00	0.00	0.00	0.00	0.00
BaO (%)	0.02	0.06	0.19	0.32	0.12	0.01	0.39	0.14	0.39	0.28	0.18	0.12	0.08	0.10	0.07	0.21
LOI (%)	4.22	5.27	8.98	9.03	5.12	6.46	6.04	10.54	7.71	5.77	8.66	4.06	3.75	9.71	5.52	3.68
Sum (%)	100.16	99.58	99.20	99.56	99.79	99.61	99.88	99.98	100.83	99.04	99.09	99.98	100.16	99.11	99.67	99.75
S (%)	<0.01	<0.01	0.01	0.01	5.11	6.62	6.74	13.28	8.69	6.65	9.82	0.03	0.02	0.10	0.23	2.72
C (%)	0.520	1.080	1.650	2.070	0.093	0.051	0.028	0.038	0.230	0.027	0.066	0.630	0.550	2.100	1.070	0.019
Ag (ppm)	0.2	0.1	0.1	0.1	0.3	0.1	0.5	0.8	1.8	0.2	0.2	0.2	0.1	0.1	<0.1	0.2
As (ppm)	2	4	5	3	14	9	28	145	44	15	11	4	6	3	3	5
Ba (ppm)	397	494	1978	2679	1207	218	3799	1029	3354	2485	1862	1009	604	921	530	1905
Bi (ppm)	<2	<2	<2	<2	4	<2	3	5	<2	<2	<2	<2	<2	<2	<2	<2
Cd (ppm)	0.4	0.4	0.5	0.4	0.4	0.4	0.5	0.4	0.5	0.6	0.4	0.4	0.4	0.4	0.4	0.4
Ce (ppm)	84	106	61	59	101	148	204	569	580	401	140	111	103	115	74	93
Cr (ppm)	70	110	43	77	131	226	185	210	154	202	234	3	3	22	3	3
Cs (ppm)	2.24	3.03	2.09	2.58	2.12	0.49	2.27	0.64	1.53	1.54	0.46	2.39	2.95	2.67	1.31	1.77
Cu (ppm)	13	20	37	10	538	25	4700	2863	23500	975	112	4	35	45	5	53
La (ppm)	41	49	30	25	48	108	133	364	403	284	111	48	49	62	35	48
Mo (ppm)	0.8	0.9	1.0	1.1	1.5	11.6	54.2	19.0	83.0	124.0	19.9	3.3	1.9	1.3	0.8	0.8
Nb (ppm)	10	15	8	8	12	12	14	11	22	14	12	13	13	7	10	15
Nd (ppm)	37	49	29	28	45	33	64	171	134	90	28	51	47	46	35	32
Ni (ppm)	7	5	11	10	3	9	7	10	36	15	107	2	2	20	4	3
Pb (ppm)	101	7	13	6	8	7	10	23	14	14	20	55	6	9	3	6
Rb (ppm)	69	118	128	139	94	7	83	23	74	57	5	89	119	129	65	70
Sb (ppm)	0.7	1.8	2.8	1.6	1.2	0.8	1.0	8.8	0.9	0.4	0.6	0.8	4.2	2.0	1.1	1.3
Sc (ppm)	12	8	19	19	10	5	8	3	7	7	3	10	9	28	7	11
Se (ppm)	<0.5	<0.5	<0.5	<0.5	1.6	2.2	7.8	6.7	3.1	6.9	8.7	<0.5	<0.5	<0.5	<0.5	1.6
Sr (ppm)	47	24	53	48	45	119	185	189	74	276	947	86	25	71	17	127
Th (ppm)	14	20	9	10	19	15	14	27	15	25	8	19	17	20	16	21
Tl (ppm)	<0.5	0.7	0.7	1.0	0.9	<0.5	<0.5	<0.5	<0.5	<0.5	<0.5	0.9	0.9	0.9	0.5	0.5
U (ppm)	3.02	4.71	2.81	2.85	5.03	3.40	13.80	14.50	4.29	3.46	2.28	3.28	4.27	4.71	4.18	7.43
V (ppm)	39	4	195	202	7	23	34	33	34	42	107	12	4	201	3	12
Y (ppm)	29	43	27	29	40	15	19	14	28	10	5	39	42	19	36	38
Zn (ppm)	165	67	213	124	15	47	17	90	74	26	49	25	43	91	53	3
Zr (ppm)	213	267	148	156	238	219	242	159	174	199	218	267	251	130	201	281

Appendix: Analytical results cont.

Hole	WT0037	WT0037	WT0037	WT0037	WT0037	WT0037	WT0038	WT0038	WT0038	WT0038	WT0038	WT0038	WT0038	WT0038	WT0038	WT0038
From (m)	136.0	160.0	186.0	212.0	226.0	256.0	50.2	71.9	89.3	125.4	154.5	175.0	190.4	202.0	229.0	243.8
To (m)	138.0	162.0	188.0	214.0	228.0	258.0	50.7	72.3	89.8	126.0	154.9	175.4	190.8	202.4	229.4	244.3
SiO2 (%)	63.45	52.01	59.50	63.56	56.10	72.74	71.55	72.53	72.48	69.57	54.90	61.91	63.10	54.92	68.25	73.54
TiO2 (%)	0.22	0.52	0.29	0.35	0.47	0.25	0.26	0.22	0.26	0.21	0.50	0.18	0.45	0.63	0.26	0.23
Al2O3 (%)	11.29	10.20	11.56	12.77	13.23	12.04	12.00	11.72	13.98	10.97	13.79	9.85	13.83	17.65	12.68	11.88
Fe2O3 (%)	14.41	19.84	14.04	11.49	13.38	6.49	3.98	4.33	2.72	8.51	17.14	15.75	11.24	15.79	9.83	5.78
MnO (%)	0.00	0.01	0.02	<0.01	0.01	<0.01	0.13	0.27	0.15	0.23	0.50	0.02	0.01	0.06	0.01	<0.01
MgO (%)	0.04	0.28	0.27	0.18	0.87	0.20	1.46	1.15	0.50	1.14	3.20	0.30	0.09	1.11	0.06	0.47
CaO (%)	0.04	0.34	0.06	0.10	0.12	0.03	1.93	1.31	1.92	0.19	0.30	0.01	0.16	0.17	<0.01	<0.01
Na2O (%)	0.05	0.12	0.12	0.19	0.44	0.27	1.51	0.12	0.26	0.18	0.56	0.13	0.17	0.26	<0.05	0.25
K2O (%)	0.23	2.67	2.91	2.85	3.89	1.98	2.62	3.40	3.94	3.07	2.38	2.58	0.79	4.23	0.37	3.33
P2O5 (%)	0.05	0.30	0.12	0.13	0.13	0.07	0.05	0.03	0.04	0.05	0.20	0.05	0.16	0.15	0.08	0.04
CuO (%)	0.02	1.39	0.04	0.06	0.11	0.09	0.00	0.00	0.00	0.06	0.06	0.01	0.01	0.01	0.01	0.30
BaO (%)	0.06	0.14	0.20	0.15	0.18	0.39	0.04	0.07	0.11	0.17	0.50	0.65	0.94	0.30	0.11	0.17
LOI (%)	9.93	11.57	10.16	7.86	11.02	5.35	4.23	4.69	4.47	5.84	6.89	9.30	8.70	5.17	7.83	4.37
Sum (%)	99.78	99.41	99.29	99.69	99.95	99.90	99.76	99.84	100.83	100.19	100.93	100.74	99.63	100.45	99.49	100.36
S (%)	10.69	14.52	8.87	8.87	8.84	5.08	0.12	0.04	0.01	0.23	0.13	11.23	8.82	1.68	7.67	4.11
C (%)	0.037	0.150	0.110	0.029	0.040	0.041	0.680	0.830	0.760	1.410	1.230	0.120	0.054	0.410	0.036	0.098
Ag (ppm)	0.2	1.3	0.2	0.3	0.2	0.2	0.1	0.1	0.1	0.3	0.2	0.3	0.3	0.2	0.1	0.3
As (ppm)	49	44	67	49	9	8	3	2	2	11	5	8	15	11	11	21
Ba (ppm)	481		1944	1558	1803	3833	386	637	988	1392	4692	6344	7986	2909	674	1592
Bi (ppm)	<2		<2	4	3	<2	<2	<2	<2	3	<2	2	<2	3	2	<2
Cd (ppm)	0.4	0.4	0.4	0.4	0.4	0.4	0.4	0.4	0.5	0.4	0.4	0.3	0.4	0.4	0.4	0.4
Ce (ppm)	145		204	188	123	110	103	103	116	232	136	180	199	76	265	78
Cr (ppm)	10		246	55	284	213	4	3	3	5	195	4	244	9	5	13
Cs (ppm)	0.45	1.55	1.69	2.46	2.57	1.84	2.39	2.25	1.97	1.96	1.85	2.35	1.13	3.57	0.65	2.47
Cu (ppm)	207	11100	277	622	1067	679	9	53	12	457	532	165	87	139	53	2400
La (ppm)	120		150	106	69	54	49	47	55	142	79	106	118	36	189	43
Mo (ppm)	4.6	10.5	10.6	8.3	6.7	6.9	1.4	0.7	0.5	2.1	2.0	1.9	7.8	1.3	11.4	6.1
Nb (ppm)	12		12	11	9	16	12	13	16	13	8	10	10	7	16	12
Nd (ppm)	30		40	69	46	47	47	46	51	78	50	72	69	36	54	27
Ni (ppm)	8		26	22	30	5	13	3	2	12	49	13	28	7	2	6
Pb (ppm)	8		12	11	9	13	9	5	11	7	6	11	4	10	7	9
Rb (ppm)	6		67	68	102	60	72	112	123	99	77	82	23	119	9	74
Sb (ppm)	2.8	1.4	0.8	0.9	0.7	1.0	1.1	1.5	1.8	3.0	3.2	1.5	2.5	2.0	0.7	1.0
Sc (ppm)	3		6	11	31	11	12	9	12	8	33	10	13	21	16	10
Se (ppm)	10.9	7.1	17.9	8.7	3.2	2.8	<0.5	<0.5	<0.5	<0.5	<0.5	1.7	3.8	10.9	3.3	12.5
Sr (ppm)	361		155	157	76	222	38	21	30	19	54	131	590	101	213	63
Th (ppm)	17		13	18	18	15	18	17	21	19	19	15	19	13	18	13
Tl (ppm)	<0.5	0.6	0.9	0.8	0.8	0.5	0.8	0.8	0.9	0.9	0.6	0.6	<0.5	0.8	<0.5	<0.5
U (ppm)	4.13	11.60	3.17	5.18	7.02	3.55	4.14	4.23	4.22	8.21	6.16	7.46	7.47	6.39	5.53	5.22
V (ppm)	28		97	97	190	12	14	4	6	28	207	35	94	217	121	42
Y (ppm)	13		7	21	27	36	36	37	42	52	23	55	16	38	22	20
Zn (ppm)	23		59	14	68	8	57	75	48	125	248	11	5	31	8	8
Zr (ppm)	234		179	201	166	305	246	235	282	232	161	194	202	157	276	235

Appendix: Analytical results cont.

Hole	WT0038	WT0038	WT0048	WT0048	WT0048	WT0048	WT0048	WT0048	WT0048	WT0048	WT0048	WT0048	WT0048	WT0048	WT0048	WT0048
From (m)	269.5	292.0	40.8	69.2	102.7	130.3	150.3	164.8	198.3	220.0	247.9	289.9	326.8	364.7	388.0	401.6
To (m)	270.0	292.4	41.1	69.5	103.0	130.6	150.8	165.2	198.7	221.0	248.4	290.5	327.7	365.5	388.7	402.2
SiO2 (%)	61.72	64.23	76.58	50.50	53.81	58.20	56.93	74.24	72.13	50.15	62.17	71.12	72.41	69.97	73.98	55.11
TiO2 (%)	0.53	0.59	0.25	0.63	0.44	0.44	0.57	0.22	0.20	0.48	0.56	0.28	0.22	0.25	0.21	0.52
Al2O3 (%)	15.43	16.01	11.73	16.89	15.40	15.63	15.10	11.91	10.37	12.60	15.75	14.37	11.54	12.43	11.48	13.21
Fe2O3 (%)	9.05	7.07	4.26	9.43	9.06	11.33	8.15	4.11	7.22	7.49	6.95	1.87	4.02	4.04	4.04	8.89
MnO (%)	0.05	<0.01	0.12	0.26	0.24	0.10	0.15	0.01	0.09	0.27	0.28	0.06	0.13	0.13	0.17	0.24
MgO (%)	2.54	0.35	1.22	3.07	2.97	2.65	2.71	1.11	1.93	4.06	1.70	1.24	1.22	1.56	1.02	4.39
CaO (%)	0.06	0.09	0.30	5.64	4.68	1.75	3.78	0.16	1.94	7.54	1.23	1.82	1.39	2.12	0.90	4.84
Na2O (%)	0.25	0.25	1.07	3.42	2.56	2.72	1.56	0.81	1.52	0.64	0.24	1.59	2.05	0.22	0.09	0.08
K2O (%)	3.14	4.33	2.44	2.00	2.56	2.01	3.26	3.01	1.62	3.11	4.51	3.37	2.90	3.55	3.26	2.86
P2O5 (%)	0.20	0.12	0.04	0.12	0.20	0.21	0.23	0.04	0.04	0.21	0.11	0.04	0.04	0.04	0.03	0.25
CuO (%)	1.25	0.03	0.00	0.00	0.04	0.00	0.01	0.00	0.03	0.00	0.01	0.00	0.00	0.00	0.00	0.00
BaO (%)	0.39	0.36	0.07	0.08	0.11	0.08	0.10	0.04	0.04	0.09	0.09	0.11	0.13	0.06	0.13	0.17
LOI (%)	5.43	5.89	2.61	8.13	7.65	4.80	7.38	3.94	2.51	13.01	6.05	4.26	4.78	5.87	4.36	9.24
Sum (%)	100.04	99.31	100.69	100.17	99.72	99.92	99.93	99.60	99.64	99.65	99.65	100.13	100.83	100.24	99.67	99.80
S (%)	3.19	5.46	0.02	0.01	0.07	0.03	0.01	<0.01	0.12	0.02	0.02	0.04	0.05	0.02	0.02	<0.01
C (%)	0.100	0.120	0.200	1.450	1.640	0.530	1.440	0.460	0.077	2.920	1.120	0.690	1.030	1.160	0.820	1.950
Ag (ppm)	0.9	0.1	0.1	<0.1	0.2	0.1	0.1	0.3	0.2	0.1	0.2	0.2	0.1	0.1	0.2	0.1
As (ppm)	6	14	1	1	2	2	3	4	2	4	3	3	3	2	4	3
Ba (ppm)	2960	3597	590	563	1029	607	716	536	510	770	842	903	1027	440	1219	1359
Bi (ppm)	<2	<2	<2	<2	<2	<2	<2	<2	<2	<2	<2	<2	<2	<2	<2	<2
Cd (ppm)	0.4	0.4	0.4	0.4	0.4	0.3	0.5	0.4	0.4	0.6	0.5	0.5	0.8	0.5	0.5	0.5
Ce (ppm)	511	121	97	46	111	114	125	94	106	119	85	112	98	103	101	136
Cr (ppm)	107	105	4	178	70	53	203	67	3	131	105	3	3	4	3	146
Cs (ppm)	2.69	2.92	2.94	1.89	2.71	2.62	3.65	1.90	2.66	2.83	2.93	2.24	1.87	2.18	1.59	1.20
Cu (ppm)	10000	145	4	30	276	29	20	167	12	14	47	3	5	3	5	15
La (ppm)	338	74	47	23	56	62	67	43	47	58	41	49	48	45	44	68
Mo (ppm)	21.0	2.0	0.7	0.6	0.5	1.0	0.7	0.8	0.9	0.5	2.1	1.0	0.7	0.9	0.7	0.7
Nb (ppm)	24	27	12	6	7	7	9	10	15	9	13	16	13	14	12	9
Nd (ppm)	137	33	46	20	41	44	54	42	48	49	40	50	45	46	47	55
Ni (ppm)	47	15	3	51	28	31	38	13	3	33	9	3	2	1	2	38
Pb (ppm)	8	11	5	7	5	3	10	187	12	15	7	77	42	13	20	7
Rb (ppm)	85	98	70	59	69	59	88	39	81	89	136	93	71	105	105	91
Sb (ppm)	0.9	0.7	0.6	1.2	1.7	1.7	1.1	0.9	1.3	1.6	1.9	1.6	1.4	1.3	1.2	1.8
Sc (ppm)	19	31	11	32	31	29	34	7	8	28	20	11	8	9	8	32
Se (ppm)	4.4	7.5	<0.5	<0.5	<0.5	<0.5	<0.5	<0.5	<0.5	<0.5	<0.5	<0.5	<0.5	<0.5	<0.5	<0.5
Sr (ppm)	276	164	37	133	105	68	77	48	26	159	40	97	50	41	22	53
Th (ppm)	21	13	15	7	20	20	20	16	19	18	15	22	17	18	17	19
Tl (ppm)	0.5	0.6	0.7	0.7	0.7	0.6	0.8	0.5	0.7	0.8	1.0	1.0	0.7	0.9	0.8	0.6
U (ppm)	21.30	3.93	4.16	1.76	4.27	4.53	4.84	4.54	4.72	4.43	3.57	4.04	3.63	3.81	4.13	4.20
V (ppm)	72	211	6	265	226	225	212	20	4	184	64	4	4	8	4	201
Y (ppm)	24	6	41	20	20	13	24	31	41	23	36	41	40	42	37	23
Zn (ppm)	140	9	62	133	168	281	188	293	171	143	122	50	204	58	102	217
Zr (ppm)	156	168	256	114	117	121	186	175	293	155	249	304	235	250	225	159

Appendix: Analytical results cont.

Hole	WT0048	WT0048	WT0048	WT0048	WT0048	WT0048	WT0050	WT0050	WT0050	WT0050	WT0050	WT0050	WT0050	WT0050	WT0050	WT0050
From (m)	412.0	430.7	440.2	463.0	476.3	487.5	39.7	61.0	87.0	92.3	131.9	159.4	173.9	186.9	198.3	228.0
To (m)	412.7	431.4	440.9	463.8	477.0	488.0	40.1	61.4	87.4	92.7	132.2	159.9	174.3	187.3	199.0	229.0
SiO2 (%)	71.07	76.05	54.81	76.18	54.98	53.19	75.69	67.94	47.78	69.27	71.32	70.51	70.58	73.77	73.56	66.53
TiO2 (%)	0.22	0.23	0.64	0.20	0.47	0.42	0.26	0.43	0.51	0.40	0.23	0.24	0.23	0.25	0.21	0.20
Al2O3 (%)	11.34	12.05	18.47	9.86	11.99	11.54	13.00	14.33	14.56	13.89	12.82	12.81	12.12	12.63	11.76	10.35
Fe2O3 (%)	7.55	3.42	13.03	6.51	17.82	15.02	2.45	4.90	12.59	4.45	4.49	4.39	8.03	4.83	6.06	12.94
MnO (%)	0.17	0.32	0.28	0.06	0.54	0.69	0.04	0.12	0.19	0.10	0.20	0.25	0.11	0.13	0.10	<0.01
MgO (%)	1.31	1.18	3.57	0.42	4.99	5.09	0.78	1.68	4.63	1.68	1.04	1.14	0.68	0.79	0.56	0.07
CaO (%)	0.09	0.11	0.28	0.11	1.03	2.87	1.04	1.52	5.53	1.94	1.47	1.50	0.16	0.11	0.19	0.01
Na2O (%)	0.26	0.21	0.14	<0.05	0.10	<0.05	1.15	1.56	2.07	0.92	0.16	0.12	0.21	0.13	0.09	0.06
K2O (%)	3.52	3.36	3.33	3.02	1.09	1.45	3.33	2.89	1.47	3.12	3.76	3.89	3.63	3.63	3.29	0.39
P2O5 (%)	0.04	0.04	0.11	0.04	0.24	0.20	0.04	0.09	0.09	0.09	0.04	0.03	0.04	0.03	0.16	0.05
CuO (%)	0.19	0.01	0.03	0.33	0.15	0.06	0.00	0.00	0.00	0.00	0.01	0.00	0.00	0.00	0.23	0.01
BaO (%)	0.13	0.23	0.16	0.28	0.11	0.17	0.03	0.04	0.00	0.10	0.11	0.10	0.10	0.21	0.45	0.04
LOI (%)	4.75	3.31	5.10	3.25	6.42	8.96	3.12	4.28	10.71	4.63	4.51	5.25	4.44	3.74	3.52	8.53
Sum (%)	100.64	100.53	99.94	100.25	99.93	99.66	100.93	99.78	100.13	100.59	100.16	100.23	100.33	100.25	100.17	99.19
S (%)	0.29	0.84	0.70	2.19	0.72	1.69	0.37	0.08	0.04	0.04	0.06	<0.01	0.02	0.02	0.65	10.14
C (%)	0.870	0.250	0.160	0.120	0.640	1.440	0.320	0.540	2.140	0.640	0.690	1.060	0.850	0.590	0.470	0.017
Ag (ppm)	0.3	0.2	0.4	1.1	1.0	0.9	0.2	0.2	0.1	0.1	0.1	0.1	0.1	0.2	0.5	0.2
As (ppm)	3	3	4	3	6	18	2	2	2	<1	1	1	4	2	4	7
Ba (ppm)	1195	2174	1689	2619	702	1431	243	541	367	826	1019	731	758	1923	4034	305
Bi (ppm)	<2	<2	3	5	2	<2	<2	<2	<2	<2	<2	<2	<2	<2	<2	<2
Cd (ppm)	0.4	0.4	0.4	0.5	0.5	0.7	0.4	0.4	0.4	0.5	0.4	0.4	0.4	0.4	0.3	0.3
Ce (ppm)	109	92	60	112	195	135	112	91	31	92	109	115	139	123	99	109
Cr (ppm)	4	5	38	3	162	167	4	13	489	3	3	3	3	96	3	172
Cs (ppm)	1.31	1.84	1.78	1.82	1.07	1.34	2.87	2.24	1.29	2.30	2.55	2.11	1.70	2.12	1.64	0.42
Cu (ppm)	1500	44	228	2600	1269	447	3	16	10	5	37	6	18	36	1800	81
La (ppm)	57	44	26	55	102	74	49	39	14	42	50	53	75	61	55	61
Mo (ppm)	1.4	0.8	1.1	7.3	1.1	1.1	0.5	0.4	0.5	0.3	0.3	0.6	1.5	15.9	1.8	2.1
Nb (ppm)	12	13	6	11	8	8	13	11	3	12	14	13	13	14	10	11
Nd (ppm)	45	39	27	47	80	55	51	40	14	41	51	55	57	54	36	38
Ni (ppm)	4	5	30	5	43	41	3	7	96	5	3	3	5	6	34	14
Pb (ppm)	6	19	21	38	124	336	14	46	6	6	5	5	5	6	9	7
Rb (ppm)	115	103	109	105	40	50	112	85	46	92	126	141	126	112	98	11
Sb (ppm)	1.0	0.8	1.3	1.2	1.5	1.4	0.7	0.7	0.8	0.6	1.5	2.0	2.5	2.5	2.0	0.8
Sc (ppm)	10	10	28	9	29	29	10	17	56	13	9	10	9	11	5	6
Se (ppm)	<0.5	2.3	1.7	2.5	<0.5	2.0	<0.5	<0.5	<0.5	<0.5	<0.5	<0.5	<0.5	<0.5	<0.5	6.2
Sr (ppm)	16	32	29	36	24	53	37	45	83	52	23	27	19	25	33	96
Th (ppm)	17	17	8	17	20	19	17	14	6	16	19	19	20	23	19	19
Tl (ppm)	0.6	0.8	0.8	0.7	<0.5	<0.5	0.9	0.8	0.5	0.9	0.9	0.9	0.9	0.9	0.6	<0.5
U (ppm)	7.08	3.60	1.57	7.67	5.69	4.96	4.42	3.55	1.39	3.60	3.85	4.58	5.60	5.77	4.83	3.18
V (ppm)	4	13	269	26	164	165	5	47	302	16	3	4	8	6	89	33
Y (ppm)	38	36	26	35	32	29	40	37	17	39	35	47	42	51	20	14
Zn (ppm)	60	117	382	40	760	746	28	74	199	72	67	59	63	73	38	11
Zr (ppm)	227	246	135	206	168	159	291	236	72	265	253	266	246	275	231	211

Appendix: Analytical results cont.

Hole	WT0050	WT0050	WT0050	WT0050	WT0050	WT0050	WT0050	WT0050	WT0050	WT0050	WT0050	WT0050	WT0050	WT0050	WT0050	WT0050
From (m)	244.8	275.3	301.4	331.4	360.4	384.3	418.6	426.9	448.7	457.0	483.4	521.1	543.7	563.0	594.5	615.4
To (m)	245.8	276.1	302.0	332.2	361.4	384.8	419.3	427.3	449.0	457.7	483.9	521.8	544.3	564.0	595.2	616.1
SiO2 (%)	69.66	66.47	57.59	73.36	66.59	80.78	80.76	66.93	68.25	66.00	76.77	76.36	59.50	60.29	77.89	57.08
TiO2 (%)	0.21	0.19	0.56	0.22	0.21	0.24	0.20	0.56	0.28	0.53	0.32	0.24	0.55	0.35	0.24	0.48
Al2O3 (%)	10.93	9.80	15.27	12.23	11.03	12.25	10.27	16.87	18.13	15.49	15.64	12.21	14.20	12.84	12.98	13.78
Fe2O3 (%)	9.41	12.57	12.41	6.03	11.87	2.21	2.95	4.36	1.35	7.02	0.63	3.46	11.75	10.77	2.21	8.36
MnO (%)	<0.01	<0.01	<0.01	<0.01	0.01	<0.01	<0.01	<0.01	0.30	<0.01	<0.01	0.11	0.75	0.52	0.03	0.65
MgO (%)	0.30	0.06	0.21	0.23	0.07	0.12	0.31	0.42	1.12	0.45	0.31	0.44	3.48	1.08	0.51	4.12
CaO (%)	0.01	0.02	0.02	0.03	0.01	0.03	0.02	0.16	2.05	0.22	0.08	0.28	0.56	1.26	0.07	3.19
Na2O (%)	0.22	0.14	1.40	0.04	0.03	0.36	0.17	0.25	<0.05	0.31	0.22	0.11	0.25	0.13	0.11	0.16
K2O (%)	2.99	0.34	3.16	2.27	0.29	1.43	2.81	4.71	0.06	4.42	4.23	3.66	2.73	3.97	4.03	3.28
P2O5 (%)	0.04	0.07	0.17	0.14	0.08	0.05	0.03	0.13	0.07	0.18	0.06	0.05	0.30	0.08	0.04	0.15
CuO (%)	0.16	0.01	0.08	1.19	0.01	0.01	0.01	0.01	0.00	0.01	0.00	0.01	0.01	0.01	0.00	0.03
BaO (%)	0.17	0.87	0.23	0.18	0.55	0.13	0.36	0.40	0.01	0.21	0.16	0.20	0.15	0.13	0.13	0.19
LOI (%)	6.07	8.80	8.76	5.01	8.73	3.08	2.04	4.36	8.19	5.62	2.21	3.45	5.78	8.09	2.47	8.35
Sum (%)	100.17	99.34	99.86	100.93	99.48	100.70	99.93	99.16	99.81	100.46	100.63	100.58	100.01	99.53	100.71	99.81
S (%)	7.08	10.18	9.42	4.97	9.46	1.61	2.20	3.12	0.37	5.33	0.15	2.02	0.41	6.28	0.75	0.15
C (%)	0.100	0.022	0.020	0.016	0.020	0.110	0.008	0.016	0.850	0.013	0.021	0.140	0.670	0.720	0.045	1.640
Ag (ppm)	0.3	0.2	0.3	0.4	0.2	0.2	0.1	0.2	0.2	0.2	0.2	0.6	0.6	0.8	0.2	0.2
As (ppm)	18	9	6	170	14	5	4	7	2	11	4	6	10	10	2	2
Ba (ppm)	1759	7830	1721	1506	5120	1170	3282	3822	171	2240	1501	1581	1382	1737	1257	1881
Bi (ppm)	2	<2	2	<2	<2	<2	<2	<2	<2	2	<2	<2	2	<2	<2	<2
Cd (ppm)	0.3	0.4	0.4	1.1	0.4	0.3	0.3	0.4	0.4	0.4	4.7	0.5	0.4	0.7	0.4	0.7
Ce (ppm)	83	213	625	329	35	63	50	64	10	121	76	125	157	66	112	96
Cr (ppm)	4	4	85	153	6	182	7	99	203	126	147	4	206	19	151	290
Cs (ppm)	2.28	0.41	2.10	1.18	0.35	1.15	2.99	2.66	0.15	2.14	2.44	1.26	0.90	1.69	1.70	1.13
Cu (ppm)	1344	116	555	9500	190	72	94	63	10	46	28	46	113	88	28	134
La (ppm)	43	149	431	221	28	43	29	32	5	57	39	56	85	39	53	47
Mo (ppm)	1.9	15.2	37.8	253.0	33.0	7.0	3.8	2.2	6.5	2.1	2.1	2.0	1.4	5.0	1.9	1.2
Nb (ppm)	11	11	20	17	18	13	16	14	14	9	17	16	9	9	15	9
Nd (ppm)	36	49	156	75	10	16	15	25	4	52	27	55	66	22	50	38
Ni (ppm)	5	3	22	19	10	4	3	15	3	25	4	5	42	7	6	53
Pb (ppm)	7	4	10	14	7	7	11	14	21	15	111	219	110	214	23	20
Rb (ppm)	81	8	77	51	6	31	74	125	1	124	115	107	89	120	121	109
Sb (ppm)	1.1	0.7	0.7	4.0	0.7	0.6	0.6	0.7	0.1	0.9	0.9	0.7	1.1	1.0	0.7	1.0
Sc (ppm)	10	5	11	6	<2	5	6	18	3	37	7	9	37	9	11	33
Se (ppm)	2.1	5.5	17.9	1.7	8.4	<0.5	2.1	5.5	<0.5	6.3	<0.5	4.2	1.9	11.0	1.4	<0.5
Sr (ppm)	100	477	174	228	300	117	64	77	33	75	39	22	17	25	14	44
Th (ppm)	16	13	20	16	2	8	12	13	6	18	18	29	24	14	18	18
Tl (ppm)	0.7	<0.5	0.5	<0.5	<0.5	<0.5	<0.5	0.9	<0.5	1.0	1.1	0.9	0.8	1.0	1.0	0.9
U (ppm)	7.27	2.82	3.72	3.14	1.41	0.93	1.72	2.86	1.60	5.10	3.43	5.08	3.85	4.46	4.60	3.57
V (ppm)	12	32	106	50	27	33	21	210	13	213	21	16	221	94	8	193
Y (ppm)	36	14	9	8	5	5	11	25	10	38	24	41	25	23	47	22
Zn (ppm)	11	10	12	42	16	6	5	7	14	7	663	46	1210	138	38	612
Zr (ppm)	222	213	160	242	233	249	206	198	364	182	333	264	181	182	269	161

Appendix: Analytical results cont.

Hole	WT0050	WT0050	WT0050	WT0050	WT0050	WT0050	WT0055	WT0055	WT0055	WT0055	WT0055	WT0055	WT0055	WT0055	WT0055	WT0055
From (m)	633.0	654.8	669.6	680.8	692.1	697.4	20.7	50.4	76.2	107.3	131.0	149.1	163.2	209.9	229.0	249.9
To (m)	633.4	655.3	670.1	681.5	692.6	698.1	21.1	50.8	76.5	107.6	131.4	149.6	163.6	210.6	229.8	250.7
SiO2 (%)	70.35	55.40	80.03	73.84	82.99	56.43	66.96	53.09	47.83	53.20	61.69	66.69	60.76	69.60	66.03	70.98
TiO2 (%)	0.17	0.50	0.27	0.24	0.23	0.47	0.55	0.46	0.59	0.61	0.20	0.19	0.54	0.24	0.32	0.36
Al2O3 (%)	9.59	13.00	14.12	12.80	12.69	12.73	15.80	13.08	16.53	16.92	10.76	9.98	14.78	12.30	13.08	13.82
Fe2O3 (%)	7.55	11.94	0.46	4.60	0.24	13.07	5.69	10.87	11.35	9.15	14.19	12.89	11.42	6.02	9.12	5.01
MnO (%)	0.50	0.56	<0.01	0.01	<0.01	0.74	0.06	0.37	0.66	0.25	0.01	<0.01	0.02	<0.01	<0.01	<0.01
MgO (%)	1.29	5.72	0.23	0.59	0.05	5.70	2.02	3.48	2.90	2.80	0.31	0.07	1.15	0.44	0.50	0.27
CaO (%)	0.94	2.63	0.02	0.07	0.01	1.42	0.86	4.82	3.39	3.12	0.01	0.02	0.19	0.10	0.06	0.11
Na2O (%)	0.08	0.11	0.14	0.12	0.06	0.12	2.01	0.15	0.13	0.20	0.07	<0.05	0.13	0.10	0.12	0.24
K2O (%)	2.79	1.72	3.77	3.61	1.01	1.37	2.64	2.95	4.69	4.40	3.29	0.16	3.34	3.40	3.43	3.68
P2O5 (%)	0.03	0.22	0.04	0.04	0.05	0.18	0.10	0.19	0.16	0.16	0.04	0.09	0.18	0.20	0.09	0.14
CuO (%)	0.03	0.01	0.00	0.01	0.00	0.04	0.00	0.04	0.01	0.01	0.15	0.01	0.75	1.21	0.21	0.08
BaO (%)	0.23	0.30	0.08	0.12	0.03	0.11	0.06	0.13	0.25	0.26	0.13	0.04	0.30	0.74	0.21	0.32
LOI (%)	6.01	7.54	1.98	3.84	2.46	7.27	3.51	10.14	11.06	8.77	8.43	9.26	6.58	4.89	6.57	4.49
Sum (%)	99.56	99.65	101.14	99.90	99.84	99.65	100.26	99.77	99.55	99.85	99.28	99.41	100.14	99.24	99.74	99.50
S (%)	3.24	0.05	<0.01	2.87	0.22	0.56	0.03	0.06	0.22	0.23	10.20	10.09	6.50	4.78	7.09	3.80
C (%)	0.660	0.940	0.019	0.013		0.840	0.270	2.230	2.580	1.750	0.066	0.036	0.059	0.020	0.110	0.028
Ag (ppm)	0.5	0.2	0.1	0.4		0.3	<0.1	0.3	0.2	0.1	0.4	0.2	0.6	1.1	0.2	0.3
As (ppm)	5	3	2	3		5	5	5	14	5	19	21	24	7	15	22
Ba (ppm)	2323	2640	702	1150	307	1139	623	1233	2139	2422	1548	138	3091	6041	1980	2779
Bi (ppm)	<2	<2	<2	<2	<2	<2	<2	<2	<2	<2	5	<2	<2	<2	<2	3
Cd (ppm)	0.4	0.5	0.4	0.4		0.4	0.4	0.4	0.5	0.4	0.3	0.5	0.4	0.6	0.5	0.5
Ce (ppm)	74	116	100	132	107	109	77	117	65	59	106	255	203	480	134	128
Cr (ppm)	7	227	135	115	154	255	23	209	53	45	4	10	272	10	17	38
Cs (ppm)	1.21	0.99	1.46	1.90		0.83	1.82	1.74	2.00	1.64	2.01	0.30	2.45	2.57	1.66	2.94
Cu (ppm)	141	32	3	39	8	278	16	257	82	51	1282	97	6000	9700	1691	487
La (ppm)	36	60	50	68	47	55	36	61	32	32	55	200	119	336	84	91
Mo (ppm)	2.0	1.2	2.1	2.1		0.8	1.0	1.3	2.0	1.3	1.1	111.0	7.9	121.0	67.1	102.0
Nb (ppm)	9	9	16	14	14	7	11	9	7	7	12	11	8	29	15	18
Nd (ppm)	31	46	42	43	48	43	38	45	32	30	50	48	68	108	41	39
Ni (ppm)	8	44	3	4	2	53	10	42	11	8	5	4	26	15	15	9
Pb (ppm)	29	9	8	15	8	15	4	28	96	4	14	11	18	14	12	17
Rb (ppm)	88	57	91	103	25	44	82	96	146	129	96	5	84	73	72	79
Sb (ppm)	0.8	1.2	0.8	0.9		1.3	1.5	2.5	2.9	1.8	1.5	0.9	1.6	0.8	1.2	1.3
Sc (ppm)	10	31	4	12	3	33	20	29	18	19	9	6	38	7	14	7
Se (ppm)	3.1	<0.5	<0.5	5.7	<0.5	2.0	<0.5	<0.5	<0.5	<0.5	1.8	11.8	2.6	3.7	7.9	6.5
Sr (ppm)	29	68	59	26	81	32	62	60	63	52	44	109	594	259	131	372
Th (ppm)	14	19	16	20	17	18	14	21	10	10	16	14	20	12	17	10
Tl (ppm)	0.8	<0.5	0.8	0.6		<0.5	<0.5	<0.5	0.6	0.6	<0.5	<0.5	<0.5	<0.5	<0.5	<0.5
U (ppm)	3.35	4.02	2.76	4.53		3.56	2.89	4.44	2.54	2.93	6.45	3.91	9.18	4.40	3.66	4.56
V (ppm)	30	187	6	10	5	198	75	188	202	196	11	92	232	55	77	59
Y (ppm)	31	23	27	38	27	21	35	21	29	29	53	14	46	25	13	32
Zn (ppm)	104	570	8	19	7	473	118	160	152	125	12	22	26	20	16	14
Zr (ppm)	187	174	293	263	275	151	220	173	140	151	223	217	178	235	235	204

Appendix: Analytical results cont.

Hole	WT0055	WT0055	WT0055	WT0056	WT0056	WT0056	WT0056	WT0056	WT0056	WT0056	WT0056	WT0056	WT0056	WT0066	WT0066	WT0066
From (m)	281.0	296.0	313.0	38.0	75.6	98.5	121.0	156.3	189.7	206.7	219.2	249.2	273.2	40.8	64.6	91.7
To (m)	281.8	296.7	313.6	38.4	76.0	98.8	121.4	156.7	190.4	207.4	220.0	250.0	274.0	41.2	65.0	92.0
SiO2 (%)	60.33	61.30	77.60	56.68	72.94	67.70	45.88	77.40	69.17	55.93	68.27	66.99	54.45	72.14	54.91	52.77
TiO2 (%)	0.52	0.55	0.26	0.60	0.24	0.21	0.46	0.24	0.20	0.71	0.22	0.30	0.45	0.28	0.44	0.62
Al2O3 (%)	15.11	15.02	12.76	16.26	12.52	11.74	12.64	12.80	10.91	19.55	11.61	11.05	13.00	14.14	12.57	16.68
Fe2O3 (%)	11.25	10.40	2.51	9.06	4.34	9.35	26.81	2.82	9.67	9.88	10.53	9.32	18.69	3.08	6.67	8.49
MnO (%)	0.01	0.05	0.01	0.15	0.19	0.29	0.22	<0.01	<0.01	0.04	<0.01	<0.01	0.01	0.06	0.48	0.14
MgO (%)	0.93	3.33	0.55	2.83	0.96	1.03	2.83	0.34	0.07	1.00	0.08	0.40	0.13	1.02	3.13	3.02
CaO (%)	0.19	0.19	0.01	2.97	0.82	0.23	0.61	<0.01	0.03	0.08	0.01	<0.01	0.11	1.36	6.69	4.48
Na2O (%)	0.12	0.13	0.16	1.68	0.11	0.09	0.07	0.25	<0.05	0.23	<0.05	0.09	0.09	2.05	0.18	0.73
K2O (%)	3.55	3.14	3.71	3.10	3.71	3.35	1.82	3.34	0.17	5.01	0.14	2.88	0.09	2.84	3.58	3.75
P2O5 (%)	0.19	0.16	0.04	0.17	0.04	0.03	0.49	0.04	0.06	0.15	0.06	0.04	0.18	0.04	0.18	0.16
CuO (%)	0.54	0.05	0.09	0.00	0.00	0.01	0.83	0.01	0.01	0.25	0.01	1.03	0.01	0.00	0.04	0.01
BaO (%)	0.42	0.18	0.22	0.04	0.17	0.08	0.20	0.30	1.09	0.60	0.21	0.55	0.38	0.09	0.17	0.06
LOI (%)	7.05	5.51	2.93	6.46	4.23	5.82	7.32	2.90	7.32	6.36	7.84	6.53	12.14	3.21	10.48	8.97
Sum (%)	100.21	100.01	100.85	100.00	100.27	99.93	100.18	100.44	98.71	99.79	98.98	99.17	99.73	100.31	99.52	99.88
S (%)	7.04	3.31	1.48	0.01	0.03	0.15	1.56	1.56	7.77	4.43	8.19	7.67	13.04	0.02	0.07	<0.01
C (%)	0.014	0.033	0.029	1.190	0.800	1.360	1.220	0.034	0.031	0.120	0.130	0.380	0.051	0.470	2.580	1.690
Ag (ppm)	0.8	0.3	0.3	0.1	0.1	0.2	1.2	0.2	0.2	0.2	0.2	0.2	0.4	0.1	0.3	0.2
As (ppm)	9	7	6	4	3	4	6	8	24	23	27	46	19	3	5	3
Ba (ppm)	4279	1813	2074	510	1522	803	1783	2848	8953	5258	1936	5097	3471	763	1671	602
Bi (ppm)	3	3	<2	<2	<2	<2	<2	<2	<2	<2	<2	2	<2	<2	<2	<2
Cd (ppm)	0.3	0.3	0.3	0.3	0.4	0.4	0.3	0.3	0.5	0.3	0.4	0.4	0.3	0.9	0.5	0.4
Ce (ppm)	158	84	127	100	111	115	252	102	74	208	110	123	235	118	107	61
Cr (ppm)	111	144	11	217	134	4	195	105	161	22	234	37	75	3	198	48
Cs (ppm)	2.36	2.32	2.70	2.26	2.05	1.97	1.01	3.20	0.45	3.59	0.42	1.22	0.32	1.72	3.19	2.33
Cu (ppm)	4300	459	1120	15	10	47	6600	64	99	1904	139	8200	233	2	189	51
La (ppm)	85	47	60	52	49	61	147	48	66	131	73	82	171	57	53	30
Mo (ppm)	8.2	4.6	2.5	1.5	1.6	1.8	2.2	1.5	58.8	17.2	25.4	75.4	7.5	1.2	1.1	1.3
Nb (ppm)	9	9	13	9	14	12	23	15	12	7	13	15	15	15	9	8
Nd (ppm)	61	36	58	40	51	47	95	50	23	69	29	33	48	54	44	30
Ni (ppm)	28	31	16	35	6	6	150	4	7	20	12	26	23	2	22	10
Pb (ppm)	10	8	12	5	6	7	9	6	4	<1.5	9	11	14	3	10	7
Rb (ppm)	116	94	135	87	115	111	58	96	5	118	4	66	3	93	116	131
Sb (ppm)	2.8	1.4	1.0	2.4	2.0	2.7	3.4	1.4	1.3	2.4	1.7	3.0	1.1	0.8	1.7	2.0
Sc (ppm)	36	33	12	35	9	7	33	12	5	31	4	16	4	12	28	20
Se (ppm)	3.6	6.6	1.4	<0.5	<0.5	<0.5	2.4	<0.5	6.3	19.3	10.2	4.8	8.6	<0.5	<0.5	<0.5
Sr (ppm)	316	35	33	46	16	14	41	494	513	402	325	131	353	72	72	97
Th (ppm)	18	19	26	16	19	17	29	19	7	7	13	11	19	20	19	11
Tl (ppm)	<0.5	<0.5	0.5	0.5	0.5	0.5	<0.5	<0.5	<0.5	<0.5	<0.5	<0.5	<0.5	<0.5	<0.5	0.6
U (ppm)	10.00	5.23	3.84	3.56	3.50	4.53	9.33	5.83	3.67	8.55	2.49	3.30	2.03	4.47	4.07	2.42
V (ppm)	232	202	28	226	6	5	773	11	33	246	40	89	47	4	178	202
Y (ppm)	37	30	76	23	40	43	39	49	17	42	10	8	6	46	20	27
Zn (ppm)	26	67	22	137	73	116	382	7	6	28	16	19	16	45	72	173
Zr (ppm)	163	176	252	169	253	228	149	277	239	137	248	172	143	304	168	149

Appendix: Analytical results cont.

Hole	WT0066	WT0066	WT0066	WT0066	WT0066	WT0066	WT0066	WT0066	WT0066	WT0066	WT0066	WT0066	WT0066	WT0066	WT0066	WT0077B
From (m)	116.3	141.8	152.2	173.0	206.4	222.6	239.3	266.3	280.1	290.1	315.1	341.3	365.0	394.4	416.5	150.0
To (m)	116.9	142.1	152.6	173.4	207.0	223.1	239.6	266.9	280.9	290.6	315.7	342.1	365.8	395.0	416.8	150.2
SiO2 (%)	70.33	54.74	54.39	69.29	72.97	60.88	60.43	69.42	68.90	57.21	59.95	62.32	64.27	57.96	59.83	64.31
TiO2 (%)	0.19	0.54	0.48	0.31	0.25	0.68	0.67	0.31	0.20	0.51	0.49	0.39	0.23	0.45	0.46	0.46
Al2O3 (%)	9.83	14.61	13.48	14.74	13.17	18.83	18.63	12.97	9.65	16.29	13.83	12.80	11.25	13.12	12.84	15.44
Fe2O3 (%)	9.33	21.02	8.30	8.15	5.47	7.56	7.63	6.61	9.24	11.89	10.97	9.83	11.70	13.84	15.42	5.70
MnO (%)	0.25	0.05	0.66	0.03	<0.01	<0.01	<0.01	0.02	0.10	0.07	0.09	<0.01	<0.01	<0.01	0.13	0.06
MgO (%)	0.94	2.78	3.89	0.51	0.39	0.60	0.59	0.73	1.11	3.21	4.47	0.47	0.56	0.47	4.83	1.50
CaO (%)	0.11	0.20	4.41	0.03	0.01	0.18	0.19	<0.01	0.13	0.41	0.42	0.56	0.38	0.17	0.18	2.72
Na2O (%)	0.15	0.09	0.12	0.14	0.18	0.49	0.21	0.16	0.10	0.12	0.10	0.12	0.06	0.20	<0.05	2.03
K2O (%)	2.79	1.97	3.54	4.33	3.86	5.46	5.59	3.49	2.73	3.47	2.18	3.70	3.48	3.94	0.63	3.13
P2O5 (%)	0.03	0.16	0.11	0.04	0.04	0.16	0.16	0.10	0.23	0.24	0.25	0.23	0.34	0.16	0.16	0.15
CuO (%)	0.00	0.00	0.01	0.00	0.04	0.00	0.01	1.88	1.40	0.11	2.18	1.39	0.64	0.01	0.26	0.00
BaO (%)	0.08	0.17	0.28	0.29	0.49	0.23	0.25	0.30	0.22	0.27	0.22	0.40	0.20	0.82	0.26	0.04
LOI (%)	6.04	3.82	10.21	2.76	4.19	3.99	5.74	4.09	5.77	5.95	5.06	7.03	7.23	8.80	4.77	4.15
Sum (%)	100.07	100.15	99.88	100.62	101.06	99.06	100.10	100.08	99.79	99.75	100.21	99.24	100.34	99.94	99.77	99.70
S (%)	0.02	0.29	0.02	0.51	3.61	4.97	4.94	3.89	4.80	3.06	2.60	7.78	8.93	10.64	0.70	<0.01
C (%)	1.520	0.180	2.440	0.110	0.031	0.070	0.110	0.078	0.430	0.210	0.140	0.110	0.020	0.023	0.089	
Ag (ppm)	0.2	0.1	0.2	0.1	0.3	0.2	0.2	1.2	0.9	0.3	1.6	2.0	0.6	0.2	0.2	
As (ppm)	2	5	6	5	7	9	6	11	7	11	9	10	11	11	4	
Ba (ppm)	731	1434	2698	2692	4355	2223	2265	2536	1471	2741	1708	3479	1737	7320	2493	323
Bi (ppm)	<2	<2	<2	<2	<2	3	2	<2	<2	<2	<2	<2	<2	2	<2	2
Cd (ppm)	0.3	0.3	0.4	0.3	0.4	0.3	0.3	0.3	0.3	0.3	0.8	0.5	0.4	0.4	0.3	
Ce (ppm)	85	96	60	86	103	53	82	342	618	174	378	469	225	169	111	106
Cr (ppm)	4	150	183	4	133	137	7	107	9	34	121	69	12	96	503	67
Cs (ppm)	1.82	1.14	1.69	2.20	2.74	2.10	3.10	1.99	1.37	2.31	1.61	2.09	2.14	2.00	0.85	
Cu (ppm)	14	25	21	19	234	244	80	15000	11200	793	17400	11100	5100	102	2100	4
La (ppm)	41	51	28	40	53	37	43	235	431	108	273	332	156	102	60	54
Mo (ppm)	0.6	0.9	0.5	0.7	6.8	1.2	3.0	9.9	8.0	2.0	25.2	19.2	60.8	8.1	1.4	
Nb (ppm)	10	7	6	14	14	1	8	22	14	8	18	20	11	9	8	11
Nd (ppm)	37	40	28	41	41	23	39	87	148	54	90	109	55	58	46	41
Ni (ppm)	3	41	36	2	5	55	4	7	15	20	24	34	90	23	114	9
Pb (ppm)	5	4	7	6	7	8	7	12	11	11	34	19	15	11	3	4
Rb (ppm)	95	63	111	132	113	69	154	87	68	86	55	88	75	97	19	99
Sb (ppm)	1.1	2.2	2.5	1.9	0.9	1.7	1.4	0.7	0.7	1.2	0.9	1.1	0.8	0.8	1.2	
Sc (ppm)	7	37	37	12	11	63	24	9	9	28	24	8	13	31	28	16
Se (ppm)	<0.5	<0.5	<0.5	<0.5	1.0	1.3	1.7	3.3	2.8	2.0	4.2	6.0	8.7	7.8	1.1	<0.5
Sr (ppm)	20	18	48	79	181	514	70	95	71	34	29	159	87	459	65	101
Th (ppm)	15	16	8	18	18	6	12	18	27	20	15	22	10	16	18	20
Tl (ppm)	<0.5	<0.5	0.5	0.7	0.6	<0.5	0.6	<0.5	<0.5	<0.5	<0.5	<0.5	<0.5	<0.5	<0.5	
U (ppm)	3.44	3.45	2.16	4.22	6.96	3.47	5.42	7.61	3.67	3.47	3.84	5.07	6.81	8.15	4.98	
V (ppm)	3	232	218	6	9	356	227	56	64	273	137	53	142	195	187	125
Y (ppm)	34	23	24	40	53	20	44	24	17	32	14	14	23	38	22	27
Zn (ppm)	79	451	273	28	12	74	16	30	37	203	492	84	45	29	144	56
Zr (ppm)	203	136	143	303	280	37	174	256	200	132	151	184	222	166	152	204

Appendix: Analytical results cont.

Hole	WT0077B	WT0077B	WT0077B	WT0077B	WT0077B	WT0077B	WT0077B	WT0077B	WT0077B	WT0077B	WT0077B	WT0077B	WT0077B	WT0077D	WT0077D	WT0077D
From (m)	165.4	185.1	204.1	239.4	285.3	319.3	368.0	418.1	454.5	524.4	541.0	568.5	583.1	607.4	622.8	632.2
To (m)	165.6	185.5	204.3	239.6	285.6	319.5	368.2	418.4	454.7	524.7	541.3	568.9	583.2	607.9	623.1	632.7
SiO2 (%)	61.63	63.77	63.64	63.30	63.42	65.20	74.28	81.92	59.34	66.73	77.87	63.57	76.91	65.31	75.52	69.48
TiO2 (%)	0.41	0.46	0.43	0.47	0.45	0.43	0.26	0.21	0.39	0.45	0.27	0.44	0.24	0.47	0.24	0.36
Al2O3 (%)	13.57	15.28	14.42	15.38	14.85	14.37	13.54	10.74	13.06	15.15	13.28	14.75	12.59	14.78	12.90	14.13
Fe2O3 (%)	7.68	5.13	5.47	5.61	5.33	4.35	2.41	0.79	3.90	4.63	1.37	5.07	0.94	4.86	1.60	2.62
MnO (%)	0.10	0.06	0.08	0.06	0.08	0.09	0.03	0.01	0.14	0.05	0.01	0.06	0.03	0.08	0.03	0.07
MgO (%)	1.88	1.59	1.50	1.59	1.43	1.27	1.39	0.47	1.33	1.44	0.65	1.72	1.11	2.42	1.00	1.37
CaO (%)	3.98	3.28	4.05	3.32	3.72	4.11	0.64	0.52	8.63	2.28	0.19	3.50	0.86	2.21	1.34	2.75
Na2O (%)	2.21	2.62	3.55	2.15	3.08	1.79	2.13	4.53	2.39	3.15	3.25	2.81	0.82	2.57	1.69	1.68
K2O (%)	2.24	2.90	2.04	3.13	2.62	2.97	2.77	0.84	2.27	2.46	2.32	2.87	3.78	2.57	3.31	3.47
P2O5 (%)	0.15	0.15	0.14	0.16	0.16	0.15	0.06	0.05	0.14	0.15	0.03	0.15	0.03	0.17	0.02	0.06
CuO (%)	0.01	0.00	0.00	0.00	0.00	0.00	0.00	0.00	0.00	0.00	0.01	0.01	0.00	0.02	0.00	0.00
BaO (%)	0.03	0.06	0.04	0.04	0.07	0.09	0.04	0.02	0.04	0.04	0.03	0.03	0.02	0.04	0.03	0.04
LOI (%)	5.53	4.11	4.69	4.46	4.49	4.88	2.44	0.99	8.19	3.40	1.44	4.78	2.89	4.26	2.59	4.16
Sum (%)	99.43	99.41	100.07	99.69	99.70	99.71	100.00	101.09	99.82	99.94	100.73	99.77	100.22	99.76	100.27	100.19
S (%)	1.19	<0.01	<0.01	<0.01	<0.01	0.03	<0.01	0.01	0.13	<0.01	0.11	0.01	<0.01	0.04	0.04	0.13
C (%)														0.620	0.290	0.540
Ag (ppm)														0.2	0.2	0.2
As (ppm)														18	3	7
Ba (ppm)	454	431	319	454	680	765	319	168	222	252	146	303	251	322	309	329
Bi (ppm)	3	<2	<2	<2	<2	<2	<2	<2	<2	<2	<2	<2	<2	<2	<2	<2
Cd (ppm)														0.4	0.3	0.5
Ce (ppm)	114	105	101	115	102	96	164	88	109	145	125	100	111	108	103	96
Cr (ppm)	75	74	67	75	71	63	80	172	74	74	65	52	90	12	58	4
Cs (ppm)														1.69	2.30	2.12
Cu (ppm)	64	3	3	2	2	3	6	6	3	4	54	91	12	191	18	5
La (ppm)	55	52	48	56	52	49	78	40	53	77	60	46	51	56	49	48
Mo (ppm)														1.2	1.3	0.9
Nb (ppm)	10	11	10	11	10	10	15	13	9	11	16	10	16	10	15	13
Nd (ppm)	46	41	42	45	43	39	70	38	44	51	47	40	47	41	44	43
Ni (ppm)	14	9	9	9	8	9	16	4	7	8	3	8	3	9	2	2
Pb (ppm)	8	4	4	4	3	4	16	10	7	2	4	3	2	3	32	76
Rb (ppm)	70	94	65	101	87	89	82	26	65	71	76	101	131	89	131	138
Sb (ppm)														1.6	1.0	0.9
Sc (ppm)	21	17	16	19	16	17	6	3	16	16	5	17	6	16	2	6
Se (ppm)	<0.5	<0.5	<0.5	<0.5	<0.5	<0.5	<0.5	<0.5	<0.5	<0.5	<0.5	<0.5	<0.5	<0.5	<0.5	<0.5
Sr (ppm)	154	153	183	143	154	117	38	74	172	83	40	119	24	64	55	101
Th (ppm)	19	21	20	21	20	19	25	20	18	21	26	20	23	20	22	19
Tl (ppm)														<0.5	<0.5	<0.5
U (ppm)														4.23	5.10	2.46
V (ppm)	155	126	113	128	114	116	11	7	106	126	8	114	6	120	5	17
Y (ppm)	28	24	24	33	29	22	39	31	42	25	37	24	37	25	33	34
Zn (ppm)	68	31	58	42	53	52	34	11	79	66	21	42	39	67	46	76
Zr (ppm)	186	208	194	212	197	195	256	213	172	205	244	197	229	190	208	246

Appendix: Analytical results cont.

Hole	WT0077D	WT0077D	WT0077D	WT0077D	WT0077D	WT0077D	WT0077D	WT0077D	WT0077D	WT0077D	WT0077D	WT0077D	WT0077D	WT0077D	WT0077D	WT0077D
From (m)	650.4	660.6	699.3	710.4	727.2	748.2	774.1	800.9	812.1	828.0	864.9	890.7	905.6	919.6	929.1	945.3
To (m)	650.6	660.9	699.7	711.0	727.6	748.6	774.4	801.1	812.4	828.2	865.2	891.0	905.9	919.9	929.5	945.7
SiO2 (%)	71.84	73.05	75.88	60.96	73.04	71.04	75.78	38.82	71.38	72.47	69.11	68.30	68.42	58.43	71.90	64.53
TiO2 (%)	0.30	0.30	0.23	0.47	0.27	0.27	0.27	0.48	0.30	0.34	0.21	0.25	0.29	0.42	0.27	0.26
Al2O3 (%)	12.59	13.69	12.09	14.98	13.71	13.47	13.24	11.60	12.57	12.23	11.55	13.36	13.66	19.87	13.10	11.77
Fe2O3 (%)	2.52	2.12	2.42	5.09	3.62	2.90	2.28	8.67	4.60	4.83	3.28	6.44	7.68	10.59	5.36	11.74
MnO (%)	0.07	0.04	0.03	0.09	0.02	0.07	0.03	0.17	0.08	0.06	0.23	0.44	0.07	<0.01	<0.01	<0.01
MgO (%)	1.60	1.28	1.54	2.60	1.52	0.94	1.04	5.51	1.51	1.11	0.93	1.27	0.90	0.41	0.33	0.37
CaO (%)	2.27	1.32	0.89	4.14	0.41	2.74	0.48	12.51	1.98	1.33	4.22	0.06	0.05	0.02	0.04	0.02
Na2O (%)	1.10	2.81	2.86	2.51	1.22	1.47	1.40	1.33	1.70	1.99	0.12	0.13	0.18	0.24	0.12	0.18
K2O (%)	3.38	2.73	1.79	2.67	3.09	3.09	3.12	2.55	2.18	2.05	3.40	3.82	3.55	5.79	3.80	3.48
P2O5 (%)	0.04	0.04	0.03	0.15	0.04	0.04	0.04	0.09	0.05	0.07	0.03	0.04	0.06	0.05	0.06	0.07
CuO (%)	0.00	0.00	0.00	0.00	0.00	0.00	0.00	0.01	0.00	0.00	0.00	0.02	0.02	0.00	0.09	0.01
BaO (%)	0.04	0.04	0.01	0.07	0.04	0.06	0.04	0.13	0.07	0.01	0.09	0.26	0.24	0.33	0.27	0.21
LOI (%)	4.34	2.69	2.40	5.87	2.56	3.85	2.24	18.43	3.86	3.44	6.61	5.54	4.89	3.61	4.07	7.25
Sum (%)	100.09	100.11	100.16	99.60	99.54	99.93	99.97	100.30	100.27	99.93	99.78	99.93	100.01	99.75	99.41	99.89
S (%)	0.30	0.09	0.09	0.06	0.05	0.00	0.03	0.01	0.04	0.07	0.01	0.07	2.19	1.28	3.29	8.62
C (%)	0.640	0.310	0.240	1.080	0.110	0.580	0.190	4.840	0.680	0.440	1.560	1.170	0.400	0.055	0.110	0.110
Ag (ppm)	0.2	0.3	0.3	0.2	0.2	0.1	0.2	0.1	0.1	0.2	0.2	0.2	0.3	0.2	0.4	0.6
As (ppm)	4	5	3	2	2	1	4	2	2	3	2	4	18	6	7	61
Ba (ppm)	358	294	238	556	561	356	276	1037	630	303	695	2149	2272	3371	2413	2166
Bi (ppm)	<2	<2	<2	2	<2	<2	<2	<2	<2	<2	<2	<2	<2	<2	3	2
Cd (ppm)	1.8	0.5	0.8	0.4	0.5	0.3	0.4	0.4	0.3	0.4	0.7	0.4	0.4	0.4	0.4	0.3
Ce (ppm)	95	100	101	99	135	111	99	27	96	87	100	97	95	104	129	140
Cr (ppm)	59	4	71	62	66	3	3	107	68	3	4	3	124	77	117	137
Cs (ppm)	2.07	1.89	1.53	2.35	2.98	2.54	3.01	2.64	1.41	1.26	1.61	2.24	1.91	3.23	2.40	2.13
Cu (ppm)	5	11	4	17	3	4	5	43	17	3	10	176	240	15	617	102
La (ppm)	46	50	47	52	62	52	43	13	42	40	45	44	45	49	64	90
Mo (ppm)	1.5	1.5	1.3	0.8	0.8	0.6	0.4	0.5	1.1	0.9	1.0	0.4	2.5	6.9	6.7	5.4
Nb (ppm)	14	14	13	10	14	15	14	2	11	11	11	14	14	18	14	12
Nd (ppm)	41	42	41	41	61	50	47	15	42	39	46	44	44	41	55	47
Ni (ppm)	3	2	2	9	4	2	2	49	3	4	2	1	3	3	5	6
Pb (ppm)	128	102	145	6	24	8	18	5	5	6	38	2	6	5	8	9
Rb (ppm)	138	113	64	94	102	108	110	89	64	57	108	124	105	170	110	90
Sb (ppm)	1.0	1.1	1.4	0.8	0.8	0.7	1.6	0.8	0.5	0.8	1.3	1.2	0.9	1.5	1.0	1.2
Sc (ppm)	4	4	3	17	10	10	11	47	11	10	9	9	11	16	15	12
Se (ppm)	<0.5	<0.5	<0.5	<0.5	<0.5	<0.5	<0.5	<0.5	<0.5	<0.5	<0.5	<0.5	4.4	<0.5	2.0	3.5
Sr (ppm)	63	97	73	97	54	86	48	149	71	40	65	23	37	45	98	68
Th (ppm)	19	23	21	19	20	20	20	4	17	16	18	22	19	27	22	16
Tl (ppm)	<0.5	<0.5	<0.5	<0.5	0.5	0.5	0.5	0.5	<0.5	<0.5	0.5	0.6	0.7	0.8	0.5	<0.5
U (ppm)	4.33	4.91	4.46	3.73	4.34	4.36	3.94	1.06	3.30	3.39	3.69	4.36	4.69	9.66	6.59	13.50
V (ppm)	11	11	7	121	6	6	4	259	15	12	4	4	11	30	19	14
Y (ppm)	32	31	29	28	42	49	39	17	36	34	39	43	43	55	59	24
Zn (ppm)	275	69	154	185	134	46	42	72	60	86	200	95	60	16	17	31
Zr (ppm)	217	231	190	201	291	308	289	49	244	251	226	272	285	397	261	244

Appendix: Analytical results cont.

Hole	WT0077D	WT0077D	WT0077D	WT0077D	WT0077D	WT0077D	WT0077D	WT0077D	WT0077D	WT0077D	WT0077D	WT0077D	WT0077D	WT0077D	WT0077D	WT0077D
From (m)	966.1	988.2	994.5	1002.9	1013.7	1022.7	1044.0	1068.9	1080.6	1098.1	1125.5	1139.6	1153.7	1176.6	1194.6	1215.9
To (m)	966.5	988.6	994.9	1003.2	1014.0	1023.0	1044.4	1069.3	1080.9	1098.5	1125.9	1140.0	1154.2	1177.1	1195.0	1216.3
SiO2 (%)	63.25	57.12	58.95	63.85	61.65	59.35	56.13	54.03	45.85	64.80	74.38	58.74	76.06	54.38	74.18	67.95
TiO2 (%)	0.53	0.38	0.42	0.47	0.49	0.70	0.55	0.48	0.33	0.55	0.30	0.58	0.24	0.54	0.30	0.37
Al2O3 (%)	15.37	11.65	14.65	16.28	13.78	8.79	15.02	13.27	8.71	16.14	15.37	15.11	12.10	14.82	13.15	13.16
Fe2O3 (%)	8.20	15.11	8.11	6.80	9.27	14.36	13.02	15.33	24.40	6.72	2.33	10.96	3.60	9.83	4.25	7.20
MnO (%)	<0.01	0.04	0.52	0.03	0.04	0.01	0.05	0.01	<0.01	<0.01	<0.01	0.08	0.04	0.54	<0.01	0.08
MgO (%)	0.57	0.71	5.12	1.81	2.17	0.82	4.18	1.08	0.42	0.84	0.31	5.30	0.55	4.68	0.29	0.96
CaO (%)	0.17	0.22	1.47	0.25	0.60	0.62	0.32	0.32	0.14	0.23	0.05	0.33	0.27	3.46	0.03	0.46
Na2O (%)	0.16	<0.05	0.06	0.15	<0.05	<0.05	0.10	0.14	0.13	0.17	0.19	0.09	0.13	0.08	0.11	0.13
K2O (%)	4.52	3.34	2.89	4.46	3.48	2.64	2.72	3.68	2.32	4.57	4.31	2.45	3.55	2.90	3.95	4.01
P2O5 (%)	0.19	0.20	0.18	0.20	0.51	0.46	0.26	0.30	0.20	0.20	0.05	0.25	0.04	0.19	0.05	0.07
CuO (%)	0.43	1.10	0.04	0.10	2.32	2.58	1.73	0.40	0.44	0.08	0.00	0.04	0.04	0.01	0.01	0.00
BaO (%)	0.42	0.18	0.13	0.21	0.27	0.27	0.29	0.77	0.65	0.43	0.21	0.18	0.20	0.20	0.12	0.20
LOI (%)	5.98	8.93	6.96	5.19	5.49	8.28	6.16	9.69	14.37	4.98	3.13	5.40	3.70	8.37	3.73	5.36
Sum (%)	99.79	98.98	99.50	99.80	100.06	98.88	100.53	99.50	97.96	99.71	100.63	99.51	100.52	100.00	100.18	99.95
S (%)	5.79	11.28	0.95	3.72	5.25	10.89	4.67	11.79	19.50	4.24	1.59	1.93	2.28	0.38	2.95	3.62
C (%)	0.067	0.880	0.025	0.071	0.073	0.028	0.016	0.010	0.012		0.030	0.110	1.490	0.023	0.330	0.800
Ag (ppm)	1.8	0.2	0.3	2.5	3.6	1.5	1.3	0.7	0.2		0.3	0.8	0.2	0.5	0.8	0.3
As (ppm)	47	7	27	11	11	33	5	8	7		9	6	7	11	8	12
Ba (ppm)	3895	1947	1338	2068	2142	2183	2501	7707	6397	4179	1760	1689	1658	1737	1272	1904
Bi (ppm)	2	3	<2	<2	<2	10	<2	6	16	<2	<2	2	5	<2	<2	<2
Cd (ppm)	0.4	0.4	0.3	0.5	0.5	0.4	0.3	0.6	0.4		0.4	0.5	0.7	0.5	0.4	0.4
Ce (ppm)	206	120	112	95	352	486	296	221	402	140	40	115	103	112	85	92
Cr (ppm)	153	26	27	31	90	15	130	96	86	243	7	134	3	135	4	4
Cs (ppm)	1.68	2.77	2.81	1.73	1.30	1.63	2.14	1.49	2.62		2.85	1.99	1.26	1.53	1.85	2.01
Cu (ppm)	3400	8800	292	764	18500	20600	13800	3200	3500	581	25	387	274	45	35	19
La (ppm)	125	88	56	52	241	348	206	146	268	69	18	57	44	57	33	40
Mo (ppm)	6.2	1.0	0.5	13.6	50.3	18.8	15.0	221.0	5.3		2.6	2.1	1.1	1.1	1.0	1.2
Nb (ppm)	10	4	8	10	21	124	23	11	12	11	17	9	13	8	12	12
Nd (ppm)	73	30	45	33	83	114	72	68	113	58	15	51	54	47	38	42
Ni (ppm)	22	18	17	15	38	125	50	29	30	19	2	33	3	31	2	2
Pb (ppm)	12	48	11	17	25	24	16	10	15	11	15	9	124	9	129	72
Rb (ppm)	104	89	77	111	90	70	71	106	70	138	108	85	107	93	112	129
Sb (ppm)	2.6	0.9	0.8	0.7	0.6	1.0	0.5	0.8	0.6		1.1	0.8	0.9	0.7	0.7	0.7
Sc (ppm)	24	22	23	26	19	12	37	33	15	33	6	35	10	30	12	13
Se (ppm)	2.7	7.1	<0.5	5.6	2.3	4.5	4.2	5.7	31.3	6.3	8.9	7.7	>50.0	1.3	11.8	25.0
Sr (ppm)	203	27	26	26	33	66	38	167	180	119	35	29	35	59	21	21
Th (ppm)	20	17	22	24	24	14	18	13	8	24	10	18	15	19	20	18
Tl (ppm)	<0.5	<0.5	0.5	<0.5	<0.5	<0.5	<0.5	<0.5	<0.5		<0.5	0.6	0.5	0.5	0.6	0.6
U (ppm)	5.00	2.33	6.53	2.98	23.00	3.54	5.33	11.20	2.86		3.97	7.71	4.25	3.14	3.97	3.77
V (ppm)	175	243	191	226	97	191	268	240	137	203	7	238	4	207	8	15
Y (ppm)	32	17	20	14	25	50	17	33	18	42	20	26	59	23	32	36
Zn (ppm)	60	409	535	248	166	57	190	93	276	45	11	743	76	665	42	64
Zr (ppm)	188	107	142	153	139	157	149	152	106	217	322	170	253	152	282	253

Appendix: Analytical results cont.

Hole	WT0077D	WT0077D	WT0077D	95WTD0090	95WTD0090	95WTD0090	95WTD0090	95WTD0090	95WTD0090	95WTD0090	95WTD0090	95WTD0090	95WTD0090	95WTD0090	95WTD0090	95WTD0090
From (m)	1229.5	1239.6	1253.7	1.0	49.5	99.4	135.5	191.3	237.0	249.0	297.0	339.0	377.0	405.0	440.0	448.0
To (m)	1229.9	1240.0	1254.1	1.4	49.9	99.8	135.8	191.6	238.0	250.0	298.0	340.0	378.0	406.0	441.0	449.0
SiO2 (%)	63.99	69.37	67.65	71.88	47.93	38.39	73.33	50.60	73.10	68.78	64.40	73.41	73.82	56.73	61.43	61.42
TiO2 (%)	0.40	0.51	0.40	0.29	0.62	0.41	0.21	0.46	0.22	0.21	0.32	0.26	0.27	0.49	0.50	0.39
Al2O3 (%)	13.23	14.30	15.11	13.56	16.30	11.75	11.35	12.58	11.80	11.25	15.13	12.61	12.78	16.30	14.95	14.52
Fe2O3 (%)	10.06	6.23	3.58	4.66	8.75	10.89	6.23	12.71	6.57	8.98	9.17	6.23	4.81	12.48	8.37	9.69
MnO (%)	0.18	0.21	0.10	0.05	0.24	0.40	0.16	0.60	0.09	0.05	0.09	<0.01	<0.01	0.03	0.07	0.02
MgO (%)	1.48	1.49	1.57	2.08	4.43	6.52	0.92	4.21	0.86	0.90	1.31	0.08	0.46	2.69	3.21	2.24
CaO (%)	0.17	0.16	1.77	0.66	6.28	10.98	0.12	4.91	0.02	0.01	0.04	0.04	0.02	0.21	0.37	0.21
Na2O (%)	0.10	0.06	0.15	1.58	1.93	0.93	0.16	0.07	0.13	0.06	0.16	0.05	0.10	0.07	0.08	0.04
K2O (%)	3.79	3.84	5.13	2.24	2.75	1.84	3.23	2.36	3.25	3.08	3.70	0.30	3.44	3.59	3.41	3.73
P2O5 (%)	0.09	0.11	0.07	0.05	0.11	0.10	0.04	0.18	0.03	0.03	0.05	0.04	0.12	0.19	0.33	0.17
CuO (%)	0.03	0.03	0.00	0.00	0.01	0.00	0.01	0.01	0.01	0.01	0.01	0.01	0.68	0.26	1.95	1.34
BaO (%)	0.16	0.20	0.16	0.08	0.06	0.03	0.09	0.23	0.33	0.23	0.36	0.02	0.42	0.23	0.20	0.22
LOI (%)	6.37	3.27	4.52	3.26	10.22	17.72	4.52	10.82	3.82	6.04	5.45	6.25	3.98	6.90	5.03	6.23
Sum (%)	100.04	99.78	100.21	100.39	99.63	99.96	100.37	99.75	100.24	99.64	100.19	99.30	100.90	100.18	99.90	100.22
S (%)	2.76	0.02	0.01	0.02	0.01	<0.01	0.01	0.01	0.27	3.79	2.16	4.74	3.01	5.41	3.28	5.75
C (%)	0.200	0.780	0.230	0.850	4.230	0.940	2.450	0.590	0.450	0.230	0.026	0.008	0.110	0.078	0.090	0.130
Ag (ppm)	0.4	0.2	0.2	0.3	0.2	0.2	0.2	0.2	0.2	0.3	0.2	1.0	0.5	1.9	1.8	1.6
As (ppm)	3	2	5	229	3	5	4	3	7	9	13	10	42	29	19	13
Ba (ppm)	1582	1614	1473	517	655	397	840	2000	3152	2590	3099	205	3466	2478	1785	2234
Bi (ppm)	<2	<2	<2	<2	<2	<2	<2	<2	<2	2	<2	<2	4	<2	<2	<2
Cd (ppm)	0.4	2.4	0.3	0.5	0.4	0.3	0.4	0.3	0.3	0.4	0.4	0.8	0.3	0.6	0.5	0.4
Ce (ppm)	95	120	112	107	35	37	96	100	101	104	96	106	389	109	283	198
Cr (ppm)	8	4	3	72	145	153	95	247	50	83	65	103	114	91	225	125
Cs (ppm)	2.13	2.99	1.63	8.14	1.77	2.41	1.38	1.61	2.05	2.07	0.55	1.71	1.98	2.37	2.31	1.54
Cu (ppm)	172	130	4	10	5	9	40	46	54	118	110	46	5400	2100	15600	10700
La (ppm)	48	59	54	50	18	18	43	52	47	51	48	62	256	68	194	136
Mo (ppm)	1.8	3.2	1.3	17.0	1.2	1.2	0.8	1.3	1.5	2.8	3.2	234.0	13.6	12.8	17.8	26.4
Nb (ppm)	11	10	16	13	5	4	12	8	12	12	15	13	25	8	20	12
Nd (ppm)	47	51	50	49	16	20	43	42	47	50	43	29	105	39	72	49
Ni (ppm)	4	8	2	3	46	50	5	49	2	3	2	5	5	19	45	30
Pb (ppm)	17	98	42	14	4	8	5	6	3	9	6	5	19	18	30	29
Rb (ppm)	123	125	180	63	83	62	111	73	102	94	113	8	79	94	91	98
Sb (ppm)	0.9	0.6	0.8	60.4	1.5	1.9	2.7	1.3	1.2	0.9	0.7	0.6	1.8	1.2	0.8	1.2
Sc (ppm)	17	16	14	11	30	30	8	32	8	10	13	7	8	34	28	18
Se (ppm)	3.3	<0.5	<0.5	<0.5	<0.5	<0.5	<0.5	<0.5	<0.5	1.1	1.7	1.1	3.9	6.5	3.8	7.7
Sr (ppm)	16	13	53	62	326	146	23	49	42	56	125	88	148	29	33	35
Th (ppm)	16	13	15	19	7	6	17	18	17	19	19	19	20	14	19	25
Tl (ppm)	0.6	0.9	0.6	2.1	0.5	0.6	<0.5	0.5	0.5	<0.5	<0.5	<0.5	<0.5	<0.5	<0.5	<0.5
U (ppm)	3.78	3.17	4.43	6.46	1.57	4.13	3.76	3.62	3.96	3.52	4.24	10.30	2.61	2.31	2.60	6.64
V (ppm)	46	32	19	12	279	226	5	202	3	5	13	16	28	308	158	100
Y (ppm)	42	47	39	40	19	19	38	21	40	52	47	18	25	26	15	9
Zn (ppm)	95	413	245	80	127	209	70	208	45	49	45	7	8	301	339	158
Zr (ppm)	225	210	330	276	112	71	233	150	247	238	304	266	258	124	156	149

Appendix: Analytical results cont.

Hole	95WTD0090	95WTD0090	95WTD0090	95WTD0090	95WTD0091	95WTD0091	95WTD0091	95WTD0091	95WTD0091	95WTD0091	95WTD0091	95WTD0091	95WTD0091	95WTD0091	95WTD0091	95WTD0091
From (m)	505.0	546.0	562.0	573.0	25.2	89.6	124.5	141.1	175.1	192.6	245.0	269.0	306.0	309.8	333.0	368.0
To (m)	506.0	547.0	563.0	574.0	25.6	90.0	124.9	141.5	175.4	192.9	246.0	270.0	307.0	310.0	334.0	369.0
SiO2 (%)	60.40	58.74	63.37	67.62	69.24	56.26	54.24	67.53	46.01	67.15	68.34	67.53	60.89	62.12	55.02	59.71
TiO2 (%)	0.47	0.49	0.50	0.32	0.40	0.50	0.43	0.19	0.49	0.18	0.28	0.23	0.53	0.50	0.63	0.46
Al2O3 (%)	13.26	13.65	13.70	12.75	12.87	14.11	11.99	10.44	13.77	9.24	13.17	11.24	15.07	14.24	17.62	16.02
Fe2O3 (%)	10.07	12.66	9.37	7.84	4.74	7.32	16.25	9.92	18.47	12.02	7.73	9.72	14.56	10.33	10.99	9.83
MnO (%)	0.07	0.23	0.04	<0.01	0.14	0.23	0.45	0.42	0.79	0.32	<0.01	<0.01	0.04	0.02	0.06	0.20
MgO (%)	2.11	1.75	1.47	0.28	2.06	3.02	3.51	1.43	3.01	1.51	0.30	0.07	1.69	0.59	1.41	3.42
CaO (%)	0.57	0.26	0.18	0.07	1.89	4.84	1.63	0.21	0.76	0.06	0.04	0.03	0.15	0.14	0.27	0.27
Na2O (%)	0.02	0.03	0.11	0.13	1.16	0.16	0.14	0.16	0.13	0.08	0.15	<0.05	0.17	0.28	0.11	0.06
K2O (%)	3.36	3.45	3.74	3.66	2.37	3.54	2.10	2.90	3.48	2.47	3.92	0.38	3.03	3.98	4.95	3.53
P2O5 (%)	0.48	0.27	0.17	0.09	0.09	0.20	0.17	0.03	0.14	0.02	0.06	0.06	0.16	0.14	0.23	0.20
CuO (%)	2.75	1.50	0.39	0.01	0.00	0.01	0.01	0.00	0.06	0.01	0.01	0.01	0.05	0.06	1.15	0.68
BaO (%)	0.29	0.23	0.47	0.28	0.10	0.22	0.10	0.18	0.44	0.56	0.25	0.04	0.42	0.27	0.37	0.23
LOI (%)	5.68	6.73	5.56	5.97	4.39	9.08	8.54	6.49	11.85	6.07	5.61	10.18	4.19	6.49	7.49	6.10
Sum (%)	99.53	100.00	99.07	99.02	99.45	99.50	99.56	99.90	99.40	99.69	99.86	99.50	100.95	99.16	100.30	100.71
S (%)	4.48	5.38	4.97	5.89	0.01	<0.01	0.19	0.12	0.24	0.29	5.34	7.35	1.79	6.73	5.82	2.97
C (%)	0.290	0.046	0.015	1.940	0.005	1.940	1.570	2.880	1.410	0.085	0.029	0.061	0.049	0.350	0.230	0.019
Ag (ppm)	1.2	0.9	0.2	0.2	0.3	0.3	0.2	0.4	0.2	0.3	0.2	0.2	0.2	0.8	0.6	2.8
As (ppm)	48	30	1	2	18	17	4	6	2	6	8	5	8	16	47	41
Ba (ppm)	2593	2097	4295	2794	879	1970	985	1903	3955	4616	2494		3990	2528	3443	2243
Bi (ppm)	<2	<2	2	2	<2	<2	5	<2	<2	<2	<2		<2	2	<2	<2
Cd (ppm)	0.6	0.4	0.3	0.4	0.4	0.3	0.4	0.4	0.3	0.4	0.4	0.4	0.3	0.4	0.6	0.7
Ce (ppm)	326	349	151	152	95	124	103	86	59	67	97		143	132	290	98
Cr (ppm)	212	210	251	185	3	175	182	4	8	4	131		180	191	107	107
Cs (ppm)	1.79	2.07	10.50	2.39	1.97	1.65	2.09	1.87	1.40	2.54	0.38	2.38	3.34	2.31	2.55	2.05
Cu (ppm)	22000	12000	3100	58	5	26	146	39	512	36	123		426	501	9200	5400
La (ppm)	224	232	100	77	46	61	54	42	28	37	45		78	69	193	51
Mo (ppm)	64.4	44.5	1.4	1.7	10.4	1.0	1.0	1.1	0.7	2.6	4.3	2.6	1.9	6.7	4.9	101.0
Nb (ppm)	24	13	11	12	12	9	8	11	6	10	14		9	9	21	8
Nd (ppm)	76	99	47	66	43	50	42	38	26	28	45		60	52	76	41
Ni (ppm)	60	30	22	13	1	29	37	8	13	7	6		29	18	22	18
Pb (ppm)	16	15	13	19	27	5	8	7	2	<1.5	7		14	16	11	21
Rb (ppm)	85	92	99	87	65	120	68	95	106	78	113		84	106	116	92
Sb (ppm)	1.2	0.9	0.2	1.8	0.8	2.1	1.8	1.9	1.3	1.2	0.9	1.5	1.2	1.1	3.3	0.8
Sc (ppm)	24	30	42	21	10	32	30	9	15	5	15		34	34	17	28
Se (ppm)	2.0	3.5	5.2	6.9	<0.5	<0.5	<0.5	<0.5	1.7	<0.5	1.5	3.2	<0.5	1.8	7.6	4.2
Sr (ppm)	40	36	56	61	60	61	29	21	66	57	63		161	117	121	27
Th (ppm)	18	18	17	21	18	21	19	17	8	11	18		20	20	13	23
Tl (ppm)	<0.5	<0.5	1.2	0.6	<0.5	<0.5	0.5	0.6	<0.5	0.5	<0.5	<0.5	<0.5	<0.5	<0.5	<0.5
U (ppm)	5.36	6.73	2.23	4.65	5.17	4.15	4.26	2.34	3.95	4.81	4.86	7.18	7.84	5.04	4.35	4.70
V (ppm)	213	215	319	89	20	211	187	5	165	4	18		182	208	133	211
Y (ppm)	19	25	18	41	35	23	19	35	29	33	40		32	38	20	20
Zn (ppm)	89	99	63	7	65	73	340	107	255	97	9		43	13	31	427
Zr (ppm)	167	167	160	225	247	171	145	212	125	185	280		187	176	160	157

Appendix: Analytical results cont.

Hole	95WTD0091	95WTD0091	95WTD0091	95WTD0091	95WTD0091	95WTD0091
From (m)	389.0	422.0	460.0	474.0	495.0	514.0
To (m)	390.0	423.0	461.0	475.0	496.0	515.0
SiO2 (%)	72.75	62.14	67.71	58.67	52.88	52.45
TiO2 (%)	0.22	0.18	0.23	0.54	0.44	0.45
Al2O3 (%)	10.11	8.63	11.24	14.67	12.37	12.88
Fe2O3 (%)	6.11	13.72	8.95	9.39	17.90	16.78
MnO (%)	0.01	<0.01	<0.01	0.03	<0.01	0.12
MgO (%)	0.36	0.43	0.46	3.12	0.63	1.10
CaO (%)	0.33	0.65	0.06	0.15	0.12	0.24
Na2O (%)	<0.05	<0.05	0.06	0.07	0.10	0.06
K2O (%)	2.80	2.42	3.11	3.31	3.49	4.00
P2O5 (%)	0.35	0.55	0.18	0.31	0.16	0.20
CuO (%)	1.73	1.38	1.78	2.38	0.14	0.48
BaO (%)	0.20	0.22	0.31	0.50	0.38	0.31
LOI (%)	4.22	9.15	6.00	6.19	11.07	10.63
Sum (%)	99.19	99.47	100.09	99.33	99.68	99.70
S (%)	4.17	10.85	5.40	5.10	11.34	11.39
C (%)	<0.005	0.033	0.095	0.007	0.170	0.690
Ag (ppm)	4.1	1.6	1.9	0.5	0.9	0.3
As (ppm)	181	30	9	14	22	2
Ba (ppm)	1330	1993	2410	3771	4006	3362
Bi (ppm)	2	4	<2	<2	3	3
Cd (ppm)	1.2	0.5	1.7	0.4	0.4	0.4
Ce (ppm)	574	416	626	791	258	148
Cr (ppm)	227	262	212	230	263	229
Cs (ppm)	1.44	2.03	1.98	1.87	1.73	1.50
Cu (ppm)	13800	11000	14200	19000	1349	3800
La (ppm)	407	287	410	520	163	84
Mo (ppm)	19.2	64.0	786.0	36.9	11.1	2.5
Nb (ppm)	11	9	17	17	9	9
Nd (ppm)	130	103	158	203	79	57
Ni (ppm)	17	88	20	31	25	27
Pb (ppm)	21	14	18	18	16	20
Rb (ppm)	64	61	76	87	95	110
Sb (ppm)	99.2	1.7	1.1	0.7	1.4	0.6
Sc (ppm)	7	17	8	40	36	34
Se (ppm)	3.8	7.8	3.6	3.0	29.2	7.6
Sr (ppm)	111	355	76	101	67	34
Th (ppm)	19	19	16	16	18	19
Tl (ppm)	<0.5	<0.5	<0.5	<0.5	<0.5	0.5
U (ppm)	21.70	6.79	5.91	15.40	10.40	4.17
V (ppm)	47	216	67	288	226	226
Y (ppm)	12	28	18	40	42	31
Zn (ppm)	32	144	19	105	27	141
Zr (ppm)	200	164	225	147	151	149

Progress report on the Mt Julia-Henty gold mine alteration study

by Tim Callaghan
Goldfields Tasmania Ltd

Introduction

Mt Julia is located on the south of the Henty Mine Lease ML7/92, approximately 1.5 km south of the Henty Gold Mine (Fig. 1). Henty style gold mineralisation was identified at the Mt Julia Prospect in December 1995 when diamond drill hole MJ005 intersected extensive sericite-silica altered volcanics within the Tyndall Group. MJ005 was the fifth hole of a systematic exploration program targeted on what was considered to be the Henty horizon. The program was initiated from the south of the mine lease and has progressed northwards.

Since this time between one and four surface diamond drill rigs have operated on the Mt Julia Prospect or between Mt Julia and Zone 96. A resource figure is currently being calculated for the Mt Julia deposit.

Geology

The Mt Julia Prospect and Henty Gold Mine are hosted within the Tyndall Group located in the footwall of the west dipping Henty Fault. The Henty Fault bifurcates into the North and South Henty Faults within the Mine lease at about 54000mN Henty Mine Grid (HMG). Extensive alteration occurs in the immediate footwall to the South Henty Fault and extends eastward higher into the overturned Tyndall Group stratigraphy.

Stratigraphy

Rocks to the east of the Henty Fault consist of the Central Volcanic Complex (CVC), Tyndall Group and Owen Conglomerate (Fig. 2). Between the North and South Henty Faults are quartz-phyric volcanics, ultramafic and mafic volcanics and black shales associated with the Henty Fault Sequence (HFS). To the west of the North Henty Fault and Henty Fault are andesitic to rhyolitic CVC, the tholeitic Henty dyke swarm and acid volcanics and sediments of the White Spur Formation.

The CVC located to the east of the South Henty Fault outcrops in the south of the Henty Mine Lease as intensely sericite-pyrite altered dacitic to rhyolitic volcanics. The boundary between the CVC and overlying Tyndall Group is not well defined in this area but is considered to be conformable.

The stratigraphy of the Tyndall Group is well defined in the vicinity of the Mt Julia Prospect. The Tyndall Group stratigraphy has been subdivided regionally by White and McPhie (1996) and consists of the Comstock Formation and Zig Zag Hill Formation. The Comstock Formation has been divided into the Lynchford Member and the Mt Julia Member (White and McPhie, 1996). Although localised rapid facies changes typify the Tyndall Group, all of these subdivisions are represented on the Mine Lease, particularly to the south.

Comstock Formation, Lynchford Member

The Lynchford Member is the basal unit of the Tyndall Group. The lowest stratigraphic units at Mount Julia and northwards on the Henty Mine Lease are intensely sericite-pyrite-carbonate altered rhyolitic coherent volcanics, siltstones and massflows that may be part of the CVC. Rare but distinctive fuchsite-sericite altered dykes are a feature of these underlying rocks. This unit appears to be continuous to the north and forms the stratigraphic footwall of the Zone 96 and Sill Zone orebodies.

Henty - Mount Julia

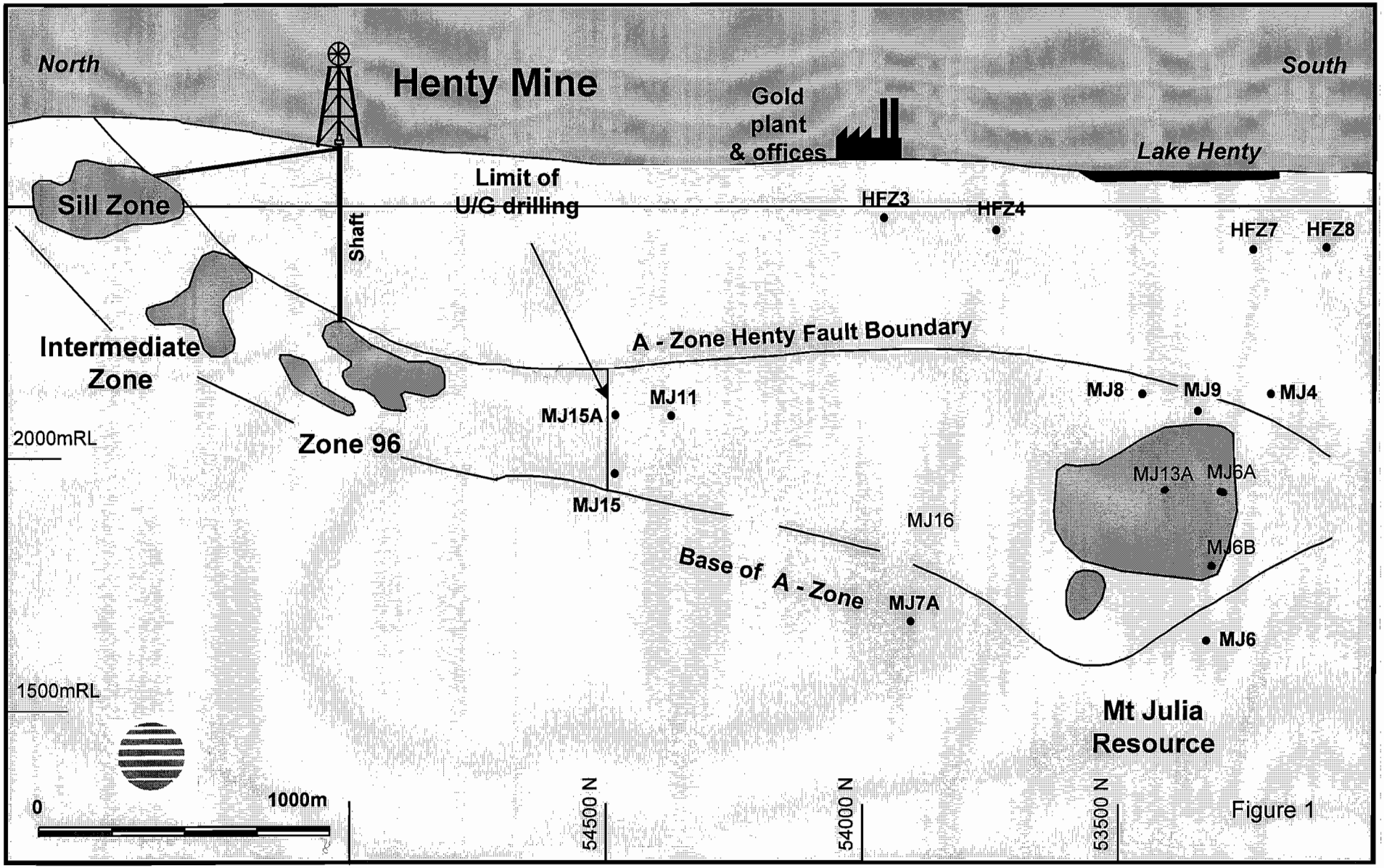

Figure 1

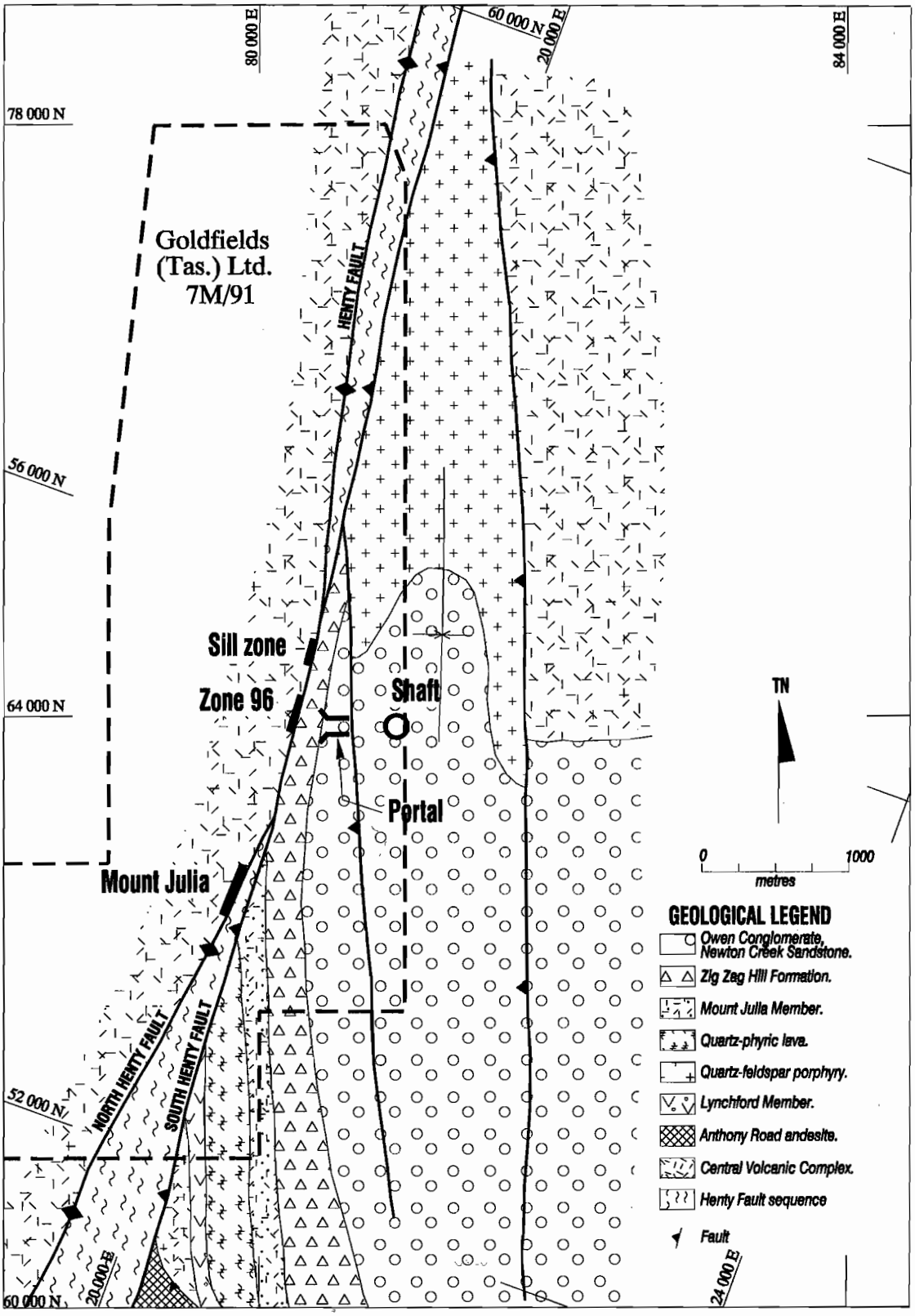
80 000 E
60 000 N
20 000 E
84 000 E
78 000 N
56 000 N
64 000 N
52 000 N
60 000 N
20 000 E
24 000 E
Goldfields
(Tas.) Ltd.
7M/91
HENTY FAULT
Sill zone
Zone 96
Shaft
Portal
Mount Julia
NORTH HENTY FAULT
SOUTH HENTY FAULT
TN
0
1000
metres
GEOLOGICAL LEGEND
Owen Conglomerate, Newton Creek Sandstone.
Zig Zag Hill Formation.
Mount Julia Member.
Quartz-phyric lava.
Quartz-feldspar porphyry.
Lynchford Member.
Anthony Road andesite.
Central Volcanic Complex.
Henty Fault sequence
Fault

At Mount Julia the bulk of the Lynchford Member consists of distinctive feldspar crystal rich sandstones with interbedded polymict, matrix supported mass flows and minor siltstones and shales. Some mass flow units contain abundant clasts to 5cm of quartz porphyritic rhyolites supported in a matrix of predominantly feldspar crystals. Quartz-feldspar crystal rich volcaniclastic sandstones, though much less common than the feldspar rich volcaniclastics are not unusual in this unit. The Lynchford Member is variably magnetic on the Henty Mine Lease due to varying amounts of detrital magnetite.

Numerous carbonate horizons occur throughout this unit. Some of the carbonates may be true chemical sediments but many appear to be pervasive carbonate alteration and partial replacement of volcaniclastic sediments. These carbonates are not uncommon within the Lynchford Member and more work is required to determine if these are hydrothermal carbonates related to mineralisation (Halley and Roberts, in press) or are similar to the carbonates seen to the south.

This base of the Lynchford Member clearly hosts the most intense alteration and mineralisation (A-Zone) at Mt Julia and northwards up to the southern end of Zone 96. Mineralisation is hosted in rhyodacitic volcanics immediately below andesitic volcaniclastics. North of Zone 96 alteration and deformation is too intense to reliably identify stratigraphic elements without the use of lithogeochemistry.

Comstock Formation, Mt Julia Member

Overlying and partially intruding the Lynchford Member in the south of the Mine Lease is a distinctive quartz-phyric rhyolite body that thickens rapidly and extends approximately 5km to the south. This rhyolite has autobrecciated and pepperitic margins and occasionally demonstrates flow banding. The rhyolite is not present over the Zone 96 and Sill Zone orebodies except perhaps as minor sills and dykes.

Overlying the rhyolite are graded volcaniclastic massflows or proximal turbidites and well sorted quartz crystal rich sandstones and minor siltstones of the Mt Julia Member. This unit was known as the Comstock Tuff by RGC and Mines Department geologists in the past (Corbett 1992).

The mass flow units contain polymict clasts of rhyolite, ripped up sediments, occasional pumice fragments and rare jasper clasts fining upwards to siltstones.

Rare cabonate beds and carbonate impregnated sediments have also been observed in this member.

The Mt Julia Member thins northwards and is not present above the Sill Zone.

Zig Zag Hill Formation

The base of the Zig Zag Hill Formation contains well sorted graded to massive epiclastic sandstones with occasional matrix supported mass flow units. The sandstones usually contain abundant quartz and altered feldspar crystals. This unit appears to be gradational with the underlying mass flow units but is better correlated with the Zig Zag Hill Formation due to the distinctive quartz porphyry clasts and intrusive quartz porphyries associated within the unit. The sandstones occassionally contain bedded magnetite horizons particularly towards the top of the massive sandstone unit in the south of the mine lease.

Overlying the sandstones are distinctive epiclastic conglomerates and coarse quartz crystal rich sandstones. The epiclastics are generally well bedded and graded and contain abundant quartz porphyry clasts derived from a contemporaneous rhyolite complex.

The Zig Zag Hill Formation also contains interbedded siliclastic conglomerates and shales identical to the overlying Newton Creek Sandstone. Mixed provenance siliclastic and volcaniclastic beds are also present becoming more common towards the top of the Zig Zag Hill Formation. An erosional channel filled with siliclastics is located just to the north of the Mt Julia prospect.

Intruding into and extruding onto the Zig Zag Hill Formation is a large quartz porphyritic rhyolite complex. The volcanic centre appears to have been in the Moxon saddle area where massive quartz porphyries occur. Jigsaw fit hyaloclasitites, dykes, sills and volcaniclastics of the same complex occur at the bottom of the shaft under Gooseneck Hill and dykes and sills of the same unit occur to the south near Mt Julia.

This complex formed a topographic high to the north and east of Henty during the Cambrian and provided much of the sediment input to the Zig Zag Hill Formation. The porphyries also intrude the

siliclastic interbeds and occur in volcaniclastics overlying them indicating that this final phase of volcanism occurred during onset of siliclastic sedimentation.

Owen Conglomerate

Overlying the Zig Zag Hill formation are the siliclastics of the Owen Conglomerate, locally represented by the Newton Creek Sandstone. These rocks are dominated by well bedded, massive clast supported siliciclastic conglomerates with lesser black shales and laminated to massive grey siliciclastic and micaceous sandstones.

Structure

The geology of the Henty Mine lease is dominated by the Henty Fault. The Henty Fault divides into North and South Henty faults in the middle of the mine lease and the intersection of these faults has a shallow southerly plunge of approximately 20° although little subsurface information regarding the North Henty fault is available. The South Henty Fault has a strong south-plunging inflexion in the vicinity of the Mount Julia deposit (Fig. 3).

The rock types to the east of the Henty Fault are controlled by a major, shallowly south plunging, asymmetric syncline centred on the siliciclastic rocks of the Owen Conglomerate and the Henty Fault. The western limb of this syncline is steeply east dipping in the south of the lease, but is overturned to the east in the northern and central regions where the synclinal axis trends into the Henty Fault. Numerous north striking, steeply west dipping brittle-ductile faults were logged in drill core and mapped in underground workings in this central part of the lease.

Most of these structures are associated with overtightening and reverse faulting of the western limb of the syncline during continued east-west compression associated with the Devonian deformation. It is possible that some of these are reactivated Cambrian faults forming the western boundary of a graben filled with the siliciclastic rocks of the Owen Conglomerate. Correlation of these faults is difficult but it appears that these are locally developed structures most prevalent in the steep limb of the syncline.

A dominant foliation (S2) of approximately 340° AMG strike and vertical to steep southwesterly dip occurs throughout the lease with the exception of the immediate vicinity of the Henty Fault, where the foliation parallels the fault.

Mineralisation is strongly controlled by the South Henty Fault which forms the upper boundary to mineralisation (Figs 3, 4), and away from which mineralisation and alteration decrease. Intensely foliated phyllosilicates associated with extensive hydrothermal alteration are always present in the immediate footwall of the fault irrespective of which stratigraphic unit is present. Mylonitisation and brecciation of altered and mineralised volcanic rocks close to the South Henty fault is a feature of the Henty deposit.

Numerous post-ductile deformation brittle faults, with several different orientations and displacements of a few metres, disrupt the rocks of the northern mine area, particularly within the Sill Zone. These types of structures are possibly present at Mt Julia but are not easily interpreted from drill core.

It is not yet fully understood what happens to the host sequence at depth. The few holes that have been drilled well below mineralisation have not intersected the ore host horizon.

Alteration

The alteration of the Mt Julia Prospect can be subdivided into three categories, footwall alteration, alteration associated with mineralisation (A-Zone) and hangingwall alteration. Alteration is similar to that of Zone 96 and the Sill Zone but is less intense and is lower in sulphide content. Alteration demonstrates distinct assymetry.

Footwall Alteration

Footwall alteration at Mt. Julia consists of intensely foliated to mylonitic sericite-pyrite-carbonate-silica (MA) altered rhyolitic volcaniclastics, lavas and sills. Minor fuchsite-sericite altered dykes are characteristic of the footwall alteration. Late carbonate veining is common throughout footwall altered rocks. Occasionally relict clastic textures of mass flows and porphyritic textures of rhyolites are preserved in an intensely sericitised and foliated matrix. Pyrite content varies from 0-2%.

GOLDFIELDS EXPLORATION

MT. JULIA PROSPECT
GEOLOGY SECTIONSECTION 53350N

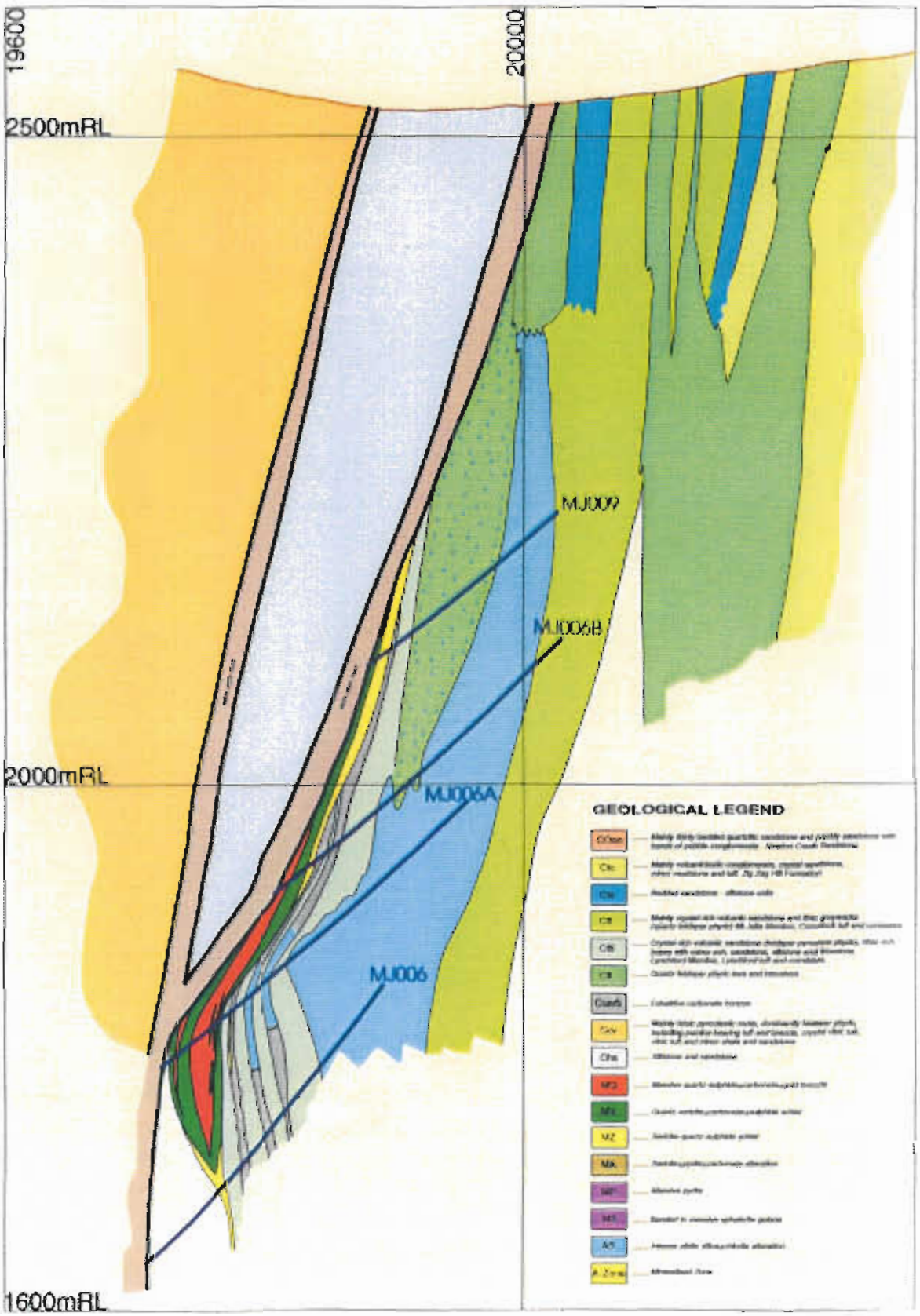

GEOLOGICAL LEGEND

COon	..... *Mainly thinly bedded quartzitic sandstone and pebbly sandstone with bands of pebble conglomerate - Newton Creek Sandstone*
Ctc	..... *Mainly volcaniclastic conglomerate, crystal sandstone, minor mudstone and tuff. Zig Zag Hill Formation*
Cts	..... *Bedded sandstone - siltstone units*
Ctt	..... *Mainly crystal-rich volcanic sandstone and lithic greywacke (quartz-feldspar phyric) Mt Julia Member, Comstock tuff and correlate*
Cttl	..... *Crystal-rich volcanic sandstone (feldspar-pyroxene phyric), lithic-rich bases with minor ash, sandstone, siltstone and limestone. Lynchford Member, Lynchford tuff and correlates.*
Ctl	..... *Quartz-feldspar phyric lava and intrusives.*
Ccarb	..... *Exhalitive carbonate horizon*
Ccv	..... *Mainly felsic pyroclastic rocks, dominantly feldspar phyric, including pumice bearing tuff and breccia, crystal vitric tuff, vitric tuff and minor shale and sandstone*
Chs	..... *Siltstone and sandstone*
MQ	..... *Massive quartz-sulphide±carbonate±gold breccia*
MV	..... *Quartz-sericite±carbonate±sulphide schist*
MZ	..... *Sericite-quartz-sulphide schist*
MA	..... *Sericite±pyrite±carbonate alteration*
MP	..... *Massive pyrite*
MS	..... *Banded to massive sphalerite galena*
AS	..... *Intense albite silica±chlorite alteration*
A-Zone	..... *Mineralised Zone*

A-Zone Alteration

A-Zone at Mt Julia is dominated by silica-sericite schists (MV) with lesser silica-carbonate alteration (MQ) and silica-sericite-pyrite (MZ) schists. This is quite different from Zone 96 where A-Zone is dominated by MZ with lesser MV and MQ, reflecting the overall lower sulphide content of the Mt Julia deposit.

MQ is an intensesly silicified and brecciated, possibly intermediate volcanic. The rock is composed dominantly of silica and carbonate veins with lesser sericite. Contacts with MV are often interfingered and gradational with increasing sericite contents. Occasional jasper clasts are preserved within both MQ and MV type alteration.

MV is an intensely silicified and sericitised indeterminate though possibly intermediate volcanic. The rock is intensely deformed and contains numerous silica-carbonate veins.

MZ often interfingers with MV and appears to be a similar rock but contains variable amounts of pyrite to 5%.

The assymetry of A-Zone is apparent as very minor massive sulphide (MS) and massive pyrite (MP) is associated with carbonate horizons concentrated near the top of the A-Zone alteration. Most of the massive sulphides appear to be massive sphalerite-galena veins with lesser disseminated and banded sphalerite and galena.

Carbonates (CB) can occur as massive, white to pink limestones but more commonly as carbonate impregnated volcaniclastics. Carbonates, although frequently occuring near the top of A-Zone, are not restricted to this position and occur at the base of A-Zone on some sections (MJ013). Jasper nodules or clasts are a feature of the sediments hosting the carbonate horizons. There is no barite associated with the carbonates or massive sulphides.

The sericite-silica-sulphide alteration overprints earlier carbonate and jasper alteration and albite-silica alteration.

Hangingwall Alteration

Rocks in the immediate hangingwall to mineralisation are strongly to intensely albite-silica (AS) and albite-silica-chlorite altered depending on the chemistry of the protolith. Albite forms zoned euhedral crystals nucleated on pre existing feldspars giving a psuedo porphyritic texture to some rocks, but more commonly occurs as pervasive fine grained albitisation of the entire rock mass. The albitisation varies from a complete, pervasive texture destructive alteration, to a bleaching of volcaniclastics with orange albitic reaction rims, to alteration of the fine-grained matrix of coherent volcanics whilst preserving most primary textures. Hangingwall alteration can extend up to 100 m above the mineralised horizon.

The alteration zone has not been closed of to the north and south. Drillholes MJ008, MJ004 and MJ009 close off the mineralisation updip and MJ006 and MJ007A close it off down dip.

Mineralisation

Mineralisation within A-Zone at Mt Julia consists of predominantly pyrite and chalcopyrite with lesser galena-sphalerite and minor gold, electrum and native bismuth. Ore grade mineralisation is confined within MV and MQ alteration with better grades generally occuring within alteration with abundant pyrite-chalcopyrite-carbonate-silica veins and breccia infill. Gold occurs as fine grained inclusions in pyrite grains associated with chalcopyrite, galena, galeno-bismuth and native bismuth from the few thin sections that have been analysed to date.

Although all of A-Zone contains anomalous gold, only a small proportion contains potential ore grade gold mineralisation. Unlike Zone 96 and the Sill Zone, not all MQ alteration contains high grade gold. Areas of barren silica-sulphide-carbonate alteration are common. Ore grade gold mineralisation is also found in MV style alteration so a resource based on geological boundaries alone is not feasible at Mt. Julia.

From the limited drilling information available it appears that several continuous zones of higher grade gold mineralisation can be defined within the A-Zone package. These areas are best defined on a geochemical basis in conjunction with geological interpretation so it will be very important to base any future mine design on resource drilling.

Geochemistry of Henty alteration

Introduction

A total of 59 samples from Mt Julia drillcore were submitted for whole rock and trace element analysis. All samples also had thin sections prepared for petrological work. Samples were from halved to quartered drill core of about 0.3 m in length. Thirty two samples were analysed for major elements by XRF at Analabs laboratories in Welshpool. Fifty five samples were sent for multi element analysis by ICP-MS at Analabs laboratories in Welshpool and by NAA at Lucas Heights. All samples were analysed for Ti and Zr by XRF at Analabs laboratories, Welshpool.

These results are combined with multielement NAA and Ti and Zr by XRF analyses on the Sill Zone, Zone 96 and Mt. Julia contained in the RGC database.

Unmineralised, less altered samples were selected from drillholes located to the south of, and below the Mt. Julia prospect. Mineralised, altered samples were obtained from within A-Zone at Mt Julia. Samples were taken above and below the A-Zone position in an attempt to determine both lateral and vertical geochemical variations associated with the alteration system.

Drillholes MJ002, MJ003, MJ004 and MJ006 intersected unmineralised Lynchford Member with distal carbonate and minor jasper alteration (Fig. 1). MJ006 passed through extensive hangingwall albite-silica (AS) alteration within the Mt Julia Member above the mineralised horizon before passing through what has been interpreted to be weakly altered unmineralised host horizon at depth (Fig. 3) and then passing into altered footwall rhyolitic volcanics. MJ006A, MJ006B and MJ013A all intersected extensively altered A-Zone alteration hosted within the base of the Lynchford Member. MJ006B and MJ013A contain significant gold mineralisation.

Altered footwall volcaniclastics were intersected in drillholes MJ006 and MJ006A. One sample of relatively unaltered footwall rocks was obtained from MJ003.

Although alteration and mineralisation at Mt Julia has many similarities with Zone 96 and the Sill Zone, there are several important differences, not least of which is the lower Au grades contained in the Mt Julia resource. A comparison of Mt Julia with these resources may provide some insight into targeting high grade mineralisation within the alteration package.

Immobile element geochemistry

Alteration within A-Zone of the Mt. Julia prospect includes extensive MV alteration (silica-sericite-carbonate ± sulphides), MQ alteration (silica-carbonate ± sulphides), lesser carbonate (CB) and MZ (silica-sericite-pyrite) and minor massive pyrite (MP) and massive sulphides (MS).

Due to the intensity of alteration, immobile element geochemistry is required to help define the stratigraphy, determine the protolith hosting A-Zone alteration and also to assist in the understanding of processes involved during alteration. Al, Ti, and the high field strength elements (HFSE) Zr, Nb and Y and the rare earth elements (REE), particularly heavy REE are generally considered to be immobile in alteration zones around a large numer of volcanogenic massive sulphides (MacLean and Kranidiotis, 1987, Maclean and Barrett, 1993). Other useful, less commonly used immobile elements include Sc, V, Th, Cr, Ni and Co. These elements and REE's Hf and Yb are more affordable for the exploration geologist as they can all be analysed cheaply by NAA along with a suite of other useful elements with Analabs Au +31 analysis instead of the more expensive XRF analysis for Ti, Al and Zr (Zr is included in the NAA suite but the detection limit is too high to be useful). This analytical technique is economical for a large number of samples such as bedrock soil geochemistry surveys whilst still providing a useful database for geochemical analysis.

Although immobile element geochemistry is best used on coherent volcanics, they have been used in this study on volcaniclastic rocks with some success. It is assumed that the immaturity of the volcaniclastics has resulted in the heavy minerals containing immobile elements (zircons, ilmenite, leucoxene, rutile and monazite) concentrating in similar ratios during resedimentation as their original volcanic source rocks.

Th, Hf, Zr and some REE are concentrated in zircons and monazite, minerals more common in felsic volcanics. Ti, Sc and V concentrate in rutile, ilmenite and iron rich phases more common in mafic

volcanics. Cr, Ni and Co are immobile elements indicative of minerals associated with ultramafic rocks such as chromite.

An examination of data indicate that Ti, Hf, Zr and to some extent Sc, V and Th have remained immobile during alteration of the host rocks at Mt. Julia (Figs 5, 8).

The MQ samples contain Sc and V concentrations too close to the detection limit to be confident of immobility of these elements during alteration although it appears as though they were in all but MQ alteration (Figs 7, 8). Sc and V were clearly immobile during the formation of the other alteration styles hosted within A-Zone and also during alteration of the footwall and hangingwall lithologies. Th is enriched relative to Ti, Sc and V in some MQ and one MV samples indicating some addition of this element during the alteration process if it is assumed MQ formed from the same protolith as the other A-Zone alteration types.

Aluminium, Niobium and Ytterium do not appear to have been as immobile as Ti, Sc, V, Th, Hf and Zr during the most intense phases of alteration at Mt. Julia Figure 9.

TiO_2/Al_2O_3 bivariate plots from the Mt. Julia data set less clearly define the different stratigraphic units present in the alteration package than Figures 5, 7 and 8. A-Zone alteration still loosely fits on a single regresion line and is again distinct from the sericitic footwall alteration and albitic hangingwall rhyolites overlying mineralisation. However MQ alteration is clearly anomalous with low Al_2O_3 contents indicative of Al depletion during the most intense silicification of the protolith, as discussed in the whole rock geochemistry section.

It appears that Y was not immobile during A-Zone alteration and not completely immobile during footwall and hangingwall alteration from the Ti/Y plot. The A-Zone alteration is not as well constrained as the footwall and hangingwall alteration perhaps indicating some mobility of Y during the most intense alteration.

Nb has behaved similarly to Y, remaining immobile during footwall and hangingwall alteration but not during A-Zone alteration. Although the A-Zone alteration products define a reasonable regression line on a Ti/Nb plot, the more intense MV and MQ alteration demonstrates a shift to lower Nb concentrations possibly indicating some depletion of this element.

From this examination it is apparent that only Ti, Hf ,V, Zr and possibly Sc and Th have remained immobile during the alteration process. The intense texture destructive A-Zone alteration, particularly MQ and MV alteration has mobilised Nb, Sc, V, Th, Y and Al, particularly during MQ alteration. These elements have remained relatively immobile during footwall sericite-pyrite alteration and hangingwall albite-chlorite alteration.

Ti/Zr plots for A-Zone alteration suggest that all of the A-Zone alteration products have been derived from the same dacitic source rock at the base of the Lynchford Member with a Ti/Zr ratio of 14.7 (Figs 5, 10). The other mafic/felsic indicator element ratios (Figs 7, 8) also suggest the protolith was intermediate between the strong rhyolitic signature of the Mount Julia Member rhyolites and footwall rhyolites, and the more mafic, possibly andesitic signature of some of the Lynchford Member volcaniclastics. Much of the Lynchford member volcaniclastics have a similar geochemical signature to the A-Zone alteration.

Although A-Zone is hosted within what appears to be a well defined stratigraphic horizon from the samples taken in this study, the Lynchford Member overlying and possibly hosting the alteration could be further subdivided as the Ti/Zr ratios vary between 5 and 44 with an average of 23.

The Lynchford Member appears to be mainly feldspar-rich crystal sandstones of andesitic to dacitic detritus but frequent mass flows containing rhyolite clasts may account for some of the differences in Ti/Zr ratios for this unit. Two groups have been defined from their geochemistry, one with similar characteristic Ti/Zr ratios to A-Zone, the other with higher Ti/Zr ratios. The group with the same immobile element geochemistry as the MZ, MV and possibly MQ alteration suggests that these may possibly be the protolith.

Other distinctive lithogeochemical groups can also be determined for the footwall rhyolites (FW) with a Ti/Zr ratio average of 6.3, the albite-silica altered Mt. Julia Member rhyolitic lavas and volcaniclastics (AS and VC) with a Ti/Zr ratio of 5.9 and the Lynchford Member (LT) volcaniclastics (Figs 3, 5, 6, 8). The footwall rhyolites, intensely albite-silica altered volcanics (AS) and unaltered volcaniclastics

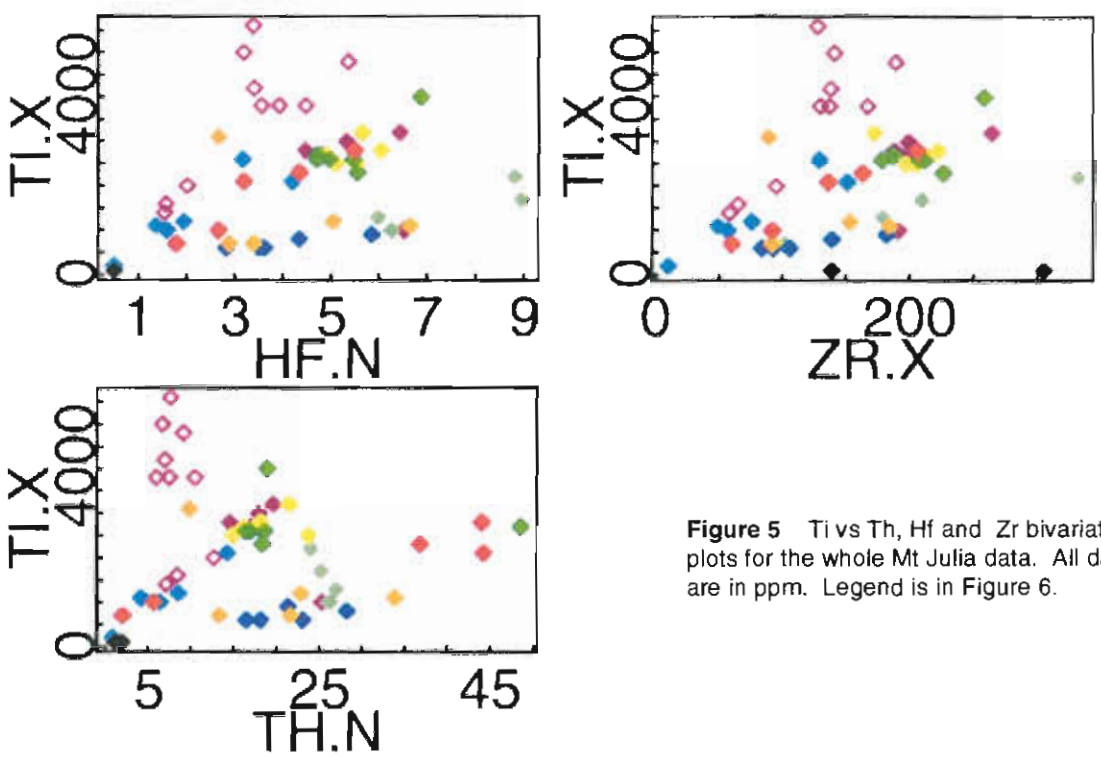

Figure 5 Ti vs Th, Hf and Zr bivariate plots for the whole Mt Julia data. All data are in ppm. Legend is in Figure 6.

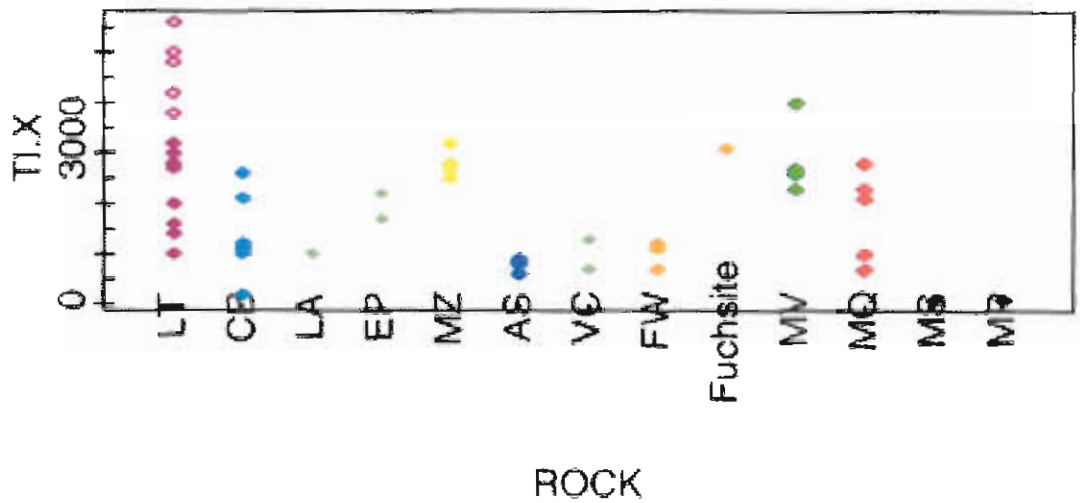

Figure 6 Legend for all figures in this chapter. The same colour code applies to plots with all the data in this document. Diamonds are Mt. Julia samples, squares are Zone 96 and circles are Sill Zone samples. LT = Lynchford Member, CB = carbonates, LA = Mount Julia Member rhyolite, EP = Mount Julia Member rhyolitic epiclastics, MZ = A-Zone silica-pyrite-sericite schist, AS = Mount Julia Member intensely albitised rhyolite, VC = Mount Julia Member volcaniclastics, FW = footwall sericite-pyrite-carbonate altered rhyolites, Fuchsite = footwall sericite-fuchsite altered dyke, MV = A-Zone silica-sericite schist, MQ = A-Zone intense silica-sulphide alteration, MS = massive sulphide, MP = massive pyrite.

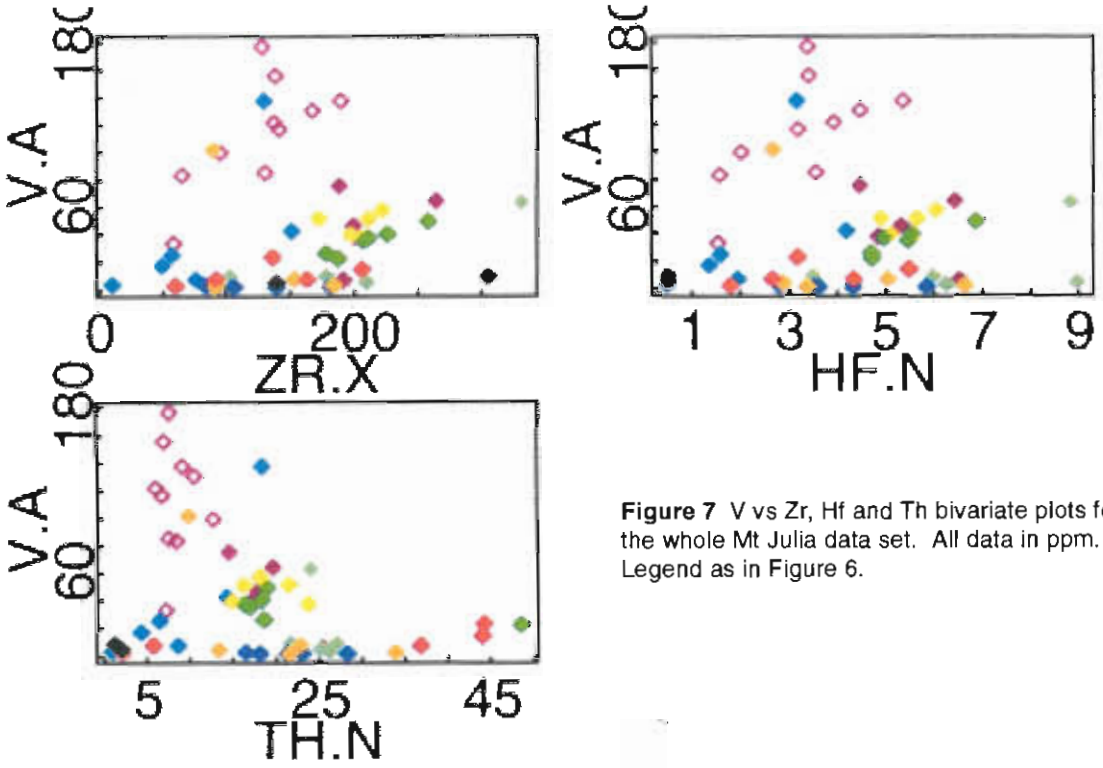

Figure 7 V vs Zr, Hf and Th bivariate plots for the whole Mt Julia data set. All data in ppm. Legend as in Figure 6.

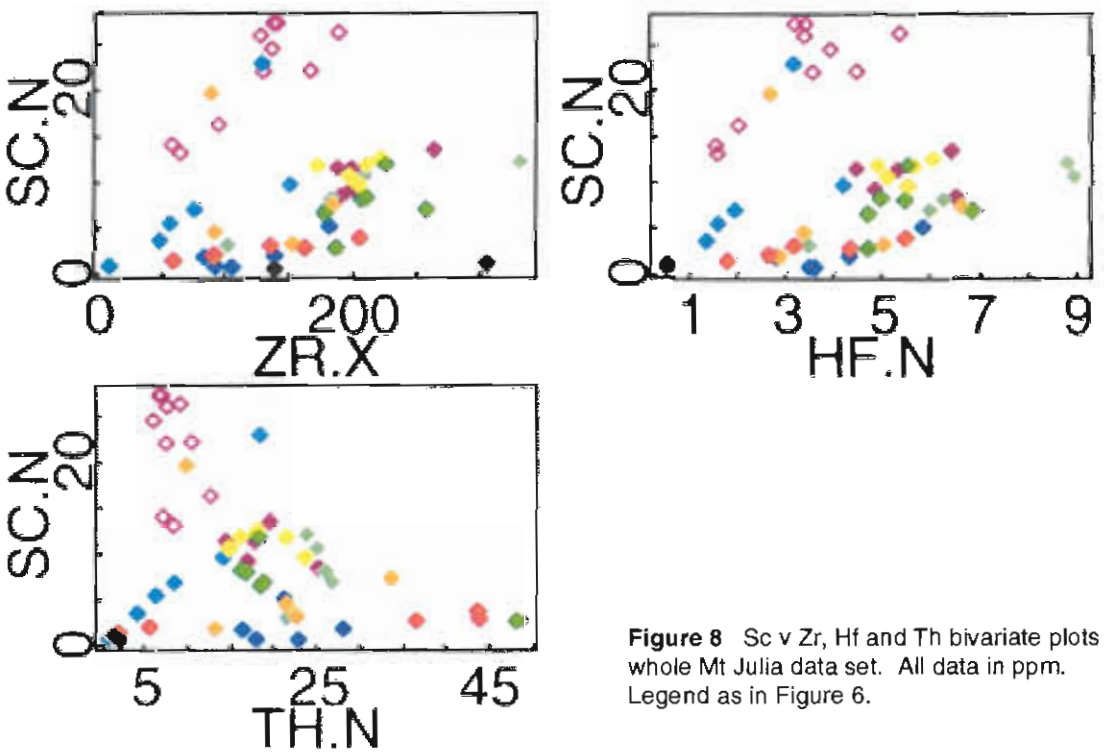

Figure 8 Sc v Zr, Hf and Th bivariate plots for whole Mt Julia data set. All data in ppm. Legend as in Figure 6.

of the Mt Julia member all plot on similar regression lines with a distinctly rhyolitic signature. They all contain very low levels of mafic indicator elements Sc, V and Ti.

What has been logged as the albite-silica (AS) altered Mt Julia Member overlying the mineralisation also appears to be derived from a single magmatic source. It is likely that the rhyolite complex and associated volcaniclastics found in the southern part of the lease dominate this sample set.

The single high titanium footwall rock that lies well above the regression line defined by the other footwall rocks is from one of the fuchsite altered dykes that commonly occur within the footwall sequence. This has a very similar geochemical signature as the Lynchford Member volcaniclastics and may be an intrusive related to this event. Most of the sericite-pyrite-carbonate altered footwall rocks at Mt. Julia appear to be derived from a common rhyolitic source, possibly the CVC.

The stratigraphic position of the A-Zone horizon is well constrained to the base of the Lynchford Member dacitic-andesitic volcaniclastics where they contact the altered footwall rocks with a rhyolitic signature. This is confirmed from the entire Henty data set (Fig. 8) where rocks from the same stratigraphic postions relative to A-Zone fit on the same regression lines defined for the stratigraphic sequence at Mt. Julia. These stratigraphic divisions are highlighted on the ternary diagram in Figure 9.

No samples from the crystal sandstones and polymict mass flows from higher in the Mt Julia Member have been analysed for this study. No samples from the Zig Zag Hill Formation or quartz-porphyries were included either. The Upper Tyndall group or Zig Zag Hill Formation has been previously studied in an Honours thesis (Large, 1995).

It has been suggested that the carbonates associated with the mineralisation and also occurring in the Lynchford Member are exhalative chemical sediments forming on the sea floor distal to the fluid source during the hydrothermal event (Halley and Roberts, in press). However textural evidence suggests that most of the carbonates are replacive with carbonate impregnating volcaniclastic sediments. If the carbonates were purely exhalative then they would have very low to below detection limits for their immobile element contents. They actually fit on the same regression lines as the Lynchford Member volcaniclastics (both geochemical subdivisions) and other A-Zone alteration products supporting the evidence suggesting that the majority of them are carbonates impregnating and replacing the volcaniclastics. Some of them have low to below detection limit values suggesting that a small proportion of the carbonates are possibly true exhalative carbonates or chemical sediments. Conversely they could have formed from intense passive addition of carbonate. No multi element data is available on the carbonates associated with Zone 96.

The Zr values for the massive sulphide and massive pyrite are erroneously high. It is highly likely that this is caused by XRF 'line overlap' of and the Pb and Zr spectra (Dunn, 1994). When titanium is plotted against Hafnium (Fig. 5), these two samples plot below the detection limit for both elements which indicates that line overlap has occurred as Hf and Zr are both concentrated in zircons. Because there are essentially no residual immobile elements in either of these rock types it is unlikely that they are replacive and must be either exhalative massive sulphides as suggested by previous workers (eg. Halley and Roberts, in press) or they are veins.

The immobile element geochemistry supports the stratigraphic interpretation of the area. A-Zone alteration is hosted in a well defined rhyodacitic volcaniclastic unit distinct from the overlying albite-silica altered rhyolites and parts of the more mafic Lynchford Member volcaniclastics and underlying footwall rhyolites.

However there are minor differences in Ti/Zr ratios of MQ alteration for the three different resources.

These differences are highlighted in Th v V, Sc, Ti and Hf bivariate plots (Fig. 10) for A-Zone analysis.

Mt Julia MQ alteration has much higher Th/V, Th/Sc and Th/Ti ratios than the other two deposits. The other notable trend in these plots is the lower Th/Ti and Th/Hf ratio of the Zone 96 and Sill Zone MQ. The Ti/Zr ratios suggest that MQ has formed from a similar protolith as the other alteration products so this must have occurred through Th addition in the Mt Julia MQ and Th depletion in the Zone 96 MQ.

Textural evidence from logging and mapping

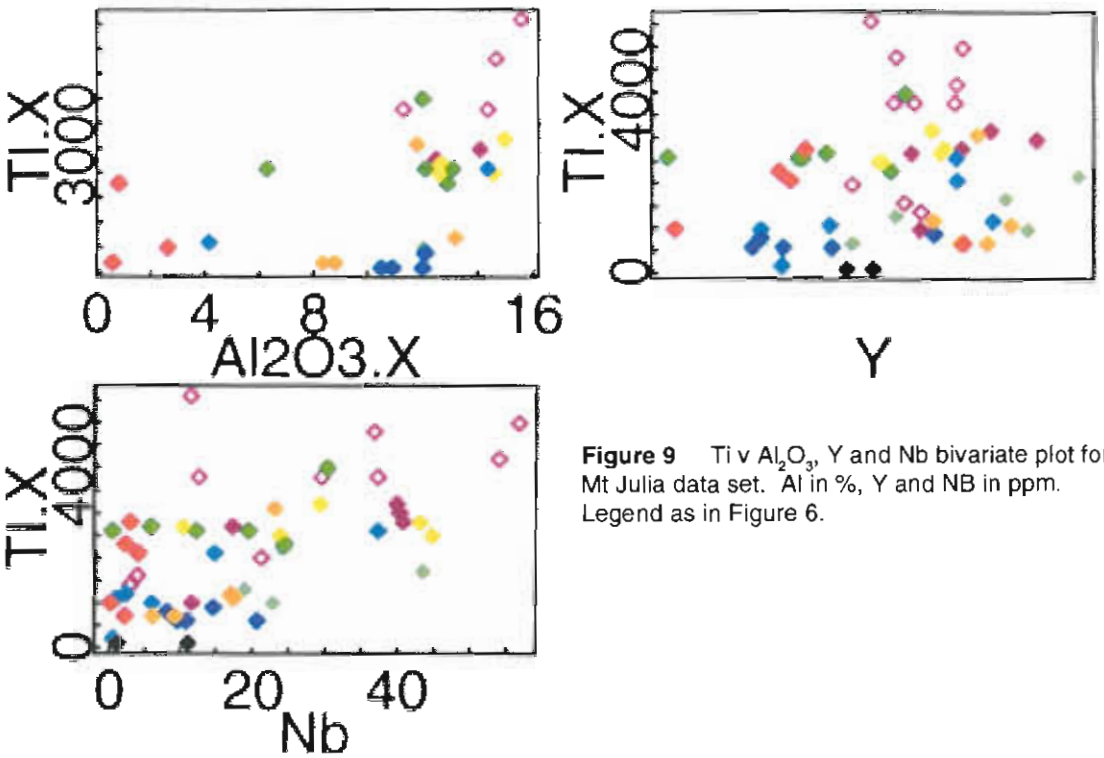

Figure 9 Ti v Al_2O_3, Y and Nb bivariate plot for Mt Julia data set. Al in %, Y and NB in ppm. Legend as in Figure 6.

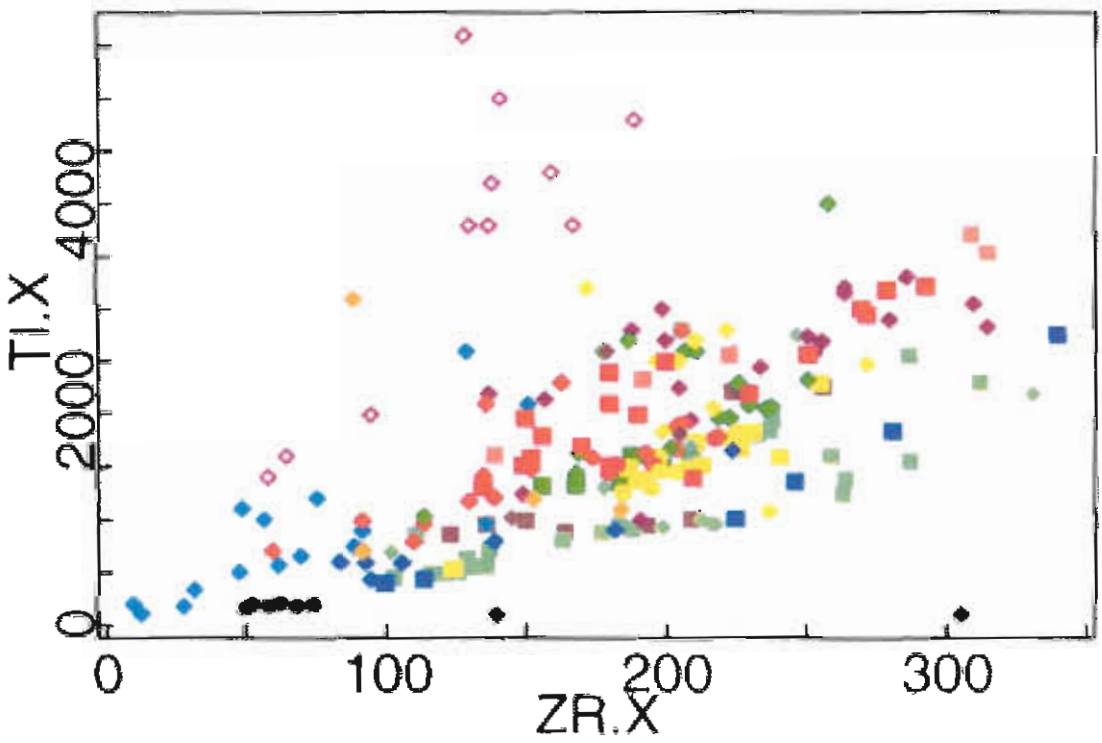

Figure 10 Ti v Zr bivariate plot for the entire Henty data set. All data in ppm, legend as in Figure 6.

supports the last hypothesis as both MQ and MV alteration overprint pre-existing jaspers and carbonates indicating formation in a common protolith (carbonate altered dacitic sandstones of the Lynchford Member). MQ and MV appear to be end members of a similar alteration process with MQ forming from the most intense alteration.

From the immobile element geochemistry it can be concluded that:

- Ti, Zr, Hf and possibly V, Sc and Th have remained immobile during both A-Zone, footwall and hangingwall alteration processes.
- Al, Y and NB have not remained immobile in the most intense A-Zone alteration, particularly MQ alteration.
- V, Sc and Th were not immobile during MQ alteration. Some Th addition has occurred in the Mt Julia MQ and Th depletion in the Zone 96 MQ. Sc and V are depleted in the MQ alteration.
- MQ and MV alteration appear to be end members of the same alteration process with MQ the most intense alteration.
- The host horizon is confined to a moderate Ti/Zr (approximately 14) dacitic volcaniclastic sandstone at the base of the Lynchford Member.
- The footwall alteration is confined to a distinct different stratigraphic unit with a much lower Ti/Zr ratio than the overlying A-Zone alteration.
- All of the overlying Mt Julia member volcaniclastics and coherent volcanics, both intensely albite-silica altered and relatively unaltered, are derived from a single rhyolitic magmatic source.
- The Lynchford Member feldspar crystal-rich sandstones and mass flows form two distinct lithogeochemical groups, a potentially rhyodacitc derived unit that hosts mineralisation at the base of the member and a more mafic (possibly andesitic) derived source.
- Mineralisation is hosted in the rhyodacitic volcaniclastic.
- The majority of the carbonates impregnate the Lynchford Member volcaniclastics of both geochemical subgroups.
- There are minor differences in the immobile element geochemistry of the A-Zone alteration products, particularly the Mt Julia MQ which can be attributed to minor dissolution and addition of some of the 'immobile' elements.

Whole rock alteration geochemistry

Figure 14 demonstrates harker diagrams for whole rock analysis of the Mt Julia drillcore.

Strong depletion of all major elements is evident in MQ with the exception of SiO_2, CaO and P_2O_5. This reflects the silica-carbonate-sulphide mineralogy of the MQ. The low concentrations of Al_2O_3 and the lack of confirmation of immobility (Figure 9) indicate that Al was leached from the protolith along with most other major and many trace elements during the alteration process.

The hangingwall lithologies, the Lynchford Member and Mt Julia Member rhyolites are strongly enriched in Na while the A-Zone alteration products and footwall alteration are strongly Na depleted. Conversely the A-Zone alteration and footwall alteration are strongly enriched in K. These relationships are better displayed on ternary diagrams in Figure 15.

The first two plots, SiO_2-K_2O-Na_2O and CaO-K_2O-Na_2O contrast the strongly Na depleted, K enriched footwall and A-Zone rocks with the strong Na enriched, low K hangingwall altered Lynchford Member and Mt Julia Member. This is a direct contrast of the sericite altered A-Zone and footwall rocks against the albite and albite-chlorite altered hangingwall.

Albitisation has strongly effected all of the stratigraphy immediately above A-Zone including the lynchford Member volcaniclastics which are dominated by an albite-chlorite mineralogy. Chlorite content is reflected in the MgO content of the Lynchford member volcaniclastics compared to the very low MgO content of the Mt Julia Member rhyolites.

MQ and some MV is strongly silica enriched and the MQ is strongly CaO enriched relative to K and Na. The CaO content is a direct indication of the carbonate content of A-zone. The minor amount of K in the MQ samples is reflective of the often gradational boundaries between MV and MQ alteration at Mt julia. These boundaries are well defined in the intensely deformed Zone 96 and Sill Zone orebodies.

On these plots (Figure 15) the two carbonate samples also contain significant quantities of albite as is reflected in their Na content. Both these samples were from hangingwall positions in distal drillholes, MJ006 and MJ002. Unfortunately there is no whole

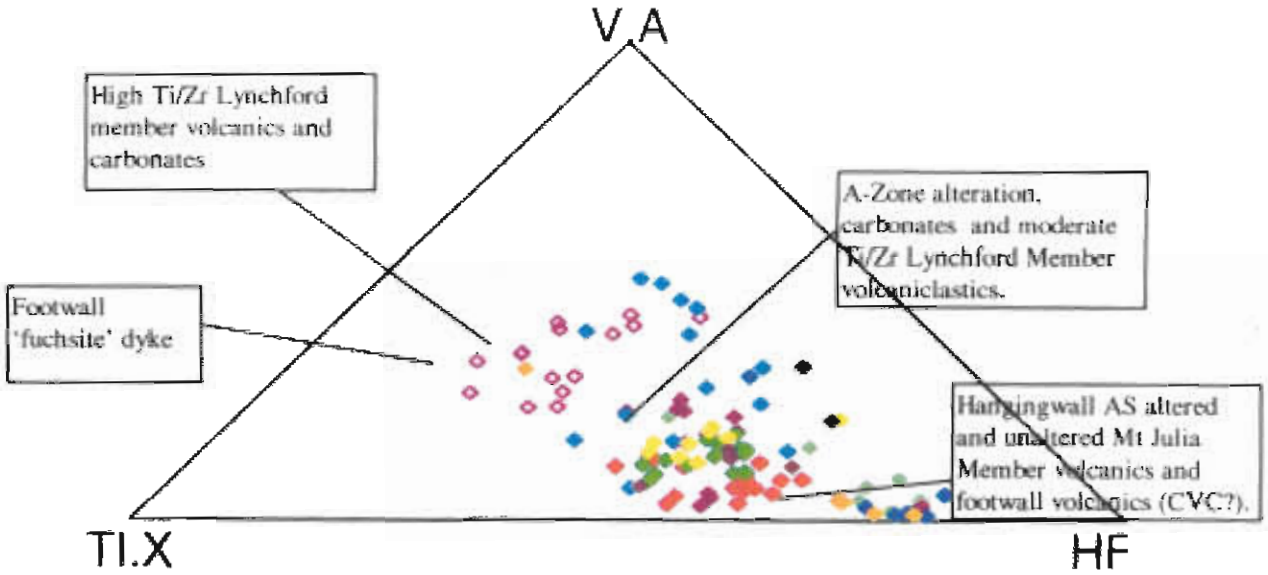

Figure 11 Ti-Hf-V ternary diagram for Mt Julia data set demonstrating the four main stratigraphic units from around A-Zone.

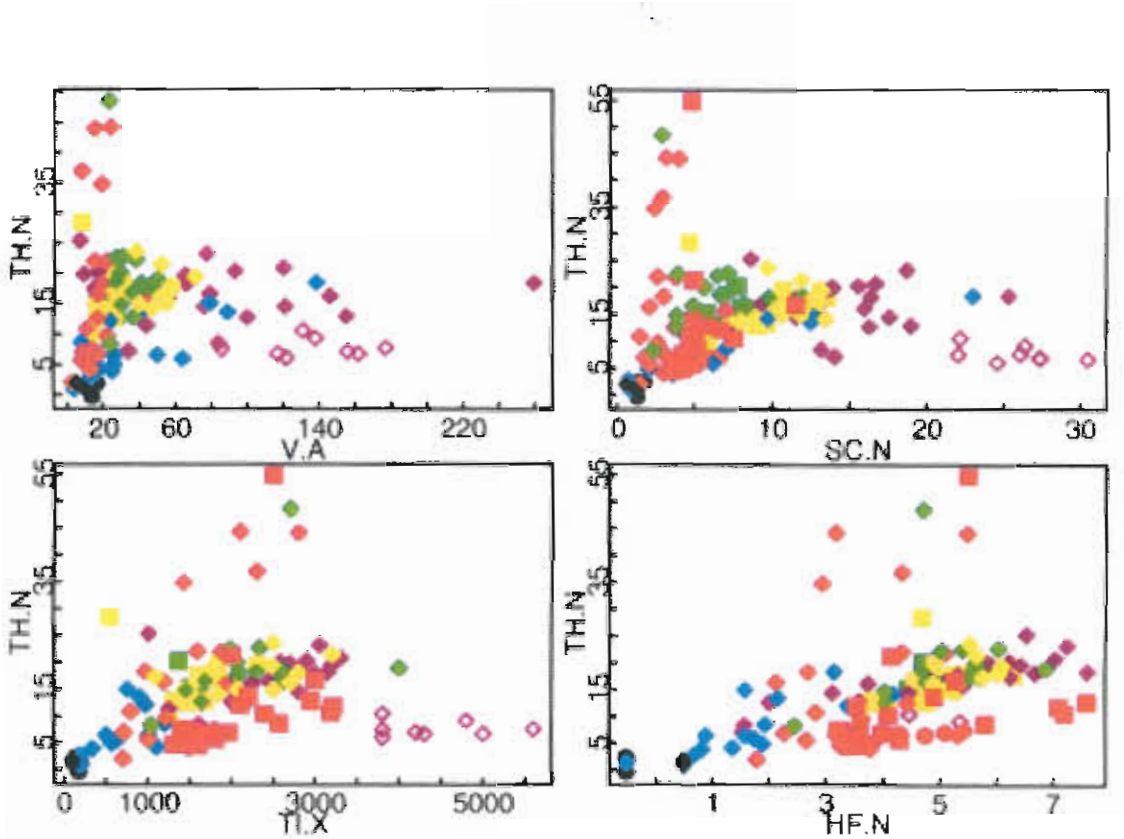

Figure 12 Bivariate plots of Th v V, Ti, Sc and Hf of A-Zone alteration in the Sill Zone, Mt Julia and Zone 96. All data in ppm.

rock data available on carbonate horizons from within A-Zone alteration but these are likely to be K enriched as they are commonly interbedded with sericite altered volcanics.

From this data it appears that carbonate alteration and albitisation predated the mineralising event. This is supported by textural evidence where later sericite alteration overprints the earlier albitic alteration as seen in both drill core and underground exposures.

The increased sulphide content of the MQ and MZ alteration compared to the MV, footwall and hangingwall alteration is also evident on the SO_3-K_2O-Na_2O plot.

From the whole rock geochemistry it can be concluded:

- Na enrichment up to 7% Na_2O has occurred in all hanginwall lithologies including volcaniclastics, coherent volcanics and carbonate rich sediments.
- K enrichment and extreme Na depletion has occurred in all A-Zone and footwall rocks.
- MQ is depleted in most elements with the exception of CaO, SiO_2, P_2O_5 and to some extent MnO.
- Chloritised Lynchford Member volcanics are also strongly albitised.

Recommended work program

Further research is required on the Mt Julia-Henty alteration study including:

- Completion of petrological work.
- Trace element geochemistry, particularly imaging of potential pathfinder elements and trace element haloes such as As, Sb, Cu, Pb, Zn, Tl, Ag, Bi and Ba.
- Further work on the whole rock geochemistry including investigation of alteration indices.
- Possibly some Carbon and Oxygen stable isotope analysis of carbonate horizons.
- Further investigation of Mt Julia mineralisation.
- Sections and longprojection defining extents of footwall, hangingwall and A-Zone alteration.
- Comparison of metal ratios between the three deposits.

References

Barrett, T J and MacLean, W H, 1993. Lithogeochemical techniques using immobile elements, *Journal of Geochemical Exploration*, 48:109-133.

Corbett, K D, 1992. Stratigraphic-volcanic setting of massive sulphide deposits in the Cambrian Mt. Read Volcanics, Tasmania, *Economic Geology*, 87:564-586.

Corbett, K D and McNeill, A, 1988. *Geological Compilation Map of the Mt. Read Volcanics and Associated Rocks, Hellyer to South Darwin Peak, 1:100 000 scale*, Tasmanian Department of Mines, Mt Read Volcanics Project Map 2.

Halley, S W and Roberts, R H, in press. Henty: A shallow water, gold rich VMS deposit in Western Tasmania, *Economic Geology*.

MacLean, W H and Kranidiolis, P, 1987, Immobile elements as monitors of mass transfer in hydrothermal alteration: Phelps Dodge massive sulphide deposit, Matagami, Quebec, Economic Geology, V82, pp951-962.

Taheri, J and Green, G R, 1991. The origin of the gold mineralisation at the Henty prospect, *Department of Resources and Energy, Division of Mines and Mineral Resources, Report* (unpublished)

White, M J and Mc Phie, J, 1996. Stratigraphy and palaeovolcanology of the Cambrian Tyndall Group, Mt. Read Volcanics, western Tasmania, *Australian Journal of Earth Sciences*, 43:147-159.

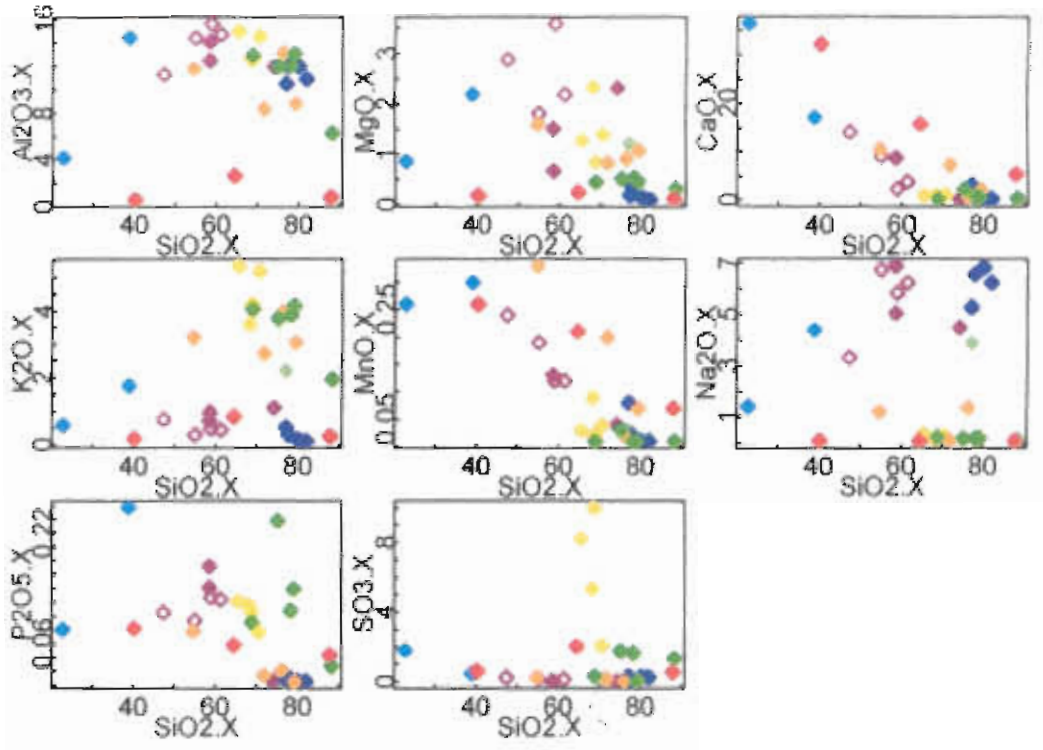

Figure 14 Harker diagrams of Mt Julia drillcore.

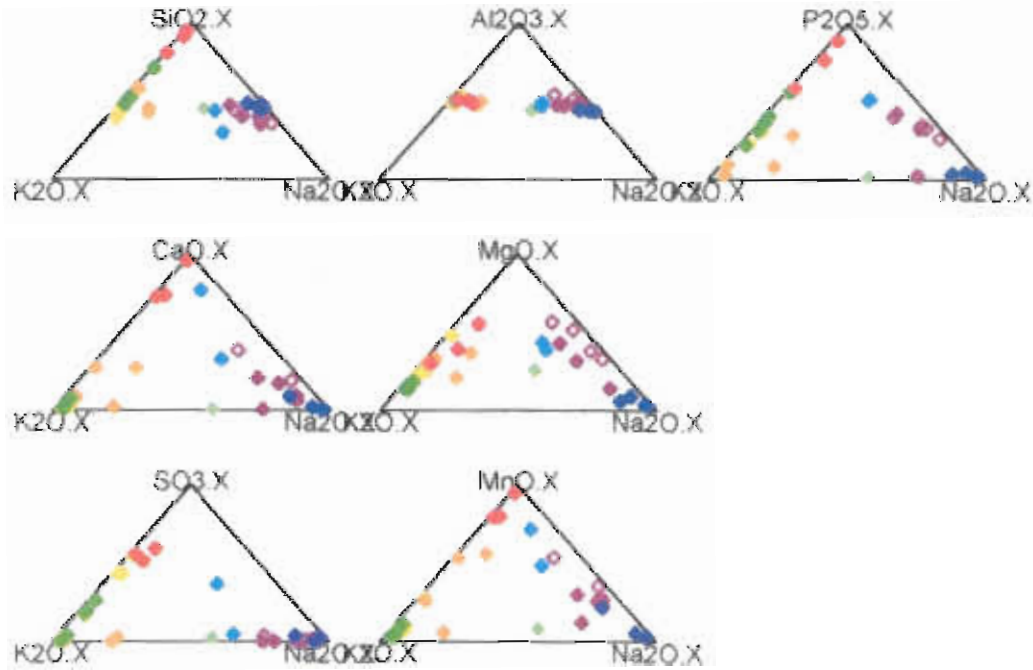

Figure 15 Ternary diagrams of Major elements in Mt Julia drill core.

Henty Gold Mine — The Zone 96 orebody: Geological and geochemical characteristics

by Jason Beckton
Goldfields (Tasmania) Ltd

Introduction

The Henty Mine is located 30km north of Queenstown in Western Tasmania. The Henty Gold Mine is the only economic deposit hosted within the Tyndall group of the Mount Read Volcanics. The Zone 96 1996 reserves are 526,000t at 26.2 g/t Au, containing 442,678 ounces of gold. Annual gold production is estimated to average 90,000 ounces over a period of 4.5 years. During the 1996–97 financial year, Henty produced 74,930t at 21.1 g/t Au, recovering 48,377 ounces (De Mark and Callaghan 1997).

Regional geology

The Henty Gold Mine lies within the Mount Read Volcanics (MRV) which also hosts the ore deposits of Hellyer, Que River, Rosebery, Hercules and Mt Lyell. The Mount Read Volcanics Belt is a 20 km wide arcuate belt of submarine and subaerial rhyolitic to basaltic lavas, intrusions, and volcaniclastics. Previous workers (Corbett and Lees 1987, Corbett 1992, White and McPhie 1996) have identified at least four lithological groups; the Central Volcanic complex which hosts most Pb-Zn-Cu-Ag-Au VHMS deposits, the Eastern quartz-porphyritic sequence, the Western volcano-sedimentary sequence and the Tyndall group which hosts the Henty Gold Mine orebodies.

Mine geology

Deposit geology is dominated by a regional structural feature, the Henty Fault. The Henty Fault is striking NW and dipping 70° to the West in the vicinity of the deposit. It is a bimodal fault with a western 'puggy' component and an Eastern mylonitic component. Central volcanics occur to the West of the deposit and mineralised Tyndall Group volcaniclastics and epiclastics occur to the East. The Tyndall group host lithologies generally trend NE and have subvertical dip (Fig. 1).

Gold mineralisation occurs within a sequence of strongly altered rocks. The alteration is strongest adjacent to the Henty fault and may be generalised as silica sericite pyrite alteration. The following styles of alteration and mineralisation.

CB Hydrothermal carbonate lenses. Average grade <1g/t Au.

MP Massive pyrite lenses also containing carbonate. Occurs primarily on stratigraphic hangingwall. Average grade 4 g/t Au.

MZ Quartz, sericite, pyrite, sulphide alteration. Forms envelope around MV and MQ. Average grade 1 g/t Au.

MV Quartz, sericite alteration. Occurs around and along strike of MQ lenses. Average grade 4 g/t Au.

MQ Massive quartz alteration. Most gold hosted within quartz-carbonate-sulphide veins forming a crackle breccia within this alteration. Average grade 40 g/t Au.

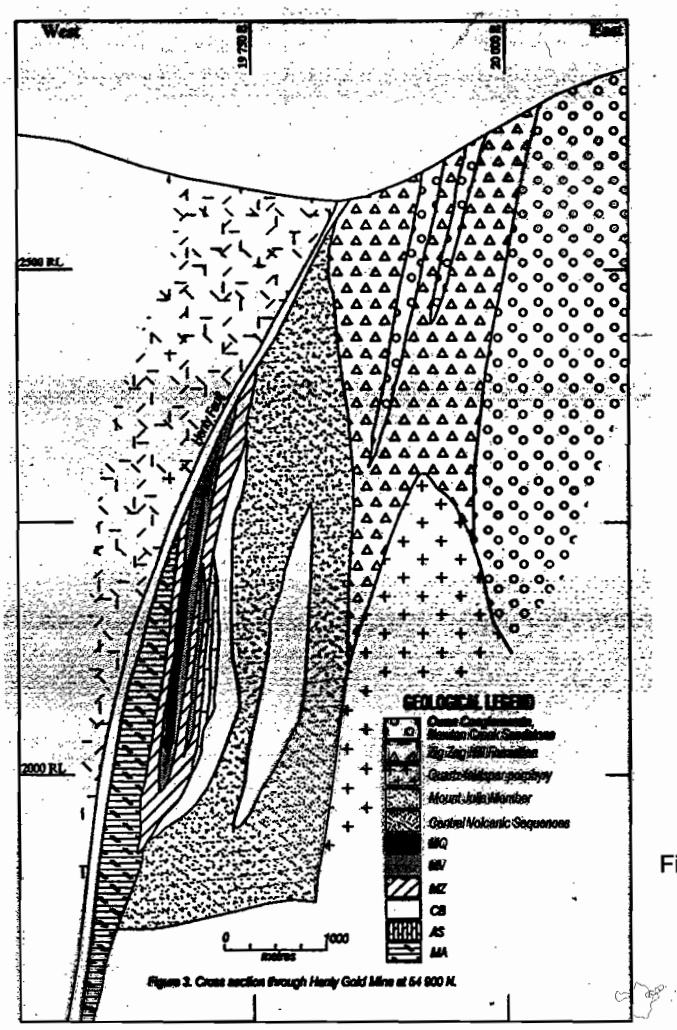

Figure 1 Deposit cross section.

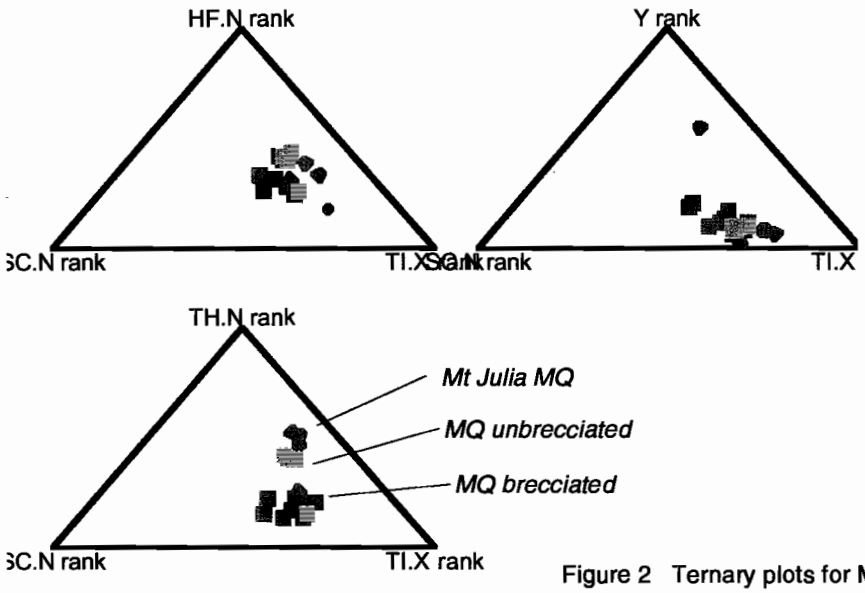

Figure 2 Ternary plots for MQ.

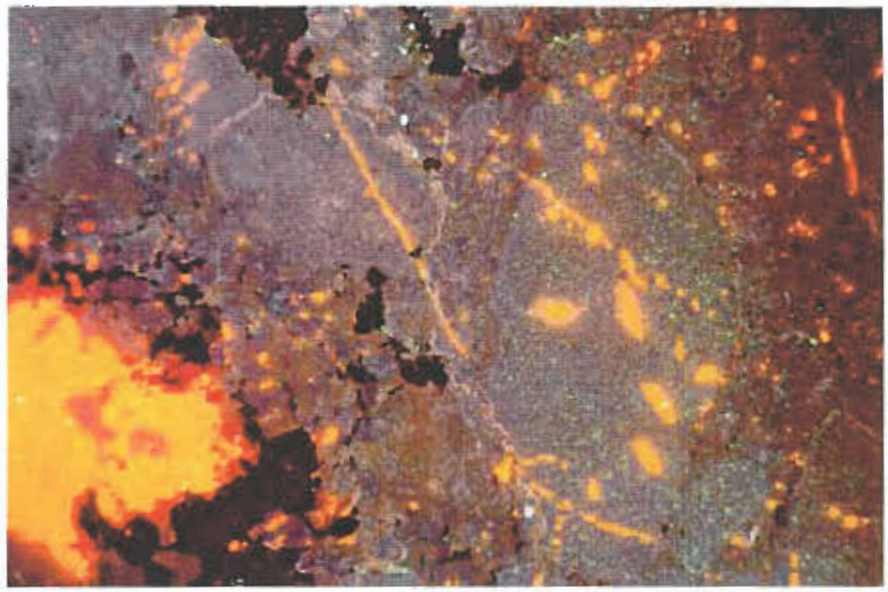

Figure 3 Ghost rhombs

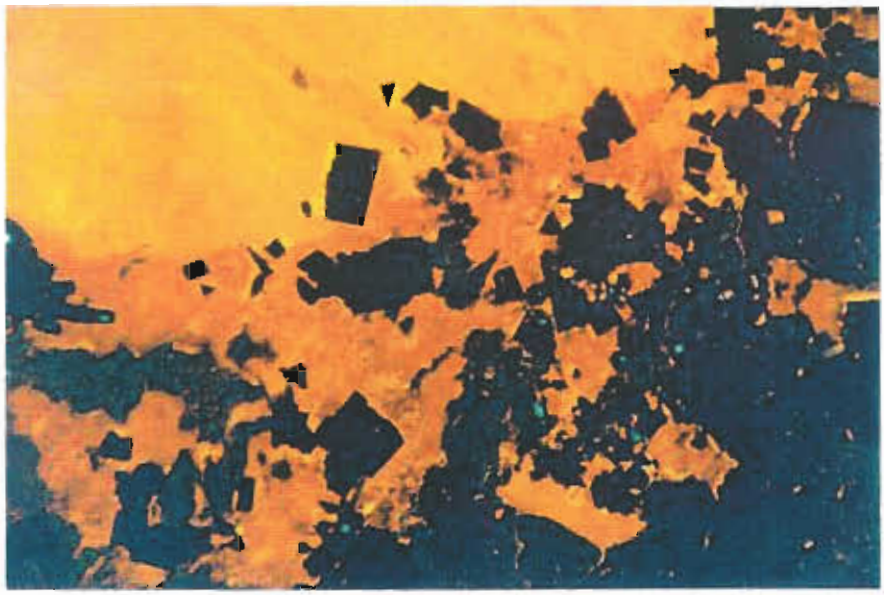

Figure 4 Late carbonate phase and qtz-cb-sulphide.

Ore genesis

Halley and Roberts (1995 in press) and Taheri and Green (1991) have suggested a shallow water, gold-rich VHMS model. A gold-rich volcanogenic Cambrian VHMS is interpreted to have formed at shallow levels. Devonian deformation was interpreted to have remobilised gold within the alteration package and resulted in high grade pods. During the Devonian deformation sericitic alteration deformed in a ductile manner. The massive quartz (MQ) alteration deformed in a brittle manner.

Bisulphide complexes are interpreted to have formed during the deformation of the alteration package, remobilising gold from high strain sericitic alteration into low strain zones within the crackle breccia of the MQ alteration.

Zone 96 1996–97 research

The principal aims of current study are to determine timing of alteration and controls on gold distribution. The Zone 96 orebody has extreme variability in both ore (MQ) grade and thickness.

Multi-element studies have been carried out to determine if there is a protolithic control on variable gold grade within the MQ. Determination of the protolith and timing of formation the MQ alteration has regional exploration implications. Texturally distinct MQ alteration types were recognised when mining in the orebody commmenced:

1. Highly brecciated 'Grey', pseudoclastic MQ. High grade (Au>20 g/t)
2. Unbrecciated 'Pink', massive MQ. Low grade (Au<20 g/t)

Ternary diagrams (pers comm. S. Halley) provide possible lithologic discrimination of the MQ alteration types. A Thorium-Scandium-Titanium plot seems to provide some discrimination (Fig. 2).

MQ alteration consists xenoblastic silica matrix which has been brecciated by quartz-carbonate-sulphide-gold veinlets. Ghost rhombs within the xenoblastic matrix appear to have been replaced (Fig. 4) by later carbonate. These rhombs and other carbonate-sulphide phases (Fig. 5) will be tested with an electron microprobe. The rhombs may be replaced quartz phenocrysts within a coherent volcanic or possibly phases within a calc silicate unit.

Fragmented jasper and late carbonate is associated with high grade, brecciated MQ. Jasper clasts contain pyrite and chacopyrite. Selvages between MQ and jasper fragments concentrate sulphide (see Fig. 6).

Mapping of alteration contacts illustrates structural relationships that could not be determined from drilling operations. The 2168 Level is an example of folding of the alteration package which is co-incident with a high grade area. Gold and sulphides are interpreted to be concentrated into Devonian fold hinges (Fig. 7).

In summary research to date is consistent with original ore genesis models with refinements that underground exposure provide.

References

Corbett KD and Lees TC 1987. Stratigraphic and structural relationships and evidence for Cambrian deformation at the western margin of the Mt Read Volcanics, Tasmania. AJES 34: 45-67.

Corbett KD 1992. Stratigraphic-volcanic setting of massive sulfide deposits in the Cambrian Mount Read Volcanics, Tasmania. Econ. Geol. 87: 564-586.

De Mark P and Callaghan T 1997. Geology and mineralisation of the Henty Gold mine, Tasmania. Proc. 3rd Int. Mining Geol. conf (in press).

Halley SW and Roberts RG in press. Henty: A shallow-water, gold-rich VMS deposit in western Tasmania.

Taheri J and Green GR 1991. The origin of the gold mineralisation at the Henty prospect. Division of Mineral Resources, Tasmania.

White MJ and McPhie J 1996. Stratigraphy and paleovolcanology of the Cambrian Tyndall Group, Mt Read Volcanics, western Tasmania. AJES 43: 147-159.

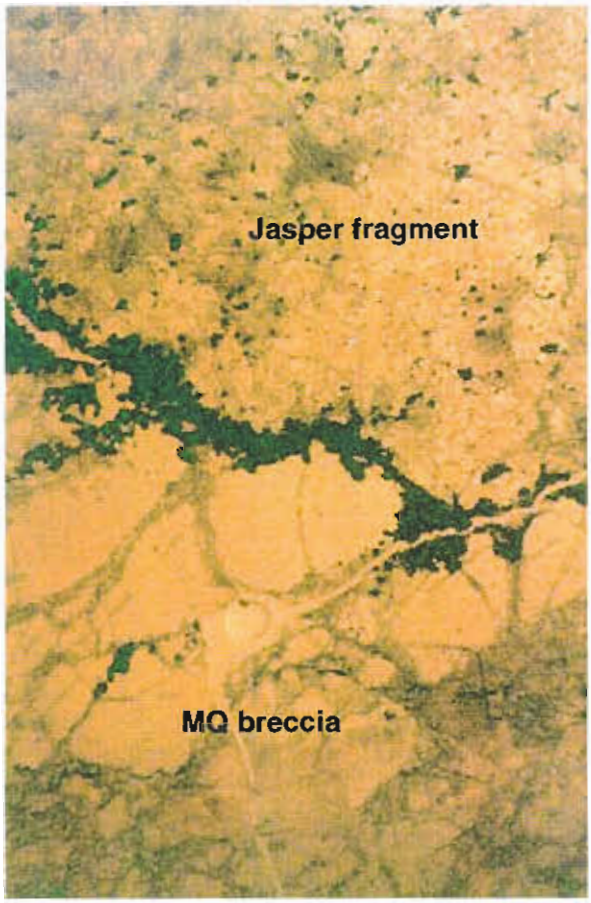

Figures 5 and 6 MQ and Jasper contacts.

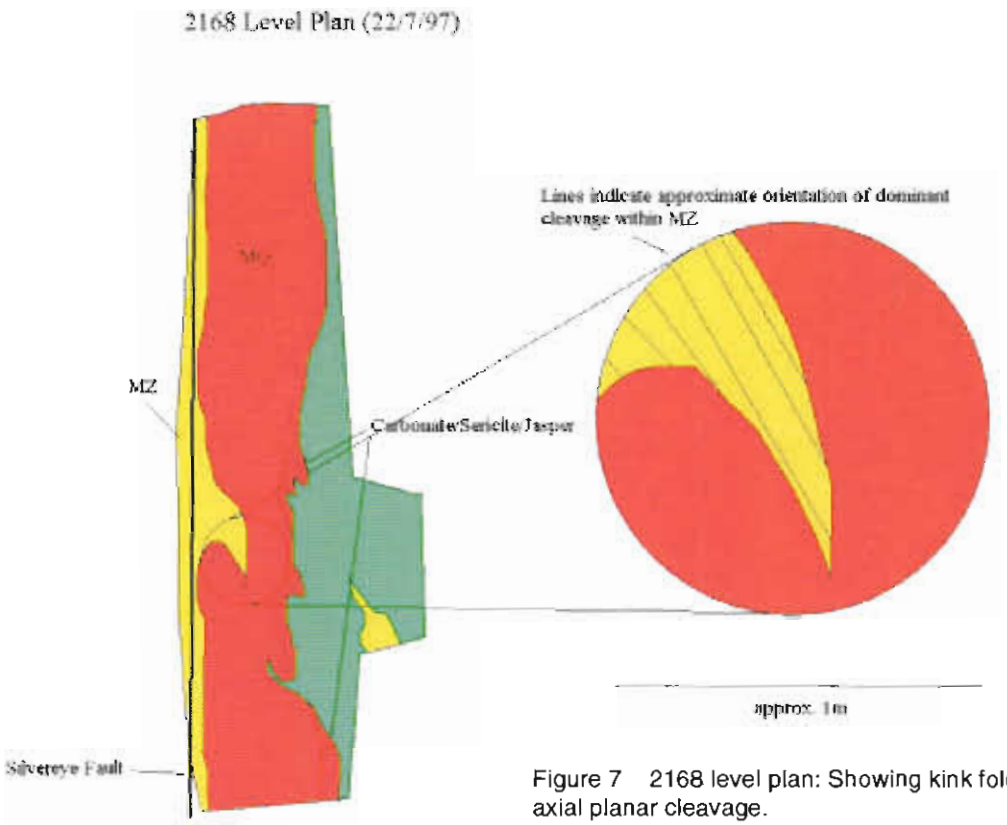

Figure 7 2168 level plan: Showing kink folding and axial planar cleavage.

The Darwin Granite–Slate Spur area: Preliminary geochemistry and a discussion of granite-related alteration

by Bill Wyman
Centre for Ore Deposit Studies, Geology Department, University of Tasmania

Abstract

This paper clarifies the classification of the Darwin granite using both geochemistry and modal mineralogy. The paper documents the island arc setting of the granite and compares it to the Elliott Bay granite to the south and to the Murchison granite to the north. The Darwin granite most nearly follows the calc-alkaline granodiorite series of (Lameyre and Bowden, 1982), and fits most criteria for the magnetite series of (Ishihara, 1981). Effects of hydrothermal alteration are pointed out as they clearly render classification schemes that rely on major element variations, such as the I-S scheme of Chappell and White (1974), virtually useless.

Hydrothermal alteration assemblages, in the Jukes–Darwin field, resemble alteration assemblages found in other intrusion-related related hydrothermal systems throughout the world. These hydrothermal alteration assemblages share many similarities with porphyry Cu-Au alteration and mineralisation assemblages (e.g. Cooke et al, 1996; Sillitoe, 1993), and may be considered a submarine analogue to porphyry-style mineralisation. Alteration assemblages near the Darwin granite are dominated by K-feldspar, chlorite, silica and sericite in various combinations and intensities. Accessory minerals include pyrite, magnetite, tourmaline, barite and chalcopyrite. Alteration assemblages appear to be most intense and widespread above the granite, and appear to drop off rapidly along the sides. Mineralisation and alteration appear to be related to the late stage intrusion of the white equigranular granite and the porphyritic white granite phase. Magnetite and tourmaline veining also appears to be related to this phase of granitic intrusion.

Introduction

The Darwin granite and Slate Spur area is located approximately 20 km south of Queenstown (Figure 1). The Darwin granite is interpreted to be a subvolcanic intrusion into the Cambrian age Mt. Read volcanics (Solomon, 1981). This granite is of particular interest to the alteration study in western Tasmania because of it's apparent association with many small Cu-Au prospects. Small Cu-Au prospects are located along the western margin of the granite and continue northward to form a continuous linear belt from the western edge of the Darwin granite through Intercolonial Spur to the Jukes prospect. This is a continuous belt of similar alteration and deposit styles approximately 15 km long and 3 km wide (Figure 2). Regional aeromagnetic data suggests that the Darwin granite, or other similar granite, underlies the entire northerly trending belt of hydrothermal alteration and Cu-Au mineralisation (Large et al., 1996; Leaman and Richardson, 1989; Payne, 1991). Hydrothermal alteration is characterised by five principal mineral assemblages: sericite, sericite-quartz, chlorite-sericite-quartz, K-feldspar-chlorite and potassium feldspar. These alteration assemblages are characteristic of granite related alteration assemblages worldwide. Accessory mineral and vein assemblages include quartz, hematite/magnetite, tourmaline, magnetite/tourmaline, minor apatite, pyrite, chalcopyrite and scheelite.

Geochemical results presented in this paper are preliminary. They are the result of analysis of rock samples collected during thirty days of field work conducted during the summers of 1995–96 and 1996–97. Detailed geologic mapping was undertaken in the Slate Spur area, west of Mount Darwin and on

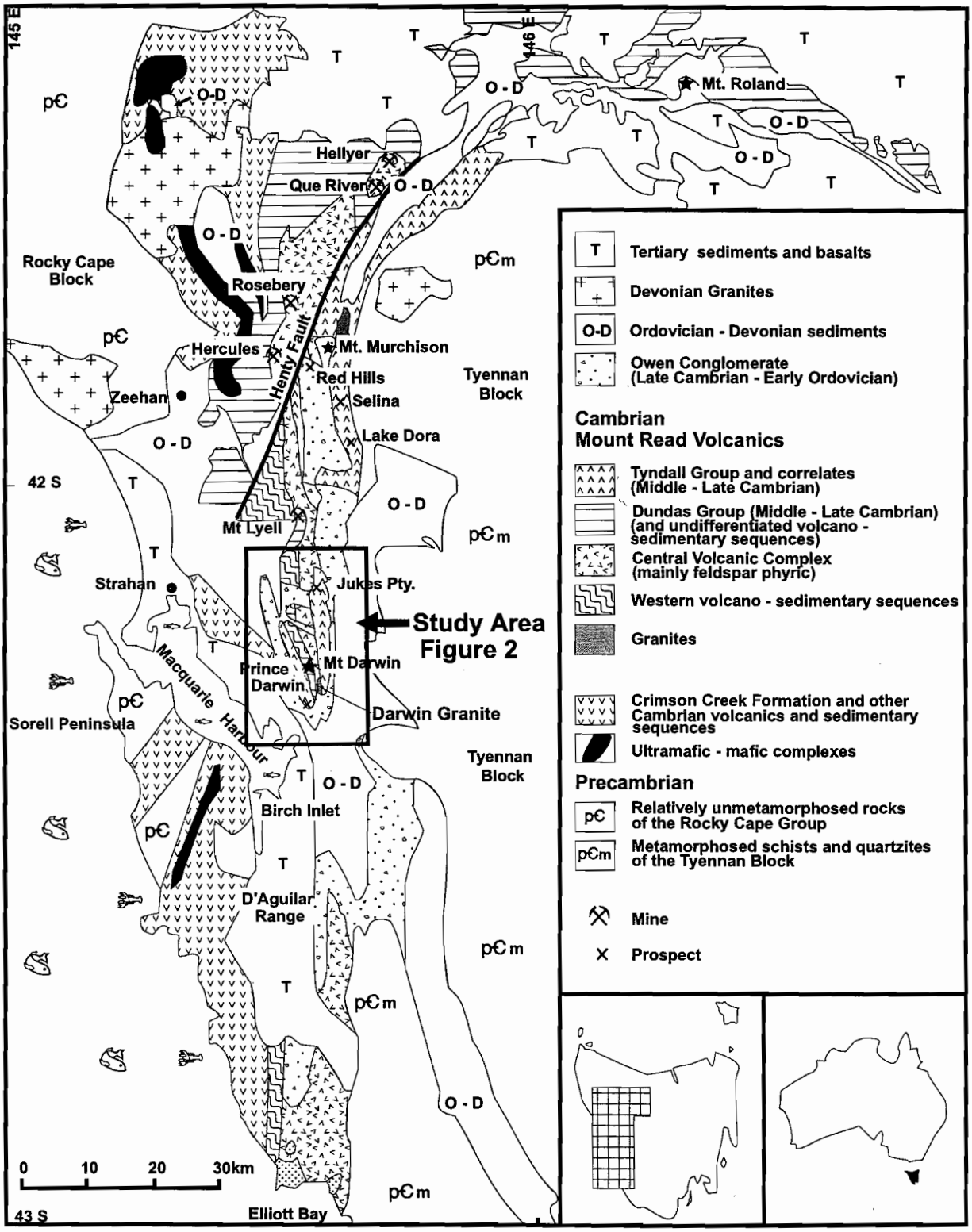

Figure 1 Location Map for the Cambrian Mt Read Volcanic Belt, western Tasmania

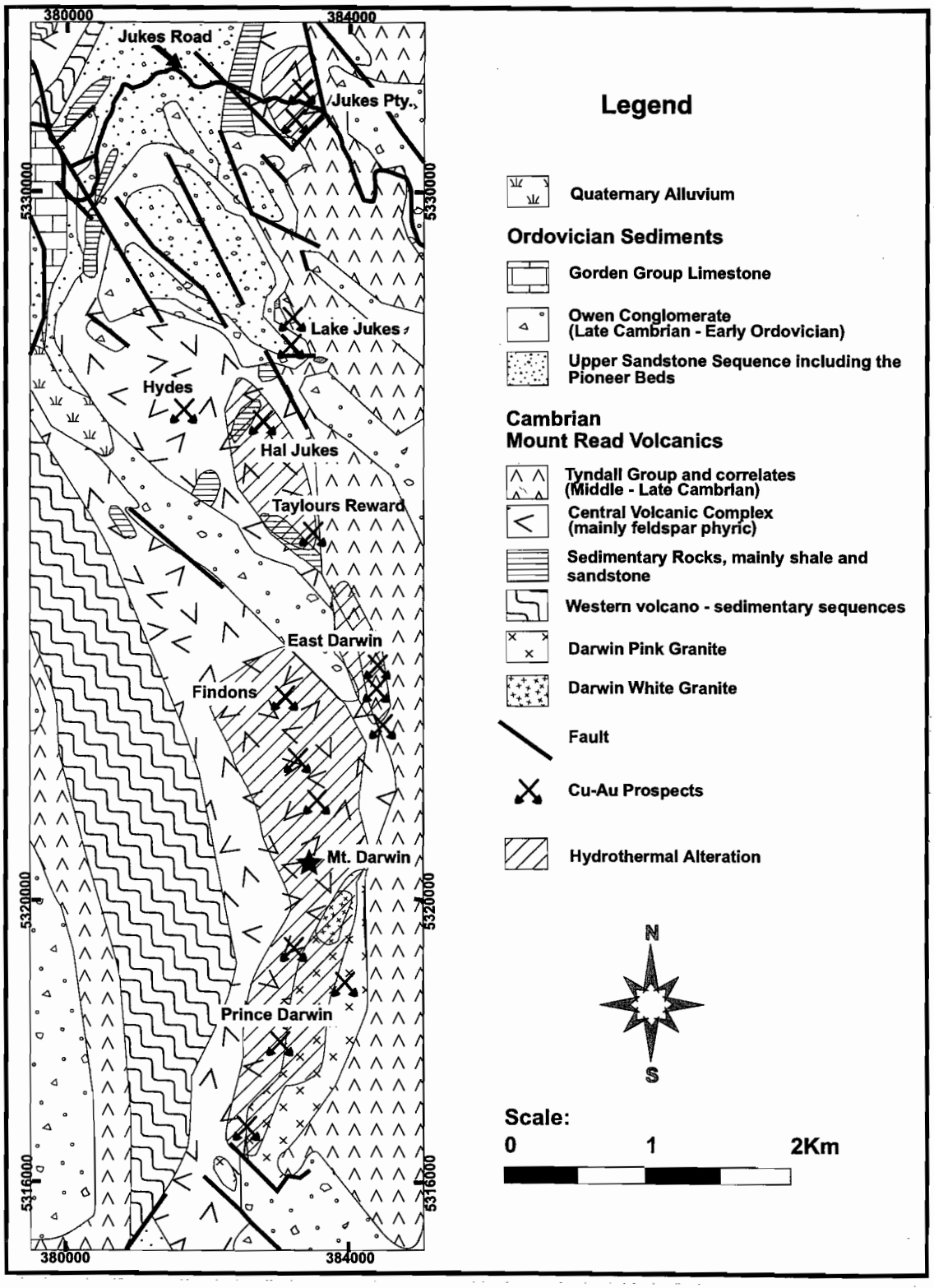

Figure 2 Study area showing locations of significant Cu-Au prospects and the extent of granite related alteration.

and around the Darwin granite itself. Detailed descriptions of the geology, alteration and volcanic facies descriptions were presented previously in (Wyman, 1996).

Geology of Mount Darwin

The Darwin granite was first studied by (Hills, 1914) who correctly described the character of two major phases of granite on the Darwin Plateau. Numerous other authors, including Solomon (1960), White (1975), and Jones (1993) have worked on various aspects of the area. Solomon (1960) and later White (1975), also recognised two phases of granite. White (1975) named them the "Pink" and "White" phases, based on their distinct mineralogy. Jones (1993) focused his research on the petrology and geochemistry of the Darwin granite and similarities to the surrounding volcanics. Jones (1993) mapped the Darwin granite at a scale of 1:5000, and identified and described both the pink and white phases, as well as several other more minor phases. Jones (1993) also described the structure and geochemistry of the granite. Gadaloff (1996) focused his studies of the Cu-Au mineralisation north of the Darwin granite and south of the Jukes prospect. Work in this study involved detailed mapping of parts of the Darwin plateau (scale 1:2500), with a focus on understanding the timing relationships of the various phases of granite intrusion to each other, the granites alteration effects on CVC rocks and geochemical relationships between the granite, the CVC and the Cu-Au mineralisation. Figure 3 is a geologic map of the Darwin granite compiled from this work and mapping from (Jones, 1993).

The Central Volcanic Complex (CVC) in the study area is dominated by volcaniclastic and mass flow deposits of rhyolitic to dacitic composition. Common, but subordinate to the volcaniclastic facies, are coherent rhyolitic and dacitic lavas. These volcanic facies are intruded by the Darwin granite, as well as quartz feldspar porphyry dykes. Detailed descriptions of the CVC volcanics are given in (Wyman, 1996) and will not be discussed further in this paper.

Classification of Granites

The Cambrian granites of western Tasmania have been studied by various authors (Abbott, 1992; Hills, 1914; Solomon, 1960; Solomon, 1981; White, 1975; Jones, 1993) and several attempts to classify them have been tried. Both Abbott (1992) and Jones (1993), concluded that the granites are strongly altered, high-K, magnetite series granites following the classification of Ishihara (1981). As pointed out by Jones (1993) and as shown later in this section, the high degree of hydrothermal alteration of the granites renders useless the I/S classification of Chappell and White (1974) and White and Chappell (1983). This inability to classify the granites using one classification but allowing the use of another, points out the ambiguity of classification schemes as a whole. None-the-less, classification does allow useful points of reference to be established that are useful for discussion purposes. This study therefor, attempted to classify the Cambrian age Murchison, Darwin and Elliott Bay granites using various classification schemes based on mode (Streckeisen, 1976), rock series (Lameyre and Bowden, 1982), source rock (Chappell and White, 1974; White and Chappell, 1983) and tectonic setting (Pearce et al., 1984). Geochemical and modal data used in the following classification attempts is both from the literature and from this study and is given in Appendix A and B.

Figure 4 is a standard QAP diagram of (Streckeisen, 1976). Overlain on this figure are various calc-alkaline trends as defined by Lameyre and Bowden (1982). Modal data from the Darwin granite (Jones, 1993) and the Murchison granite (Abbott, 1992; Polya, 1981) are plotted. Modal data for the Elliott Bay granite has not been calculated. Both the Murchison and Darwin granite series plot clearly within the granite and granodiorite fields of Streckeisen (1976) and most nearly fit the calc-alkaline-granodiorite trend (line B) of Lameyre and Bowden (1982). This trend, and the calc-alkaline monzonite trend (line C) are frequently associated with major porphyry copper mineralisation (Lameyre and Bowden, 1982).

Chappell and White (1974) and White and Chappell (1983), developed a classification system to distinguish between granites formed from partial melting of sedimentary rocks and those formed from

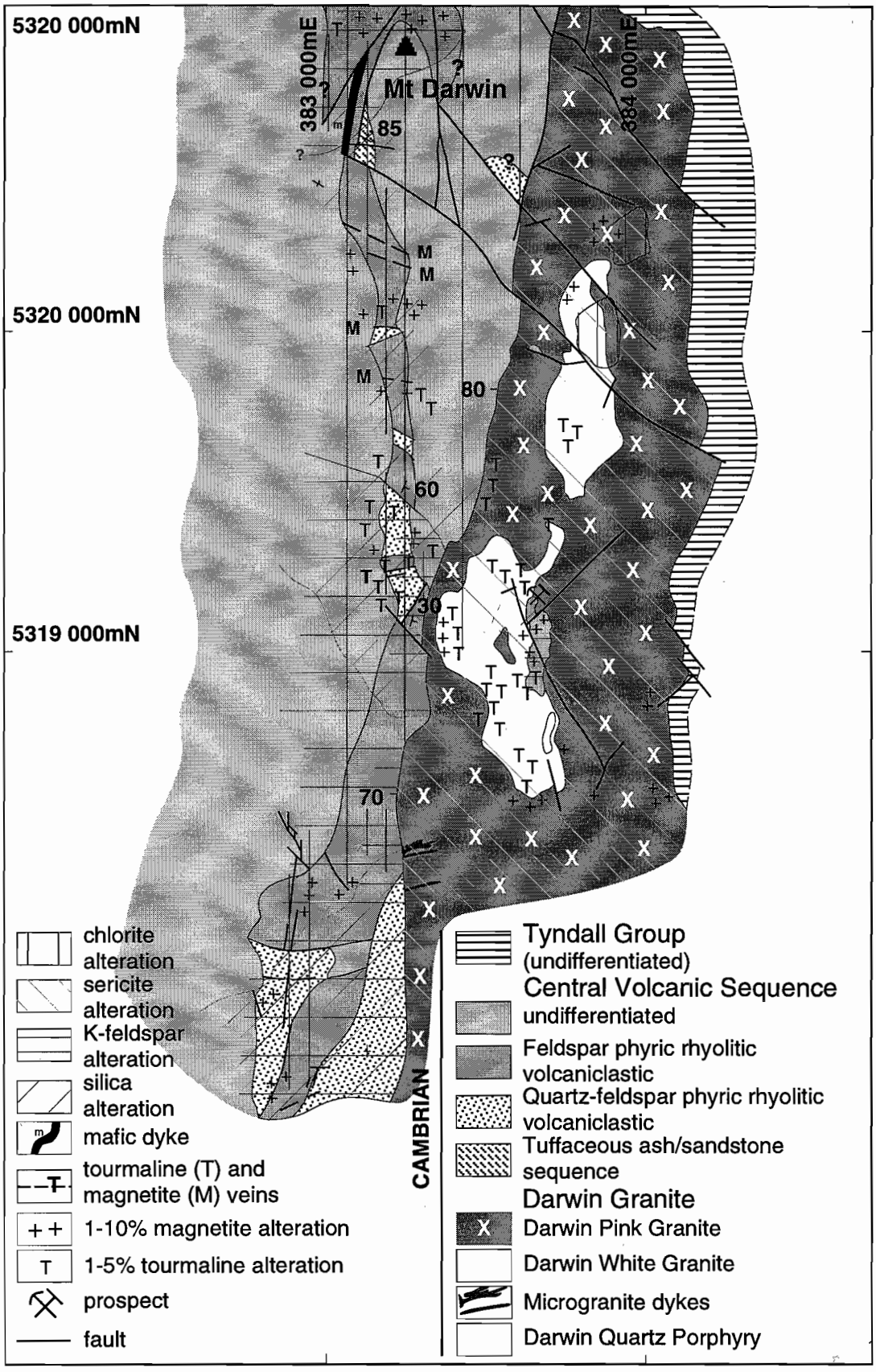

Figure 3 Geologic map of the northern half of the Darwin granite showing hydrothermal alteration in relation to the geology.

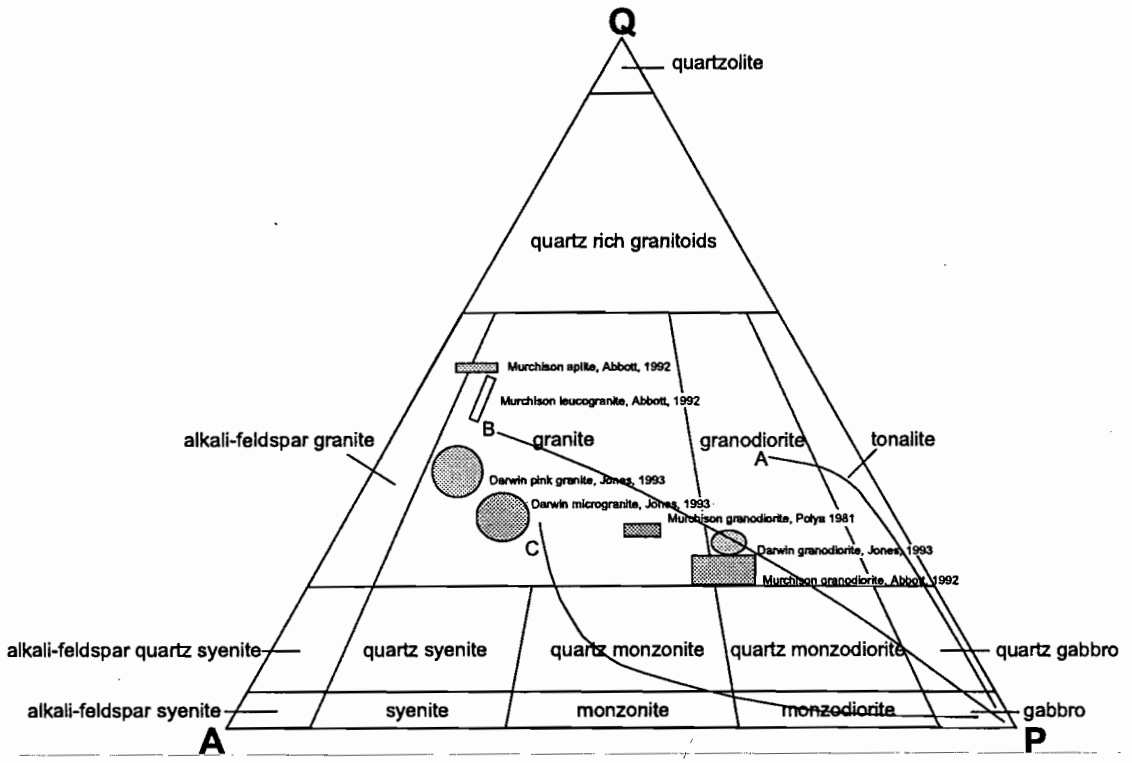

Figure 4 QAP diagram showing the modal classification of both the Darwin granite and the Murchison granite, after Streckeisen (1974). Darwin granite data is from Jones (1993) and Murchison granite data is from Polya (1981) and Abbott (1992).

partial melting of igneous source rocks. Bekinsale (1979) expanded on the classification and a summary of the characteristics is shown in Table 1, which compares the source rock characteristics with the Murchison, Darwin and Elliott Bay granites. The effects of hydrothermal alteration clearly affect those parts of the classification that rely on sodium, potassium or calcium and modal mineralogy. The Cambrian granites should be I-type granites (Ishihara, 1981; White and Chappell, 1983) however sodium and calcium depletion as a result of hydrothermal alteration, in both the Darwin and Elliott Bay granites result in classification as an S-type granite. S-type criteria met as a result of hydrothermal alteration are: Na_2O < 3.2%, $Al_2O_3/(Na_2O+K_2O+CaO)$ ratio higher than 1.1, and no normative diopside nor normative corundum in the Darwin granite and only trace of normative diopside in the Murchison and Elliott Bay granites (Appendix B). Similarities to I-type are also met and include: (1) Linear or near linear immobile element variation diagrams such as P_2O_5, TiO_2 and Zr vs SiO_2 (Figures 5–7) and Ti vs Zr (Figure 8). Hydrothermal alteration produces much more scatter in plots involving more mobile elements such as Rb and Y (Figures 9–10). (2) Low initial $^{87}Sr/^{86}Sr$ ratios (< 0.708). Initial $^{87}Sr/^{86}Sr$ ratios in the Darwin granite vary from 0.703 to 0.709 (Appendix C). (3) All three granites contain abundant magnetite, very little ilmenite and accessory hornblende and sphene. ^{18}O data for the granites is currently unavailable. About the only result that can be concluded from the application of the Chappell and White (1974) and White and Chappell (1983) criteria is that they are not applicable in hydrothermally altered rocks.

This initial I-S classification of Chappell and White (1974) and White and Chappell (1983) has been extended by Loiselle and Wones (1979) and Collins et al. (1982) by the introduction of A-type granites and M-type granites (White, 1979) as subdivisions of I-type granites. These two new granite subdivisions attempt to distinguish granites of anorogenic and oceanic arc settings respectively (Pitcher, 1993). S-type granites are currently assumed to be a product of cordilleran and post-orogenic uplift regimes (Bekinsale, 1979; Pitcher, 1983). A type granites can be further subdivided into metaluminous, and peralkaline subtypes. A-type peralkaline granites appear to be derived from the mantle via fractional crystallisation of basic magmas and metaluminous

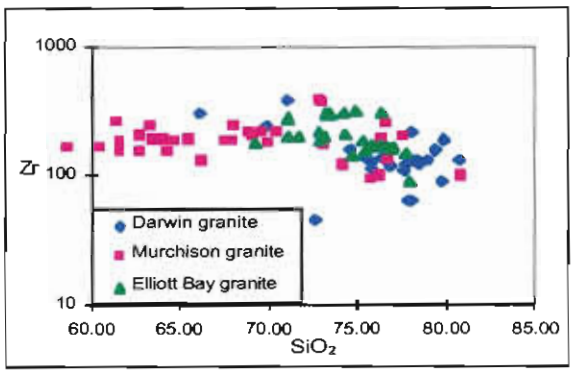

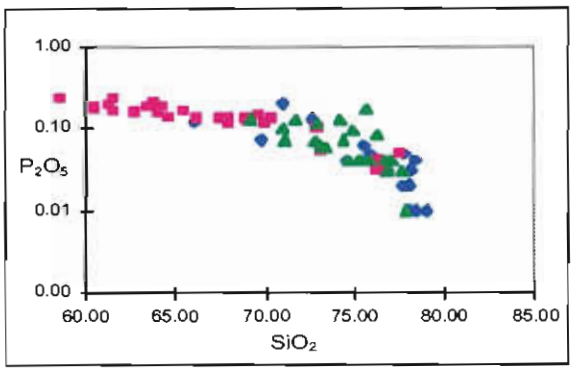

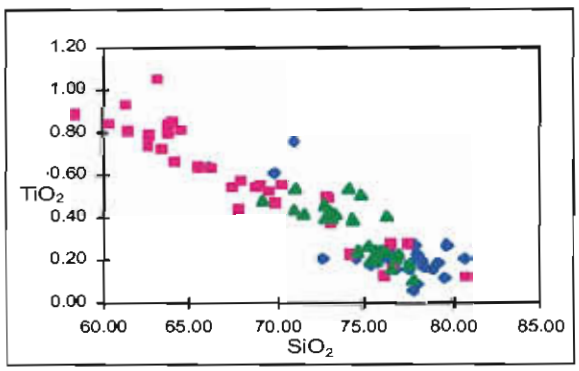

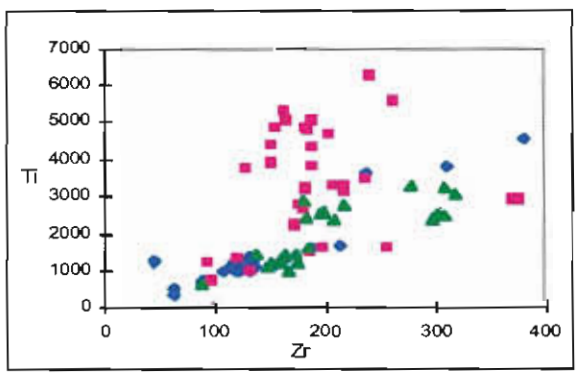

Figures 5–8 Linear or near linear immobile element variation diagrams of P_2O_5, TiO_2 and Zr vs SiO_2 and Ti vs Zr

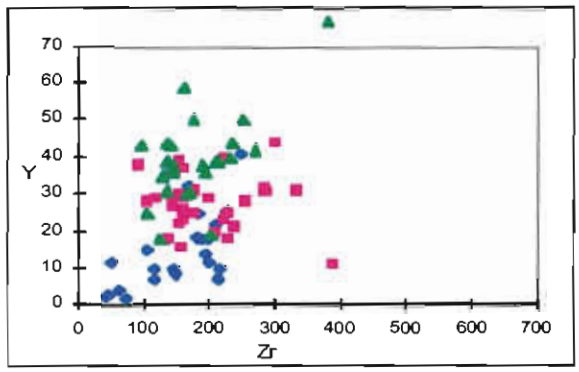

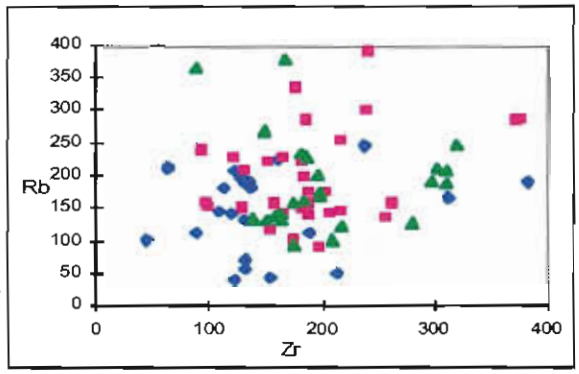

Figures 9–10 Hydrothermal alteration produces scatter in plots involving more mobile elements such as Rb and Y

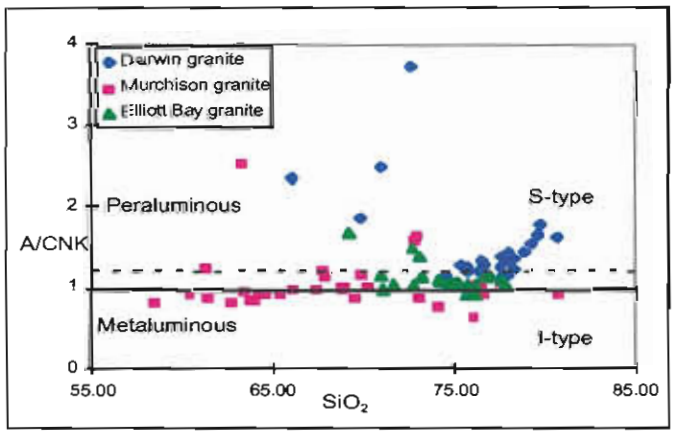

Figure 11 A/CNK vs. SiO2 plot of Shand (1947) and showing the I-S boundary of Chappell and White (1974).

types are derived from residual I-type sources. To safely and accurately apply the A-M subgroup classifications, the nature of the source material must be known with some certainty. Since this is rarely the case, the use of these subdivisions seems inappropriate and will not be further discussed in this study.

Ishihara (1981) classified granites as magnetite series or ilmenite series. Table 2 summarises the criteria for the two series. This classification is also applicable to the effusive equivalents of the granites. Magnetite series granites are associated with major sulfide mineralisation, whereas the ilmenite series granites are associated with cassiterite and wolframite mineralisation. The two granite series are considered to have resulted from the prevalence of different oxygen fugacaties during evolution of the granite magmas, in which dissociation of water in the hydrous magma is the main oxidizing agent for the magnetite series magmas and incorporation of crustal carbon is the most essential reducing agent for the ilmenite series magmas. The magnetite series can be correlated with I-type granitoids and the ilmenite series with both the I and S-type. Ishihara (1981) stated that even as little as one grain of magnetite should be enough to classify the granite as belonging to the magnetite series. In Australia, S-types are typically ilmenite series, but I-types are divisible into the magnetite and the ilmenite series (Ishihara, 1981). In the western Pacific, since Jurassic time, I-type magnetite series granites are associated with the inner marginal seacoast, face toward the marginal basin and are dominated by sulfide mineralisation (Ishihara, 1981). The Darwin, Murchison and Elliott Bay granites fit the criteria very well to be classified as magnetite series by the Ishihara classification.

Shand (1947) classified granites according to their alumina saturation. The system uses the ratio A/CNK (molar Al_2O_3 / (Na_2O+K_2O+CaO)) which can change from greater than one to less than one in igneous rocks. A/CNK will equal 1 in rocks with quartz and two or more feldspars only but rocks with additional mineral phases will shift the ratio above or below unity. For example, rocks with hornblende will shift the ratio below 1 while rocks with garnet will shift the ratio above 1. The A/CNK/SiO_2 relationship for the Darwin, Murchison and Elliott Bay granites is shown as Figure 11. The I/S-type boundary of Chappell and White is also shown for reference. While the Murchison granite overlaps the metaluminous and I-type boundary the Darwin and Elliott Bay granites are clearly within the peraluminous field and S-type granite field. This shift is a result of sodium and calcium depletion in the Darwin and Elliott Bay granites as a result of hydrothermal alteration. This classification is therefor probably not useful except in very fresh and unaltered rocks. A variations of this theme was introduced by Clarke (1992) and is reproduced in Table 3. Clarke's classification uses Shand (1947) terminology but adds mineralogical and other chemical data in support of each class. Clarke (1992) also adds tectonic setting and mineral deposit associations to the classification. These associations agree very nicely with the interpreted tectonic setting of the Mt. Read volcanics and the associated mineral deposits

Since the primary source material for the granitic melt is related to tectonic setting, any useful classification scheme should give tectonic setting information that is in agreement with the surrounding interpreted geological setting. The Mt. Read volcanics have been interpreted to be volcanic arc that has been accreted onto continental crust, therefor a tectonic setting classification scheme applied to the Cambrian granites should reflect this setting. Several authors have tried to classify granites using various chemical discrimination diagrams that could separate various tectonic settings (Pearce et al., 1984; Pitcher, 1993; Clarke, 1992). The classification scheme of Pearce et al. (1984) appears to be the most workable for this study since good trace element data is available. Pearce et al. (1984) used trace elements and rare earth's in an attempt to distinguish between ocean ridge granites (ORG), volcanic arc granites (VAG), within plate granites (WPG) and collisional granites (COLG). ORG was further subdivided into groups a–d but for the purposes of this study will not be discussed. Pearce et al. assumed that Rb, Y, and Nd were not as mobile in granitic rocks due to the apparent lack of alteration in granites relative to basalts. Even though it has been shown that the Darwin, Murchison and Elliott Bay granites have been hydrothermally altered, Rb, Y, and Nd are plotted in Figures 12–17 in Rb-Y-Nb vs. SiO2 space. The Murchison granite shows the most clear degree of evolution based on SiO_2 content with a range from 58–78%. The Darwin and Elliott Bay granite have a much more restricted range of SiO_2 values and

Table 1 Characteristic Features of I- and S-type granites compared to the Darwin, Murchison and Elliott Bay granites. (See Bekinsale, 1979; Chappell and White, 1974; Jones, 1993; Pitcher, 1993.)

I-Types	Cambrian Granites	S-Types
Relatively high sodium, Na_2O normally >3.2% in felsic varieties, decreasing to > 2.2% in more mafic types	Darwin granite: **average 2.876 wt.%** Murchison granite: average 3.086 wt.% Elliott Bay granite: average 2.653 wt.%	Relatively low sodium, Na_2O normally <3.2% in rocks with approx. 5% K_2O, decreasing to <2.2% in rocks with approx. 2% K_2O
Mol $Al_2O_3/(Na_2O+K_2O+CaO)<1.1$	Darwin granite: **average 1.578** Murchison granite: average 1.03 Elliott Bay granite: average 1.125	Mol $Al_2O_3/(Na_2O+K_2O+CaO)>1.1$
C.I.P.W. normative diopside or <1% normative corundum	Darwin granite: **NO normative diopside or corundum** Murchison granite: 0.29% av. normative diopside, no corundum Elliott Bay granite: trace normative diopside, no corundum	>1.1% C.I.P.W. normative corundum
Tend to be the acid end of a broad compositional spectrum from basic to acid	Darwin granite: **granodiorite to granite** Murchison granite: granodiorite to granite Elliott Bay granite: granite only to date	Tend to occur in restricted ranges of only acidic compositions
Regular inter-element variations within plutons; linear or near linear variation diagrams	Darwin granite: **linear or near linear variation diagrams** Murchison granite: linear or near linear variation diagrams Elliott Bay granite: linear or near linear variation diagrams	Variation diagrams more irregular
Magmas with relatively high oxygen fugacity; Relatively high ferric/ferrous ratios; characterised by magnetite	Darwin granite: **abundant magnetite** Murchison granite: abundant magnetite Elliott Bay granite: abundant magnetite	Magmas with relatively low oxygen fugacity; Relatively low ferric/ferrous ratios; characterised by ilmenite
Low initial $^{87}Sr/^{86}Sr$ ratios (< 0.708)	Darwin granite: **0.703-0.709** Murchison granite: 0.710 Elliott Bay granite: not available	High initial $^{87}Sr/^{86}Sr$ ratios (> 0.708)
Normal range of $\delta^{18}O$ values (approx. 6-10 ‰ SMOH	Darwin granite: **magnetite values -3.4 - +6.9** Murchison granite: not available Elliott Bay granite: not available	Enriched in ^{18}O ($\delta^{18}O$ values approx. ≥ about 10 ‰ SMOH)
Hornblende and sphene commonly present	Darwin granite: **minor hornblende and sphene** Murchison granite: abundant hornblende and sphene Elliott Bay granite: minor hornblende and sphene	Muscovite, monazite, cordierite and garnet are commonly present

Table 2 Characteristics of Magnetite vs Ilmenite Series granites after Ishihara (1981)

Magnetite Series	Ilmenite Series
Magnetite content > 0.1 vol. percent	Magnetite and ilmenite content < 0.1 vol. percent
Magnetic susceptibility higher than 1×10^{-4} emu/g	Magnetic susceptibility less than 1×10^{-4} emu/g
In calc-alkaline granites, Fe_2O_3/FeO ratio > 0.5	In calc-alkaline granites, Fe_2O_3/FeO ratio < 0.5
Positive $\delta^{34}S$ values	Negative $\delta^{34}S$ values
Low $\delta^{18}O$ values	High $\delta^{18}O$ values
Depletion in lithophile elements	Enrichment in lithophile elements
Accessory magnetite(0.1-2 vol. %), ilmenite, sphene, epidote, hematite, pyrite and chalcopyrite	Accessory ilmenite, pyrrhotite, graphite, monozite, garnet and muscovite
Biotite with high Fe_2O_3/ FeO and low refractive index	Biotite with low Fe_2O_3/ FeO and high refractive index
Intrusive sequences in which Fe/(Fe + Mg) for amphiboles and biotites decreases with increasing SiO_2 content of the host rocks	Intrusive sequences in which Fe/(Fe + Mg) for amphiboles and biotites increases with increasing SiO_2 content of the host rocks
Associated with base metal sulfides, sheelite, gold and silver, porphyry molybdenum and copper, and Kuroko-type VHMS deposits	Cassiterite, wolframite, beryl, and fluorite mineralisation

Ref. Ishihara,1981,

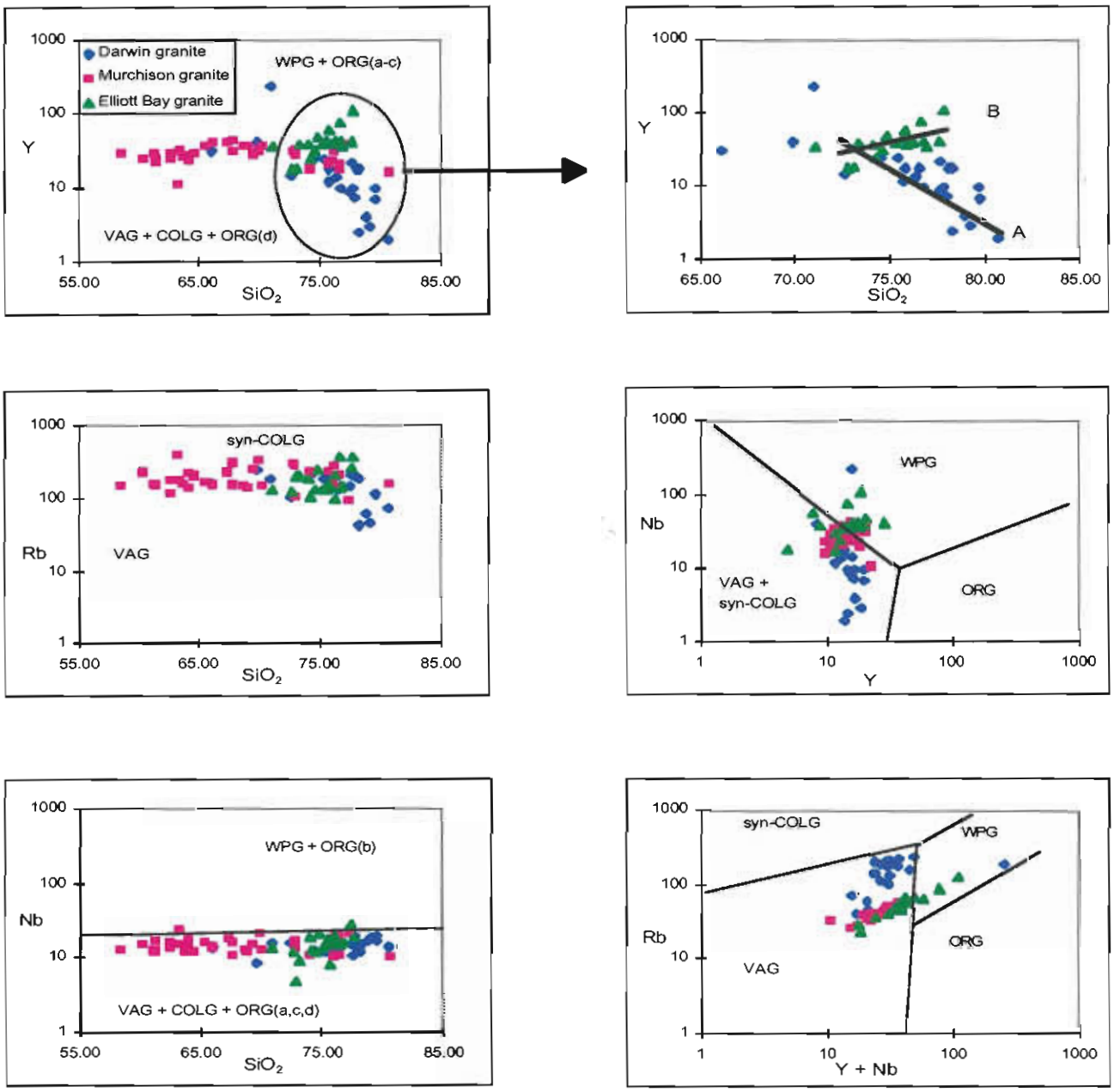

Figures 12-17 Rb, Y, and Nd are plotted in Rb-Y-Nb vs. SiO_2 space. All three granites appear to overlap the field boundaries between syn-collisional granites and volcanic arc granites.

therefore granite types. This may however be an artifact of erosion and degree of sampling. All three granites appear to overlap the field boundaries between syn-collisional granites and volcanic arc granites. The increase in Rb in Figure 13 may be explained by a slight increase in Rb due to increased mobility during hydrothermal alteration in all three of the granites. Since Rb substitutes for K in potassic alteration, the effect of hydrothermal alteration would be to increase the Rb content forcing the points on the diagram up toward the syn-COLG line resulting in erroneous results. Y and Nb have been demonstrated to be weakly mobile during hydrothermal alteration as shown in Figures 9–10. This weak mobility becomes less apparent when plotted on log scale variation diagrams as the small increases and decreases are a factor of 2 or so and not an order of magnitude. In Figure 12, the Murchison granite shows linear Y relationship parallel to the field boundary separating VAG + COLG + ORG (D) from WPG + ORG (a–c). At SiO_2 levels less 73% , the Y content is most likely controlled by partitioning into calcic plagioclase or hornblende (Atherton and Tarney, 1979). Both the Darwin and Elliott Bay granites show variable Y contents beginning at about 73% SiO_2 (Figure 15). The Darwin granite follows Line A. This systematic decrease, after 73% SiO_2, is probably due to increased fractionation of the granite and stripping out of Y by some mineral phase. The plot of Zr vs. SiO_2 (Figure 5) is flat suggesting that the mineral is not zircon. In addition the high SiO_2 values above 78% SiO_2 are probably not magmatic values and result from to increased SiO_2 due to loss of other mineral phases or increased silica as a result of hydrothermal alteration. The increasing trend along Line B for the Elliott Bay granite is unexplained and will be the subject of further thought. All three granites plot within the volcanic arc granite field in Figure 14 and 17 and demonstrate Nb depletion characteristic of volcanic arc granites (Pearce et al., 1984). Figure 14 also suggests that the Nb content in the granites is not related to SiO_2 content and therefor must be controlled by partitioning into some other mineral phase.

A compilation of petrographic descriptions from this research was presented in Wyman (1996)

Alteration

The gross effects of hydrothermal alteration have been mentioned above and include sodium and calcium depletion and local potassium increases. This style of alteration, in and around the Darwin granite, has many characteristics of hydrothermal alteration found in and around other mineralised granite systems worldwide. Alteration assemblages are dominated by K-feldspar, chlorite, sericite, and silica with lesser amounts of carbonate, pyrite, magnetite and other accessory minerals. Lack of outcrop restricts the amount of geologic mapping that can be done, and in most places it is difficult to accurately define distinct zones. Crude zoning is seen, however, on Mt. Darwin and the ridge south from Mt. Darwin to the contact with the Darwin granite. This Zoning is shown on Figure 18 in relation to the geology. Descriptions of the megascopic and petrologic characteristics of alteration in the various units mapped in this study were presented in Wyman (1996).

Sericite alteration

Sericite alteration of groundmass is typically weak to moderate. Sericite forms small aggregates as replacements of groundmass feldspar and often outlines interlocking groundmass grains. Sericite can also occur as small micro-veinlets cross-cutting both the groundmass as well as individual phenocrysts. Sericite is typically seen as the first sign of alteration in feldspar phenocrysts. It typically replaces the feldspar along cleavage plains or via fractures. Cores and blebs of unaltered relict feldspar with preserved twinning are typical.

Sericite-chlorite alteration

Three domains of sericite with lesser chlorite are found (1) irregular blebs in the groundmass (0.02–0.05 mm) with some larger masses to 0.2 mm, (2) irregular masses in phenocrysts, and (3) in veins with quartz or other minor accessories. Chlorite is most common as an accessory in phenocryst replacement where it can form coarse aggregrates related to fractures or fine interlocking mosiacs with sericite. Sericite-chlorite alteration is common in rocks with moderate to intense alteration. Phenocryst replacement is destructive to crystallographic structure, twinning is not preserved.

Chlorite-sericite alteration

Chlorite occurs as irregular blebs of varying size in the groundmass that is previously sericite or chlorite-sericite altered. Complete groundmass replacement is uncommon. This alteration is related to increased fracture density and early hydrothermal activity. Chlorite and sericite replace plagioclase, biotite and other ferromagnesian mineral phenocrysts. Chlorite is typically the dominant replacement mineral although sericite is a common accessory and is in part, probably overprinted by this later event. This phase of alteration is pre K-feldspar alteration and generally accompanied by only one additional accessory mineral, magnetite. Evidence for the timing of this alteration includes, chlorite veins that have cut sericite/chlorite altered rhyolites. These veins show diffuse chlorite alteration boundaries with chlorite replacing sericite/chlorite altered volcanics.

Chlorite alteration

Chlorite replaces small groundmass size feldspar laths. This alteration overprints previously sericite and/or K-feldspar alteration that did not alter the fine groundmass feldspar laths. This alteration is seen behind small solution fronts. Large irregular masses of chlorite also occur as cores of magnetite and iron oxides. This appears to be a phase of magnetite replacing large masses of chlorite, or the chlorite may have pseudomorphed an early mineral or relict mineral after the magnetite.

K-feldspar alteration

Hydrothermal K-feldspar appears to be confined to the area near Jukes Prospect and is seen only weakly at Mt. Darwin. It is typically moderate to intense, texturally destructive and turns the rocks pink. Phenocrysts in the K-Feldspar altered rocks are typically sericite-chlorite, or chlorite-sericite altered. K-feldspar alteration is almost always associated with weak chlorite alteration and is believed to have overprinted it. K-feldspar alteration only occurs without other alteration assemblages in the groundmass of the most intensely altered rocks. The most common accessory alteration assemblages found in association with K-feldspar alteration in order of abundance are chlorite, sericite and silica.

Discussion of alteration

The alteration assemblages at Mt. Darwin are dominated by K-feldspar, chlorite, silica and sericite in various combinations and intensities. Accessory minerals include pyrite, magnetite, tourmaline, barite and chalcopyrite. Table 4 compares the alteration assemblages found at Mt. Darwin to the porphyry Cu-Au style alteration assemblages found in other intrusion related hydrothermal systems. These criteria are discussed at length in the literature by numerous authors including (Cooke et al., 1996; Sillitoe, 1993; Titley, 1982; Titley, 1993) and others. The comparison in Table 4 demonstrates numerous similarities between the alteration assemblages at Mt. Darwin and porphyry Cu-Au deposits.

The Darwin granite is interpreted as plunging to the north under the CVC rocks (Leaman and Richardson, 1989; Payne, 1991; Large et al., 1996). K-feldspar and chlorite alteration assemblages are dominant, and magnetite, and even barite veins, occur along the entire projected northward trend of the granite, 15 km to the north. These alteration assemblages, combined with geophysical evidence from Leaman and Richardson (1989) and Payne (1991), appear to be strong evidence that there is a buried granite, at least as far north as Jukes. Also this is strong evidence that alteration is most intense and widespread near the top of the granite, and although there is intense alteration along the sides of the granite, it is confined to less than 1 km.

Discussion

The Darwin granite can only be classified as a highly fractionated granite of the magnetite series. Trace element geochemistry also supports an island arc setting. Alteration assemblages, in and around the Darwin granite, resemble alteration assemblages found in other granite related hydrothermal systems throughout the world. Alteration assemblages appear to be most intense and widespread above the granite, and appear to drop off rapidly along the sides. Mineralisation and alteration appear to be related to the late stage intrusion of the white equagranular granite and the porphyritic white granite phase. Magnetite and tourmaline veining also appears to be related to this phase of granitic intrusion. Hydro-

Table 3 Tripartite chemical classification of granitic rocks from Clarke (1992)

The Granitiod Family QAP 60% > Quartz > 20% Alkali-feldspar/(Alkali-feldspar + Plagioclase) = 1			
	Peraluminous	Metaluminous	Peralkaline
Definition (Shand, 1947)	A > CNK	CNK > A > NK	A < NK
Characteristic minerals	aluminosilicates, cordierite, garnet, topaz, tourmaline, spinel, corundum	orthopyroxene, clinopyroxene, cummingtonite, hornblende, epidote	fayalitic olivine, aegirine, arfvedsonite, riebeckite
Other common minerals	biotite, muscovite	biotite, minor muscovite	minor biotite
Oxide minerals	ilmenite, tapiolite	magnetite	magnetite
Accessory minerals	apatite, zircon, monazite	apatite, zircon, titanite, allanite	apatite, zircon, titanite, allanite, fluorite, cryolite, pyrochlore
Other chemical features	F/Cl > 3		Low CaO, Al2O3, H2O, K, Zr, Nb, Ta, ΣREEs, Y, F/Cl < 3
Isotopic compositions $^{87}Sr/^{86}Sr_i$ εNd_i	 0.7050-0.7200 generally << 0	 0.7030-0.7080 approx. 0	 0.7030-0.7120 highly variable
Typical mineral deposits	aplite-pegmatite-greisen; polymetallic Sn-W-U-Mo-Cu and Be-B-Li-P	porphyry Cu-Mo	Sn-W-U-Mo and rare metal (Nb-Ta) greisens
General plate tectonic environment	continent-continent collision tectonics involving thickened continental crust	subduction related continental and island arc	post-tectonic or anorogenic extension resulting in intracontinental ring complexes

From Clarke, 1992

Table 4 Comparison of alteration assemblages at Mt. Darwin with typical porphyry Cu-Au alteration assemblages

Mt. Darwin/Darwin granite	Typical Porphyry Cu-Au System
K-Feldspar Alteration Characterised by K-feldspar, chlorite, silicification, pyrite, magnetite, sericite and stockworks of quartz and quartz K-feld veins and replacement of primary quartz and feldspar phenocrysts, and destruction of all primary textures. The style is both selectively pervasive and pervasive.	**Potassic(Biotite-K-Feldspar), or Potassium Silicate alteration.** Characterised by orthoclase, biotite, muscovite and commonly, sericite. Veins in this zone and containing these minerals are paired with quartz and frequent sulfides. Magnetite is common(5-10 vol. %) The style is both selectively pervasive and pervasive.
Chlorite Alteration Both pre and post K-feldspar alteration. Occurs with quartz, minor carbonate, sericite, minor K-feldspar and magnetite and pyrite. Close to intense K-Feld alteration this zone contains abundant pyrite. The style is both vein and pervasive.	**Propylitic Alteration.** This style contains epidote, carbonate, various zeolites, albite, chlorite and quartz. Qtz. + Carb. + Chlorite veins are typical. The style is both vein and pervasive.
Chlorite-Sericite Alteration Pale green sericite and minor chlorite replace feldspar phenocrysts in altered volcanics at Jukes. Other accessory minerals in this zone are minor carbonate, magnetite, pyrite and quartz. The style is pervasive.	**Intermediate Argillic Alteration** Pale green overprint to K-silicate zones. Accessory minerals include sericite, chlorite, minor carbonate magnetite, quartz and pyrite. The style is both vein and pervasive.
Sericite-Chlorite Alteration Contains sericite and quartz with minor chlorite. The style is pervasive.	**Phyllic(sericitic).** Commonly this zone contains pyrite and quartz and lesser chlorite. Only weakly developed in gold rich systems. The style is both vein and pervasive.
Sericite Alteration Most common minerals are sericite and quartz. Clay assemblages are destroyed due to the age of the deposit and metamorphic effects but may be represented by the sericite-quartz assemblages. Pyrite is a trace levels. The style is pervasive.	**Advanced-Argillic(Alunite-Pyrophyllite).** High volumes of pervasive quartz and alunite with kaolin and pyrophyllite. Barite and native sulfur appear in late stage open space fillings. Metal poor. The style is both vein and pervasive.
Additional Features	
Only two plutons recognised to date. This may be a function of erosion as multiple plutons have been recognised in the Murchison granite.	Clusters of Plutons
No district scale base metal zoning	District scale base metal zoning
Shallow crustal emplacement(1-2 km)	Shallow crustal emplacement(1-2 km)
Emplaced in coeval volcanic sequences in volcano-plutonic arc	Commonly emplaced in coeval volcanic sequences in volcano-plutonic arcs
Equagranular with minor porphyritic phases	Generally porphyritic monzonite to quartz diorite compositions. Equagranular precursors to ore bearing stocks
Stocks are I-type, magnetite series and calc-alkaline with highly variable K_2O/SiO_2	Stocks are I-type, magnetite series and calc-alkaline with highly variable K_2O/SiO_2
Hydrothermal Breccia at Jukes contains high Cu-Au, although no hydrothermal breccias are recognised at Mt. Darwin.	Hydrothermal Breccias are common and carry high Cu-Au

fracturing above the granite, resulted in emplacement of the alteration assemblages, veins and mineralisation.

Regional aeromagnetic data suggests that the Darwin granite underlies the entire northerly trending belt of hydrothermal alteration and Cu-Au mineralisation (Large et al., 1996; Leaman and Richardson, 1989; Payne, 1991). The eastern margin of the intrusion is an erosional unconformity with Cambrian Tyndall Group volcanics and therefore no hydrothermal alteration remains exposed on that side. Magnetite and tourmaline veins, copper mineralisation and hydrothermal alteration overprint the pink granite phase of the Darwin granite and appear to be related to the later white granite phase.

The Jukes–Darwin field has numerous similarities to 'porphyry-style' mineralisation including:

* Collisional event in the middle Cambrian, followed by a period of bimodal volcanism (Crawford and Berry, 1992)
* Calc-alkaline magnetite-series granite emplaced post-obduction
* Cambrian granite-related Cu-Au vein mineralisation associated with potassic and intermediate argillic (chlorite) alteration (Cooke et al., 1996)
* The presence of tourmaline breccias and magnetite veins
* Multiple intrusions
* Shallow crustal emplacement

Unfavourable elements for Cambrian 'porphyry-style' mineralisation in the Jukes–Darwin field include:

* No porphyritic stock recognised to date: unless the quartz-feldspar porphyry dykes represent an as yet unrecognized stock.
* Lack of quartz-diorite to monzodiorite intrusions
* Large scale zoned alteration systems not known (except for Mt. Lyell)
* Sulfides have heavy $\delta 34S$ values (Gadaloff, 1996)
* Barite veins
* Submarine volcanism

It is possible that Cu-Au mineralisation in the Jukes–Darwin field is low grade 'porphyry-style', but the submarine setting favours rapid inundation by seawater, thus explaining the isotopic character of the sulfides (Wyman et al., 1997). Early seawater inundation diluted and dissipated the Cu-Au-bearing magmatic-hydrothermal fluids, producing intermediate argillic (chlorite-sericite) alteration, and preventing the development of extensive Cu-Au stockwork mineralisation.

REFERENCES

Abbott, P. D. B., 1992, Geology of a barite-galena occurrence exposed in the Anthony Power development tunnel, western Tasmania: Unpub. BSc (Hons) thesis, University of Tasmania, 62 p.

Atherton, M. P., and Tarney, T., 1979, Origin of Granite Batholiths: Geochemical evidence: Kent, Shiva Publishing Limited, p. 148.

Bekinsale, R. D., 1979, Granite magmatism in the Tin Belt of south-east Asia, in Atherton, M. P. a. T., J., ed., Origin of Granite Batholiths: Geochemical Evidence: Orpington, Kent, Shiva Publishing Ltd, p. 34-44.

Chappell, B. W., and White, A. J. R., 1974, Two Contrasting Granite Types: Pacific Geology, v. 8, p. 173-174.

Clarke, D. B., 1992, Granitiod Rocks, Chapman and Hall, 283 p.

Collins, W. J., Bearns, S. D., White, A. J. R., and Chappell, B. W., 1982, Nature and origin of A-type granite with particular reference to Southeastern Australia: Contributions to Mineralogy and Petrology, v. 10, p. 189-200.

Cooke, D. R., Heithersay, P. S., Wolfe, R., and Calderon, A. L., 1996, Concepts and Exploration Criteria for Australian and SW Pacific Porphyry Cu-Au deposits, Coursework Manual 5: Master of Economic Geology, CODES, University of Tasmania.

Crawford, A. J., Corbett, K. D., and Everard, J. L., 1992, Geochemistry of the Cambrian volcanic - hosted massive sulfide - rich Mount Read Volcanics, Tasmania, and some tectonic implications: Economic Geology, v. 87, p. 597-619.

Gadaloff, C., 1996, Cambrian Copper-Gold Vein Mineralisation in the East Darwin Area, Western Tasmania: Unpub. B.Sc.(Honours) thesis, University of Tasmania.

Hills, C. L., 1914, The Jukes-Darwin mining field: Bulletin of the Geological Survey of Tasmania, v. 16.

Ishihara, S., 1981, The granitoid series and mineralization: Economic Geology, v. 75th Anniv. Vol., p. 458-484.

Jones, A. T., 1993, The geology, geochemistry and structure of the Mt. Darwin - South Darwin Peak area, western Tasmania: Unpub. B.Sc.(Honours) thesis, University of Tasmania, 120 p.

Lameyre, J., and Bowden, P., 1982, Plutonic Rock Types Series: Discrimination of Various Granitiod Series and Related Rocks: Journal of Volcanology and Geothermal Research, v. 14, p. 169-186.

Large, R. R., Doyle, M., Raymond, O., Cooke, D., Jones, A., and Heasman, L., 1996, Evaluation of the role of Cambrian granites in the genesis of world class VHMS deposits in Tasmania: Ore Geology Reviews, v. 10, p. 215-230.

Leaman, D. E., and Richardson, R. G., 1989, The granites of west and North-west Tasmania, a geophysical interpretation: Bulletin Geological Survey of Tasmania, v. 66, p. 146.

Loiselle, M. C., and Wones, D. R., 1979, Characteristics and Origins of Anorogenic Granites, Geological Society of America, 11: Abstracts with Programs, p. 468.

Payne, B., 1991, Geophysical interpretation of the Mt. Sedgewick - Red Hills area, western Tasmania: Unpub. B.Sc.(Honours) thesis, University of Tasmania, 107 p.

Pearce, J. A., Harris, N. B. W., and Tindle, A. G., 1984, Trace Element Discrimination Diagrams for the Tectonic

Interpretation of Granitic Rocks: Journal of Petrology, v. 25, p. 956-983.

Pitcher, W. S., 1983, Granite: typology, geological environment and melting relationships, *in* Atherton, M. P. a. G., C.D., ed., Migmatites, Melting and Metamorphism: Nantwich, Shiva Publications, p. 277-287.

Pitcher, W. S., 1993, The Nature and Origin of Granite: London, Blackie Academic and Professional, 316 p.

Polya, D. A., 1981, The geology of Murchison Gorge: Unpub. B.Sc.(Honours) thesis, University of Tasmania.

Shand, S. J., 1947, Eruptive Rocks. Their Genesis, Composition, Classification, and their Relation to Ore Deposits: New York, J. Wiley & Sons, 488 p.

Sillitoe, R. H., 1993, Gold-rich porphyry copper deposits: Geologic model and exploration implications, *in* Kirkham, R. V., Sinclair, W.D., Thorpe, R.I., and Duke, J.M., ed., Mineral Deposit Modeling: Geological Association of Canada, Special Paper, p. 465-478.

Solomon, M., 1960, The Dundas group in the Queenstown area: Papers and Proceedings of the Royal Society of Tasmania, v. 94, p. 33-49.

Solomon, M., 1981, An introduction to the geology and metallic ore deposits of Tasmania: Economic Geology, v. 76, p. 194-208.

Streckeisen, A., 1976, To Each Plutonic Rock its proper name: Earth-Science Reviews, v. 12, p. 1-33.

Titley, S. R., 1982, The Style and Progress of Mineralization and Alteration in Porphyry Copper Systems: American Southwest, *in* Titley, S. R., ed., Advances in Geology of the Porphyry Copper deposits: Southwestern North America, Univ. Ariz. Press.

Titley, S. R., 1993, Characteristics of Porphyry Copper Occurrence in the American Southwest, *in* Kirkham, R. V., Sinclair, W.D., Thorpe, R.I., and Duke, J.M., ed., Mineral Deposit Modeling: Geological Association of Canada, Special Paper, p. 433-464.

White, A. J. R., 1979, Source Rocks of Granite Magmas. Lecture notes from GSA Symposium: Geological Society of America 92nd Annual Meeting, San Diego, California, U.S.A., 1979, p. 539.

White, A. J. R., and Chappell, B. W., 1983, Granitoid types and their distribution in the Lachlan Fold Belt, southeastern Australia, Memoir 159, Geological Society of America, p. 21-34.

White, N. C., 1975, Cambrian volcanism and mineralisation, SW Tasmania: Unpub. Ph.D. thesis, University of Tasmania, 339 p.

Wyman, B., 1996, The Darwin Granite-Slate Spur Area: Geology, Volcanic Facies Analysis and Alteration Petrography, Studies of VHMS-related alteration: geochemical and mineralogical vectors to ore: CODES Centre for Deposit Studies, AMIRA/ARC project P439.

Wyman, B., Cooke, D. R., and Large, R. L., 1997, Granite Related Copper-Gold Mineralisation in the Southern Mt Read Volcanics, Western Tasmania, Australia: Third International Mining geology conference, Launceston, Tasmania, Australia, 10-14 November, 1997, in press.

Appendix A Geochemical data from the Darwin granite

Sample Number	41174	41372	41373	41374	41375	840200	GS1	GS2	GS3	GS4	GS5	GS6	GS7	B2028	B2033
Reference	White, 1975	White, 1975	White, 1975	White, 1975	White, 1975	Crawford et al, 1992	Jones, 1993	Jones, 1993	Jones, 1993	Jones, 1993	Jones, 1993	Jones, 1993	Jones, 1993	Wyman, 1996	Wyman, 1996
SiO2	75.41	77.81	79.67	79.26	72.61	76.58	78.07	77.70	78.35	80.74	79.76	75.80	76.42	69.87	78.00
TiO2	0.18	0.06	0.12	0.19	0.21	0.22	0.23	0.19	0.20	0.21	0.27	0.19	0.21	0.61	0.09
Al2O3	13.86	12.84	13.41	14.07	9.73	14.52	13.43	12.57	13.07	14.73	14.17	13.78	13.74	14.35	12.72
Fe2O3	1.65	0.75	0.70	0.61	13.48	1.74	1.80	2.74	1.93	0.41	2.46	1.98	1.55	6.74	0.62
MnO	0.00	0.00	0.00	0.00	0.24	0.02	0.01	0.01	0.00	0.01	0.10	0.00	0.00	0.03	0.01
MgO	0.35	0.08	0.27	0.09	1.27	0.38	0.58	0.35	0.33	0.22	0.31	0.41	0.33	1.16	0.12
CaO	0.17	0.17	0.08	0.56	0.15	0.28	0.04	0.05	0.02	0.30	0.19	0.09	0.10	0.01	0.24
Na2O	2.73	2.98	3.01	4.09	0.06	3.15	1.19	0.19	1.04	3.82	3.09	2.23	2.45	0.13	3.00
K2O	5.47	5.27	2.66	1.10	2.06	4.66	6.68	7.92	7.23	1.97	2.33	6.86	6.63	6.82	5.22
P2O5	0.06	0.02	0.00	0.00	0.13	0.03	0.03	0.05	0.04	0.00	0.00	0.05	0.04	0.07	0.01
Total(Volatile Free)	99.90	99.98	99.92	99.99	99.95	101.58	102.06	101.78	102.21	102.42	102.69	101.38	101.48	99.80	100.02
S					NA									0.26	<0.01
Sc	1	2			8	3	3	4	3			2	3	14	<2
Tl					NA										
V	27	26	17	24	156	21	19	20	18	2	4	16	17	53	2
Cr	20	30	22	23	0	1	3	2	2	3	4	2	3	4	2
Co							WC Mill	WC Mill	WC Mill	WC Mill	WC Mill	WC Mill	WC Mill		
Ni	1	2			0	1	2	3	2	2	3	5	5	2	1
Cu					NA		7	97	28	6	11	14	8	29	7
Zn					NA		42	316	42	19	48	17	18	41	24
As					NA		<3	<3	<3	<3	<3	<3	<3	13	<3
Br							1.2	1.5	<1	<1	<1	1.9	1		
Rb	185	215	115	47	105	135	196	211	190	74	116	200	195	249	213
Sr	130	56	96	183	4	138	48	59	52	115	75	67	58	51	26
Zr	138	65	90	156	46	132	134	124	134	134	190	128	137	239	65
Nb	12	20	17	19	16	14	13	11	12	14	20	12	13	8.6	16.7
Mo					NA										
Ag															
Cd															
Sn					NA		1.8	4.5	2.7	1.1	3.8	2.4	1.4	5.7	1.1(<1.5)
Sb															
Cs															
Ba	896	234	748	100	468	1385	1240	3152	1941	416	444	1348	1151	2105	88
La	103	43	37	33	NA	44.7	69.8	80.2	55.8	3.9	4.7	57.9	65.2	42	19
Ce					NA	89.5	115.1	132.9	99.9	6.4	8.5	96.4	106.3	95	33
Nd						26.5								44	9
Y	25	10	10	3	15	18	18	22	18	2	7	12	14	41	8
W							WC Mill	WC Mill	WC Mill	WC Mill	WC Mill	WC Mill	WC Mill		
Tl															
Pb	23	8	25	43	5		50	327	196	14	19	6	6	14	10
Bi					NA		<1.5	<1.5	<1.5	<1.5	<1.5	<1.5	<1.5	5.9	<2
Th					NA		32	37	35	41	45	39	44	13	33
U					NA		4.8	11.6	4.8	0.9	1.7	7.4	8.6	3.3	7.7

Appendix A (cont.)

Sample Number	B2040	B2043	B2045	B2046	B2053	B2054	B2061	L8	L7
Reference	Wyman, 1996	Wyman, 1996	Wyman, 1996	Wyman, 1996	Wyman, 1996	Wyman, 1996	Wyman, 1996		
SiO2	75.83	78.95	74.59	77.96	76.78	77.58	78.37	71.03	66.14
TiO2	0.19	0.16	0.21	0.28	0.16	0.16	0.17	0.76	0.64
Al2O3	13.13	13.95	13.25	13.58	13.46	12.91	13.73	14.52	13.48
Fe2O3	1.90	0.33	1.06	1.32	0.79	0.72	0.53	7.08	13.05
MnO	0.01	0.01	0.01	0.05	0.01	0.01	0.02	0.05	0.07
MgO	0.34	0.23	0.27	0.29	0.19	0.16	0.14	1.25	1.40
CaO	0.07	0.39	0.01	0.57	0.03	0.03	1.00	0.26	0.18
Na2O	1.90	4.19	0.33	4.62	2.30	2.06	4.70	0.15	0.15
K2O	6.46	1.78	9.92	1.31	6.03	6.17	1.31	4.71	4.75
P2O5	0.04	0.01	0.04	0.02	0.03	0.02	0.01	0.20	0.12
Total(Volatile Free)	99.87	100.00	99.70	99.99	99.79	99.82	99.99	100.00	100.00
S	<0.01	<0.01	0.01	0.01	0.01	0.01	<0.01		
Sc	3	<2	5	3	4	2	1		
Ti								4456	3836
V	16	<1.5	14	26	8	7	2		
Cr	2	2	4	2	2	2	2		
Co									
Ni	<1	<1	2	<1	1	1	<1		
Cu	7	2	4	3	7	6	3		
Zn	32	11	11	42	13	12	21		
As	<3	<3	<3	<3	<3	<3	<3		
Br									
Rb	182	61	227	53	146	148	43	191	168
Sr	68	241	103	135	51	61	205	11	23
Zr	115	133	162	216	121	110	123	382	312
Nb	13.4	17.2	12.4	21.8	15	15.2	14.8	16	14
Mo									
Ag									
Cd									
Sn	2.8	1.8	2.8	1.3(<1.5)	2.1	2.3	2.0		
Sb									
Cs									
Ba	1127	185	2502	114	1759	1736	211		
La	72	2	74	36	50	30	5		
Ce	134	4	139	56	110	65	9		
Nd	41	3	55	19	37	20	3		
Y	18	4	25	12	10	9	3	238	32
W									
Tl									
Pb	8	3	8	5	<1.5	2	9		
Bi	<2	<2	<2	<2	<2	<2	<2		
Th	32	44	19	41	42	40	36		
U	4.5	1.5	4.1	4.8	3.5	5.2	1.5		

Appendix A (cont.)

Sample Number	B2019	B2019 D	B2020	B2022	B2022 D	B2025	B2026	B2027	B2029	B2030	B2031	B2032	B2035	B2037
SiO2	77.34	77.31	74.71	76.04	76.04	69.58	3.65	76.52	22.31	50.61	78.54	67.81	56.33	75.75
TiO2	0.16	0.16	0.24	0.44	0.43	0.23	0.09	0.18	0.05	0.19	0.20	0.67	0.18	0.22
Al2O3	12.48	12.52	13.42	14.77	14.77	17.79	0.51	13.28	0.53	27.03	12.92	14.60	12.38	12.32
Fe2O3	0.85	0.83	4.15	2.23	2.23	6.17	95.47	1.34	76.85	15.59	3.47	8.63	27.20	1.30
MnO	0.01	0.01	0.09	0.01	0.00	0.01	0.01	0.01	0.01	0.02	0.01	0.03	0.02	0.01
MgO	0.19	0.19	0.99	0.65	0.66	4.26	0.06	0.43	0.06	4.30	0.46	1.31	2.39	0.20
CaO	0.04	0.04	0.83	0.01	0.01	0.54	0.02	0.01	0.01	0.33	0.01	0.01	0.13	0.01
Na2O	1.92	1.91	0.09	0.79	0.80	1.26	0.05	0.16	0.05	1.85	0.09	0.12	0.97	0.24
K2O	6.88	6.87	5.32	5.01	5.02	0.15	0.16	7.81	0.08	0.08	4.23	6.48	0.36	9.63
P2O5	0.02	0.02	0.06	0.02	0.02	0.01	0.03	0.03	0.09	0.01	0.02	0.07	0.04	0.04
Total (Volatile Free)	99.89	99.86	99.91	99.97	99.98	100.01	100.05	99.77	100.03	100.00	99.95	99.73	99.99	99.73
S	0.01		0.09		<0.01	0.01	0.01	0.01	<0.01	<0.01	<0.01	0.01	0.1	0.02
Sc	2		5		11	20	<2	5	8	46	7	16	18	3
Tl														
V	11		29		39	136	187	6	18	103	6	56	75	7
Cr	2		5		3	17	11	3	6	8	3	4	12	3
Co														
Ni	<1		2		1	5	7	1	5	4	1	2	16	2
Cu	4		48		2	14	33	33	33	36	116	27	8	4
Zn	10		48		83	56	32	11	6	50	19	47	25	12
As	<3		<3		<3	8	4	8	25	<3	<3	<3	<3	<3
Br														
Rb	143		199		184	6	9	222	3	3	163	260	15	209
Sr	50		26		16	84	16	66	15	100	10	49	76	92
Zr	116		145		272	142	6	161	10	54	174	268	71	179
Nb	14.6		14.2		15.9	6.9	<2	13.6	2.6	2.6	15.3	10	8.2	9.5
Mo														
Ag														
Cd														
Sn	2.1		8.8		1.9	7.3	0.4(<3)	7.2	1203.4	39.4	16.0	7.5	12.2	3.4
Sb														
Cs														
Ba	1323		877		354	36	63	2179	54	25	550	2339	139	2676
La	30		49		39	19	14	41	5	9	43	41	14	27
Ce	62		96		85	37	7	99	3	10	102	94	23	62
Nd	19		34		36	12	4	38	5	3	44	45	7	18
Y	11		24		29	9	60	33	648	8	32	44	266	65
W														
Tl														
Pb	5		4		5	224	62	10	16	45	5	4	7	13
Bi	<2		<2		<2	2.4	5.9	<2	17.4	<2	<2	<2	<2	<2
Th	26		31		14	15	<2	21	3	13	25	12	16	46
U	2.5		5.5		3.2	2.8	15.5	4.7	11.6	2.7	5.1	4	6.9	7.8

Appendix A (cont.)

Sample Number	B2038	B2044	B2047	B2048	B2049	B2050	B2051	B2052	B2060		
SiO2	71.35	65.52	76.29	68.01	72.36	64.82	63.85	63.96	98.42		
TiO2	0.27	0.67	0.52	0.67	0.41	0.72	0.88	0.14	0.01		
Al2O3	14.59	15.56	9.25	14.66	13.99	17.05	16.27	20.85	0.47		
Fe2O3	2.96	6.40	7.62	6.31	0.84	8.66	5.87	9.83	0.77		
MnO	0.01	0.03	0.01	0.03	0.01	0.05	0.01	0.01	0.01		
MgO	0.92	1.84	1.72	1.65	0.21	2.71	1.31	3.25	0.02		
CaO	0.01	0.01	0.02	0.01	0.01	0.01	0.01	0.22	0.01		
Na2O	0.30	0.22	0.15	0.17	0.29	0.06	0.33	1.58	0.05		
K2O	9.27	9.35	4.31	8.07	11.49	5.80	10.96	0.10	0.31		
P2O5	0.04	0.05	0.05	0.11	0.06	0.07	0.06	0.04	0.01		
Total (Volatile Free)	99.72	99.65	99.94	99.69	99.67	99.95	99.55	100.00	100.09		
S	0.01	0.03	0.51	<0.01	0.01	0.01	0.05	<0.01	<0.01		
Sc	8	20	14	17	2	27	21	32	<2		
Ti											
V	13	135	70	50	5	154	122	30	<1.5		
Cr	3	8	6	2	3	66	2	2	2		
Co											
Ni	3	9	2	3	2	16	3	7	<1		
Cu	8	22	7	6	5	247	21	3	<1		
Zn	89	55	44	149	10	111	119	20	2		
As	<3	<3	5	<3	<3	<3	<3	<3	<3		
Br											
Rb	259	241	159	216	227	290	219	2	8		
Sr	80	90	21	82	85	16	97	63	2		
Zr	223	213	175	270	318	219	264	54	7		
Nb	16.4	9.9	7.8	9.7	14.2	8.7	9.9	5.1	1		
Mo											
Ag											
Cd											
Sn	5.2	7.6	14.3	12.8	5.0	5.3	6.0	148.1	3.0		
Sb											
Cs											
Ba	2463	2939	648	2728	3017	812	4479	28	98		
La	40	102	15	67	5	37	41	<2	<2		
Ce	88	200	31	124	17	77	88	<4	<4		
Nd	35	75	15	46	3	32	44	<2	<2		
Y	46	33	22	35	94	30	31	373	12		
W											
Tl											
Pb	31	17	6	7	5	22	22	2	<1.5		
Bi	<2	<2	<2	<2	<2	<2	<2	<2	<2		
Th	25	11	9	12	9	12	10	13	<1.5		
U	6.5	3.9	2.5	4.1	5.7	3.5	3.7	4.1	<1.5		

Appendix A (cont.)

Sample Number	B1077	B1079	B1080	B1085	B1087	B1089	B1091	B1092	B1093	B1095	B1096	B1098	B1099	B2001
SiO2	76.80	70.00	74.46	76.64	82.64	82.68	76.42	68.11	75.79	81.77	71.33	77.78	80.71	75.53
TiO2	0.21	0.65	0.35	0.38	0.16	0.28	0.25	0.63	0.25	0.17	0.43	0.21	0.25	0.26
Al2O3	12.68	16.11	13.41	13.28	10.89	9.97	12.26	14.99	13.59	10.23	14.55	13.01	12.50	12.80
Fe2O3	1.54	3.41	3.87	2.76	1.55	1.77	2.94	8.47	1.52	1.37	5.34	1.29	1.44	3.62
MnO	0.01	0.10	0.03	0.01	0.01	0.01	0.01	0.03	0.01	0.01	0.01	0.01	0.01	0.02
MgO	0.35	1.65	0.69	1.26	0.60	0.76	0.37	1.73	0.38	0.29	0.98	0.31	0.44	0.49
CaO	0.02	0.12	0.04	0.01	0.01	0.01	0.01	0.19	0.02	0.01	0.02	0.01	0.01	0.02
Na2O	2.46	5.08	3.73	0.06	0.05	1.16	0.10	2.21	2.29	1.54	2.23	1.23	0.15	2.41
K2O	5.77	2.72	3.27	5.40	4.09	3.32	7.49	3.40	5.98	4.51	4.95	5.99	4.44	4.68
P2O5	0.03	0.07	0.06	0.02	0.02	0.03	0.03	0.16	0.03	0.03	0.03	0.03	0.02	0.03
Total(Volatile Free)	99.87	99.92	99.91	99.82	100.03	99.99	99.88	99.93	99.86	99.92	99.88	99.87	99.96	99.86
S	<0.01	0.01	<0.01	<0.01	<0.01	0.01	0.01	<0.01	0.01	<0.01	<0.01	0.01	<0.01	0.01
Sc	6	18	11	7	4	9	9	16	9	4	11	6	8	9
Tl														
V	7	101	8	41	11	2	<1.5	44	2	10	18	7	3	2
Cr	2	70	2	23	3	2	2	3	2	3	6	2	1	1
Co														
Ni	2	12	1	9	1	1	2	2	1	1	3	1	<1	1
Cu	3	2	3	6	1	1	21	27	4	3	4	4	2	3
Zn	81	99	40	27	26	13	17	88	14	22	37	32	21	21
As	<3	<3	<3	<3	<3	<3	4	<3	<3	3	<3	<3	<3	<3
Br														
Rb	190	102	116	249	188	140	189	151	151	145	184	198	177	145
Sr	93	137	78	4	3	20	16	45	57	35	33	34	3	54
Zr	173	366	273	226	117	285	274	280	267	142	306	167	253	273
Nb	15.7	15	12.6	14.7	11.8	13.9	11.7	9.7	13.7	11	11.7	15.6	13.4	13.1
Mo														
Ag														
Cd														
Sn	3.1	3.2	2.0	3.1	2.2	3.4	3.3	6.8	2.2	2.8	3.5	1.6	2.2	1.1(<1.5)
Sb														
Cs														
Ba	1179	754	794	1689	390	401	1303	801	1349	889	949	1194	392	1189
La	36	55	79	47	45	55	45	44	53	46	45	43	57	25
Ce	73	107	158	112	102	127	99	95	123	100	91	110	123	64
Nd	37	53	75	47	41	57	44	45	52	41	40	42	48	29
Y	29	44	58	24	25	47	40	42	43	33	31	33	35	38
W														
Tl														
Pb	6	8	2	4	13	3	16	2	4	16	4	35	4	3
Bi	<2	<2	<2	<2	<2	<2	<2	<2	<2	<2	<2	<2	<2	<2
Th	25	16	19	22	16	21	18	14	21	19	15	23	19	20
U	4.4	4.4	4	4.4	2.9	6.4	5.2	4.5	4.4	5.3	2.9	3.9	5	3.8

Appendix A (cont.)

Sample Number	B2002	B2003	B2005	B2013	B2014	B2017	B2017 D
SiO2	76.23	75.77	75.09	84.33	74.18	77.35	77.37
TiO2	0.24	0.32	0.22	0.17	0.28	0.20	0.20
Al2O3	12.83	13.56	14.37	10.35	13.04	12.33	12.37
Fe2O3	2.74	2.79	2.00	1.09	3.64	1.29	1.29
MnO	0.01	0.01	0.01	0.01	0.06	0.01	0.01
MgO	0.51	0.76	0.59	0.38	0.48	0.27	0.26
CaO	0.03	0.02	0.01	0.01	0.17	0.01	0.01
Na2O	2.55	2.24	1.57	0.06	3.63	0.27	0.24
K2O	4.71	4.40	6.04	3.57	4.32	8.01	8.01
P2O5	0.03	0.05	0.02	0.02	0.05	0.04	0.04
Total(Volatile Free)	99.87	99.91	99.92	100.00	99.86	99.79	99.81
S	<0.01	<0.01	<0.01	<0.01	<0.01	0.01	
Sc	8	11	7	4	10	6	
Ti							
V	<1.5	5	10	7	5	10	
Cr	1	2	3	3	1	2	
Co							
Ni	1	2	2	2	2	1	
Cu	52	2	3	1	3	5	
Zn	20	21	20	17	50	80	
As	<3	<3	<3	<3	<3	<3	
Br							
Rb	141	146	223	163	131	246	
Sr	49	34	27	3	142	36	
Zr	263	274	178	131	267	155	
Nb	12	13.1	15.5	13.2	13.1	13.2	
Mo							
Ag							
Cd							
Sn	5.9	3.5	3.5	3.2	3.2	2.0	
Sb							
Cs							
Ba	1135	1001	820	334	1199	1799	
La	49	54	41	46	117	51	
Ce	111	114	93	98	114	119	
Nd	49	54	36	40	107	47	
Y	40	44	32	27	83	30	
W							
Tl							
Pb	3	<1.5	5	<1.5	4	4	
Bi	<2	<2	<2	<2	<2	<2	
Th	21	20	27	16	19	22	
U	4.6	5.1	6	2.4	3.8	4	

Appendix B ACNK and normative mineralogy for the Darwin granite

Sample Number	41174	41372	41373	41374	41375	840200	GS1	GS2	GS3	GS4	GS5	GS6	GS7	B2028
A	0.136	0.126	0.132	0.138	0.095	0.142	0.132	0.123	0.128	0.144	0.139	0.135	0.135	0.141
C	0.003	0.003	0.001	0.010	0.003	0.005	0.001	0.001	0.000	0.005	0.003	0.002	0.002	0.000
N	0.044	0.048	0.049	0.066	0.001	0.051	0.019	0.003	0.017	0.062	0.050	0.036	0.040	0.002
K	0.058	0.056	0.028	0.012	0.022	0.049	0.071	0.084	0.077	0.021	0.025	0.073	0.070	0.072
A/CNK	1.29	1.18	1.68	1.57	3.73	1.35	1.45	1.40	1.36	1.64	1.78	1.22	1.21	1.88
Qz	35.12	38.34	47.95	46.66	50.27	35.62	40.47	41.38	40.20	45.41	45.78	32.89	33.47	33.84
Or	32.40	31.16	15.73	6.52	12.33	27.16	38.74	46.09	41.89	11.39	13.46	40.04	38.69	40.64
Ab	23.19	25.23	25.48	34.67	0.52	26.27	9.91	1.60	8.62	31.57	25.49	18.63	20.46	1.13
An	9.43	6.10	15.27	16.77	20.44	11.56	11.35	9.91	9.43	16.82	17.48	7.25	6.81	18.55
Ne														
Cpx	-7.63	-4.66	-12.35	-11.89	-17.89	-8.81	-9.51	-8.62	-8.21	-12.41	-14.31	-6.07	-5.59	-16.24
Di	-2.55	-0.93	-6.20	-3.97	-2.92	-3.02	-4.16	-1.94	-2.37	-9.02	-3.19	-1.97	-1.94	-4.63
Hd	-5.08	-3.73	-6.16	-7.92	-14.98	-5.79	-5.36	-6.68	-5.83	-3.39	-11.12	-4.09	-3.65	-11.61
Opx	6.73	3.55	7.57	6.80	31.43	7.43	8.26	8.74	7.30	6.76	11.21	6.46	5.42	19.65
En	2.05	0.63	3.54	2.07	4.56	2.32	3.34	1.77	1.91	4.72	2.24	1.91	1.72	5.07
Fs	4.68	2.92	4.03	4.73	26.87	5.11	4.93	6.97	5.39	2.03	8.97	4.55	3.70	14.57
Olivine														
Fo														
Fa														
Mt	0.27	0.12	0.11	0.10	2.20	0.28	0.28	0.43	0.31	0.06	0.39	0.31	0.25	1.09
Il	0.35	0.12	0.23	0.37	0.41	0.42	0.43	0.36	0.37	0.39	0.50	0.36	0.40	1.16
Cm	0.00	0.00	0.00	0.00	0.00	0.00	0.00	0.00	0.00	0.00	0.00	0.00	0.00	0.00
Ap	0.11	0.04	0.00	0.00	0.24	0.05	0.06	0.09	0.07	0.00	0.00	0.09	0.07	0.13
Sum	99.97	99.99	100.00	100.00	99.93	99.98	99.98	99.97	99.98	100.00	100.00	99.97	99.98	99.96

Sample Number	B2033	B2040	B2043	B2045	B2046	B2053	B2054	B2061	L8	L7
A	0.125	0.129	0.137	0.130	0.133	0.132	0.127	0.135	0.142	0.132
C	0.004	0.001	0.007	0.000	0.010	0.001	0.001	0.018	0.005	0.003
N	0.048	0.031	0.068	0.005	0.074	0.037	0.033	0.076	0.002	0.002
K	0.055	0.069	0.019	0.105	0.014	0.064	0.066	0.014	0.050	0.050
A/CNK	1.15	1.28	1.46	1.17	1.35	1.30	1.27	1.25	2.50	2.36
Qz	38.60	36.81	43.91	32.78	41.80	37.91	39.81	41.87	41.21	32.84
Or	30.83	38.31	10.53	58.87	7.74	35.72	36.56	7.74	28.01	28.41
Ab	25.36	16.10	35.46	2.82	39.11	19.55	17.49	39.76	1.28	1.28
An	5.85	8.24	13.99	5.38	12.50	8.60	7.76	12.54	25.19	22.34
Ne										
Cpx	-4.02	-6.97	-9.75	-4.71	-8.31	-7.29	-6.54	-6.37	-21.56	-19.29
Di	-1.29	-2.04	-7.40	-1.92	-2.99	-2.86	-2.49	-2.92	-6.33	-3.67
Hd	-2.73	-4.93	-2.35	-2.79	-5.32	-4.43	-4.06	-3.45	-15.22	-15.63
Opx	3.07	6.73	5.47	4.19	6.39	5.01	4.46	4.02	22.80	30.78
En	0.90	1.78	4.01	1.58	2.10	1.80	1.55	1.71	6.07	5.23
Fs	2.17	4.95	1.46	2.62	4.29	3.21	2.90	2.31	16.74	25.56
Olivine										
Fo										
Fa										
Mt	0.10	0.31	0.05	0.17	0.21	0.13	0.12	0.09	1.15	2.13
Il	0.17	0.37	0.31	0.41	0.52	0.31	0.30	0.33	1.45	1.23
Cm	0.00	0.00	0.00	0.00	0.00	0.00	0.00	0.00	0.00	0.00
Ap	0.02	0.07	0.02	0.07	0.04	0.05	0.04	0.02	0.36	0.22
Sum	99.99	99.98	99.99	99.98	99.99	99.98	99.99	99.99	99.89	99.94

Appendix C Strontium and neodymium data for the Southern Mt. Read Volcanics

Sample Number	Unit/Location	Rock Type	epsilon Nd (init)CHUR	87Sr/86Sr (T=initial)	Refrence
GS-7	Darwin granite	Granite	**-4.99**	**0.703293**	Stoltz, 1997 pers. comm.
JD13	Darwin granite	Granite	**-2.8**	**0.709282359**	Crawford, 1997 pers. comm.
TO4137	Murchison Granite	Granite	**-4.7**	**0.709782831**	Crawford, 1997 pers. comm.
AR1	Tyndall Group	?	**-4.7**	0.709829878	Crawford, 1997 pers. comm.
AR4	Tyndall Group	?	**-5.0**	0.710386573	Crawford, 1997 pers. comm.
W93	Queenstown Reservoir	Andesite	**0.0**	0.708536276	Crawford, 1997 pers. comm.
M189	Crown Hill	Andesite	**-2.2**	0.708707651	Crawford, 1997 pers. comm.
Z632	Crown Hill	Hnbl. Andesite	**-0.2**	0.708272923	Crawford, 1997 pers. comm.
HR23	Halls Rivulet	Andesite	**-5.8**	0.715336688	Crawford, 1997 pers. comm.
39233	Mt.Lyell	Andesite	**-1.6**	0.709355803	Crawford, 1997 pers. comm.
AR6	?	Hnbl. Andesite	**-0.7**	0.708797065	Crawford, 1997 pers. comm.
Y75	Yolande River	Felsic porph.	**-7.7**	0.699719738	Stoltz, 1997 pers. comm.
Z488	Western Volc. Seq.	Rhyolite porph.	**-8.5**	0.723061812	Stoltz, 1997 pers. comm.
109452	Prince Lyell Apatite-Magnetite veins	Apatite	**-3.54**	0.708979	Stoltz, 1997 pers. comm.
109454	Prince Lyell Apatite-Magnetite veins	Apatite	**-4.14**	0.70901	Stoltz, 1997 pers. comm.
Garfield	Garfield Apatite-Magnetite veins	Apatite	**-1.2**		Halley, 1996 pers. comm.
Garfield	Garfield Apatite-Magnetite veins	Apatite	**-1.3**		Halley, 1996 pers. comm.

Sample Number	Unit/Location	Rock Type	epsilon Nd (init)CHUR	87Sr/86Sr (T=initial)	Refrence
GS-7	Darwin granite	Granite	**-4.99**	**0.703293**	Stoltz, 1997 pers. comm.
JD13	Darwin granite	Granite	**-2.8**	**0.709282359**	Crawford, 1997 pers. comm.
TO4137	Murchison Granite	Granite	**-4.7**	**0.709782831**	Crawford, 1997 pers. comm.
AR1	Tyndall Group	?	**-4.7**	0.709829878	Crawford, 1997 pers. comm.
AR4	Tyndall Group	?	**-5.0**	0.710386573	Crawford, 1997 pers. comm.
W93	Queenstown Reservoir	Andesite	**0.0**	0.708536276	Crawford, 1997 pers. comm.
M189	Crown Hill	Andesite	**-2.2**	0.708707651	Crawford, 1997 pers. comm.
Z632	Crown Hill	Hnbl. Andesite	**-0.2**	0.708272923	Crawford, 1997 pers. comm.
HR23	Halls Rivulet	Andesite	**-5.8**	0.715336688	Crawford, 1997 pers. comm.
39233	Mt.Lyell	Andesite	**-1.6**	0.709355803	Crawford, 1997 pers. comm.
AR6	?	Hnbl. Andesite	**-0.7**	0.708797065	Crawford, 1997 pers. comm.
Y75	Yolande River	Felsic porph.	**-7.7**	0.699719738	Stoltz, 1997 pers. comm.
Z488	Western Volc. Seq.	Rhyolite porph.	**-8.5**	0.723061812	Stoltz, 1997 pers. comm.
109452	Prince Lyell Apatite-Magnetite veins	Apatite	**-3.54**	0.708979	Stoltz, 1997 pers. comm.
109454	Prince Lyell Apatite-Magnetite veins	Apatite	**-4.14**	0.70901	Stoltz, 1997 pers. comm.
Garfield	Garfield Apatite-Magnetite veins	Apatite	**-1.2**		Halley, 1996 pers. comm.
Garfield	Garfield Apatite-Magnetite veins	Apatite	**-1.3**		Halley, 1996 pers. comm.

Background alteration in the Mount Black Volcanics: textures, mineralogy and geochemistry.

by Cathryn Gifkins
Centre for Ore Deposit Studies, Geology Department, University of Tasmania

Summary

All units of the Mount Black and Sterling Valley Volcanics have been variably modified by the combined effects of different alteration styles. The most common alteration assemblages within the volcanics are, silicification, feldspar ± quartz, sericite, sericite-chlorite ± carbonate ± quartz, carbonate, chlorite, chlorite-epidote ± carbonate and sphene. The wide distribution of many of these alteration styles and the remote location from known mineralisation suggests that these alteration assemblages are the product of regional processes rather than focussed hydrothermal events associated with mineralisation.

Background or regional style alteration is not a blanket style alteration. Instead regional processes produce a complex pattern of overlapping alteration styles and intensities. The distribution of alteration styles and their intensities is partly controlled by the geochemical signature and the permeability of the rocks. Mafic volcanic units tend to undergo alteration to more mafic assemblages which include chlorite and epidote while more felsic units are altered dominantly by sericite, feldspar and to a lesser extent chlorite. Ultimately the permeability is related to both the texture and the chemical stability of a rock. In a pile of glassy volcanic rocks the texture and hence porosity can vary considerably over a short distance due to both the primary volcanic textures and the post-depositional modification of these textures.

The complex and discontinuous nature of an originally glassy silicic volcanic pile like the Mount Black Volcanics has resulted in the patchy distribution of the different regional alteration facies. An individual unit with a constant primary geochemical signature may have vastly different primary volcanic, devitrification and hydration textures. Post-depositional alteration may highlight these textural differences. For example fracture controlled polyphase feldspar-quartz and chlorite-sericite alteration occurs in the dense perlitic core of a rhyolite flow. In the flow-banded margin of the flow individual bands are dominated by feldspar-quartz or sericite-chlorite alteration. In deposits where the margins are highly vesicular or pumiceous the sericite-chlorite altered bands have undergone subsequent compaction. The associated rhyolitic hyaloclastite at the flanks and top of the flow are much more strongly altered. Feldspar-quartz, sericite-chlorite, chlorite and carbonate assemblages are all commonly present. The patchy distribution of these alteration phases may result in an apparently polymictic volcaniclastic breccia.

Introduction

This study is intended to characterise the background alteration textures, mineralogy and chemistry related to regional scale processes in the volcanic pile remote from the ore in a massive sulphide district. Glassy volcanic rocks typically undergo a complex and diverse history of post-depositional modification which involves both wide spread regional processes as well as smaller focussed processes such as mineralising hydrothermal cells.

Textural changes begin immediately after eruption from the magma chamber. Emplacement or depositional processes may produce distinctive textures such as flow-banding, autobrecciation in coherent

deposits and grading, bedding or welding in clastic deposits. Post deposition processes such as devitrification and hydration effect the texture of the volcanic glass producing spherulites, lithophysae, micropoikolitic texture (snowflake texture) and perlitic fractures. These primary and secondary volcanic textures may be accentuated or obscured by later changes. The later post-depositional processes commonly affect not only the texture but the mineralogy and chemistry. Devitrification, hydration, hydrothermal and diagenetic alteration, burial and compaction, tectonic deformation and metamorphism have all acted to modify the primary facies. Each process is influenced by the existing deposit texture and mineralogy but also modifies and overprints this. Thus the texture, mineralogy and geochemistry of volcanic rocks evolves by a series of steps, however the steps are not necessarily discrete and many overlap making the recognition of individual phases complicated. The result of this series of alteration processes operating is often a complex pattern of two or more phase alteration assemblages which may enhance or destroy pre-existing textures in the volcanic rock.

Although regional scale or background alteration does not generally involve as large deviations in the chemical signature as alteration related to hydrothermal systems associated with mineralisation, it is significant, complex and texturally diverse. By studying the style and amount of textural and mineralogical changes in the rocks of the Mount Black Volcanics, away from known mineralisation, we are assuming that these changes cannot reasonably be related to the mineralising episode.

Regional geology and stratigraphy

The rocks of the Mount Black and Sterling Valley Volcanics compose a significant part of the northern Central Volcanic Complex (CVC), in the Mount Read Volcanic Belt. They unconformably overlie the Rosebery–Hercules sequence to the west and are truncated by the Henty Fault zone to the east. Regionally the Mount Black Volcanics represent a large open syncline. The western or upper most part of the Mount Black Volcanics and the Rosebery–Hercules sequence form the eastern limb of the adjacent anticline to the west. This NNE trending regional anticline extends for 20 km from Hercules in the south to Pinnacles in the north. The Sterling Valley Volcanics occur in the core and on the western limb of a regional anticline which extends from the north of Mount Block and is truncated to the south by the Henty Fault.

The local stratigraphy to the Hercules and Rosebery mineralisation has been divide from base to top by Allen (1991, 1993, 1994) (Fig. 1a) into; i) footwall pyroclastics which are dominated by very thick feldspar-phyric, pumice-rich, mass flow units with minor massive dacite and autoclastic breccias, ii) "host rock" or transitional stratified volcaniclastics that are composed of bedded siltstones and tuffaceous sandstones, iii) black slate and iv) hangingwall epiclastics which are massive thick-bedded quartz and feldspar, crystal-, lithic-, and pumice-rich volcaniclastic sandstones and breccias.

The Mount Black Fault separates the quartz-phyric volcaniclastic mass-flow units of the Rosebery–Hercules Hangingwall from the Mount Black Volcanics. The original stratigraphic relationship between the Mount Black Volcanics and the Rosebery–Hercules hangingwall is uncertain.

The Mount Black Volcanics are a several kilometre thick package of feldspar-phyric massive, flow-banded and flow-brecciated lavas and sills of generally rhyolitic to dacitic composition with minor andesite. Variable proportions of lithic and/or pumice-rich volcaniclastic breccias, shard-rich sandstones and siltstones, and crystal-rich sandstones are interbedded with, or intruded by the more coherent units. The facies distribution and contact relationships are quiet complex reflecting the large volume of laterally discontinuous high relief lava domes and the high proportion of lava-like intrusive bodies. These intrusions are interpreted to be shallow sills which were coeval with the continuing volcaniclastic activity and extrusion of lavas. The lavas and intrusions have similar mineralogy, geochemistry and primary volcanic textures and are best differentiated based on their contact relationships. Establishing a stratigraphy for the Mount Black Volcanics is made more complicated by the lack of thick laterally continuous clastic units that may be used as marker horizons.

Stratigraphically at the top of the Mount Black Volcanics the facies are dominated by flow-banded and brecciated rhyolite lavas and pumice-rich rhyolitic breccias intruded by thick feldspar porphyritic dacitic sills (Fig. 1b). Below this the volcanics are dominated by massive red-brown to grey feldspar±hornblende porphyritic dacitic to andesitic and less commonly rhyolitic lavas, sills and thick piles of autoclastic debris.

Conformably underlying the Mount Black Volcanics to the east is a package of basaltic to dacitic volcanics, locally known as the "Sterling Valley Volcanics" (Fig. 1b). These are composed of numerous monomict and polymict basaltic to andesitic mass-flow breccias, basaltic to dacitic lavas and sills, laminated basaltic sandstones and rare tuffaceous siltstones. The Sterling Valley Volcanics and Mount Black Volcanics are in stratigraphic contact and appear to petrographically and chemically related.

Summary of main lithofacies

The characteristics of the main facies, their facies associations and alteration styles within the Mount Black and Sterling Valley Volcanics are summarised in Table 1. For more detailed descriptions of the lithofacies see Gifkins et al (1996a). The following brief descriptions are accompanied by Plates 1 to 6, that show some of the main textural and alteration characteristics of the lithofacies.

Feldspar porphyritic rhyolite to rhyodacite lavas and sills are commonly massive to flow-banded and flow-brecciated (Plate 1a, b, f). The rhyolites typically have 3–10% euhedral plagioclase phenocrysts of 1–2 mm in diameter but can also be aphyric. The plagioclase phenocrysts often form glomero-porphyritic aggregates in a siliceous groundmass with interstitial carbonate and chlorite. Internal primary volcanic and devitrification textures include; perlitic fractures, snowflake or micropoikolitic textured groundmass, spherulite-rich flow-bands, densely microspherultic groundmass or amygdales. The presence of spherulites and micropoikolitic textures which are the product of high temperature devitrification indicate that the rhyolites were originally coherent volcanic glass (Lofgren, 1971 and McPhie et al, 1993). The margins of many of the flow-banded rhyolites and rhyodacites contain highly vesicular or pumiceous bands which have undergone strong compaction and phyllosilicate alteration producing chlorite-rich foliated bands and lenses. The contacts may be marked by peperite textures, inclusions of fine grained siltstone which have mixed with the lava as it flowed over or intruded into wet sediment (Plate 1g).

Associated with many of the rhyolites and rhyodacites are **feldspar-phyric autobreccias and hyaloclastite.** Flow breccias and hyaloclastite are syn-eruptive volcaniclastic deposits formed by non-explosive fragmentation processes, flow-brecciation and quench fragmentation respectively. Fragmentation occurs at the margins of moving lavas, domes and sills and less commonly may form bands within a individual coherent unit. Deposits of hyaloclastite are recognised on the basis of curviplanar clast margins which are typical of quench brecciation (Pichler, 1965). The blocks produced by flow brecciation and quenching may be enclosed within the non-fragmented magma, deposited on the flanks of a moving flow, or are free to be redeposited by sedimentary processes.

The deposits are typically monomicitic, massive, poorly sorted and vary from matrix supported aggregates of rotated clasts to clast supported breccias with jigsaw fit textures. Although the clasts are often genetically related they may have a variety of internal textures. These breccias may be composed of dense originally glassy fragments, that now contain perlitic fractures, spherulites or are vesicular (Plate 2a, b, d, e, f). A range of fine banded clasts vary from pumiceous to flow-banded. This variation in vesiculation and the association with vesicular coherent facies suggests that many of these pumiceous clasts were not derived from a large explosive eruption but are the product of autoclastic fragmentation of the more vesicular or pumiceous margins of the flow or sill (Fink and Manley, 1987, Gifkins et al., 1996b). However, not all the pumice lithic breccias can be related to effusive volcanism. Some lithic-rich pumice breccias are interpreted to be the down slope redeposition of pyroclastic tube pumice deposits and dense glassy lava debris. The pumice clasts are both compacted and uncompacted.

Feldspar-quartz porphyritic rhyolite sills are thick, massive, densely microspherultic feldspar-

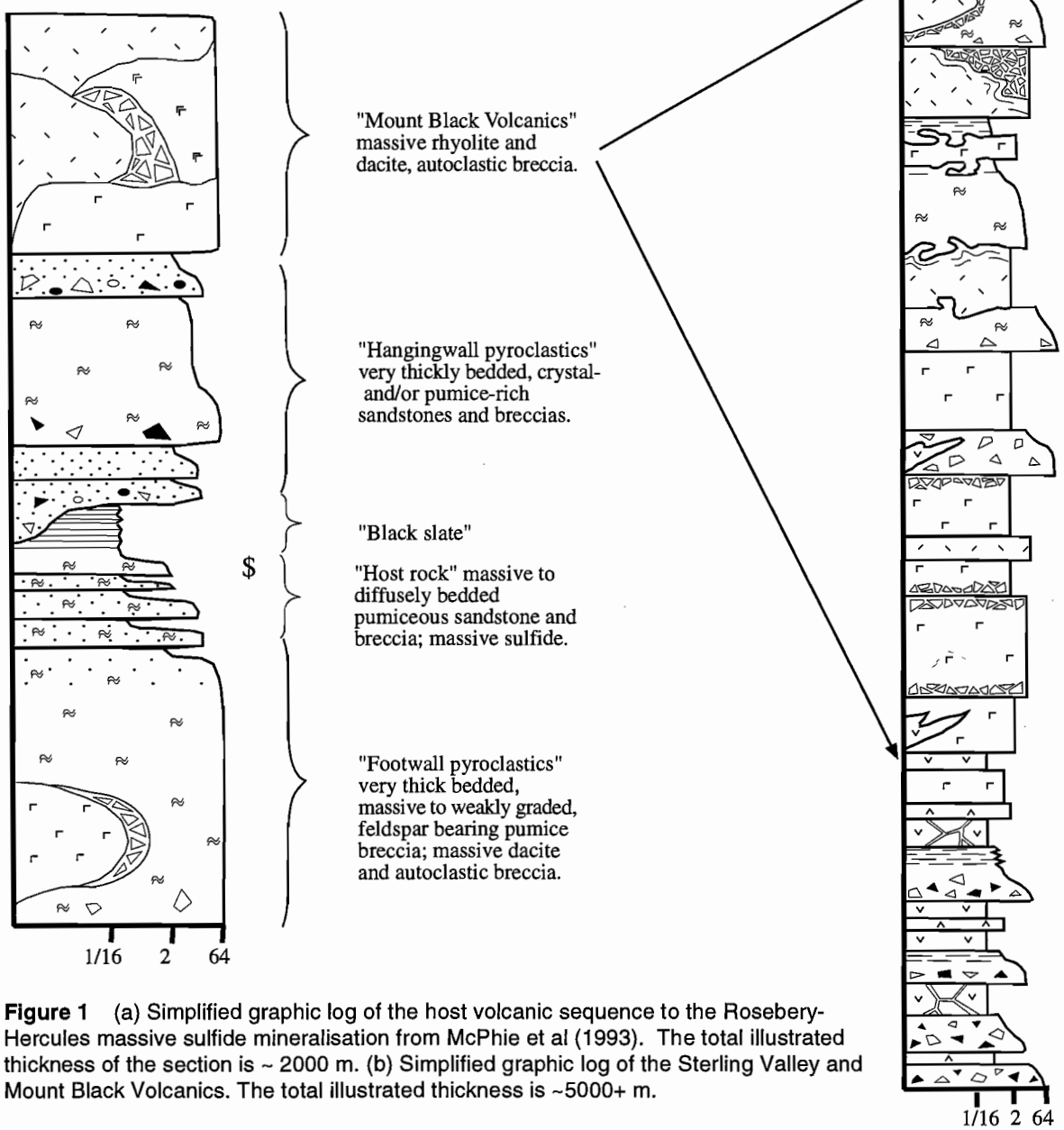

Figure 1 (a) Simplified graphic log of the host volcanic sequence to the Rosebery-Hercules massive sulfide mineralisation from McPhie et al (1993). The total illustrated thickness of the section is ~ 2000 m. (b) Simplified graphic log of the Sterling Valley and Mount Black Volcanics. The total illustrated thickness is ~5000+ m.

quartz porphyritic units that occur at random positions in the stratigraphy. They generally contain 5–10%, 1–2mm total crystals.

Rhyolitic feldspar-phyric pumice-rich breccias, sandstones and siltstones are dominated 3–10%, 2mm plagioclase porphyritic pumice, plagioclase crystal fragments and shards (Plate 3). They also contain rare dense volcanic clasts that occur largely towards the base of the thick normally graded units. The dense volcanic lithic clasts were originally glassy and include perlitic glass, spherulitic and flow-banded to massive plagioclase porphyritic and aphyric rhyolite. In handspecimen the breccias contain dark phyllosilicate-rich lenticular patches, 1–5 cm long aligned roughly in the plane of regional bedding and are set in a paler feldspar-quartz rich domain. These lenses comprise of compacted pumice which resemble fiamme in welded ignimbrites. The quartz-feldspar domains contain relic uncompacted tube pumice. The pumice tubes are defined by sericitic alteration along the tubes while the glassy walls are replaced by feldspar (Plate 3d). The uncompacted nature of these pumices indicates that the deposits were originally non-welded and that the feldspar alteration occurred very early, prior to compaction. In areas of strong deformation the flattened tube pumices become stretched and transposed in the cleavage resulting in a foliated fabric which resembles eutaxitic texture in welded primary pyroclastic deposits (Allen, 1988; Plate 3b, c.

In outcrop the breccia deposits are normally graded with sharp bases and finely stratified tops suggesting deposition by mass flow. The sandstones are massive to diffusely bedded and may represent the tops of unrecognised pumice-rich breccias or reworked pumiceous deposits. The tuffaceous siltstones are commonly siliceous, pale grey to buff coloured and weakly laminated or cross bedded. Sedimentary structures within the siltstones are typical of turbidite deposits and indicate the below wave base environment of deposition for parts of the Mount Black Volcanics.

Feldspar crystal-rich sandstones are composed of predominantly euhedral and angular plagioclase crystal fragments and lesser proportions of broken quartz crystals, fine plagioclase porphyritic pumice clasts and dense glassy lithics. They contain feldspar crystal contents averaging 30 to 60%. In hand-specimen the distribution of the crystals appears uneven. They are commonly massive bodies up to tens of metres in thickness and are occasionally normally graded.

Feldspar porphyritic dacite lavas and sills are the dominant facies type in the Mount Black Volcanics. They are typically thick, massive, weakly vesicular, blocky and red-brown to grey-green in colour (Plate 4a, b). They can be aphyric but most commonly contain 0–25% 1–3 mm zoned euhedral plagioclase phenocrysts that often form glomero-porphyritic aggregates up to 5mm in diameter in the siliceous groundmass. The glomeroporphyritic clusters contain interstitial chlorite, magnetite, epidote and sphene and rarely carbonate. The groundmass is recrystallised granophyric and occasionally contains microspherulites or micro-poikolitic texture, but more commonly contains arcuate perlitic fractures (Plate 4h). The perlitic fractures are commonly highlighted by polyphase alteration where the fractures are defined by dark chlorite±epidote alteration while the unfractured cores are feldspar±quartz altered. The presence of both microspherulites and perlitic fractures reflect the originally glassy nature of the groundmass.

Feldspar-hornblende porphyritic dacite sills or lavas are massive, blocky, medium brown, with 10–30% total crystal content (Plate 5a). 1–2 mm euhedral plagioclase phenocrysts and 1 mm prismatic hornblende crystals, rare quartz and accessory sphene are present in a finer grained groundmass. The groundmass has a fine sandy texture reflecting the high density of microspherulites and/or micro-poikolitic quartz (Plate 5b). The feldspar-hornblende phyric dacites are occasionally flow-banded or contain flow aligned phenocrysts. Many of the feldspar-hornblende porphyritic dacites, particularly along Pieman Rd, contain fine arcuate perlitic fractures (Plate 5c, d).

Feldspar porphyritic andesitic and basaltic lavas and sills are massive, blue-green, with 5–20%, 2–2.5mm plagioclase and minor hornblende phenocrysts and abundant fine grained opaques. The dark groundmass is composed of interlocking needles of plagioclase and hornblende or actinolite ("felt textured") and is strongly pervasively altered by chlorite ± magnetite and epidote. The margins of lavas are commonly quench or flow fragmented and

Table 1 Characteristics of the main lithofacies, their facies associations and alteration styles within the Mount Black and Sterling Valley Volcanics. For more detailed descriptions of the lithofacies see Gifkins (1996).

FACIES	DISTRIBUTION	VOLCANIC TEXTURES	OTHER TEXTURES	ASSOCIATIONS	ALTERATION STYLES	ALTERATION TEXTURES
Fsp porphyritic rhyolite lavas and sills	western portion of MBV	massive, flowbanded, amygdaloidal, pumiceous, perlitic, spherulitic or micropoikolitic	compaction foliation in pumiceous or highly vesicular bands	flow-brecciated or quench brecciated volcaniclastic debris	ser, fsp, chl+bt,fsp+bt, ser+chl, CO_3, chl	pervasive, patchy, dominal, wispy, banded, fracture controlled, selective alteration of phenocrysts
Fsp>qtz porphyritic rhyolite sills	random with N-S orientation	massive, rarely flow-banded, denesly microspherultic or micropoikolitic			fsp+qtz	pervasive
Rhyolitic pumice breccias	western portion of MBV	massive to normally graded deposits of fsp porphyritic tube pumice clasts and fsp crystal fragments, rare dense lithics	compaction foliation, S_0 parallel styolites	graded and laminated pumiceous and shard-rich sandstones and siltstones	fsp+qtz, ser+chl, CO_3, ser, chl+bt	patchy, pseudo eutaxitic textures, chl+bt styolites
Rhyolitic lithic pumice breccias	western portion of MBV	feldspar phyric, massive and normally graded deposits of tube pumice and dense perlitic and spherulitic glassy clasts, fsp crystal fragments	compaction of pumiceous clasts	sometimes associated with an adjacent rhyolitic lava/sill which has a flow-banded and pumiceous margin	fsp+qtz, ser, ser+chl,	domainal flow-bands, patchy, clast selective, alteration rinds around clasts
Siltstones and sandstones	rare, throughout	dominately composed of juvenile volcanic material (shards, crystals, lithics) and rhyolitic to basaltic in composition.	laminations, grading and cross bedding, wispy lenses of compacted pumice clasts	commonly occurs as reworked top of a graded volcaniclastic breccia	ser+chl, ser, chl	pervesive, bedding controlled alteration
Fsp porphyritic dacite lavas and sills	wide spread throughout MBV	massive, densely mirospherultic or micropoikolitic, vesicular or perlitic		flow-brecciated or quench brecciated volcaniclastic debris	fsp+qtz, ser weak chl, ep	pervasive, fracture controlled, nucleated on spherulites or micropoikolitic quartz, selective alteration of plagioclase crystals
Fsp>hbl porphyritic dacite sills or lavas	wide spread throughout MBV	massive, densely microspherultic or micropoikolitic, more rarely perlitic and highly vesicular		rarely with pumiceous quench brecciated fsp-hbl porphyritic debris	fsp+qtz, ser+chl	pervasive, fracture controlled, selective replacement of phenocrysts
Aphyric andesites	Sterling Valley	massive		insitu hyaloclastite	chl+ep, fsp, ser+chl	fine grained massive alteration, rarely fracture controlled
Fsp±hbl porphyritic andesites	Sterling Valley and Sterling Saddle	massive, perlitic fractures, peperitic contacts			ser+chl, chl+ep, ser	pervasive or fracture controlled alteration
Basaltic lavas	Sterling Valley	massive, insitu quench fragmented, glassy fine grained margins			chl+ep±CO_3	pervasive
Mafic breccias	Sterling Valley	massive to graded with diffusely laminated tops, composed of angular blocky clasts of andesite ±(dacite, basalt and scoria) Clasts have glassy rinds and commonly perlitic		graded and diffusely laminated, coarse to fine grained mafic sandstones	chl+ep, chl+ser, chl, weak fsp	selective alteration of clasts, pervasive alteration of finer grained matrix
Fine to medium grained basaltic dykes (Henty dyke suite)	cross cutting stratigraphy east of the Mount Black Fault	massive, chilled margins, aphyric or fsp±px porphyritic, commonly weakly vesicular		strong chlorite alteration selvage	chl+ep+CO_3	pervasive

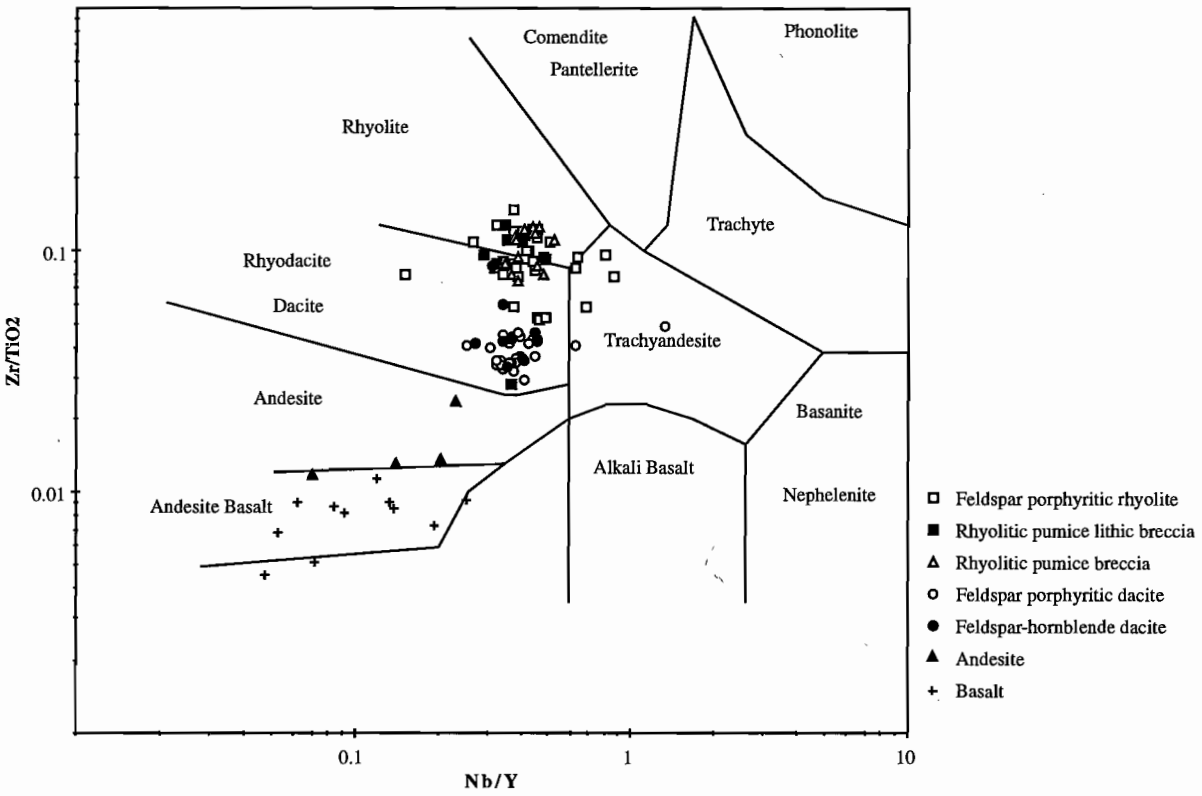

Figure 2 Discrimination diagram of Nb/Y versus TiO_2 for the Mount Black and Sterling Valley Volcanics (after Winchester and Floyd, 1977). This depicts the composition of the main lithofacies.

Plate 1: Feldspar porphyritic rhyolites.

a) Sample 039799 from DDH 120R. This is a sample of least altered, massive, 15% feldspar porphyritic rhyolite. Weak pervasive feldspar alteration of the groundmass and weak selective sericite alteration of the feldspar phenocrysts is evident in handspecimen.

b) Sample R17 from Mount Black summit, is a finely flow-banded, 15% feldspar porphyritic rhyolite. Individual flow-bands are feldspar-quartz altered or sericite-chlorite altered. Some of the sericite-chlorite altered bands were originally highly vesicular or pumiceous and have been compacted.

c) Sample PR9 from the Pieman Rd, is a massive, densely microspherulitic, 5% feldspar prophyritic rhyolite. A fine sandy texture in handspecimen suggests that the groundmass might be either densely microspherulitic or micropoikolitic. Pervasive, moderate pink, feldspar-quartz alteration.

d) Sample 039789 from DDH 120R, is a massive, perlitic, 2% feldspar porphyritic, rhyolitic insitu hyaloclastite. Intense, pink, feldspar alteration destroys the primary volcanic textures, however in areas of chlorite alteration the perlitic texture can still be recognised.

e) Sample 039749 from DDH 128Ris a massive, 8% feldspar porphyritic, perlitic, rhyolite. Patchy pink feldspar-quartz alteration and green-grey sericite-chlorite alteration are partly controlled by perlitic fracture.

f) Sample 039715 from DDH 128R. This 5% feldspar porphyritic, rhyolitic, autoclastic breccia contains angular blocky clasts of feldspar porphyritic and aphyric rhyolite and wispy pumice clasts in a finer grained matrix. The matrix is altered to patchy feldspar-sericite. Feldspar alteration haloes exist around the blocky rhyolite clasts. The pumice and dense glassy rhyolite clasts are selectively chlorite or feldspar-chlorite altered.

g) Sample 039704 from DDH 128R is a 5% feldspar phyric, blocky, rhyolitic, peperite with strong carbonate alteration. The intense carbonate alteration occurs in the sediment component of the peperite and as alteration fronts progressing outwards into the dark coherent feldspar phyric rhyolite. The feldspar crystals are replaced by carbonate that is dusted with green sericite.

h) Sample 039725 from DDH 128R is a massive, 20% feldspar porphyritic rhyolite. Pervasive moderate sericite-chlorite alteration in this sample destroys many of the primary volcanic textures, however the porphyritic nature is still evident. The feldspar phenocrysts are weakly, secondary pink, feldspar altered.

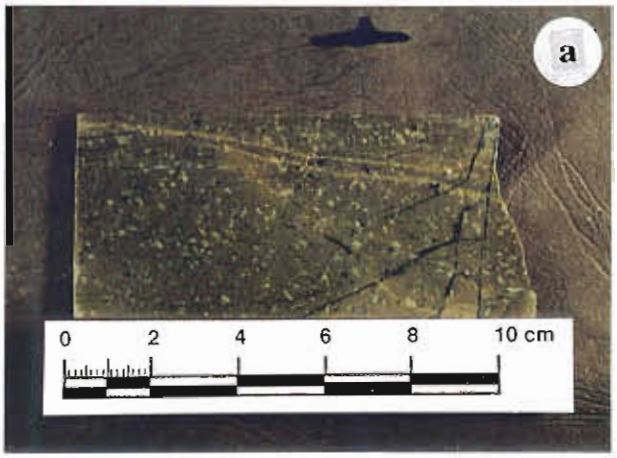
a
0 2 4 6 8 10 cm


b
0 2 4 6 8 10 cm


c
0 2 4 6 8 10 cm


d
0 2 4 6 8 10 cm

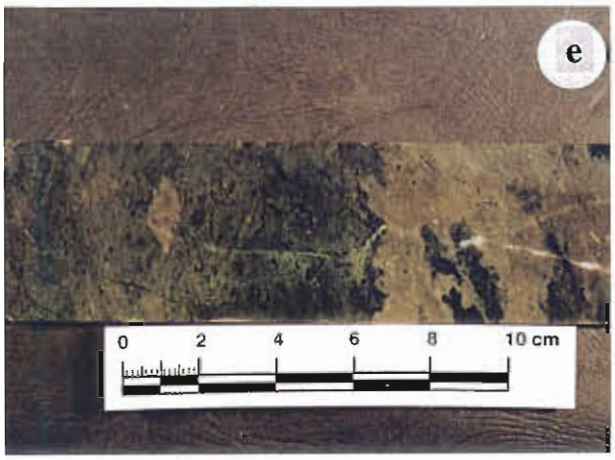
e
0 2 4 6 8 10 cm


f
0 2 4 6 8 10 cm


g
0 2 4 6 8 10 cm


h
0 2 4 6 8 10 cm

Plate 2: Feldspar phyric, rhyolitic, pumice bearing lithic breccias.

a) This photograph of a finely flow-banded rhyolitic autobreccia outcrop comes from the eastern flank of Mount Read. The breccia is massive, poorly sorted and clast supported. The blocky angular, flow-banded clasts can be seen at high angles to one another on the weathered surface of the outcrop.

b) Sample PR26 is a massive, glassy rhyolitic breccia from the Pieman Rd. This breccia is poorly sorted and clast supported. It is composed of abundant originally glassy rhyolite clasts that have classical and ladder perlite fractures. Many of the clasts are vesicular to pumiceous. All the clasts in this sample are interpreted to be the product of quench fragmentation of a rhyolitic dome which was extruded onto the seafloor. The massive, poorly sorted and clast supported nature of the outcrop is consistent with the clasts having been redeposited only a short distance down slope. Sericite ± chlorite alteration is pervasive, while patchy and selective white to pale pink feldspar-quartz alteration highlights many of the larger clasts. This two phase alteration assemblage gives the sample the appearance of being a polymictic, matrix supported breccia.

c) From left to right samples 039783-039782-039790-039792 from DDH 120R are variably altered rhyolitic, pumice lithic breccia. These samples represent part of a thick, normally graded mass flow deposit. 039783 is dominated by pervasive sericite and lesser white feldspar alteration. The other samples show increasing pink feldspar alteration and decreasing sericite from left to right. Rare dark chlorite-rich lenses or fiamme are also evident.

d) This sample from DDH 78R at 174.3m is a 7% feldspar phyric, rhyolitic, pumice-rich lithic breccia. Strong domainal pink feldspar and chlorite-sericite alteration are prominent. The darker chlorite-sericite altered clasts or domains are clearly feldspar porphyritic, while the feldspar alteration has destroyed the porphyritic texture.

e) Sample R112 (x2.5 PPL). This is a photomicrograph of rhyolitic pumice-rich lithic breccia from the southern side of Mount Black. In the photomicrograph number of angular perlitic clasts, feldspar crystal fragments and chlorite-sericite altered vesicular fragments can be recognised. The finer grained clasts which compose the matrix are dominantly pervasively sericite ± feldspar altered while the large dense originally glassy fragments are feldspar-quartz altered.

f) Sample 039711 from DDH 128R is a 10% feldspar phyric, finely flow-banded autoclastic rhyolite breccia. The dense blocky rhyolite clasts are massive porphyritic and flow-banded. Domainal feldspar-quartz and sericite-chlorite alteration highlights the crystalline and glassy bands in the clasts. Massive clasts are generally feldspar-quartz altered and the finer grained matrix is strongly sericite±chlorite altered. The feldspar phyric nature of the matrix is easily recognised in the sericitic domains.

g) Sample R30 is from the Mount Black summit area (x1.5, PPL). This photomicrograph captures the insitu flow-brecciation of a finely flow-banded, weakly feldspar porphyritic rhyolite. Pervasive feldspar-quartz alteration.

h) Sample 039783 is from DDH 120R (x2.5, PPL). The photomicrograph of variably vesicular clasts is from a sample of rhyolitic pumice-rich lithic breccia. At the base of the photograph is a dense perlitic rhyolite clast. Above this are moderately vesicular and highly vesicular rhyolite clasts. The vesicle walls are defined by a fine dusting of sericite or opaques. The dense clasts and glassy vesicle walls are feldspar-quartz altered, although some of the more pumiceous clasts show patchy phyllosilicate alteration.


a


b
PR26
0 2 4 6 8 10 cm


c


d
0 2 4 6 8 10 cm

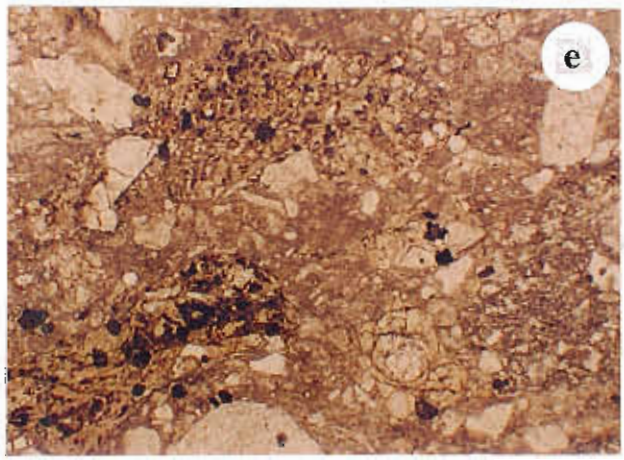
e


f
0 2 4 6 8 10 cm


g


h

Plate 3: Feldspar phyric, rhyolitic, pumice-rich breccias.

a) Sample PR6 from the Pieman Rd is a feldspar phyric tube pumice breccia. Strong pink feldspar alteration and patchy chlorite-sericite alteration dominate the sample. Pumice in the feldspar-rich domains are uncompacted, while pumice in the chlorite-sericite altered domains have undergone compaction and are crenulated by the later regional cleavage. The orientation of the chlorite-sericite rich lenses or fiamme can be used to determine the bedding parallel compaction foliation.

b) Sample 039717 from DDH 128R. This rhyolitic pumice breccia has strong domainal feldspar and sericite-chlorite alteration more typical of the pumice breccias. The dark phyllosilicate-rich lenses or fiamme are clearly feldspar phyric and define a foliation at low angle to the core.

c) Sample EHP319 538.6m is from a very thick pumice-breccia to the east of south Hercules. This rhyolitic pumice breccia has large uncompacted pink-white fibrous tube pumices which can be seen without a handlens. The pink feldspar alteration is associated with disseminated magnetite and dark chlorite-rich fiamme and is similar to many of the pumice breccias observed away from the ore environment in the Rosebery and Hercules footwall.

d) Sample EHP319 538.6m (x1.5, PPL). This photomicrograph shows well preserved feldspar altered tube pumices at high angles to one another. The tubes are defined by fine sericite, while the glassy walls are composed of fine granophyric feldspar and quartz. The primary plagioclase crystals are replaced by chlorite.

e) Sample 039720 from DDH 128R is an example of the fine grained stratified top of the thick normally graded rhyolitic pumice breccias. The laminations are discontinuous, have uneven thicknesses and are typically variably altered.

f) Sample 039796 from DDH 120R. This is a handspecimen of fine grained laminated shard-rich siltstone. Shards are well preserved in the feldspar-quartz altered domains, however only the feldspar phyric nature of the deposit can be recognised in the more sericite-chlorite rich domains.

g) Sample 039796 from DDH 120R (x5, PPL). This photomicrograph is from the feldspar-quartz altered domain in the top right-hand corner of the previous photograph. It shows well preserved feldspar altered, angular shards in fine grained mosaic of feldspar-quartz-sericite.

h) Sample PR11 from the Pieman Rd (x5, PPL). In this photomicrograph patchy chlorite and carbonate rhombs are replacing the originally feldspar altered shards in the groundmass of a pumice breccia. The feldspar-quartz altered shards are hosted within a fine grained matrix of feldspar, quartz and sericite.


a
0
2
4
6
8
10


b
0
2
4
6
8
10 cm


c
0
2
4
6
8
10 cm

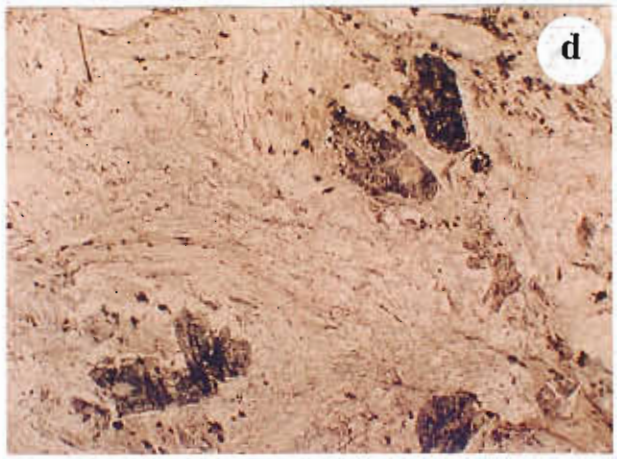
d


e
0
2
4
6
8
10 cm


f
0
2
4
6
8
10 cm

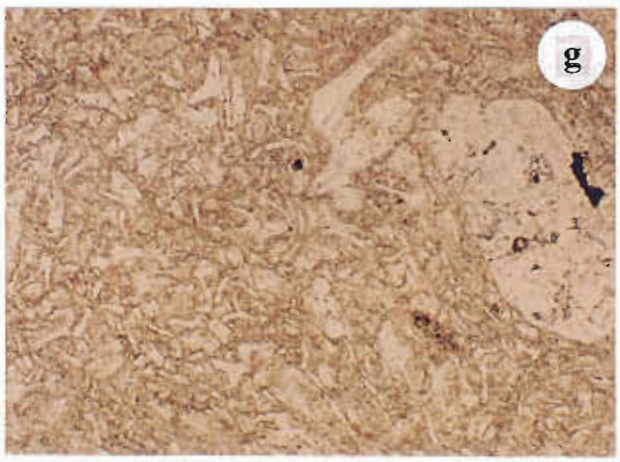
g


h

Plate 4: Feldspar porphyritic, dacite lavas and sills.

a) Sample M67 from the Murchison Highway is an example of the most voluminous lithofacies in the Mount Black Volcanics. This massive feldspar porphyritic dacite is considered to be one of the least altered rocks in the Mount Black Volcanics. Pervasive weak feldspar alteration of the groundmass is overprinted by weak fracture controlled chlorite alteration.

b) Sample PR17 from the Pieman Rd is a typical massive weakly feldspar porphyritic sill of the Mount Black Volcanics. This sample has a fine grained micropoikolitic textured groundmass and is weakly pervasively red-brown secondary feldspar altered.

c) These samples from DDH 112R at 358.9m and 363.1m respectively are from the base of a dacitic lava flow. The upper sample in the photograph is finely brecciated. The clasts have fine grained chilled margins and curviplanar edges typical of quench fragmentation. The sample has been interpreted as insitu hyaloclastite at the base of a lava flow which has extruded into the water. The second sample is a peperitic mixture, of dacite lava clasts and pumiceous sandstone, at the very base of the flow. Clasts of the underlying pumiceous sediments have been incorporated into the base of the flow as it travelled along the wet unconsolidated sediments on the seafloor.

d) Sample M90 from the Murchison Highway south of Mount Black, is a typical crystal-rich feldspar porphyritic dacite of the Mount Black Volcanics. The groundmass of this sample is moderately pervasively chlorite altered. The feldspar phenocrysts are largely pristine.

e) Sample PR51 from the Pieman Rd is an example of the more variable alteration that occurs in some of the coherent originally glassy dacites. Fine perlitic fractures in the groundmass of this sample have acted as permeable pathways for fluid during alteration. Perlitic fractures have increased the porosity of the coherent dacite and this is reflected by the complex, overprinting, feldspar, sericite and chlorite-rich alteration phases.

f) These four samples of a massive sandy dacite are from DDH 80R between 351 m and 394 m. This photograph illustrates the variety of alteration assemblages that commonly pervasively alter the massive dacites. From left to right the alteration styles are; weak feldspar-sericite, moderate feldspar-quartz, mottled pink feldspar and chlorite and moderate sericite accompanied by chlorite-magnetite replacement of the feldspar phenocrysts.

g) Sample PR56 from the Pieman Rd is an example of strong domainal two phase alteration in a coherent perlitic dacite. This dacite has a fine perlitic fractures throughout the groundmass and abundant curviplanar fractures which define blocky clasts. The deposit is interpreted to be an insitu quench breccia. The distribution of the two phases of alteration; red feldspar-quartz and dark green epidote-chlorite; has been controlled by the quench fracture pattern.

h) The photomicrograph of PR1 (x2.5, PPL) is dominated by fine arcuate overlapping perlitic fractures, that are highlighted by fine grained sericite. The perlite cores are feldspar-quartz altered..


a
0 2 4 6 8 10 cm


b
0 2 4 6 8 10 cm


c
0 2 4 6 8 10 cm

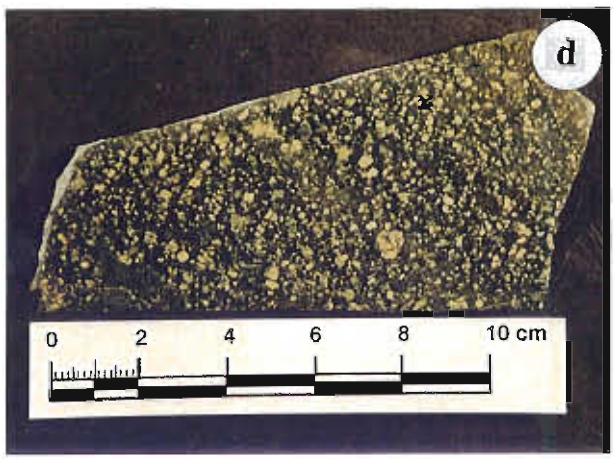
d
0 2 4 6 8 10 cm

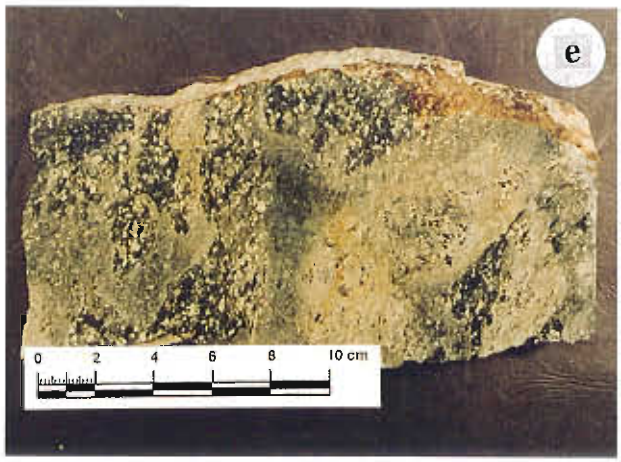
e
0 2 4 6 8 10 cm


f
0 2 4 6 8 10 cm


g
0 2 4 6 8 10 cm


h

Plate 5: Feldspar-hornblende porphyritic dacites and basaltic dykes of the Henty Dyke Swarm.

a) Sample PR58 from the Pieman Rd is an example of coherent, massive, feldspar-hornblende porphyritic dacite of the Mount Black Volcanics. The groundmass is weakly feldspar altered and the hornblende phenocrysts are replaced by chlorite-epidote.

b) Photomicrograph of the densely spherulitic groundmass of a massive dacite. Radiating fibres of feldspar and quartz exhibit radial extinction patterns. The spherulites are partly recrystallised and are dusted with fine grained sericite. Sample 040612 (x2.5, crossed polars).

c) Sample PR57 from the Pieman Rd is a massive, perlitic, feldspar-hornblende porphyritic dacite with fracture controlled polyphase alteration. The two dominant alteration facies are; red feldspar-quartz and dark green chlorite-epidote. The alteration is controlled by fine perlitic fractures in the groundmass.

d) The photomicrograph of sample PR57 covers both a feldspar-quartz rich domain on the left side of the photograph and a chlorite-epidote rich domain on the right side. No textures are evident in the strongly feldspar altered domain, however perlitic fractures are recognisable near the middle of the photograph in the chlorite-epidote domain. The feldspar phenocrysts are becoming progressively replaced by chlorite and epidote along the crystal cleavage.

e) Sample 039712 is a fine grained, weakly vesicular basaltic dyke of the Henty Dyke Suite. The right hand side of the photograph shows a fine grained sheared intrusive contact. The white spots are carbonate filled amygdales. The basaltic dyke is strongly chlorite-epidote-carbonate altered.

f) Photomicrograph of M39, a basaltic dyke similar to 039712, on the Murchison Highway near Sterling saddle. It is a fine grained, weakly feldspar porphyritic basalt. The feldspar phenocrysts are zoned and altered to chlorite-epidote. The groundmass is a mass of fine interlocking needles of feldspar, pyroxene, chlorite and epidote. The brown-green chlorite patches in the top of the photomicrograph are elongated chlorite filled amygdales. (x5, PPL).

g) Sample 040631 is of one of the coarser grained basaltic dykes of the Henty Dyke Suite. The white patches are feldspar phenocrysts and the dark blebs are round chlorite filled amygdales. The groundmass is pervasively chlorite-epidote altered and this is overprinted by pink feldspar bearing veins.

h) Photomicrograph of sample M42, a coarse grained basaltic dykes. (x5, PPL).


a
0 2 4 6 8 10 cm


b


c

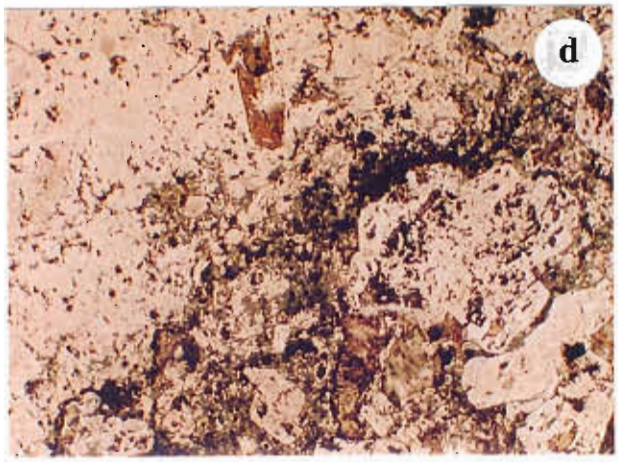
d


e

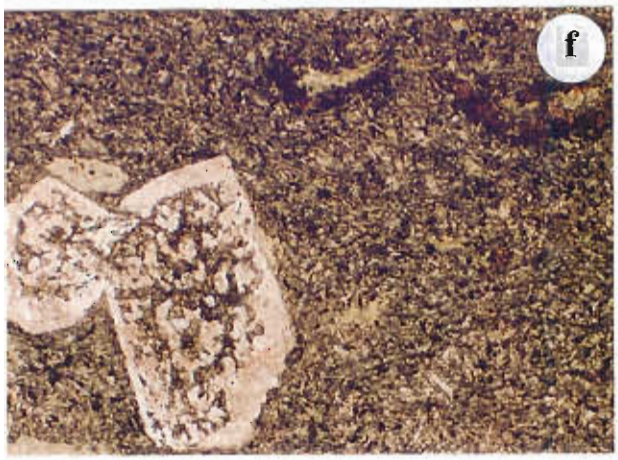
f

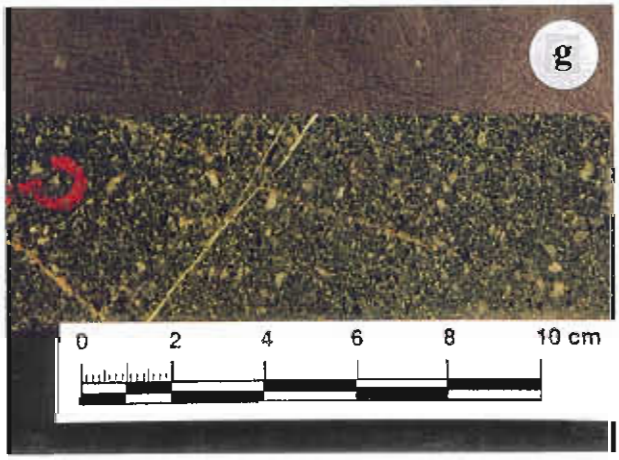
g
0 2 4 6 8 10 cm

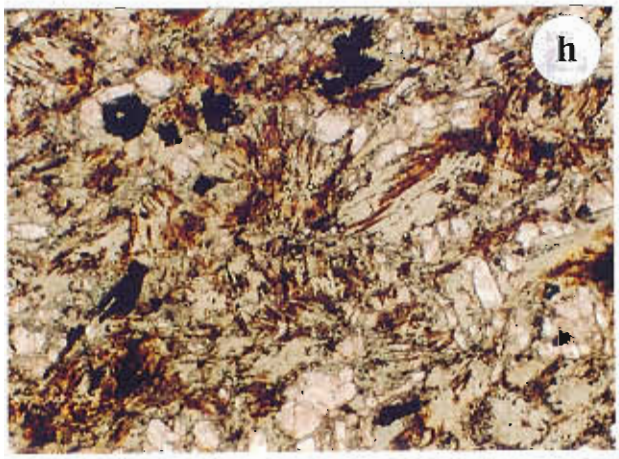
h

Plate 6: Mafic breccias, andesitic and basaltic lavas and sills of the Sterling Valley Volcanics.

a) This sample from DDH STP218 at 85.5 m in the Sterling Valley is typical of the polymictic mafic breccias. It is from a poorly sorted, clast supported normally graded unit. The sample is composed of blocky, angular, feldspar porphyritic dacitic to basaltic clasts that have curviplanar margins typical of quench fragmentation. The alteration style is characterised by pervasive chlorite-sericite-epidote.

b) Photomicrograph of the same mafic breccia ("as above") is from STP218 at 113.6 m. In thin section a number of trachytic basalt clasts, fine massive andesite clasts, perlitic glassy dacite fragments and feldspar crystals can be recognised. (x1.5, PPL).

c) This sample from DDH STP 218 at 127 m is a medium grained, poorly stratified, mafic sandstone.

d) Sample M9, from the Murchison Highway, is typical of the feldspar-hornblende porphyritic andesites of the Mount Black and Sterling Valley Volcanics. It is coarse grained massive and pervasively chlorite-sericite-epidote altered.

e) Photomicrograph of massive feldspar-hornblende porphyritic andesite from DDH STP 218 at 16.5 m. (x1.5, PPL).

f)Sample M6, from the Murchison Highway near the Henty Fault Zone, is an example of a massive, fine grained, aphyric andesite. The alteration is pervasive chlorite-epidote.

g) Sample M7, from the Murchison Highway, is a typical Sterling Valley lava, a medium grained feldspar porphyritic basaltic lava. The margin in the upper left of the sample is fine grained and perlitic. The groundmass is strongly chlorite altered.

h) This sample of a fine grained basalt in DDH STP 234 at 129.4 m is massive and strongly chlorite-epidote altered giving it a similar appearance to the Henty dyke basalts however reworking and quench fragmentation at the top of the deposit indicate the extrusive origin of this basaltic lava.


a
0 2 4 6 8 10 cm

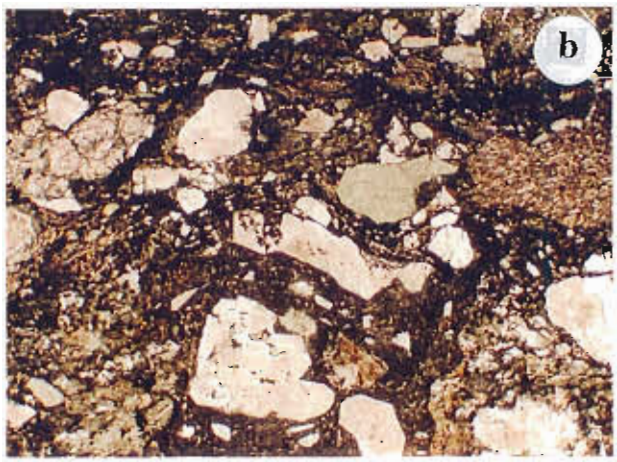
b

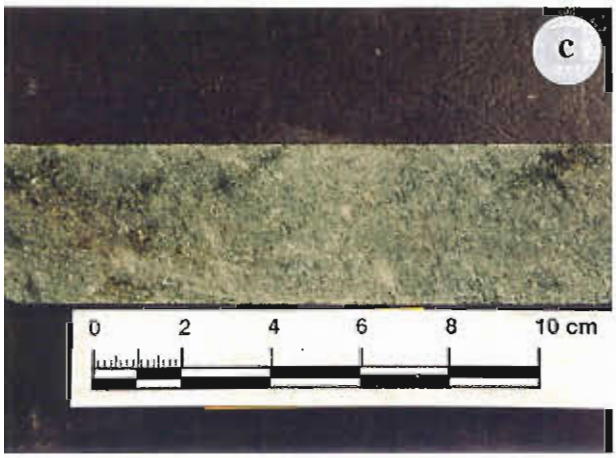
c
0 2 4 6 8 10 cm


d
0 2 4 6 8 10 cm

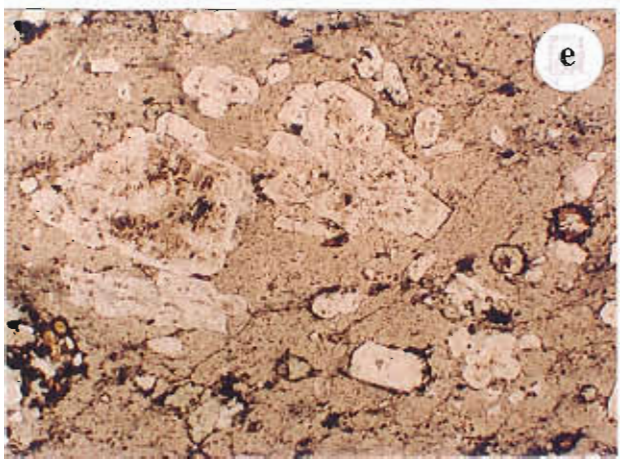
e


f
0 2 4 6 8 10 cm


g
0 2 4 6 8 10 cm

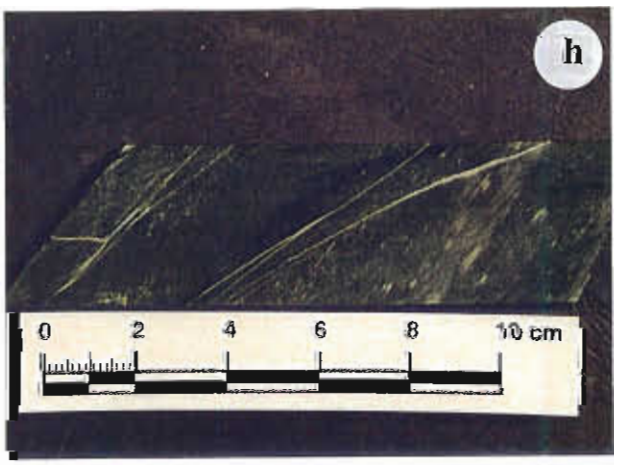
h
0 2 4 6 8 10 cm

associated with thick, massive to normally graded mass flow deposits of andesitic to basaltic re-sedimented hyaloclastite. Many units contain irregular clasts of silicified diffusely laminated and massive siltstone which were probably incorporated as the unit flowed over or intruded into a siltstone unit (peperite). Other units are clearly intrusive sills occurring within the mass flow deposits and having intrusive upper contacts.

Fine grained, aphyric andesitic and basaltic lavas and sills are massive units that rarely contain autoclastic material (Plate 6f, h). They occur mostly as sills within the Sterling Valley Volcanics, intruding into the mass flow deposits. In thin section fine interlocking laths of feldspar and actinolite are visible.

Polymictic and monomictic andesitic to basaltic breccias and sandstones are normally graded thick units that were deposited by mass flow processes. The mafic breccias and sandstones vary from monomictic to polymictic and comprise of angular, aphyric and feldspar ± hornblende/pyroxene porphyritic, lava clasts ranging from basaltic to dacitic in composition (Plate 6a, b, c). They also contain abundant angular and broken feldspar crystals and very rare quartz fragments in a chlorite-rich matrix. The clasts range in texture from highly vesicular or scoriaceous to dense quenched lava, trachytic clasts and coarsely porphyritic clasts. Clasts commonly have fine grained chilled, curviplanar margins indicating that they were sourced from a carapace of quench fragmented debris which was deposited in a subaqueous environment.

Weakly vesicular basalt dykes of the Henty Dyke Swarm are generally massive, fine to medium grained aphyric to weakly (3%) feldspar ±pyroxene porphyritic (Plate 5e, f, g, h). They form irregular branching dark green bodies, rarely more than one metre wide and have fine grained sharp irregular contacts interpreted to be intrusive. They commonly contain calcite-chlorite-quartz filled amygdales with a groundmass of "felt textured" interlocking feldspar laths and prismatic chlorite altered needles.

Primary geochemistry

Major and trace element analyses for 119 samples from the Mount Black and Sterling Valley Volcanics and 4 samples of the Rosebery Hangingwall are presented in Appendix 1. The chemical composition of the volcanics in the Mount Black Volcanics varies widely indicating that most elements have been mobile during the regional Greenschist facies metamorphism and alteration (McNeill and Corbett, 1989). However immobile elements Ti, Zr, Nb and Y define linear trends when plotted against one another, see Gifkins (1996), with only minor scatter. Some of the scatter observed is due to the inclusion of the Henty Dyke suite into the data set rather than mobility of Zr or Ti. Hence the immobile elements Ti, Zr and Nb and relatively immobile Y can be used to discriminate the primary volcanic compositions. Previous studies (Large et al, 1989) have been used as a guide to divide the Mount Black and Sterling Valley volcanics into compositional suites based on Ti/Zr ratios. Large et al (1989) defined the following categories fro the CVC coherent volcanics:

	Ti/Zr
Rhyolite	4 to 12
Dacite	12 to 20
Andesite	20 to 60
Basaltic	60 to 120+

The Winchester and Floyd (1977) style discrimination diagram plot of Zr/TiO_2 versus Nb/Y (Fig. 2), for the analysed samples indicates that the Mount Black–Sterling Valley Volcanic package spans a broad range of compositions from basalt to rhyolite, while the Henty Dyke Suite is composed only of basalts. Interestingly all of pumice-rich breccia samples plot in a tight cluster as rhyolites to rhyodacites, depicting that they represent homogenous monomictic volcaniclastic units of similar composition. From the regional mapping it appears that only three or four individual pumice-rich units exist and that they are displaced by large volumes of dacite and rhyolite intrusions. Of the pumice-lithic rich breccias all but one sample plots in the rhyolite-rhyodacite field. The more dacitic to andesitic sample, M45, is from near the gradational contact between the Mount Black and Sterling Valley Volcanics and reflects the

increasingly more mafic composition of the volcanics lower in the stratigraphy. The interpretation that the rhyolitic pumice breccias, lavas and syn-sedimentary sills represent explosive and effusive products of the single volcanic centre is supported by compositional similarities. The TiO_2 vs Zr plot (Fig. 3a) shows a possible four linear trends can be defined. The indicates that at least four suites of rocks are present and that Ti and Zr are relatively immobile for each suite. The rhyolite lavas, sills and pumice-breccias all belong to a single linear trend.

Both the Sterling Valley basalt lavas and sills and the Henty Dyke Suite basaltic dykes plot together in the andesite-basalt field of Winchester and Floyd discrimination diagram but are separated by the TiO_2 vs Zr diagram.

The plots of Nb vs Zr (Fig. 3b), Nb vs Y (Fig. 3c) and Al_2O_3 vs TiO_2 (Fig. 3d) show a linears trend which suggests that the primary chemical variation in the Mount Black Volcanics and Sterling valley Volcanics is the result of magmatic fractionation of a single parent magma.

The Mount Black–Sterling Valley volcanic package have petrographically been divided into five broad facies which can be described now in terms of their geochemistry:

1. The rhyolite and rhyodacites are typified by very low (<0.5%) TiO_2, low Ti/Zr ratios of 5–8, although a few samples have Ti/Zr ratios of 10–12 and high silica (typically 68–80% SiO_2). The silica percentage is not a good guide to composition as it is clearly mobile during the post-depositional changes. Sample 39701 has a Ti/Zr ratio of 7.8 typical of a Mount Black Rhyolite but only 11.38% silica! In handspecimen this sample is intensely carbonate altered.

   The rhyolites and rhyodacites of the Mount Black package show affinities with the Suite I Crawford et al (1992). They have silica values greater than 58% and Ti/Zr ratios between 5–35. However the low, medium or high K affinities of the any of the Mount Black package have not been determined due to the high mobility of K_2O.

2. The feldspar±hornblende dacites are characterised by moderate TiO_2 values (0.41–0.72%) , moderate Ti/Zr ratios of 12–19 and high silica 56–70% SiO_2. These rocks share affinities with Suite I and Suite II rocks of Crawford et al (1992). They have higher P_2O_5 contents than the rhyolites, rhyodacites and feldspar-porphyritic dacites. From the TiO_2 vs Zr plot it can be suggested that two suites of dacite exist within the Mount Black Volcanic package. The first group includes the feldspar-hornblende porphyritic dacites and feldspar porphyritic dacites. They have lower TiO_2 values (0.41–0.53%), low Ti/Zr ratios (12–15) and high SiO_2 values of 65–70%.

3. The second suite of dacites is feldspar porphyritic only dacite, with TiO_2 values of (0.58–0.71%), high Ti/Zr ratios (16–19) and lower SiO_2 values of (56–61). This group of feldspar only porphyritic dacites are equivalent to Suite I (Crawford et al, 1992).

4. Only four Mount Black andesite samples were analysed making characterisation of the primary geochemistry difficult. They appear to have a wide range of TiO_2 values (0.53–0.96%), variable Ti/Zr ratios from 20–53, silica values of 44–69% and low Nb <7 ppm.

5. The basaltic group of samples includes both the Henty Dyke Suite samples and samples of basaltic lava from the Sterling Valley Volcanics. The basaltic suite is characterised by generally high TiO_2 values greater than 60%, Ti/Zr 64–135, low Nb < 3 ppm and low SiO_2 37–50%. These are Suite IV rocks of Crawford et al (1992) and are considered to be similar to subduction zone basalts erupted during the early stages of arc splitting and back-arc basin development.

Stratigraphy and volcanic architecture

The schematic stratigraphy and volcanic architecture are ways of displaying the relationship between facies within the volcanic pile. The volcanic architecture of the Mount Black Volcanics highlights the discontinuous nature of the facies and their complex internal textures (Fig. 4). A single unit which has a

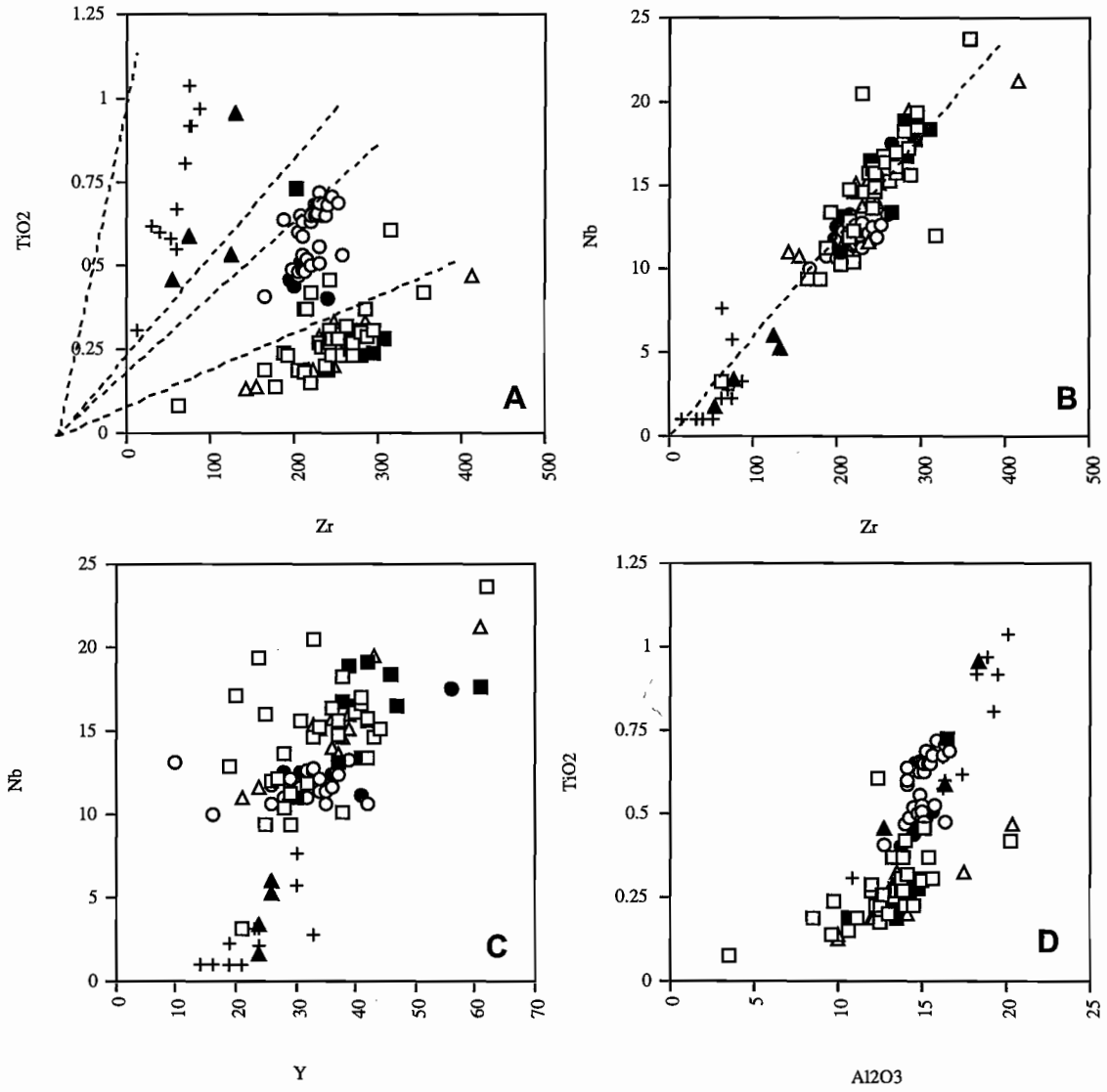

LEGEND

- ○ Feldspar porphyritic dacite
- □ Feldspar porphyritic rhyolite
- ■ Rhyolitic pumice lithic breccia
- △ Rhyolitic pumice breccia
- ● Feldspar-hornblende dacite
- ▲ Andesite
- \+ Basalt

Figure 3 (a) TiO_2 versus Zr plot differentiates the rhyolites, feldspar±hornblende porphyritic dacites, feldspar porphyritic dacites and basalts. The different geochemical suites plot on separate linear trends. (b) the Nb versus Zr plot shows a positive linear trend which indicates the preservation of primary Zr/Nb ratios. (c) Nb versus Y diagram shows a positive linear trend with some scatter due to minor mobility of Y. (d) TiO_2 versus Al_2O_3 diagram shows a positive linear trend indicating that Al_2O_3 is largely immobile.

similar primary geochemical signature (Ti/Zr, see primary geochemistry section) may display a wide variety of primary volcanic and post-depositional textures, it may also be extrusive, intrusive or both. The schematic volcanic architecture also depicts lava-like intrusions scattered throughout the volcanic pile like raisins in a pudding.

The Sterling Valley Volcanics are the lowest exposed part of the stratigraphy in the study area. They conformably and gradationally underlie the Mount Black Volcanics and appear to be petrographically and chemically related. The conformable nature of Mount Black-Sterling Valley Volcanics contact means that the volcanic stratigraphy and architecture of the area will be discussed as a single package of volcanics (Fig. 1b).

The Sterling Valley Volcanics are a thick succession of mass-flow deposits, extrusive lavas and intrusive shallow sills which record the eruptive history and erosional events of one or more mafic volcanic centres. The volcanic centre was predominantly basaltic but also produced more fractionated magmas which were extruded into the submarine environment. Quenching of the hot lava during extrusion brecciated the andesitic to basaltic magma and this debris was redeposited down slope by mass-flow events. The quenched lava clasts indicate that part of the source volcano was subaqueous or that lava flowed into the sea from a summit that emerged above sea level. The base of the volcano has been removed by displacement along the Henty Fault. The regional significance of the Sterling Valley Volcanics is that they are the structural relic of the medial facies association of a large marine mafic volcano that was active early in the eruptive history of the CVC.

The mafic to intermediate activity of the Sterling Valley Volcanics was followed by the emplacement of the basal succession of the Mount Black Volcanics, a thick pile of intermediate lavas and sills. These feldspar-hornblende porphyritic dacites, pre-dated the more felsic lavas and pumiceous debris, may represent a period of intermediate lava dome or cryptodome formation. The margins of the sills and lavas are commonly autobrecciated, but little redeposition of this autoclastic material has occurred.

Following this was a period of complex extrusion and shallow intrusion of coherent felsic lavas and sills coeval with the deposition of felsic pumiceous mass-flow units. The felsic lavas and shallow intrusions were commonly autobrecciated during emplacement and quench fragmented as they came into contact with seawater or wet unconsolidated sediment. Clastic debris derived from the coherent lavas remained in-situ, was deposited on the flanks of the moving flow or redeposited by mass-flow forming poorly sorted, normally graded breccias. The best evidence for the environment of emplacement of the Mount Black Volcanics and Sterling Valley Volcanics is the presence of facies and sedimentary structures typical of a subaqueous setting. Finely laminated and cross-bedded tuffaceous siltstones have been deposited by turbidites in below wave base conditions. Rare mudstones also indicate that background conditions to the volcanic activity were relatively quiet marine. During this phase densely spherulitic, massive to faintly flow-banded, feldspar±hornblende phyric dacite sills swarmed throughout the felsic and intermediate Mount Black succession and into the upper part of the Sterling Valley Volcanics.

The final volcanic event recorded in the Mount Black Volcanics and Sterling Valley Volcanics is the intrusion of a series of mafic dykes that are correlated with the Henty Dyke Swarm.

The important points from the volcanic architecture (Fig. 4) are that; in the Mount Black and Sterling Valley Volcanics the principal volcanic facies are silicic, intermediate and mafic lavas and sills. The lavas are commonly glassy and are associated with thick piles of insitu and resedimented hyaloclastite or an abundance of flow-banded autobrecciated debris. The sills are largely massive conformable, syn-volcanic intrusions. Most of the intrusions are lava-like in texture and were emplaced into water-saturated unconsolidated sediment probably only a few metres to a kilometre below the seafloor. The contacts of these intrusives are typically peperitic. The lavas and sills can only be distinguished based on contact relationships and many appear to be both partly extrusive and partly intrusive. Less prominent are a variety of juvenile volcaniclastic deposits. Two main types of subaqueous volcaniclastic deposits occur. One is composed dominantly of relatively dense to highly vesicular lava clasts and is related to the emplacement of lava

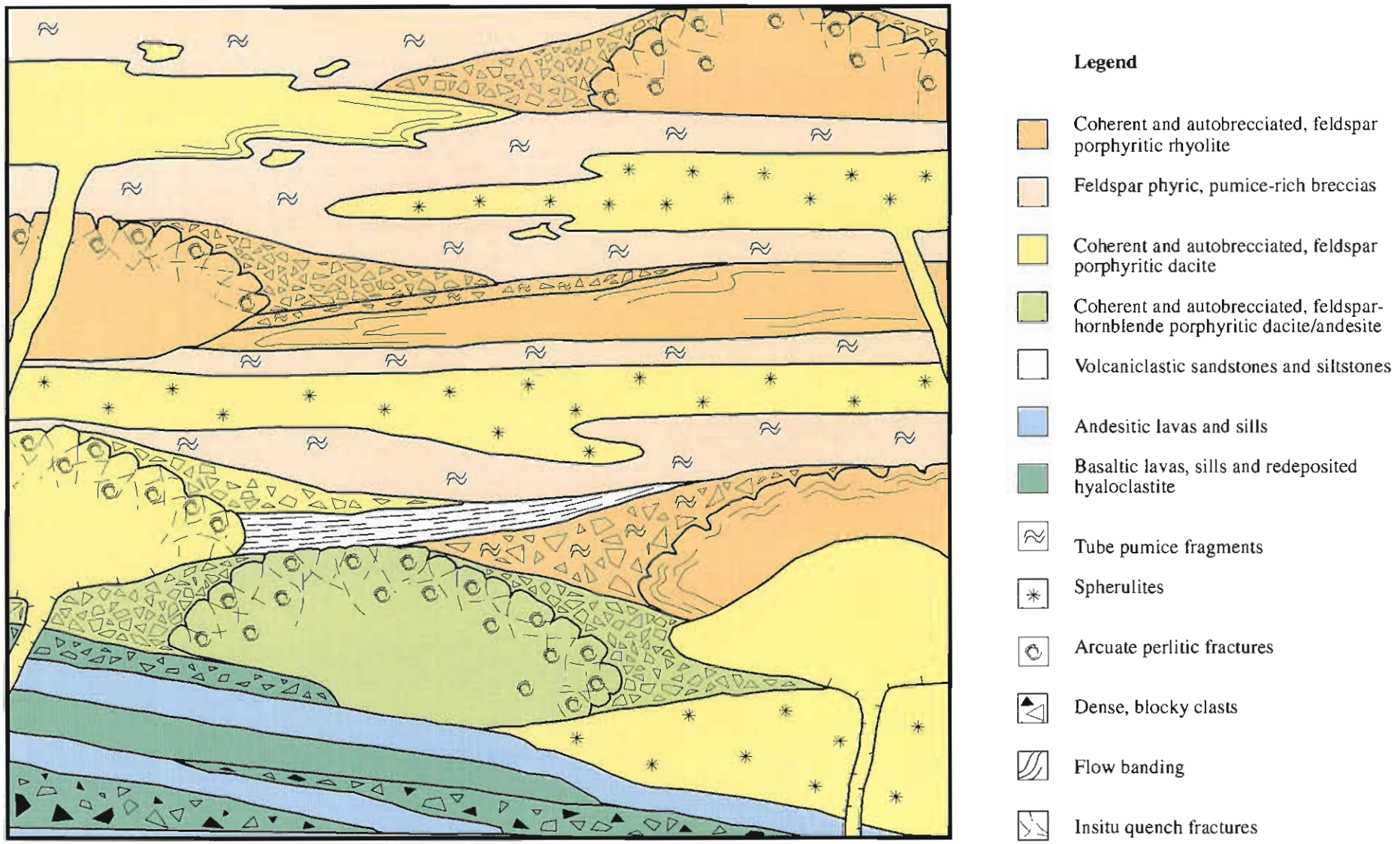

Figure 4: Schematic facies architecture of the submarine Mount Black Volcanic succession. Showing the relationships between the main lithofacies and variations in the internal texture of many of the facies.

flows or domes. The other type is dominated by pumice and was produced by explosive eruptions. Sedimentary facies such as black mudstone are very limited indicating that ongoing volcanic activity probably swamped any background sedimentation.

Styles of alteration, petrology and geochemistry

Alteration of the Mount Black and Sterling Valley Volcanics is attributed to regional scale processes and is more intense in the more porous units such as the volcaniclastics and glassy margins of coherent units. The most common alteration minerals include; feldspar, quartz, chlorite, sericite, epidote, carbonate (calcite), pyrite and magnetite. Eight main alteration styles have been identified, two of these; feldspar ± quartz and sericite-chlorite ± epidote; are particularly widespread, regionally extensive alteration styles.

The major and trace element data has been assessed with the aim of determining chemical changes associated with the main alteration styles and the difference in the intensity and styles of alteration in volcaniclastic versus coherent units. The Mount Black and Sterling Valley Volcanics display a wide range of Na_2O, K_2O and Ishikawa Alteration Index (Ishikawa et al, 1976) values which partly reflects the variation in primary geochemistry, and partly the different alteration types.

The Ishikawa et al (1976) Alteration Index = $(100(K_2O+MgO)/ (K_2O+MgO+Na_2O+CaO)$ for the majority of the samples falls in a narrow window of 25–70. Unaltered arc-related rocks are assigned a window of 20–50 (Stolz et al, 1996) which suggests that the bulk of the Mount Black Volcanics are only weakly altered. By comparing the AI to the major element trends it is possible to qualify the alteration mineralogy. This alteration index does not account for carbonate alteration and hence strongly carbonate altered rocks will plot in the unaltered window. To overcome this problem the Chlorite/carbonate/pyrite Index of Large (1996) was introduced. Chlorite/pyrite/carbonate Index = $(100(MgO+FeO)/(MgO+FeO+Na_2O+K_2O)$. Figure 5, shows a plot of Ishikawa Alteration Index against Chlorite/carbonate/pyrite Index. The least altered rhyolites of Large (1996) plot toward the centre of the diagram in a box with 25<AI<50 and 18<CI<35. This suggests that the majority of the Mount Black rhyolite lavas, sills and pumice breccias are only weakly altered. However two samples of feldspar porphyritic rhyolite that are dominated by intense carbonate alteration plot towards calcite on the CI axis.

Main alteration styles

Silicification is widespread and pervasive occurring most notably within the high level dacitic sills. Silicification is also associated with major faults and shear zones throughout the sequence. The volcanic package generally shows a linear trend of increasing TiO_2 with decreasing SiO_2, (Fig. 6), which suggests that the silica mobility has been quiet limited. However, the percentage of SiO_2 of many of the samples is higher or lower than would be predicted for the composition according to the Ti/Zr ratios. Many of the units with Ti/Zr of 12–20 (Large, 1996) suggesting dacitic composition have SiO_2 contents over 68% which would suggest that they were rhyolites, demonstrating that silica has been mobilised during at least one of the regional scale post-depositional events.

Feldspar±quartz alteration in handspecimen is characterised by a pink colouration due to the presence of albite dusted with hematite and varies in intensity and texture. Feldspar alteration may be selective, or domainal in character, forming pink feldspar-rich zones. It occurs as overgrowths on the margins of plagioclase crystals, replaces along fractures within the plagioclase crystals and may partially replace primary plagioclase phenocrysts (Plate 1h). Fine grained feldspar also occurs as laths enclosed in micropoikolitic quartz scattered throughout the groundmass of coherent units and replaces the glassy walls of uncompacted pumice fragments and glass shards (Plate 2g and h). The replacement of pumice fragments by a competent mineral phase has occurred pre compaction, suggesting that the feldspar alteration was either early diagenetic or that feldspar replaces an early diagenetic mineral phase. It is commonly associated in both coherent and clastic rocks with chlorite-sericite or sericite alteration producing a distinctive pink and green polyphase alteration patterns.

In the massive, coherent units pink-green alteration is patchy, forming a contrasting green and pink mottled pattern on a scale of 2–20 cm, while in

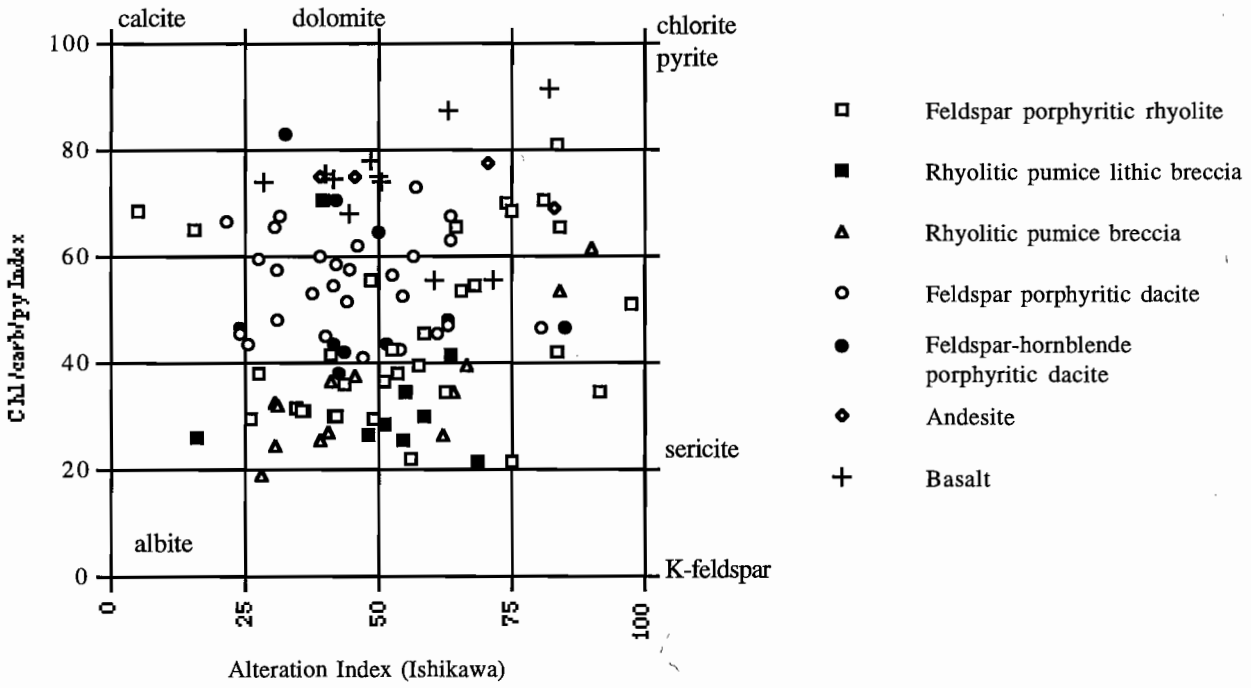

Figure 5 Alteration Index (Ishikawa et al, 1976) versus Chlorite/carbonate/pyrite Index (Large et al, 1996) plot for the Mount Black and Sterling Valley Volcanics.

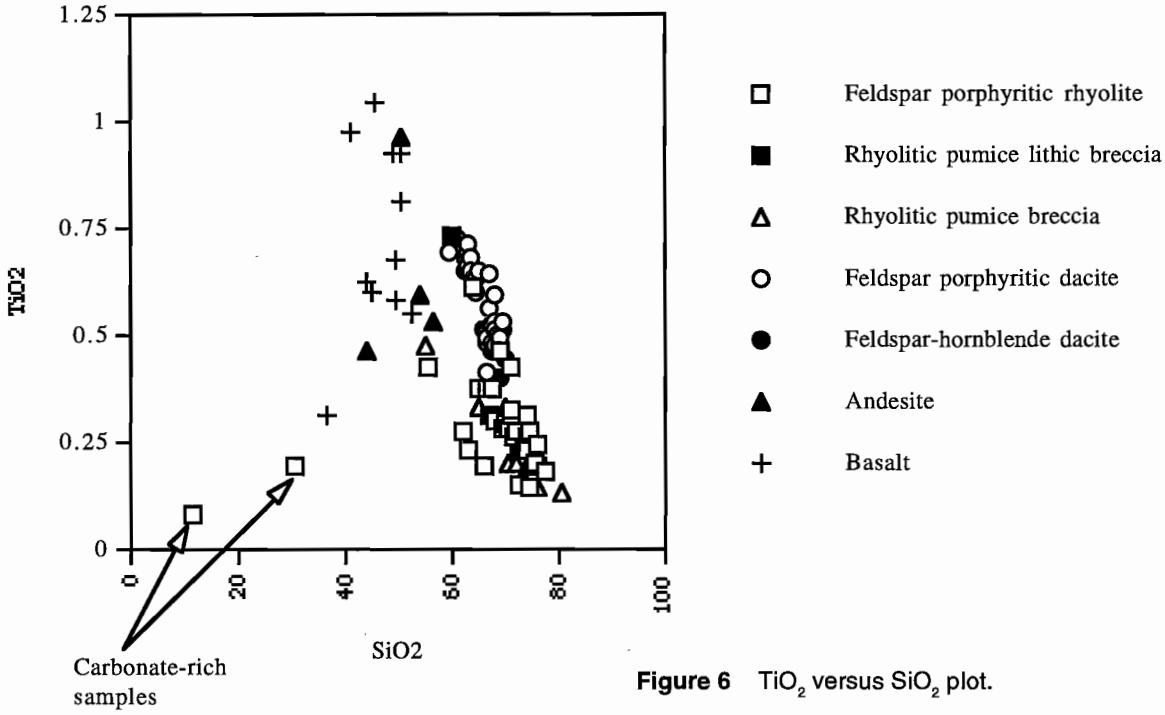

Figure 6 TiO_2 versus SiO_2 plot.

the flow-banded units the pink and green alteration is confined to individual bands where sericite-chlorite defines the originally glassy flow-bands and feldspar-quartz the spherulitic flow-bands (Plate 1d, e and b). False clastic and polymictic textures are often developed in the coherent flow-banded units by this two phase alteration and primary clastic textures in the volcaniclastic units are enhanced. In many of the autobreccias and hyaloclastite feldspar-quartz alteration forms pink halos or rinds around lithic clasts set in a green sericite-chlorite groundmass (Plate 1f). The pumice-rich units are also pink-green altered, with original pumice textures being preserved in the pale feldspar-quartz altered domains while in the sericite-chlorite domains only the porphyritic nature of the original pumice clasts can be determined (Plate 2a, b and c). Quartz-feldspar is also a very common vein assemblage.

A marked increase in Na_2O is associated with feldspar alteration and this is reflected in low values for the Ishikawa Alteration Index. Na_2O depletion is accompanied by decreases in K_2O, Rb, Cs, Ba (Stolz et al, 1987).

Fine grained **muscovite or sericite** is one of the most common minerals in these rocks and is probably the result largely of the Greenschist facies metamorphism rather than hydrothermal alteration. Fine grained white muscovite is a pervasive weak disseminated phase in most of the volcanic package. It is scattered as disseminated grains throughout the recrystallised quartz-felspathic groundmass of many of these coherent units, giving a green-grey colouration to the Mount Black dacites (Plate 4d). Commonly fine grained muscovite dusts or partially to completely replaces the primary plagioclase crystals. It also rims feldspar phenocrysts, spherulites and micropoikolitic quartz. Although this alteration phase is widespread in the Mount Black and Sterling Valley Volcanics it is rarely strong enough to mask primary volcanic textures. Muscovite also commonly forms along cleavage and fracture surfaces.

Hydrothermal sericite alteration is normally associated with the addition of potassium and this is only evident in the more intensely altered samples. A large number of the rocks analysed have amounts of potassium similar to those in unaltered arc related rocks. Strong sericite alteration is correlated with high K_2O and high values for the Alteration Index, (Fig. 7).

Sericite-chlorite±carbonate±quartz±pyrite alter-

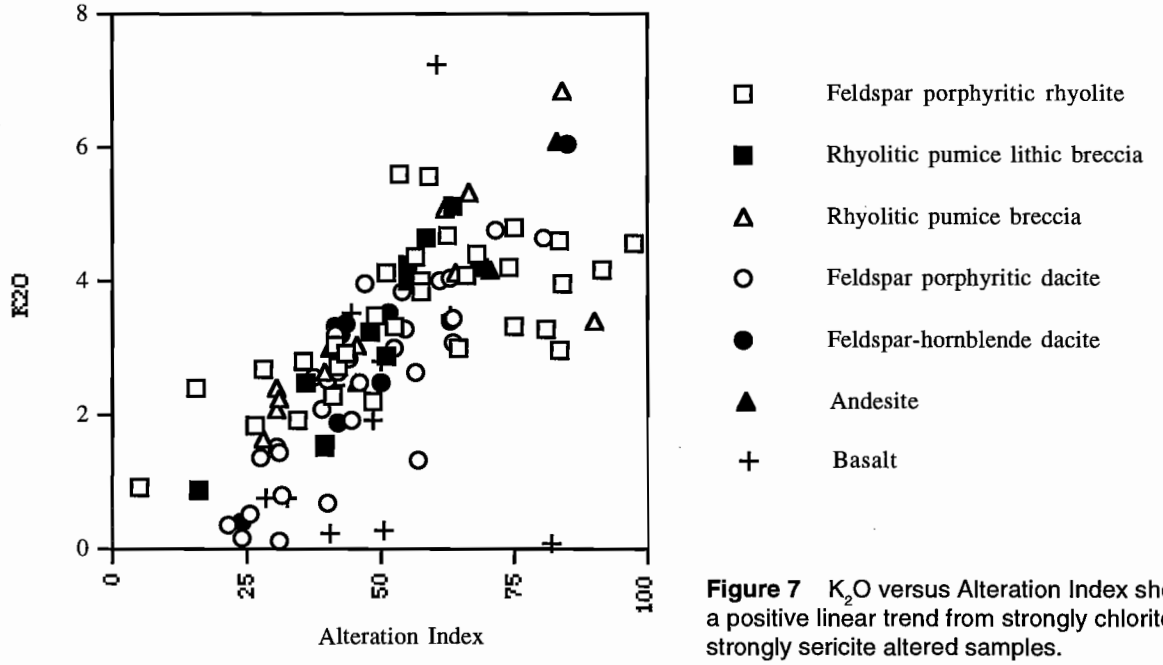

Figure 7 K_2O versus Alteration Index shows a positive linear trend from strongly chlorite to strongly sericite altered samples.

ation occurs in coherent flow-banded lavas and sills, autobreccias, hyaloclastite and pumiceous breccias (Plates 1b, e, f, 2d, f , 3b, 4e, g, 5c). Pale green, variably silicified and chloritised, it is often non-homogenous alteration producing patches or lenses of dark green chlorite-sericite in a paler feldspar-rich composition. These dark lenses typically form in pumiceous debris with carbonate-sericite altered feldspar phenocrysts but they can also form in individual flow-bands of a coherent unit or the flow-banded clasts of autoclastic deposits. This is common in the Mount Black rhyolites where weak pervasive sericite-quartz-chlorite alteration overprints an earlier feldspar-chlorite ± epidote phase. Partial to complete pseudomorphing of the ferromagnesian phases by chlorite is also common. In the more rhyolitic units sericite-chlorite alteration tends to be patchy set in quartz-feldspar rich domains. Within the chlorite-sericite rich domains the phenocrysts are preserved but other primary volcanic textures are largely destroyed.

Chlorite is generally less abundant than the sericite, and pyrite, chlorite and quartz are accessory and do not always occur along with sericite-chlorite alteration. Volcaniclastic units typically display the most intense sericite alteration.

Samples with high AI and high K_2O are strongly sericite altered and low K_2O samples are chlorite altered (Fig. 7). Depletion in CaO, Na_2O and Sr associated with enrichment's in Cs, Sb, Tl.

Carbonate alteration is fine grained, either disseminated, replacing or rimming feldspar phenocrysts. Carbonate rhombs have been observed to replace the shard-rich matrix of some of the pumice breccias and pumiceous sandstones (Plate 3h). Carbonate more commonly occurs in veins associated with chlorite or quartz that appear to have been activated during the Devonian metamorphism. Carbonate alteration is generally weak, however more intense carbonate alteration masks primary volcanic textures resulting in a fine grained massive homogenous pale.

At least two types of **chlorite** alteration can be determined. A dark (hydrothermal) chlorite and magnetite phase and a paler green (metamorphic) chlorite. The dark chlorite ± magnetite alteration is very widespread occurring in almost all units in a number of different forms. Most commonly as patchy to pervasive disseminated fine grained aggregates in the groundmass of the rocks throughout the volcanic package. It also occurs commonly as fibrous and fine grained material interstitial to the crystals in glomeroporphyritic clusters and between micro-spherulites and micropoikolitic quartz in the groundmass of coherent lavas and sills. It can rim individual feldspar phenocrysts in many of the coherent units (Plate 5b). In the hornblende porphyritic rocks chlorite ± magnetite commonly pseudomorphs the hornblende crystals. Less commonly chlorite ± magnetite alters the primary plagioclase crystals, often only replacing the core of zoned crystals or altering along the crystal cleavage (Plate 5d). It occurs as pervasive fine grained aggregates between the feldspar and hornblende laths in the basalts of the Sterling Valley Volcanics. Chlorite -rich assemblages also commonly fill vesicles or vugs. Chlorite±magnetite occurs in the pumice-rich volcaniclastics as styolitic textures parallel to the compaction foliation (Plate 3f). Chlorite alteration halos are also associated with mafic dykes and sills and with brittle fractures and faults throughout the region. Chlorite commonly highlights both early syn-volcanic fractures, ie, perlitic fractures (Plate 4g and 5c), and later hydraulic and tectonic fractures. The magnetite associated with this alteration phase occurs as blebs or euhedral pseudomorphs in the ground-mass. These blebs are often concentrated along grain boundaries.

The brown-green chlorite appears to be an earlier phase regularly being overprinted by the blue-green chlorite ± magnetite. It is fine grained and disseminated and often associated with weak sericite alteration.

The felsic rocks of the Mount Black volcanics display only limited chlorite alteration while the more mafic units of the Sterling Valley Volcanics and Henty Dyke Suite contain substantially more chlorite-CO_3± ser alteration. This is most common as vesicle fill, late-brittle fractures and faults throughout the region or vein assemblages. It also occurs as moderately strong pervasive alteration. Strong chlorite alteration is associated with low K_2O and high Alteration Index values (Fig. 7).

Chlorite-epidote±feldspar alteration is largely associated with the more basic rocks of the Sterling Valley Volcanics. It completely replaces hornblende and partially alters primary plagioclase. It also occurs as weak fine grained irregular patches in the

groundmass of many of the coherent dacites, andesites and basalts. Epidote filled fractures are less common.

Sphene is a weak alteration phase in fine grained irregular patches which often concentrate along grain boundaries. Sphene is commonly replaced by leucoxene.

Controls on the distribution of regional alteration styles

The main regional scale alteration facies have a patchy distribution and vary considerably in intensity throughout the Mount Black and Sterling Valley Volcanics. The distribution and intensity of the alteration styles in part can be related to the texture and geochemical signature of the volcanics. However this is not necessarily the primary volcanic texture and chemistry, as many post-depositional processes have acted to affect the texture, mineralogy and geochemistry of the volcanic units. The present alteration assemblages reflect the combined effects of different post-depositional processes; devitrification, hydration, hydrothermal and diagenetic alteration, diagenetic compaction and metamorphism; on the primary mineralogy's and textures. Thus the composition and texture of the volcanic facies evolves by a series of steps, however the steps are not necessarily discrete and many overlap making the recognition of individual phases complicated. Despite the complex series of steps, the current mineral assemblage in many of the volcanics reflects primary variations in composition.

The original composition of the volcanic units has exerted a strong control on the less intense alteration assemblage and textures formed. Within the more felsic rhyolites, rhyodacites and dacites the primary volcanic, devitrification and hydration textures are varied, discontinuous and often complexly related. Subsequent alteration textures observed within the felsic rocks appear complex and patchy due to these primary and secondary variations in texture. The alteration of the more mafic units (andesites and basalts) is typically more uniformly pervasive, reflecting the more massive style of volcanic deposits.

The alteration assemblages which dominate in felsic rocks versus mafic rocks are also partly controlled by the primary volcanic composition. The silicic volcanics are dominated by feldspar-quartz, sericite- chlorite and carbonate alteration assemblages while more mafic rocks are typically dominated by chlorite, epidote and carbonate assemblages.

Permeability and competency contrasts formed by primary volcanic processes, quenching, hydration, and devitrification have had a significant role in the porosity of the rocks, fluid flow during post-depositional processes and ultimately in the distribution of different alteration facies. Alteration is strongly controlled by fluid pathways, in the coherent facies it is controlled by the fractures which are generally produced by quenching, flow and hydration and by the distribution of more crystalline versus glassy textures, such as spherulites and flow-banding. In the massive lavas and sills alteration has progressed as fronts moving outward from the primary fractures, perlitic fractures and chilled margins towards the unaltered domains. Alteration in clastic facies is controlled by the distribution of matrix to clasts. There is a significant difference between the style of alteration in coherent lavas and sills compared with the alteration textures developed in volcaniclastic deposits.

The earliest alteration phases present in the current assemblages are feldspar-quartz and sericite alteration. These assemblages appear to be related to diagenetic alteration and compaction. The evidence for this comes from the pumice-rich breccias where uncompacted pumice clasts and glass shards are preserved by feldspar-quartz alteration. This alteration is usually patchy with domains of feldspar-quartz alteration and phyllosilicate-rich domains. The quartz-feldspar domains contain relic uncompacted tube pumice, glassy walls are feldspar-quartz altered and the tube vesicles are defined by sericite. The phyllosilicate altered domains have been flattened by compaction producing fiamme like-textures in which only the primary phenocrysts can still be recognised. The pumice clasts and shards can only have remained uncompacted during burial if they were altered to a more competent mineral phase than glass prior to compaction. Whether this competent alteration phase was the feldspar-quartz alteration or whether this alteration style completely replaces a competent diagenetic phase has not been ascertained. This early feldspar-quartz alteration has also weakly altered the originally glassy groundmass

of many of the massive spherulitic or micropoikolitic sills and lavas, while in the flow-banded units pink feldspar alteration is confined to individual bands. In many of the autobreccias and hyaloclastite quartz-feldspar alteration forms pink halos or rinds around lithic clasts set in a green sericite-chlorite rich groundmass.

Although the feldspar dominated alteration assemblage is not clearly controlled by the permeability it has significantly affected the subsequent patterns of permeability and porosity in the volcanic pile. It forms irregular patches or domains in both the volcaniclastic and coherent facies but is usually more in intense in the volcaniclastics. As a result later alteration phases occur in the next most porous or reactive portion.

The different alteration facies result from different alteration stages, even though the time between stages may be very short. Within flow-banded and spherulitic lavas and sills the quartz-feldspar-rich bands, nodules and devitrification textures (spherulites) have been recrystallised and replaced during the early feldspar-quartz alteration. In contrast the glassy domains have been replaced by phyllosilicate assemblages dominated by sericite and chlorite. The phenocrysts are more prominent in these darker phyllosilicate-rich bands and give the false impression that the darker domains are more phenocryst-rich than the paler quartz-feldspar domains (Plate 1b). The alternating pink and green altered flow-bands can resemble folded, thinly bedded, volcaniclastic rocks with crystal-rich phyllosilicate layers and crystal-poor siliceous layers.

Polyphase alteration of perlitic glass is another good example of successive alteration styles developing in the most permeable zone. Perlitic fractures in many of the originally glassy lavas, sills and piles of autoclastic material, have been highlighted by sericite-chlorite alteration and the enclosed core has been altered by paler quartz-feldspar±sericite. The alteration has enhanced the fractures creating a contrast in composition and colour between the fractures and the areas that they enclose, resulting in a pseudoclastic texture (Plate 4e, 4g, 4h, 5c and 5d). The more advanced that the prominent fracture controlled alteration the more matrix supported the resulting alteration texture.

Pseudoclastic textures are common particularly in the more felsic units and can develop an apparently polymictic appearance. The apparent polymictic character can be due to a number of features; phenocrysts in the dark phyllosilicate domains can appear more prominent than those in the quartz-feldspar altered domains; differences in the intensity of alteration and hence colour within individual units; and overprinting alteration assemblages in the same unit.

In summary it appears that the alteration in glassy coherent lavas and sills evolves towards matrix supported monomict and polymict textures typical of volcaniclastic mass flow deposits. With increasing alteration the false clastic textures converge to produce textures similar to those of welded pyroclastic deposits (Allen, 1988).

In autobreccias and hyaloclastite alteration is also commonly polyphase and the preservation of pre-existing textures is controlled by the intensity of the alteration phases. In weak to moderately altered deposits the primary clastic texture is enhanced by the alteration stages and this often imparts a polymictic appearance (Plate 1f). The alteration is matrix and fracture controlled in a similar manner to the fracture controlled alteration in coherent lavas and sills. In more intensely altered units the primary nature of the unit becomes obscured.

Conclusions

The Mount Black Volcanics represent a thick pile of silicic to intermediate, subaqueous, glassy, lavas and sills with abundant associated flow and quench brecciated debris and minor feldspar porphyritic pumice-rich breccias. The intrusive nature of many of these units explains why they cannot be correlated with each other and occur through thick intervals of the stratigraphy like "raisins in a pudding".

The Sterling Valley Volcanics represent a thick pile of mafic to intermediate, subaqueous, lavas, sills and redeposited hyaloclastites.

The Mount Black and Sterling Valley Volcanics are a conformable suite of rocks which span a broad range of compositions from basaltic to rhyolitic. This range of primary compositions shows a linear trend and may reflect the magmatic fragmentation of a single parent magma. The facies within this succession can be divided into five main petrological and geochemical suites:

1. Feldspar porphyritic rhyolitic to rhyodacitic, lavas, sills, autoclastic debris and thick pumice-rich deposits.
2. Feldspar ± hornblende porphyritic dacite lavas, sills and glassy autoclastic debris.
3. Feldspar porphyritic dacite sills and lavas.
4. Feldspar-hornblende porphyritic andesite lavas and/or sills.
5. Aphyric to weakly feldspar porphyritic basaltic lavas and sills.

The basaltic dykes of the Henty Dyke suite show affinities with the basaltic lavas and sills of the Sterling Valley Volcanics.

Petrology and geochemistry of the alteration suggests that eight major styles of alteration are present in the Mount Black and Sterling Valley Volcanics. The widespread occurrence of these alteration assemblages which have been sampled away from known mineralisation suggests that they are the product of regional events rather than localised hydrothermal activity. These main alteration styles are:

1. silicification
2. feldspar ± quartz
3. sericite
4. sericite-chlorite ± carbonate ± quartz
5. carbonate
6. chlorite
7. chlorite-epidote ± carbonate
8. sphene

Of these alteration styles the feldspar-quartz and sericite alteration are thought to be related to early diagenetic alteration processes. The prevasive sericite alteration is probably largely the result of the regional Greenschist facies metamotphism.

Many of the alteration styles in felsic rocks are texturally enhancing. The patterns of permeability and competence contrasts in the felsic rocks have a marked effect on the alteration patterns. Both chlorite and sericite dominated alteration assemblages appear to be strongly controlled by fluid pathways, except in areas of intense alteration. The dominant fluid pathways include volcaniclastic deposits, originally glassy bands in flow-banded lavas, insitu breccia (autobreccia and hyaloclastite), perlitic fractures, hydraulic breccias and fractures or joints. Feldspar-quartz alteration can be patchy or perveasive in permeable volcaniclastcs, while in coherent units it is either weakly pervasive or stronglly controlled by the fracture porosity.

The alteration of the andesites and basalts is more uniformly pervasive although varying in intensity. The mafic units generally have a pervasively altered groundmass and partial to complete replacement of the primary phenocrysts. Although they appear intensely altered, the Alteration Index suggests that they are relatively unaltered and the present mineral assemblage, plagioclase-chlorite-epidote ± sphene ± actinolite may be largely the result of the Greenschist facies metamorphism.

References

Allen, R.L., 1994. Synvolcanic, sub-seafloor replacement model for Rosebery and other massive sulphide ores. Contentious issues in Tasmanian geology. Ed by Cooke, D.R. and Kitto, P.A. in Geol Soc of Aust Abstracts 39, 31-34.

Allen, R.L., 1993. Geological cross-section and interpretation, 1320mN Rosebery mine north end. Unpubl report to Pasminco Exploration, Tasmania.

Allen, R.L., 1991. Structure, stratigraphy and volcanology of the Rosebery-Hercules Zn Pb Cu Au Massive Sulphide District Tasmania: Results 1988-1990. Unpubl report to Pasminco Exploration, Tasmania.

Allen, R.L., 1988. False pyroclastic textures in altered silicic lavas, with implications for volcanic-associated mineralisation. Econ. Geol. 83: 1424-1446.

Crawford, A.J., Corbett, K.D. and Everard, J.L., 1992. Geochemistry of the Cambrian volcanic-hosted massive sulfide-rich Mount Read Volcanics, Tasmania, and some tectonic implications. Econ Geol v.87, 597-619.

Fink, J. and Manley, C., 1987. Origin of pumiceous glassy textures in rhyolitic flows and domes. Geol. Soc. Am Spec. Pap. 212, 77-88.

Gifkins, C.C., Allen, R.A., Stolz, A.J. and Duhig, N.,1996a. Mount Black to Murchison Gorge: Preliminary volcanic facies analysis and alteration styles. AMIRA Project P439 Report 2, May 1996. Unpubl.

Gifkins, C.C., Allen, R.A. and McPhie, J., 1996b. Fiamme associated with silicic lavas and intrusions. EOS, Transactions, AGU, v.77, No.22, p W125.

Ishikawa, Y., Sawaguchi, T., Iwaya, S. and Horiuchi, M., 1976. Delineation of prospecting targets for Kuroko deposits based on modes of volcanism of underlying dacite and alteration haloes. Mining Geology, 26, 105-117 (in Japanese with English abstract).

Large, R.R., 1996. The Hercules-Mt Read traverse: Relationships between volcanic mineralogy, alteration and geochemistry. AMIRA Project P439, October 1996: 153-233.

Large, R., Doyle, M., Raymond, O., Cooke, D., Jones, A. and Heasman, L., 1996. Evaluation of the role of Cambrian granites in the genesis of world-class VHMS deposits in Tasmania. Accepted in Ore Geology reviews.

Large, R.R., Crawford, A.J. and Duhig, N., 1989. Primary alteration chemistry of the Mount Read Volcanics. AMIRA Project

P210, November 1989: 38-45.
Lofgren, G., 1971. Experimentally produced devitrification textures in natural rhyolitic glass. Geol Soc Am Bull. v. 82:111-124.
McNeill, A.W. and Corbett, K.D., 1989. Geology of the Tullah-Mt Block area. Mt Read Volcanics Project Geological Report 2.
McPhie, J., Doyle, M. and Allen, R.L., 1993. Volcanic Textures: a guide to the interpretation of textures in volcanic rocks. p198.
Pichler, H., 1965. Acid Hyaloclastites. Bull. Volc. 28, 293-310.
Stolz, J., Allen, R., Gifkins, C., McPhie, J. and Blake, M., 1997. Petrographic and geochemical characteristics of alteration from the Macintosh Dam-Anthony Road-Mt Black traverse, Mt Read Volcanic Belt.
Stolz, A.J., Large, R. and Duhig, N., 1996. Progress report on the utilisation of the Mount Read Volcanics database. AMIRA Project P439 Report 2, May 1996. Unpubl.
Winchester, J.A. and Floyd, P.A., 1977. Geochemical discrimination of different magma series and their differentiation products using immobile elements. Chemical Geology, v. 20, p. 325-344.

Appendix 1

	39701	39704	39711	39714	39717	39719	39725	39726	39728	39731	39745	39749	39752	39754	39764	39770
SiO2	11.38	30.57	69.67	69.77	71.37	70.18	68.02	72.28	71.64	69.54	70.45	71.9	69.42	56.03	71.96	71.69
TiO2	0.08	0.19	0.28	0.29	0.29	0.33	0.3	0.27	0.26	0.28	0.28	0.27	0.53	0.58	0.26	0.26
Al2O3	3.56	8.47	14.8	12.04	13.23	13.46	15	13.07	12.8	13.71	13.43	13.46	15.71	14.34	13.66	14.23
Fe2O3	0.77	1.7	2.88	3.74	2.74	2.74	2.71	2.8	3.22	4.03	2.4	3.05	4.18	7.02	2.42	1.89
MnO	0.04	0.04	0.08	0.18	0.07	0.08	0.1	0.11	0.43	0.1	0.13	0.11	0.04	0.21	0.03	0.02
MgO	1.55	2.99	0.8	1.31	0.69	0.82	0.83	0.62	0.7	0.58	0.66	0.73	1.12	3.43	0.45	0.43
CaO	44.7	29.12	1.44	2.77	2	2.74	1.7	1.56	1.96	1.33	2.8	1.46	0.33	5.79	0.94	1.23
Na2O	0.12	<0.05	2.5	0.03	4.43	2.7	1.6	4.47	1.52	3.18	3.49	3.25	1.04	0.55	3.96	4.2
K2O	0.92	2.4	3.98	4.07	2.21	2.99	4.68	2.05	4	4.09	2.8	2.89	4.61	3.29	4.2	3.83
P2O5	0.02	0.05	0.04	0.05	0.06	0.07	0.06	0.04	0.06	0.06	0.05	0.05	0.1	0.12	0.04	0.04
LOI	36.16	25.27	3.32	5.49	2.71	3.64	3.5	2.36	3.69	3.07	3.7	2.49	2.51	7.94	1.26	1.8
Total	99.3	100.8	99.79	99.74	99.8	99.75	98.5	99.63	100.28	99.97	100.19	99.66	99.59	99.3	99.18	99.62
S	<0.01	0.01	0.01	0.38	0.01	0.02	<0.01	0.01	0.07	1	0.01	0.04	0.14	0.01	<0.01	<0.01
Total C	10.1	6.4	0.35	0.89	0.46	0.61	0.44	0.35	0.67	0.28	0.57	0.31	0.054	1.32	0.13	0.23
Alteration Index	5.22	15.60	54.82	65.77	31.08	41.19	62.54	30.69	57.46	50.87	35.49	43.46	80.70	51.45	48.69	43.96
Trace Elements (ppm)																
Sc	-	-	6	7	5	6	5	4	5	5	5	4	13	20	5	5
V	<1.5	<1.5	4	16	10	12	8	7	7	7	7	7	54	134	4	4
Cr	2	2	2	2	3	3	3	2	2	2	2	2	6	129	2	2
Ni	2	1	1	2	1	<1	2	1	1	1	1	1	2	70	1	1
Cu	3	3	2	5	2	3	3	2	5	4	16	14	12	11	2	2
Zn	12	25	23	29	23	37	34	41	84	22	22	21	59	129	13	13
As (ICP)	1	<	1	3	7	8	11	11	14	20	11	12	13	84	18	17
Rb	40	85	178	203	84	119	183	76	184	113	107	113	179	121	143	120
Sr	312	279	94	48	167	104	84	108	95	86	111	96	37	132	132	136
Y	21	25	46	37	37	36	38	39	33	41	42	43	10	32	52	38
Zr	63	165	309	288	230	248	280	250	233	254	246	244	259	186	268	271
Nb	3.2	9.4	18.4	15.6	13.7	14	18.3	15.1	14.6	16.7	15.7	14.6	13.2	12	16.6	16.6
Mo(ICP)	0.4	0.4	1.9	1.1	1	1.1	1.8	0.7	1.2	2.1	0.5	2.6	18.1	2.4	1	0.6
Ag(ICP)	0.3	0.2	0.2	0.2	0.1	0.1	0.2	0.2	0.3	0.1	0.1	0.1	0.2	0.3	0.2	0.1
Cd(ICP)	0.3	0.4	0.4	0.4	0.5	0.6	0.5	0.6	0.7	0.6	0.5	0.6	0.6	0.6	0.6	0.6
Sb(ICP)	0.6	1.3	1.7	3.5	0.8	0.8	1.1	0.8	2.6	1.3	0.9	1.1	2	2	0.5	0.4
Cs(ICP)	0.9	1.93	3.05	8.34	2.19	1.47	2.61	1.88	3.56	1.86	1.19	1.57	3.47	3.42	2.3	1.95
Ba	134.1	302.7	1042.6	645.1	698.2	725.5	1105.1	440.2	875.2	918.1	611.5	921.7	1426.9	1184.6	937.6	858.8
La	14	23	53	44	50	21	37	19	25	27	43	51	10	30	52	41
Ce	25	59	118	95	106	51	93	44	59	62	93	103	26	67	109	92
Nd	17	27	49	42	46	23	39	19	26	27	40	45	12	27	46	39
Tl(ICP)	<	<	0.6	0.7	<	<	<	<	0.6	<	<	<	0.7	0.6	0.5	<
Pb	2	4	4	68	4	3	2	3	170	7	3	2	43	18	5	3
Bi (ICP)	<	<	<	0.4	0.2	0.2	0.1	<	0.2	0.8	0.1	0.2	0.1	2.1	0.4	0.2
Th (ICP)	3.65	11.9	17.9	17.4	11.3	15.7	19.5	17.8	17.2	19.5	13.9	15.7	20.1	14.5	15	13.7
U(ICP)	0.12	0.3	4.61	4.31	3.44	3.32	4.55	4.39	3.86	4.48	4.19	4.28	5.15	4.37	4.32	3.34

Total Fe as Fe2O3, LOI = loss on ignition, Alteration Index = 100(MgO+K2O)/(MgO+K2O+CaO+Na2O)

39771	39775	39779	39780	39781	39782	39783	39784	39785	39786	39787A	039787B	039788A	039788B	39789	39790	39792	39793
72.57	73.76	74.94	71.81	70.6	74.05	74.4	76.5	36.69	72.48	66.09	45.29	49.33	62.97	74.01	72.57	76.08	54.93
0.25	0.25	0.19	0.2	0.2	0.19	0.19	0.19	0.31	0.24	0.19	1.04	0.67	0.23	0.23	0.23	0.19	0.47
13.63	13.37	12.05	14.1	14.13	12.12	12.05	12.09	10.87	14.27	11.11	20.12	16.31	14.47	12.21	13.4	10.66	20.37
2.21	2.57	1.48	1.8	2.1	1.79	1.85	1.76	15.87	2.19	3.04	8.6	11.71	3.15	2.17	2.45	1.67	7.17
0.02	0.16	0.13	0.13	0.25	0.07	0.07	0.02	0.69	0.15	0.21	0.21	0.21	0.15	0.09	0.05	0.09	0.06
0.4	1.04	0.44	0.59	0.55	0.54	0.34	0.43	10.1	0.5	0.68	2	2.73	1.03	0.49	0.63	0.47	2.6
1.17	1.09	2.2	2.6	1.82	2.35	2.3	0.59	7.87	0.85	5.8	5.32	4.94	4.92	2.41	1.66	2.39	0.69
4.04	0.03	2.53	<0.05	1.65	2.82	3.88	4.11	<0.05	3.06	2.89	0.66	2.78	0.79	4.07	3.9	4.71	1.1
4	4.59	2.62	4.12	5.07	2.97	2.39	3.11	3.45	4.23	2.66	7.21	3.52	5.57	1.82	2.47	0.88	6.83
0.04	0.04	0.03	0.03	0.03	0.03	0.03	0.02	0.05	0.04	0.03	0.23	0.13	0.04	0.03	0.04	0.03	0.08
1.58	3.19	3.41	4.72	3.18	2.97	2.67	1.12	13.52	2.39	6.71	9.25	7.38	6.39	3.08	2.45	2.76	4.97
99.91	100.09	100.02	100.1	99.58	99.9	100.17	99.94	99.42	100.4	99.41	99.93	99.71	99.71	100.61	99.85	99.93	99.27
<0.01	0.03	0.01	0.02	0.01	<0.01	0.01	0.01	0.01	0.01	<0.01	0.03	0.01	0.01	0.01	0.02	0.01	2.08
0.2	0.23	0.53	0.55	0.48	0.52	0.48	0.23	3	0.32	1.63	1.87	1.37	1.26	0.57	0.32	0.59	0.13
45.79	83.41	39.28	63.99	61.83	40.44	30.64	42.96	63.11	54.75	27.76	60.63	44.74	53.61	26.28	35.80	15.98	84.05
4	5	4	5	5	3	5	3	42	6	7	39	28	7	5	6	4	9
5	7	2	<1.5	<1.5	<1.5	2	<1.5	218	3	33	399	218	18	3	3	3	15
2	2	2	2	2	2	2	2	1326	2	2	4	14	2	2	1	2	8
1	5	1	1	1	1	1	1	266	1	1	3	22	3	<1	1	<1	3
4	3	4	30	24	3	4	2	7	4	5	187	55	3	2	2	1	5
18	60	18	36	51	14	24	18	182	29	51	78	139	26	19	18	27	74
18	16	15	19	16	16	16	15	30	18	18	24	20	17	15	16	17	24
112	371	127	187	185	117	95	82	271	151	100	354	181	191	76	95	34	283
155	24	69	41	68	93	108	93	129	91	187	127	194	131	113	104	144	51
39	31	33	36	39	38	34	36	21	42	38	30	30	40	36	40	37	61
265	269	237	249	244	219	223	228	14	295	205	75	62	271	258	262	210	414
15.8	15.7	15.4	15.8	16	14.6	15.1	14.9	<1	19.1	10.2	5.8	7.6	16.1	16.4	16.5	13.1	21.3
1	1.1	1.5	0.6	1.6	2.6	0.9	0.8	0.4	1	0.5	18.8	3.1	1.4	1.1	4.7	0.9	2.6
0.2	0.2	0.2	1.1	0.5	0.2	0.2	0.1	0.2	0.2	0.2	0.3	0.2	0.2	0.2	0.2	0.1	0.3
0.6	0.6	0.6	0.7	0.7	0.6	0.6	0.6	0.4	0.6	0.8	0.5	0.5	0.7	0.6	0.6	0.5	0.9
0.5	1.9	2.1	18.4	6.1	0.9	0.7	0.7	0.8	4.4	2	5	2.4	1.6	1.8	1.1	1.1	2.1
1.63	6.78	2.91	4.36	2.72	2.03	1.56	1.64	13.2	2.2	2.55	7.76	8.23	4.06	1.08	1.74	0.62	4.91
986.2	380.9	430.5	692.9	1378.7	730.3	652.6	1162.9	282.1	1346.2	795.2	1623.1	773.2	1598.5	513.3	859.8	279.7	1639.4
46	34	6	45	36	41	19	36	8	25	22	22	16	35	38	37	48	74
107	75	13	102	83	89	44	82	13	59	57	46	38	88	86	83	102	156
43	32	6	44	35	37	19	34	6	24	22	20	17	37	36	34	45	70
<	1.5	0.5	0.7	0.7	<	<	<	1.4	0.6	<	1.3	1	0.6	<	<	<	0.9
5	4	6	11	19	3	4	2	2	6	8	5	8	6	4	2	4	5
0.1	<	0.1	<	<	<	<	<	<	0.1	<	0.9	0.2	<	<	<	<	4.1
14.7	16.1	12.7	16.1	16.6	13.3	13.6	15.5	10.4	16.5	13.6	11.8	8.43	14.2	11.9	13.9	9.68	21.6
4.38	6.26	4.33	4.54	4.98	4.3	4.16	4.83	0.27	6.05	4.13	0.89	1.39	4.85	4.15	4.05	3.07	5.69

39795	39796	39797	39798	39799	39800	40603	40604	40605	40606	40607	40608	40609	40611	40612	40613	40614	40615
55.65	80.53	65.06	76.09	69.01	67.31	70.76	66.98	43.77	49.58	56.39	62.15	73.33	74.38	75.96	70.82	67.49	71.04
0.42	0.13	0.33	0.14	0.4	0.31	0.31	0.31	0.46	0.58	0.53	0.27	0.23	0.14	0.24	0.42	0.37	0.32
20.31	9.97	17.52	10.03	13.75	15.31	14.56	15.05	12.72	16.25	15.09	11.97	14	9.7	9.77	13.99	13.31	14.2
5.69	0.96	3.84	1.96	3.21	4.95	2.8	5.15	18.84	12.6	13.36	13.03	2.49	7.94	3.9	3.36	6.51	2.01
0.18	0.1	0.14	0.23	0.24	0.06	0.05	0.06	1.44	0.31	0.15	0.05	0.06	0.12	0.1	0.09	0.6	0.07
1.6	0.27	0.92	0.52	0.84	1.5	0.86	1.27	2.53	5.39	2.76	0.68	0.47	0.86	0.98	1.02	1.61	0.78
2.5	1.64	1.63	3.46	2.56	0.48	0.72	0.35	1.37	5.41	1.16	0.59	0.97	0.9	2.01	1.71	1.03	2.3
2.51	3.22	1.47	0.8	2.85	0.85	3.18	3.3	1.44	2.8	0.65	1.12	3.08	0.06	1.37	2.21	0.04	3.01
5.54	1.63	5.29	3.02	3.19	6.03	4.64	5.11	4.16	2.77	6.06	4.2	3.45	3.26	2.2	3.3	3.93	3.01
0.08	0.02	0.07	0.03	0.07	0.06	0.05	0.05	0.1	0.12	0.11	0.05	0.04	0.02	0.03	0.09	0.09	0.05
4.79	1.89	3.52	3.91	3.71	2.46	1.72	1.87	12.9	4.12	2.96	5.04	2.1	2.29	3.21	2.96	4.46	3.28
99.27	100.36	99.79	100.19	99.83	99.32	99.65	99.5	99.73	99.93	99.22	99.15	100.22	99.67	99.77	99.97	99.44	100.07
<0.01	0.01	0.02	0.01	0.01	0.02	<0.01	0.5	<0.01	0.01	0.44	5.09	0.2	0.04	0.16	0.06	0.19	0.01
0.42	0.36	0.34	0.78	0.64	0.1	0.13	0.009	3.43	0.39	0.18	0.11	0.19	0.19	0.43	0.31	0.56	0.46
58.77	28.11	66.70	45.38	42.69	84.99	58.51	63.61	70.42	49.85	82.97	74.05	49.18	81.10	48.48	52.43	83.81	41.65
8	1	5	3	9	5	5	4	25	25	27	6	5	5	5	10	9	5
15	2	8	3	23	7	8	6	185	240	176	15	2	11	10	36	35	8
3	2	2	1	2	3	3	3	17	24	15	2	2	2	2	5	33	3
2	<1	2	<1	1	1	2	2	12	34	12	7	2	1	2	2	5	2
4	1	2	1	4	3	2	31	12	7	1400	1300	162	52	3	9	29	4
68	12	47	27	75	41	21	45	60	188	106	35	20	91	51	42	2900	27
16	16	15	15	16	18	18	27	24	20	28	59	18	17	18	17	32	20
223	69	220	122	118	196	120	160	151	149	230	137	113	131	80	123	162	117
87	68	52	66	190	49	86	87	62	419	42	43	79	24	96	140	18	155
62	21	43	28	34	56	61	39	24	16	26	33	37	29	29	27	32	34
357	143	285	155	240	266	293	281	55	53	125	230	246	179	188	221	216	263
23.7	11	19.5	10.7	11.6	17.5	17.7	18.9	1.7	1	6	20.5	14.9	9.4	11.3	12.2	11.9	15.3
4.8	1.1	1.5	1	0.6	0.5	0.9	1.8	1.1	0.8	0.6	1.8	2.6	7.8	1.3	4.1	6.7	0.6
<	0.1	0.1	0.2	0.2	0.1	0.1	0.2	0.2	0.2	0.8	0.8	0.3	0.4	0.2	0.2	0.5	0.2
0.6	0.5	0.6	0.5	0.7	0.6	0.6	0.6	0.5	0.4	0.4	0.6	0.6	0.7	0.5	0.5	9.2	0.6
1.1	0.5	0.9	0.6	1.4	1.7	0.8	3.1	7.5	1.6	1.3	1.2	0.8	1.4	1.8	1.5	3.9	2
3.12	0.76	2.47	1.38	3.43	4.98	1.82	4.46	8.06	5.38	4.89	1.68	1.45	2.06	1.5	2.86	4.11	2.87
1371.8	386.7	1295.8	673.5	877.6	2004.2	1711.2	1727.9	743.2	365.1	1597.2	2173.8	1179.5	688.6	697.3	1273.9	1931.3	2120.3
62	16	31	25	42	38	49	37	24	14	21	73	29	30	27	34	52	46
137	34	76	57	84	88	114	84	46	34	50	145	66	60	53	77	107	109
62	13	30	22	36	37	48	35	17	16	18	60	27	24	24	31	42	44
0.7	<	0.7	<	<	0.7	<	0.9	0.7	0.8	1	<	<	<	<	<	0.8	<
<1.5	2	<1.5	2	3	<1.5	1	2	9	8	2	21	4	22	7	2	26	4
0.3	0.1	<	<	<	0.2	<	4.9	0.4	0.6	1.2	9.8	0.9	0.3	0.3	0.1	0.6	0.1
20.9	9.38	21.3	10.6	14.5	18.8	16.7	16.1	8.1	7.62	9.98	11.3	13.7	11.5	12.5	13.7	13.9	13.8
6.72	3.67	6.52	3.52	3.87	5.54	5.55	5.64	1.52	1.62	2.93	8.65	6.35	5.75	5.02	5.05	3.92	5.06

40616	40617	40618	40621	40624	40626	40631	40635	109R1	109R2	109R3	109R4	109R5	109R8	109R10	109R11	M4	M6
71.57	75.37	68.25	67.53	64.07	45.08	44.11	68.01	73.89	63.8	70.82	66.38	65.01	72.56	66.32	73.64	62.51	53.86
0.37	0.34	0.34	0.52	0.63	0.6	0.62	0.47	0.26	0.61	0.31	0.37	0.37	0.15	0.41	0.23	0.68	0.59
13.35	14.17	14.32	14.51	15.12	16.33	17.44	13.96	12.6	12.37	15.64	13.89	15.43	10.6	12.82	12.56	15.66	16.34
3.65	1.09	2.27	4.37	5.35	9.34	8.14	4.57	3.37	11.46	2.52	8.22	6.97	6.78	8.74	4.6	6.54	7.79
0.08	0.03	0.11	0.06	0.1	0.34	0.17	0.09	0.12	0.33	0.05	0.18	0.1	0.14	0.16	0.11	0.1	0.13
1.12	0.44	0.72	1.3	2.21	6.09	9.03	1.44	0.83	2.62	0.78	1.78	1.09	1.21	1.37	0.66	2.74	6.02
1.28	0.42	3.19	2.38	4.17	9.45	8.98	1.68	1.27	1.06	0.33	0.83	0.86	1.44	1.76	0.07	4.61	8.73
3.96	4.56	3.98	3.56	3.7	2.57	2.66	4.27	3.15	0.05	4.46	1.82	1.73	0.05	0.99	0.07	1.78	2.9
2.06	2.3	3.3	3.95	2.55	2.44	1.91	2.52	2.26	2.96	2.69	3	4.38	3.31	3.43	4.53	1.85	1.5
0.07	0.05	0.06	0.13	0.13	0.14	0.06	0.12	0.05	0.2	0.05	0.1	0.06	0.04	0.12	0.04	0.1	0.06
2.58	1.22	3.09	1.2	2.17	7.5	6.83	2.96	2.45	3.6	1.78	3.16	3.82	3.25	3.44	2.69	3.39	2.47
100.09	99.99	99.63	99.51	100.2	99.88	99.95	100.09	100.25	99.06	99.43	99.73	99.82	99.53	99.56	99.2	99.96	100.39
0.04	0.02	0.13	0.01	0.04	0.05	0.01	0.01	0.02	0.16	0.01	0.05	0.01	0.22	0.11	0.11	<0.01	<0.01
0.34	0.063	0.53	0.005	0.14	1.13	0.83	0.29	0.25	0.19	0.09	0.22	0.59	0.33	0.34	0.23	0.07	0.03
37.77	35.49	35.92	46.92	37.69	41.51	48.45	39.96	41.15	83.41	42.01	64.33	67.87	75.21	63.58	97.37	41.80	39.27
11	7	9	10	14	34	35	10	4	14	4	6	5	3	8	3	17	33
22	13	16	70	106	244	195	66	17	34	12	42	22	9	65	2	129	176
31	5	3	6	20	53	373	6	3	4	2	7	4	2	6	2	43	67
4	3	2	1	4	53	137	2	2	6	1	4	3	3	3	2	9	34
8	3	11	4	8	198	57	2	2	6	2	5	3	3	5	9	11	73
512	46	435	51	75	164	109	45	32	112	26	70	24	50	47	24	104	81
19	20	22	22	22	22	20	22	1	<	<	<	<	1	<	5	5	2
70	83	96	102	73	116	87	72	93	125	113	120	179	123	142	175	84	69
265	109	406	242	280	279	317	129	107	28	127	57	53	24	41	6	263	268
43	38	39	34	34	19	14	32	25	26	24	19	20	28	16	42	34	24
266	259	254	216	221	41	32	206	242	317	295	214	285	221	167	193	225	77
10.6	12.8	10.8	12.2	11.4	<1	<1	11.7	16	12	19.4	12.9	17.2	10.4	10	13.4	12.0	3.4
1.1	1.4	1.5	3.1	1	1.6	0.6	0.3	10.5	2.5	1.7	3.2	3.6	5.5	3.4	0.8	0.9	0.5
0.3	0.4	0.3	0.2	0.1	0.2	0.2	0.2	0.1	0.2	0.1	0.2	0.1	0.1	0.2	0.2	0.2	0.1
1.9	0.7	2.1	0.6	0.5	0.5	0.4	0.5	0.4	0.4	0.4	0.4	0.4	0.4	0.3	0.3	0.1	0.4
2.9	2.1	1.4	0.7	1.5	3.1	0.8	0.5	0.9	0.7	1.3	1	1.9	0.6	0.8	1.1	1.2	1.2
1.82	1.87	2.25	1.21	1.79	6.5	4.01	1.81	2.12	2.01	2.17	2.13	2.97	1.9	3.39	2.37	1.32	2.79
1675.8	1273.2	1745	958.1	732.7	620	372.5	697.3	737.2	727.1	697.5	779.1	1119.1	948.8	854.5	1160.3	429	410
39	46	41	46	30	13	4	41	147	19	39	51	9	59	30	49	40	15
83	102	94	89	71	33	12	87	308	40	82	103	23	123	57	117	81	33
34	43	40	37	31	19	5	37	113	14	29	39	9	44	21	46	35	13
<	<	0.5	<	<	0.6	<	<	<	<	<	<	0.6	<	0.5	0.6	0.7	<
40	45	96	4	11	48	6	4	2	<1.5	3	3	3	3	4	4	147	10
0.3	0.6	0.2	0.1	0.2	0.1	<	<	0.2	0.2	<	<	<	0.4	0.2	0.2	0.1	<
10.2	14.5	11.5	15.1	12.4	9.17	3.85	12.3	19.3	13.8	18.2	18.7	21.7	20.6	15.7	16.3	13.4	4.39
3.19	4.89	4.24	4.9	3.25	1.2	0.36	4.3	6.99	5.4	6.85	6.15	8.72	6.36	3.98	5.96	3.24	1.07

M7	M9	M10	M19	M24	M25	M29B	M3O	M33	M39	M42	M45	M46	M50	M59	M60	M63	M67
50.66	50.49	65.89	59.68	66.52	67.63	68.15	49.22	62.93	52.39	40.87	60.15	70.08	64.1	63.06	69.98	64.92	67.73
0.92	0.96	0.51	0.69	0.49	0.46	0.59	0.92	0.68	0.55	0.97	0.73	0.44	0.65	0.71	0.8	0.65	0.48
18.32	18.39	15.70	16.59	15.3	14.87	14.09	19.56	16.28	14.87	18.93	16.55	14.49	14.69	16.39	12.65	15.5	15.14
10	10.36	4.70	8.76	4.36	4.33	4.66	11.74	5.83	10.30	15.08	7.43	3.82	6.41	6.85	5.79	5.64	4.95
0.19	0.16	0.08	0.09	0.06	0.07	0.11	0.18	0.07	0.21	0.29	0.12	0.06	0.09	0.13	0.1	0.09	0.1
4.38	4.73	1.35	4.58	1.22	1.33	1.66	4.01	3.1	7.29	13.46	3.08	1.68	2.78	3	2.46	3.12	1.58
8.64	6.46	0.77	1.11	2.17	3.04	3.03	7.6	1.15	6.09	0.49	4.47	1.04	2.96	0.85	0.59	1.3	1.59
4.03	2.19	3.81	3.3	3.78	3.48	2.7	2.28	1.96	5.07	2.51	2.58	5.54	2.27	3.44	2.6	5.91	5.09
0.73	2.46	3.49	1.29	3.35	3.3	2.83	0.76	4.74	0.24	0.08	1.53	0.4	2.45	2.62	1.86	0.1	1.42
0.1	0.11	0.13	0.12	0.12	0.13	0.08	0.09	0.12	0.05	0.1	0.08	0.09	0.1	0.13	0.12	0.1	0.12
2.61	3.7	2.88	4.04	1.9	1.43	2.05	4	3.23	2.83	7.77	3.44	2.22	3.64	3.08	2.9	2.51	1.87
100.58	100.01	99.33	100.25	99.27	100.07	99.95	100.36	100.09	99.89	100.55	100.16	99.86	100.14	100.26	99.85	99.84	100.07
0.04	0.09	0.06	0.03	0.11	0.03	0.02	0.03	0.1	0.06	0	0.11	<0.01	0.01	<0.01	<0.01	<0.01	<0.01
0.03	0.11	0.09	0.08	0.07	0.03	0.04	0.04	0.08	0.14	0.07	0.14	0.04	0.24	0.04	0.04	0.06	0.08
28.74	45.39	51.33	57.10	43.44	41.52	43.93	32.56	71.60	40.26	81.86	39.54	24.02	50.00	56.71	57.52	30.87	30.99
35	29	9	19	8	7	15	33	15	35	55	21	7	16	19	20	18	8
292	271	65	159	60	54	114	300	133	201	265	158	45	120	149	147	136	61
83	61	4	50	5	5	46	107	28	67	1181	37	5	49	24	227	49	4
54	31	2	11	2	2	7	47	5	36	335	12	2	10	5	43	10	2
163	112	4	6	5	3	17	123	8	48	6	52	3	10	6	3	3	4
82	118	63	95	47	38	67	104	58	119	396	104	64	61	162	147	108	75
10	1	1	3	<	1	3	2	6	3	5	4	<	3	<	2	2	2
28	84	97	79	90	88	88	27	224	5	7	47	21	62	119	69	4	46
385	267	134	115	214	265	233	360	128	228	177	377	325	192	141	111	160	253
24	26	36	32	26	32	28	23	33	19	24	30	28	31	29	19	27	28
76	132	213	253	206	197	211	78	242	62	88	204	200	233	247	182	238	207
2.2	5.3	12.4	12.6	11.8	11.8	11.0	3.2	12.5	2.3	3.2	11.0	12.5	12.5	11.9	10.4	12.1	12.2
0.9	0.5	0.4	0.4	0.3	0.5	0.3	0.4	0.3	0.6	0.3	0.6	0.3	0.3	0.3	1.9	1	0.6
0.2	0.1	<	0.1	<	<	0.1	<	0.2	<	<	<	<	0.1	0.1	<0.1	<0.1	<0.1
0.1	0.2	<	<	0.1	0.2	<	0.1	<	0.1	<	0.1	<	<	2.9	0.1	<0.1	0.2
1.5	1	0.4	3.2	0.7	0.7	1.3	0.7	1.8	0.9	4.4	1.8	1	0.5	2.4	0.9	0.6	1
1.44	1.56	1.29	4.56	0.93	0.94	1.28	1.07	3.3	0.33	0.79	0.96	0.91	0.87	2.47	1.31	0.27	1.64
285	1017	968	88	755	878	813	423	1175	85	32	562	123	664	761	483	42	362
9	15	46	35	30	34	26	8	25	11	12	25	37	25	26	21	27	28
19	33	81	69	63	73	63	24	61	22	23	59	71	55	56	40	56	63
10	15	38	31	29	30	26	12	24	12	16	26	33	25	22	17	26	26
<	<	<	<	<	<	0.7	<	1	<	<	<	<	<	0.7	0.9	<0.5	<0.5
16	20	4	6	13	11	10	7	13	5	14	16	5	8	29	10	9	11
<	<	0.3	<	<	<	0.1	<	<	<	<	0.1	<	<	<	<0.1	<0.1	0.1
3.37	6.81	16	15.6	15.3	14	12.6	3.46	15.1	3.97	4.81	12.5	16.1	14.1	14.2	9.05	14.5	16
1.18	1.86	3.54	3.76	3.56	3.33	3.04	1.14	3.86	1.18	0.94	3.15	3.18	3.48	3.47	2.02	3.49	3.25

M69B	M73	M77	M78	M79	M80	M81	M84	M85	M86	M89	M90	M98	M103	M105	M112	M114	M116
50.29	68.85	66.65	74.18	63.48	64.55	62.58	66.77	61.05	62.81	64.53	62.98	68.53	73.19	73.93	75.3	75.48	77.62
0.81	0.49	0.48	0.25	0.68	0.6	0.65	0.56	0.72	0.65	0.63	0.69	0.5	0.25	0.31	0.2	0.19	0.18
19.29	14.96	16.41	13.65	15.6	14.11	15.18	14.83	15.89	15.34	14.87	15.32	14.76	13.72	13.72	13.02	13.49	12.54
11.66	3.93	4.15	2.12	6.03	4.87	6.2	5.32	7.59	6.33	6.08	5.6	4.34	2.4	2.66	1.61	1.45	2.01
0.21	0.06	0.03	0.02	0.08	0.09	0.09	0.07	0.1	0.09	0.09	0.1	0.06	0.04	0.11	0.01	0	0.01
6.42	2.01	2.03	0.5	2.15	2.21	2.82	2.56	3.57	3.03	2.75	2.21	1.38	0.52	0.61	0.35	0.42	0.6
0.77	0.34	0.24	0.4	5.59	5.39	3.53	2.02	2.69	4.92	1.73	5.62	1.09	0.18	0.18	0.03	0.03	0.01
5.77	6.54	7.07	3.66	3.49	2.29	2.66	3.52	3.66	3.42	3.42	3.61	3.33	3.71	4.63	1.7	2.11	0.42
0.25	0.16	0.5	3.85	0.36	3.2	2.46	1.92	0.66	0.77	2.97	1.33	3.83	4.26	1.91	4.79	4.2	4.16
0.1	0.1	0.12	0.04	0.1	0.11	0.11	0.08	0.1	0.11	0.11	0.13	0.12	0.05	0.05	0.03	0.02	0.02
4.48	1.97	1.95	1.3	2.38	2.73	2.79	2.5	4.04	2.36	2.77	2.22	1.76	1.08	1.6	1.85	2.31	2.15
100.05	99.41	99.63	99.97	99.94	100.15	99.07	100.15	100.07	99.83	99.95	99.81	99.7	99.4	99.71	98.89	99.7	99.72
<0.01	<0.01	<0.01	<0.01	<0.01	<0.01	<0.01	<0.01	<0.01	<0.01	<0.01	0.01	<0.01	<0.01	<0.01	0.01	<0.01	<0.01
0.06	0.06	0.05	0.1	0.04	0.27	0.07	0.04	0.17	0.02	0.04	0.11	0.02	0.01	0.07	0.16	0.35	0.05
50.49	23.98	25.71	51.72	21.66	41.33	46.03	44.71	39.98	31.30	52.62	27.72	54.10	55.13	34.38	74.82	68.34	91.71
45	10	10	4	15	13	17	12	16	15	16	13	10	4	4	4	4	3
318	61	63	13	139	108	132	109	145	132	143	113	68	8	6	<1.5	3	2
11	6	5	5	30	39	55	29	64	40	45	27	7	2	2	2	2	2
29	3	2	2	10	6	11	6	11	8	8	6	2	1	<1	2	2	1
10	3	2	4	8	11	8	5	5	5	5	6	5	3	35	14	30	10
280	87	68	32	60	49	86	71	86	92	71	99	91	33	33	18	26	28
<	<	<	<	5	4	<	6	6	6	<	5	3	<	2	17	<	1
19	7	20	118	16	104	86	76	22	36	77	44	150	122	78	298	153	171
152	147	94	121	406	216	240	188	205	283	226	305	157	142	152	41	56	10
33	26	39	20	31	30	32	29	30	32	35	37	32	40	44	42	47	37
70	212	214	192	228	205	222	231	230	209	211	231	220	207	244	238	241	214
2.8	11.8	13.3	10.5	11.6	11.5	11.5	12.2	11.3	11.0	11.4	12.4	12.6	14.7	15.1	15.8	16.5	14.8
0.4	0.5	0.3	0.2	1	0.8	0.2	0.5	0.4	0.6	0.2	0.9	0.2	0.7	1.1	0.3	0.3	0.4
<	<0.1	<0.1	<	<0.1	<0.1	<	<	0.1	<	<	<	<	<	<	0.1	0.4	0.1
<	0.1	0.2	<	<0.1	0.1	<	<	<	<	<	0.2	0.2	<	<	<	<	<
2.2	1	0.4	0.6	1.4	0.4	0.6	0.7	0.5	1	0.5	1.4	1.3	0.5	1.3	2.1	1	1
1.54	0.47	0.68	2.24	0.9	1.31	1.27	1	0.49	0.93	1.18	1.32	3.94	3.43	2.04	3.84	2.05	2.5
78	71	91	942	102	715	595	499	213	223	871	400	889	1133	551	932	1613	858
47	22	53	23	27	27	27	23	24	29	30	30	37	50	42	43	41	32
104	42	110	50	64	60	59	58	55	62	63	68	78	91	89	94	92	71
47	21	47	16	29	26	26	25	23	30	30	32	33	43	37	39	37	31
<	<0.5	<0.5	<	<0.5	<0.5	<	<	<	<	<	<	0.6	0.6	<	1.7	1	0.9
34	12	8	11	30	8	19	16	18	18	11	30	34	11	19	17	13	12
<	<0.1	<0.1	<	0.1	<0.1	<	0.1	<	<	<	<	<	<	<	0.4	1.9	<
5.97	16.6	16	19.3	14.2	13.7	8.57	15.3	13.5	13.5	13.3	14.2	18.4	20.1	18.4	21.6	21.2	16.9
2.06	3.23	2.41	3.84	3.47	3.47	1.9	3.89	3.36	3.31	3.32	3.56	4.08	4.07	4.65	4.8	4.71	4.35

M117	M120	M121	M134	MBE96-8	MY	MB96-35	MB96-37	MB96-38	MB96-39	MB96-40	MB96-41	MB96-42	MB96-43	MB96-44	MB96-45	MB96-46
62.72	63.11	63.67	68.17	62.71	66.94	74.58	68.89	68.13	73.89	74.24	74.03	66.68	69.5	71.51	73.78	71.55
0.65	0.66	0.65	0.51	0.71	0.64	0.27	0.46	0.53	0.27	0.23	0.3	0.49	0.51	0.36	0.26	0.3
14.97	14.95	15.12	15.04	15.01	14.11	13.85	15.12	14.98	13.7	13.93	13.74	14.21	14.95	15	13.1	13.87
5.91	6.12	5.92	4.83	5.96	5.82	2.08	4.11	5.5	2.22	2.15	2.38	6.09	4.6	3.15	4.79	5.74
0.09	0.1	0.12	0.03	0.1	0.08	0.01	0.02	0.1	0.02	0.01	0.01	0.37	0.14	0.02	0.02	0.12
2.67	2.43	2.61	1.67	2.62	2.81	0.38	1.23	1.18	0.37	0.49	0.46	1.34	1.42	0.89	0.64	1.06
4.28	6.29	4.19	0.36	4.29	1.74	0.13	0.08	0.25	0.41	0.04	0.04	0.9	0.21	0.06	0	0.02
3.06	2.66	3.18	3.24	3.46	1.64	3.54	3.66	2.83	3.46	3.21	3.95	2.94	2.62	3.8	0.06	0.48
2.64	1.51	2.08	3.97	3.61	3.05	4.34	3.83	4.04	4.31	2.88	3.24	3.27	3.39	2.53	3.98	3.4
0.11	0.09	0.1	0.12	0.11	0.1	0.03	0.09	0.14	0.04	0.02	0.05	0.13	0.13	0.05	0.03	0.04
2.32	2.4	2.29	1.71	1.77	3.18	1.11	2.12	2.22	1.25	2.71	1.79	3.23	2.42	2.23	3.09	2.94
99.42	100.32	99.93	99.65	100.35	100.11	100.32	99.61	99.9	99.94	99.91	99.99	99.65	99.89	99.6	99.75	99.52
<0.01	<0.01	<0.01	<0.01	0.13	<0.01	<0.01	<0.01	<0.01	<0.01	0.02	<0.01	0.01	0.02	0.02	<0.01	0.01
0.11	0.04	0.04	0.04	0.06	0.17											
41.98	30.57	38.89	61.04	44.56	63.42	56.26	57.50	62.89	54.74	50.91	48.11	54.56	62.96	46.98	98.72	89.92
16	18	16	12	22	16	4	11	11	3	5	4	11	11	6	4	4
126	126	124	73	157	143	4	60	83	3	3	12	77	81	12	7	18
51	47	47	9	31	46	2	11	8	2	3	3	7	7	3	2	4
8	8	9	2	8	10	1	3	3	2	2	1	3	3	1	1	1
9	5	4	3	37	22	2	3	18	4	3	3	6	7	6	35	14
57	64	92	63	47	68	17	36	32	19	23	21	75	40	38	33	70
13	8	<	<	1	4	<	<	<	<	<	1	<	<	<	4	2
70	39	56	136	115	127	136	138	157	140	121	112	135	129	103	170	154
233	352	315	170	205	131	96	122	103	104	78	112	100	78	98	4	8
33	33	36	33	33	26	41	28	35	62	38	41	42	41	40	25	24
225	228	227	231	186	188	270	243	212	269	282	266	199	209	282	254	238
12.1	12.0	11.7	12.8	9.7	10.7	17	13.6	10.7	16.1	16.8	13.4	10.6	11.1	16	13.7	11.6
0.5	0.3	0.2	0.5	0.2	0.3	0.5	0.4	1.7	0.6	0.7	0.8	0.9	0.2	0.4	1	0.2
<	<	<	<	0.1	0.1	<	<	<	<	<	<	<	<	<	<	0.1
0.2	0.2	<	<	0.1	0.2	<	<	0.3	0.2	<	<	0.1	0.4	<	<	<
0.8	1.1	0.9	1.1	1	0.5	0.4	0.7	0.5	0.5	0.6	0.9	0.7	0.9	0.4	0.9	1.4
0.59	0.41	0.82	4.46	1.14	1.71	1.98	2.98	2.9	2.35	1.99	2.36	4.06	2.57	1.17	1.46	1.53
562	515	568	1176	809	742	988	817	876	947	787	942	696	711	606	931	703
32	31	34	42	27	25	57	38	54	174	47	54	47	49	41	32	41
70	70	70	88	62	47	102	80	113	289	82	107	95	101	74	72	82
31	32	33	35	28	20	45	31	47	131	42	44	39	45	37	29	32
<	<	<	0.7	0.6	0.6	<	0.5	<	<	<	<	<	<	<	0.9	0.9
7	22	5	8	20	29	3	3	2	3	8	7	4	2	3	5	7
<	<	<	<	<	0.3	<	0.3	<	<	<	0.1	<	<	0.3	2.6	2.1
13.8	13.9	13.6	17.9	10.3	11.4	22	21.4	19.6	22	23.3	22.3	18.4	19.3	20.6	25.1	18.4
3.45	3.41	3.34	4.25	2.64	3.36	5.4	5.01	4.59	5.05	5.21	5.73	4.35	4.66	4.98	5.79	3.91

Rosebery alteration study and regional alteration studies in the Mount Read Volcanics: The record of diagenetic alteration in the strongly deformed, felsic volcaniclastic succession enclosing the Rosebery and Hercules massive sulphide deposits

by Rodney L. Allen
Volcanic Resources, Stavangar, Norway

Drill core logging, petrography and geochemistry of the Rosebery drill cores are now at a stage where regional diagenetic alteration can be distinguished from local hydrothermal and tectonic alteration stages. The results have important implications for both the Rosebery alteration study and for the regional alteration studies of the Mount Read Volcanics and elsewhere, so a contribution focussing on diagenetic alteration is presented here.

This documentation of alteration in the Rosebery–Hercules area results from detailed study of the Rosebery and Hercules mine sequences over a number of years, in addition to the recent studies of AMIRA project P439.

Introduction

The Rosebery and Hercules ore deposits are strongly deformed, Zn-Pb-Cu-Ag-Au massive sulphide deposits that occur in a Cambrian felsic volcaniclastic succession of low metamorphic grade. Recently there has been debate as to whether the deposits are synvolcanic and formed on the seafloor (Green et al., 1981) or below the sea floor (Allen, 1991, 1994b), or whether they formed much later in dilational structures during compressional deformation (Aerden, 1994). The ore deposits contain alteration assemblages related to ore formation, regional diagenesis, tectonic deformation, metamorphism and subsequent granite intrusion. However, there is disagreement in distinguishing these alteration events and in the interpretation of their relative importance in ore formation.

Volcanic-hosted massive sulphide deposits (VHMS) are generally interpreted to have formed at the discharge site of a high temperature (300°C) submarine hydrothermal system. The discharge of such a hydrothermal system produces alteration zones at successively lower temperatures outward from the ore deposit. In contrast, diagenetic alteration is related to the regional geothermal gradient in the depositional basin. Temperatures range from near 0°C at the seafloor to 250°C at 2–10 km depth, the precise depths of particular isotherms depending on the geothermal gradient. The resulting diagenetic alteration pattern is generally a sequence of flat-lying zones (layers), each characterised by a particular mineral assemblage that formed within a particular temperature range. It is generally inferred that the high temperature hydrothermal ore-related alteration either grades outward into synchronous, low temperature, diagenetic alteration, or is subsquently enveloped by diagenetic alteration after the ore deposit and host rocks are buried deeper beneath younger strata in the depositional basin.

This contribution aims to clarify the character, intensity, timing and distribution of synvolcanic diagenetic alteration in the Rosebery-Hercules area, and the relationship between this diagenetic alteration, local hydrothermal carbonate alteration associated with the massive sulphide deposits, and deformation fabrics.

Changes in whole rock and mineral chemistry related to the diagenetic alteration are currently being explored and will be reported in the future.

Structure and stratigraphy of the altered succession

The Rosebery and Hercules ore deposits occur in a belt of moderately to strongly deformed rocks adjacent to the Rosebery thrust fault at the western margin of the Central Volcanic Complex of the Mount Read Volcanics. The ore deposits occur on the eastern limb and in the hinge of an anticline that forms the hangingwall to the Rosebery fault.

Two main regional foliations, one main generation of folding and several generations of faulting are recognized (Allen, 1991, 1994a). The earliest foliation (S1) is a spaced, stylolitic foliation expressed by concentrations of sphene, leucoxene, and sericite or chlorite. S1 is generally parallel to bedding, has no known related folds, and is interpreted by Allen (1990, 1991, 1994a) and Allen and Cas (1990) as a diagenetic compaction and dissolution foliation. Development of S1 may have continued into the early stages of compressional deformation. However, S1 is clearly overprinted and folded by the main strong, pervasive, regional cleavage, S2. S2 is axial planar to the main folds (F2) and is coplanar with a strong stretching lineation (L). S2 grades into, or is overprinted by, strong local foliation related to major brittle-ductile faults. Faults and shear zones are common, and several generations of movement are recognized along the major faults (Allen, 1991).

The lowest stratigraphic unit exposed in the Rosebery–Hercules area is a greater than 800 m thick, poorly stratified, rhyolitic to dacitic pumice deposit, with subordinate coherent to hyaloclastic sills (Footwall Volcanics; Allen, 1991, 1994a). This unit is overlain by a well stratified, up to 300 m thick, succession of black mudstone and rhyolitic pumiceous mass flow units (Hangingwall Volcaniclastics). These are in turn overlain by more than 1 km of rhyolitic pumice breccias, lavas and dacitic intrusions known informally as the Mount Black Volcanics (Allen, 1991, 1994a). Locally, a 0–50 m thick package of stratified, felsic, crystal-pumice-lithic sandstones and siltstones occurs at the boundary between the Footwall Volcanics and Hangingwall Volcaniclastics. This package is termed "host rock" by Rosebery Mine staff and the Transitional Stratified Volcaniclastics (TSV) by Allen (1991, 1994a,b). Ore lenses occur within the top of the Footwall Volcanics pumice breccia and within the lower part of the Transitional Stratified Volcaniclastics (Allen, 1991, 1994b).

The pumiceous units of the Footwall Volcanics and Hangingwall Volcaniclastics are mainly interpreted as submarine mass flow deposits, that were fed directly (syneruptively) from large, subaerial to shallow water, magmatic pyroclastic eruptions (Allen, 1990, 1991, 1994a) and Allen and Cas (1990). The Transitional Stratified Volcaniclastics is interpreted mainly as slightly to moderately reworked pyroclastic debris, derived mainly from the Footwall Volcanics pumice deposit (Allen, 1991, 1994a).

Primary textures of the altered rocks

Altered, rhyolitic to dacitic pumice and glass shards are the main constituents of the Footwall Volcanics and Hangingwall Volcaniclastics throughout the Rosebery–Hercules area. The pumice and shard textures are remarkably well preserved in hand specimen and thin section, despite the strong deformation and long history of alteration. The textures are well preserved due to widespread replacement by mechanically competant minerals such as feldspar, prior to deformation (Allen, 1990, 1991, 1994a,b; Allen and Cas, 1990). The replaced pumice and glass shards were then variably flattened, stretched and recrystallized during the deformation (by foliation and stretching lineation), but were not penetratively foliated and texturally destroyed. In contrast, pumice and shard textures are poorly preserved where they were replaced by incompetant, easily foliated, phyllosilicate-rich assemblages.

Apart from the mudstones, depositional units in the Footwall Volcanics and Hangingwall Volcaniclastics are very thick beds (mainly 50–200 m thick) with coarse, clast-supported, poorly to moderately sorted breccia texture of pumice clasts (pumice breccia) and subordinate glass shard matrix. Poorly vesicular lithic clasts are scattered irregularly throughout the footwall pumice units, but comprise <1% of the rock. In the Hangingwall Volcaniclastics lithic clasts are concentrated in the lower third of each mass flow unit where they typically form 5–30% of the unit. The tops of many beds are normal graded from breccia to sand-size and composed of

clast-supported pumice shreds and glass shards. The Transitional Stratified Volcaniclastics comprise thick to thin beds of planar-stratified, clast-supported, moderately to well sorted, fine breccia to sand-size pumice, shards, volcanic feldspar and minor quartz crystals, and 2–10% lithic clasts.

Green et al. (1981) interpreted the footwall pumice deposits as welded pyroclastic flow deposits and the fiamme-like lenses (phyllosilicate lenses in the S1 foliation) as a welding-compaction foliation. However, Allen (1990, 1991, 1994a, b) and Allen and Cas (1990) noted that within tectonically weakly deformed feldspar, quartz and carbonate altered domains the pumice and shard textures are unflattened and non-welded. They reinterpreted the fiamme-like lenses and the associated S1 fabric as a post-depositional, diagenetic compaction foliation formed during burial of the pumice deposits.

The pumice clasts are porphyritic, with plagioclase and minor pyroxene phenocrysts in the footwall, and plagioclase, quartz and minor K-feldspar and biotite in the hangingwall. Each phenocryst is surrounded by a clot of highly vesicular round-vesicle pumice texture, which grades outward into slightly less vesicular, fibrous tube-vesicle pumice. The tube-vesicle pumice generally forms most of the pumice clast. The bubble walls of the pumice framework are mainly very thin (much thinner than the adjacent vesicle diameter) except for a relatively thick rim of altered glass directly around the phenocrysts. Glass shards include straight stick-like shards derived from tube-vesicle pumice and triangular-cuspate shards derived from round-vesicle pumice.

By comparison with texturally similar, unlithified, non-welded, pumice-rich, lithic-poor ignimbrite and airfall deposits, the initial porosity and density of the Rosebery–Hercules pumice breccia units can be estimated to 50–70% and 0.7–1 kg3/m3 respectively (Allen, 1987, chapter 5 part 2). The mean porosity and density of individual rhyolitic pumice clasts from large magmatic pyroclastic eruptions is 77% and 0.55 kg3/m3 respectively (Wilson et al., 1980; Sparks, 1978; Allen, 1987).

Backstripping the alteration events

Table 1 lists the alteration assemblages and alteration generations recognised in the Footwall Volcanics, Transitional Stratified Volcaniclastics and Hangingwall Volcaniclastics in this study. Different alteration types were distinguished according to mineralogy, alteration texture, and overprinting relationships with respect to foliations and other alteration types. The relative timing of each alteration type is shown in Table 1 as both the maximum time span possible according to overprinting relationships (widely spaced dashes), and the interpreted most likely timing (closely spaced dashes).

The alteration assemblages that are easiest to categorise are those that are unaffected or only very weakly affected by S2 foliation and F2 small folds, and are consequently post-main deformation in timing. These alterations are vein related and comprise the last quartz-carbonate vein sets associated with the S2–F2 deformation or later reactivation of S2 (19 in Table 1), and various granite-related assemblages related to intrusion of Devonian granites that underlie the area (20 in Table 1).

Earlier alteration assemblages that are strongly foliated by S2 and also overprint S1 are regarded as broadly syntectonic. However, both pre- and syn-S2 alteration assemblages can be equally strongly deformed and recrystallized. Consequently, it can be difficult to prove whether a deformed alteration assemblage is syn- to post-S1 and pre-S2, or is syn-S2 in origin. Distinct syn-tectonic syn-S2 alteration comprises anastomosing to subplanar sericitic S2 foliation domains, most quartz-carbonate and carbonate veins, the fine chloritic veinlet networks that infill brittle breccia zones adjacent to thrust faults, and some greenschist metamorphic assemblages (13–18 in Table 1). Strong sericite, quartz (silicification) and chlorite alteration associated with the massive sulphide mineralization range from strongly deformed and overprinted by S2, to areas of less deformed, syn- to late-S2 recrystallization and remobilization. Although the strong sericite, quartz and chlorite alterations are commonly foliated and folded by S2–F2 and locally preserve layering parallel to S1 and bedding, no indisputable direct evidence has yet been observed as to whether the alteration

Table 1 Alteration types and their relative timing, Rosebery-Hercules area

Regional + ORE RELATED alteration	Time -------> | S1 | S2 |
Deposition of pumice breccia	-
(1) Smectite (montmorillonite) (glass surfaces)	--- - - -
(2) SPHEROIDAL MN-CARBONATE (concentric layered, concretionary)	---- - - - - -
(3) Mordenite-clinoptilolite (replaces glass)	----- - - - - - -
Sphene-leucoxene±hematite	- --------- - - - - -
(4) ?Analcite (replaces mordenite-clinoptilolite)	----- - - - -
Adularia-quartz (overgrowths on plag phenos)	----- - - - - -
(5) Burial compaction, sericite fiamme	- - - - ------- - -
(6) SPOTTY MN-CARBONATE (not concretionary)	--- - - - - - -
SUB-NODULAR MN-CARBONATE VEINS	--- - - - - - -
(7) SERICITE ±QUARTZ-CARBONATE-LEUCOX	----- - - - - - - - -
(8) QUARTZ-Py±SERICITE ±Sp-Gn-Cpy	--- - - - - - - - - -
(9) CHLORITE ±QUARTZ ±Py-Sp-Gn-Cpy	--- - - - - - - - - -
(10) Calcite impregnation ± sp (hangingwall, pre/syn-S1)	- - --- - - - -
(11) Albite (replaces adularia, analcite; deep subseafloor)	- - - ------ - -
(12) Stylolitic S1	- --------- -
Chlorite/sericite pseudofiamme	- --------- -
(13) Metamorphic albite-chl-epid-carb-mag-leucox	- - ---------- -
Metamorphic biotite + retrograde chlorite	- - ---------- -
(14) Reactivated S1 ±sericite or chlorite	- --- - -
(15) Syn-S2 sericite-pale carbonate (cleavage related)	- --------- -
(16) Syn-S2 quartz-pale carbonate ±ser±sp-py-gn veins	- --------- -
(17) Pre/syn-S2 dark carbonate-apatite ±arspy veins, patches	- - - - - - - --- -
(18) Syn-S2 network chlorite veins (fault-related)	- - ------ -
(19) Late/post-S2 quartz-carbonate veins, bleached selvages	- ---- - -
(20) Post-S2 biot-tour, chl-mag, carb-fluor-apat-tour-arspy veins (with sericite-dark carbonate vein selvages)	--- - -
	| S1 | S2 |

---------- Interpreted main growth interval
- - - - - Time span that is possible from overprinting relationships

and mineralization is pre-, syn- or post-S1 (Table 1). Other indirect evidence (see below) strongly suggests that these alterations and mineralization are pre- to syn-S1.

Two lines of evidence suggest that some of the syn- and post-tectonic alteration types have a "closed system" behaviour in the sense that they result from recrystallization and remobilization of earlier alteration minerals rather than the introduction of new chemical components to the area. First, petrographically similar chlorites, sericites and dark Fe-Mn bearing carbonates occur repeatedly in different alteration generations. The similarity of these different generations of minerals is currently being tested by microprobe analysis of individual minerals (see preliminary report in this volume). Second, the composition of many syn- to late-tectonic veins changes according to the alteration in the rocks that the veins cross. For example, veins are chlorite-rich where they cross a patch of chlorite alteration and then become quartz-rich in an adjacent area of quartz-sericite alteration. This suggests that components in the wall rocks were "sweated" into veins during the deformation, rather than the veins being the source of the wallrock alteration.

Finally, the alteration assemblages that are regional in distribution and pre-date or are synchronous with the stylolitic S1 foliation are here defined as diagenetic (1, 3–5, 11–12 in Table 1). Alterations that show similar timing relationships but which are only local in distribution are related to discrete local hydrothermal alteration systems (2, 10 in Table 1) or the cooling of particular volcanic emplacement units.

Diagenetic alteration

All original glass surfaces of the pumice and glass shards, including bubble walls, invariably have a thin film (≤ 10 μm) of sericite, with or without chlorite. These sericite films are overprinted by all other alteration types and foliations, and occur regardless of which other alteration types have replaced the rest of the pumice and shards. Consequently, the sericite films are interpreted as the relic of an extremely early clay alteration that attacked all glass surfaces soon after deposition of the pumiceous strata.

The next alteration that is well preserved, regional in extent and pre-dates the S1 stylolitic fabric is feldspar. The feldspar typically comprises diffuse, cream to pink spots of relatively coarse grained albite ± orthoclase, 5–20 mm in diameter, centred on original igneous plagioclase phenocrysts, and a fine grained mosaic of feldspar and quartz between the spots. Locally, the coarse grained feldspar has replaced most of the rock. Within the feldspar altered domains, feldspar has partially replaced the original plagioclase phenocrysts, infilled cracks in the phenocrysts, and completely replaced the pumice and shard texture around the phenocrysts, except for the thin sericite films described above. The replacement by feldspar is not only texturally non-destructive, but has commonly sealed the pumice into competant spots and patches that have resisted subsequent deformation.

The feldspar alteration is mainly albite, but in the least deformed and least hydrothermally altered rocks throughout the area, there are relict cores of orthoclase within the albite altered domains (Allen and Cas, 1990). The orthoclase occurs within the plagioclase phenocrysts, in fractures in the phenocrysts and as thin rims up to 1 mm wide enclosing each phenocryst. The K-feldspar rims are in turn enclosed by albite. The K-feldspar is generally untwinned and optically homogeneous without subgrains. The outer edge of the K-feldspar halo is irregular, locally ragged and grades outward into complex twinned (interpenetrating, cross-hatched) and simple to lamellae twinned albite. These textures are attributed to replacement of K-feldspar by albite. Similar textures of K-feldspar alteration nucleated on feldspar phenocrysts and K-feldspar alteration overprinted by albitisation occur in some porphyry copper deposits (e.g. Gustafson and Hunt, 1975). Henneberger and Browne (1988) also noted a similar texture of adularia alteration at the young Ohakuri geothermal system, New Zealand. The adularia initially formed a rim on plagioclase phenocrysts, and then replaced the phenocryst starting at the rim and along fractures and cleavages.

The feldspar alteration textures indicate that there were two stages of feldspar alteration (Table 1). First, a potassium feldspar, probably adularia or orthoclase, nucleated on the igneous plagioclase phenocrysts and grew outwards, replacing the surrounding

pumice to form K-feldspar spots or more extensive areas of replacement. Close to the plagioclase phenocrysts, the K-feldspar replaced both the pumice framework (original glassy bubble walls) and all original porosity such as cracks in the phenocrysts and the interior of vesicles. At greater distance from the phenocrysts the replacement by feldspar was incomplete or the replacement was by fine grained feldspar plus quartz. At a later stage, but still prior to S1 stylolitic foliation, the K-feldspar was extensively replaced by albite.

Locally, the K-feldspar or albite that replaces the pumice framework and vesicles, preserves relicts of fan-shaped fibrous texture and mosaics of blocky to tabular subgrains. The fibrous textures are not common feldspar textures or crystal shapes, and are not spherulitic devitrification of glass because they occur within vesicles as well as the original glass bubble walls. Consequently, the textures suggest that at least locally the feldspar has replaced and pseudomorphed earlier minerals. Considering the fan-radiating fibrous texture, and the structure and composition of common diagenetic minerals that could be replaced by feldspar, the precurser minerals were probably zeolites.

Comparison with other diagenetic studies

There are several studies of diagenetic alteration that are relevant to the Rosebery–Hercules area. The most important studies are those of the Neogene marine basins of the Japan volcanic arc. These basins are broadly analogous to the Rosebery–Hercules area in their extensional back-arc to intra-arc tectonic setting, mainly marine depositional environments, abundance of pumiceous felsic strata, and the association with massive sulphide mineralization (the Kuroko deposits in the Japanese case). The Neogene marine basins in Japan show a consistent pattern of vertical diagenetic zoning, comprising from top to bottom: (1) a weak clay zone in which the rocks are composed of fresh glass and variable smectite-opal alteration, and no zeolites, (2) mordenite-clinoptilolite (plus smectite-opal) zone, the first zeolitic alteration zone, (3) analcite-heulandite zone, (4) laumontite-albite zone and (5) albite zone (Iijima, 1974; Utada et al., 1974; Utada, 1991; Ogihara, 1996). The composition of these and other zeolites that are common in felsic volcanic rocks are listed in Table 2. Neogene lacustrine caldera basins in the Japan volcanic arc display a similar vertical diagenetic zonation, except that the zeolite species tend to have less alkalic, more calcic compositions and the calcic zeolite wairakite (Table 2) occurs with albite in the highest grade diagenetic zone (zone 5 above; Utada, 1991). Saline-alkaline lacustrine successions are less analogous to the Rosebery–Hercules area, and are characterised by clinoptilolite and/or analcite zeolitic zones, K-feldspar, boron-bearing minerals, and evaporites (Stamatakis et al., 1996; Temel and Gündogdu, 1996; Gündogdu et al., 1996). Gündogdu et al. (1996) noted that K-feldspar formed after clinoptilolite and before analcite, and formed by direct replacement of glass rather than by diagenetic transformation of clinoptilolite.

Examples of felsic pumiceous rocks with extensive feldspar alteration analogous to that in the Rosebery–Hercules area include the Recent Ohakuri geothermal system in New Zealand (Henneberger and Browne, 1988), the Devonian–Carboniferous Iberian Pyrite Belt (Munhá et al., 1980), and the Early Proterozoic Bergslagen district, Sweden (Frietsch, 1982; Lagerblad and Gorbatschev, 1985). At Ohakuri, a subaerial and lacustrine, rhyolitic pumice succession has alteration zoned from (1) weak smectite, to (2) mordenite-clinoptilolite (plus smectite and opal), to (3) quartz-adularia, and (4) silicification (Henneberger and Browne, 1988). Henneberger and Browne (1988) determined that the mordenite-clinoptilolite-smectite assemblage formed essentially by hydration of volcanic glass by neutral pH water at ≤ 100°C. They suggest that the mordenite-clinoptilolite-smectite assemblage was converted to quartz-adularia by the pervasive movement of alkaline chloride type water at 130–190°C. Henneberger and Browne (1988) also showed that with increasing intensity of alteration, the porosity of the pumiceous rocks progressively decreased and the density increased. The mean porosity and dry density of the fresh unaltered pumice deposit were measured as 40% and 1.1 kg3/m3 respectively, whereas the mean values for the mordenite-clinoptilolite alteration zone were 35% and 1.3, and for the quartz-adularia zone were 13% and 1.9.

Table 2 Diagenetic and hydrothermal alteration minerals common in felsic volcanic rocks (in marine and terrestrial geothermal systems)

Phyllosilicates		
	Clays	
	Smectite group	= $(0.5Ca,Na)_{0.7}(Al,Mg,Fe)_4[(Si,Al)_8O_{20}](OH)_4.nH_2O$
	Montmorillonite	(Ca and Na varieties ±K)
	Illite (mica-clay) group	= $(K,H_3O)(Al,Mg,Fe)_2(Si,Al)_4O_{10}[(OH)_2,H_2O]$
	Kaolinite group	= $Al_4(Si_4O_{10})(OH)_8$
	Micas	
	Sericite	= $KAl_2(AlSi_3O_{10})(OH)_2$
	Chlorite	= $(Mg,Fe^{+2},Fe^{+3})_6AlSi_3O_{10}(OH)_8$
	Other phyllosilicates	
	Talc	= $Mg_3(Si_4O_{10})(OH)_2$
	Pyrophyllite	= $Al_2Si_4O_{10}(OH)_2$
Zeolites		
	Calcic zeolites	
	Heulandite	= $(Ca,Na_2,K_2).(Al_2Si_7O_{18}).8H_2O$; Ca>(Na+K)
	Laumontite	= $CaAl_2Si_4O_{12}.4H_2O$
	Wairakite	= $CaAl_2Si_4O_{12}.2H_2O$
	Alkalic zeolites	
	Analcite	= $Na(AlSi_2O_6).H_2O$
	Clinoptilolite	= $(K,Na,Ca,Mg)_{2\text{-}3}Al_3Si_{15}O_{36}.12H2O$; (Na+K)>Ca
	Range includes Na-rich, Na-K type, and K-rich	
	Mordenite	= $(K_2,Na_2,Ca,Mg)(AlSi_5O_{12})_2.7H_2O$
	Range includes Na-rich and K-Na type	
Silica	Opal	= $SiO_2.nH_2O$
	Quartz	= SiO_2
	Cristobalite	= SiO_2
Feldspars		
	Kspar (adularia)	= $KAlSi_3O_8$
	Albite	= $NaAlSi_3O_8$
Carbonates		
	Calcite	= $CaCO_3$
	Dolomite	= $CaMg(CO_3)_2$
	Ankerite	= $Ca(Fe,Mg)(CO_3)_2$
	Rhodochrosite	= $MnCO_3$
Sulphates		
	Alunite	= $(Na,K)Al_3(SO_4)_2(OH)_6$
	Anhydrite	= $CaSO_4$
	Gypsum	= $CaSO_4.2H_2O$
Other minerals		
	Epidote	= $Ca_2(Al,Fe)_3Si_3O_{12}(OH)$
	Sphene	= $CaTiO(SiO_4)$
	Leucoxene	= TiO_2 (fine grained rutile)

In the Iberian Pyrite Belt, Munhá et al. (1980) reported extensive, strong K-feldspar (adularia) alteration of marine felsic volcanic rocks. In Bergslagen, the thick, felsic volcanic succession has an upper zone of K-feldspar alteration up to 2 km thick, and an underlying zone of albite alteration (Frietsch, 1982; Lagerblad and Gorbatschev, 1985). Munhá et al. (1980) and Lagerblad and Gorbatschev (1985) attributed the feldspar alteration to alkali exchange reactions between initially glassy volcanic rocks and sea water convecting through the volcanic pile. They used experimental studies and thermodynamic data to argue that in the upper parts of the volcanic pile, at temperatures lower than 150°C, Na in the glassy rocks was exchanged for K from the sea water, resulting in Na depletion and formation of K-feldspar and K-rich smectites. At greater depths in the volcanic pile, at temperatures above 150°C, the exchange reaction favours fixation of Na from the modified sea water to form albite, and depletion of K from the rocks. These authors did not discuss the relationship between zeolites and the feldspar zones, presumably because no evidence of former zeolites was identified in the rocks.

These studies of diagenetic alteration help clarify the diagenetic mineral transformations in the Rosebery–Hercules area. The first stage of diagenetic or hydrothermal alteration of felsic pumice and glass shards in both marine and terrestrial environments is the development of thin films of smectite clay (montmorillonite) and opal on all glass surfaces (Iijima, 1974, Henneberger and Browne, 1988). Consequently, the texturally identical sericite films coating the surfaces of pumice and shards in the Rosebery–Hercules area are interpreted as metamorphosed equivalents of original smectite±opal films. In both marine and terrestrial environments, the second stage of diagenetic alteration commonly involves replacement of the remaining glass and infilling of porosity by low temperature zeolites. The zeolites that replace glass at this early, low temperature diagenetic stage are generally mordenite and clinoptilolite (Iijima, 1974; Utada et al., 1974; Abe and Aoki, 1975; Henneberger and Browne, 1988; Utada, 1991; Stamatakis et al., 1996; Temel and Gündogdu, 1996; Gündogdu et al., 1996; Ogihara, 1996). Mordenite and clinoptilolite commonly occur together. Mordenite typically forms fan-radiating fibrous aggregates, whereas clinoptilolite is characterised by aggregates of blocky-tabular crystals. Both minerals can also form fine grained massive replacements of glass. Considering the morphology of mordenite and clinoptilolite, and that they characteristically form in felsic pumiceous rocks directly following initial smectite-opal alteration of glass surfaces, it is concluded that the local pseudomorphs within the feldspar alteration in the Rosebery–Hercules area are of mordenite and clinoptilolite. The Rosebery–Hercules pumice units could have been extensively replaced by mordenite and clinoptilolite at this early stage. It can be concluded that the K-feldspar alteration post-dated an earlier mordenite-clinoptilolite stage. However, there is insufficient evidence to determine how much of the K-feldspar formed by transformation of mordenite-clinoptilolite as opposed to direct replacement of glass.

Zonation of diagenetic alteration

This study indicates that the Rosebery–Hercules rocks successively experienced stages of smectite±opal, mordenite-clinoptilolite, adularia-quartz, and albite-quartz diagenetic alteration. By comparison with other diagenetic alteration systems, these alteration assemblages that characterise each alteration stage, should also have existed vertically as a set of diagenetic alteration zones. However, in this study no distinct regional vertical or lateral zonation of diagenetic alteration has been observed in the Rosebery–Hercules area. An albite-quartz-sericite-sphene/leucoxene±chlorite±epidote assemblage with minor relics of K-feldspar occurs at all stratigraphic levels. This assemblage is interpreted as the highest grade diagenetic alteration (or its greenschist facies metamorphosed equivalent), which initially developed deep in the volcanic pile. The assemblage is equivalent to the deepest diagenetic zone of Utada (1991) in the Neogene basins of Japan, or the deep albite zone in Bergslagen. The occurrence of this single high grade diagenetic zone throughout the volcanic succession, indicates that the region had a very high geothermal gradient, and also that as new strata accumulated and burial depth increased, the diagenetic zones progressed up through the

stratigraphy until the whole Rosebery–Hercules succession was overprinted by the basal, highest grade diagenetic zone.

Comparison with diagenetic zoning in the Neogene basins of Japan, suggests that a regional diagenetic analcite zone could have been present in the Rosebery–Hercules succession. The analcite zone would have occured between the mordenite-clinoptilolite and albite zones (cf. Iijima, 1974; Utada, 1991; Ogihara, 1996). However, there is no definite petrographic evidence for analcite in the Rosebery–Hercules rocks, and it is possible that K-feldspar alteration developed instead of analcite due to different chemistry of the pumice deposits or different chemistry of the diagenetic brine.

Relation of ore-associated carbonate alteration to diagenetic alteration

The earliest formed ore-related carbonate alteration is the spheroidal Mn-carbonate alteration (Table 1). This alteration type comprises 0.2 mm – 1 cm diameter, finely concentric layered, carbonate spheroids, set in an intensely sericite-altered matrix (Allen and Large, 1996). This alteration type only occurs directly above, below or laterally adjacent to strong mineralization. Remarkably, the very best preserved and least deformed glass shard and pumice textures in the entire Rosebery–Hercules area occur within these carbonate spheroids. The shards and pumice are preserved as strongly sericite altered structures completely enclosed by fine grained carbonate. All of the original glass surfaces of the shards and pumice have been replaced by sericite, and in some cases the entire glass framework has been replaced by sericite. Remaining parts of the glass framework are replaced by carbonate. During the main S2–F2 deformation, the carbonate spheroids behaved as rigid spots; they were partly dismembered and extended in the stretching lineation, but remained internally unfoliated. The enclosing sericitic matrix was strongly foliated and all primary textures were obliterated. The deformation style of the carbonate spheroids and the remarkable preservation of shards and pumice within them, indicate that the spheroids formed before any significant regional deformation and clearly before cleavage development (S2). The lack of S1 foliation and any evidence for precursor zeolite or feldspar alteration within the spheroids, suggests that the spheroids grew after initial diagenetic or hydrothermal smectite alteration of the shards and pumice (now sericite) but prior to zeolite alteration, K-feldspar alteration, compaction and S1 stylolite development (Table 1).

These observations indicate that ore-related carbonate alteration commenced soon after the onset of diagenetic alteration.

Other spotty Mn-carbonate alteration textures, without fine concentric concretionary internal structures, also occur preferentially adjacent to mineralization (Allen and Large, 1996). However, locally this alteration type contains relics of feldspar-quartz altered pumice, and the textural relationship is interpreted as carbonate replacement of the feldspar. The feldspar relics vary from K-feldspar to albite, and could represent K-feldspar that was albitised before or after the carbonate alteration. Consequently, at least some spotty carbonate formed after or during a stage of diagenetic or hydrothermal feldspar alteration, and later than the spheroidal carbonate (Table 1).

Spotty carbonates are commonly overprinted by strong sericite alteration and the strongly mineralized quartz-sericite and chlorite-quartz alteration that in part forms the orebodies (Table 1). These overprinting relationships indicate that the main stage of mineralization followed formation of the spotty carbonates. Therefore the beginning of ore-related alteration and mineralization is very well constrained.

The end of ore formation is less well constrained.

Evolution of diagenetic alteration in the Rosebery–Hercules area

The data presented above indicate that the Rosebery–Hercules area was part of a dynamic high-grade diagenetic alteration system that evolved through recognizable prograde stages, but which also advanced rapidly up through the stratigraphy as strata accumulated. Each pumiceous deposit in the stratigraphic succession experienced initial smectite ± opal alteration immediately after deposition. This alteration was succeeded by zeolite stages (now poorly preserved), a K-feldspar stage, and finally an

albite stage. Because diagenetic assemblages are strongly temperature dependent (Utada, 1991), studies of young basins can be used to estimate the temperatures of diagenetic alteration stages in the Rosebery–Hercules area. Smectite (montmorillonite) growth probably commenced at very low temperatures and continued up to 140°C (Simmons and Browne, 1996). Above 140°C the smectites would have been converted to illite and sericite. Zeolite growth (mordenite-clinoptilolite) probably started at 40–50°C (cf. Utada, 1991, Ogihara, 1996) and continued up to 130°C. K-feldspar alteration probably occured at temperatures up to 190°C and mainly below 150°C (cf. Henneberger and Browne, 1988; Munhá et al., 1980), whereas albite alteration occured above 150°C (cf. Munhá et al., 1980) and up to 250°C or more.

Overprinting relationships and the stratigraphic extent of the diagenetic assemblages, suggest that the diagenetic alteration system initially preceded ore formation, then continued during ore formation, and probably also continued after ore formation had ceased.

Implications for studies of ore genesis and alteration

(1) Diagenetic alteration around massive sulphide deposits can have a complex history and provide important information about the timing and origin of the ore deposit.

(2) Diagenetic paragenesis and relationships to hydrothermal alteration, mineralization, and deformation fabrics can with care be determined even in ancient, strongly altered and deformed rocks.

(3) Diagenetic alteration should be identified and separated from ore-related alteration, because the early, shallow-level diagenetic alteration, and especially K-feldspar alteration, can result in increased K, Al and depleted Na±Ca±Mg in rocks near the top of the stratigraphy, regardless of proximity to ore. Subsequently, deeper-level diagenetic alteration can prograde up through the stratigraphy and result in decreased K and increased Na. Changes in other elements such as Si, Fe, Mn and ore metals can also be related to diagenetic alteration.

(4) It is commonly inferred that hydrothermal alteration related to massive sulphide mineralization is purely a very early event and is subsequently overprinted by regional diagenetic alteration after deep burial of the ore deposit. This study and the data of Iijima (1974) indicate that the geometrical and timing relationships between the diagenetic and hydrothermal alteration are complicated. It appears in the Kuroko deposits and at Rosebery that the ore-related alteration post-dated the earliest stage of diagenesis, then proceded parallel with the next stages of diagenetic alteration, overprinted early to middle diagenetic stages (such as mordenite-clinoptilolite and K-feldspar), then finally was outlived by the diagenetic system, which continued up through the hangingwall stratigraphy.

(5) The dominant diagenetic mineral assemblages in the Rosebery–Hercules area (feldspar-quartz) and the well preserved vitroclastic rock textures, indicate that the stratigraphic succession was rapidly overprinted by relatively high grade diagenetic alteration. This indicates the region had a very high geothermal gradient, possibly higher than in the Neogene Kuroko-bearing basins of Japan, and amongst the highest recorded in studies of young marine basins (> 100°/km). This evidence for a high geothermal gradient suggests that the diagenetic alteration system is a symptom and indicator (?regional vector) toward "very hot" basins that are favourable for submarine hydrothermal mineralization.

(6) The textural changes associated with diagenetic alteration in the Rosebery–Hercules area and comparison with studies of young alteration systems, indicate that large changes in rock porosity and density occured during diagenetic alteration. These changes presumably influenced the progress of hydrothermal alteration and mineralization.

References

Abe, H. and Aoki, M. 1975. Experiments on the hydrothermal alteration of mordenite rocks in sodium carbonate solution, with reference to analcimization around Kuroko deposits. Economic Geology, v. 70, p. 770-780.

Aerden, D. 1994. Formation of the Rosebery and Hercules ore deposits, Tasmania by syntectonic mobilization of metals and wallrock replacement about structural traps. Contentious issues in Tasmanian Geology symposium 1994, Geological Society of Australia Tasmanian Division, Extended Abstracts volume, p. 83-88.

Allen, R. L. 1987. Subaqueous volcanism, sedimentation and the geological setting of Zn-Cu-Pb massive sulphide deposits, Benambra, S.E. Australia. Ph.D. thesis, Monash University, 284 p.

Allen, R. L., 1989, Unpublished geological plans and sketches filed with Pasminco Mining Rosebery (partly reproduced in Allen and Hunns, 1990).

Allen, R. L. 1990. Subaqueous welding, or alteration, diagenetic compaction and tectonic dissolution? IAVCEI International Volcanological Congress, Mainz, Germany, Abstracts volume.

Allen, R. L., 1991, Stratigraphy, structure, volcanology and ore genesis of the Rosebery - Hercules ZnPbCuAu massive sulphide district, Tasmania. Unpublished report to Pasminco Exploration, Melbourne Australia. 3 volumes.

Allen, R. L. 1994a. Volcanic facies analysis indicates large pyroclastic eruptions, sill complexes, synvolcanic grabens, and subtle thrusts in the Cambrian "Central Volcanic Complex" volcanic centre, western Tasmania. Contentious Issues in Tasmanian Geology Symposium, Geological Society Australia Tasmania Division, Hobart. Abstracts number 39, p. 31-3.

Allen, R. L. 1994b. Synvolcanic, subseafloor replacement model for Rosebery and other massive sulphide ores. Contentious Issues in Tasmanian Geology Symposium, Geological Society Australia Tasmania Division, Hobart. Abstracts number 39, p. 89-91.

Allen, R. L. and Cas, R. A. F. 1990. The Rosebery controversy: Distinguishing prospective submarine ignimbrite-like units from true subaerial ignimbrites in the Rosebery-Hercules ZnCuPb massive sulphide district, Tasmania. 10th Australian Geological Convention. Geological Society Australia, Abstracts 25, p. 31-32.

Allen, R. L., and Hunns, S. R., 1990, Geology of the Hercules and South Hercules orebodies, and Hercules excursion stops. In, Corbett, K. & Large, R. eds. Excursion guide E1 - The Mount Read Volcanics and associated ore deposits, p. 15-27. 10th Australian Geological Convention, Hobart.

Allen, R.L. and Large, R.R. 1996. Rosebery Alteration Study. AMIRA-ARC project P439, Report 3, October 1996, p. 143-152.

Frietsch, R. 1982. Alkali metasomatism in the ore-bearing metavolcanics of central Sweden: Geological Survey of Sweden, series C, v. 791, 54 p.

Green, G.R., Solomon, M. and Walshe, J.L. 1981. The formation of the volcanic-hosted massive sulphide ore deposit at Rosebery, Tasmania. Econ. Geol. 76, 304-338.

Gustafson, L.B. and Hunt, J.P. 1975. The porphyry copper deposit at El Salvador, Chile. Economic Geology, v. 70, p. 857-912.

Gündogdu, M.N., Yalcin, H., Temel, A. and Clauer, N. 1996. Geological, mineralogical and geochemical characteristics of zeolite deposits associated with borates in the Bigadic, Emet and Kirka Neogene lacustrine basins, western Turkey. Mineralium Deposita, v. 31, p. 492-513.

Henneberger, R.C and Browne, P.R.L. 1988. Hydrothermal alteration and evolution of the Ohakuri hydrothermal system, Taupo Volcanic Zone, New Zealand. Journal of Volcanology and Geothermal Research, v. 34, p. 211-231.

Hill, A., and Orth, K., 1995, Textures and origins of carbonate associated with the volcanic-hosted massive sulphide deposit at Rosebery, Tasmania: AMIRA-ARC project P439, Report 1, November 1995, p. 129-141.

Iijima, A. 1974. Clay and zeolitic alteration zones surrounding Kuroko deposits in the Hokuroku District, Northern Akita, as submarine hydrothermal-diagenetic alteration products. Mining Geology Special Issue, no. 6, p. 267-289.

Lagerblad, B., and Gorbatschev, R. 1985. Hydrothermal alteration as a control of regional geochemistry and ore formation in the central Baltic Shield: Geologische Rundschau, v. 74, p. 33-49.

Munhá, J., Fyfe, W.S. and Kerrich, R. 1980. Adularia, the characteristic mineral of felsic spilites. Contributions to Mineralogy and Petrology, v. 75, p. 15-19.

Ogihara, S. 1996. Diagenetic transformation of clinoptilolite to analcime in silicic tuffs of Hokkaido, Japan. Mineralium Deposita, v. 31, p. 548-553.

Simmons, S.F. and Browne, P.R.L. 1996. Smectite, *in* Thompson, A.J.B. and Thompson J.F.H. eds. Atlas of alteration, Geological Association of Canada, Mineral Deposits Division, p. 96.

Sparks, R. S. J. 1978. The dynamics of bubble formation and growth in magmas: A review and analysis. J. Volcanol. Geotherm. Res. 3, 1-37.

Stamatakis, M.G., Hall, A. and Hein, J.R. 1996. The zeolite deposits of Greece. Mineralium Deposita, v. 31, p. 473-481.

Temel, A. and Gündogdu, M.N. 1996. Zeolite occurrences and the erionite-mesothelioma relationship in Cappadocia, central Anatolia, Turkey. Mineralium Deposita, v. 31, p. 539-547.

Utada, M. 1991. Zeolitization in the Neogene formations of Japan. Episodes, v. 14, p. 242-245.

Utada, M., Minato, H., Ishikawa, T. and Yoshizaki, Y. 1974. The alteration zones surrounding Kuroko-type deposits in Nishi-Aizu District, Fukushima Prefecture, with emphasis on the analcime zone as an indicator in exploration for ore deposits. Mining Geology Special Issue, no. 6, p. 291-302.

Wilson, L., Sparks, R. S. J. & Walker, G. P. L. 1980. Explosive volcanic eruptions-IV. The control of magma properties and conduit geometry on eruption column behavoir. Geophys. J. R. Astr. Soc. 63, 117-148.

Carbonate and muscovite mineral chemistry, Rosebery VHMS deposit, Tasmania

by Ross Large, Rod Allen and Michael Blake
Centre for Ore Deposit Studies, Geology Department, University of Tasmania

Summary

Microprobe analyses on samples from DDH 120R at the Rosebery north-end show a systematic variation in the chemistry of muscovites and carbonates relative to volcanic stratigraphy and ore position. These preliminary results indicate the potential to use both muscovite chemistry and carbonate chemistry as vectors to ore.

Comparison of data from PIMA, FTIR and microprobe analyses indicate a good correlation between muscovite spectra and muscovite chemistry. The FTIR is shown to provide accurate information on the substitution of Fe and Mg into the octahedral Al site of muscovite.

Introduction

This is the first report on a detailed study of mineral chemistry in the alteration system to the Rosebery VHMS deposit; in particular the footwall, hangingwall and ore horizon alteration mineral chemistry related to the K lens and adjacent A-B lens systems. The purpose of this study is to:

- relate mineral chemistry of carbonates, feldspars and phyllosilicates to mineral textures and paragenesis at the diagenetic and hydrothermal stages of alteration;
- relate mineral chemistry to whole rock and trace element geochemistry;
- investigate mineral chemical zonation relative to the ore lenses and alteration system;
- investigate the effect of later metamorphism and veining on mineral chemistry;
- determine mineral chemical vectors to ore.

This initial investigation is on samples from DDH 120R through the hangingwall, ore horizon and footwall sequence (Allen et al., 1996, Large and Allen, 1997). Twenty samples were selected which represent the various rock types and alteration facies. Rod Allen had previously undertaken detailed petrological and paragenetic studies on these samples and marked-up the minerals for microprobe analysis. The analyses were undertaken by Mike Blake, under the direction of Brendan Griffin at the University of Western Australia using a CAMECA SX50 electron microprobe.

Petrography and analytical data

Detailed petrographic descriptions of each sample are provided in Appendix 1 (at end of volume). A summary of the microprobe spot positions and photograph of the mineral textures relative to each analysed spot are also given in this appendix. A full spreadsheet of the analytical data is given in Appendix 2 (p. 167).

Previous work on DDH 120R

DDH 120R was selected for detailed mineral chemistry studies because it provides a complete section through the Rosebery Mine stratigraphy, from 350m above the ore horizon to 100 m below the ore horizon. Previous reports by Allen et al. (1996) and, Large and Allen (1997) provide details on the volcanic facies and lithogeochemistry of the drill hole.

Some downhole lithogeochemical variations relevant to this mineral chemical study are shown in Figure 1 (Ti/Zr and Zn), Figure 2 (MnO and CO_2) and Figure 3 (K_2O and AI).

Muscovite chemistry at Rosebery

Occurrence of muscovite

Fine grained muscovite (locally termed sericite) is a major mineral phase in both the altered and "unaltered" volcanic rocks at Rosebery. Based on petrographic studies, supported by the K_2O data in Figure 3, it is apparent muscovite is elevated in the host volcanics immediately surrounding the ore lens. The altered dacitic pumice breccia unit enclosing the ore lens contains from 30 to 50 wt% muscovite, whereas the footwall rhyolite pumice breccias contain 10 to 40 wt% muscovite, typically increasing toward the ore lens. The relatively unaltered hangingwall volcanic sandstones and volcaniclastics vary from 8 to 25 wt% muscovite.

Chemical variation in muscovite

"Ideal" muscovite has the formulae

$$K_2Al_4[Si_6Al_2O_{20}](OH,F)_4$$

Principal isomorphous substitution in the muscovite structure is as follows (Deer et al., 1996)

For K:	Na, Rb, Cs, Ca, Ba.
For octahedral Al:	Mg, Fe^{2+}, Fe^{3+}, Mn, Li, Cr, Ti, V.
For (OH):	F.

In the present study only some of these potential substitutions could be analysed: Na, Ca, Mg, Fe_{total}, Mn, Cr and Ba. Further studies will be required when the UTas microprobe is operational, especially for Ba and Rb.

At Rosebery, the main chemical variation in muscovite composition is due to substitution of Fe and Mg for octahedral Al. This feature is clearly shown in Figure 4, where the number of Al atoms in the structure are plotted against Fe and Mg atoms. This calculation is based on a total of seven (7) cation atoms in the structure of muscovite, i.e., K(Al, Fe, Mg)$_2$ [Si_3AlO_{10}](OH)$_2$

The Rosebery muscovite varies in composition from near pure muscovite (0.05 Fe + Mg atoms) towards phengite with up to a maximum of around 0.5 Fe + Mg atoms in the structure (Fig. 4).

It is noteworthy that muscovite from the ore horizon shows a fairly consistent chemistry with 0.2 to 0.4 Fe + Mg atoms. The hangingwall muscovite is generally (but not always) lower in Fe + Mg (<0.25 Fe + Mg atoms) while the footwall muscovite typically shows elevated values of greater than 0.4 Fe + Mg atoms. The spread in footwall muscovite analyses at right angles to the phengite line in Fig. 4 may be due to a high Fe^{3+}/ Fe^{2+} ratio in the muscovite in these samples (Ron Berry, pers. comm.)

Most of the muscovites show negligible Na substitution in the K site (Fig. 5). However ten analyses on this plot trend toward the paragonite end member indicating mixing on the microscale between muscovite and paragonite. This feature usually indicates fine grained intergrowths rather than complete solid solution (Ron Berry, pers. comm.). A further four analyses trend towards albite indicating fine muscovite-albite intergrowths.

Downhole variations in muscovite chemistry DDH 120R

Variations in the chemistry of muscovite related to stratigraphic position and proximity to the massive sulphide ore lens are shown in Figures 6 to 12. Individual microprobe analyses are plotted as single points. In some samples only one muscovite grain was analysed, while other samples have multiple grain analyses. The spread of points at a given depth (e.g., 1422m) shows the variation in chemistry for several mineral grains from the same sample.

Fe content (Fig. 6): The most Fe-rich muscovite occurs deep in the footwall altered zone. There is a

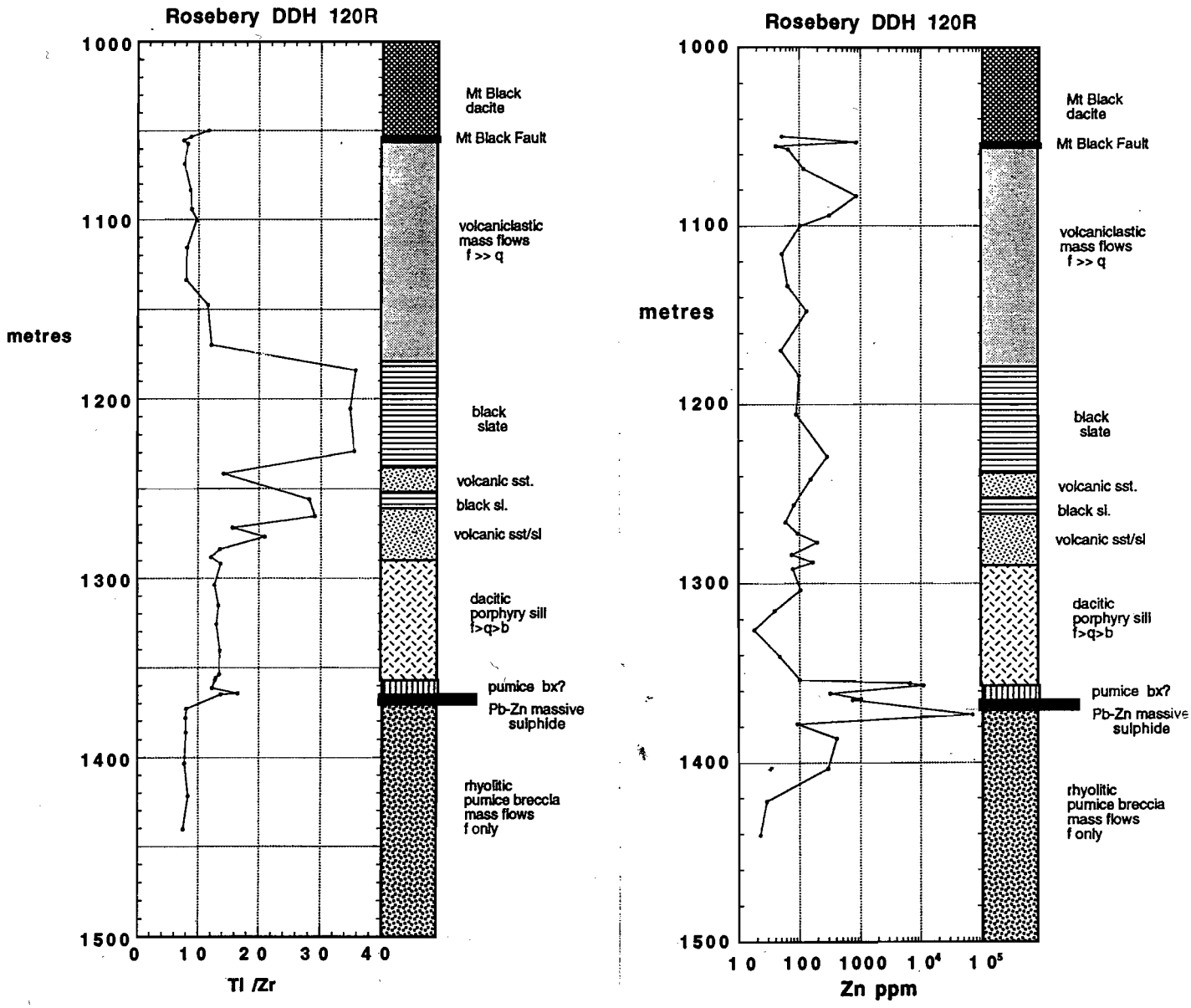

Fig. 1 DDH 120R downhole Ti/Zr and Zn ppm (Report 4, p.273)

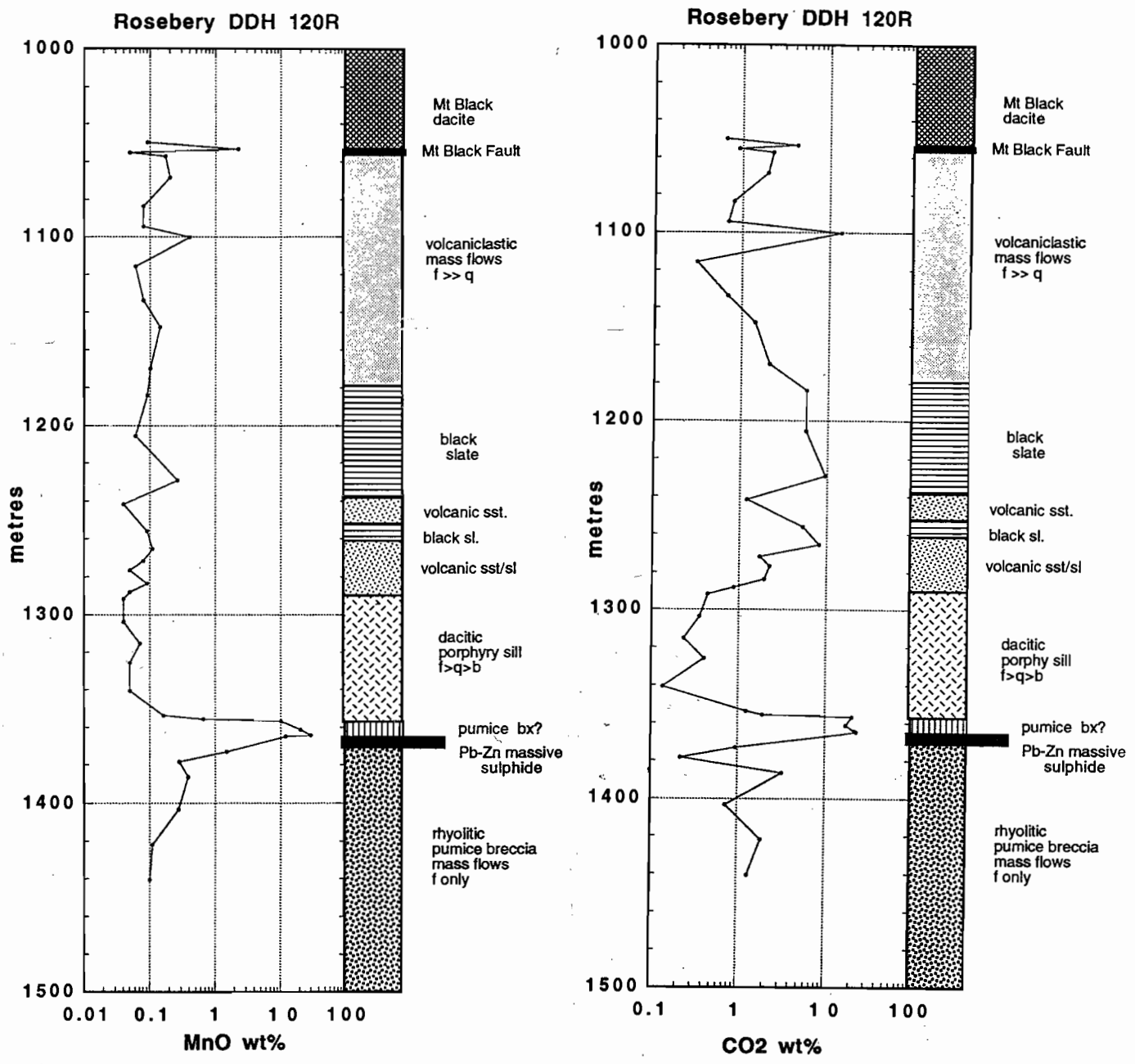

Fig. 2 DDH 120R downhole MnO and CO_2 (Report 4, p.275 and 277).

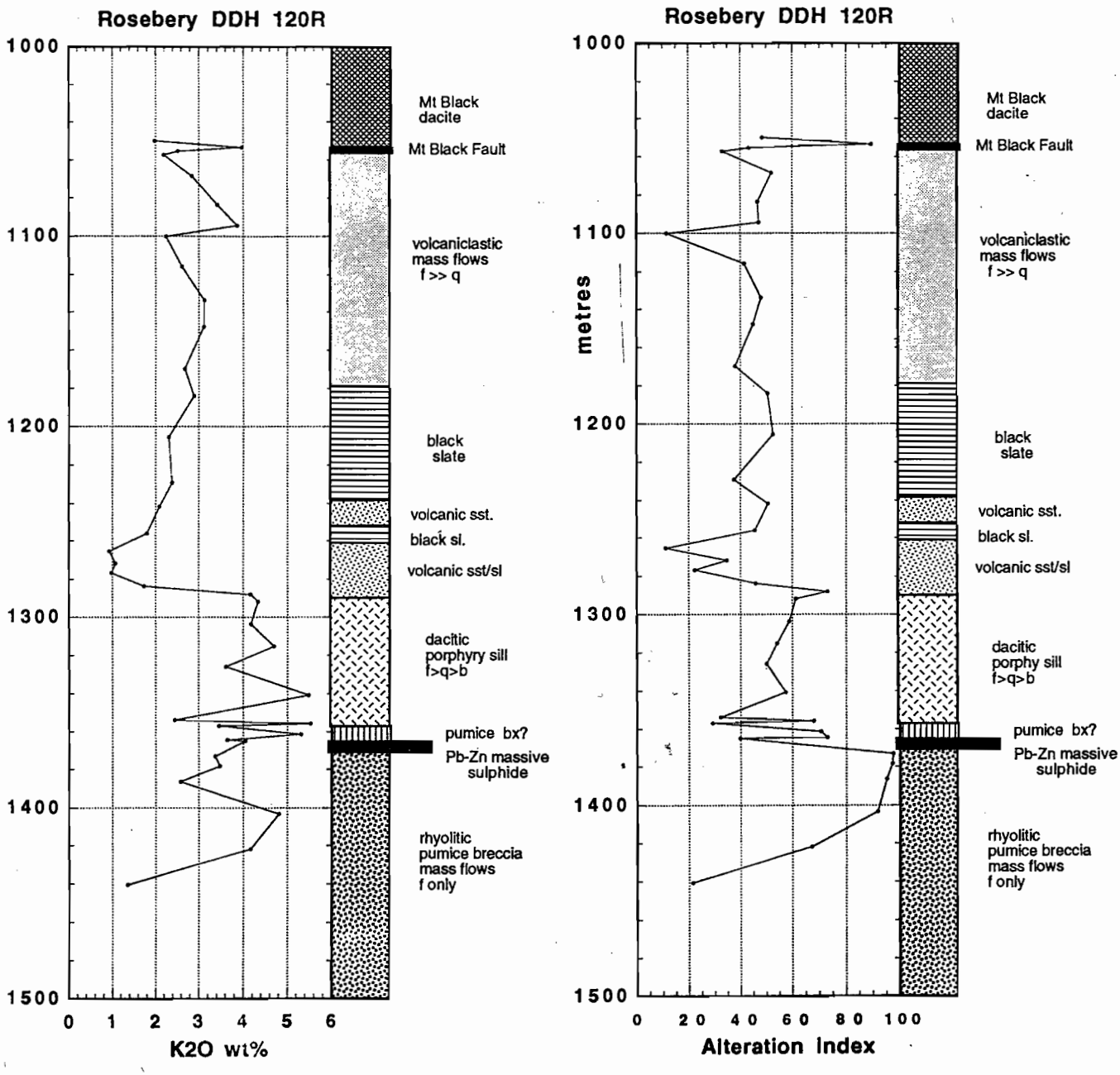

Fig. 3 DDH 120R downhole K_2O and AI (Report 4, p.276).

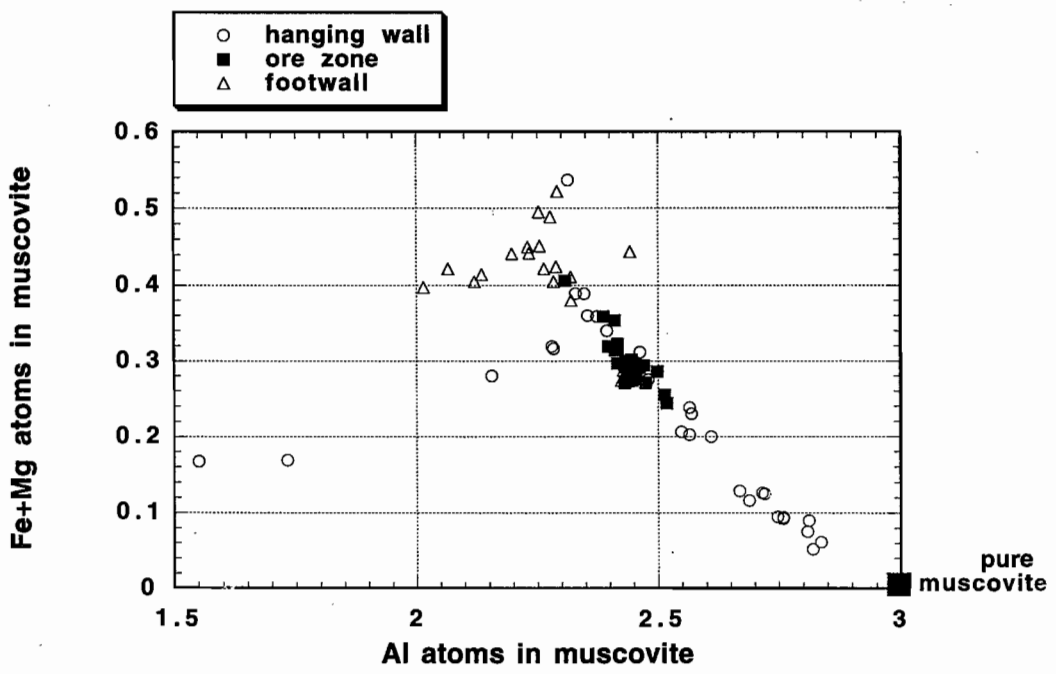

Fig. 4 Substitution of Fe and Mg for octahedral Al in the Rosebery muscovites from DDH 120R.

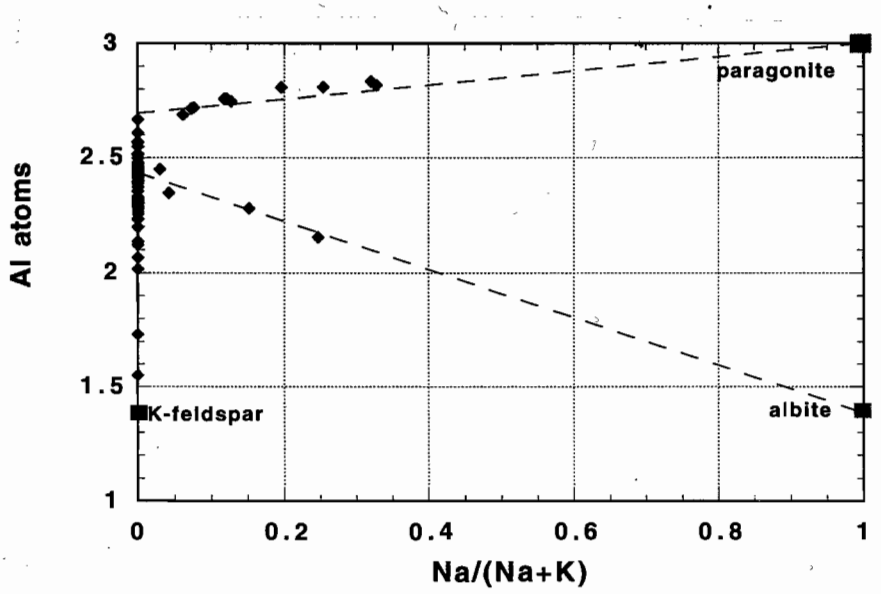

Fig. 5 Variation in Na/(Na + K) ratio for the Rosebery muscovites. This plot shows that ten analyses are mixtures of muscovite and paragonite while a further four show mixing between muscovite and albite.

general decrease in the Fe content of muscovite passing up through the altered footwall to the ore position. The Fe-poor muscovites in the hangingwall between 1220m and 1300m are those which display mixing with paragonite (Fig. 5).

Mg content (Fig. 7): The most Mg-rich muscovite (>0.2 atoms in octahedral site) occur in the ore horizon and immediate footwall altered zone. Mg-poor muscovite (<0.2 atoms Mg in OS) are typical of the hangingwall volcanic sandstones and volcaniclastics.

Ba content (Fig. 9): Muscovite from the hanging-wall volcaniclastic suite exhibits Ba contents of less than 0.02 atoms in the structure. Ore horizon muscovite is anomalous with a wide range in Ba content, with many analyses above 0.04 atoms per K site. Note that the Ba microprobe analyses require **further** verification due to the overlap of Ba and Ti peaks used in the analysis.

Si/Al ratio (Fig. 10): The atomic ratio of Si/Al in the muscovite structure generally varies from 1 to 1.8. One sample at 1150 metres downhole shows anomalously high values of >2.2. This suggests a fine mineral intergrowth between muscovite and quartz?

K/Al ratio (Fig. 11): The K/Al atomic ratio shows a parallel variation with the Fe + Mg atomic substitution. Highest values (>0.4 atomic K/Al) occur in the altered footwall volcanics and at the top of the drillhole below the Mt Black Fault.

Na/(Na + K) ratio: This ratio measures the paragonite component of the muscovite. Up to 30 mole% paragonite is present in muscovite in the hangingwall sediments above the dacite porphyry. Muscovite in the ore zone and footwall contains no measurable Na.

Discussion of muscovite mineral chemistry

Fine grained muscovite ("sericite") at Rosebery exhibits a consistent variation in chemistry that may be related to stratigraphic position and hydrothermal mineralising processes. The effect of metamorphism and recrystallisation during the Devonian is unknown but, at this stage, it is assumed to have little influence on the current mineral chemistry. Characteristics of the muscovite from the unaltered hangwall, ore zone and altered footwall are listed below.

Ore zone muscovite: generally but not always has the following chemistry:
- elevated Ba substituting for K (>0.02 atoms)
- intermediate Fe + Mg (0.2–0.4 atoms per OS)
- elevated Mg (≥0.2 atoms per OS)
- Na/Na + K <0.05.

Footwall alteration zone muscovite:
- intermediate Ba (0.01–0.03 atoms)
- elevated Fe + Mg (≥0.4 atoms per OS)
- elevated Mg (≥0.2 atoms per OS)
- Na/Na + K <0.05.

Hangingwall unaltered zone:
- low Ba
- variable Fe + Mg (0 to 0.4 atoms per OS)
- low Mg (0 to 0.2 atoms per OS)
- Na/Na + K up to 0.35.

Comparison of PIMA, FTIR and microprobe analytical data for muscovite

Ten samples were selected from DDH 120R to compare the response of muscovite from the PIMA system with the Fourier Transform Infra Red (FTIR) spectrometer system at the University of Tasmania. PIMA investigates the wavelength range 1300–2500 nm (clay minerals and carbonates), while the FTIR investigates the wavelength range 2000–25,000 nm (clays, carbonates and other silicites).

PIMA: The PIMA analyses were undertaken by AGSO on crushed powder samples selected from DDH 120R. The spectra (2040–2545 nm) for each sample are shown in Figure 13.

The downhole variation in the PIMA muscovite 2200 nm wavelength peak (Al-OH) shows a good correlation with the trend of the Al atomic distribution in muscovite based on the microprobe analyses (Fig. 14). Although the same samples were not analysed in each case, the correlation between the two data sets is exceptionally good.

FTIR: The FTIR analyses were undertaken at the Central Science Laboratory (Tas. Uni.) on crushed powder samples. A complete spectra from the FTIR for sample 120R-1288.1 is shown in Figure 15. The downhole variation in the FTIR 2760 muscovite peak for the ten samples studied shows a similar pattern

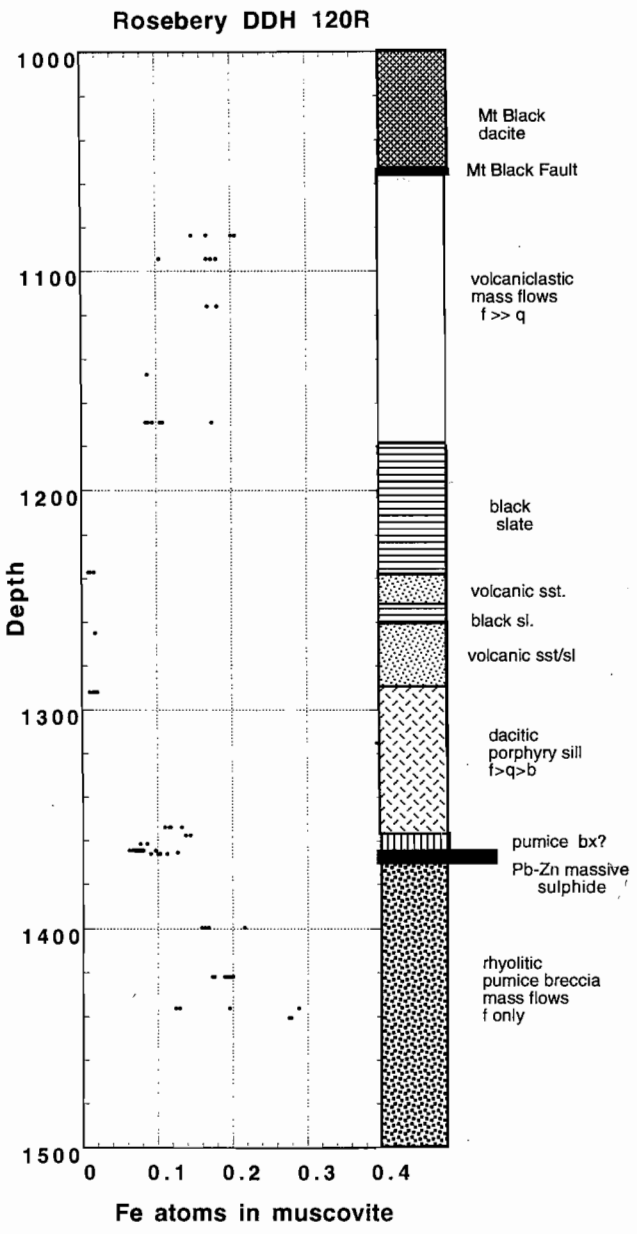

Fig. 6 Downhole variation in Fe atoms in muscovite, DDH 120R. Calculated on the basis of seven (7) cation atoms in the structure of muscovite.

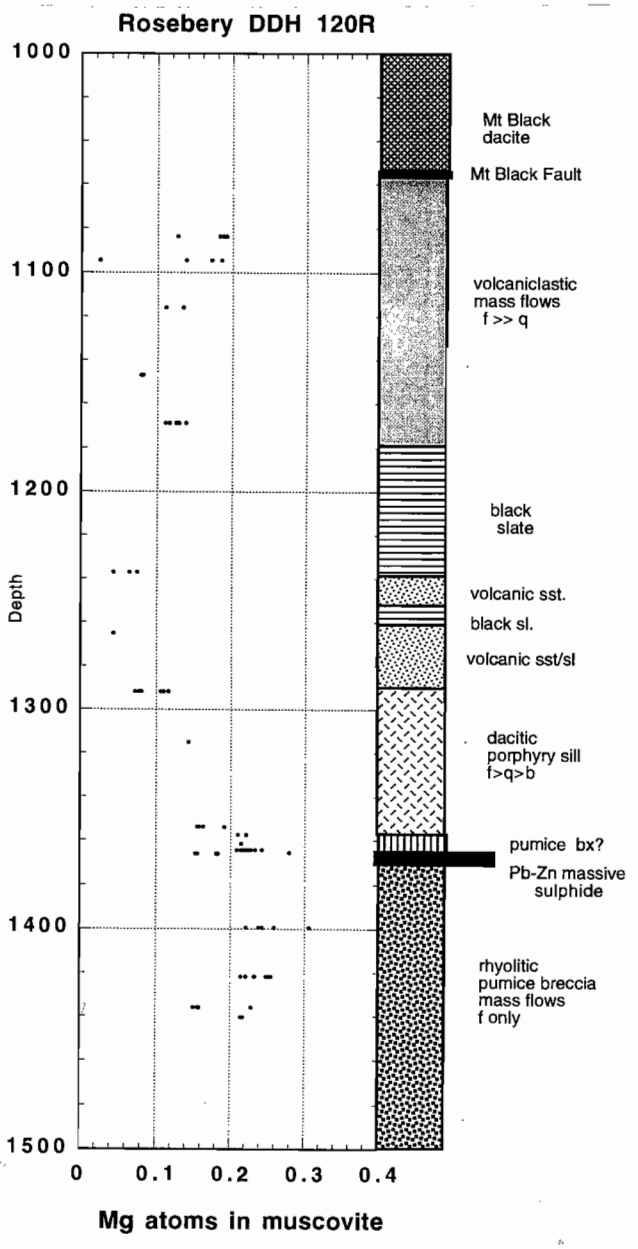

Fig. 7 Downhole variation in Mg atoms in muscovite, DDH 120R. Calculated on the basis of seven (7) cation atoms in the structure of muscovite.

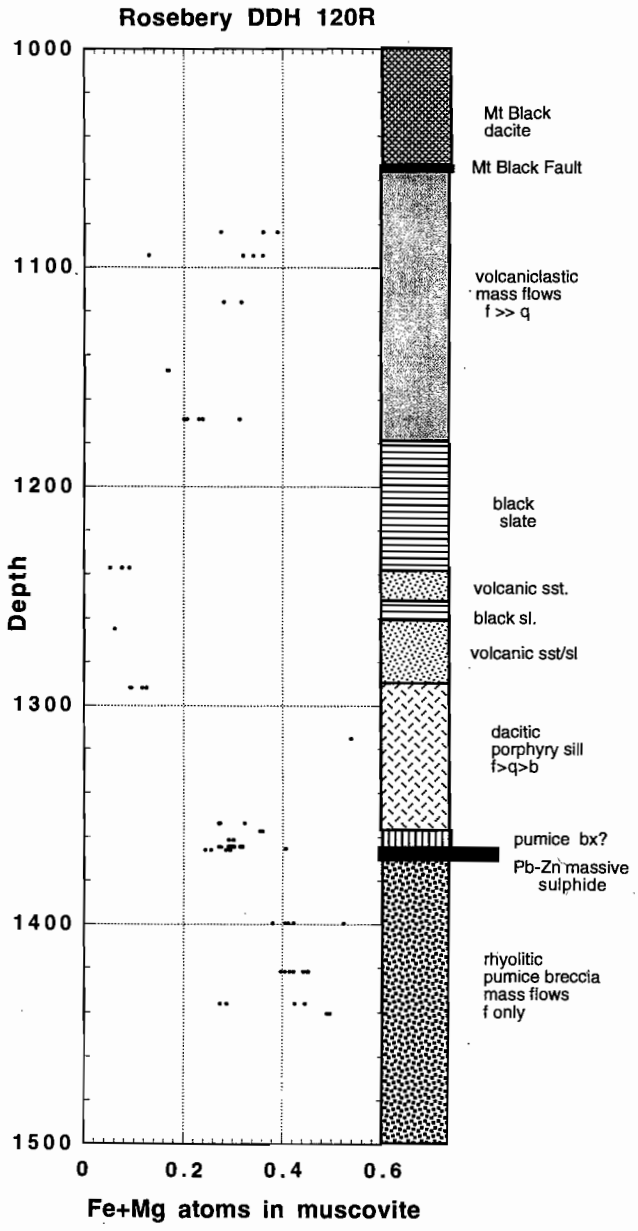

Fig. 8 Downhole variation in Fe + Mg atoms in muscovite, DDH 120R. Calculated on the basis of seven (7) cation atoms in the structure of muscovite.

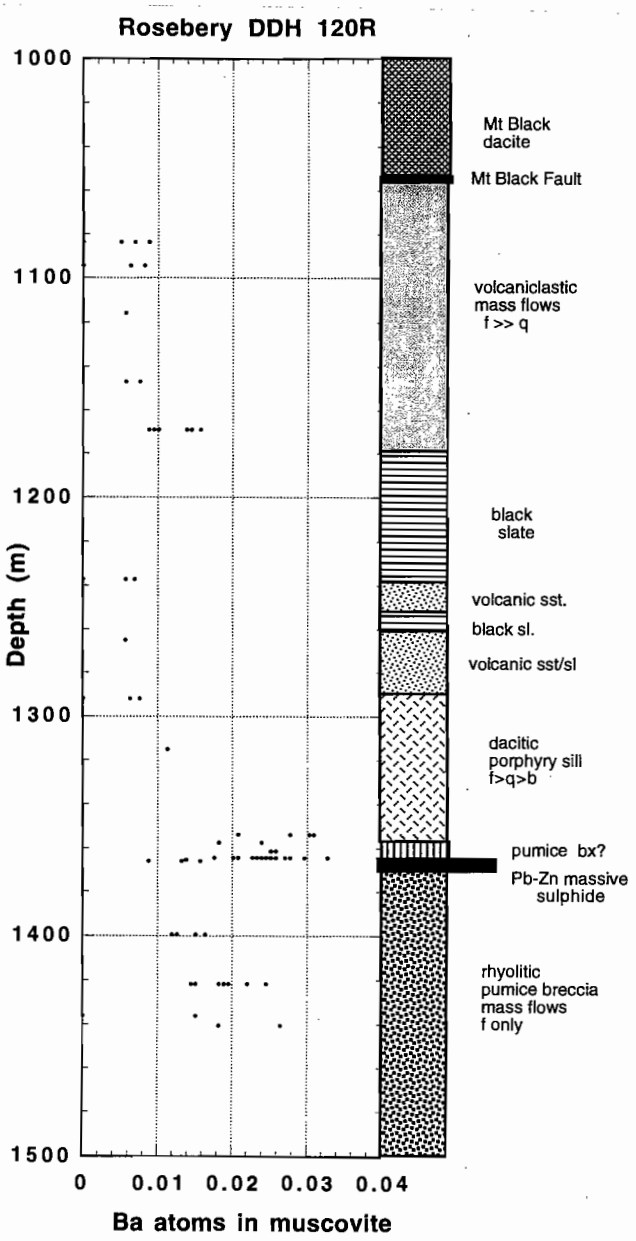

Fig. 9 Downhole variation in Ba atoms in muscovite, DDH 120R. Calculated on the basis of seven (7) cation atoms in the structure of muscovite. Note this data requires verification due to peak overlap of Ba and Ti.

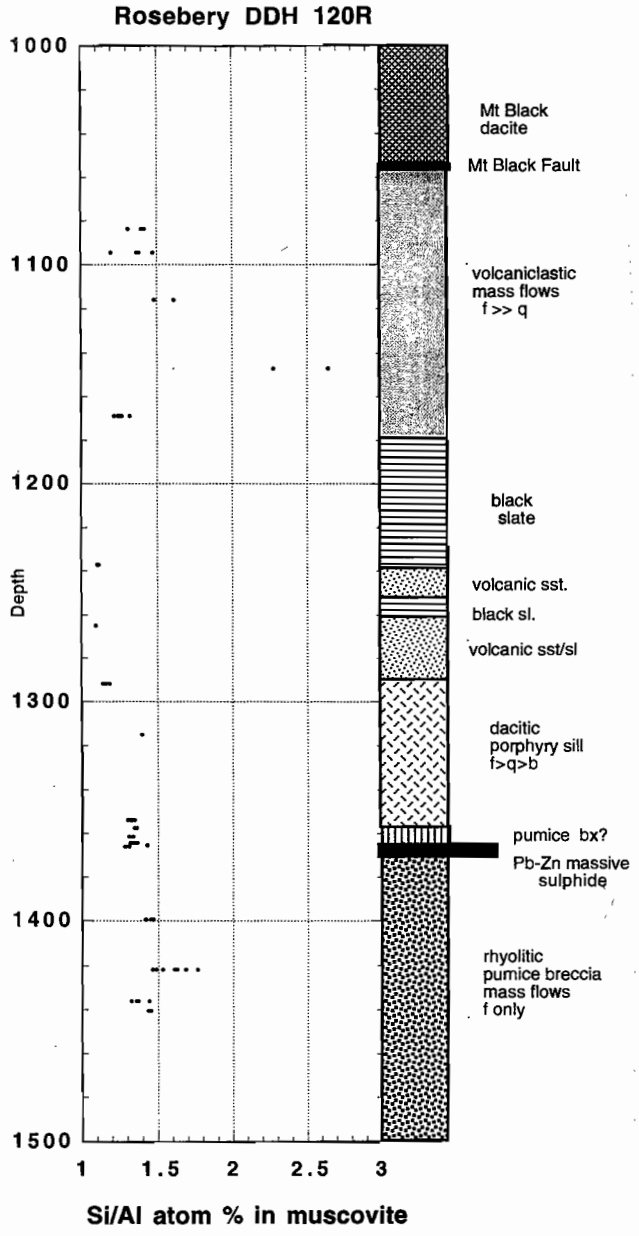

Fig. 10 Downhole variation in Si/Al in muscovite, DDH 120R.

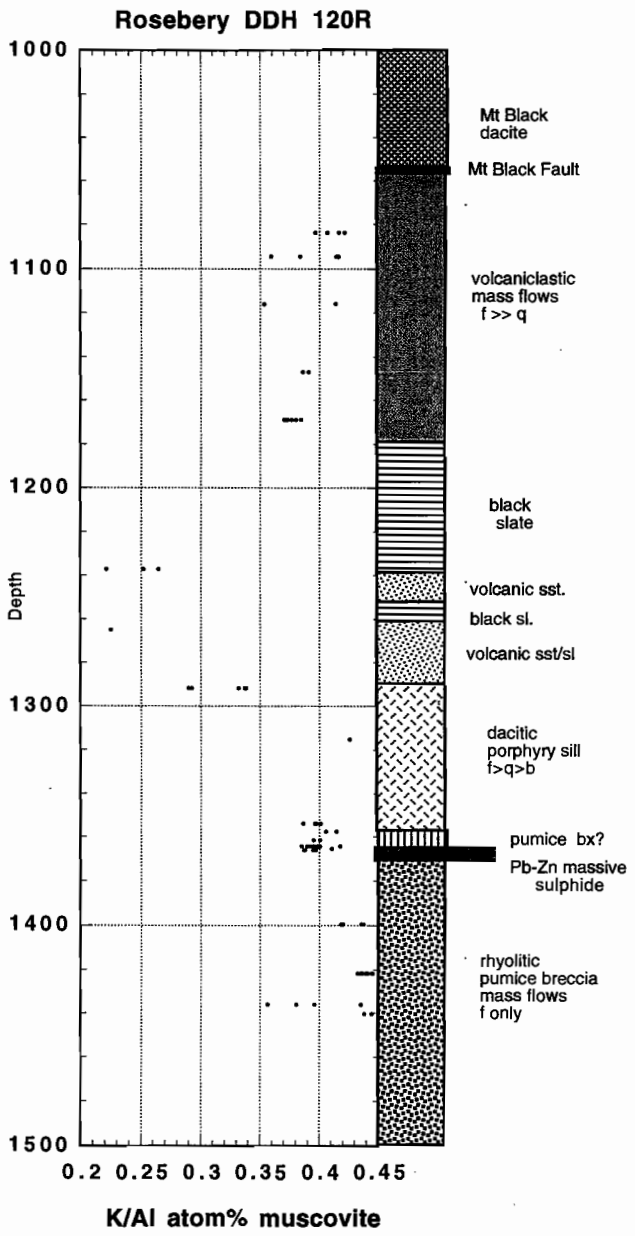

Fig. 11 Downhole variation in K/Al atomic ratio in muscovite, DDH 120R.

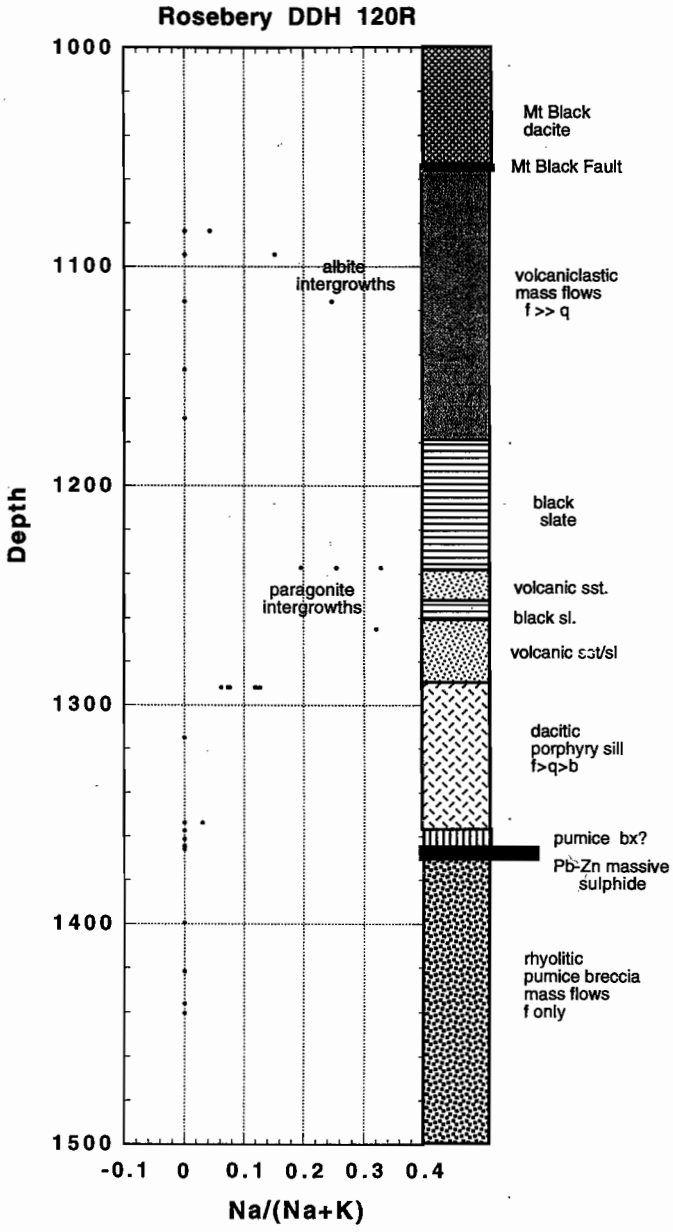

Fig. 12 Downhole variation in Na/Na + K atomic ratio in muscovite, DDH 120R.

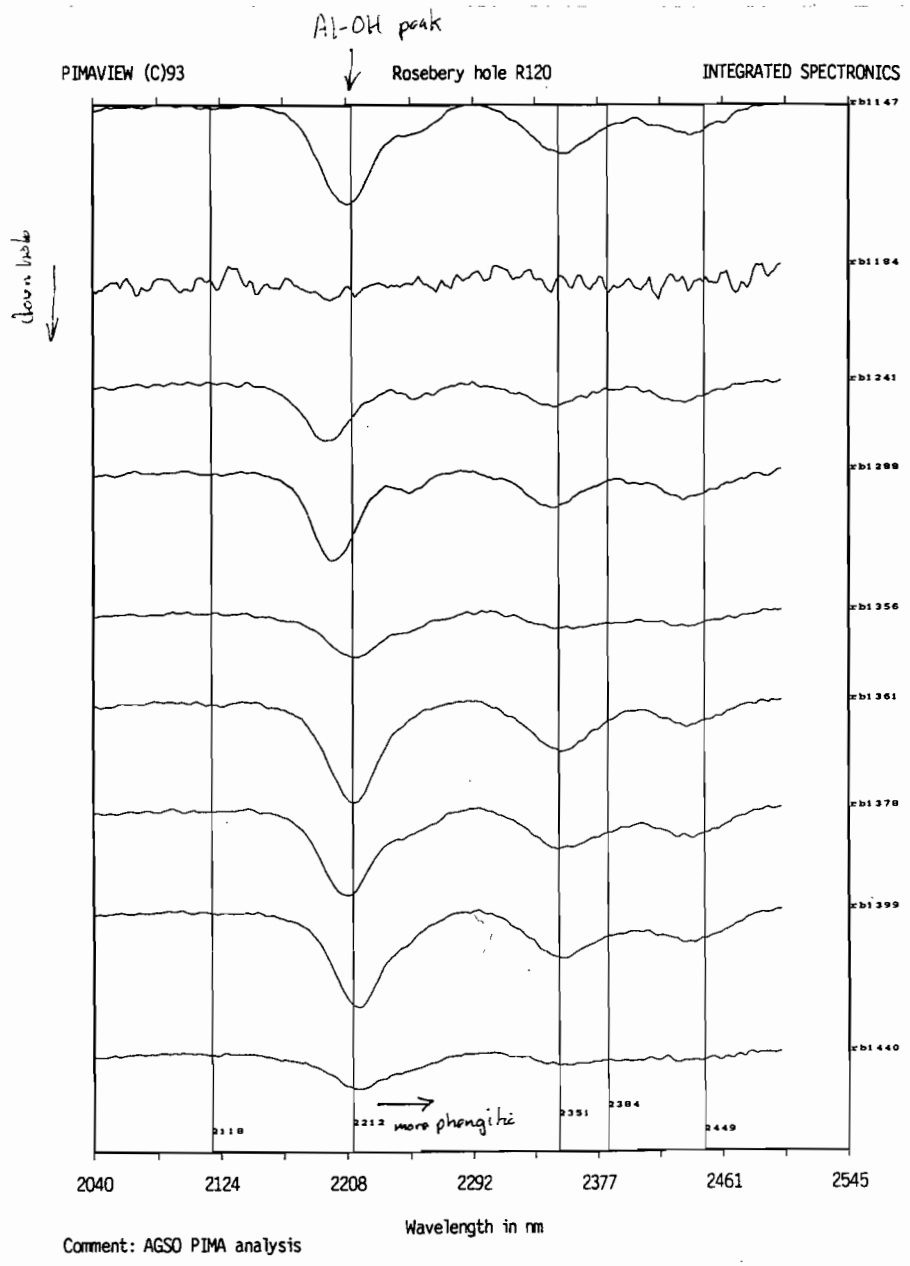

Fig. 13 Stacked PIMA spectra for samples from DDH 120R. The PIMA analyses were performed by AGSO.

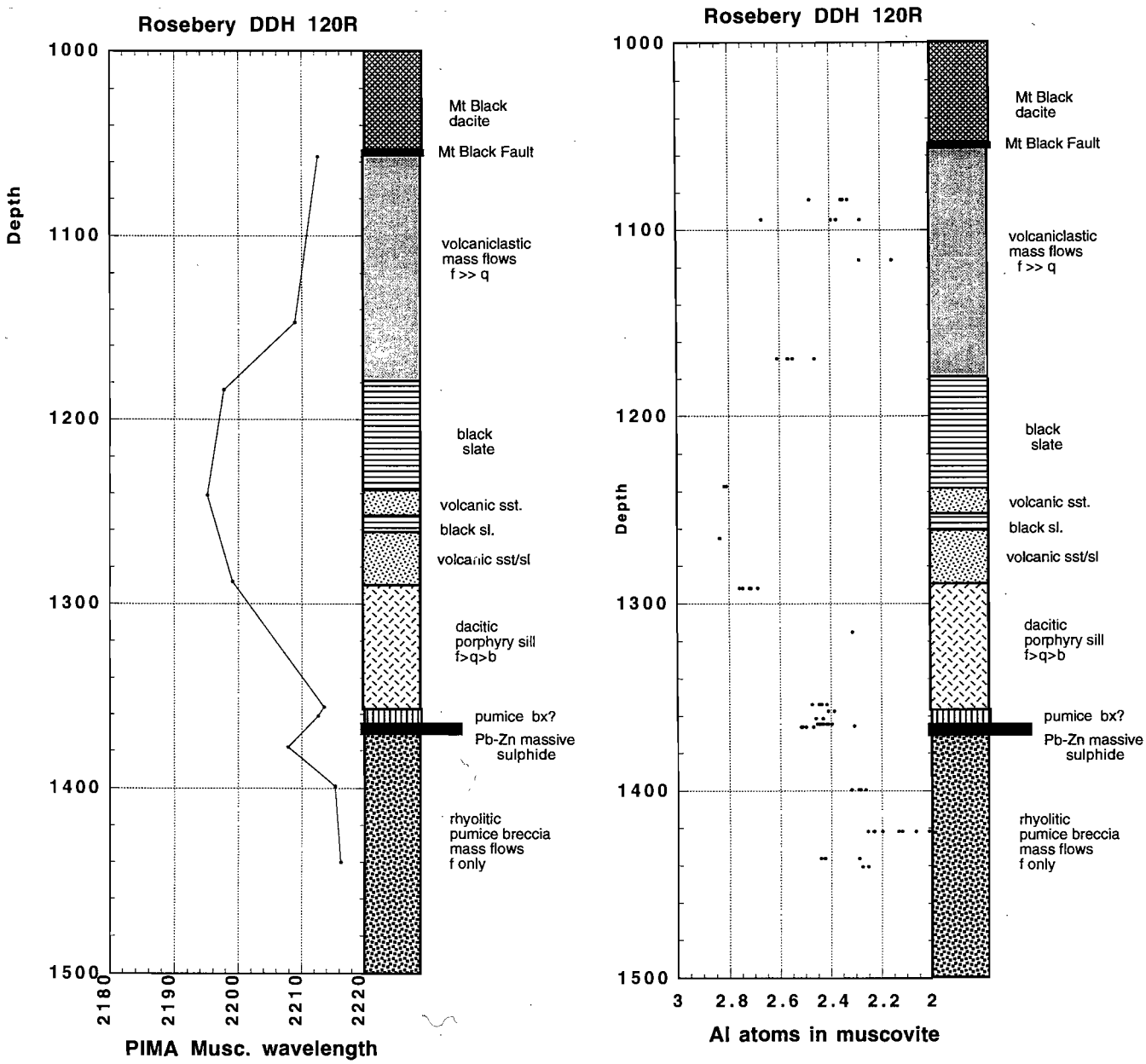

Fig. 14 Comparison of downhole PIMA (2200 nm Peak) with microprobe Al atomic distribution in muscovite.

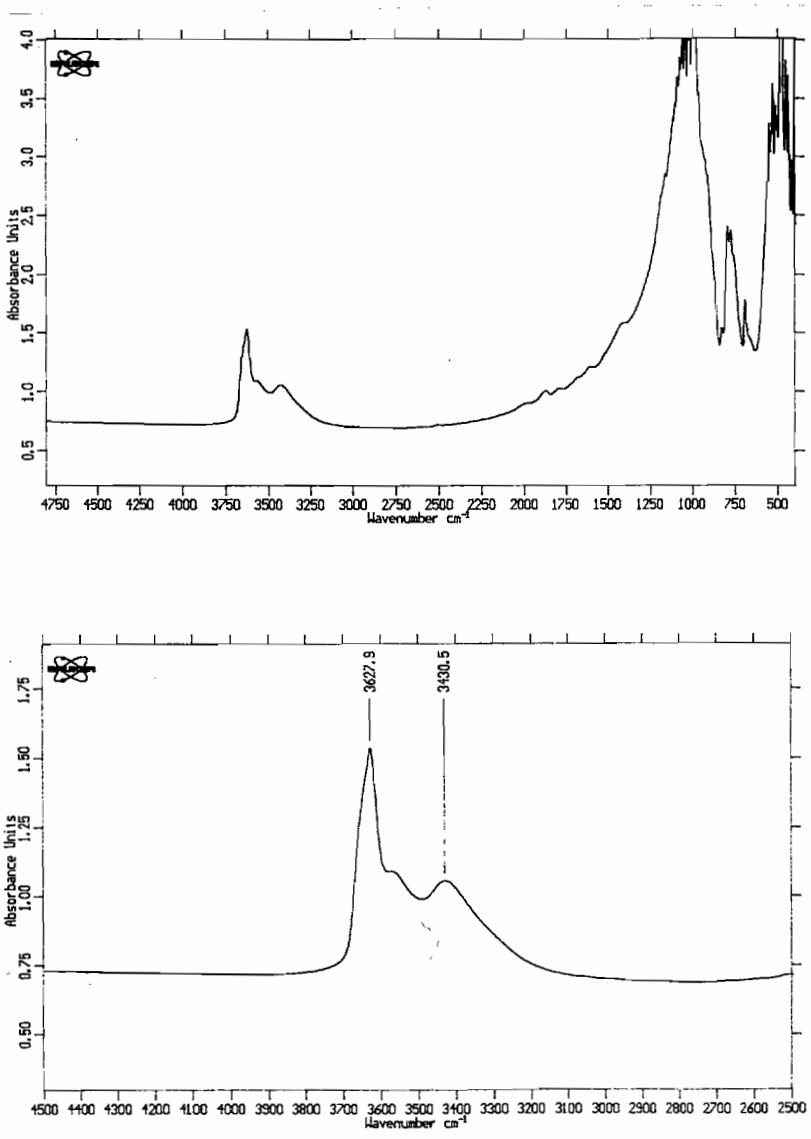

Fig. 15 FTIR spectra for sample 120R-1288.1. The muscovite peak investigated in this study is at 3627.9 cm^{-1} wavenumber (2756.5 nm). The adjacent peak at 3430.5 cm^{-1} is related to chlorite.

to the PIMA 2200 muscovite peak data and correlates well with the microprobe Al atomic distribution (Fig.16). A particularly good linear correlation between the FTIR muscovite wavelength (2760 Peak) and the mean microprobe Al atomic distribution is exhibited by the combined data (Fig. 17).

Carbonate chemistry

Previous studies by Brathwaite (1974) and Khin Zaw (1991) reported a manganese-rich suite of carbonates, including the following minerals in order of abundance: rhodochrosite ($MnCO_3$), ferroan rhodochrosite [(Mn,Fe) CO_3], kutnahorite [$CaMn(CO_3)_2$], dolomite [$CaMg(CO_3)_2$] and calcite ($CaCO_3$).

Plots of the microprobe data from this study (Fig. 18) show that the carbonates in DDH 120R fall into three main groups.

Group 1: rhodochrosite-ferroan rhodochrosite with up to 50 mole % $FeCo_3$;
- dominantly carbonates from the dacitic pumice breccia ore horizon below the porphyry sill;
- also includes some footwall carbonate alteration (ferroan rhodochrosite with 20 to 40 mole % $FeCO_3$).

Group 2: kutnahorite -ankerite
- dominantly ore horizon carbonates with some footwall carbonates at the ankerite end of the spectrum.

Group 3: calcite
- confined principally to the hangingwall volcanics and volcaniclastics above the base of the dacitic porphyry sill. The deepest sample in the footwall (70m below the ore lens) also contains calcite.

Downhole variation in carbonate chemistry is shown in Figures 19, 20, 21 and 22. These plots clearly show the marked change in carbonate chemistry between the hangingwall sequence and the ore-horizon/footwall sequence below the porphyry sill. These chemical features are summarised below:

Hangingwall carbonate: always calcite with very minor substitution of $FeCO_3$ (<3 mole %), $MnCO_3$ (<3 mole %) and $MgCO_3$ (<2 mole %).
It is interesting that the most Mn-poor and "purest" calcites were found in the volcanic sandstone and black slate overlying the dacite porphyry. These lithologies also host the most Fe,Mg-poor muscovite, with highest paragonite component.

Ore horizon: within the ore lens and overlying dacitic pumice breccia unit the carbonates are Mn-rich varieties (>20 mole % $MnCO_3$): rhodochrosite, ferroan rhodochrosite and ferroan kutnahorite.

Footwall alteration zone: carbonate compositions are similar to the ore-horizon but with examples concentrated at the Fe-rich end of the spectrum; ferroan rhodochrosite and ankerite.

Further work

- PIMA/FTIR study of muscovite chemistry in other drill holes around K lens.
- Further microprobe analyses on muscovites and carbonates in samples from DDH R4452, 131R, 113RDI and 109R.
- Preliminary evaluation of chlorite chemistry in DDH 120R.

Conclusions

Microprobe analyses have shown a systematic variation in muscovite and carbonate mineral chemistry relative to stratigraphy and ore position at Rosebery. The major mineral chemical variations are summarised below.

Muscovite

- Variations in muscovite chemistry at Rosebery are controlled by substitution of (1) Fe and Mg into the Al octahedral site, and (2) Na and Ba into the K site.

- Muscovite in the ore zone and dacitic pumice breccia host horizon have an intermediate phengitic composition with 2–2.5 Al atoms and 0.2–0.4 Fe + Mg atoms in the octahedral site. They show both enrichment in Ba and Mg and have a very low Na/Na+K ratio.

- Muscovites in the hangingwall volcanics and volcaniclastics has a markedly different chemistry. They contain low Ba, low Mg and elevated Na/Na+K. The phengitic component (Fe+Mg atoms in OS) is variable, increasing upwards toward the Mt Black fault.

- Muscovite in the footwall alteration zone shows similarities to the ore horizon muscovite, exhibiting a phengitic composition with low Na/Na+K ratio. Mg content of muscovite increases upwards to the ore horizon, whereas the Fe content shows the reverse trend.

- Downhole PIMA and FTIR data of the muscovite peak wavelengths show good correlation with one another and the mineral chemistry. An excellent linear correlation occurs between FTIR muscovite wavelength (2760 nm peak) and the mean microprobe Al atomic distribution in muscovite.

Carbonate

- Mn-rich carbonates in DDH 120R are restricted to the ore horizon dacitic pumice breccia and the footwall alteration zone.

- All hangingwall lithologies, above the base of the dacitic quartz porphyry, contain calcite with a low $MnCO_3$ component (<3 mole %).

- Two Mn-carbonate compositional groups are present in the ore zone and footwall alteration system;
  (1) rhodochrosite-ferroan rhodochrosite
  (2) kutnahorite-ankerite

- The most Mn,Fe-poor carbonate in DDH 120R is found in the volcanic sandstone and black slates above the porphyry sill, and is associated with the paragonitic muscovite assemblage.

General

Trends of increasing phengitic component of muscovite toward the top of the drill hole (1050–1100 m), indicated by both the microprobe data and FTIR data, suggest the possibility of the Mt Black Fault marking a potential stratiform VHMS ore position. This unlikely proposal is supported by weakly anomalous levels of other geochemical vectors: Tl, Sb, MnO, AI, CPCI and As at the position of the Mt Black Fault.

Acknowledgments

Thanks to Ron Berry for assistance in interpretation of the muscovite analyses.

References

Allen, R.L., Duhig, N. and Large, R.R., 1966, Rosebery alteration study : AMIRA Project P439; Report 2 : May 1996, p. 95-118.

Brathwaite, R.R., 1974, The geology and origin of the Rosebery Ore Deposit, Tasmania. Economic Geology, V69, p. 1086-1101.

Deer, W.A., Howie, R.A. and Zussman, J., 1996, An introduction to the Rock Forming Minerals : Longman, 528p.

Khin Zaw, 1991, The effect of Devonian metamorphism and metasomatism on the mineralogy and geochemistry of the Cambrian VMS deposits in the Rosebery-Hercules district, Western Tasmania : Unpub. PhD thesis, University of Tasmania, 342p.

Large, R.R. and Allen, R.L., 1997, Preliminary report on the Rosebery lithochemical halo study : AMIRA Project P437, Report 4, May 1997, p. 259–330.

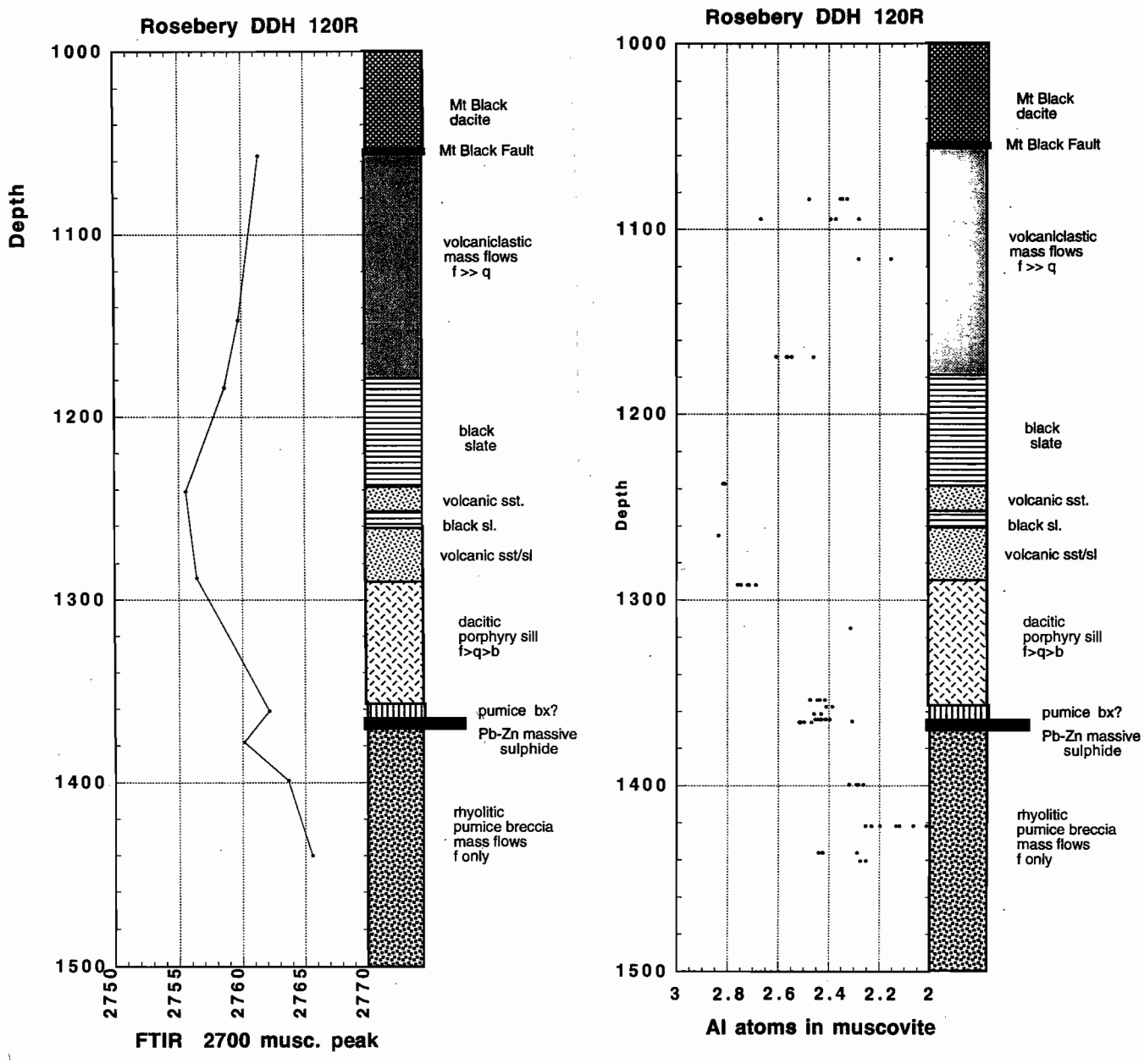

Fig. 16 Comparison of downhole FTIR (2760 nm Peak) with microprobe Al atomic distribution in muscovite.

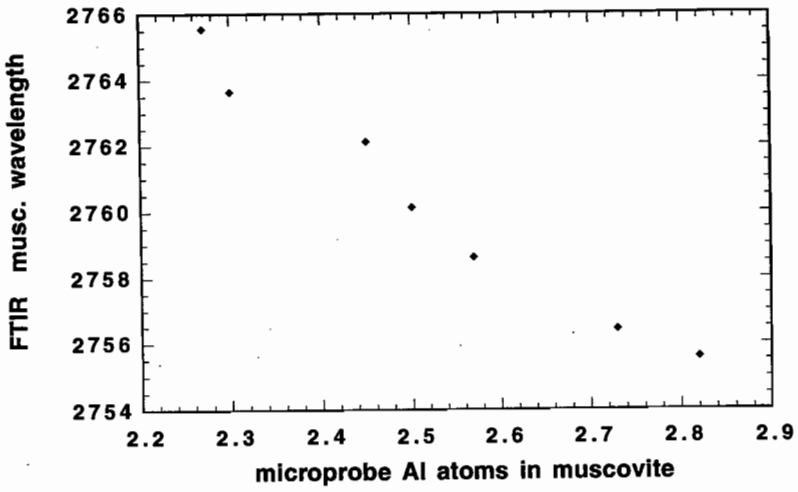

Fig. 17 Linear correlation between FTIR muscovite wavelength (2760 nm peak) and Al atomic distribution calculated from mean microprobe analyses on muscovite.

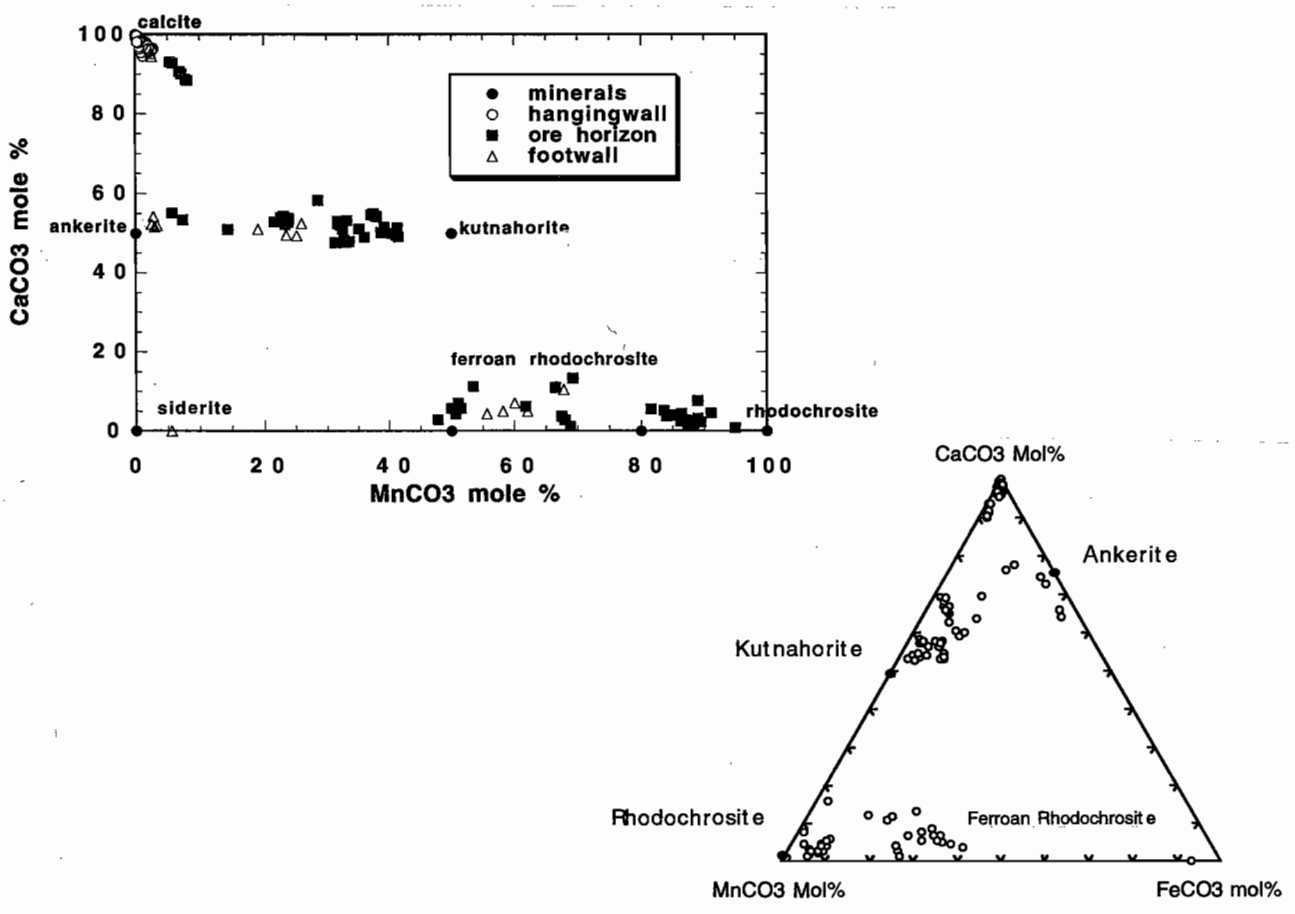

Fig. 18 Rosebery DDH 120R carbonate microprobe analyses showing the three major groups:
- rhodochrosite-ferroan rhodochrosite
- kutnahorite-ankerite
- calcite.

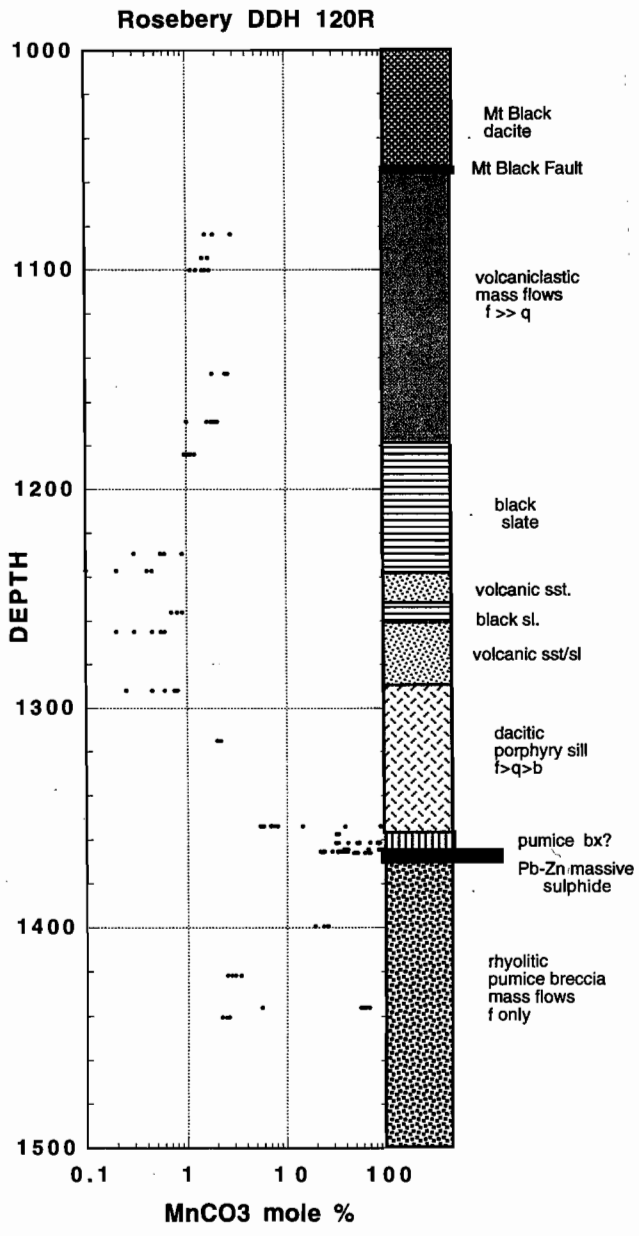

Fig. 19 $MnCO_3$ content of carbonates in DDH 120R from microprobe data.

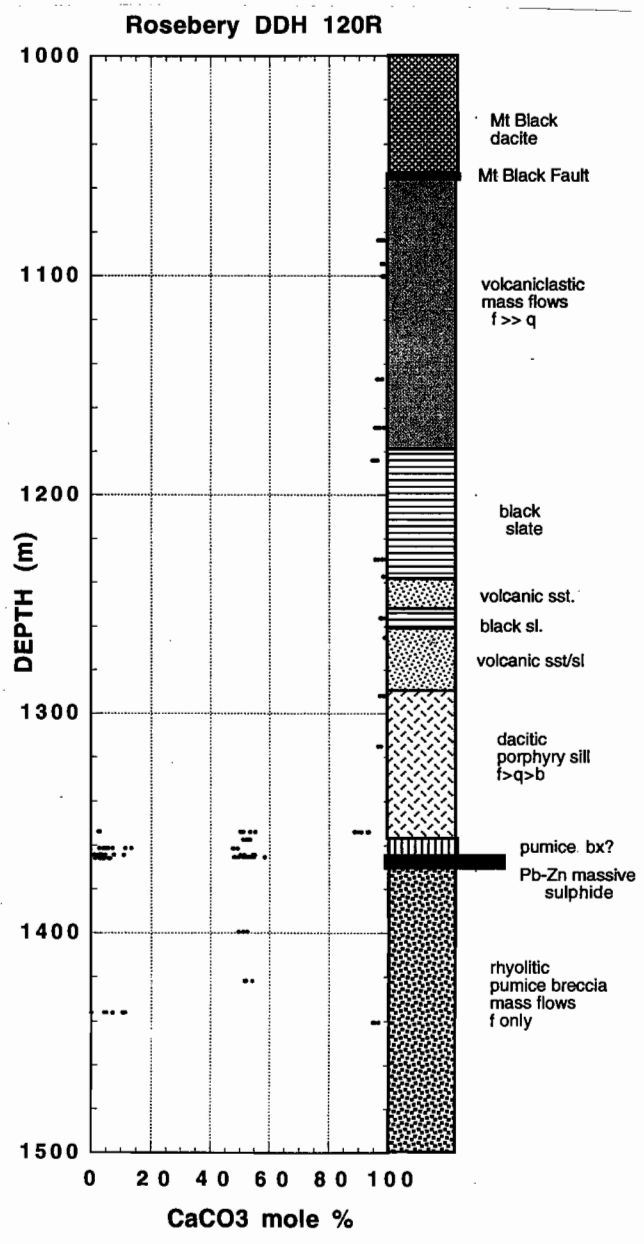

Fig. 20 $CaCO_3$ content of carbonates in DDH 120R from microprobe data.

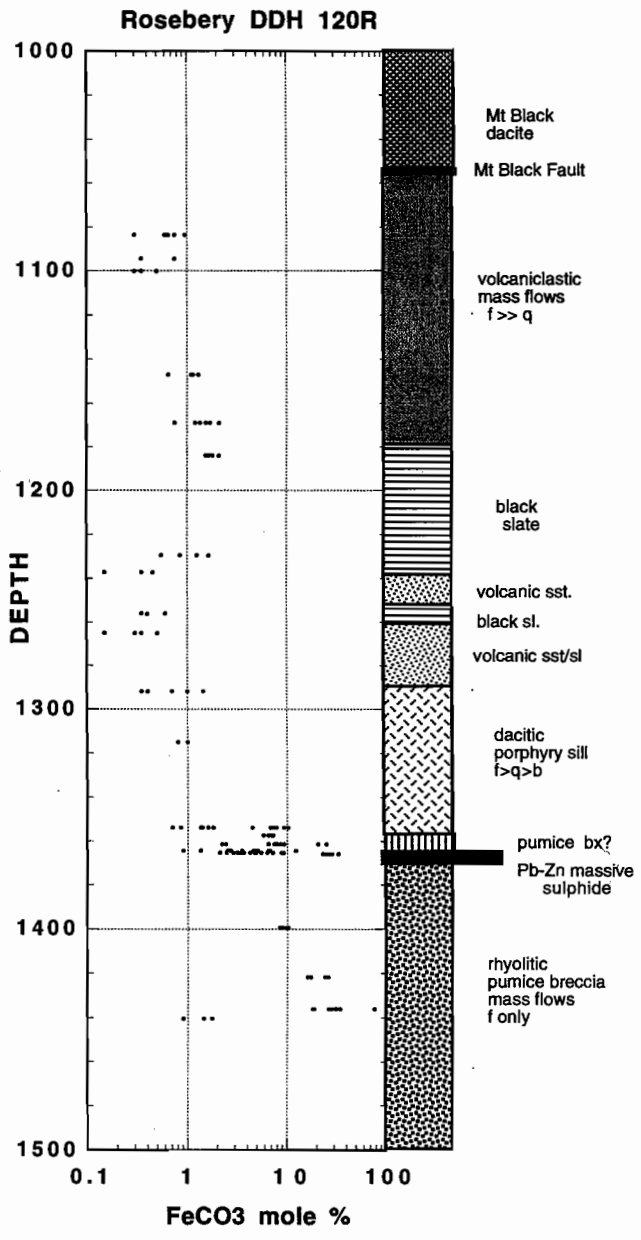

Fig. 21 $FeCO_3$ content of carbonates in DDH 120R from microprobe data.

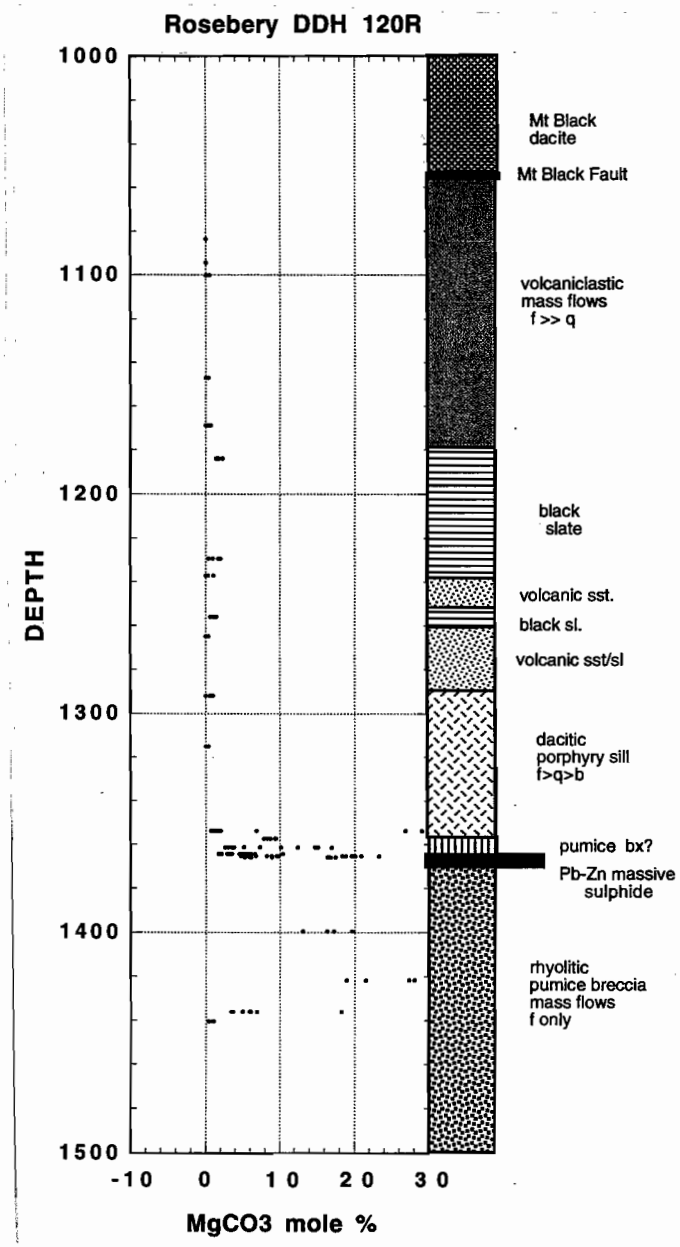

Fig. 22 $MgCO_3$ content of carbonates in DDH 120R from microprobe data.

Appendix 2

120R Probe Results

Carbonate Data

Sample	Area	depth	Description	FeCO3	MnCO3	MgCO3	CaCO3	NICO3	SIO2	Al2O3	Carb total
120R-1083.7	A3 C1	1083.7	coarse carbonate in diffuse, foliated vein	0.76	3.32	0	99.23	0	0	0	103.31
120R-1083.7	A3 C2	1083.7	coarse carbonate in diffuse, foliated vein	0.9	3.26	0	97.53	0	0	0	101.69
120R-1083.7	A2 C1	1083.7	coarse carbonate patch in matrix	0.71	2.12	0	98.62	0	0	0	101.45
120R-1083.7	A2 C2	1083.7	coarse carbonate patch in matrix	1.11	3.18	0	95.23	0	0	0	99.52
120R-1083.7	A2 C3	1083.7	coarse carbonate patch in matrix	0.34	1.8	0	99.12	0	0	0	101.26
120R-1094.5	A4 C1	1094.5	coarse carbonate patch or vein	0.4	1.91	0	100.03	0	0	0	102.35
120R-1094.5	A4 C2	1094.5	coarse carbonate patch or vein	0.87	1.72	0	99.51	0.35	0	0	102.45
120R-1100.3	A4 C1	1100.3	coarse grained carbonate in matrix	0.37	1.46	0	99.46	0	0	0	101.29
120R-1100.3	A4 C2	1100.3	coarse grained carbonate in matrix	0.39	1.28	0	100.25	0	0	0	101.91
120R-1100.3	A2 C1	1100.3	coarse grained carbonate patch in matrix	0.32	1.25	0	99.59	0	0	0	101.16
120R-1100.3	A2 C2	1100.3	coarse grained carbonate patch in matrix	0.58	1.98	0	98.3	0	0	0	100.86
120R-1100.3	A1 C1	1100.3	coarse grained, foliated carbonate in vein	0.35	1.86	0.42	101.66	0	0	0	104.29
120R-1100.3	A1 C2	1100.3	coarse grained, foliated carbonate in vein	0.37	1.7	0	101.51	0	0	0	103.58
120R-1147	A1 C1	1147	carbonate patch within altered feldspar	1.34	3	0	96.39	0	0	0	100.73
120R-1147	A1 C2	1147	carbonate patch within altered feldspar	1.52	2.8	0	95.84	0	0	0	100.16
120R-1147	A2 C1	1147	carbonate patch within altered feldspar	0.79	2.09	0	99.41	0	0	0	102.29
120R-1147	A2 C2	1147	carbonate patch within altered feldspar	1.29	2.93	0.36	97.14	0	0	0	101.72
120R-1169	A1-C1	1169	carbonate grain within feldspar	0.89	1.18	0	100.23	0	0	0	102.3
120R-1169	A1-C2	1169	carbonate grain within feldspar	1.6	2.41	0	97.98	0	0	0	101.99
120R-1169	A3 C1	1169	ranular carbonate in pressure shadow of feldsp	1.42	1.93	0.4	100.85	0	0	0	104.6
120R-1169	A3 C2	1169	ranular carbonate in pressure shadow of feldsp	2.42	2.19	0.61	95.96	0	0	0	101.17
120R-1169	A3 C3	1169	ranular carbonate in pressure shadow of feldsp	1.97	2.33	0.46	96.09	0	0	0	100.85
120R-1169	A3 C4	1169	ranular carbonate in pressure shadow of feldsp	1.58	2.12	0.38	98.44	0	0	0	102.52
120R-1169	A3 C5	1169	ranular carbonate in pressure shadow of feldsp	1.84	2.06	0.33	99.96	0	0	0	104.19
120R-1184.0	A2 C1	1184	carbonate within quartz vein	1.81	1.26	1.23	96.93	0	0	0	101.23
120R-1184.0	A1 C1	1184	vein carbonate	1.92	1.15	1.25	95.41	0	0	0	99.73
120R-1184.0	A1 C2	1184	vein carbonate	2.11	1.2	1.53	96.3	0	0	0	101.14
120R-1184.0	A3 C1	1184	vein carbonate	2.47	1.38	1.9	95.8	0	0	0	101.55
120R-1184.0	A3 C2	1184	vein carbonate	1.81	1.1	1.53	96.57	0	0	0	101
120R-1229.3	A1 C1	1229.3	coarse carbonate in vein	1.87	0.99	1.67	93.71	0	0	0	98.24
120R-1229.3	A1 C2	1229.3	coarse carbonate in vein	1.42	0.7	1.42	95.91	0	0	0	99.45
120R-1229.3	A2 C1	1229.3	fine carbonate in vein	0.98	0.6	0.77	96.37	0	0	0	98.73
120R-1229.3	A2 C2	1229.3	fine carbonate in vein	0.65	0.34	0.27	96.09	0	0	0	97.34
120R-1237	R4 C1	1237	coarse vein carbonate	0.5	0.5	0.86	96.23	0	0	0	98.09
120R-1237	R4 C2	1237	coarse vein carbonate	0.37	0.45	0	97.05	0	0	0	97.88
120R-1237	A2 C2	1237	foliated matrix carbonate	0	0.53	0	101.16	0	0	0	101.69
120R-1237	A2 C3	1237	foliated matrix carbonate	0.42	0	0.27	101.26	0	0	0	101.95
120R-1237	A1 C1	1237		0	0.23	0	101.28	0	0	0	101.51

PROB120R.xls

Appendix 2 cont.

120R Probe Results

Carbonate Data

Sample	Area	depth	Description	FeCO3	MnCO3	MgCO3	CaCO3	NiCO3	SiO2	Al2O3	Carb total
120R-1241	A3 C1	1241	carbonate altered feldspar	0.81	0.5	0.48	95.73	0.33	0	0	97.85
120R-1241	A1 C1	1241	coarse carbonate in carb-pyrite vein	0.84	0.92	0	100.53	0	0	0	102.29
120R-1241	A1 C2	1241	coarse carbonate in carb-pyrite vein	1.65	0.7	0.84	95.1	0	0	0	98.28
120R-1241	M082	1241	coarse carbonate in carb-pyrite vein	1.13	0.31	0.48	96.84	0	0	0	98.75
120R-1256.0	A2 C1	1256	coarse qtz - carbonate vein	0.45	0.81	1	97.84	0	0	0	100.1
120R-1256.0	A2 C2	1256	coarse qtz - carbonate vein	0.69	1	1.15	96.28	0	0	0	99.13
120R-1256.0	A1 C1	1256	recrystallised foliated vein carbonate	0.42	0.92	0.54	98.17	0	0	0	100.06
120R-1256.0	A1 C2	1256	recrystallised foliated vein carbonate	0.68	1.05	0.86	96.76	0	0	0	99.35
120R-1265	A2 C1	1265	coarse S2 vein carbonate	0.61	0.73	0.33	103.07	0	0	0	104.74
120R-1265	A2 C2	1265	coarse S2 vein carbonate	0	0.24	0	103.07	0	0	0	103.31
120R-1265	A1 C1	1265	foliated matrix carbonate	0.44	0.34	0	100.14	0	0	0	100.91
120R-1265	A1 C2	1265	foliated matrix carbonate	0.6	0.63	0.31	102.51	0	0	0	104.05
120R-1265	A1 C3	1265	foliated matrix carbonate	0.37	0.53	0	101.21	0	0	0	102.12
120R-1291.8	A2 C1	1291.8	carbonate grains within plag phenocryst	0.44	0.92	0.5	97.98	0	0	0	99.84
120R-1291.8	A2 C2	1291.8	carbonate grains within plag phenocryst	0.42	0.83	0.59	97.12	0	0	0	98.95
120R-1315	A3 C1	1315	early foliated qtz - carb veinlet	0.95	2.32	0	99.12	0	0	0	102.39
120R-1315	A3 C2	1315	early foliated qtz - carb veinlet	1.19	2.54	0.31	99.05	0	0	0	103.1
120R-1353.8	A1 C1	1353.8	carbonate patch in feldspar pressure shadow	0.79	6.64	0.56	91.82	0	0	0	99.82
120R-1353.8	A1 C2	1353.8	carbonate patch in feldspar pressure shadow	2.03	9.06	1.44	86.59	0	0	0	99.12
120R-1353.8	A2 C1	1353.8	carbonate within plag phenocryst	1.6	8.1	1.05	88.18	0	0	0	98.92
120R-1353.8	A2 C2	1353.8	carbonate within plag phenocryst	0.97	6.06	0.56	91.18	0	0	0	98.77
120R-1353.8	A3 C1	1353.8	matrix carbonate	1.53	7.79	0.86	89.34	0	0	0	99.52
120R-1353.8	A3 C2	1353.8	matrix carbonate	1.82	8.8	1.42	86.27	0	0	0	98.31
120R-1357.4	A1 C1	1357.4	coarse recrystallised vein carbonate	7.69	33.97	6.65	47.93	0	0	0	96.24
120R-1357.4	A1 C2	1357.4	coarse recrystallised vein carbonate	7.5	33.66	6.42	49.07	0	0	0	96.65
120R-1357.4	A3 C1	1357.4	early coarse carbonate vein	7.66	33.74	6.84	48.73	0	0	0	96.97
120R-1357.4	A3 C2	1357.4	early coarse carbonate vein	7.53	34.64	7.4	47.52	0	0	0	97.09
120R-1357.4	A2 C1	1357.4	recrystallised carbonate spheroid	6.98	34.2	7.3	48.37	0	0	0	96.85
120R-1357.4	A2 C2	1357.4	recrystallised carbonate spheroid	6.31	35.74	6.19	49.91	0	0	0	98.14
120R-1361.4A	A1 C1	1361.4	interlocking carb within early qtz-carb vein	5.68	39.01	5.52	46.55	0	0	0	96.76
120R-1361.4A	A1 C2	1361.4	interlocking carb within early qtz-carb vein	4.74	40.71	5.29	45.98	0	0	0	96.72
120R-1361.4A	A2 C1	1361.4	concentric layered carbonate spheroid	11.61	7.73	25.89	54.32	0.29	0	0	99.83
120R-1361.4A	A2 C2	1361.4	concentric layered carbonate spheroid	7.37	87.14	1.46	2.32	0	0	0	98.3
120R-1361.4A	A2 C3	1361.4	concentric layered carbonate spheroid	11.87	6.56	24.55	55.39	0	0	0	98.37
120R-1361.4A	A2 C4	1361.4	concentric layered carbonate spheroid	8.95	16.33	22.33	50.57	0	0	0	98.18
120R-1361.4A	A2 C5	1361.4	concentric layered carbonate spheroid	10.79	8.52	25.38	53.76	0	0	0	98.46
120R-1361.4A	A2 C6	1361.4	concentric layered carbonate spheroid	6.86	88.81	1	2.05	0	0	0	98.72
120R-1361.4B	A1 C1	1361.4	recrystallised (late S2) carb within foliated vein	6.71	88.39	1.97	4.03	0	0	0	101.1

PROB120R.xls

Appendix 2 cont.

120R Probe Results — Carbonate Data

Sample	Area	depth	Description	FeCO3	MnCO3	MgCO3	CaCO3	NiCO3	SiO2	Al2O3	Carb total
120R-1361.4B	A1 C2	1361.4	recrystallised (late S2) carb within foliated vein	22.39	57.88	11.65	10.62	0	0	0	102.54
120R-1361.4B	A1 C3	1361.4	recrystallised (late S2) carb within foliated vein	27.18	55.81	13.59	6.73	0.35	0	0	103.66
120R-1361.4B	A1 C4	1361.4	recrystallised (late S2) carb within foliated vein	8.05	84.05	3.91	5.03	0	0	0	101.04
120R-1361.4B	A1 C5	1361.4	recrystallised (late S2) carb within foliated vein	9.73	35.15	10.25	46.64	0	0	0	101.77
120R-1361.4B	A1 C6	1361.4	recrystallised (late S2) carb within foliated vein	10.42	36.55	8.28	46.14	0	0	0	101.39
120R-1361.4B	A2 C1	1361.4	concentric layered carbonate spheroid	8.23	87.43	2.28	3.57	0	0	0	101.51
120R-1361.4B	A2 C2	1361.4	concentric layered carbonate spheroid	7.73	86.73	2.91	4.69	0	0	0	102.06
120R-1361.4B	A2 C3	1361.4	concentric layered carbonate spheroid	8.05	88.6	2.63	2.28	0	0	0	101.57
120R-1361.4B	A2 C4	1361.4	concentric layered carbonate spheroid	2.45	45.51	5.92	47.02	0	0	0	100.89
120R-1361.4B	A2 C5	1361.4	concentric layered carbonate spheroid	2.61	74.16	11.86	12.44	0	0	0	101.07
120R-1364.4B	A3 C1	1364.4	carbonate in altered plagioclase phenocryst	0.92	95.99	2.11	0.73	0.48	0	0	100.22
120R-1364.4B	A4 C1	1364.4	carbonate in early carb-qtz vein	3.89	44.26	4.93	47.75	0	0	0	100.83
120R-1364.4B	A4 C2	1364.4	carbonate in early carb-qtz vein	2.77	40.9	4.1	52.41	0	0	0	100.19
120R-1364.4B	A6 C1	1364.4	carbonate grain	5.08	91.24	3.76	1.73	0	0	0	101.81
120R-1364.4B	A7 C1	1364.4	carbonate in early carb-qtz vein	2.81	41.78	4.35	52.1	0	0	0	101.04
120R-1364.4B	A7 C2	1364.4	carbonate in early carb-qtz vein	12.77	69.55	8.03	10	0	0	0	100.35
120R-1364.4B	A7 C3	1364.4	carbonate in early carb-qtz vein	2.86	44.83	3.81	48.77	0	0	0	100.25
120R-1364.4B	A8 C1	1364.4	partially recrystallised carbonate spheroid	1.39	89.88	1.57	6.66	0	0	0	99.49
120R-1364.4B	A8 C2	1364.4	partially recrystallised carbonate spheroid	4.73	91.27	2.47	2.87	0	0	0	101.34
120R-1364A	A1 C1	1364.4	arbonate spheroid enclosing feldspar phenocry	6.95	90.61	2.68	2.48	0	0	0	102.72
120R-1364A	A1 C2	1364.4	arbonate spheroid enclosing feldspar phenocry	2.84	94.09	1.3	4.09	0	0	0	102.31
120R-1364A	A1 C3	1364.4	arbonate spheroid enclosing feldspar phenocry	5.05	90.33	5.04	1.07	0	0	0	101.49
120R-1364A	A2 C1	1364.4	carbonate spheroids	6.74	87.61	3.45	3.62	0	0	0	101.43
120R-1364A	A2 C2	1364.4	carbonate spheroids	5.26	89.68	4.45	2.39	0	0	0	101.79
120R-1364A	A2 C3	1364.4	carbonate spheroids	7.02	87.32	4.16	3.46	0	0	0	101.96
120R-1365.4A	A1 C1	1365.4	carbonate within deformed carbonate vein	6	39.45	7.72	46.71	0	0	0	99.88
120R-1365.4A	A1 C2	1365.4	carbonate within deformed carbonate vein	5.39	38.67	7.21	49.05	0	0	0	100.32
120R-1365.4A	A2 C1	1365.4	vein carbonate	3.95	44.81	4.7	47.21	0	0	0	100.68
120R-1365.4A	A2 C2	1365.4	vein carbonate	4.05	43.12	4.62	49.43	0	0	0	101.22
120R-1365.4A	A6 C1	1365.4	vein carbonate	3.56	41.25	3.83	52.07	0	0	0	100.7
120R-1365.4A	A6 C2	1365.4	vein carbonate	3.4	40.56	3.93	52.18	0.35	0	0	100.42
120R-1365.4B	A1 C1	1365.4	carbonate aggregate ? replacing feldspar	5.39	26.67	16.56	51.93	0	0	0	100.54
120R-1365.4B	A1 C2	1365.4	carbonate aggregate ? replacing feldspar	4.87	27.33	15.41	53.32	0	0	0	100.93
120R-1365.4B	A2 C1	1365.4	coarse dusty brown carbonate	3.31	27.36	16.48	53.92	0	0	0	101.07
120R-1365.4B	A2 C2	1365.4	coarse dusty brown carbonate	2.84	26.1	17.61	53.98	0	0	0	100.52
120R-1365.4B	A3 C1	1365.4	irregular vein carbonate aggregates	7.82	35.4	6.63	49.91	0	0	0	99.76
120R-1365.4B	A3 C2	1365.4	irregular vein carbonate aggregates	7.02	31.49	5.44	55.98	0	0	0	99.92
120R-1365.4B	A4 C1	1365.4	dusty brown matrix carbonate	4.18	26.39	15.75	54.03	0	0	0	100.34

PROB120R.xls

Appendix 2 cont.

120R Probe Results

Carbonate Data

Sample	Area	depth	Description	FeCO3	MnCO3	MgCO3	CaCO3	NICO3	SIO2	AI2O3	Carb total
120R-1365.4B	A4 C2	1365.4	dusty brown matrix carbonate	2.42	24.79	19.53	52.78	0	0	0	99.52
120R-1365.4B	A5 C2	1365.4	syn tectonic carbonate vein	9.66	36.82	7.84	45.91	0	0	0	100.24
120R-1365.4B	A5 C2	1365.4	syn tectonic carbonate vein	10.26	36.39	8.05	46.95	0	0	0	101.64
120R-1365.4B	A5 C3	1365.4	matrix carbonate near vein	3.97	27.44	16.9	52.94	0	0	0	101.25
120R 1366.0	A2 C1	1366	carbonate surrounded by sphalerite	24.61	71.23	4.56	2.5	0	0	0	102.9
120R 1366.0	A2 C2	1366	carbonate surrounded by sphalerite	23.76	70.16	4.68	3.37	0	0	0	101.98
120R 1366.0	A2 C3	1366	carbonate surrounded by sphalerite	35.68	51.19	12.9	2.78	0	0	0	102.56
120R 1366.0	A2 C4	1366	carbonate surrounded by sphalerite	29.34	54.08	13.86	5.39	0	0	0	102.67
120R 1366.0	A3 C1	1366	carbonate surrounded by sphalerite	25.68	71.15	4.01	1.09	0	0	0	101.93
120R 1366.0	A3 C2	1366	carbonate surrounded by sphalerite	30.86	54.64	13.15	4.07	0	0	0	102.72
120R 1366.0	A4 C1	1366	carbonate surrounded by sphalerite	24.71	65.71	7	5.8	0	0	0	103.22
120R 1366.0	A4 C2	1366	carbonate surrounded by sphalerite	28.31	55.63	13.32	5.41	0	0	0	102.67
120R-1399.5	A2 C1	1399.5	coarse carbonate probably replacing feldspar	10.23	28.3	13.51	48.53	0	0	0	100.57
120R-1399.5	A2 C2	1399.5	coarse carbonate probably replacing feldspar	11.08	26.54	14.28	48.78	0	0	0	100.68
120R-1399.5	A3 C1	1399.5	coarse carbonate probably replacing feldspar	9.45	29	10.73	50.94	0	0	0	100.12
120R-1399.5	A3 C2	1399.5	coarse carbonate probably replacing feldspar	11.74	21.79	16.48	50.8	0	0	0	100.81
120R-1421.8	A1 C1	1421.8	carbonate alteration in feldspar phenocryst	27.92	3.52	18.36	52.37	0	0	0	102.17
120R-1421.8	A1 C2	1421.8	carbonate alteration in feldspar phenocryst	30.07	3.92	16.02	52.26	0	0	0	102.27
120R-1421.8	A5 C1	1421.8	carbonate alteration in feldspar phenocryst	18.95	3.24	23.73	56.05	0	0	0	101.97
120R-1421.8	A5 C2	1421.8	carbonate alteration in feldspar phenocryst	20.53	2.98	24.26	53.78	0	0	0	101.55
120R-1436.2	A1 C1	1436.2	carbonate alteration in feldspar phenocryst	35.95	58.6	4.68	3.98	0	0	0	103.21
120R-1436.2	A1 C2	1436.2	carbonate alteration in feldspar phenocryst	29.13	64.07	3.74	4.48	0	0	0	101.43
120R-1436.2	A2 C2	1436.2	vein carbonate	62.49	4.57	10.89	0	0	0	0	77.95
120R-1436.2	A3 C1	1436.2	vein carbonate	18.94	70.49	2.78	9.48	0	0	0	101.68
120R-1436.2	A3 C2	1436.2	vein carbonate	19.6	69.64	2.63	10.23	0	0	0	102.1
120R-1436.2	A4 C1	1436.2	vein carbonate	27.32	62.68	5.27	6.43	0	0	0	101.7
120R-1436.2	A4 C2	1436.2	vein carbonate	32.5	60.83	4.52	4.59	0	0	0	102.44
120R-1440.5	A3 C1	1440.5	carbonate alteration within feldspar	1.65	2.8	0.75	94.02	0	0	0	99.22
120R-1440.5	A5 C1	1440.5	carbonate patches on feldspar phenocryst	1.05	2.54	0.33	97.09	0	0	0	101.01
120R-1440.5	A5 C2	1440.5	carbonate patches on feldspar phenocryst	2.06	3.08	0.92	96.71	0	0	0	102.77

Appendix 2 cont.

120R Probe Results — Sericite Data — 20-10-97

Sample	Depth	Area	Description	SiO2	BaO	Al2O3	Cr2O3	Fe2O3	FeO	MnO	MgO	CaO	Na2O	K2O	Cl	Oxide total
120R-1083.7	1083.7	A1 S1	sericite alteration of feldspar phenocryst	48.2	0	31.12	0	0	2.61	0	1.26	0	0	11.4	0	94.59
120R-1083.7	1083.7	A1 S2	sericite alteration of feldspar phenocryst	48.36	0.4	29.31	0	0	3.63	0	1.81	0	0.32	11.01	0	94.66
120R-1083.7	1083.7	A3 S1	sericite in diffuse foliated vein	48.61	0.49	29.07	0	0	3.54	0	1.86	0	0	11.17	0	94.52
120R-1083.7	1083.7	A3 S2	sericite in diffuse foliated vein	48.35	0.27	29.26	0	0	2.94	0	1.89	0	0	11.38	0	93.97
120R-1094.5	1094.5	A1 S2	matrix sericite	34.03	1.44	17.15	1.66	0	12.35	0.84	0.52	12.42	0.31	0	0	80.08
120R-1094.5	1094.5	A3 S1	fine sericite, matrix	48.45	0.47	30.05	0	0	2.97	0	1.71	0	0	11.5	0	94.94
120R-1094.5	1094.5	A3 S2	fine sericite, matrix	48.62	0.47	29.83	0	0	3.09	0	1.84	0	0	11.46	0	95.1
120R-1094.5	1094.5	A5 B1	? biotite alteration of feldspar phenocryst	47.27	0	33.49	0	0	1.85	0	0.24	0	0	11.11	0	93.96
120R-1094.5	1094.5	A5 B3	? biotite alteration of feldspar phenocryst	50.4	0.34	29.01	0	0	3.24	0	1.39	0.12	1.21	10.27	0	95.83
120R-1115.9	1115.9	A3 S2	matrix sericite	52.35	0.34	27.51	0	0	3.05	0	1.12	0.1	1.93	8.97	0	95.22
120R-1115.9	1115.9	A3 S3	matrix sericite	49.6	0.31	28.38	0	0	3.19	0	1.32	0	0	10.84	0	93.5
120R-1147	1147	A3 S2	sericite rich matrix patch	65.85	0.36	21.16	0	0	1.7	0	0.85	0	0	7.53	0	97.29
120R-1147	1147	A3 S3	sericite rich matrix patch	62.59	0.45	23.34	0	0	1.68	0	0.86	0	0	8.42	0	97.14
120R-1169	1169	A2-SER1	foliated sericite in matrix	47.79	0.54	32.01	0	0	1.69	0	1.1	0	0	11.36	0	94.25
120R-1169	1169	A2 M2	foliated sericite in matrix	47.92	0.9	32.69	0	0	1.88	0	1.26	0	0	11.25	0	95.5
120R-1169	1169	A2 M3	foliated sericite in matrix	47.94	0.81	32.48	0	0	1.53	0	1.16	0	0	11.29	0	94.85
120R-1169	1169	A4 S1	elongate sericite altered domain	47.96	0.56	30.79	0	0	3.07	0	1.37	0	0	10.55	0	94.05
120R-1169	1169	A4 S2	elongate sericite altered domain	47.29	0.79	32.93	0	0	1.58	0	1.11	0	0	11.26	0	94.61
120R-1169	1169	A4 S3	elongate sericite altered domain	47.47	0.49	32.27	0	0	1.94	0	1.28	0	0	11.33	0	94.56
120R-1237	1237	A3 S1	sericite in elongate ?pumice clast	45.75	0.38	35.09	0	0	0.15	0	0.42	0	2.3	7.18	0	91.1
120R-1237	1237	A3 S2	sericite in elongate ?pumice clast	45.41	0.32	34.92	0	0	0.28	0	0.73	0	1.82	8.12	0	91.46
120R-1237	1237	A3 S3	sericite in elongate ?pumice clast	45.51	0	34.76	0	0	0.2	0	0.63	0.12	1.36	8.49	0	91.07
120R-1241	1241	A2 S1	sericite in strongly altered feldspar	46.08	0	33.92	0	0	0.26	0	0.78	0	0.87	9.07	0	90.98
120R-1241	1241	A2 S2	sericite in strongly altered feldspar	45.57	0.34	33.91	0	0	0.29	0	0.75	0	0.81	9.16	0	90.68
120R-1241	1241	A3 S1	altered feldspar crystal	45.68	0.41	34.01	0	0	0.34	0	0.7	0	0.83	9.18	0	90.97
120R-1241	1241	A3 S2	altered feldspar crystal	39.13	0.27	33.67	0	0	6.82	0	4.99	0.17	4.11	1.87	0	90.91
120R-1265	1265	A3 S2	sericite in elongate ?pumice clast	47.13	0.34	36.64	0	0	0.33	0	0.44	0.11	2.36	7.61	0	94.81
120R-1291.8	1291.8	A3 S1	moderately coarse groundmass sericite	46.03	0	33.73	0	0	0.26	0	1.08	0	0.57	10.5	0	92.17
120R-1291.8	1291.8	A3 S2	moderately coarse groundmass sericite	46.21	0.36	33.81	0	0	0.18	0	1.14	0	0.54	10.36	0	92.44
120R-1291.8	1291.8	A3 S3	moderately coarse groundmass sericite	46.63	0	33.39	0	0	0.18	0	1.04	0	0.45	10.43	0	92.12
120R-1315	1315	A2 S1	mod coarse matrix sericite	46.37	0.61	28.17	0	0	6.76	0	1.38	0	0	11.07	0	94.09
120R-1315	1315	A2 S3	mod coarse matrix sericite	64.84	0.52	17.92	0	0	0	0	0	0	0	16.83	0	99.88
120R-1353.8	1353.8	A2 S1		46.54	1.69	29.87	0	0	2.02	0	1.52	0	0.22	10.65	0	91.76
120R-1353.8	1353.8	A3 S1	matrix sericite	46.97	1.13	29.58	0	0	2.28	0	1.85	0	0	10.86	0	92.17

Appendix 2 cont.

120R Probe Results — Sericite Data — 20-10-97

Sample	Depth	Area	Description	SiO2	BaO	Al2O3	Cr2O3	Fe2O3	FeO	MnO	MgO	CaO	Na2O	K2O	Cl	Oxide total
120R-1353.8	1353.8	A3 S2	matrix sericite	46.42	1.49	29.55	0	0	1.88	0	1.56	0	0	10.94	0	91.18
120R-1353.8	1353.8	A4 S1	matrix sericite	82.96	0	8.54	0	0	0.43	0	0.28	0	1.13	2.55	0	95.89
120R-1353.8	1353.8	A4 S2	matrix sericite	45.85	1.64	29.92	0	0	1.97	0	1.48	0	0	10.95	0	91.08
120R-1357.4	1357.4	A2 S1	sericite within deformed carbonate spheroic	45.67	1.28	28.5	0	0	2.33	0	2.09	0	0	10.91	0	90.21
120R-1357.4	1357.4	A2 S2	sericite within deformed carbonate spheroic	45.8	0.99	28.87	0	0	2.43	0	1.99	0	0	10.81	0	90.45
120R-1361.4B	1361.4	A3 S1	sericite matrix to carbonate spheroids	47.84	1.46	30.96	0	0	1.37	0	2.13	0	0	11.3	0	94.41
120R-1361.4B	1361.4	A3 S2	sericite matrix to carbonate spheroids	46.82	1.37	29.77	0	0	1.48	0	2.07	0	0	11	0	91.9
120R-1364.4B	1364.4	A1 S1	sericite matrix to carbonate spheroids	48.51	1.13	30.43	0	0	1.24	0	2.26	0	0	11.2	0	94.27
120R-1364.4B	1364.4	A1 S2	sericite matrix to carbonate spheroids	48.01	1.3	30.67	0	0	1.36	0	2.13	0	0	11.27	0	94.16
120R-1364.4B	1364.4	A2 S2	sericite of glass shard within carb spheroid	48.39	1.42	31.09	0	0	1.2	0.19	2.09	0	0	11.05	0	94.8
120R-1364.4B	1364.4	A2 S2	sericite of glass shard within carb spheroid	47.53	1.39	30.39	0	0	1.39	0.85	2.15	0	0	10.96	0	94.656
120R-1364.4B	1364.4	A3 S1	ser altered plag within carb spheroid	48.13	1.15	30.18	0	0	1.43	0	2.31	0	0	11.16	0	94.362
120R-1364.4B	1364.4	A4 S1	sericite near carbonate - qtz vein	47.72	1.51	30.59	0	0	1.26	0	2.22	0	0	11.05	0	94.352
120R-1364.4B	1364.4	A4 S2	sericite near carbonate - qtz vein	47.94	1.84	30.83	0	0	1.36	0	2.25	0	0	11.2	0	95.416
120R-1364.4B	1364.4	A4 S3	sericite near carbonate - qtz vein	48.07	0.97	29.93	0	0	1.7	0	2.19	0	0	11.54	0	94.402
120R-1364.4B	1364.4	A4 S4	sericite near carbonate - qtz vein	48.17	1.4	30.36	0	0	1.29	0	2.41	0	0	11.19	0	94.824
120R-1364.4B	1364.4	A5 S1	sericite matrix to carbonate spheroids	48.18	1.66	30.52	0	0	1.09	0	2.08	0	0	11.13	0	94.656
120R-1364.4B	1364.4	A5 S2	sericite matrix to carbonate spheroids	47.97	1.44	30.85	0	0	1.42	0	2.16	0	0	11.1	0	94.94
120R-1364.4B	1364.4	A6 S1	matrix	47.82	1.33	30.36	0	0	1.32	0.14	2.17	0	0	11.15	0	94.292
120R-1364.4B	1364.4	A6 S2	matrix	47.83	1.28	30.4	0	0	1.17	0.15	2.23	0	0	11.04	0	94.098
120R-1364.4B	1364.4	A7 S1	repeat of A4	48.42	1.57	30.81	0	0	1.3	0	2.17	0	0	11.2	0	95.466
120R-1365.4B	1365.4	A4 S1	sericite in matrix carbonate aggregate	49.43	0.77	29.32	0	0	2.28	0.15	2.81	0.14	0	11.11	0	96.014
120R 1366.0	1366	A1 S1	coarse white mica associated with ZnS	47.42	0.88	31.27	0	0	1.82	0	1.81	0	0	11.4	0	94.602
120R 1366.0	1366	A1 S2	coarse white mica associated with ZnS	47.37	0.72	30.67	0	0	1.97	0	1.78	0	0	11.24	0	93.75
120R 1366.0	1366	A5 S1	large zone of sericite	47.89	0.49	31.6	0	0	1.77	0	1.54	0	0	11.29	0	94.576
120R 1366.0	1366	A5 S2	large zone of sericite	47.74	0.5	31.55	0	0	1.61	0	1.52	0	0	11.3	0	94.224
120R-1399.5	1399.5	A3 S1	sericite in carbonate altered matrix	47.72	0.83	28.48	0	0	3.79	0	3.01	0	0	11.05	0	94.878
120R-1399.5	1399.5	A4 S1	matrix	48.54	0.92	29.06	0	0	2.97	0	2.41	0	0	11.23	0	95.128
120R-1399.5	1399.5	A5 S1	sericite in altered feldspar domain	49.09	0.68	28.36	0	0	2.87	0	2.57	0	0	11.45	0	95.024
120R-1399.5	1399.5	A7 S1	matrix sericite	48.73	0.72	28.47	0	0	2.93	0	2.35	0	0	11.46	0	94.66
120R-1399.5	1399.5	A7 S2	matrix sericite	48.25	0.83	28.83	0	0	2.78	0	2.17	0	0	11.61	0	94.468
120R-1421.8	1421.8	A1 S1	matrix sericite	51.29	0.86	27.05	0	0	3.57	0	2.15	0	0	10.98	0	95.904
120R-1421.8	1421.8	A2 S1	matrix sericite	48.65	1.06	28.18	0	0	3.49	0	2.5	0	0	11.47	0	95.352
120R-1421.8	1421.8	A3 S1	intense sericite alteration	53.5	0.85	25.78	0	0	3.18	0	2.24	0	0	10.4	0	95.946

Appendix 2 cont.

120R Probe Results — Sericite Data — 20-10-97

Sample	Depth	Area	Description	SiO2	BaO	Al2O3	Cr2O3	Fe2O3	FeO	MnO	MgO	CaO	Na2O	K2O	Cl	Oxide total
120R-1421.8	1421.8	A3 S2	intense sericite alteration	51.66	1.06	26.99	0	0	3.1	0	2.34	0	0	11.09	0	96.242
120R-1421.8	1421.8	A3 S3	intense sericite alteration	49.84	1.12	27.64	0	0	3.42	0	2.47	0	0	11.04	0	95.526
120R-1421.8	1421.8	A4 S1	intense sericite alteration	49.7	1.04	28.31	0	0	3.39	0	2.53	0	0	11.64	0	96.614
120R-1421.8	1421.8	A4 S2	intense sericite alteration	52.27	1.24	26.35	0	0	3.39	0	2.35	0	0	10.82	0	96.422
120R-1421.8	1421.8	A5 S1	matrix to carb altered feldspar	49.2	1.39	28.08	0	0	3.46	0	2.54	0.11	0	11.26	0	96.036
120R-1436.2	1436.2	A1 S1	sericite carbonate alteration of feldspar	47.75	0	30.62	0	0	5.1	0	1.55	0	0	10.08	0	95.1
120R-1436.2	1436.2	A1 S2	matrix to altered feldspar	49.3	0	30.59	0	0	2.2	0	1.5	0	0	10.75	0	94.34
120R-1436.2	1436.2	A6 S1	sericite near chlorite alteration outside vein	48.33	0.85	28.46	0	0	3.44	0	2.24	0	0	11.43	0	94.746
120R-1436.2	1436.2	A6 S2	sericite near chlorite alteration outside vein	49.24	0	30.78	0	0	2.3	0	1.58	0	0	11.25	0	95.15
120R-1440.5	1440.5	A2 S1	sericite in altered feldspar fracture	47.46	1.01	28.07	0	0	4.77	0	2.09	0	0	11.51	0	94.908
120R-1440.5	1440.5	A5 S1	matrix sericite near altered feldspar phenocry	48.26	1.49	28.19	0	0	4.91	0	2.15	0	0	11.4	0	96.404

PIMA-II spectral analysis of hydrothermal alteration associated with the Hellyer VHMS deposit: new results*

by K. Yang†, J.F. Huntington†, J.B. Gemmell and R. Fulton

Summary

Further results of the spectral study of the altered and unaltered samples from the Hellyer Zn-Pb deposit are presented in this report. The data show that the hydrothermal alteration system at Hellyer can be spectrally characterised using the PIMA-II portable infrared spectrometer.

Compositional variation of muscovite has been identified spectrally in this study. For muscovite at Hellyer, wavelength of the Al-OH absorption was found to vary between 2190 to 2225 nm, corresponding approximately to Al(vi)# at 0.95–0.65. The long Al-OH wavelengths (> 2216 nm) are characteristic of the muscovite in the most intensely altered rocks. In terms of rock types, the ore-hosting volcaniclastic rocks (i.e. HVS) tend to have the longest Al-OH (2216–2225 nm), the footwall andesites (i.e. FPS) show the medium Al-OH wavelengths (2210–2220 nm), and the hangingwall basalts (PLS) display the shortest Al-OH (2190–2216 nm).

Observed in several drill-holes, the mineralised volcanics (with high Pb, Zn and Cu contents) are characterised by muscovite with relatively longer Al-OH wavelengths, whereas the surrounding altered, but unmineralised, rocks show shorter Al-OH wavelengths. This finding suggests that in exploration the Al-OH wavelength could be used as a parameter for assessing alteration intensity and potential mineralisation.

Chlorite also shows a wide range of cation composition. Based on the observed Fe-OH wavelength range (2250–2264 nm), the Mg# value for chlorite in the altered volcanics is estimated at 0.7–0.2. The composition variation, however, does not appear to be related to the alteration intensity or mineralisation.

In two drill-holes from the northern part of the alteration system, an K-feldspar (Ba-bearing) enriched interval has been found in the altered footwall. The textures indicate the K-feldspar as hydrothermal in origin.

In the unaltered volcanic rocks, the metamorphic effects are spectrally shown as either zoisite or prehnite-dominated assemblages.

Introduction

While the overall goal of the P435 project is to develop the techniques of spectrally mapping hydrothermal alteration/mineralisation systems, the specific aims of the present study at Hellyer are to:

1. Identify and (semi)quantify major phyllosilicate minerals and thus delineate the alteration zones. As qualitatively identifying minerals with PIMA-II is a well-established method, our emphasis has been placed on (semi) quantitatively determining mineral abundances with spectral data.

In collaboration withCSIRO/AMIRA Project P435
Mineral Mapping with Field Spectroscopy for Exploration

* Modified from *Spectral Signatures of Hydrothermal Alteration in the Volcanic Rocks at Hellyer, Tasmania* by K. Yang, J.F. Huntington, R.N. Phillips, J.B. Gemmell and R. Fulton (August 1997), CSIRO/AMIRA Project P435 Final Report

† CSIRO, Division of Exploration and Mining

Figure 1 Plan showing the locations of analysed drillholes.

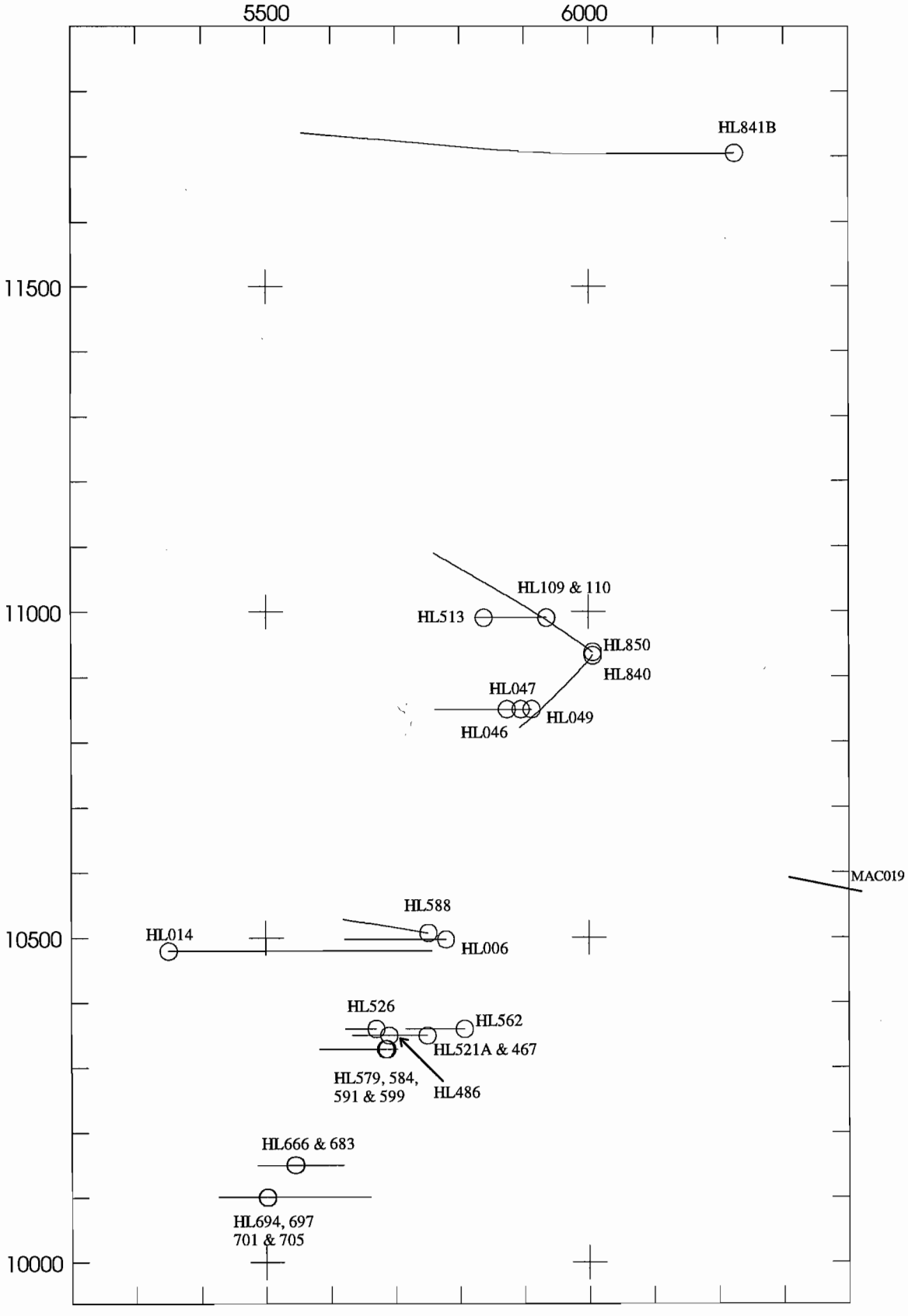

2. Recognise possible compositional variations of a particular alteration mineral and determine their relationship with alteration/mineralisation. Although the Hellyer deposit has been extensively studied in previous work (Jack, 1989; Gemmell and Large, 1992) little detailed data have been available with regard to the compositional variations of the main alteration minerals such as muscovite and chlorite.

Samples and methods

Samples from 34 diamond drill-holes, comprising 293 pulverised composite samples (each representing a 2-metre interval) and 1216 core splits (Table 1), were spectrally measured using the PIMA-II portable infrared spectrometer. The plan showing the distribution of the analysed drill-holes is enclosed in Figure 1. For each pulverised sample, one spectrum was collected; for each peace of core sample, two to four spectra, depending on the degree of heterogeneity of the sample as could be visually recognised, were obtained.

For part of the samples studied, geochemical data were made available by Aberfoyle Exploration and the Centre for Ore Deposit and Exploration Studies (CODES), University of Tasmania. These geochemical data were used as references for the spectrally extracted (semi)quantitative mineralogical data (e.g. relative mineral abundance). To check the spectral data, additional mineral chemistry (by electron microprobe) and whole-rock potassium content (by gamma-ray spectrometry) were analysed in this study at CSIRO DEM, North Ryde.

The PIMA-II measures hemispherical reflectance between 1300 nm and 2500 nm (short-wave infrared or SWIR) relative to a spattered gold reflectance standard. The spectral resolution is approximately 7–10 nm, with a sampling interval of 2–4 nm. No sample preparation is required. Each spectral measurement takes about 30 seconds.

Processing reflectance spectra (e.g. smoothing spectra, generating hull quotient and second-derivative spectra, and gaussian deconvolution) and extracting various spectral parameters (e.g. wavelengths and intensities of absorption features) were carried out automatically with the software package XSPECTRA, which is developed by CSIRO DEM. Mineralogical interpretation of the SWIR spectra was made manually with reference to the USGS Spectral Library and CSIRO spectral collections.

Absorption intensities used as parameters for relative mineral abundance were derived from either the hull quotient or the second-derivative spectra. We have found that the two types of parameters are agreeable very well, except that for a minor to trace spectral feature (i.e. very low mineral abundance) the hull quotient as an abundance parameter functions not as well as the second-derivative. Therefore, second-derivatives have been used as the preferred abundance parameter in this study.

Wavelengths of the interested absorption features were measured on the hull quotient spectra. For some minor and all trace features, since the wavelength of absorption minima could not be accurately determined, the related samples were not plotted in those figures involving wavelength data.

Only phyllosilicates and, in some cases, carbonates and feldspar were interpreted from the PIMA-II spectra. Other minerals that may be also present in the samples, such as plagioclase, quartz and sulfides, were not considered, as they showed either very weak or no absorption features in the SWIR region.

Results and interpretation

Previous results from this study have been reported in Yang et al. (1996a) and Yang et al. (1996b). New results are reported below.

Muscovite Microprobe Analysis

To examine the relationship between the Al-OH wavelength and the octahedral cation composition for muscovite, chemical composition of muscovite was analysed using electron microprobe. The results are listed in Table 2 and plotted in Figure 2.

There is no apparent correlation between the microprobe and the spectral data, and this is probably due to:

- The composition of muscovite varies significantly within a sample (Fig. 2). The electron microprobe analysis determines the composition of individual muscovite grains, whereas the spectral data obtained by PIMA-II reflect the weighted average muscovite composition of individual samples. This

Table 1 Sample list.

drill-hole	sample type	depth (m)	number of samples
HL006	core	292.0 to 482.4	59
HL 014	pulp	4.9 to 226.5	14
HL 028	pulp	139.6 to 265.8	12
HL046	core	104.9 to 318.1	53
HL047	core	147.3 to 313.0	51
HL049	core	278.9 to 315.2	16
HL 055	core	83.3 to 342.3	31
HL 057	pulp	222.6 to 322.3	10
HL109	core	43.9 to 143.0	33
HL110	core	1.8 to 162.7	32
HL 306	pulp	0 to 505.4	49
HL467	core	122.0 to 230.0	59
HL486	core	52.5 to 169.0	132
HL513	core	105.4 to 135.9	17
HL521A	core	77.4 to 239.0	41
HL526	core	58.1 to 166.1	48
HL562	core	39.0 to 249.5	69
HL579	core	20.0 to 131.0	56
HL584	core	28.8 to 160.3	45
HL588	core	66.0 to 108.9	48
HL591	core	48.4 to 149.0	28
HL599	core	57.6 to 146.8	48
HL601	core	22.2 to 122.0	46
HL666	core	73.0 to 199.0	50
HL683	core	109.0 to 272.0	46
HL694	core	111.5 to 345.5	77
HL697	core	53.5 to 339.0	77
HL701	core	113.0 to 194.1	24
HL705	core	84.8 to 178.0	40
HL840	pulp	171.8 to 393.0	53
HL841B	pulp	500.6 to 1133.5	80
HL 850	pulp	169.8 to 511.9	27
MAC019	pulp	462.6 to 790.9	42
MAC031	core	104.1 to 165.0	6

Table 2 Electron microprobe analyses of m,uscovite.

Sample	Depth (m)	No.	Na_2O	FeO	Cr_2O_3	V_2O_3	BaO	K_2O	CaO	TiO_2	MgO	Al_2O_3	SiO_2	Total
HL841B	509.7-514.2	1(2)	0.44	0.54	0.13	0.13	0.114	8.18	0.14	0.06	1.07	34.48	49.46	94.74
HL841B	509.7-514.2	2	0.70	0.50	0.22	0.12	0.21	9.34	0.07	0.06	0.71	33.73	44.80	90.46
HL841B	509.7-514.2	3	0.30	0.66	0.32	0.12	0.24	8.42	0.42	0.11	0.83	32.27	44.10	87.79
HL841B	509.7-514.2	4	0.61	0.52	0.17	0.13	0.24	8.34	0.13	0.08	0.62	34.26	45.28	90.38
HL841B	514.2-523.2	1	0.77	4.61	0.49	0.07	0.27	6.06	0.11	0.12	3.43	30.36	40.89	87.18
HL841B	514.2-523.2	2	0.92	2.30	0.43	0.11	0.30	7.04	0.16	0.06	2.15	34.05	45.94	93.46
HL841B	514.2-523.2	3	0.55	0.86	0.07	0.08	0.16	7.25	0.59	0.07	1.11	34.26	46.78	91.78
HL841B	514.2-523.2	4	0.65	0.72	0.19	0.11	0.39	7.82	0.64	0.06	0.84	36.80	48.56	96.78
HL841B	514.2-523.2	5	0.42	0.50	0.08	0.07	0.27	9.05	0.10	0.12	0.71	35.01	46.70	93.03
HL841B	560.5-563.6	1	0.28	0.67	0.13	0.11	0.04	7.17	0.13	0.10	0.63	34.77	44.72	88.75
HL841B	916.1-923.4	1	0.69	0.64	–	0.08	0.17	9.38	0.17	0.09	0.75	37.23	48.80	98.00
HL841B	916.1-923.4	1	0.40	0.59	0.01	0.05	0.09	9.22	0.14	0.12	0.77	35.49	49.12	96.00
HL841B	916.1-923.4	2	0.43	0.60	0.10	0.13	0.19	9.88	0.10	1.35	0.77	36.62	49.21	99.38
HL841B	916.1-923.4	2	0.45	0.66	0.10	0.03	0.18	9.98	0.09	1.04	0.73	34.45	47.01	94.72
HL841B	916.1-923.4	3	1.12	2.65	0.02	0.04	--	6.92	0.10	0.03	2.14	34.46	47.34	94.82
HL841B	916.1-923.4	3	0.87	1.09	0.02	0.11	--	8.58	0.07	0.12	0.96	33.86	46.09	91.77
HL841B	538.0	1	0.93	0.45	0.10	0.07	0.27	8.38	0.13	0.07	0.60	39.04	50.79	100.83
HL841B	538.0	2	0.63	3.13	0.29	0.18	0.23	7.62	0.08	0.18	2.94	33.91	44.95	94.14
HL841B	538.0	3	1.33	0.91	0.17	0.14	0.19	7.41	0.18	0.27	1.40	34.13	51.34	97.47
HL841B	595.4	1	0.21	0.79	--	0.10	0.32	8.51	0.09	0.09	1.21	35.31	50.39	97.02
HL841B	595.4	2	0.25	0.61	0.24	0.16	0.54	7.82	0.10	0.09	0.95	34.43	46.11	91.30
HL841B	595.4	3	0.18	0.90	0.33	0.08	0.47	8.32	0.22	0.32	0.94	33.00	46.00	90.76
HL840	252.0		0.02	1.46	0.01	0.06	0.89	5.78	0.02	0.21	2.65	30.46	50.77	92.33
HL840	252.0	1	0.06	0.97	–	0.07	0.43	8.55	0.03	0.14	2.12	29.49	47.07	88.93
HL840	252.0	2	0.11	1.24	0.05	0.08	0.91	9.82	–	0.16	2.35	28.95	45.99	89.66
HL840	252.0	3	0.07	1.17	0.01	0.04	1.05	9.82	0.01	0.17	2.46	29.63	48.77	93.20
HL840	252.0	4	0.09	0.91	0.01	0.11	0.12	8.67	0.05	0.09	2.11	30.22	48.99	91.37
HL840	252.0	5	0.09	1.01	–	0.02	0.66	9.98	–	0.16	2.37	28.90	48.46	91.65
HL840	252.0	6	0.05	1.27	0.04	0.02	0.71	6.84	0.06	0.12	2.75	28.39	50.93	91.18
HL840	252.0	7	0.02	1.58	0.01	0.03	0.85	4.22	0.04	0.14	2.80	30.08	52.72	92.49
HL840	252.0	8	0.12	1.73	0.03	0.02	0.98	10.11	0.03	0.19	2.42	25.23	44.03	84.89
HL666	162.0	1	0.31	2.01	0.03	0.08	0.23	8.28	0.04	0.11	1.18	29.94	40.27	82.48
HL666	162.0	2	0.19	2.79	0.02	0.06	0.19	7.54	0.13	0.12	1.31	31.12	44.06	87.53
HL666	162.0	3	0.24	2.69	–	0.11	0.16	6.87	0.04	0.07	1.56	29.09	40.3	81.13
HL666	162.0	4	0.21	2.28	–	0.04	0.42	8.97	0.07	0.11	1.18	33.72	44.63	91.63
HL666	162.0	5	0.18	3.52	0.01	0.09	0.12	8.32	0.08	0.11	1.55	33.93	45.71	93.62
HL666	162.0	6	0.27	1.01	–	0.05	0.14	9.68	0.16	0.06	0.83	30.69	43.14	86.03
HL666	162.0	7	0.27	1.54	–	0.04	0.27	10.01	0.09	0.16	0.85	34.14	43.71	91.08
HL694	144.0	1	0.28	2.19	0.02	0.03	1.00	8.10	0.31	0.17	2.73	29.11	52.00	95.94
HL694	144.0	2	0.12	2.10	–	0.04	0.94	8.69	0.06	0.15	2.74	28.88	49.86	93.58
HL694	144.0	3	0.08	2.16	–	--	0.83	8.83	0.07	0.13	2.70	28.90	51.15	94.85
HL694	144.0	4	0.35	1.96	–	0.07	1.14	8.76	0.05	0.12	2.64	28.26	50.46	93.81
HL694	144.0	5	0.12	1.13	0.03	0.09	0.61	8.82	0.06	0.16	2.17	30.14	48.73	92.06
HL694	144.0	6	0.11	0.68	0.04	0.06	0.63	7.98	0.01	0.09	1.80	30.10	47.93	89.43
HL694	144.0	7	0.11	0.82	0.01	0.06	0.46	8.95	0.07	0.09	2.05	29.98	47.96	90.56
HL694	144.0	8	0.10	0.98	–	0.04	0.41	8.85	0.05	0.09	1.84	30.03	47.25	89.64
HL694	144.0	9	0.08	0.93	0.04	0.03	0.57	8.72	0.04	0.09	2.00	29.56	47.52	89.58
HL840	124.0	1	0.06	3.15	0.14	0.14	0.67	10.27	0.08	0.2	3.01	26.67	48.73	93.12
HL840	124.0	2	0.07	3.29	0.07	0.11	0.56	10.27	0.09	0.27	3.16	26.46	50.22	94.57
HL840	124.0	3	0.05	2.02	0.10	0.09	0.31	7.23	0.55	0.12	2.92	28.17	51.53	93.09
HL840	124.0	4	0.05	3.63	0.10	0.11	0.56	8.81	2.62	0.22	3.39	26.35	47.77	93.61
HL840	124.0	5	0.03	5.89	0.10	0.09	0.34	8.14	0.15	2.28	4.69	22.84	41.16	85.71
HL840	124.0	6	0.05	3.19	0.07	0.07	0.50	9.69	0.08	0.21	3.00	27.3	49.91	94.07
HL840	124.0	7	0.04	2.41	0.16	0.13	0.64	9.39	0.21	0.17	2.60	27.91	48.87	92.53
HL840	124.0	8	0.25	2.29	0.01	0.08	0.13	8.56	0.05	0.08	1.26	33.06	43.04	88.81
HL840	124.0	9	0.20	3.45	--	0.02	0.21	7.17	0.07	0.07	1.74	31.64	45.95	90.52
HL840	124.0	10	0.11	1.63	--	0.04	0.33	4.92	0.04	0.11	1.14	35.97	49.50	93.79
HL840	124.0	11	0.25	0.95	0.03	0.08	0.29	8.66	0.07	0.09	0.75	34.37	47.51	93.05
HL840	124.0	12	0.05	2.42	--	0.05	0.26	2.87	0.08	0.08	1.42	35.34	48.45	91.02
HL840	124.0	13	0.20	3.49	0.01	0.08	0.25	7.31	0.06	0.05	1.69	28.01	50.94	92.09

*Numbers in brackets indicate the number of analysis made on one grain.
-- undetected.

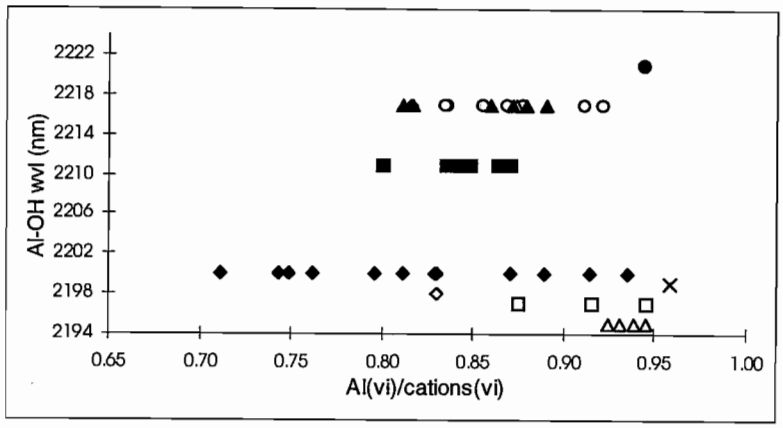

Figure 2. Comparison between microprobe analysis and the Al-OH wavelength (wvl) for muscovite. Open squares = 919.7 m of HL841B; solid squares = 252 m of HL840, open circles = 162 m of HL666, solid circles = 562 m of HL841B, open triangles = 512 m of HL841B, solid triangles = 144 m of HL694, open diamonds = 519 m of HL841B, solid diamonds = 124 m of HL840, cross = 538 m of HL841B. vi = six-fold coordinated cations in the octahedral sites.

is probably why the correlation between the two sets of data shown in Figure 2 seems so poor, since for each sample there is only one Al-OH wavelength value corresponding to several microprobe analyses.

- As observed under the electron microscope, muscovite occurs as very fine sheets, commonly associated with chlorite, quartz or feldspar. The analytical results, therefore, were to various degrees contaminated by the associated minerals. Furthermore, for some drill-holes, only pulverised samples were available, and the quality of the analysis was probably also affected by the very fine grain size of the material, even without the contamination from other minerals.

Grain mounts, made from pulverised samples, were used for microprobe analysis. The very fine grain size of the material, along with the common association of muscovite with other phases like chlorite, quartz and feldspar has probably affected to some extent the quality of the analysis and exaggerated the composition differences between muscovite grains.

Chlorite composition variations

Fe-OH wavelength of chlorite is the spectral parameter for chlorite Mg# {Mg/(Mg+Fe)}, with the longer wavelength corresponding to lower Mg# (Pontual 1994; Yang et al. 1996c). Wavelength variations for chlorite Fe-OH in the sampled footwall and hangingwall rocks are displayed in Table3, Figure 3 to 5, respectively, and summarised as follows:

- In the altered footwall, there does not appear to be a consistent trend of wavelength variation for chlorite in relation to alteration zoning. HL840, for example, shows chlorite of more Fe-rich (Fe-OH wavelength (2258 nm) in the sulfide-rich, intensely altered siliceous zone (170–270 m) than in sericite and sericite-chlorite zones, whereas in HL841B relatively Mg-rich chlorite (Fe-OH wavelength < 2256 nm) tends to develop in the two sulfides-rich intervals. Vertically in HL306, the chlorite in the siliceous core appears to be more Mg-rich than in the other zones (Fig. 3).

- Similarly in the hangingwall, while chlorite in HL014, HL028 and HL055 shows a decrease in Fe-OH wavelength toward the contact with footwall, the chlorite in HL057 appears to behave in the opposite way (Fig. 4).

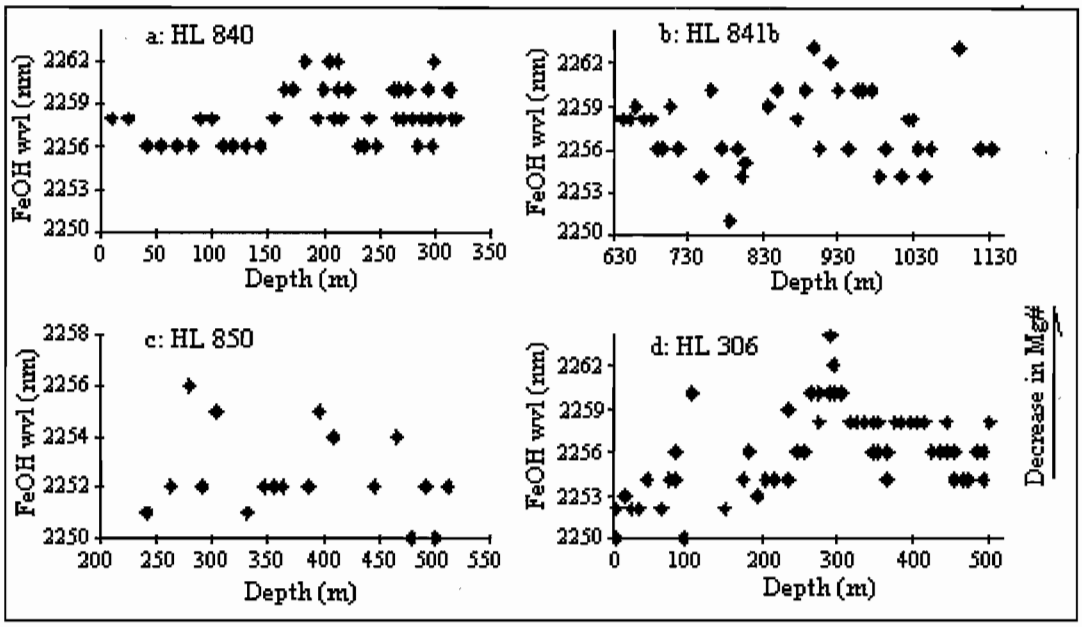

Figure 3. Wavelength variations of the chlorite Fe-OH in the altered footwall. Longer Fe-OH wavelength indicates higher Mg/(Mg+Fe). Only those samples with an identifiable Fe-OH feature are plotted.

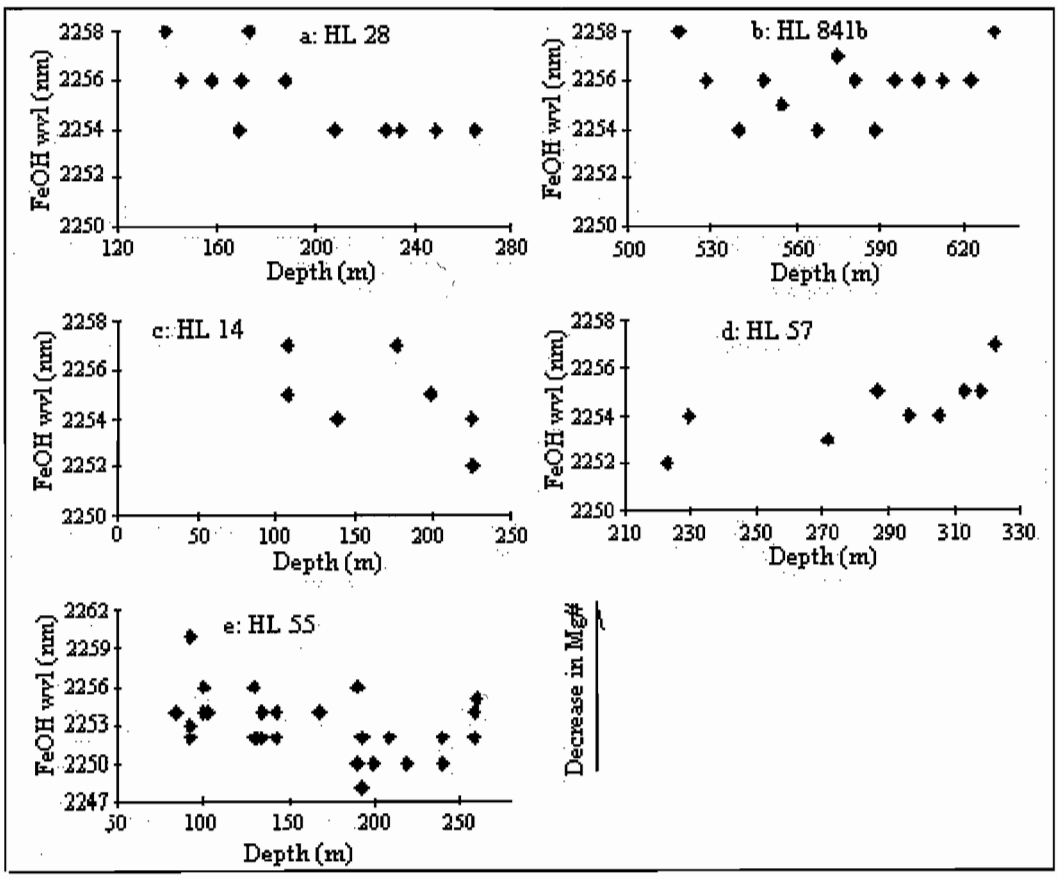

Figure 4. Wavelength variations of the chlorite Fe-OH feature in the altered hangingwall. Longer Fe-OH wavelength indicates higher Mg/(Mg+Fe). Only those samples with an identifiable Fe-OH feature are plotted. More than one datum point at a depth represents multiple measurements on a single sample.

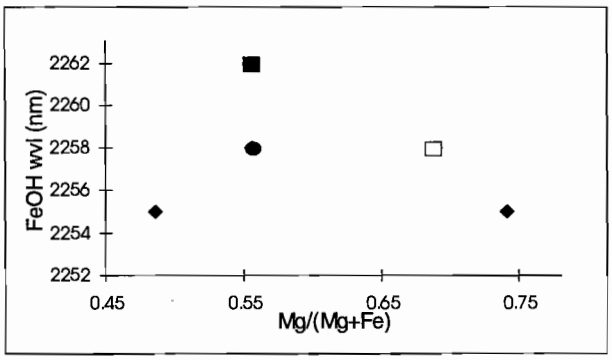

Figure 5. Relationship between the Fe-OH wavelength and Mg# for chlorite. Each datum point is the average of 1-4 analyses on individual chlorite. Datum points with same a pattern belong to a same sample.

Table 3 Electron microprobe analyses of chlorite in HL841B samples.

Sample #	Depth (m)	Grain #	Na_2O	FeO	Cr_2O_3	V_2O_3	BaO	K_2O	CaO	TiO_2	MgO	Al_2O_3	SiO_2	Total
626325	509.7-514.2	1	0.04	18.90	0.01	0.07	0.08	0.45	0.25	0.03	13.40	21.72	25.02	79.97
626333	560.5-563.6	1	–	19.33	–	0.03	–	0.04	0.21	0.02	13.07	22.30	24.15	79.15
626333	560.5-563.6	2	0.01	20.34	0.27	0.03	0.01	0.04	0.14	0.03	14.12	22.11	26.69	83.79
626333	560.5-563.6	3	0.03	21.06	–	0.03	–	0.08	0.15	0.03	12.16	21.69	21.63	76.86
626361	779-793.6	1	0.05	14.88	0.06	0.07	–	0.08	0.04	0.05	18.53	18.33	26.19	78.28
626366	803.7-810.9	1	–	11.33	0.22	0.08	0.11	0.63	0.09	–	18.69	17.05	27.85	76.05
626366	803.7-810.9	1	–	10.78	0.21	0.10	–	1.87	0.07	0.02	16.67	18.02	28.11	75.85
626366	803.7-810.9	2	0.04	17.24	0.01	0.01	0.05	0.45	0.14	0.04	9.15	19.25	22.82	69.20
626380	916.1-923.4	1	0.05	17.69	0.01	0.04	0.17	0.52	0.12	0.02	12.36	22.79	27.58	81.35
626380	916.1-923.4	1	0.01	18.56	0.02	0.01	0.02	0.23	0.10	0.02	12.97	21.29	25.79	79.02

Table 4 Electron microprobe analyses of dickite in HL841B samples.

Sample #	Depth (m)	Type	Na_2O	FeO	Cr2O3	V_2O_3	BaO	K_2O	CaO	TiO_2	MgO	Al_2O_3	SiO_2	Total
HL 2	595.4	aggregate	0.31	0.55	0.13	0.01	0.07	0.07	0.09	–	0.22	29.68	35.08	66.21
HL 2	595.4	aggregate	0.72	0.47	0.02	0.02	–	0.02	0.15	–	0.14	22.98	25.63	50.15
HL 2	595.4	aggregate	0.27	1.04	0.04	–	0.12	0.08	0.13	0.02	0.3	31.06	35.59	68.65
HL 2	595.4	vein	–	0.43	–	–	0.02	0.01	0.07	–	0.04	25.13	27.12	52.82
HL 2	595.4	vein	–	0.03	0.04	–		0.02	0.03	–	0.04	21.01	21.46	42.63

- It appears that in a single drill hole the composition of chlorite (Fe-OH wavelength) in the hangingwall does not vary as much as in the footwall.

- Chlorite Mg#, estimated from our data for Mg#–Fe-OH wavelength correlation from Fimiston, WA, is 0.7–0.2 (Fe-OH wavelength 2250–2264 nm) for the altered footwall, and 0.7–0.3 (Fe-OH wavelength 2250–2260 nm) for the hangingwall rocks.

There are not enough electron microprobe analyses of chlorite to compare with the Fe-OH wavelength data. There appears to be a negative correlation in Figure 5, if the datum point with the lowest Mg# is rejected as an outlier. More composition data are certainly needed to derive a factual spectra–composition correlation.

Muscovite/chlorite abundance ratio

Abundance ratio of muscovite and chlorite can be (semi)quantitatively determined by the second derivative ratio of Al-OH and Fe-OH features. Variations in abundance ratio may better display the zoning expressed by changes in muscovite and chlorite abundances:

- In HL840, a central muscovite-rich zone is enveloped by chlorite-rich zones (Fig. 6a).

- In HL841B, a zig-zag pattern developed on a background of decreasing muscovite/chlorite ratio indicates that while the western part of the alteration system is more chlorite-rich than the eastern part, however there are locally muscovite-enriched portions (sub-zones?) (Fig. 6b).

- In HL306, while the general trend shows a decrease in muscovite relative to chlorite with depth, there is an interval at approximately 300 to 420 m depth that is extremely enriched with chlorite (Fig. 6d).

- HL850 samples are mainly micaceous, as indicated

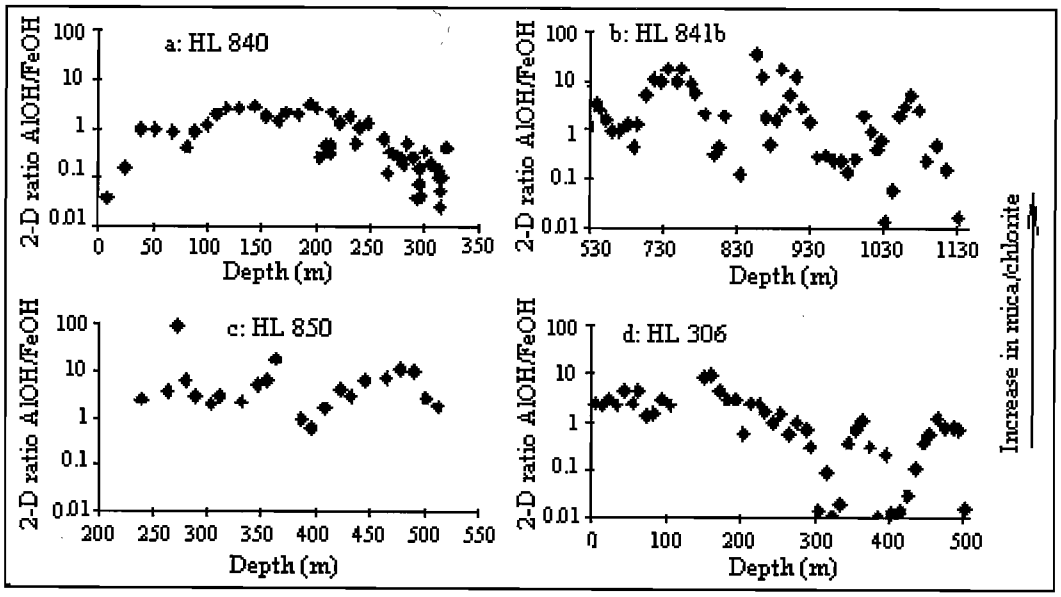

Figure 6. Variations in 2-D ratio of the Al-OH and Fe-OH features in footwall samples.

by the 2-D ratio > 1 for most samples. The muscovite/chlorite ratio change is relatively small, without an obvious trend (Fig. 6c).

- Generally, values of high (> 1) to very high (> 10) 2-D Al-OH/Fe-OH ratio are more likely to be found in the altered footwall than in the hangingwall samples. For example, most samples from four of the five drill holes in hangingwall have the 2-D values < 1. This suggests that footwall alteration produced higher muscovite and lower chlorite than the hangingwall alteration.

- Increase in muscovite relative to chlorite towards the contact with the footwall is also a common trend in the altered hangingwall, as shown in HL014, HL028 and HL055 (Fig. 7).

Potassium feldspar

K-feldspar is present locally within the altered footwall volcanics at Que River (McGoldrick & Large, 1992), but little has been reported of hydrothermal K-feldspar in the footwall alteration system at Hellyer. In this study, an K-feldspar enriched interval (?zone) was found in the altered footwall in both HL840 (approximately at 142–247 m depth).and HL841B (at 741–870.3 m depth).

K-feldspar could not be spectrally identified with the PIMA-II, as its diagnostic absorptions are not in the SWIR wavelength range. A potassium-deficiency, however, was found by comparing the spectrally-indexed muscovite abundance and the chemically-analysed whole-rock K content, and this K-deficiency suggests the presence of an additional K-bearing mineral in the concerned intervals (Figs 8, 9).

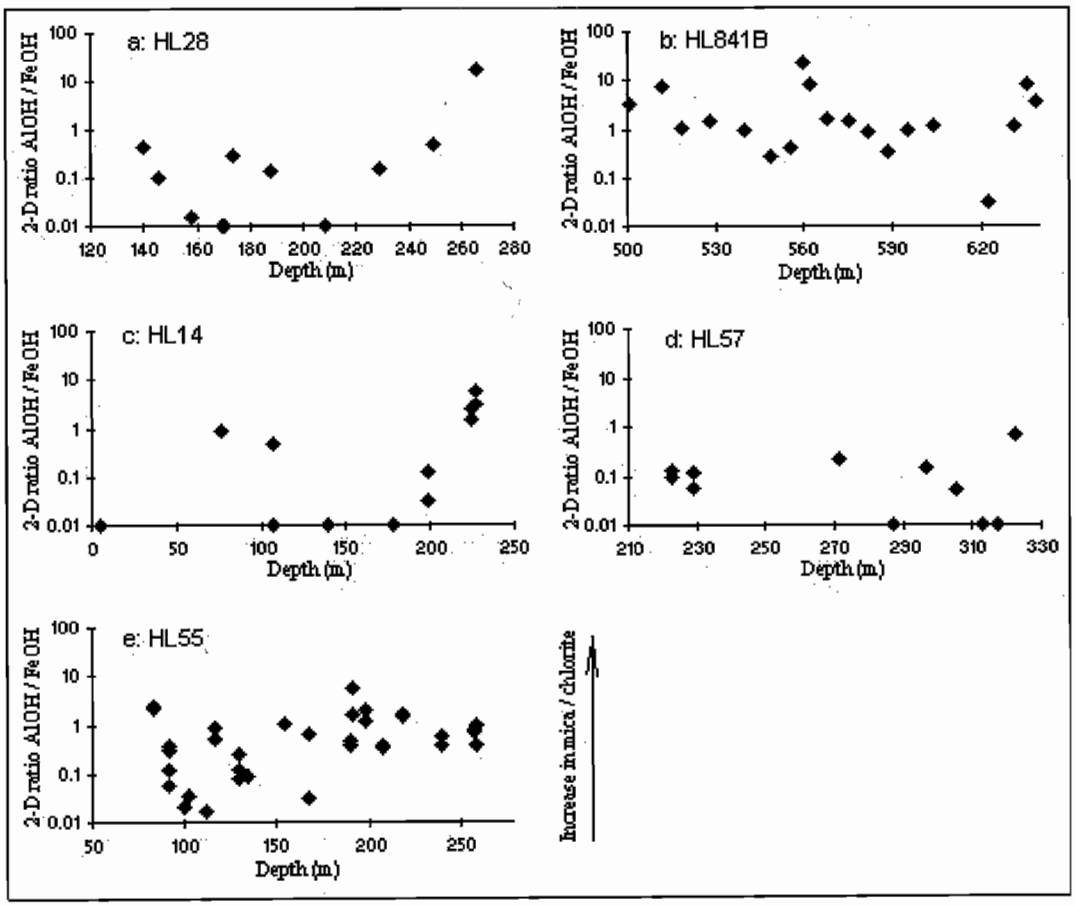

Figure 7. Variations in 2-D ratio of the Al-OH and Fe-OH features in hangingwall samples.

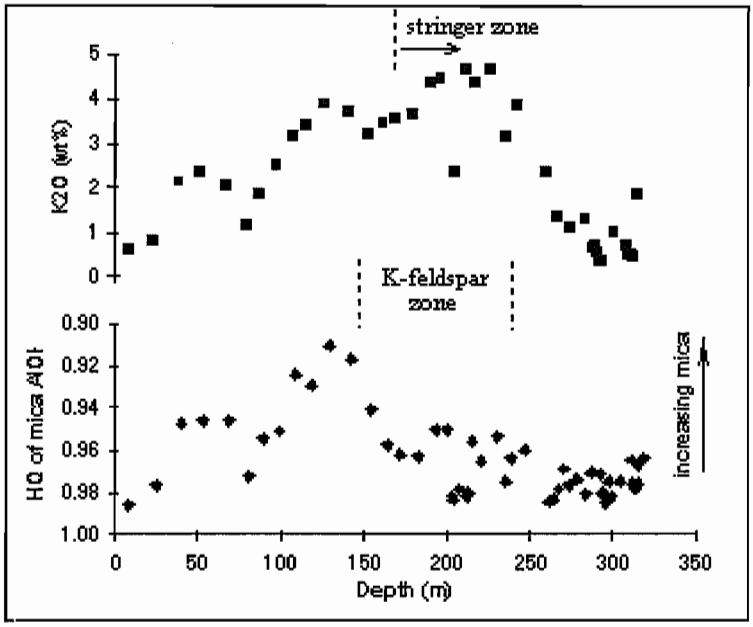

Figure 8. Variations in whole-rock K_2O and muscovite content in HL840 (within FPS). The K-feldspar zone occurs in the interval where the trend of muscovite abundance does not match that of whole-rock K content.

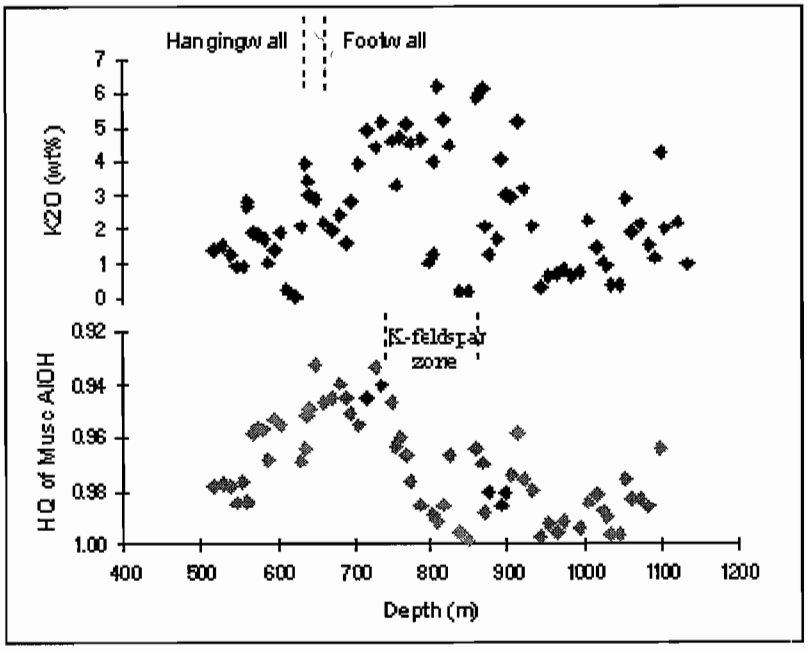

Figure 9. Variations in whole-rock K_2O and muscovite content in HL841B. The K-feldspar zone occurs where the trend of muscovite abundance does not match that of whole-rock K content. Host rocks of the K-feldspar zone range from basalt, andesite to minor dacite, including volcaniclastics.

In HL841B, the host rocks for the identified K-feldspar are dominantly andesitic and basaltic in composition, including lava, volcaniclastics and polymict. The host rocks of the K-feldspar zone in HL840 are mainly andesitic (lava and volcaniclastics), some are so intensely altered that no original lithology could be recognised (in drill log referred to as highly altered).

To confirm the suspected K-feldspar, several pulverised core samples were selected from both drill holes and grain mounts were prepared for microprobe work. Under the electron microprobe, abundant K-feldspar in the samples were found that were ultimately associated with (i.e. replacing or replaced by) muscovite, albite or quartz (Fig. 10). The textures indicate a hydrothermal, rather than magmatic, origin for the K-feldspar.

Microprobe analysis of K-feldspar shows various amounts of BaO, from 0.1 to 7.6 wt% (Table 5), similar to the secondary K-feldspar found at Que River (McGoldrick & Large, 1992).

Most K-feldspar in the identified interval is not likely to have been derived from a primary magmatic precursor, since the andesitic and basaltic host rocks are not expected to contain any significant primary K-feldspar.

Carbonates

Carbonates are shown mainly by a major CO_3 absorption between 2320 and 2340 nm, a wavelength region where both chlorite and muscovite also absorb significantly. Therefore, when coexisting with chlorite and/or muscovite, carbonates are difficult to identify spectrally, due to the feature overlap with the other two minerals. For this reason, we have tried to look at carbonates mainly in unpulverised core splits, in which we could focus the spectrometer onto carbonate veins and large aggregates.

Members of the dolomite-ankerite series $\{CaMg(CO_3)_2–Ca(Mg,Fe)(CO_3)_2\}$ appear to be the main hydrothermal carbonate minerals (Fig. 11). These carbonate species were found in both the footwall and the hangingwall sequence.

Dickite

Dickite was found only at 595.4 m depth (hangingwall basalt) in HL841B (Fig. 12). Wavelength of the shoulder feature at 2180–2182 nm, as well as the wavelength spacing (27–29 nm) of the OH doublet near 1400 nm indicates the phase as dickite rather than kaolinite. Observed with optical microscopy, this sample is rich in kaolin clay that occurs as aggregates, probably psuedomorphing former plagioclase. In places, dickite veins are also present. The dickite appears to be hydrothermal, instead of weathering, in origin.

The greenish colour of the dickite-rich sample needs to be noted. The green colour is similar to what would be referred to as 'fuchsite', and indeed this sample was logged as fuchsite-bearing. However, neither the PIMA-II spectra nor the optical microscopy revealed any significant muscovite. Instead, dickite was found as the dominant alteration mineral, and microprobe analysis showed trace Cr contained in the dickite (Table 5). We therefore suspect that it is the Cr-bearing dickite that makes the sample greenish.

Kaolin clay is uncommon at Hellyer, and has not been previously reported. Kaolin (likely dickite), however, was found in the altered volcanics at Que River (Offler & Whitford, 1992), about 3 km south of Hellyer.

Metamorphic signatures

Gemmell and Large (1992) and Whitford et al. (1984) have found that the hydrothermal alteration assemblages in the Que River–Hellyer region have been little affected by the regional prehnite-pumpellyite facies metamorphism. Two types of metamorphic assemblages have been spectrally documented in this study.

Prehnite + calcite

The samples with recognisable prehnite are all from the hangingwall basalt. The absorption by prehnite is spectrally shown by several distinct features (Fig. 13).

From our limited data, calcite appears to be the main carbonate species in the hangingwall basalt, and so probably is metamorphic rather than hydrothermal. The calcite spectra are characterised by a major CO_3 absorption at 2336–2340 nm, with a shoulder feature near 2300 nm (Fig. 14).

Six MAC031 samples from the hangingwall basalt (PLS) were spectral analysed. All the six samples show a Fe-OH absorption near 2250 nm, which is

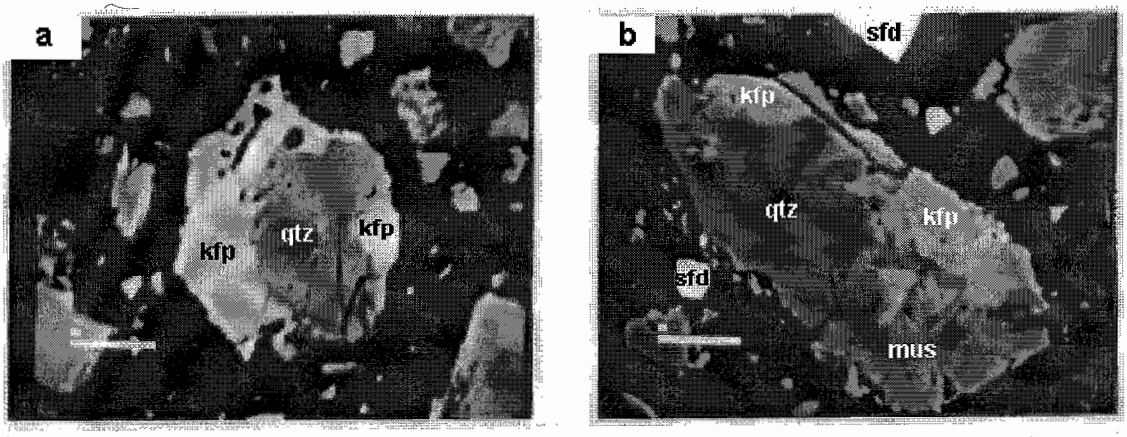

Figure 10. Backscatter electron image of secondary K-feldspar. kfp = K-feldspar, qtz = quartz, mus = muscovite, sfd = sulfide. Length of the scale bar is 10 (m.

Table 5 Electron microprobe analyses of K-feldspar in the footwall samples.

Sample #	depth (m)	Na2O	FeO	Cr2O3	V2O3	BaO	K2O	CaO	TiO2	MgO	Al2O3	SiO2	Total
HL841B	807.3	0.24	0.76	nd	nd	0.11	15.92	0	0.06	0.65	18.16	64.25	100.15
HL841B	807.3	0.26	1.22	0.02	0.03	0.21	15.92	0.03	0.03	1.13	18.31	64.75	101.91
HL841B	786.3	0.27	0.18	nd	nd	1.36	14.04	nd	0.02	nd	17.89	61.30	95.06
HL841B	786.3	0.20	1.69	0.02	nd	0.26	12.95	0.03	0.02	2.72	19.32	64.03	101.24
HL840	252.0	0.30	0.15	nd	nd	6.70	13.18	0.02	nd	0.05	20.13	61.17	101.70
HL840	252.0	0.17	0.11	0.01	0.04	7.62	7.36	0.03	0.01	0.09	20.85	63.08	99.37
HL840	252.0	2.65	0.25	0.01	nd	0.63	10.93	0.01	nd	nd	18.18	65.46	98.12

nd = not detected. Each analysis is for a single grain of K-feldspar.

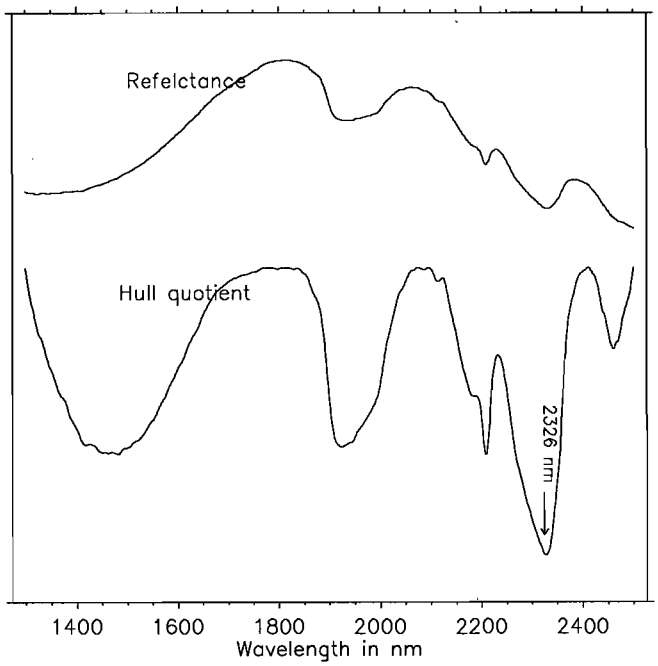

Figure 11. Spectra of a carbonate vein in the HL841B sample at 595.4 m (core split). The major absorption at 2326 nm may indicate dolomite-ankerite as the main carbonate species. The two features near 2200 nm are from dickite in the rock cut by the carbonate vein.

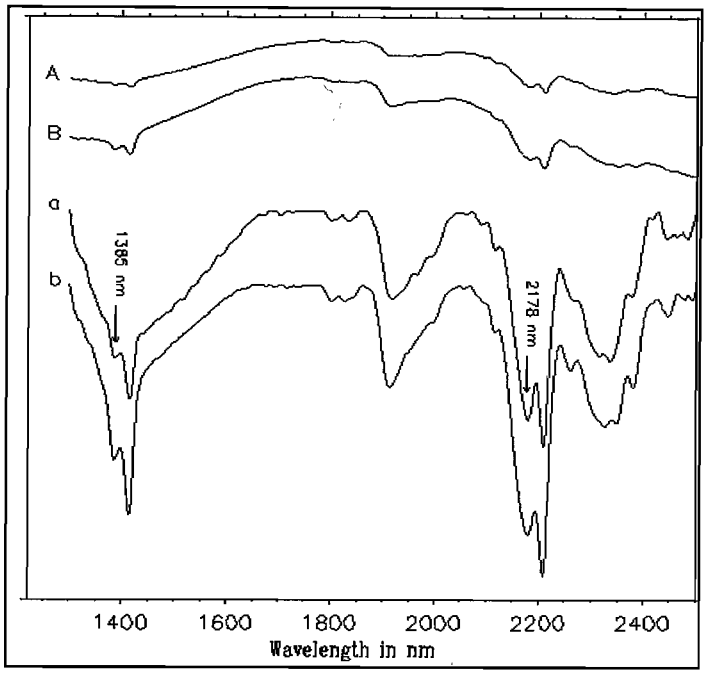

Figure 12. Spectra of HL841B sample at 595.4 m. A and B are reflectance spectra, and a and b are hull quotient spectra. The two absorptions diagnostic of dickite are marked by arrows. The asymmetry for the feature around 1900 nm and the fall-off in reflectance at 1650-1450 nm are due to carbonates that account for approximately 30 to 40% by volume of the rock.

caused by prehnite in the upper two samples and by chlorite in the lower four samples (Fig. 15). Muscovite is detectable only in sample. The wavelength of the absorption feature at 2336–2340 nm suggests calcite as the main carbonate species in all samples except one, in which the wavelength at 2334 nm may suggest dolomite as the main carbonate species. A change, therefore, is spectrally evident from the metamorphic (prehnite + calcite), through the slightly altered (prehnite + calcite + chlorite) to the moderately altered (chlorite + muscovite) samples.

Zoisite + calcite

Zoisite, as a regional metamorphic mineral, was found also in the hangingwall basalt. In the upper part of drill-hole HL697, the metamorphic assemblage of zoisite+ calcite is dominant down to 66 m depth, and then chlorite becomes significant and increases with depth (Fig. 16). Development of the chlorite water feature near 2000 nm clearly indicates the chlorite domination in samples from 73.4 m.

Implications

The spectral data of two drill-holes (MAC031 & HL697) confirms that the regional prehnite-pumpellyite facies metamorphism did not affect, to any significant degree, the hydrothermal alteration at Hellyer.

The spectral data, on the other hand, indicates that the hydrothermal alteration peripheral to the Hellyer mineralisation system is dominated by chlorite. As clearly demonstrated in these two two drill-holes, in the alteration this chlorite-rich assemblage changes, through a transition zone, to a metamorphic assemblage. It should be noted that the chlorite-dominated alteration assemblage is far more extensive than the Hellyer mineralisation system. The relationship between this chlorite-rich alteration and the pipe-shaped Hellyer alteration system has not been mentioned in the literature.

Conclusions

The samples spectrally analysed in this study include various lithologies present at Hellyer. They cover variably altered and unaltered volcanics and sedimentary rocks. From the spectral data obtained, we can make a synthesis on some mineralogical and geological issues that may be of significance to exploration.

1. Alteration zoning in the footwall can be better characterised by the PIMA-II spectral data than the hangingwall.

2. The spectrally revealed zoning pattern in the footwall is generally agreeable with what has been summarised by Gemmell and Large (1992), but locally a more complex zoning may be present.

3. The Al-OH wavelength of muscovite is a good index for mineralisation. The implied Fe and/or Mg-rich muscovite with longer Al-OH wavelength occurs within or proximal, whereas the relatively Fe and Mg-poor muscovite peripheral, to orebody. This finding suggests that the Al-OH wavelength data may be used directly for mapping in exploration. From the data obtained so far, a special attention should be paid to the altered rocks with the Al-OH wavelength > 2210nm (i.e. approximately more than 20% of octahedral Al replaced by mainly Fe and Mg), which may be mineralised; the footwall volcanics with Al-OH wavelength < 2205nm (less than 15% octahedral Al replaced by Fe and Mg) are not likely to be sulfide-rich.

4. Chlorite composition, though also highly variable, does not appear to show any correlation with mineralisation, and therefore is less significant in directly indicating the mineralisation. The Mg# value of chlorite, estimated by the Fe-OH wavelength, ranges from 0.7–0.2 for the altered footwall and 0.7–0.3 for hangingwall volcanics.

5. Secondary potassium feldspar is enriched locally in the footwall alteration system. The K-feldspar enriched zone tends to be associated with intense silicification and sericitisation.

6. Hydrothermal dickite may be present in the altered hangingwall rocks. The dickite contains trace Cr, and thus the host rocks may appear

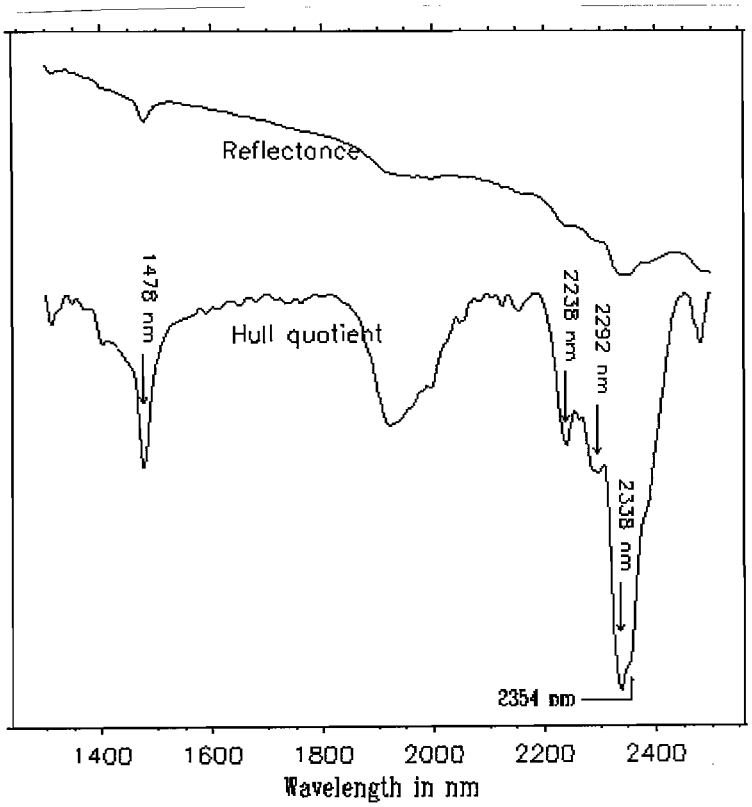

Figure 13. Spectra of calcite-prehnite vein HL055 at 154.2 m depth. The features at 1478 nm, 2238 nm and 2292 nm are from prehnite; the major feature at 2338 nm is from prehnite and possibly calcite.

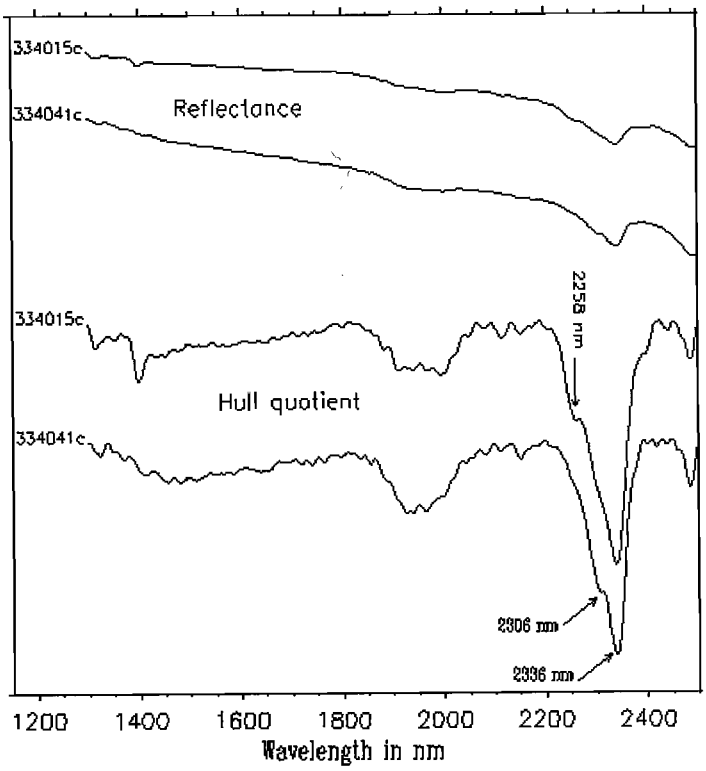

Figure 14. Spectra of the carbonate-rich parts of two HL055 samples (core splits). Carbonates in sample 334015 (100 m) are in vein, and in 334041 (207.6 m) as infillings of vesicles. Calcite is indicated by the CO_3 absorption minimum at 2336 nm. The feature near 2256 nm belongs to chlorite.

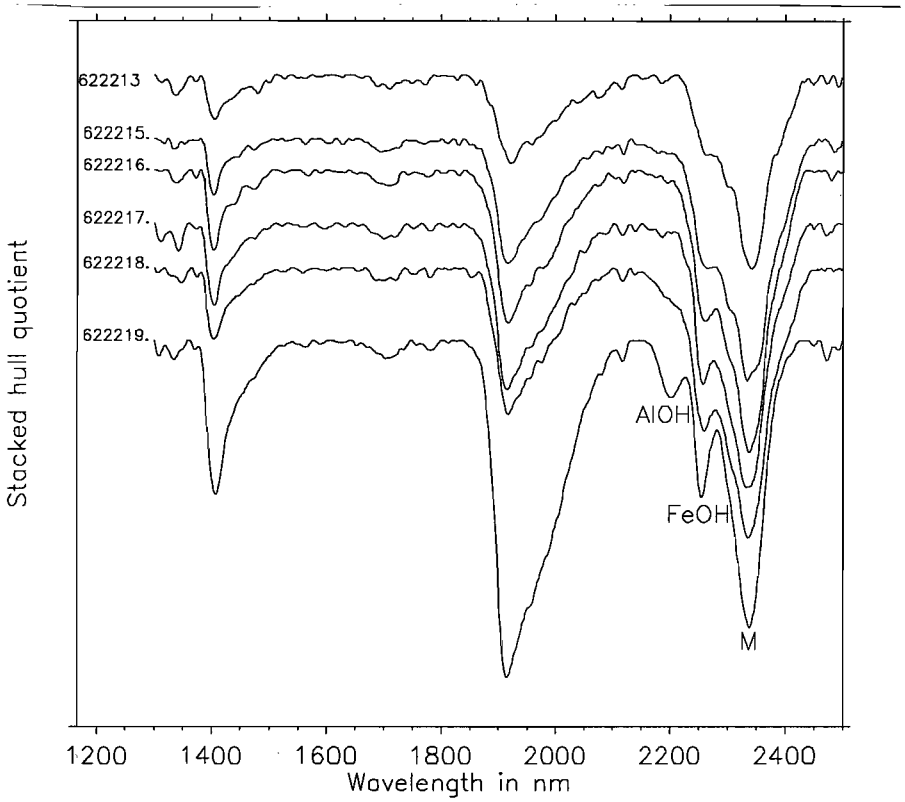

Figure 15. Hull quotient spectra for MAC031 samples. Al-OH and Fe-OH are absorption features of muscovite and chlorite, respectively. Feature M is the mixture of CO3 absorption of carbonates and Mg-OH of chlorite.

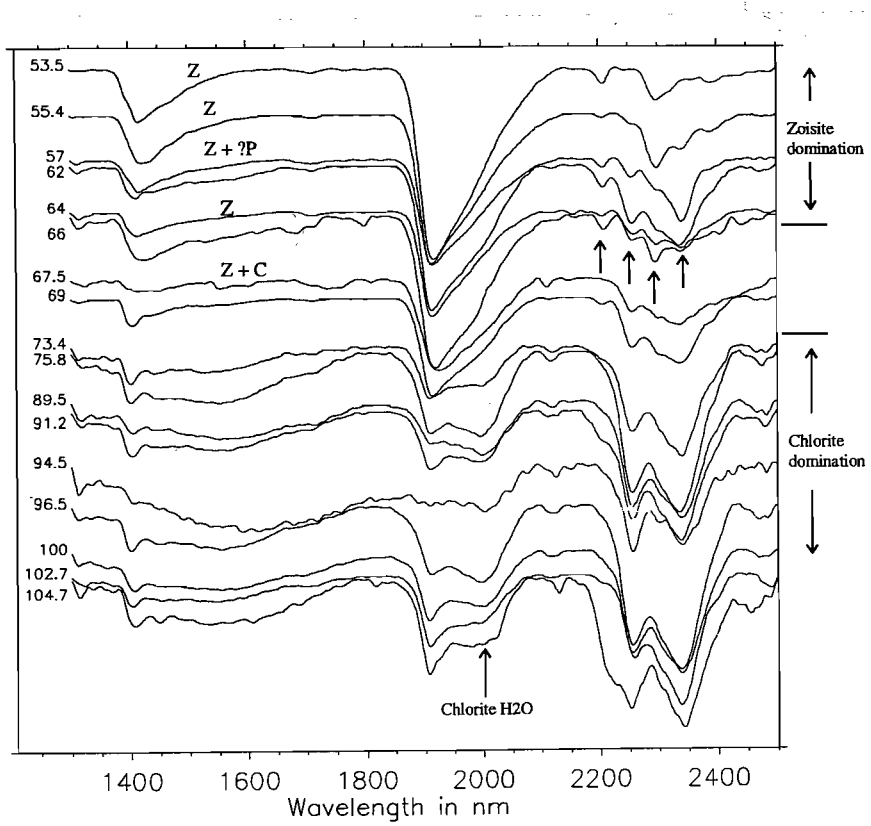

Figure 16. SWIR spectra of the upper part of HL697. The zoisite absorption features are marked by arrows. For the zoisite-bearing samples: Z = zoisite, P = prehnite, C = chlorite.

greenish but should not be mistaken as 'fuchsitic' alteration.

7. An intensified carbonate feature at 2320–2340 nm, along with a weak chloritic Fe-OH feature at 2250–2260 nm, is the spectral signatures of the immediate country volcanics.

References

Gemmell, J.B. and Large, R.R., 1992, Stringer system and alteration zones underlying the Hellyer volcanic-hosted massive sulfide deposit, Tasmania, Australia. Econ. Geol. v. 87, p. 620–649.

Jack, D.J., 1989, Hellyer host rock alteration. unpub. M.Sc. Thesis, Department of Geology, University of Tasmania.

Large, R.R., 1992, Australian volcanic-hosted massive sulfide deposits: features, styles, and genetic models. Econ. Geol., v. 87, p. 471–510.

McArthur G.J. and Dronseika E.V. 1990. Que River and Hellyer zinc-lead-silver deposits. In Geology and mineral deposits of Australia and Papua New Guinea (Ed. F.E. Hughes), pp.1229–1239, The Australasian Institute of Mining and Metallurgy, Melbourne.

McGoldrick, P.J. and Large, R.R., 1992, Geologic and geochemical controls on gold-rich stringer mineralisation in the Que River Deposit, Tasmania. Econ. Geol., v. 87, p. 667–685.

Offler, R. and Whitford, D.J. 1992, Wall-rock alteration and metamorpism of a volcanic-hosted massive sulfide deposit at Que River, Tasmania: petrology and mineralogy. Econ. Geol., v. 87, p. 686–705.

Pontual, S., 1994, Influence of composition on the spectral response in the chlorite and biotite-phlogopite mineral groups. Internal CSIRO DEM Consultancy Report. Summary Report: Phase 3C.

Yang, K., Huntington, J.F., Gemmell, J.B. and Fulton, R., 1996a, PIMA-II spectral analysis of alteration associated with the Hellyer VHMS deposit: preliminary results, AMIRA Project P439, May 1996, p. 171–178.

Yang, K., Huntington, J.F., Gemmell, J.B. and Fulton, R., 1996b, PIMA-II spectral analysis of alteration associated with the Hellyer VHMS deposit: progress report, AMIRA Project P439, October 1996, p. 307–318.

Yang, K., Huntington, J.F., Scott, K.M. and Mason, P., 1996c, Pilot spectral analysis of samples from the Ardlethan tin deposit, NSW, CSIRO Exploration and Mining Report 136 R, 33 pp.

Whitford, D.J., Creelman, R.A. and Ramsden, A.R., 1984, Petrological, geochemical and mineragraphic studies at Que River and Hellyer, Part 6. CSIRO Division of Mineralogy Report 1544R, pp38.

Preliminary geochemical data from the Dobson Creek–White Spur traverses

by Wally Herrmann, Rod Allen and Jocelyn McPhie
Centre for Ore Deposit Studies, Geology Department, University of Tasmania

Introduction

Four short traverses across the Central Volcanic Complex–White Spur Formation contact were mapped and sampled in April, 1997 to determine the lateral extents of trace element geochemical anomalies and contrasting alteration styles, which had been observed in association with the contact, on the earlier Hercules and Hall Rivulet Canal regional traverses.

Preliminary interpretations of volcanic facies and alteration style were presented in the previous P439 Report 4, (Allen et al., 1997).

XRF analyses for major and some trace elements were "in progress" at CODES during mid October and probably will not beat the deadline for publication in P439 Report 5. Petrographic thin sections have been prepared and will be described and interpreted in conjunction with major element data.

This report presents and briefly comments on the currently available ANALABS data for Ag, As, Bi, Mo, Cd, Sb, Cs, Tl, Th, U (ICP-Ms) and CO_2 (Leco).

Geochemistry

The (sorted) analyses are tabulated with the sample locations, abbreviated lithological descriptions and formation names, in Table 2. An additional column: "Strat Level", lists the approximate stratigraphic levels of the samples above (+) or below (-) the observed base of the White Spur Formation (WSF).

Most of the Bi and Tl values are only marginally above their detection limits and are of doubtful reliability. Additional standard and duplicate samples (in a sub set of Hellyer samples which were run in the same analytical batch) suggest that the ICP-MS method has lately been unreliable for As, Cs, Tl & Th; this problem is currently being followed up with Analabs.

Notwithstanding the doubts about accuracy, the correlation matrix, in Table 1, indicates reasonably strong +ve correlations (r >0.6) between the elements As-Ag-Sb-Cd and weaker +ve correlations (r ~0.4 to 0.6) between Tl-As,Ag,Sb and Mo-Ag,Cd,Sb (but no correlation between Tl & Mo!). There are no strong negative correlations.

Selected elements are illustrated as line graphs, for each traverse, plotted against estimated stratigraphic level, in Figure 2.

No particular geochemical pattern relative to stratigraphic position is evident except on Traverse 1 where sample WS97-34 records the coincident maxima in Ag, As, Sb, Cd, Mo and Tl, with a ragged halo of As and (faint) Tl? in WSF to the west. This anomalous sample is from a basal, pumiceous crystal-lithic rich volcaniclastic breccia (containing mudstone clasts) within the WSF, about 5m west of the CVC contact. The rock was reported to be intensely silicified with ~5% pyrite>galena in veinlets and disseminated streaks.

The anomalous geochemical values are comparable with those associated with the Rosebery ore horizon (Large & Allen, 1997) but considerably lower than those reported from the Hercules–Mt Read traverse (Large, 1996). Further comments, about the style and significance of alteration and mineralisation near the contact on White Spur Traverse 1, may be warranted when the major and other trace element data becomes available.

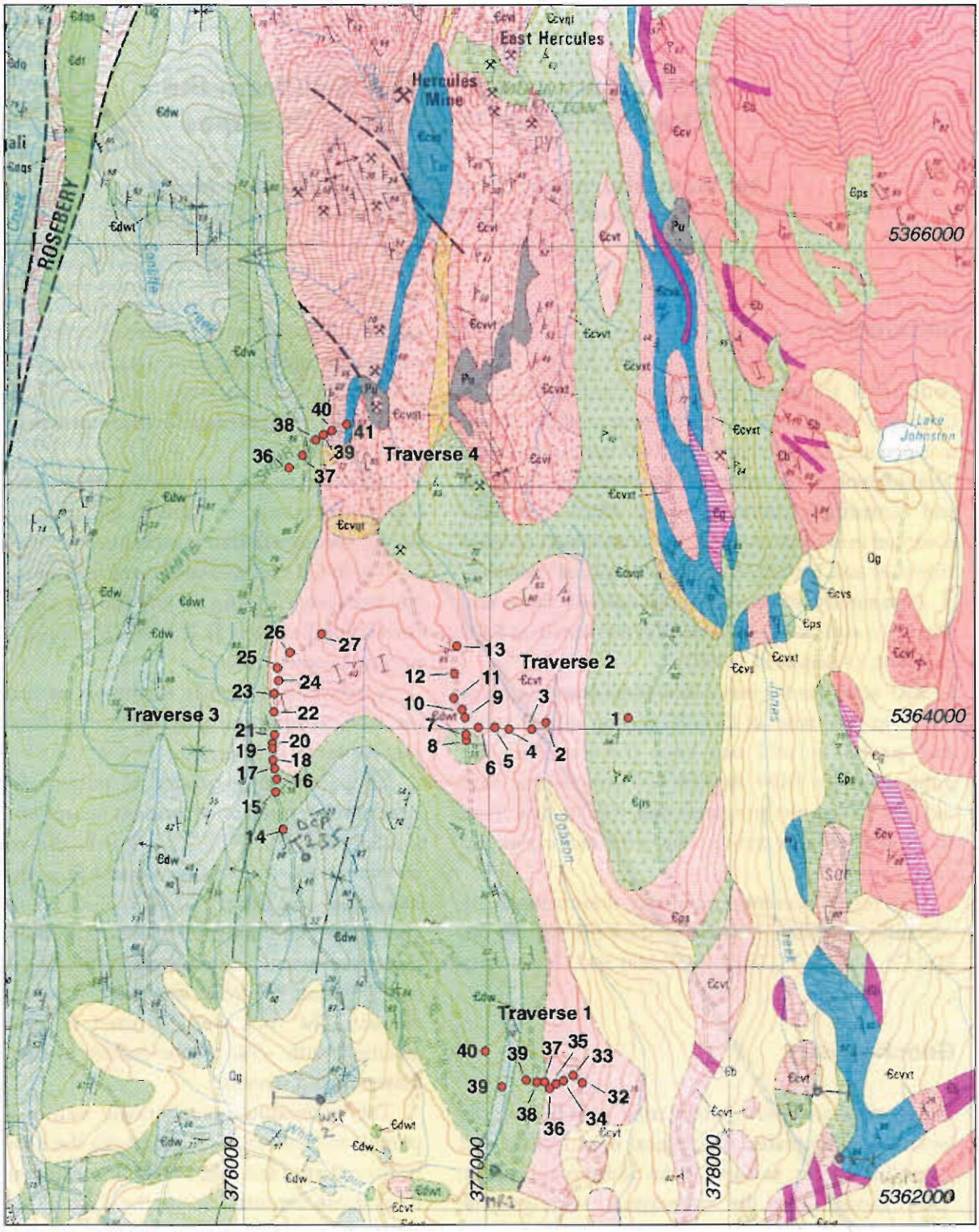

Figure 1 Locations of White Spur traverses 1–4 and sample numbers. Scale 1:25,000.

References

Allen, R.L.A., McPhie, J., Gifkins, C. and Blake, M. 1997. Dobson Creek - White Spur area "step out" traverses: Preliminary report. AMIRA/ARC Project P439, Report 4, May 1997, p343-346.

Large, R.R., 1996. The Hercules-Mt Read traverse: relationships between volcanic mineralogy, alteration and geochemistry. AMIRA/ARC Project P439, Report 3, Oct 1996, p153-233.

Large, R.R. and Allen, R.L.A., 1997. Preliminary report on the Rosebery lithochemical halo study. AMIRA/ARC Project P439, Report 4, May 1997, p259-330.

Table 1 Correlation Matrix; White Spur, Sample Nos: WS97-1 to WS97-46

	Ag	As	Bi	Mo	Cd	Sb	Cs	Tl	Th	U	CO_2	Th/U
Ag	1.00											
As	0.59	1.00										
Bi	0.11	-0.03	1.00									
Mo	0.50	0.34	0.31	1.00								
Cd	0.86	0.61	-0.03	0.48	1.00							
Sb	0.90	0.62	-0.09	0.45	0.83	1.00						
Cs	-0.07	-0.29	-0.15	-0.19	-0.15	0.00	1.00					
Tl	0.41	0.49	-0.26	-0.05	0.37	0.43	0.01	1.00				
Th	-0.04	0.27	0.03	0.01	0.01	-0.05	-0.04	0.24	1.00			
U	0.24	0.46	0.00	0.19	0.27	0.23	-0.09	0.24	0.85	1.00		
CO_2	-0.05	0.02	-0.06	-0.08	-0.07	-0.04	0.02	0.06	-0.25	-0.28	1.00	
Th/U	-0.30	-0.23	-0.01	-0.21	-0.25	-0.35	0.13	0.11	0.00	-0.49	0.23	1.00

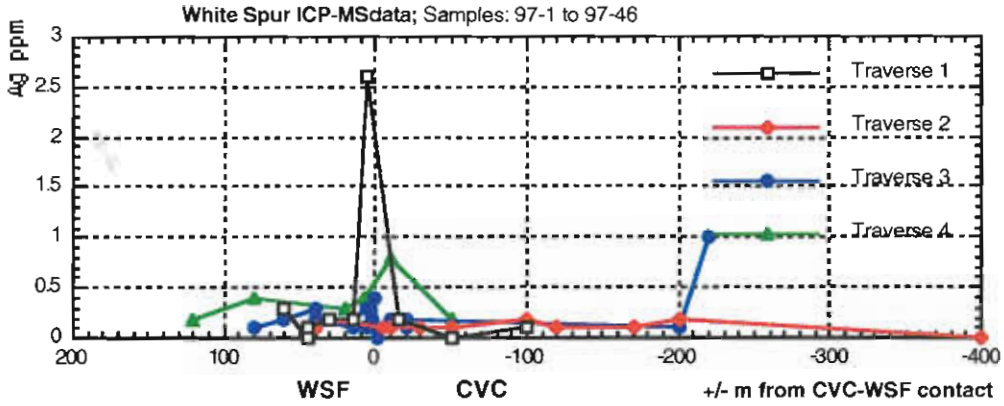

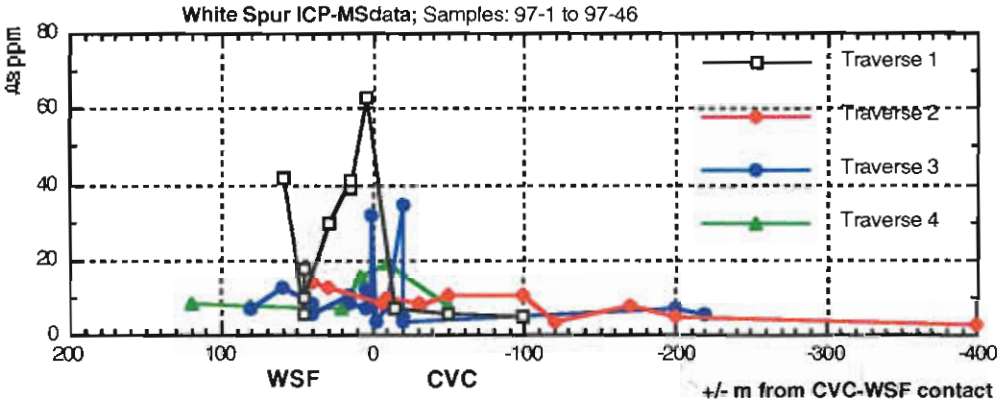

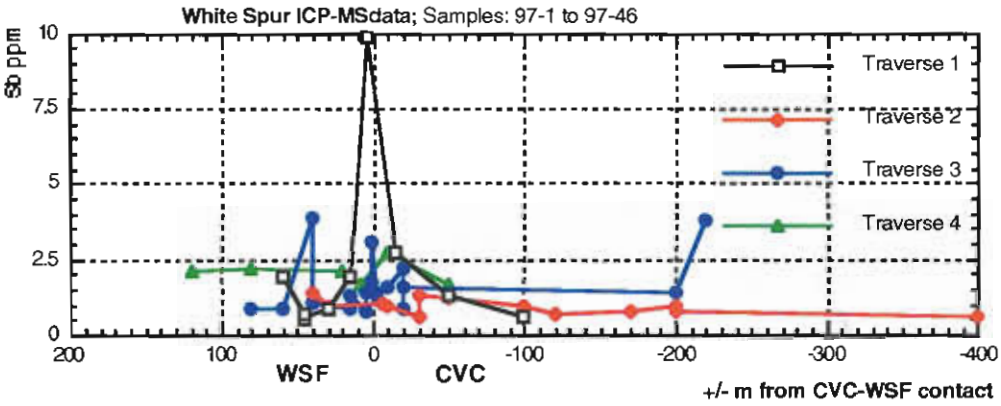

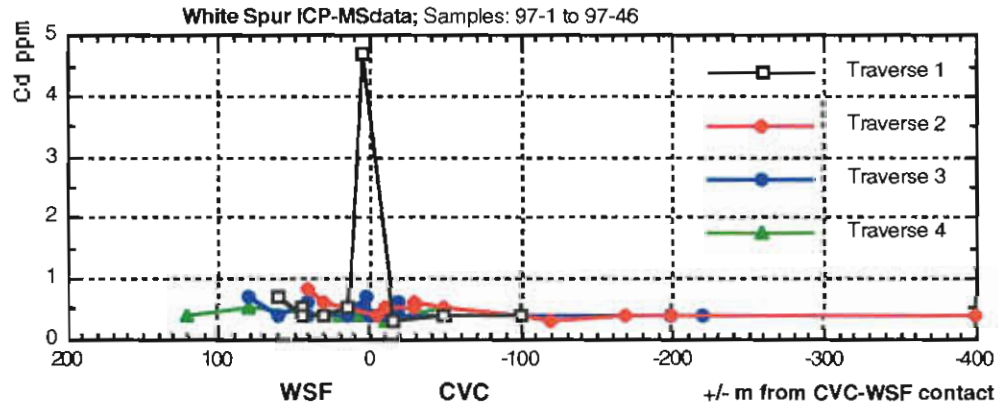

Figure 2 Line Graphs: Selected trace elements, White Spur Traverses.

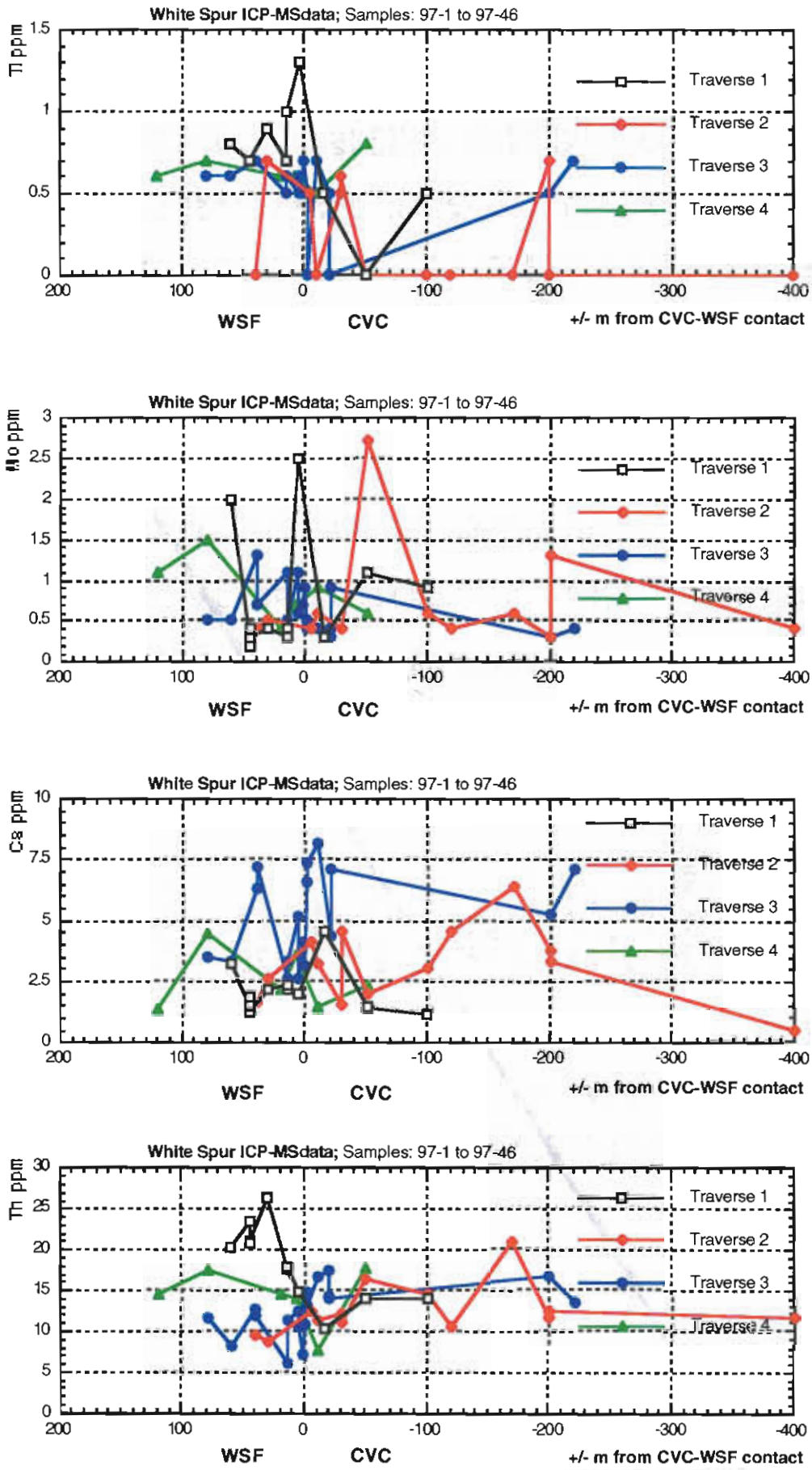

Figure 2 (cont.) Line Graphs: Selected trace elements, White Spur Traverses.

Table 2 **WHITE SPUR TRAVERSES: ICP-MS Data** RLA & JMcP April 1997 Analabs: PE028773 [WS97-1sorted] 15/10/97 1 of 1

Field No.	icpms no.		T	No	FMN	Strat Level (m) (above or below contact)	Lithology	Ag GS201	As GS201	Bi GS201	Mo GS201	Cd GS201	Sb GS201	Cs GS201	Tl GS201	Th GS201	U GS201	CO2 OM612	Th/U calc
		Method																	
		L Detection						0.1	1	0.1	0.1	0.1	0.1	0.05	0.5	0.05	0.05	0.02	
		U Detection						500	1000	1000	1000	1000	1000	1000	1000	1000	1000	75	
		Unit						ppm	ppm	ppm	ppm	ppm	ppm	ppm	ppm	ppm	ppm	%	
WS97-33	RA 037		1	CVC		-15	Fs (lithic) PuBx	0.2	7	0.1	0.3	0.3	2.7	4.56	0.5	10.3	3.81	1.36	2.7
WS97-32	RA 035		1	CVC		-50	Fs PuBx (Mt&Ep)	<	6	0.2	1.1	0.4	1.3	1.42	<	13.9	3.93	0.12	3.5
WS97-31	RA 034		1	CVC		-100	Fs PuBx (Mt&Ep)	0.1	5	0.1	0.9	0.4	0.6	1.19	0.5	13.9	3.76	0.36	3.7
WS97-34	RA 038		1	WSF		5	QF-lith PuBx+PyGn	2.6	63	<	2.5	4.7	9.9	1.92	1.3	14.8	6.81	0.05	2.2
WS97-35	RA 039		1	WSF		15	QF? ser PuBx	0.2	39	0.1	0.4	0.5	1.9	2.18	1	17.7	5.62	0.55	3.1
WS97-35	RA 017	duplicate	1	WSF		15	QF? ser PuBx	0.2	41	0.1	0.3	0.5	1.9	2.3	0.7	17.9	5.64	0.62	3.2
WS97-36	RA 040		1	WSF		30	Q (lith) ser PuBx	0.2	30	0.1	0.4	0.4	0.9	2.13	0.9	26.3	7.41	0.11	3.5
WS97-37	RA 041		1	WSF		45	Bdd Slst-Sst	0.1	10	<	0.3	0.4	0.6	1.29	0.7	21	6.42	0.06	3.3
WS97-39	RA 044		1	WSF		45	Bdd Slst-Sst	0.1	18	0.1	0.4	0.5	0.5	1.87	0.7	20.9	6.59	0.05	3.2
WS97-40	RA 045		1	WSF		45	Bdd Slst-Sst	<	6	0.1	0.2	0.4	0.7	1.48	0.7	23.6	6.03	0.13	3.9
WS97-38	RA 043		1	WSF		60	dk gry Slst-Sst	0.3	42	0.1	2	0.7	1.9	3.22	0.8	20.2	7.1	0.73	2.8
WS97-9	RA 010		2	CVC		-5	Fs PuBx	0.1	9	0.2	0.4	0.4	1.1	4.06	0.5	12.4	4.2	0.34	3.0
WS97-6	RA 006		2	CVC		-10	Fs PuBx	0.1	10	0.2	0.6	0.5	1	3.16	<	11.4	3.1	0.66	3.7
WS97-10	RA 011		2	CVC		-30	Fs PuBx	0.1	8	0.2	0.4	0.6	1.3	4.55	0.6	11	3.52	0.12	3.1
WS97-11	RA 012		2	CVC		-30	fg Fs PuBx	0.1	9	0.2	0.4	0.5	0.6	1.5	0.5	12.2	4.24	0.05	2.9
WS97-5	RA 005		2	CVC		-50	Fs PuBx-Sst	0.1	11	0.2	2.7	0.5	1.2	1.95	<	16.4	5	0.34	3.3
WS97-4	RA 004		2	CVC		-100	Fs PuBx	0.2	11	0.2	0.6	0.4	1	3.04	<	14.5	4.54	0.15	3.2
WS97-12	RA 013		2	CVC		-120	Fs PuBx	0.1	4	0.1	0.4	0.3	0.7	4.56	<	10.4	3.82	0.40	2.7
WS97-3	RA 003		2	CVC		-170	Fs PuBx	0.1	8	0.4	0.6	0.4	0.8	6.35	<	20.8	5.65	0.18	3.7
WS97-2	RA 002		2	CVC		-200	Fs PuBx	0.2	5	0.1	1.3	0.4	0.8	3.3	<	12.4	4.02	0.42	3.1
WS97-13	RA 014		2	CVC		-200	Fs PuBx	0.2	5	0.1	0.3	0.4	1	3.72	0.7	11.7	3.68	0.59	3.2
WS97-1	RA 001		2	CVC		-400	QFp spher Rhy	<	3	<	0.4	0.4	0.6	0.45	<	11.7	3.46	0.19	3.4
WS97-7	RA 008		2	WSF		30	xt-Pu-lith Bx	0.2	13	0.1	0.5	0.6	1	2.57	0.7	8.56	2.45	0.09	3.5
WS97-8	RA 009		2	WSF		40	mg QF Sst	0.1	14	0.2	0.4	0.8	1.4	1.57	<	9.36	3.44	0.07	2.7
WS97-18	RA 020		3	CVC		-2	Fs PuBx, wd	<	4	<	0.5	0.4	1.3	7.33	<	13.2	4.5	0.11	2.9
WS97-24	RA 026		3	CVC		-2	Fs PuBx	<	4	0.1	0.4	0.4	1.4	6.53	0.5	14.7	4.5	0.11	3.3
WS97-21	RA 023		3	CVC		-10	Fs PuBx (wd)	0.2	8	<	0.4	0.4	1.6	8.11	0.7	16.7	5.44	0.29	3.1
WS97-19	RA 021		3	CVC		-20	Fs PuBx, wd	0.2	4	0.3	0.9	0.4	1.6	7.11	<	13.9	4.83	0.12	2.9
WS97-25	RA 027		3	CVC		-20	Fs PuBx	0.1	5	0.1	0.3	0.6	0.9	4.38	0.5	14.1	4.73	0.77	3.0
WS97-26	RA 028		3	CVC		-20	Fs PuBx wd	0.2	35	0.1	0.4	0.5	2.2	4.33	0.5	17.5	4.67	0.40	3.7
WS97-27A	RA 029		3	CVC		-200	Fs PuBx fr	0.1	7	0.1	0.3	0.4	1.4	5.26	0.5	16.6	4.22	0.17	3.9
WS97-27B	RA 030		3	CVC		-220	Fs PuBx wd	1	6	<	0.4	0.4	3.8	7.11	0.7	13.5	4.18	0.40	3.2
WS97-20	RA 022		3	WSF		1	QFxt-lith Bx	0.4	32	0.2	0.9	0.4	3.1	3.15	0.7	10.7	3.61	0.16	3.0
WS97-17	RA 019		3	WSF		2	QFxt Sst or PuBx	0.2	8	<	0.7	0.7	1.8	4.08	0.5	7.06	2.18	0.40	3.2
WS97-16	RA 018		3	WSF		5	QFxt Sst or PuBx	0.1	12	<	0.6	0.5	1.4	2.58	0.6	10.5	1.89	0.12	5.6
WS97-23	RA 025		3	WSF		5	Pu>xt mg Sst	0.3	7	0.1	1.1	0.5	0.8	5.1	0.5	12.5	4.17	0.17	3.0
WS97-15	RA 016		3	WSF		15	QF fg PuBx	0.2	9	0.1	0.5	0.4	1.3	3.27	0.6	11.3	2.77	0.11	4.1
WS97-22	RA 024		3	WSF		15	QFxt rich Sst	0.1	11	<	1.1	0.4	0.9	2.57	0.5	6.15	1.32	0.14	4.7
WS97-14	RA 015		3	WSF		40	lam blk slate	0.2	6	0.1	0.7	0.4	1.1	7.13	0.7	11.9	3.87	0.20	3.1
WS97-28	RA 031		3	WSF		40	blk Mudst	0.3	9	0.2	1.3	0.6	3.9	6.29	0.7	12.6	3.98	0.59	3.2
WS97-29	RA 032		3	WSF		60	mic Sst (mudst)	0.2	13	0.2	0.5	0.4	0.9	3.32	0.6	8.1	1.54	4.54	5.3
WS97-30	RA 033		3	WSF		80	QF xt rich Sst	0.1	7	0.1	0.5	0.7	0.9	3.5	0.6	11.6	3.19	1.21	3.6
WS97-42	RA 047		4	CVC		-10	Q-ser Schist	0.8	19	0.1	0.9	0.3	2.7	1.46	0.5	7.67	3.68	0.44	2.1
WS97-41	RA 046		4	CVC		-50	Fs-Pu cg Sst	0.2	8	0.2	0.6	0.5	1.7	2.29	0.8	17.8	5.65	0.14	3.2
WS97-43	RA 048		4	WSF		8	fg volc Sst	0.4	16	0.1	0.7	0.4	1.7	3.56	0.6	14	4.6	0.10	3.0
WS97-44	RA 049		4	WSF		20	QFPu-lith Bx	0.3	7	0.3	0.4	0.4	2.1	2.1	0.6	14.5	3.32	0.12	4.4
WS97-45	RA 050		4	WSF		80	gry ser Slst	0.4	8	0.4	1.5	0.5	2.2	4.4	0.7	17.3	5.15	0.14	3.4
WS97-46	RA 051		4	WSF		120	QFxt PuBx	0.2	9	0.1	1.1	0.4	2.1	1.35	0.6	14.4	4.15	0.14	3.5
GSS-5	RA 007	standard						4.2	381	32.9	5.1	0.8	38.6	12	0.9	21.7	5.82	IS	3.7
GSS-5		expected values						4.4	412	41	4.6	0.45	35.4	15	1.6	22.7	6.5		3.5

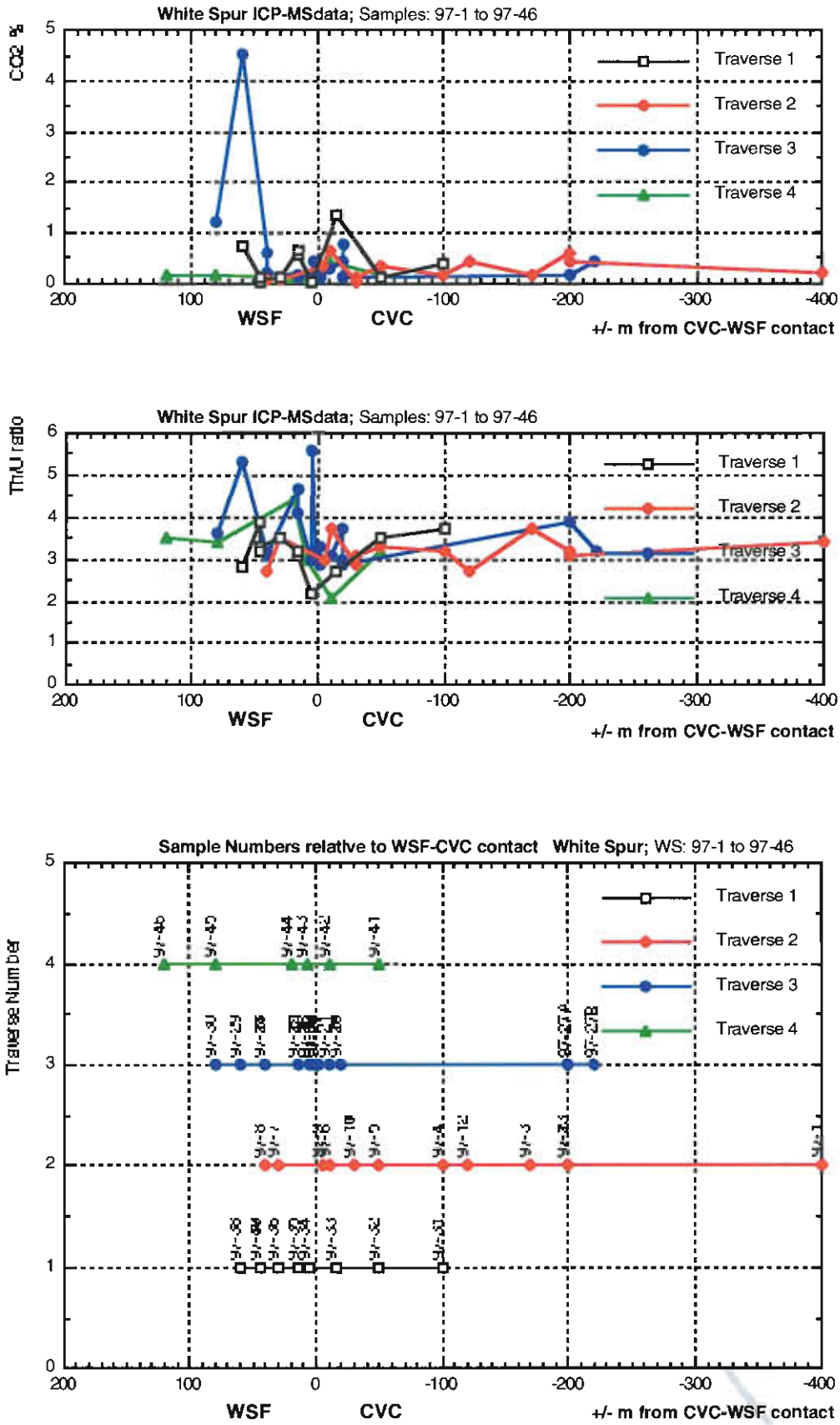

Figure 2 (cont.) Line Graphs: Selected trace elements, White Spur Traverses.

Alteration geochemistry of the sub-seafloor replacement style Highway–Reward deposit, Mount Windsor Subprovince

by Mark Doyle
Centre for Ore Deposit Studies, Geology Department, University of Tasmania

Summary

Geochemical studies of hydrothermal and diagenetic alteration associated with the Cu-Au-rich Highway-Reward massive sulfide deposit in the Cambro-Ordovician, Mount Windsor Subprovince are discussed. Alteration in the footwall and hanging wall is similar and characterised by patterns of depletion (Na_2O, CaO, MgO) and enrichment (K_2O, Rb/Sr) which provide vectors to ore. Rb/Sr ratios are generally higher in the hanging wall alteration halo than the footwall and may discriminate the ore position. Sills and cryptodomes in the host succession to mineralisation range in composition from high-silica dacite to rhyolite and are similar to comparable facies in the remainder of the Trooper Creek Formation. The results of this analysis have application to other sub-seafloor replacement type VHMS deposits hosted by syn-sedimentary intrusion-dominated volcanic centres.

Introduction

Hydrothermal alteration is increasingly being recognised in the hanging wall of volcanic-hosted massive sulfide (VHMS) deposits (e.g. Large, 1992). There are few detailed descriptions of the mineralogical and geochemical characteristics of this style of alteration. Halos of subtle hydrothermal alteration have been mapped above VHMS deposits which are interpreted to have formed at the seafloor (e.g. Hellyer; Jack, 1989). Pipes or plumes of intense hanging wall alteration are characteristic of sub-seafloor massive sulfide deposits, and can extend from tens to hundreds of metres into the hanging wall volcanic succession (e.g. South Hercules, Khin Zaw and Large, 1995; Ansil, Galley et al., 1995; Highway–Reward, Doyle, 1997a,b). Detailed studies of the volcanic facies, mineralisation and alteration at Highway–Reward provide a framework for geochemical studies of alteration associated with a syn-genetic sub-seafloor replacement style massive sulfide deposit.

The principal intention of this research is to document (1) the primary geochemistry of lavas and intrusions which host the Highway–Reward massive sulfide mineralisation; (2) the chemical changes which characterise each alteration zone; and (3) differences in the geochemistry of footwall and hanging wall alteration associated with the massive sulfide deposit.

Review of previous work

A detailed analysis of the Highway–Reward deposit, in the Mount Windsor Subprovince of Queensland, has provided insights into the characteristics of sub-seafloor replacement style, Cu-Au-rich VHMS deposits hosted by lava- and intrusion-dominated volcanic centres. The character, setting and geometry of the submarine host succession, and genetic links between volcanic, alteration and mineralisation processes have been addressed in previous reports (Doyle, 1995, 1997a) and are briefly reviewed in the following summary sheet.

Geochemistry

Sampling and analytical techniques

The new trace- and major-element data (Appendix 1) relate to a suite of variable altered, coherent lavas and intrusions sampled from drill core in the host

Table 1 **Summary sheet for the Highway–Reward deposit**

Location: 35 km south of Charters Towers in north Queensland

Resource:

Highway	Primary — 1.2 m.t. @ 5.5% Cu, 6.5 g/t, Ag, 1.2 g/t Au
	Oxide — 0.07 m.t. @ 6.04 g/t Au
Reward	Primary — 0.2 m.t. @ 3.5% Cu, 13 g/t Ag, 1 g/t Au
	Supergene — 0.3 m.t. @ 11.6% Cu, 21 g/t Ag, 1.8 g/t Au
	Oxide — 0.1 m.t. @ 33 g/t Ag, 6.49 g/t Au

Volcanic belt: Mt Windsor Subprovince (Highway Member, Trooper Creek Formation)

Age of volcanism: Cambro-Ordovician

Facies associations: Hosted by a rhyolitic to dacitic intrusion-dominated sequence, that includes sedimentary facies, turbiditic sandstone and pumiceous and crystal-rich sandstone-breccia (Table 2). Contact relationships and phenocryst mineralogy, size and percentages indicate the presence of more than thirteen distinct porphyritic units in a volume of 1x1x0.5 km (Table 3). The peperitic upper margins to most porphyritic units demonstrate their intrusion into wet unconsolidated sediment. Syn-sedimentary sills, cryptodomes and partly extrusive cryptodomes have been recognised (Figs. 1, 2; Doyle, 1997a,b). These represent a proximal facies association from intrabasinal, non-explosive, syn-sedimentary intrusion-dominated magmatism.

Ore composition: Dominantly pyrite Cu-Au type

Mineralisation types: The mineralisation can be divided into five principal types on the basis of mineralogy, textures and relationships to the host rocks. These are: (1) discordant pyrite-chalcopyrite pipes; (2) veins, disseminations, discordant bands and strata-bound lenses of pyrite-sphalerite±galena±barite; (3) footwall quartz-pyrite stringer veins; (4) hanging wall quartz-pyrite stringer veins; and (5) gossanous breccia.

Surface expression: The Reward orebody occurs under 100 m combined thickness of Tertiary fluviatile sediments (Campaspe Formation) and weathered gossanous volcanics (e.g. Beams et al., 1989). The Highway orebody is located approximately 200 m NNW of the Reward orebody beneath the abandoned Highway open pit. Prior to development the Highway orebody was marked by a gossan at surface.

Structural/lithofacies control: The Highway and Reward pyrite-chalcopyrite pipes are discordant to bedding, but parallel to S4, and have a plunge sub-parallel to a sub-vertical mineral lineation (cf. Berry et al., 1992). It is possible that the D4 faults reactivated pre-existing structures that controlled the initial deposition of the pyrite pipes (Berry et al., 1992; Huston, 1992) and acted as conduits for rising magma. The location, distribution, form and shape of massive sulfide mineralisation and alteration are closely related to inferred initial patterns of permeability in the host rocks. The lavas and intrusions focussed hydrothermal fluids along the discrete mineralising pathways. Others formed an impermeable barrier promoting sub-seafloor ponding of hydrothermal fluids and replacement (Doyle, 1997a,b).

Alteration: The Highway and Reward orebodies occur within a well developed discordant alteration envelope. The envelop extends from at least 150 m below the orebodies to over 60 m above the Highway pipe (Fig. 1B). Broadly the alteration envelope has a mineralogical zoning which is defined by assemblages of sericite, chlorite-sericite, quartz-chlorite-sericite, chlorite ± anhydrite, quartz-sericite ± pyrite, albite ± K-feldspar ± sericite-chlorite-quartz and hematite ± chlorite-sericite-quartz. A quartz-sericite ± pyrite zone is centred beneath the pyrite pipes and, on some sections, extends into the hanging wall succession. Small domains of intense chlorite ± anhydrite alteration occur within the footwall quartz-sericite ± pyrite zone and along some margins of the pipes. Quartz-sericite ± pyrite alteration gives way laterally and vertically to domains of sericite-chlorite ± quartz and chlorite-sericite alteration. Beyond the hydrothermal alteration halo, rocks of rhyolitic to dacitic composition contain various assemblages of feldspar (albite), calcite, sericite, chlorite, quartz and hematite (Fig. 2B).

Discussion: Laing (1988) and Beams et al. (1989, 1990) proposed two episodes of ore deposition at Highway-Reward: a Cambro-Ordovician event which deposited syn-genetic sphalerite-rich mineralisation, and a Siluro-Devonian syn-deformational episode which produced discordant pyrite-chalcopyrite pipes. The textural and structural evidence presented by Laing (1988) and Beams et al. (1989, 1990) is inconclusive and not diagnostic of a syn-kinematic origin for the pyrite pipes. Rather the available evidence suggests that the pyrite-chalcopyrite pipes and strata-bound lenses formed together and are syn-genetic, sub-seafloor replacements of the host sediment, syn-volcanic intrusions, partly extrusive cryptodomes and volcaniclastic units (Doyle, 1997a, b).

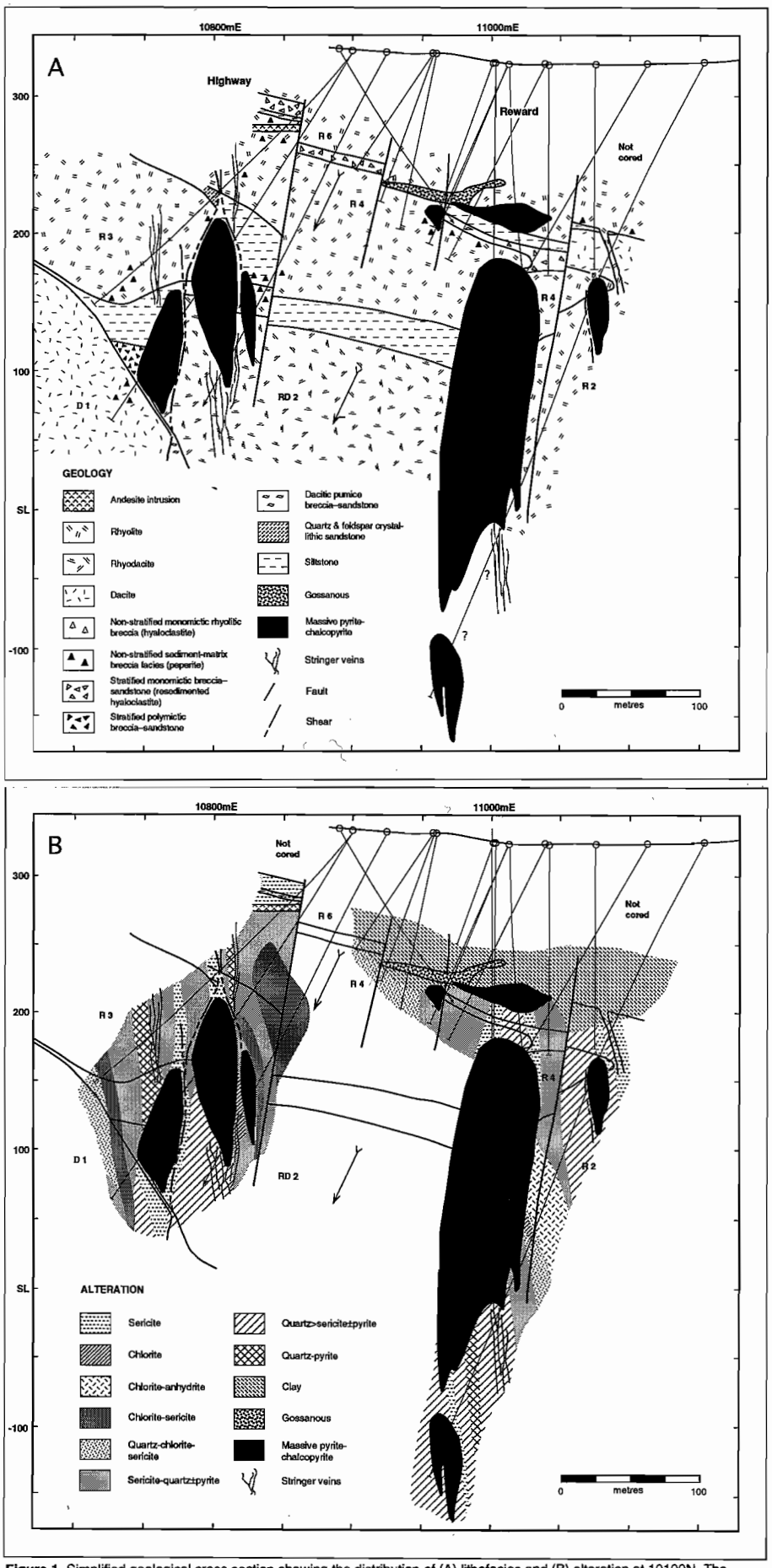

Figure 1. Simplified geological cross section showing the distribution of (A) lithofacies and (B) alteration at 10100N. The position of the massive sulfide bodies is also shown. In section (B), the boundaries on the main lithological units are illustrated. Dacite D1, rhyodacite RD2 and rhyolites R2-4 and R6 occur on section 10100N.

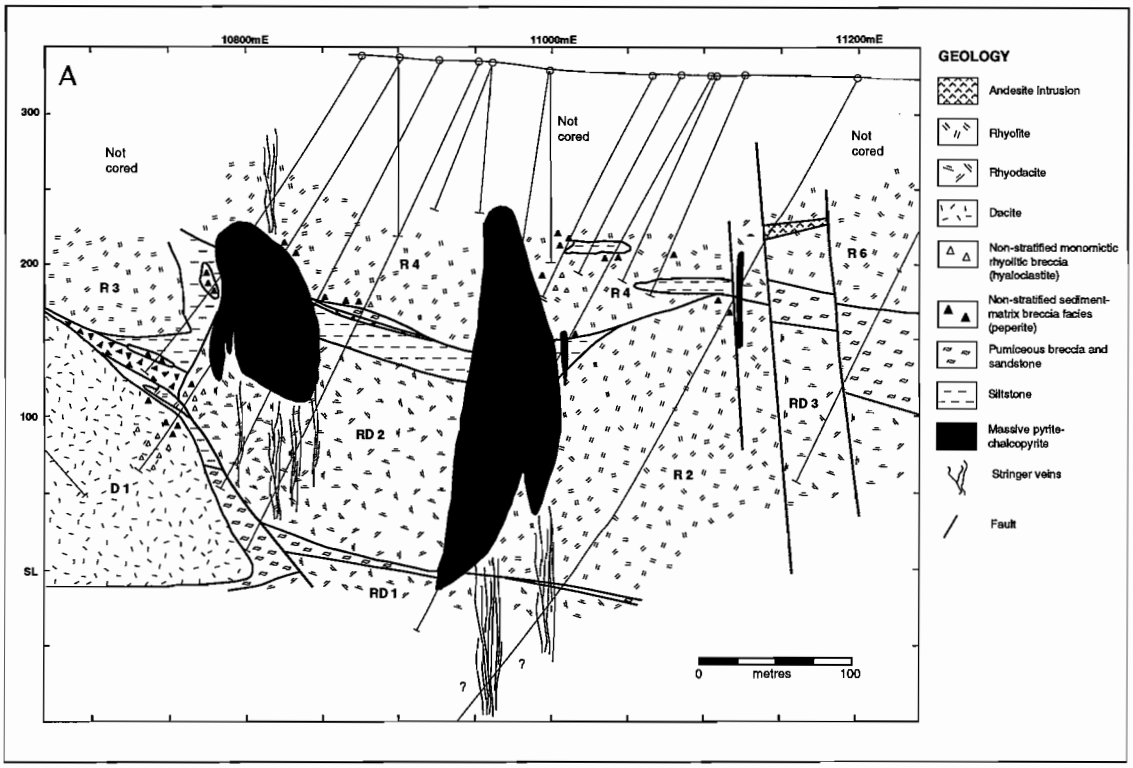

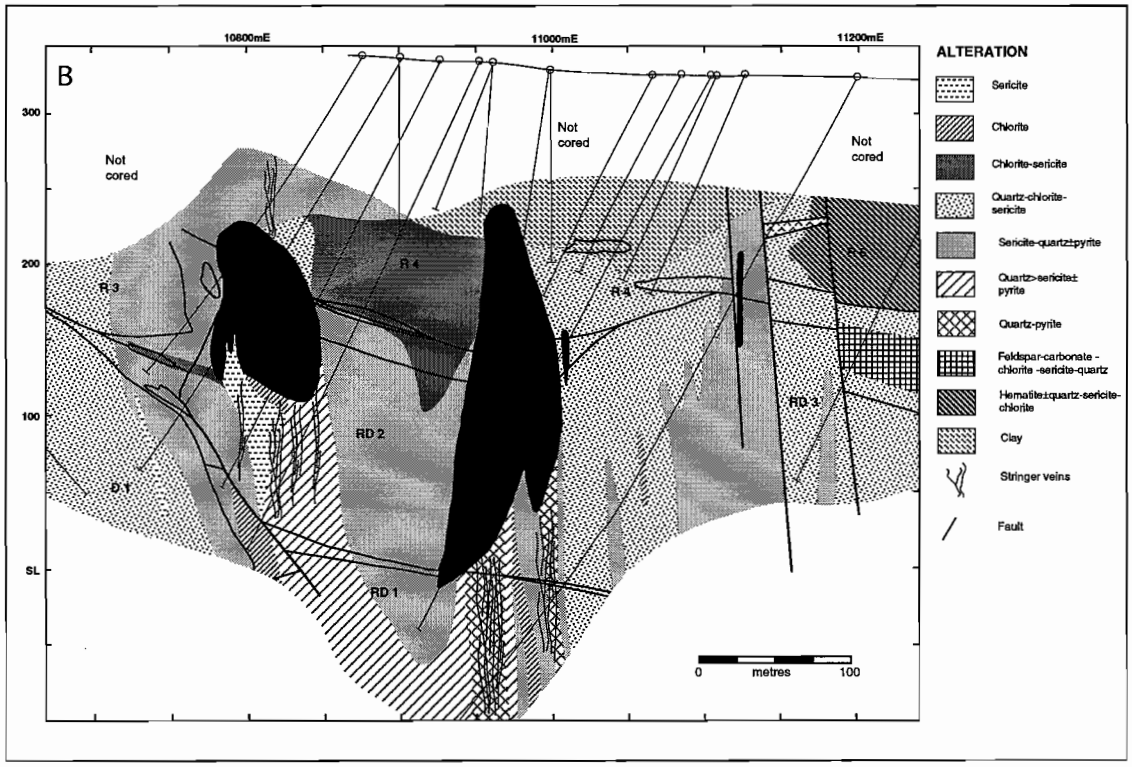

Figure 2. Simplified geological cross section showing the distribution of (A) lithofacies and (B) alteration at 10150N. The position of the massive sulfide bodies is also shown. Boundaries of the main lithological units are illustrated in both (A) and (B). Dacite D1, rhyodacites RD1-RD3 and rhyolites R2-4 and R6 are exposed on section 10150mN.

sequence to the Highway–Reward deposit. Rocks were first crushed in a jaw crusher, and a hand picked separate of chips free of oxidised or weathered rinds, veins or amygdales was powdered in a tungsten carbide disc mill. Major element and most trace element concentrations were determined on a Philips automated XRF spectrometer at the University of Tasmania using standard fused disc and pressed pellet techniques (Norrish and Chappell, 1977). The major element analyses have been recalculated to 100% anhydrous to remove variations caused by differing loss on ignition values. Some trace elements (As, Cd, Sb, Cs, Mo, Tl, Bi, U and As) were determined by ICP-MS at ANALABS facilities in Perth. Samples (0.2 g) were digested in aqua regia/perchloric acid/hydrofluoric acid using ANALABS method 201.

Element mobility

In the study area, the Seventy Mile Range Group has been affected by regional deformation and prehnite-pumpellyite to greenschist facies metamorphism, and hydrothermal alteration is locally intense. Therefore all samples selected for this study have undergone some degree of mineralogical readjustment. The variable mobility of elements during low-grade metamorphism and hydrothermal alteration is relatively well documented (e.g. MacLean and Kranidiotis, 1987; Whitford et al., 1989; Rollinson, 1993). Elements considered to be essentially immobile during these styles of alteration include the high field strength elements such as Ti, Zr and Nb. Also generally useful are P, Sc and Th. The concentrations of the large ion lithophile elements (including K, Rb, Ba and Sr) are unlikely to reflect original magmatic concentrations. The absence of a negative correlation between Ti/Zr and SiO_2 (Fig. 3A), suggests that the SiO_2 abundances in these rocks do not often reflect primary concentrations. This is clearly the case for samples with SiO_2 contents greater than 77 wt%.

Compositions

Regional lithogeochemical studies of coherent volcanic rocks within the Seventy Mile Range Group were undertaken by Berry et al. (1992), Stolz (1995) and Doyle (1997b). Stolz (1995) subdivided the Seventy Mile Range Group into four igneous suites. These correspond to discrete stratigraphic units within the three major volcanic-bearing formations (oldest to youngest; Puddler Creek Formation, Mount Windsor Formation, Trooper Creek Formation) of the Seventy Mile Range.

The new data for the Trooper Creek Formation are comparable with trends identified within the formation throughout the remainder of the Seventy Mile Range Group (e.g. Stolz, 1995; Doyle 1997b). On a plot of Zr/TiO_2 versus Nb/Y the samples range in composition from rhyodacite to andesite (Fig. 3B). Some lavas and intrusions classified as rhyolite petrographically (because they contain 5–7 modal percent quartz phenocrysts, 1–7 mm across) plot in the high-silica dacite field (Fig. 3C). These samples are characterised by having greater than 70 wt% SiO_2 but higher Ti/Zr ratios than rhyolitic lavas from the Mount Windsor Formation (Stolz, 1995). Other lavas and intrusions in the Trooper Creek Formation that generally contain less than 1 modal percent quartz phenocrysts (mapped as rhyodacite and dacite) also plot in the high-silica dacite field or as andesite (Fig. 3B, C; cf. Stolz, 1995).

Overall the range of compositions from high-silica dacite to andesite fall along linear trends which are consistent with the wider sample set reported by Stolz (1995) and Doyle (1997b) (e.g. Fig. 3D–F). The compositions of coherent rocks from the hanging wall (rhyolites 6 and 8) and footwall (dacite 1, rhyodacites 1–3, rhyolites 1–4) of the Highway–Reward deposit are similar and do not appear to vary stratigraphically.

The silicic coherent rocks at Highway–Reward (Trooper Creek Formation) are distinguishable from rhyolites, rhyodacites and dacites in the Mount Windsor Formation by their higher P/Zr and Ti/Zr values. In a plot of TiO_2 vs. Th the former are also generally lower in Th and higher in TiO_2 (Fig. 3G; Stolz, 1995). In the area between Highway–Reward and Trooper Creek prospect, the Mount Windsor Formation rhyolite, rhyodacite and dacite intervals also typically have lower Fe_2O_3 concentrations and higher Y and Rb abundances. Samples from Highway–Reward generally display similar trends to the remainder of the Trooper Creek Formation.

Analyses of volcaniclastic rocks at Highway–Reward were limited to in situ and resedimented hyaloclastite and pumice-crystal breccia and sandstone. The samples of pumice-crystal breccia and sandstone are feldspar-bearing (154/335), feldspar > quartz-bearing (805/213.6 and 259.9) or quartz- and feldspar-bearing (814/251). In plots of

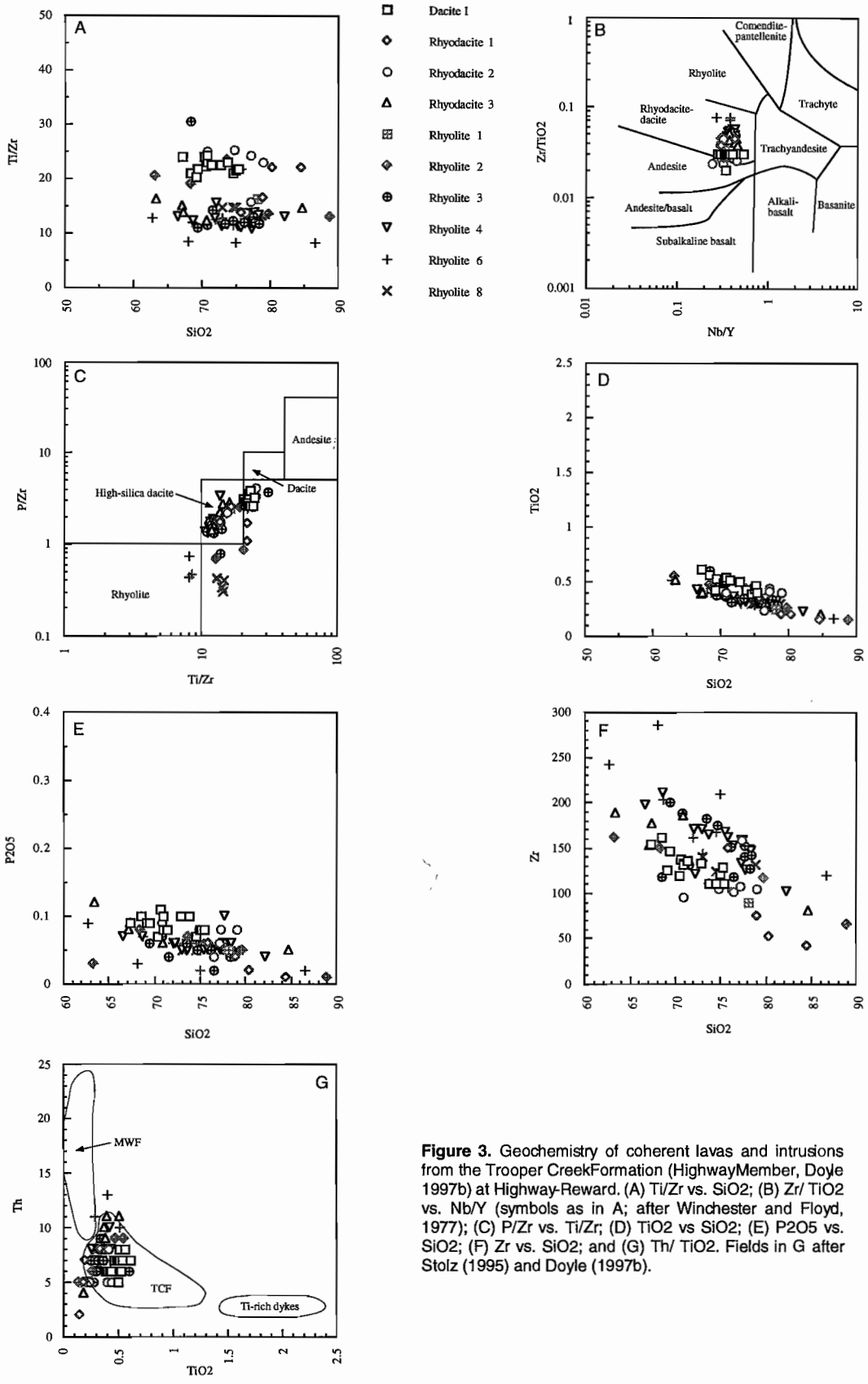

Figure 3. Geochemistry of coherent lavas and intrusions from the Trooper CreekFormation (HighwayMember, Doyle 1997b) at Highway-Reward. (A) Ti/Zr vs. SiO2; (B) Zr/ TiO2 vs. Nb/Y (symbols as in A; after Winchester and Floyd, 1977); (C) P/Zr vs. Ti/Zr; (D) TiO2 vs SiO2; (E) P2O5 vs. SiO2; (F) Zr vs. SiO2; and (G) Th/ TiO2. Fields in G after Stolz (1995) and Doyle (1997b).

Table 2. Summary of the principal lithofacies in the host succession to the Highway-Reward deposit.

Lithofacies	Characteristics	Interpretation
Massive rhyolite to dacite	Aphyric or evenly porphyritic; columnar and tortoise shell jointing; massive or flow banded	Coherent facies of cryptodomes and syn-sedimentary intrusions
Non-stratified rhyolitic to dacitic breccia	Monomictic; poorly sorted; blocky to ragged clasts; clast- to matrix-supported; gradational into coherent facies and/or peperite	Autobreccia and in situ hyaloclastite
Non-stratified sediment-matrix breccia facies	Rhyolitic to dacitic; blocky, ragged and globular-shaped clasts; clast- to matrix-supported; jigsaw-fit texture in matrix-poor breccia; matrix may be siltstone, sandstone or pumice breccia; present along the upper or lower contacts of massive andesite to rhyolite facies; 0.1–1 m thick	Peperite (cf. Busby-Spera and White, 1987; Brooks, 1995)
Stratified, monomictic rhyolitic to dacitic breccia facies	Thick (0.5-11 m), internally massive or graded beds; clast-supported; blocky to elongate jagged clasts; often associated with hyaloclastite, peperite and coherent lava	Gravity-driven collapse and resedimentation of unstable hyaloclastite (cf. Dimroth et al., 1978). Deposits from high-concentration sediment gravity flows
Siltstone-matrix rhyolitic to dacitic breccia	Stratified; polymictic, matrix- to clast-supported; thick (< 7 m); internally massive or normally graded; blocky to ragged clasts locally with jigsaw-fit fabric; siltstone matrix and intraclasts	Gravity-driven collapse of unstable hyaloclastite or peperite from the margins of subaqueous lavas or cryptodomes; deposition from high-concentration sediment gravity flows (? debris flows)
Graded dacitic to rhyolitic pumice breccia and sandstone	Essentially monomictic; normally graded; non-welded; 1–80 m thick; equant to ragged tube pumice, crystal fragments, shards and sparse angular lithic clasts	Resedimentation of subaerial or shallow submarine pyroclastic pumice into a deeper submarine setting; syn-eruptive; down-slope transport by high-concentration turbidity currents
Stratified crystal-rich volcanic sandstone	Essentially monomictic; massive or weakly normally graded; grain supported; rich in crystal fragments and pumice with lesser shards and lithic clasts; 1-50 m thick	Syn-eruptive; crystal concentration during eruption and transportation; deposition from high-concentration, granular turbidity currents
Vitric-crystal-lithic sandstone	Planar, laterally continuous beds; thin (15-70 cm) massive to normally graded crystal-vitric-lithic sandstone and interbedded siltstone; dominantly volcanic; some beds contain non-volcanic detritus	Sandstone beds are deposits from low concentration turbidity currents (Bouma Ta-Te); siltstone predominantly from suspension sedimentation
Massive to laminated siltstone	Laminated or thinly bedded intervals up to 160 m thick; planar, even, continuous beds; in some cases laminae drape small irregularities such as outsize pumice clasts	Predominantly suspension sedimentation; in part water-settled volcanic ash; deposited below storm wave base

Table 3 Form, dimensions and phenocryst populations for sills, cryptodomes and partly extrusive cryptodomes at Highway-Reward.

Unit	Form	Dimensions (m)		Quartz	Feldspar			
		Length	Width	Thickness	%	size (mm)	%	size (mm)
Dacite 1	cryptodome	250	300	>300	—	—	5	0.5-1.5
Rhyodacite 1	sill	150	>250	>100	2-3	0.5-2	6-7	1-2
Rhyodacite 2	cryptodome	175	≥275	50-150	sparse	< 1	2-3	0.5-1.5
Rhyodacite 3	?	>50	>75	>80	2	0.5-3	8-10	1-3
Rhyolite 1	sill	?	?	?	9-10	0.5-4	?	?
Rhyolite 2	cryptodome	>100	>125	120-170	10-12	1-3	6	1-2
Rhyolite 3	cryptodome	175	5 - >150	20-100	6-7	1-3	7	1-3
Rhyolite 4	partly ext.	312	>300	40-120	6-7	1-4	7	1-2
Rhyolite 5	sill	38	25-140	5-10	6-7	1-6	7-8	1-3
Rhyolite 6	sill	150	>300	25 to >60	7	0.5-2	5	1-2
Rhyolite 7	?	>37	>60	>30	4-5	1-3	5	1-3
Rhyolite 8	sill	75	>300	35 to >85	6-7	0.5-7	7	1-2
Rhyolite 9	cryptodome	?	>350	>225	6	1-3	10-12	1-2

P/Zr vs. Ti/Zr and Th vs. TiO_2 the pumice breccia-sandstone samples fall within the field of the Trooper Creek Formation. On a Zr/ TiO_2 vs. Nb/Y plot the samples can be classified as rhyodacites and dacites.

Andesite dykes

Unaltered andesite dykes cross-cut massive sulfide mineralisation at Highway–Reward. The dykes at Highway–Reward plot along a similar trend to data for the Mount Windsor Formation and Trooper Creek Formation suggesting they are probably cogenetic with other lavas and intrusions in the Seventy Mile Range Group (Doyle, 1997b).

Alteration geochemistry

In this section the geochemical data have been assessed in order to: (1) determine the chemical changes which characterise each alteration assemblage and zone; and (2) distinguish any differences in the geochemistry of intense alteration in the footwall and hanging wall to the pyrite pipes.

Alteration facies

The alteration envelope surrounding the Highway–Reward deposit is defined by assemblages of quartz-sericite ± pyrite, chlorite ± anhydrite, sericite, sericite-chlorite-quartz, chlorite-sericite, feldspar (albite & K-feldspar) ± carbonate ± chlorite ± sericite ± quartz, and hematite±quartz±sericite ± chlorite (Doyle, 1997a,b). A quartz-sericite ± pyrite zone occurs beneath the pyrite pipes and extends into the hanging wall lithofacies to more than 60 m on some sections. Within the quartz-sericite ± pyrite zone either quartz or feldspar can be the dominant phase. Quartz-dominant alteration is more widespread in the footwall stringer zone. The most intense and texturally destructive alteration occurs within this zone, and in some cases, in quartz-sericite-altered hanging wall lithofacies. Small domains of chlorite ± anhydrite alteration occur within the quartz-sericite±pyrite zone and along the margins of the pyrite pipes. Sericite-alteration occurs throughout the mineralised zone, but is most common within shear zones at the margins of the pyrite pipes. The quartz-sericite±pyrite zone is enclosed by domains of sericite-chlorite-quartz and chlorite-sericite alteration. Fifty to two hundred metres away from the orebodies, felsic volcanic rocks have altered to assemblages of feldspar (albite & K-feldspar) ± carbonate ± chlorite ± sericite ± quartz, and hematite ± quartz ± sericite ± chlorite (Doyle, 1997a,b).

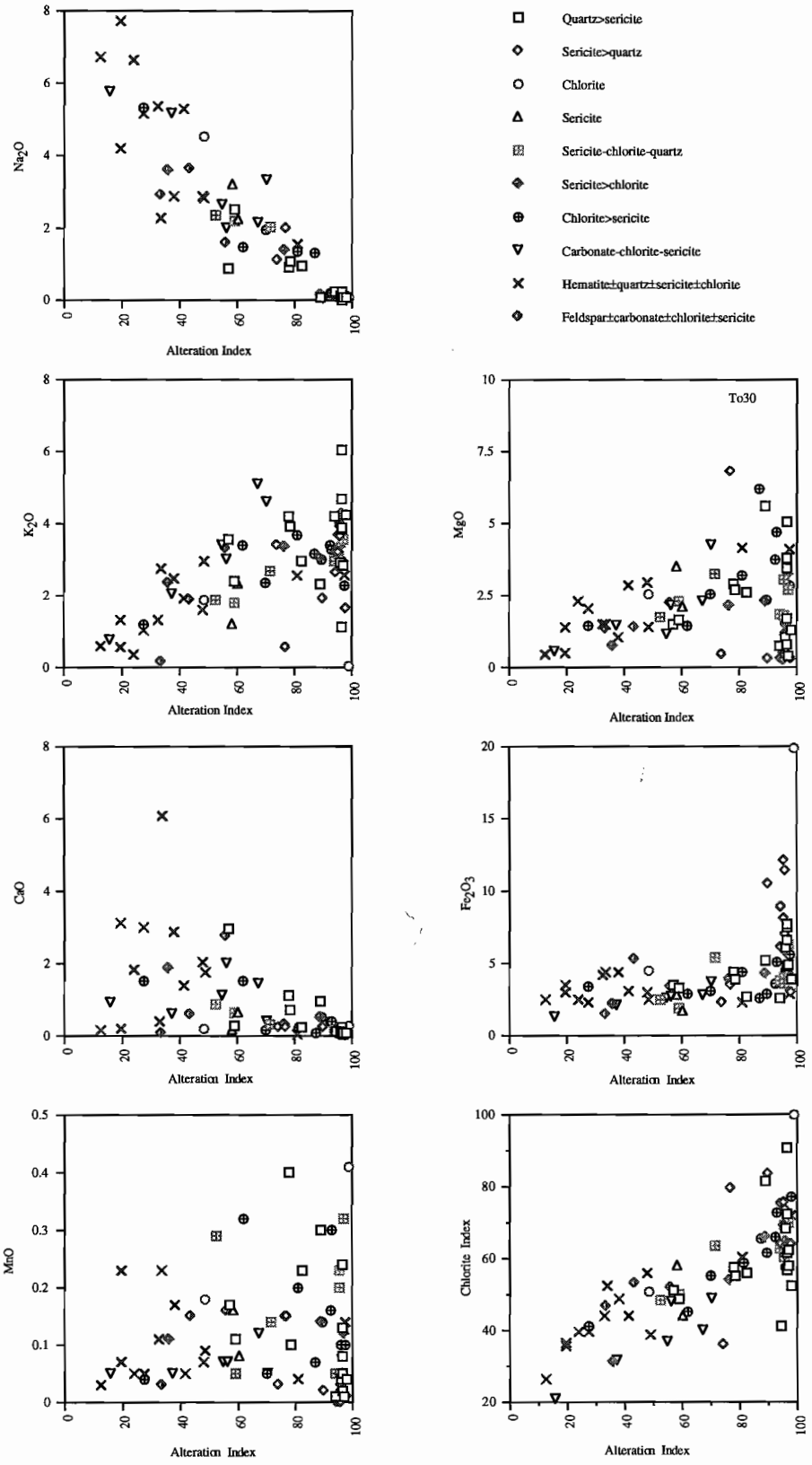

Figure 4. Variation of Na_2O, K_2O, MgO, CaO, Fe_2O_3, MnO and Chlorite Index as a function of Ishikawa Alteration Index

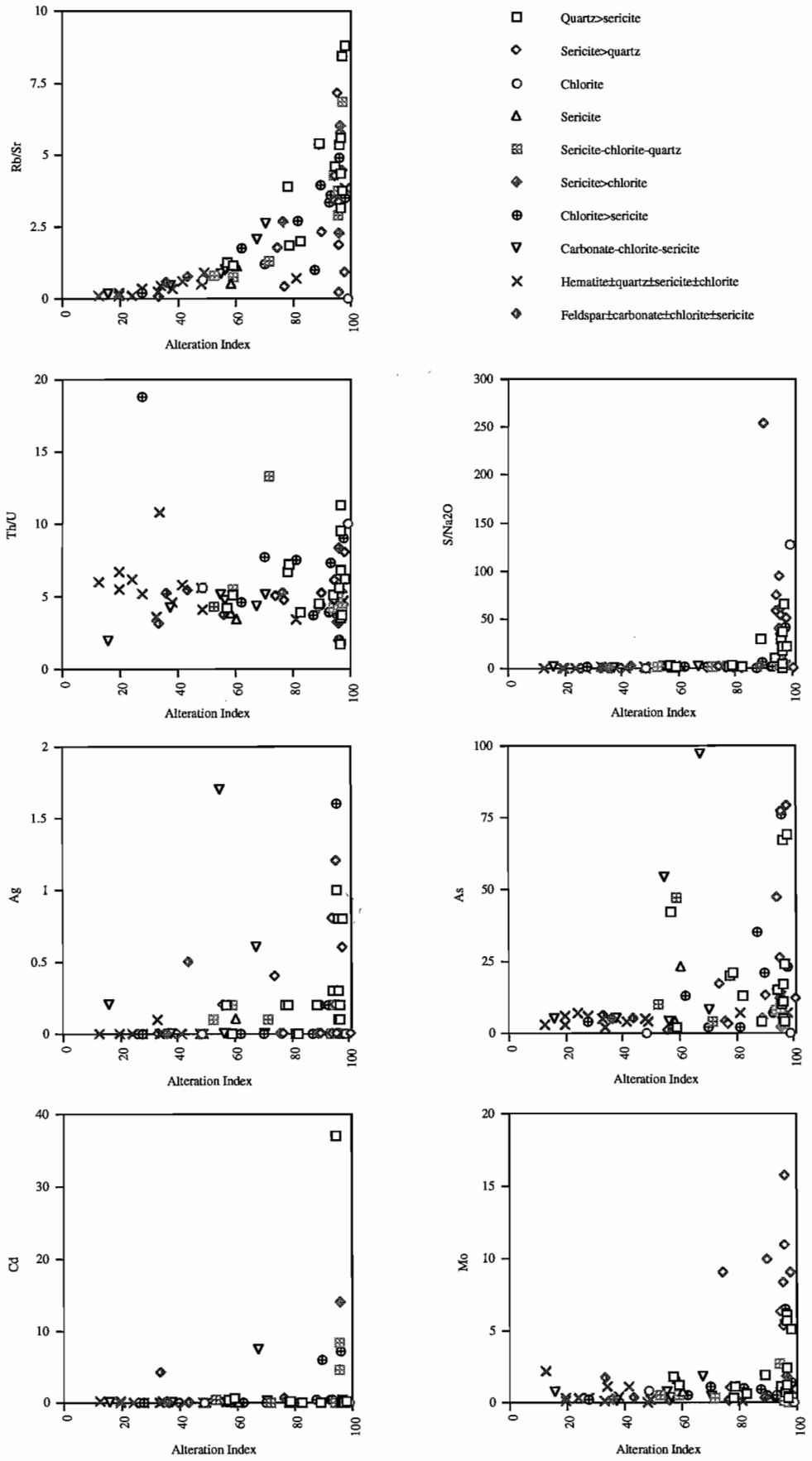

Figure 5. Variation of Rb/Sr, Th/U, S/Na_2O, Ag, As, Cd and Mo as a function of Ishikawa Alteration Index

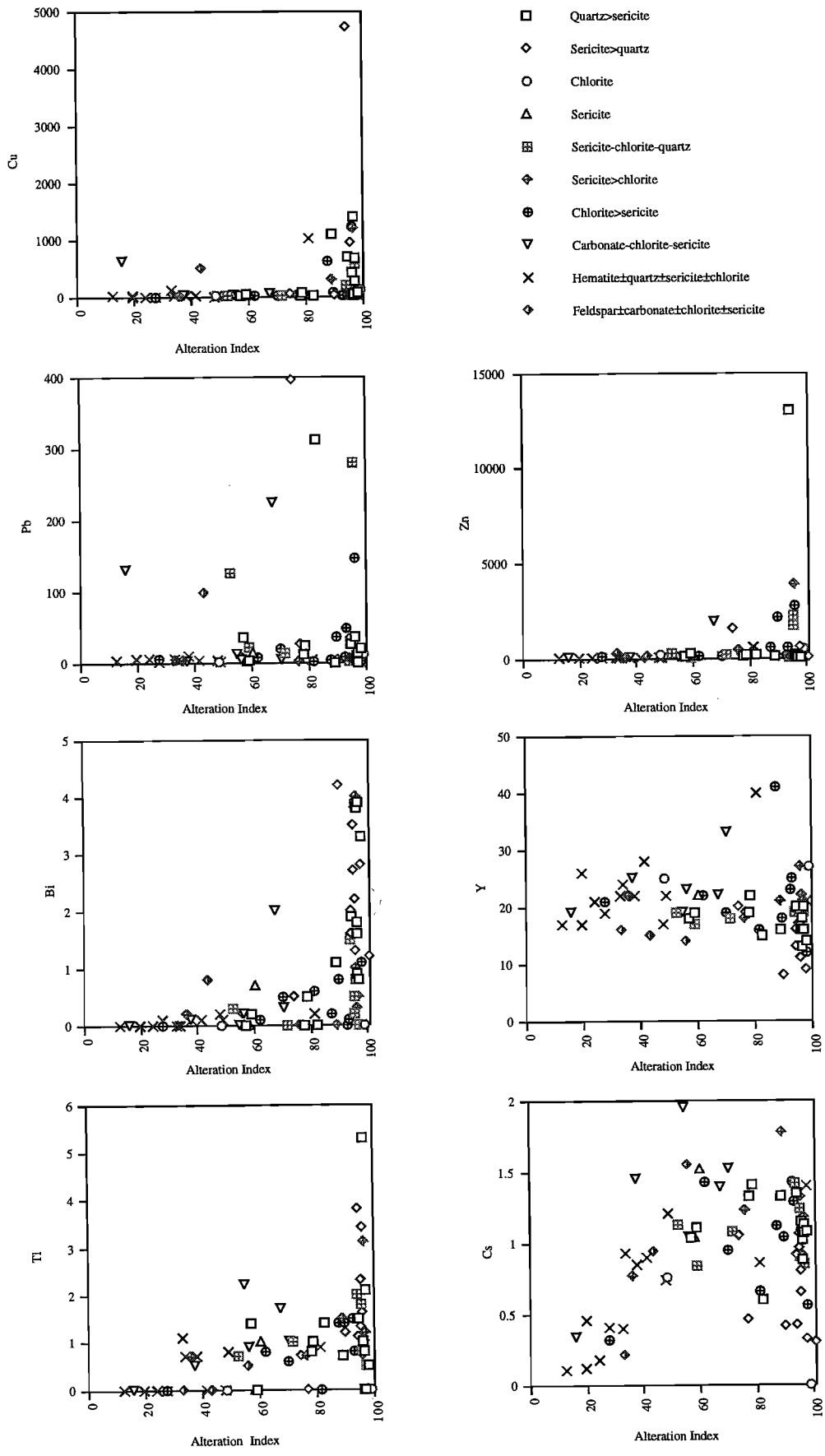

Figure 6. Variation of Cu, Pb, Zn , Bi, Y, Tl and Cs as a function of Ishikawa Alteration Index

Quartz > sericite ± pyrite

The relatively uniform patterns of depletion (Na_2O, MnO, MgO and CaO) and enrichment of (K_2O) within this sample population is reflected in high values for the Ishikawa (1983) Alteration Index (74–100; average 93; Fig. 4). Rb/Sr shows covariance with the Ishikawa Alteration Index (i.e. AI=100(MgO+K_2O)/(MgO+K_2O+Na_2O+CaO)) (Fig. 5). The Chlorite Index (CI) was defined by Large et al. (1996) as CI = (100 (MgO+FeO)/(MgO+FeO+Na_2O+K_2O). CI values for samples from Highway–Reward show similar patterns to the AI (Fig. 4). Concentrations of Bi, S and Fe_2O_3 are elevated in sericite > quartz ± pyrite-altered samples with AI values greater than 90 (Figs 5, 6). In addition, there are sporadic enrichments in Ag, As, Cd, Mo, Sb, Cu, Zn and Pb. There is a broad range of values for Tl, Y, As, Sb, Sc, V, Ni, Th/U, P_2O_5, MnO, and Al_2O_3, but most are within background levels.

Sericite > quartz ± pyrite

Samples showing this style of alteration are often geochemically distinct from those which have altered to quartz > sericite ± pyrite. Sericite > quartz ± pyrite-altered samples are typically enriched in Mo, Ni and Fe_2O_3, show elevated S/Na_2O, and are depleted in Rb/Sr, Cs and Al_2O_3 (Figs 4–6). Y, Ag and possibly MgO are also often low compared to the majority of the more quartz-rich samples. Alteration Index values for sericite > quartz ± pyrite-altered samples range from 56 to 97 (69% greater than 95; Fig. 4). Similar concentrations of Tl, As, Th/U, Bi, Cd, Sb, Se, Sc, V, Cu, Zn, Pb, Na_2O, K_2O, P_2O_5 and MnO occur within samples from both groups. Rare samples contain anomalous Cu, Zn and/or Pb (Fig. 6).

Chlorite ± anhydrite

Analyses of intensely chlorite-altered rock were limited to a single sample (REM 154/335 m) from the footwall of the Highway orebody. The sample has very low Na_2O, K_2O, CaO and extremely high MgO (26.9 wt%) and Fe_2O_3 resulting in a high AI (98) and CI (99) values (Fig. 4). Also enriched are P_2O_5, Al_2O_3 and MnO. Ratios of S/ Na_2O and Th/U are high, whereas the Rb/Sr ratio is very low. Concentration of Se, Ni, Cu, Zn and Pb are within background levels.

Sericite

Sericite altered samples are characterised by having elevated Se. All other elements (Tl, Y, Ag, As, Bi, Cd, Mo, Sb, Se, Cs, Sc, V, Ni, Cu, Pb and ratios (S/ Na_2O, Rb/Sr, Th/U) fall within the range of background levels. One sample has high Zn (216 ppm). AI values for samples which are sericite-altered range from 58 to 60 reflecting moderate concentrations of Na_2O, K_2O, MgO and CaO.

Sericite-chlorite-quartz alteration

As there is a wide range in the proportion of minerals and alteration intensity among samples showing sericite-chlorite-quartz alteration, the geochemical signatures accordingly display considerable variability. A broad spread of MgO, K_2O, Na_2O and CaO values is reflected in the AI (52–96; Fig. 4). Concentrations of Y, Ag, Mo, Sb, Se, Cs, Sc, and ratios of S/ Na_2O and Th/U are consistently within background levels. Tl, Bi, Cd, V, Cu, Zn, Pb, P_2O_5, MnO and ratios of Rb/Sr are high in some samples with AI values greater than 90. One sample (600/195.5 m) has anomalous As.

Sericite > chlorite

These rocks typically have concentrations of Tl, Ag, As, Mo, Sb, Sc, V, Ni, K_2O, P_2O_5, MnO, Al_2O_3 and Fe_2O_3 within the range of background levels. Some display sporadic enrichment in Tl, Y, Bi, Cd and Cs (Fig. 6). The AI values for samples which are sericite > chlorite-altered range from 27 to 97. A few samples (47/103.2 m; 128/139.3 m; 113/161.3; 118/124.4 m) with AI greater than 80 contain elevated Cu and Zn. Samples display a broad range of Na_2O, MgO and CaO values and ratios of Rb/Sr and Th/U.

Chlorite > sericite

Samples which are affected by this style of alteration display sporadic enrichment in Y, Ag, As, Bi, Cd, Mo, Sb, Se, Cu, Zn and Pb. Ratios of S/Na_2O and Th/U are also elevated in a few samples. Th/U, Cs, MgO, CaO, Na_2O, K_2O and P_2O_5 vary widely within the sample set resulting in a broad range in AI values (36–97). Rb/Sr shows covariance with the AI. Values for all other elements (e.g. Tl, Sc, V, Ni, MnO, Al_2O_3, Fe_2O_3) are consistently at background levels.

Feldspar (albite & K-feldspar) ± carbonate ± chlorite ± sericite ± quartz

The alteration assemblage within these samples is found throughout the Trooper Creek Formation and interpreted as the greenschist facies equivalent of early diagenetic minerals (Doyle, 1997a,b). The assemblage is preferentially found within formerly glassy volcanic rocks (including lavas, intrusions and pumice breccia units) and can be considered as background alteration. Samples which display this style of alteration are moderately enriched in Na_2O and contain low concentrations of K_2O, Rb and Ba relative to hydrothermally altered samples. Concentrations of these elements are reflected in low values for the AI and in plots of S/ Na_2O and Rb/Sr (Fig. 4). Rb/Sr ratios mirror the AI, reflecting the depletion of K_2O and Rb relative to Sr. Typically these rocks also have low concentrations of chalcophile elements including Cu, Pb, Zn, As, Ag, Tl, Sb and Mo. The exception is one sample (REM 506/149.2 m) which has elevated Cu (487 ppm), Pb (98 ppm), Zn (119 ppm), Ag (0.5 ppm) and Bi (0.8 ppm). Enrichment in this sample may be attributed to overprinting sericite-chlorite alteration. One other exception is sample (HMO 52/130.3 m) which has elevated concentrations of Cd, Mo, Zn, SiO_2 and low Al_2O_3, which may also be due to overprinting alteration.

Carbonate-chlorite-sericite ± albite

Minor carbonate occurs throughout the alteration envelope as a replacement of feldspar. In some cases, carbonate minerals have also replaced part of the groundmass. Al values for samples which are carbonate-chlorite-sericite ± albite-altered range from 16 to 70 reflecting a broad range in concentrations of Na_2O, K_2O, MgO and CaO. Concentrations of Tl, Y, Ag, As, Bi, Cd, Mo, Sb, Se, Sc, V, Ni, P_2O_5, MnO and Fe_2O_3 and ratios of S/ Na_2O and Th/U are generally within background levels. However, there are some exceptions: (1) sample (803/127.1 m) is enriched in Tl, Ag, As, Bi, Sb, V, Zn, Pb and Al_2O_3; (2) sample (800/143.4 m) contains elevated Y, Ag, and Al_2O_3; (3) sample (814/314.1 m) contains the highest Ag of all the samples analysed and is also enriched in Tl, As and Sb; and (4) anomalous Cu and Pb characterise sample 814/140.1, although the AI is only 16. Overall, values for the various Alteration Indices are relatively low.

Hematite ± quartz ± sericite ± chlorite

Hematite-rich alteration is also regionally distributed and interpreted to have deposited from low temperature fluids circulating through the volcanic package (Doyle, 1996; Doyle, 1997a, b). Domains of hematite, chlorite-sericite and chlorite-carbonate often generate patchy and mottled textures. As the proportions of minerals varies widely between samples, chemical patterns associated with this style of alteration display significant variability. Na_2O values range from around 0.1 to 7.7 wt% and K_2O concentrations from 0.5 to 10 wt % (Fig. 4). These elemental variations are reflected in the AI (12 to 97). The progressive increase in AI is accompanied by enrichment in MgO, Cs, Bi and Rb/Sr. Rare samples are enriched in Y (52/126.6 m), Th/U (804/127.5 m), V (814/185.35 m), Cu (52/126.6 m) and Zn (52/126.6 m). The samples typically have low concentrations of S, Tl, Ag, As, Bi, Cd, Mo, Sb, Se, Ni and Pb. They display a broad range in Sc, V, P_2O_5, CaO and MnO values. Surprisingly, Fe_2O_3 contents are not elevated above background levels.

Variations in alteration chemistry between the footwall and hanging wall

At Highway, a zone of strong hydrothermal alteration extends for at least 60 m into the hanging wall volcanic succession. A similar, but less well preserved, alteration plume extents above the Reward pyrite-pipe. As sampling was undertaken on selected cross-sections through the orebody, the spatial variability in geochemical data can be evaluated.

Na_2O and CaO

Sodium and CaO are consistently depleted to values mostly less than 0.1 wt% Na_2O and 1 wt% CaO in the footwall and hanging wall lithofacies (Fig. 7). Depletion in these elements extends to at least 100 m below the Highway and Reward pipes and 40 m above the Highway orebody. Stringer vein-style mineralisation and strong silica-sericite alteration extends for at least 90 m north (10300N) and 150 m south (9850N) of the Highway and Reward pipes. However, the extent of the Na_2O and CaO halo is poorly constrained and further sampling is required. The halo occurs in quartz-sericite-altered samples 12 m south of the pyrite-pipes. CaO depletion is recorded in DDH 600/195.5 m, 90 m north of the Reward pipe.

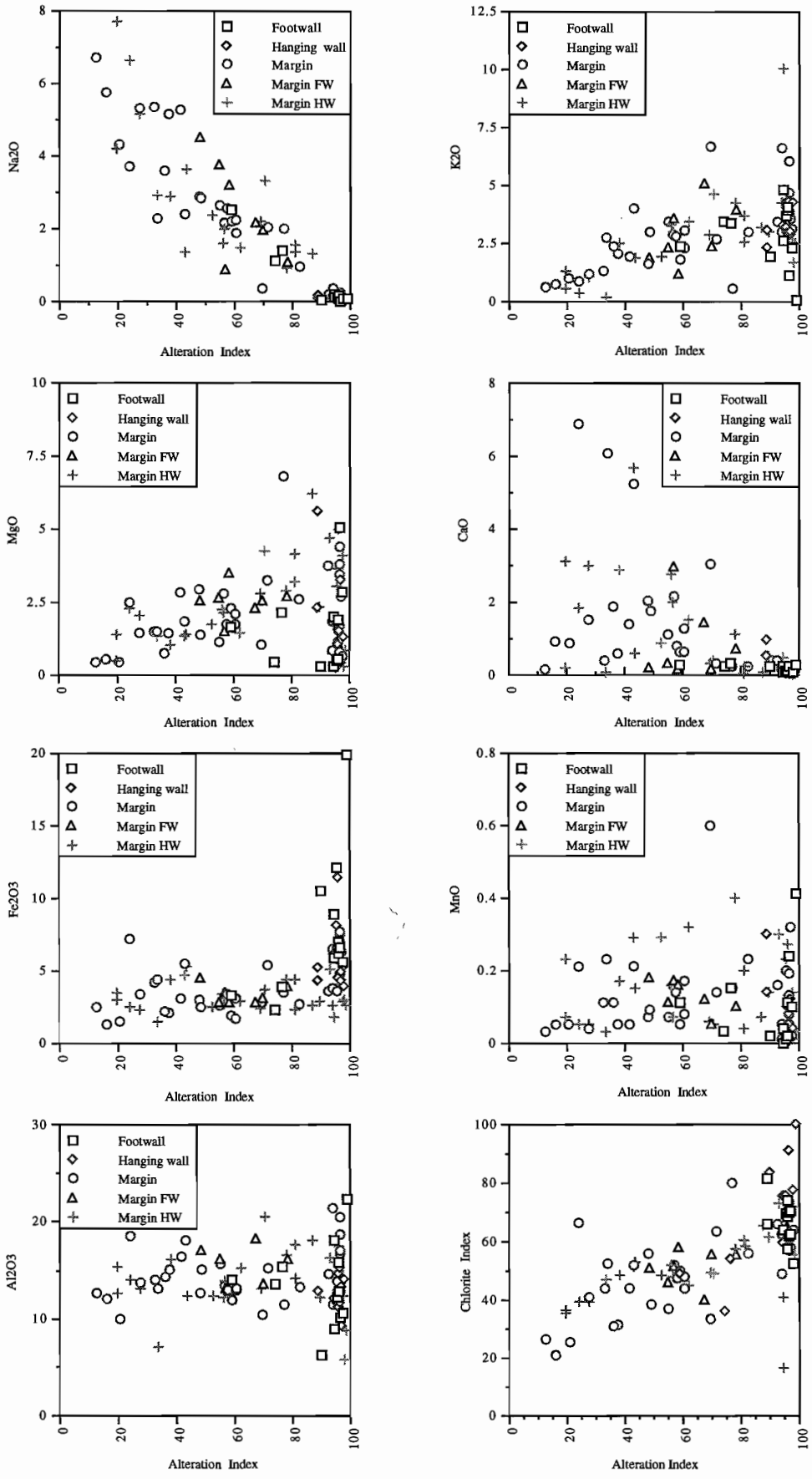

Figure 7 . Variation of Na_2O, K2O, MgO, CaO, Fe_2O_3, MnO, Al_2O_3 and Chlorite Index as a function of Ishikawa Alteration Index.

However, Na_2O values for this sample are within the range of background levels. Sodium is generally elevated (around 1–8 wt%) in lithologies marginal to the orebodies, but some samples exhibit strong depletion to values of 0.1 to 0.9 wt%. CaO concentrations are more sporadic and range from 0.04 to 6.9 wt%

MgO and K_2O

Intense footwall and hanging wall alteration are characterised by high K_2O, coupled with depletion MgO, although the elemental patterns are more erratic than for Na_2O and CaO (Fig. 7). Hanging wall alteration has more uniform concentrations of K_2O and MgO than lithofacies in the footwall.

Alteration Indices

The AI is consistently high within hanging wall lithofacies (89–97), and although values for footwall samples are generally greater than 90, rare samples have values as low as 59. Alteration Index values for the remainder of the sample population range from 12 to 98 (Fig. 7). The highest values are for samples altered to assemblages of sericite-quartz (19%), chlorite-sericite (23%), sericite-chlorite-quartz (48%) and hematite-sericite-quartz (<1%). In hanging wall lithofacies, CI values range between 52 and 81. As the alteration mineralogy in the footwall lithofacies varies, CI patterns are more erratic (35–99). The highest values (99) occur within the chlorite-altered pumice breccia from beneath the Highway orebody. CI values for samples marginal to the orebodies vary widely (16–79), but are mostly less than 60.

Rb/Sr ratio

High Rb/Sr ratios are also a good indicator of intense hydrothermal alteration, and because values are generally higher in the hanging wall (mostly 4.2 to 8.7) than the footwall (1.1 to 4.5), may discriminate the ore position (Fig. 8). The exception is one intensely quartz-sericite-altered sample (113/77.3 m) from the hanging wall to the Highway pipe which has a Rb/Sr ratio of 1.1. Variable Rb/Sr (0.05–5.5) in porphyries marginal to the orebodies relate to different alteration assemblages and intensities. A few samples with elevated Rb/Sr and AI values fall within the field defined by hanging wall samples.

Cu, Pb, Zn

Copper exhibits strong enrichment to values of up to 4706 ppm in hanging wall lithofacies. Anomalous values of greater than 200 ppm Cu and AI > 80 occur within a few samples from the footwall and margins of the orebodies. The highest values for Pb (>50 ppm) and Zn (>100 ppm) are in lithofacies from the footwall, hanging wall and margin of the deposit with AI values greater than 50 (Fig. 9).

Ag, Mo, As, Bi, S/ Na_2O

Anomalous values of greater than 0.3ppm Ag, 4ppm Mo, 1ppm Bi and ratios of S/ Na_2O exceeding 10 are limited to samples with AI values of greater than 80 (Figs. 8,9). These include samples from the footwall and hanging wall and lithofacies distal (>400 m) to the pyrite pipes.

MnO, Al_2O_3 *and* P_2O_5

MnO, Al_2O_3 and P_2O_5 values for footwall and hanging wall lithofacies generally fall with the range of background levels, with sporadic enrichment and depletion at AI values greater than 90 (Fig. 7). MnO values greater than 0.4 wt% occur as intense chlorite alteration in dacitic pumice breccia beneath the Highway orebody.

Th/U, Tl, Sb and As

Stolz et al. (1996), Large (1996) and Large and Allen (1997) demonstrated that the Th/U ratio and concentrations of Tl, Sb and As are useful in defining the ore position at Hercules and Rosebery. Th/U ratios in the footwall and hanging wall of the Highway–Reward deposit are generally within the range of background concentrations (3–8; Fig. 8). The most anomalous Th/U ratios (8–15) occur in lithofacies in the footwall and away from the orebodies. Tl, Sb and As patterns are erratic with no clear trends of enrichment or depletion in the footwall and hanging wall lithofacies.

Other elements

Samples from the footwall and hanging wall display a broad range in V, Y, Ni, Nb, Ce, La Cd, Cs, Sc and Se values which are consistent with the remainder of the sample population. Anomalous concentrations of greater than 0.5 ppm Bi are largely restricted to

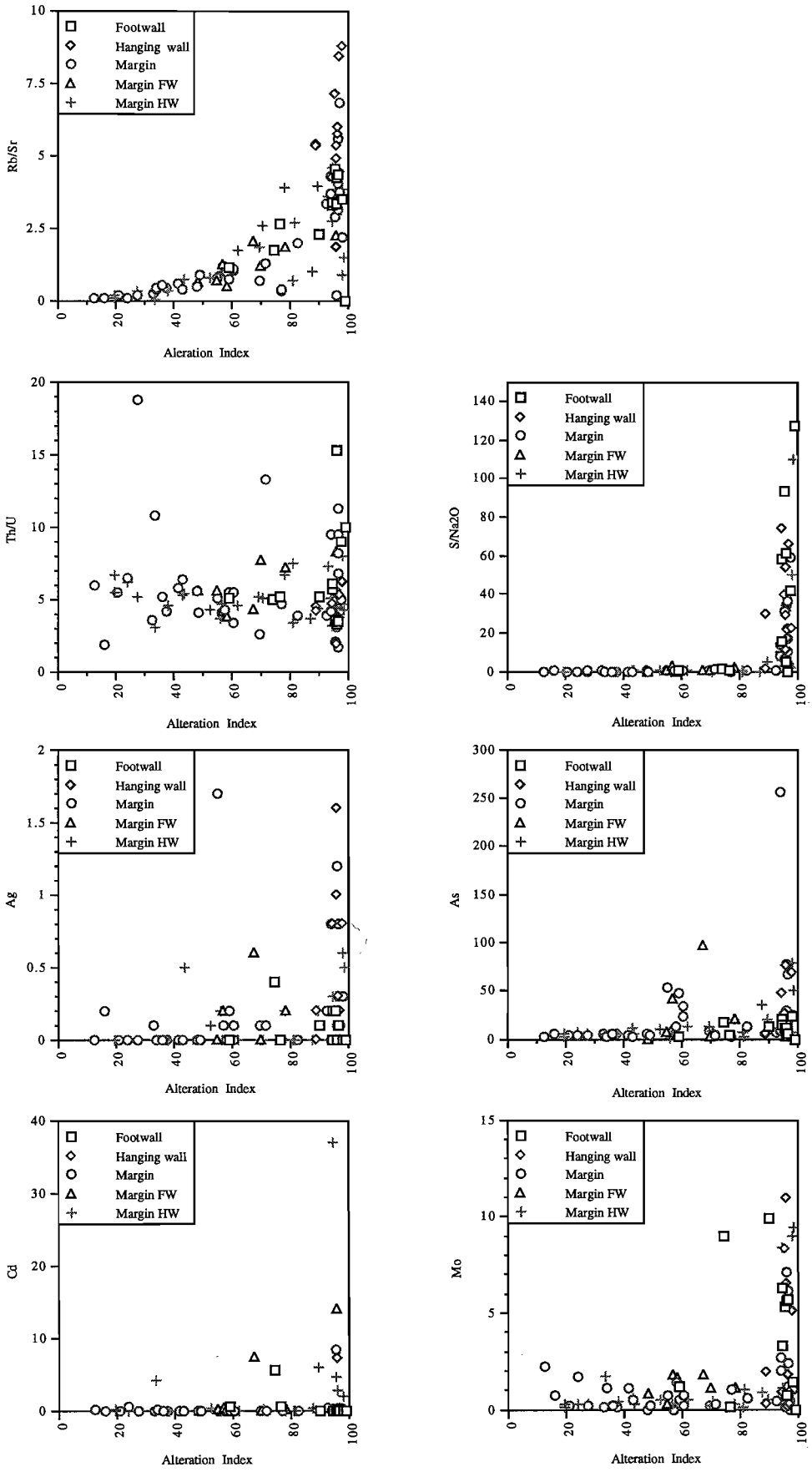

Figure 8 Variation of Rb/Sr, Th/U, S/Na_2O, Ag, As, Cd and Mo as a function of Ishikawa Alteration Index.

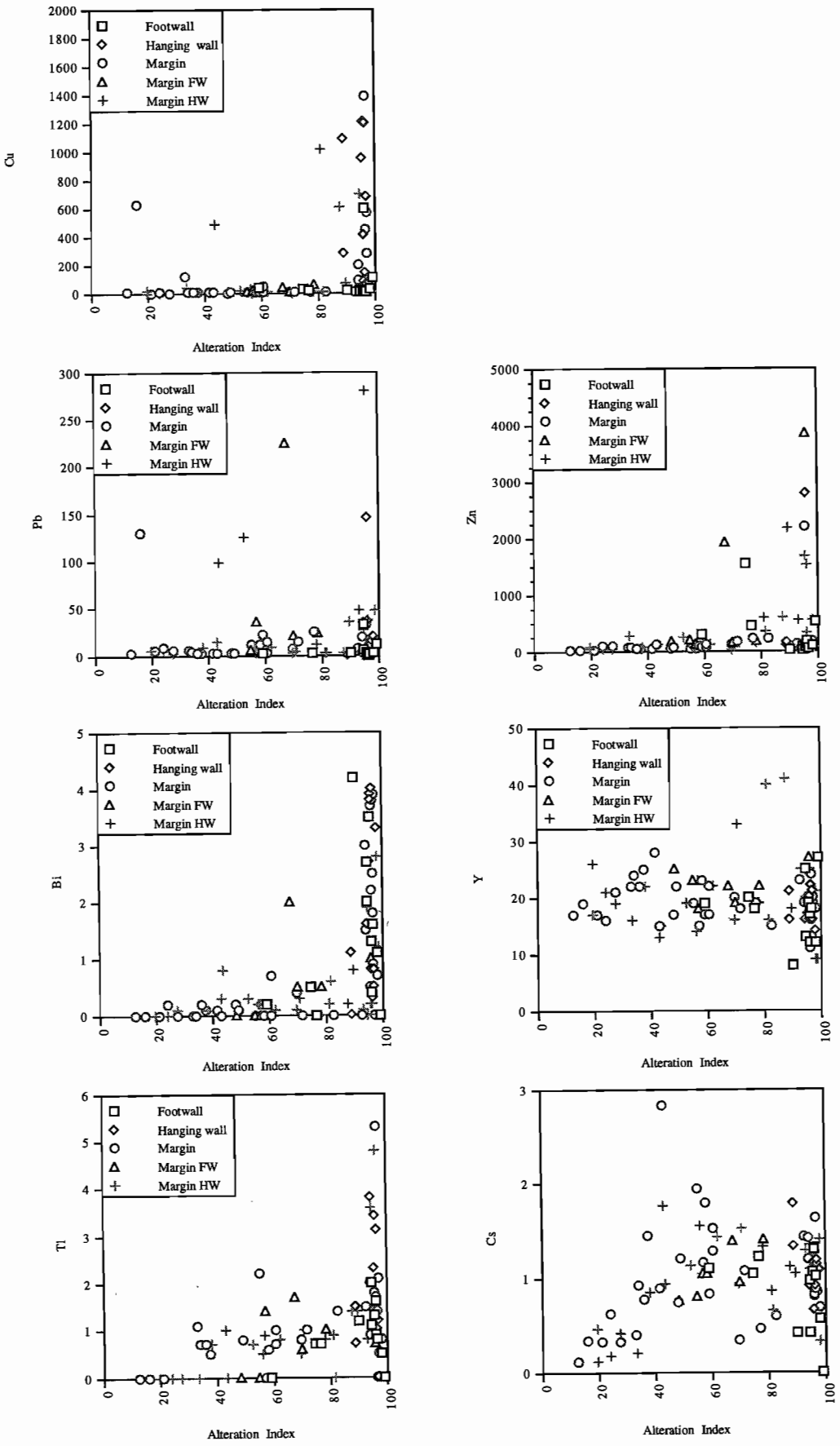

Figure 9 Variation of Cu, Pb, Zn, Bi, Y, Tl and Cs as a function of Ishikawa Alteration Index.

samples with high (>80) AI values. These samples are mostly from the footwall and hanging wall of the orebodies, but some are from lithofacies distal to mineralisation (e.g. 814/613.1 m).

Conclusions

A detailed analysis of the Highway-Reward VHMS deposit has provided insights the geochemical characteristics of hydrothermal alteration associated with sub-seafloor replacement style VHMS deposits. The principal findings of the research are:

- The Highway-Reward massive sulfide deposit is hosted by a syn-sedimentary intrusion-dominated volcanic package emplaced in a submarine (below storm wave base) environment.
- The sills and cryptodomes range in composition from high-silica dacite to rhyolite.
- Compositions of coherent rocks from the footwall and hanging wall are similar, and comparable with felsic lavas and intrusions in the remainder of the Trooper Creek Formation (e.g. Stolz, 1995; Doyle, 1997a,b).
- The footwall and hanging wall alteration haloes are characterised by depletion in Na_2O, CaO and MgO, coupled with high K_2O values.
- The Na_2O and CaO haloes extend to at least 40 m into the hanging wall package and 100 m below the pyrite pipes.
- The Ishikawa (1983) Alteration Index, Chlorite Index (Large et al., 1996) and Rb/Sr ratio also provide vectors to mineralisation.
- Rb/Sr ratios are generally higher in the hanging wall alteration halo than the footwall, and may discriminate the ore position.
- Tl, Sb, As and Th/U have been used to define the favourable horizon at Hercules and Rosebery (e.g. Stolz et al., 1996). At Highway-Reward, patterns for these elements are erratic with no clear trends of enrichment or depletion.

References

Beams S., Laing W. and O'Neill D., 1989. The exploration history and geology of the polymetallic Reward deposit, Mt Windsor Volcanic Belt, north Queensland. North Queensland Gold '89 Conference, Townsville, Queensland, 95-102.

Beams S.D., Laurie J.P. and O'Neill D.M., 1990. Reward polymetallic sulfide deposit. In: Hughes, F. E. (ed.) Geology of the mineral deposits of Australia and Papua New Guinea. Australasian Inst. Mining Metall. Mon., 14: 1339-1543.

Berry R.F., Huston D.L., Stolz A.J., Hill A.P., Beams S.D., Kuronen U. and Taube A., 1992. Stratigraphy, structure, and volcanic-hosted mineralisation of the Mount Windsor Subprovince, north Queensland, Australia. Econ. Geol., 87: 739-763.

Brooks E.R., 1995. Palaeozoic fluidisation, folding, and peperite formation, northern Sierra Nevada, California. Can. J. Earth Sci., 32: 314-324.

Busby-Spera C.J. and White J.D.L., 1987. Variation in peperite textures associated with differing host-sediment properties. Bull. Volc., 49: 765-775.

Dimroth E., Cousineau P., Leduc M. and Sanschagrin Y., 1978. Structure and organisation of Archean basalt flows, Rouyn-Noranda area, Quebec, Canada. Can. J. Earth Sci., 15: 902-918.

Doyle M.G., 1995. Preliminary investigation of alteration at the Highway and Reward deposits, Mount Windsor Volcanics, Queensland. AMIRA - P439, Report 1: 149-160

Doyle M.G., 1996. Volcanic influences in the formation of iron oxide-silica deposits in a volcanogenic-massive sulfide terrain, Mount Windsor Volcanic belt, Queensland. AMIRA - P439, Report 3: 87-142.

Doyle M.G., 1997a. Alteration associated with sub-seafloor replacement style massive sulfide deposits: evidence from the Cambro-Ordovician Highway-Reward deposit, Mount Windsor Subprovince. AMIRA - P439, Report 4: 231-257.

Doyle M.G., 1997b. A Cambro-Ordovician submarine volcanic succession hosting massive sulfide mineralisation: Mount Windsor Subprovince, Queensland. [Unpub. Ph.D thesis]. University of Tasmania, 261 pp.

Galley A.G., Watkinson D.H., Jonasson I.R. and Riverin G., 1995. The subsea-floor formation of volcanic-hosted massive sulfide: Evidence from the Ansil deposit, Rouyn-Noranda, Canada. Econ. Geol., 90: 2006-2017.

Huston D.L., 1992. Geological and geochemical controls on mineralisation at the Reward deposit: detailed studies of the Highway pipe. [unpub.] CODES, University of Tasmania. 31 pp.

Ishikawa, Y., Sawaguchi, T., Iwaya, S. and Horiuchi, M., 1976. Delineation of prospecting targets for Kuroko deposits based on modes of volcanism and underlying dacite and alteration haloes. Mining Geology, 26: 105-117.

Jack D.J., 1989. Hellyer host rock alteration [Unpub. M.Sc. thesis]. University of Tasmania, 182 pp.

Khin Zaw and Large R.R., 1992. The precious metal-rich South Hercules mineralisation, western Tasmania: A possible subsea-floor replacement volcanic-hosted massive sulfide deposit. Econ. Geol., 87: 931-952.

Laing W.P., 1988. Structure of the Reward deposit, north Quensland. Unpublished report to Terra Search Pty. Ltd.

Large R.R., 1992. Australian volcanic-hosted massive sulfide deposits: features, styles, and genetic models. Econ. Geol., 87: 471-510.

Large, R.R., 1996. The Hercules-Mt Read traverse: relationships between volcanic mineralogy, alteration and geochemistry: AMIRA - P439, Report 3: 153-234.

Large, R.R., Stolz, A.J. and Duhig, N., 1996. Preliminary assessment of MRV geochemical databases in terms of possible vectors to ore. AMIRA - P439, Report 2. 197-209.

Large, R.R and Allen, R. 1997. Preliminary report on the Rosebery lithogeochemical halo study. AMIRA - P439, Report 4. 259-330.

MacLean W.H. and Kranidiotis P., 1987. Immobile elements as monitors of mass transfer in hydrothermal alteration: Phelps Dodge massive sulfide deposit, Matagami, Quebec. Econ. Geol., 82: 951-962.

Norrish K. and Chappell B.W., 1977. X-ray fluorescence spectrography. In: Zussman, J. (eds.) Physical methods in determinative mineralogy. New York, Academic Press, 161-214.

Rollinson H., 1993. Using geochemical data: evaluation, presentation, interpretation. Longman scientific and technical, 352 pp.

Stolz A.J., 1995. Geochemistry of the Mount Windsor Volcanics: Implications for the Tectonic setting of the Cambro-Ordovician volcanic-hosted massive sulfide mineralisation in Northeastern Australia. Econ. Geol., 90: 1080-1097.

Stolz J., Allen, R., Gifkins, C., McPhie J. and Blake M., 1997. Petrographic and geochemical characteristics of alteration from the Macintosh Dam-Anthony Road-Mt Black traverse, Mt Read Volcanic Belt. AMIRA - P439, Report 4, 1-25.

Whitford D., McPherson W.P.A. and Wallace D.B., 1989. Geochemistry of the host rocks to the volcanogenic massive sulfide deposits at Que River, Tasmania. Econ. Geol., 84: 1-21.

Winchester J.A., and Floyd, R.A., 1977. Geochemical discrimination of different magma series and their differentiation products using immobile elements. Chem. Geol. 20: 325–344.

Appendix 1: Major (wt%) and trace (ppm) element analyses – Highway-Reward deposit, Mount Windsor Subprovince

Sample	36/123.5	36/197	36/349.9	39/403.8	40/210	47/103.2	47/320.7	52/130.3	52/126.6 m	52/187.5 m	113/77.3 m	113/112.3 m	113/135.45 m	113/161.3 m	113/178.9 m	116/182.8	118/124.4 m
Lithology	Rhyodacite 3	Rhyolite 2	Rhyolite 1	Rhyodacite 2	Rhyolite 4	Rhyolite 6	Rhyolite 4	Rhyolite 6	Rhyolite 6	Rhyolite 4	Rhyolite 3	Rhyolite 3	Rhyolite 3	Rhyolite 3	Rhyolite 3	Rhyolite 4	Rhyolite 3
Section	10200N	10200N	10200N	10100N	9975N	10025N	10025N	10025N	10025	10025N	10075N	10075N	10075N	10075N	10075N	10137.5N	10025N
Position	MAR/HW	MAR/HW	FW	MAR/FW	FW	HW/MAR	FW/MAR	MAR/HW	HW/MAR	MAR	HW	HW	HW	HW/MAR	HW/MAR	HW/MAR	HW/MAR
SiO2	84.75	88.89	78.12	77.29	78.45	68.06	75.88	86.6	74.93	78.23	71.53	76.50	78.33	69.46	76.23	68.7	78.45
TiO2	0.19	0.14	0.24	0.41	0.32	0.4	0.29	0.16	0.28	0.30	0.31	0.27	0.25	0.37	0.30	0.43	0.28
Al2O3	8.74	5.79	10.57	11.62	13.51	18.07	12.83	7.2	14.24	12.48	12.63	11.59	11.23	16.23	13.03	17.41	12.24
Fe2O3	2.55	3	5.57	5.83	2.28	2.53	2.75	1.5	2.25	3.57	11.33	8.03	6.03	5.06	4.00	3.87	2.89
MnO	0.03	0.01	0.1	0.03	0.03	0.07	0.16	0.03	0.04	0.20	<0.01	<0.01	0.04	0.30	0.23	0.13	0.14
MgO	0.81	0.26	2.84	1.06	0.45	6.16	3.49	1.33	4.14	1.80	0.36	0.25	1.01	4.66	3.02	5	2.33
CaO	0.04	0	0.06	0.09	0.23	0.05	0.15	0.06	0.03	0.06	0.01	0.01	0.07	0.39	0.17	0.14	0.51
Na2O	0.01	0.04	0.06	0.1	1.11	1.32	3.17	2.91	1.54	0.18	0.15	0.15	0.09	0.20	0.12	0.21	0.11
K2O	2.5	1.63	2.28	3.36	3.39	3.16	1.17	0.16	2.54	3.12	3.64	3.18	2.90	3.28	2.86	3.54	2.98
P2O5	0.05	0.01	0.05	0.08	0.06	0.03	0.05	0.02	0.02	0.06	0.04	0.02	0.04	0.06	0.05	0.07	0.05
LOI	2.36	2.33	3.72	3.62	2.57	4.83	2.38	1.24	3.44	3.05	7.12	5.44	3.58	4.06	3.13	4.19	2.98
Total	100	100	100	100	100	100	100	100	100	100	100	100	100	100	100	100	100
P/Zr	2.74	0.67	2.43	2.21	1.78	0.46	1.36	0.73	0.43	1.84	1.46	0.79	1.44	1.37	1.49	1.45	1.58
Ti/Zr	14.29	12.91	16.02	15.57	13.01	8.39	10.83	8.03	8.05	12.24	14.01	13.63	11.86	10.99	11.86	12.23	11.75
Nb/Y	0.39	0.41	0.41	0.30	0.41	0.38	0.45	0.39	0.27	0.40	0.32	0.35	0.43	0.40	0.41	0.45	0.39
Alt. index	98.51	97.93	97.71	95.88	74.13	87.18	58.40	33.41	80.99	95.35	96.06	95.52	95.91	93.12	95.32	96.06	89.57
Chl. index	55.30	63.93	77.04	64.57	35.73	65.32	57.88	46.61	60.18	60.34	73.56	69.15	68.22	72.62	68.93	69.34	61.44
Mn-CB index	11.93	5.65	31.18	10.13	10.54	14.34	28.74	10.50	9.93	38.28	0.28	0.29	14.07	49.62	44.95	27.75	38.65
Sc	7	5	8	17	9	12	9	4	9	7	7	8	7	9	8	13	7
V	22	14	24	36	25	14	23	6	11	19	39	20	16	28	19	30	20
Cr	NA	NA	NA	NA	NA	NA	NA	NA	<1	2	2	2	2	3	2	NA	2
Ni	4	6	3	2	3	3	3	5	1	<1	2	3	<1	1	<1	4	<1
Cu	10	93	25	83	26	603	2	32	1015	11	71	944	403	3	48	5	66
Zn	56	538	92	3841	1543	576	216	264	589	2184	80	36	158	531	1654	323	2157
Pb	48	18	2	<1.5	396	3	2	4	3	32	5	5	36	48	280	<1.5	36
Rb	51.1	32	45.4	78.5	68	75.4	29.8	4.1	61	66	64	57	64	75	71	68.9	67
Sr	35	36	13	35	39	79	61	104	89	23	35	8	12	21	19	23	17
Y	9	9	12	27	20	41	19	16	40	20	20	17	16	25	19	25	18
Zr	80	65	90	158	147	286	161	120	210	148	131	118	127	200	151	211	142
Nb	4	4	5	8	8	15	9	6	11	8	6	6	7	10	8	11	7
Ba	2853	2122	865	1547	1347	1445	419	213	924	1881	1444	839	1152	986	939	5181	1062
Th	4	5	5	8	8	13	7	5	11	7	7	5	7	8	6	8	6
Ag	0.5	0.6	<0.1	<0.1	0.4	<0.1	<0.1	<0.1	<0.1	0.2	<0.1	0.2	1	<0.1	0.3	0.1	0.2
As	51	79	23	2	17	35	4	6	7	7	14	26	10	8	11	6	21
Bi	1.2	2.8	1.1	1	0.5	0.2	<0.1	<0.1	0.2	0.5	3.8	2.7	0.8	0.1	0.2	0.2	0.8
Cd	0.1	2	<0.1	14	5.5	0.3	<0.1	4.1	<0.1	8.3	<0.1	<0.1	<0.1	0.3	4.6	0.1	5.9
Mo	9.4	9	1.4	0.8	9	0.9	1.6	1.7	0.1	0.1	10.9	8.3	0.7	0.5	0.4	0.7	0.5
Sb	1.6	3	0.6	0.5	0.6	1.4	0.5	1.1	1.2	0.8	1.1	4.2	2.3	0.6	1.2	1.4	2.3
Se	<1	<1	<1	<1	<1	3	5	4	<1	<1	1	1.5	<1	<1	<1	<1.5	<1
Cs	0.58	0.32	0.56	0.91	1.05	1.12	1.04	0.21	0.86	0.9	0.65	0.96	1.15	1.29	1.24	1.11	1.04
Tl	<0.5	<0.5	0.5	0.7	0.7	1.4	<0.5	<0.5	0.9	1.8	3.4	2.3	1	0.8	0.8	4.8	1.4
U	0.95	0.63	0.56	0.97	1.62	3.56	1.86	1.63	3.28	1.45	3.76	1.57	1.25	1.1	1.38	1.81	1.39
S	1.1	2.01	2.51	3.35	1.42	0	-0.01	0	<0.01	1.2	8.03	5.87	2.6	0.04	0.35	0.13	0.51
La	9.9	9.7	18.4	16.4	7.4	33.4	15.7	11.1	19	16	24	22	12	28	12	19.7	14
Ce	25.4	25.8	33.3	38.5	25.1	72.6	32.4	24.3	47	39	50	47	26	35	26	52.6	31
Nd	11.1	12.9	14.6	17.2	10.2	32.3	15.2	10.3	23	13	23	18	10	17	11	24.3	12

Ag, Cd, Sb, Cs, Mo, Tl, Bi, U and As by ICP-MS; remainder by XRF

[1] Total Fe as Fe_2O_3

[2] Analyses recalculated to 100% anhydrous

Appendix 1: N

Sample	118/128.1 m	118/162.5 m	123/179.2 m	128/139.3 m	132/122.4 m	132/142.95 m	132/148.05 m	140/97.8	140/248.2	144/157.08	144/316.3	148/268.8	151/163.4	151/258.3	151/350.5	154/170.2 m	154/208.8 m
Lithology	Rhyolite 3	Rhyolite 3	Rhyolite 4	Rhyolite 3	Rhyolite 3	Rhyolite 3	Rhyolite 3	Rhyolite 4	Rhyolite 3	Rhyolite 4	Rhyodacite 2	Rhyodacite 1	Rhyolite 4	Rhyodacite 2	Dacite 1	Rhyolite 4	Rhyodacite 2
Section	10025N	10025N	10075N	10075N	10050N	10050N	10050N	10100N	10100N	10100N	10100N	10200N	10050N	10050N	10050N	10150N	10150N
Position	HW/MAR	HW/MAR	MAR	HW	HW/MAR	HW/MAR	HW/MAR	HW	HW/MAR	MAR/HW	FW	FW/MAR	MAR	MAR	FW	MAR	MAR
SiO2	77.59	77.70	77.51	74.63	70.76	64.24	73.45	72.24	68.49	77.32	76.43	75.86	66.66	79.02	70.88	73.72	77.16
TiO2	0.33	0.28	0.31	0.36	0.36	0.23	0.35	0.31	0.6	0.28	0.23	0.34	0.42	0.4	0.51	0.31	0.43
Al2O3	14.21	12.35	13.16	14.66	14.93	18.08	15.18	12.88	17.69	12.41	10.08	13.57	17.07	11.49	15.87	14.58	12.79
Fe2O3	2.55	2.49	1.62	4.47	6.64	4.65	2.81	5.18	4.32	2.9	6.59	3.08	6.93	3.72	6.12	3.52	4.75
MnO	0.01	0.29	0.08	0.10	0.27	0.29	0.32	0.3	0.2	0.14	0.24	0.05	0.19	0.05	0.11	0.16	0.02
MgO	0.75	1.73	2.09	1.54	3.62	1.35	1.44	5.6	3.19	4.1	5.01	2.51	4.36	1.84	1.87	3.71	0.80
CaO	0.10	0.88	0.63	0.06	0.08	5.68	1.50	0.94	0.24	0.07	0.23	0.16	0.16	0.15	0.12	0.40	0.09
Na2O	0.21	2.36	2.23	0.18	0.20	1.33	1.47	0.06	1.35	0.09	0	1.93	0.13	0.16	0.13	0.17	0.08
K2O	4.19	1.88	2.30	3.95	3.07	3.94	3.40	2.31	3.67	2.55	1.12	2.36	3.78	2.96	4.04	3.38	3.81
P2O5	0.06	0.05	0.06	0.05	0.07	0.20	0.06	0.06	0.1	0.05	0.04	0.06	0.07	0.08	0.08	0.05	0.06
LOI	3.31	2.63	2.88	3.71	3.85	6.11	3.56	3.59	3.8	3.37	4.16	2.88	4.64	2.98	3.36	3.61	4.09
Total	100	100	100	100	100	100	100	100	100	100	100	100	100	100	100	100	100
P/Zr	1.82	1.59	1.71	1.30	1.70	9.10	1.49	2.16	3.69	1.38	1.72	1.75	1.55	3.32	2.62	1.37	2.56
Ti/Zr	12.95	11.77	11.76	12.16	11.34	14.47	11.58	15.33	30.38	10.59	13.62	13.66	12.81	22.82	22.92	11.27	24.03
Nb/Y	0.36	0.37	0.39	0.45	0.43	0.43	0.41	0.41	0.35	0.41	0.32	0.45	0.36	0.31	0.54	0.38	0.46
Alt. index	94.15	52.62	60.49	95.80	95.95	43.02	61.94	88.78	81.18	97.65	96.38	69.97	96.56	93.93	95.94	92.56	96.28
Chl. index	40.90	48.29	43.94	57.40	74.56	51.25	44.89	81.24	58.50	71.76	90.71	55.18	73.05	62.44	63.89	65.97	56.57
Mn-CB index	4.37	46.98	24.35	21.16	46.13	61.88	49.19	62.44	30.85	35.77	70.13	13.33	34.51	17.24	22.63	35.59	7.23
Sc	8	6	8	8	9	5	10	7	6	9	10	11	12	10	14	8	10
V	22	18	20	26	29	14	24	20	17	21	24	31	30	23	42	22	30
Cr	2	2	1	2	3	1	2	NA	NA	NA	NA	NA	NA	NA	NA	2	2
Ni	<1	<1	<1	1	<1	<1	<1	4	3	3	3	4	3	2	6	1	1
Cu	698	13	43	1204	12	2	2	1083	3	24	6	4	444	197	592	6	1385
Zn	13028	233	104	2760	1524	81	112	92	330	132	38	139	160	43	171	120	90
Pb	26	125	14	145	37	15	8	<1.5	2	<1.5	1	20	2	2	2	7	10
Rb	92	46	50	88	70	107	81	59	29.3	57.7	64.7	48.3	80.5	64.5	93.1	70	78
Sr	20	61	46	18	20	231	47	11	11	15	15	41	20	15	22	21	14
Y	20	19	22	19	24	13	22	16	16	21	18	19	24	19	12	23	13
Zr	152	141	158	175	188	97	183	121	118	159	101	149	197	105	133	165	107
Nb	7	7	9	8	10	6	9	6	6	9	6	9	9	6	7	9	6
Ba	1213	1944	1382	1190	954	982	883	1952	406	927	992	635	2128	1234	2523	1791	2222
Th	9	6	8	7	9	12	8	6	6	7	5	8	10	6	7	7	5
Ag	0.3	0.1	0.1	1.6	<0.1	<0.1	<0.1	0.2	<0.1	<0.1	0.1	<0.1	0.1	<0.1	<0.1	0.2	0.8
As	15	10	23	76	13	11	13	4	2	7	5	2	5	8	5	7	17
Bi	1.9	0.3	0.7	3.9	0.4	0.3	0.1	1.1	0.6	<0.1	1.6	0.5	2.5	1.5	0.4	<0.1	3.8
Cd	37	0.4	<0.1	7.2	2.8	<0.1	<0.1	<0.1	<0.1	<0.1	<0.1	<0.1	0.1	<0.1	<0.1	0.3	0.3
Mo	1.1	0.5	0.7	6.5	0.7	0.6	0.5	1.9	1	0.9	5.7	1.1	26	2.7	0.7	0.4	6.1
Sb	4.1	1.3	2.2	4.9	1.1	2.1	0.8	1.6	0.6	1.1	0.7	0.4	0.9	0.7	0.8	0.8	1.3
Se	<1	<1	<1	<1	<1	<1	<1	<1.5	2	<1.5		1 20	<1	<1	<1	<1	1.1
Cs	1.35	1.13	1.52	1.09	1.08	1.77	1.43	1.33	0.66	1.4	1.02	0.95	1.63	1.42	1.3	1.43	1.07
Tl	1.5	0.7	1	0.8	0.9	1	0.8	0.7	<0.5	0.5	0.8	0.6	1.4	2	0.9	1.5	5.3
U	1.79	1.42	2.4	3.57	2.96	2.29	1.74	1.36	0.8	1.49	1.44	1.04	1.22	1.43	0.46	1.83	3.06
S	2.16	0.12	0.51	2.02	0.73	0.07	0.1	1.76	0.57	0.18	-0.01	0.7	1.36	1.26	0.65	0.01	2.89
La	19	12	25	17	15	25	15	8.9	11	19.9	13.4	14.9	17.8	7.5	8.1	15	14
Ce	37	32	55	37	37	52	32	25.7	24.2	40.3	27.1	32.1	37.8	18.2	23.5	35	35
Nd	16	12	21	14	15	21	13	14	10	17.9	14	14.5	16.1	8.5	10.1	13	11

Ag, Cd, Sb, C

[1] Total Fe as

[2] Analyses re

Appendix 1: M

Sample	154/280	154/297.6 m	154/335 m	506/149.2 m	506/224.53 m	515/218.5	551/87.7 m	551/115 m	551/130.85 m	551/301.4 m	551/313.5	558/141.85 m	558/171.9 m	558/240 m	560/124.4	560/316.3	600/184.3
Lithology	Rhyodacite 2	Rhyodacite 2	Dacitic pum. bx	Rhyolite	Rhyolite	Rhyodacite 3	Rhyolite 4	Rhyolite 4	Rhyolite 4	Dacite 1	Dacite 1	Rhyolite 4	Rhyolite 4	Dacite 1	Rhyolite 4	Dacite 1	Rhyolite 8
Section	10150N	10150N	10150N	10400N	10400N	10200N	10100N	10100N	10100N	10100N	10100N	10200N	10200N	10200N	10150N	10150N	10300N
Position	FW	FW	FW	MAR/HW	MAR/HW	MAR	HW	HW	HW	FW	FW	HW	HW	MAR	HW	FW/MAR	MAR
SiO2	74.88	70.66	29.48	74.30	69.17	63.45	82.26	77.35	76.49	72.88	75.2	72.09	77.77	70.41	75.49	68.49	74.95
TiO2	0.44	0.40	0.72	0.34	0.34	0.51	0.22	0.26	0.29	0.50	0.46	0.36	0.29	0.48	0.31	0.56	0.3
Al2O3	12.8	12.23	22.25	12.43	16.58	21.35	9.28	11.56	12.83	15.36	13.97	15.22	12.10	15.27	13.27	17.07	11.55
Fe2O3	6.99	12.07	19.81	5.25	4.34	6.43	4.87	6.16	4.22	3.85	3.29	6.30	6.06	5.39	4.27	4.41	3.43
MnO	0.02	0.01	0.41	0.15	0.40	0.01	0.01	0.08	0.14	0.15	0.11	0.05	<0.01	0.14	0.12	0.18	0.15
MgO	0.54	0.50	26.88	1.40	2.90	0.82	0.38	1.46	2.30	2.11	1.65	1.44	0.29	3.24	3.23	2.55	6.78
CaO	0.11	0.11	0.25	0.59	1.11	0.14	0.05	0.06	0.52	0.30	0.27	0.09	0.15	0.31	0.11	0.19	0.22
Na2O	0.08	0.09	0.05	3.61	0.90	0.33	0.05	0.10	0.14	1.39	2.52	0.13	0.06	2.03	0.08	4.52	1.98
K2O	3.92	3.65	0.01	1.85	4.19	6.59	2.84	2.90	3.03	3.35	2.37	4.26	3.19	2.66	2.94	1.86	0.56
P2O5	0.08	0.09	0.14	0.09	0.08	0.12	0.04	0.05	0.05	0.10	0.08	0.06	0.10	0.07	0.05	0.1	0.06
LOI	4.83	7.60	13.8	3.37	4.31	5.91	4.31	3.25	3.39	2.86	2.6	4.31	4.42	4.06	3.25	2.42	3.12
Total	100	100	100	100	100	100	100	100	100	100	100	100	100	100	100	100	100
P/Zr	3.32	4.04	3.67	5.09	2.44	2.77	1.77	1.71	1.50	3.40	2.73	1.62	3.33	2.66	1.31	2.71	2.12
Ti/Zr	25.10	24.97	25.65	25.65	13.43	16.15	12.80	11.75	11.53	22.40	21.58	12.57	13.72	23.99	11.12	20.84	14.57
Nb/Y	0.33	0.25	0.33	0.30	0.34	0.47	0.37	0.39	0.37	0.42	0.38	0.37	0.40	0.39	0.41	0.35	0.30
Alt. index	95.91	95.43	98.91	43.59	77.85	94.04	96.88	96.31	89.01	76.33	59.03	96.28	94.25	71.61	97.01	48.36	76.94
Chl. index	63.07	75.26	99.87	52.88	57.21	48.84	62.23	69.97	65.82	53.98	48.53	61.85	63.87	63.30	70.08	50.54	79.53
Mn-CB index	7.19	5.57	98.67	27.25	50.05	3.35	5.12	22.99	37.27	28.01	21.88	12.37	4.41	26.27	30.25	23.78	40.38
Sc	11	9	16	12	12	20	5	6	7	12	14	9	6	11	8	17	10
V	25	22	59	56	32	52	16	18	21	36	18	35	21	30	22	49	29
Cr	NA	2	3	5	2	NA	2	2	2	2	NA	3	2	3	NA	NA	NA
Ni	4	1	5	1	2	4	2	<1	1	2	4	1	<1	2	3	3	3
Cu	6	9	102	487	3	90	673	1194	277	15	36	140	4706	10	60	1	3
Zn	106	54	522	119	136	24	27	70	133	431	295	108	43	170	145	162	211
Pb	<1.5	3	12	98	12	19	<1.5	2	<1.5	2	3	8	34	14	<1.5	2	25
Rb	66.9	68	<1	44	93	113.2	59	60	64	74	59.2	86	55	54	66.4	44.1	12.4
Sr	20	15	9	62	24	31	7	10	12	28	53	15	13	42	15	68	35
Y	17	19	27	15	19	19	16	18	21	18	19	22	16	18	21	25	19
Zr	105	95	169	80	150	189	102	133	152	133	128	170	125	120	167	161	123
Nb	6	5	9	5	7	9	6	7	8	8	7	8	7	7	9	9	6
Ba	1291	1132	21	1526	1557	2110	1418	1546	1358	1003	787	2446	1583	908	1241	515	260
Th	5	5	10	5	7	11	5	8	7	7	7	8	7	7	8	8	7
Ag	<0.1	0.2	_	0.5	0.2	0.8	0.2	0.2	<0.1	<0.1	<0.1	0.3	0.8	0.1	<0.1	<0.1	<0.1
As	12	12	_	5	20	256	4	5	5	4	2	16	47	4	4	<1	3
Bi	1.3	3.5	_	0.8	<0.1	3	0.8	0.3	<0.1	<0.1	0.2	4	1.6	<0.1	0.5	<0.1	<0.1
Cd	0.1	<0.1	_	<0.1	<0.1	<0.1	<0.1	<0.1	<0.1	0.6	0.6	<0.1	0.2	<0.1	<0.1	<0.1	<0.1
Mo	5.6	5.3	_	0.3	0.3	2	0.3	0.1	0.3	0.1	1.2	1.8	0.9	0.3	0.9	0.8	1
Sb	0.5	0.4	_	0.6	1	4	0.6	0.9	1.1	1.1	0.8	1.3	3.4	0.6	0.7	0.3	0.4
Se	<1	1.2	1.5	<1	<1	<1	1.1	<1	<1	<1	<1	<1	<1	<1	<1	<1	<1
Cs	1.32	1.06	_	0.94	1.33	1.2	1.13	0.91	1.78	1.23	1.11	1.12	0.91	1.08	1.18	0.76	0.46
Tl	1.6	1.3	_	<0.5	0.8	0.9	<0.5	1	1.5	0.7	<0.5	3.1	3.8	1	1.2	<0.5	<0.5
U	1.54	1.39	_	0.94	1.06	1.16	1.37	1.52	1.67	1.37	1.38	2.15	1.49	0.53	1.51	1.43	1.51
S	4.89	8.39	6.37	2.44	0.64	4.54	3.27	1.67	0.11	0.02	0.26	2.77	4.42	1.83	0.11	0	0
La	12.7	15	21	23	15	26.1	14	14	18	15	17.4	9	16	17	20.6	19.1	16.7
Ce	26.1	31	35	48	36	57.7	24	29	39	34	35.9	26	33	35	41.6	39.3	30.2
Nd	12.5	16	16	22	13	23	11	10	14	13	16.6	9	13	15	17	18.7	12.4

Ag, Cd, Sb, C

[1] Total Fe as

[2] Analyses re

Appendix 1: N

Sample	600/195.5 m	600/241.1 m	600/380.2 m	800/127.6	800/140.2	800/140.4 m	800/143.4 m	800/162.3 m	800/242	801/141 m	801/291.2	803/62	803/85.5 m	803/127.1 m	803/286 m	803/314.7 m	804/39.8 m
Lithology	Rhyolite 8?	Rhyolite 8?	Rhyolite 8?	andesite	Rhyolite 6	Rhyolite 6	Rhyolite 6	Rhyolite 6	Rhyodacite 3	Rhyolite	Rhyodacite 3	Dacite 1	Dacite 1	Dacite 1	Dacite 1	Dacite 1	Dacite 1
Section	10300N	10300N	10300N	10150N	10150N	10150N	10150N	10150N	10150N	10025N	10025N	10150N	10150N	10150N	10150N	10150N	10300N
Position	MAR	MAR	MAR	MAR	MAR	MAR/HW	MAR/HW	MAR/HW	MAR	MAR/HW	MAR	MAR	MAR	MAR/FW	MAR/FW	MAR/FW	MAR/HW
SiO2	78.86	74.57	73.05	59.49	68.63	73.08	62.70	71.97	67.39	73.95	67.22	74.94	75.47	67.28	70.88	71.43	69.43
TiO2	0.29	0.30	0.34	0.38	0.4	0.30	0.51	0.34	0.4	0.34	0.38	0.43	0.40	0.61	0.53	0.51	0.52
Al2O3	12.00	12.68	13.74	18.51	16.37	13.09	20.43	14.02	18.62	13.82	16.72	13.04	12.97	18.26	16.20	16.16	16.13
Fe2O3	1.83	2.96	3.38	7.16	3.08	2.22	3.64	2.46	4.8	2.62	7.48	3.4	3.02	2.76	3.82	2.73	4.40
MnO	0.05	0.07	0.04	0.21	0.05	0.05	0.05	0.05	0.13	0.07	0.08	0.14	0.17	0.12	0.10	0.11	0.17
MgO	2.29	2.91	1.42	2.47	2.81	2.02	4.25	2.30	3.41	2.15	3.78	1.75	1.74	2.26	2.68	2.64	1.05
CaO	0.64	2.01	1.51	6.86	1.37	2.97	0.39	1.82	0.12	2.00	0.1	0.79	1.25	1.41	0.72	0.31	2.87
Na2O	2.19	2.86	5.30	3.69	5.27	5.15	3.32	6.64	0.17	1.97	0.18	2.54	1.88	2.14	1.08	3.75	2.86
K2O	1.79	1.58	1.17	0.86	1.9	1.04	4.60	0.35	4.68	3.00	3.85	2.79	3.02	5.06	3.90	2.28	2.47
P2O5	0.05	0.05	0.05	0.33	0.07	0.06	0.09	0.06	0.09	0.07	0.08	0.08	0.08	0.09	0.10	0.08	0.09
LOI	2.65	3.61	2.39	3.09	3.12	3.37	3.64	2.42	4.14	4.53	5.25	2.8	3.13	4.07	4.35	2.68	4.45
Total	100	100	100	100	100	100	100	100	100	100	100	100	100	100	100	100	100
P/Zr	1.70	1.83	1.60	16.78	1.51	1.88	1.68	1.65	2.23	1.94	2.29	2.89	3.23	2.66	3.17	2.65	2.83
Ti/Zr	13.06	14.55	14.51	26.55	11.84	12.52	12.58	12.50	13.64	12.59	14.95	21.34	21.66	24.00	24.16	22.32	21.59
Nb/Y	0.42	0.39	0.33	0.32	0.37	0.40	0.37	0.40	0.46	0.34	0.45	0.30	0.35	0.39	0.35	0.34	0.38
Alt. index	59.02	48.01	27.59	23.99	41.50	27.40	70.43	23.88	96.54	56.54	96.46	57.69	60.39	67.40	78.56	54.76	37.98
Chl. index	49.69	55.65	40.86	66.20	43.77	39.36	48.75	39.27	61.44	47.62	72.28	47.43	47.67	39.73	55.17	45.81	48.43
Mn-CB index	22.44	38.10	22.86	66.32	20.69	36.03	10.32	24.97	22.65	35.46	18.26	29.12	37.17	26.96	25.12	19.31	46.07
Sc	8	9	9	7	11	9	12	9	16	9	15	12	10	15	13	12	13
V	25	25	30	55	29	19	38	19	51	24	60	33	30	44	39	55	38
Cr	2	2	2	NA	NA	2	3	2	NA	2	NA	NA	1	3	2	2	2
Ni	<1	<1	2	3	3	1	1	1	3	1	3	4	<1	2	1	2	1
Cu	6	<2	<2	8	1	<2	<2	<2	42	<2	5	4	3	33	56	7	3
Zn	65	47	78	83	48	34	70	38	72	36	72	89	69	1910	151	198	61
Pb	22	3	6	9	3	2	4	5	4	3	2	11	3	224	23	6	9
Rb	37	37	27	33.1	61.7	31	127	8	99.4	78	72	56.8	60	100	74	48	63
Sr	51	80	150	550	110	102	49	142	23	80	23	57	57	49	41	73	185
Y	17	17	21	16	28	19	33	21	18	23	16	23	17	22	22	23	22
Zr	132	124	140	86	203	143	242	161	176	164	152	121	111	154	131	136	146
Nb	7	7	7	5	10	8	12	9	8	8	7	7	6	9	8	8	8
Ba	825	518	296	208	414	237	984	92	1843	728	1046	950	757	2055	2207	602	625
Th	8	8	9	12	10	7	10	7	11	7	9	6	6	7	7	8	8
Ag	0.2	<0.1	<0.1	<0.1	<0.1	<0.1	<0.1	<0.1	0.3	<0.1	0.1	<0.1	<0.1	0.6	0.2	<0.1	<0.1
As	47	5	4	4	4	6	8	7	67	4	11	13	34	97	21	7	5
Bi	0.2	0.2	<0.1	0.2	0.1	0.1	0.3	<0.1	0.9	0.2	1.8	<0.1	<0.1	2	0.5	<0.1	0.1
Cd	<0.1	<0.1	<0.1	0.6	<0.1	<0.1	0.2	<0.1	<0.1	<0.1	<0.1	<0.1	<0.1	7.3	0.1	0.2	<0.1
Mo	0.5	<0.1	0.2	1.7	1.1	0.3	0.4	0.3	1.2	0.3	2.4	1.4	0.2	1.8	1.1	0.3	0.4
Sb	0.9	1	0.4	1	0.8	0.7	1.6	0.8	1.4	0.7	0.3	1.5	1.3	3.1	1.5	0.4	1.1
Se	<1	<1	<1	<1	<1	<1	<1	<1	<1	<1	<1	<1	<1	<1	<1	<1	<1
Cs	0.84	0.74	0.32	0.62	0.9	0.41	1.52	0.18	1.02	1.04	0.88	1.8	1.28	1.39	1.41	0.8	0.85
Tl	<0.5	<0.5	<0.5	<0.5	<0.5	<0.5	1	<0.5	<0.5	0.9	0.8	0.6	0.7	1.7	1	<0.5	0.7
U	1.47	1.43	0.48	1.87	1.74	1.36	1.97	1.13	0.98	1.51	1.34	1.4	1.11	1.64	0.98	1.43	1.33
S	0.42	0.01	0.01	0	0	<0.01	<0.01	<0.01	0.72	<0.01	3.05	0.38	0.31	1.43	2.12	0.77	<0.01
La	20	12	17	26.4	23.5	18	21	18	12.4	23	25	22.4	12	15	17	17	14
Ce	42	30	37	50.3	46.2	34	46	42	28.7	52	50.8	45.1	25	37	40	32	33
Nd	17	12	15	24.7	18.7	16	19	17	14.5	21	21.9	21.5	10	14	15	16	13

Ag, Cd, Sb, C

[1] Total Fe as

[2] Analyses re

Appendix 1: M

Sample	804/80.4 m	804/127.5	804/141.6 m	804/177.5	804/320.8 m	805/160.05	805/160.85m	805/213.6 m	805/259.9 m	807/126.56	807/178.3 m	807/280.8	807/319	807/360.2 m	807/434.7	807/460.5	807/481.1 m
Lithology	Dacite 1	Dacite 1	Dacite 1	andesite	Dacite 1	rhyolite	Rhyodacite 3	Fld>qtz pum bx	Fld>qtz pum bx	Rhyolite 6	Rhyolite 2	Rhyolite 2	Rhyolite 2	Rhyolite 2	Rhyodacite 1	Rhyodacite 1?	Rhyodacite 1
Section	10300N	10300N	10300N	10300N	10300N	10200N	10200N	10200N	10200N	10150N	10150N	10150N	10150N	10150N	10150N	10150N	10150N
Position	MAR/HW	MAR	MAR/HW	MAR	MAR/FW	MAR	MAR/HW	MAR/HW	MAR/HW	HW	MAR	MAR	MAR	FW	FW	FW	FW
SiO2	74.58	69.15	70.67	62.09	73.82	76.63	70.88	74.08	75.89	75.89	63.23	79.71	73.71	68.34	84.5	80.41	78.94
TiO2	0.38	0.42	0.50	0.29	0.42	0.3	0.37	0.26	0.31	0.38	0.55	0.26	0.43	0.47	0.15	0.19	0.20
Al2O3	12.71	13.07	15.85	18.12	13.18	12.68	15.34	12.21	13.20	14.02	20.45	10.58	13.94	18.02	4.7	6.23	8.87
Fe2O3	2.96	4.4	1.76	5.45	3.50	2.41	3.48	3.40	2.40	3.81	7.70	5.36	6.51	5.87	8.94	10.49	8.84
MnO	0.23	0.23	0.05	0.21	0.17	0.03	0.07	0.16	0.06	0.04	0.05	0.02	0.01	0.04	0.01	0.02	<0.01
MgO	0.47	1.5	0.41	1.84	1.47	0.41	1.37	2.21	2.76	1.29	1.68	0.65	0.58	1.98	0.19	0.28	0.30
CaO	3.10	6.05	0.46	5.23	2.94	0.16	0.20	2.74	0.29	0.05	0.04	0.04	0.07	0.21	-0.01	0.21	0.06
Na2O	4.20	2.27	0.16	2.4	0.86	6.7	7.70	1.59	2.20	0.07	0.23	0.05	0.15	0.19	0	0.03	0.11
K2O	1.30	2.73	10.02	3.94	3.55	0.58	0.53	3.30	2.83	4.24	6.04	3.07	4.25	4.79	1.41	1.91	2.62
P2O5	0.07	0.09	0.11	0.23	0.10	0.05	0.06	0.05	0.06	0.06	0.03	0.05	0.07	0.08	0.01	0.02	0.04
LOI	3.44	6.7	1.93	5.68	4.90	0.46	1.00	3.90	2.55	3.48	6.04	5.13	4.86	4.93	4.74	5.81	5.49
Total	100	100	100	100	100	100	100	100	100	100	100	100	100	100	100	100	100
P/Zr	2.88	3.15	3.60	10.42	3.76	1.52	1.42	2.42	2.29	2.48	0.87	1.86	2.76	2.49	1.07	1.68	2.50
Ti/Zr	20.88	20.21	22.05	18.05	22.98	12.56	12.05	16.60	15.72	21.57	20.41	13.32	23.29	18.80	21.99	21.90	16.32
Nb/Y	0.36	0.28	0.37	0.35	0.34	0.46	0.38	0.37	0.41	0.49	0.37	0.31	0.33	0.33	0.34	0.36	0.31
Alt. index	19.45	33.71	94.33	43.10	56.90	12.61	19.34	56.05	69.19	97.88	96.63	97.64	95.64	94.39	100.63	90.12	94.46
Chl. index	36.26	52.20	16.38	51.54	51.17	26.16	35.38	51.92	49.42	52.26	57.87	63.69	59.40	59.29	85.38	83.36	75.15
Mn-CB index	49.48	62.55	8.76	53.62	51.29	5.94	9.98	46.82	15.36	9.45	8.49	7.14	3.72	11.32	6.00	17.45	_
Sc	11	14	10	6	11	8	9	9	8	11	14	10	11	12	4	5	7
V	26	31	35	31	28	22	30	30	32	41	61	40	43	42	21	32	24
Cr	2	NA	2	NA	2	NA	3	3	2	NA	4	NA	NA	31	NA	NA	3
Ni	4	3	1	2	<1	5	1	1	1	4	2	3	4	2	34	6	3
Cu	15	4	8	6	15	4	<2	22	3	67	274	24	13	16	10	11	8
Zn	41	66	22	105	110	19	63	63	20	49	96	163	9	68	14	12	10
Pb	5	4	2	3	35	3	6	9	3	19	13	6	7	32	3	3	6
Rb	28	60.7	104	100.5	65	5	5	68	73	96.3	123	46.2	75.9	92	22	29.7	47
Sr	153	151	38	275	52	77	91	75	40	11	33	21	23	28	8	13	14
Y	17	24	19	15	18	17	26	14	16	14	20	18	18	25	6	8	13
Zr	110	125	137	96	111	143	186	94	119	106	161	117	111	149	41	52	75
Nb	6	7	7	5	6	8	10	5	7	7	7	6	6	8	2	3	4
Ba	273	925	5034	1941	1279	252	187	667	399	1229	2779	1031	2234	3683	628	1404	865
Th	6	6	5	12	6	7	10	5	7	7	9	6	6	9	2	5	7
Ag	<0.1	<0.1	0.3	<0.1	0.2	<0.1	<0.1	0.2	<0.1	0.8	0.1	0.3	0.1	0.2	<0.1	0.1	<0.1
As	6	2	19	3	42	3	3	1	13	69	24	25	30	20	12	13	15
Bi	<0.1	<0.1	<0.1	<0.1	<0.1	<0.1	<0.1	0.2	0.1	3.3	3.9	0.7	3.7	2.7	1.2	4.2	2
Cd	<0.1	0.1	<0.1	<0.1	0.4	0.1	0.2	<0.1	<0.1	0.1	0.2	<0.1	<0.1	<0.1	<0.1	<0.1	<0.1
Mo	0.3	1.1	8.4	0.5	1.8	2.2	0.1	0.1	0.2	5.1	0.4	1	7.1	3.3	4.8	9.9	6.3
Sb	0.8	1.1	1.2	0.8	1.1	0.8	0.9	0.7	0.9	1.6	0.8	0.8	1.7	2	0.8	1.2	0.6
Se	<1	<1	<1	<1	<1	<1	<1	<1	<1	<1	1	<1	<1	<1	1	2.3	5.3
Cs	0.46	0.93	1.09	2.83	1.04	0.11	0.12	1.55	0.94	1.08	1.07	0.69	0.82	0.97	0.3	0.41	0.42
Tl	<0.5	0.7	3.6	0.8	1.4	<0.5	<0.5	0.5	0.5	0.5	2.1	0.8	1.7	2	2.1	1.2	1.1
U	1.11	0.56	1.57	1.88	1.44	1.17	1.51	1.38	1.35	1.13	0.95	1.22	2.91	1.59	1.1	0.97	1.16
S	<0.01	0	0.86	0	2.28	-0.01	<0.01	0.01	0.38	1.54	5.16	2.96	4.62	2.97	6.52	7.6	6.39
La	13	17.8	17	24	16	12.9	24	16	16	9.8	23	21.8	21	20	8	11	11
Ce	29	39.5	45	55.3	31	26.8	46	32	34	26.4	56	41.6	48	52	15.2	23.9	19
Nd	13	17.6	12	25.8	12	13.6	21	13	14	10.5	21	17.2	23	18	5.6	9.9	7

Ag, Cd, Sb, C

[1] Total Fe as

[2] Analyses re

Appendix 1: M

Sample	809/262.1 m	809/289.1 m	814/140.1 m	814/177.8 m	814/185.35 m	814/251 m	814/314.1 m	814/357.3 m	814/381.7 m	814/481.3 m	814/613.1 m	814/630.76 m	814/766.5 m
Lithology	Rhyolite 6?	Rhyolite 4?	Rhyolite	Rhyolite	Rhyolite	Qtz & fld pum	Rhyolite	Rhyolite	Rhyolite	Rhyolite	Rhyodacite 3?	Rhyodacite 3?	Andesite dyke
Section	9850N	9850N											
Position	MAR	MAR											
SiO2	74.53	73.06	73.24	78.35	72.84	81.63	73.01	74.92	73.25	72.42	75.36	76.85	52.09
TiO2	0.32	0.31	0.35	0.31	0.34	0.24	0.38	0.24	0.31	0.44	0.28	0.27	0.58
Al2O3	14.30	15.12	15.05	12.04	13.99	10.00	15.63	10.36	13.48	14.07	13.13	13.24	19.92
Fe2O3	2.15	2.45	2.09	1.29	4.18	1.50	2.59	2.79	2.85	6.22	5.75	2.61	9.35
MnO	0.11	0.09	0.05	0.05	0.11	0.05	0.07	0.60	0.16	0.32	0.03	0.23	0.18
MgO	0.72	1.39	1.41	0.53	1.46	0.41	1.15	1.01	2.78	2.68	1.14	2.60	4.66
CaO	1.86	1.75	0.57	0.89	0.38	0.88	1.10	3.01	2.14	0.16	0.12	0.24	10.67
Na2O	3.60	2.82	5.15	5.74	5.34	4.31	2.61	0.34	2.15	0.05	0.10	0.95	2.24
K2O	2.35	2.94	2.04	0.74	1.31	0.94	3.40	6.67	2.83	3.53	4.00	2.94	0.12
P2O5	0.06	0.05	0.06	0.05	0.06	0.04	0.06	0.05	0.06	0.12	0.07	0.06	0.18
LOI	2.63	3.51	1.90	1.84	1.53	1.49	3.85	3.51	4.09	3.04	4.32	2.76	4.26
Total	100	100	100	100	100	100	100	100	100	100	100	100	100
P/Zr	1.61	1.34	1.55	1.48	1.57	1.55	1.97	2.58	2.41	5.66	2.84	2.23	15.57
Ti/Zr	11.44	11.02	12.03	12.24	11.90	12.25	16.26	16.30	16.58	27.20	15.05	13.30	70.44
Nb/Y	0.40	0.41	0.34	0.42	0.39	0.38	0.36	0.25	0.42	0.29	0.54	0.43	0.26
Alt. index	36.03	48.71	37.61	16.08	32.65	20.63	55.08	69.60	56.65	96.76	95.89	82.36	27.06
Chl. index	30.83	38.47	31.42	20.74	43.95	25.10	36.70	33.45	51.75	69.81	60.63	55.99	84.69
Mn-CB index	33.45	31.77	13.12	17.82	18.38	20.92	23.40	56.12	42.67	48.51	9.49	39.19	84.04
Sc	9	8	9	8	9	6	11	6	9	16	9	9	25
V	22	22	28	31	69	18	44	16	32	69	26	30	181
Cr	2	2	2	2	3	2	3	2	3	13	2	2	22
Ni	<1	2	1	1	2	1	1	2	2	1	7	<1	1
Cu	3	2	2	623	112	<2	6	8	10	570	40	10	12
Zn	32	61	42	19	73	11	35	114	31	112	67	221	51
Pb	3	2	2	130	6	5	11	7	5	<1.5	5	311	45
Rb	66	84	51	11	21	22	81	83	74	82	3	62	81
Sr	130	95	118	107	87	121	101	123	62	12	17	31	554
Y	22	22	25	19	22	17	19	20	15	19	11	15	14
Zr	168	170	173	151	169	115	139	88	113	96	113	121	50
Nb	9	9	9	8	9	6	7	5	6	5	6	6	4
Ba	604	692	317	335	364	344	1065	4948	362	1206	1502	1574	59
Th	8	7	8	7	9	6	8	2	6	4	6	6	7
Ag	<0.1	<0.1	<0.1	0.2	0.1	<0.1	1.7	0.1	0.1	0.1	1.2	<0.1	<0.1
As	5	4	5	5	5	4	54	9	8	3	77	13	11
Bi	0.2	0.1	0.1	<0.1	<0.1	<0.1	<0.1	0.4	0.2	<0.1	2.2	<0.1	0.2
Cd	<0.1	<0.1	<0.1	<0.1	<0.1	<0.1	<0.1	<0.1	<0.1	<0.1	0.1	<0.1	0.2
Mo	0.2	0.2	0.1	0.7	0.1	0.2	0.7	0.2	<0.1	<0.1	15.7	0.6	0.4
Sb	0.5	0.5	0.5	0.7	0.5	0.9	2.8	0.3	0.7	0.5	1.4	1	0.8
Se	1	<1	<1	2.3	1	1.1	<1	<1	<1	<1	<1	<1	1.1
Cs	0.77	1.21	1.45	0.34	0.4	0.33	1.95	0.34	1.16	0.85	0.8	0.6	0.56
Tl	0.7	0.8	0.5	<0.5	1.1	<0.5	2.2	0.8	<0.5	0.5	0.9	1.4	<0.5
U	1.55	1.73	1.92	3.71	2.5	1.11	1.57	0.77	1.48	0.97	1.95	1.56	0.96
S	<0.01	<0.01	<0.01	0.09	0.06	<0.01	0.85	0.1	0.2	0.12	3.45	0.18	0.03
La	20	15	19	19	10	12	10	16	13	13	9	16	14
Ce	41	34	41	38	24	22	21	42	24	26	22	40	30
Nd	18	15	19	17	14	11	10	7	11	10	8	14	14

Ag, Cd, Sb, C

[1] Total Fe as

[2] Analyses re

Final Report of AMIRA-ARC project P439 — May 1998

Studies of VHMS related alteration: geochemical and mineralogical vectors to ore

Suggested Chapter Headings — 10 October 1997

Executive Summary (stand alone report) *WH*

Introduction

Project objectives and comparison with outcomes

Organisation of report *WH*

Part 1 Interpretation of altered volcanic textures and geochemistry

Ch 1 Primary geochem of unaltered submarine? volcanics - *MRV, MWV, Benambra?*

Compositional range and variability, comparisons with modern least altered volcanics

Typical examples of mainly coherent facies with photos & micrographs in a standardised format for presentation of analyses (including $\partial^{18}O_{wr}$, REE?) alteration indices, box plots etc.

Comparisons of co-magmatic coherent and volcaniclastic facies

Implications for melt sources and tectonic settings?? *AJC, JS, RLA?*

Ch 2 Diagenetic & Metamorphic "background" alteration (unrelated to VHMS

Textural-mineralogical-geochemical -isotopic & etc. changes

Physico-chemical conditions, phase equilibria?

Volcanic facies controls

Typical examples: photos, micrographs, analyses, alteration indices, box plots etc. in standard format *CG, MD, RLA, JMcP*

Ch 3 Overview of VHMS related alteration types

Expanding upon the P439 research proposal; outlining the seven main facies of alteration, as currently understood, and their typical textural-mineralogical-geochemical features.

Alteration zonation, volcanic facies/structural controls, physico-chemical conditions.

JBG, DC, MD & RRL

Ch 4 Techniques of Interpretation *(illustrated by exemplary data sets)*

4.1 Lithogeochemical Techniques

Useful elements (including REE & isotopes?), analytical methods, costs, precision, standards) - *full treatment? or reference to Rollinson, 1993 ?*

Immobile element ratios: as a mapping tool in pervasively altered rocks

Mobile mass changes: comparison of Isocon, B&McL and PER methods

Simple vectors eg: Na_2O, Mn, Tl, Py, $\partial^{18}O$ etc.

Alteration Indices : AI, CCPI, CO_3I (and others, based on mobile mass changes?)
Box plots: for discrimination of diagenetic, synvolcanic hydrothermal, post volcanic hydrothermal and metamorphic styles
Mass change zonation: useful vectors? *WH, RRL? MB?*

4.2 Mineralogical Techniques
Microprobe analyses
PIMA & comparison with other spectrometers *MB, RF, et al?*

PART 2 Case studies of Australian VHMS related alteration systems

Ch 5 Alteration in the Mount Read Volcanics

5.1 MRV regional geology, alteration mineralogy and geochemistry
GIS plots of selected data from MRV geochem database and regional traverses
Relationships of alteration to volcanic facies, *syn-volcanic granites*, VHMS deposits
RLA, BW, MB, RRL, JMcP

5.2 Hellyer footwall: ZnPbCu, zoned, focussed, structurally controlled, in largely coherent mafic volcanics *JBG*

5.3 Hellyer hangingwall: in mafic volcanics *RF*

5.4 Rosebery: ZnPbCu , zoned? stratabound, in permeable felsic volcaniclastics
RLA, MB, RRL?

5.5 Western Tharsis: disseminated Cu-Au, granite connection?? *DH*

5.6 Henty: Au rich, shallow water? felsic volcanics, stratabound extreme silicification and Al_2O_3 mobility? *TC & JB*

Ch 6 Alteration in the Mount Windsor Volcanics

6.1 Highway-Reward: Cu-Au, sub sea floor replacement VHMS, structural control? *MD*

6.2 Thalanga: sea floor ZnPbCu, zoned FW alteration, stratabound? , facies control?, felsic volcanics, successful application of $\partial^{18}O$ exploration? *HP, AHP? WH? SH? CRM?*

6.3 Waterloo & Agincourt: contrasting high grade MS and low grade disseminated styles; *is alteration zonation sufficiently known?* *TM (doubtful)*

6.4 Liontown: REE and $\partial^{18}O$ alteration vectors *CRM*

6.5 Gydgie: a barren? system *MB, GD, JS?*

6.6 Ironstone formations in the MWV *MD & GD*

Ch 7 Gossan Hill: an Archean ZnCu, sub seafloor VHMS *RS*

Ch 8 A review of VHMS hydrothermal alteration and exploration vectors

8.1 Comparison of ***Australian*** systems discussing controls of volcanic facies, primary composition, structure, water depth, source of fluids, water/rock ratios, physico-chemical factors & etc. Opportunity for arm waving.
All contributions welcome

8.2 New exploration vectors *WH, RRL et al?*

Sample number: 96-120R-1094 Rock and thin section description

Location: Drill hole 120R, 1094.5 m; north end Rosebery mine

Hand specimen and summary: Lower crystal-lithic-rich part of Hangingwall Unit 3a pumice breccia mass flow unit. Plagioclase»qtz phenocrysts and lithic clasts enclosed by moderately-poorly preserved pumice and glass shards. Weak-moderate q-ser and biot-chl alteration. Disseminated Sp. Alteration mainly comprises extensive mosaic of fine grained feld>qtz»ser-carb-clinoz, and weak ser-altered feld phenocrysts. Biot ?overprints ser. The rock has minor qtz>carb veinlets.

Mineral percentages in thin section:

plagioclase	?50%	)__	75%
quartz	?25%	)	
sericite	7-10%		
biot		5%	
chlorite	3%		
carbonate	3-5%		
sphene-leucox	3%		
opaques (sp)	1%		
zircon	trace		

Primary textures: 35% 1.5 mm plag » qtz crystals, and several lithic clasts, enclosed by pumice-glass shard matrix. Pumice and shard textures only locally well preserved. One fine-grained, siliceous, aphyric rhyolite lithic with 5% streaky amygdales. One feld-biot-ser-rich, 10% feld-porphyritic, relict perlitic, felsic lava lithic. This lithic contains a few 0.12mm zircons.

Tectonic fabrics: One strong foliation expressed by orientation of matrix sericite and clinozoisite, beard pressure shadow growths on phenocrysts, and folding, elongation and partial transposition of pumice texture. Qtz crystals have undulose extinction and moderate subgrain development.

Alteration, veins: Rock has similar secondary feldspar alteration to that described in samples 96-120R-1 and 2, however, the fine grained recrystallization of originally coarse secondary feldspar is more advanced. Plagioclase phenocrysts are relatively well preserved, with only weak replacement by sericite»carb. Pale brown biot occurs in sericitic areas, including in the matrix and within the feldspar phenocrysts, and appears to replace sericite. The biot is commonly intergrown with chl and appears altered/retrograded to the chl. Minor, deformed, foliated, ²0.5mm qtz>carb»ser veinlets.

Sphene is abundant, and is both irregularly disseminated throughout, and occurs as diffuse stylolitic "veins" (S1 foliation), which are strongly foliated and folded by S2-F2. The sphene is locally moderately fresh brown, but mainly partly granular and partly very fine cloudy; the latter is probably leucoxene (fine grained rutile) and gives the aggregates their white opaque colour in hand specimen.

Carbonate is clean, almost clear (?Fe/Mn-poor).

Opaques are mainly irregular dissemination/impregnation of streaky (foliated) sphalerite. Sp appears pre- to early-S2.

Interpretation/important relationships: Sphalerite is disseminated rather than vein related, and appears pre-S2. Fine grained feld±qtz and ser alterations post-date feld replacement of pumice. Earliest preserved feld replacement of pumice is untwinned optically continuous feld; this replaced/recrystallized to twinned coarse grained plag (albite), then in turn changes to fine grained plag±qtz mosaics. Minor carbonate is scattered throughout, but is concentrated in qtz-carb veinlets. Biotite-chl alteration appears to be the latest alteration stage, and could be Devonian granite-related.

Mineral Probe Results

Carbonates

Sample	Area	Description
120R-1094.5	A4 C1	coarse carbonate patch or vein
120R-1094.5	A4 C2	coarse carbonate patch or vein

Area	FeCO3	MnCO3	MgCO3	CaCO3	Carb total
A4 C1	0.4	1.91	0	100.03	102.35
A4 C2	0.87	1.72	0	99.51	102.45

White Micas

Sample	Area	Description
120R-1094.5	A1 S2	matrix sericite
120R-1094.5	A3 S1	fine sericite, matrix
120R-1094.5	A3 S2	fine sericite, matrix
120R-1094.5	A5 B1	? biotite alteration of feldspar phenocryst
120R-1094.5	A5 B3	? biotite alteration of feldspar phenocryst

Area	SiO2	TiO2	Al2O3	Cr2O3	Fe2O3	FeO	MnO	MgO	CaO	Na2O	K2O	Cl	Oxide total
A1 S2	34.03	0.8	17.15	1.66	0	12.35	0.84	0.52	12.42	0.31	0	0	80.08
A3 S1	48.45	0.26	30.05	0	0	2.97	0	1.71	0	0	11.5	0	94.94
A3 S2	48.62	0.26	29.83	0	0	3.09	0	1.84	0	0	11.46	0	95.1
A5 B1	47.27	0	33.49	0	0	1.85	0	0.24	0	0	11.11	0	93.96
A5 B3	50.4	0.19	29.01	0	0	3.24	0	1.39	0.12	1.21	10.27	0	95.83

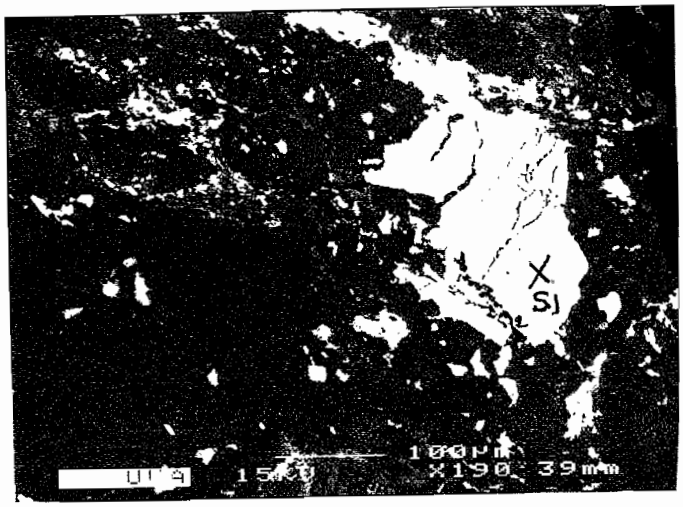

120R - 1094·5 AREA 1

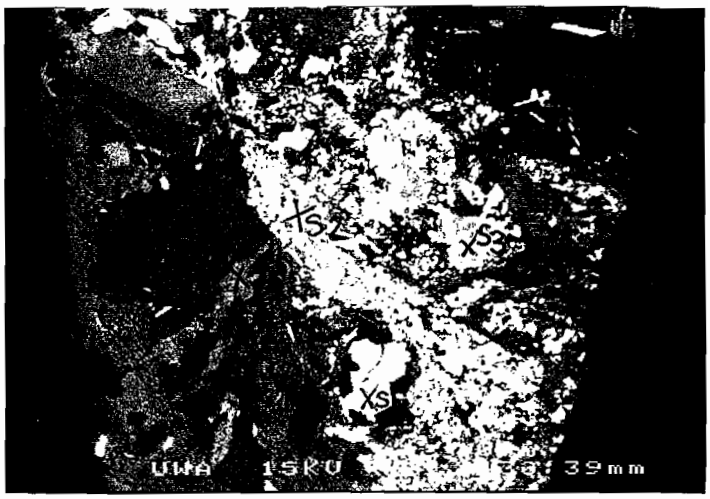

120R - 1094·5 AREA 2

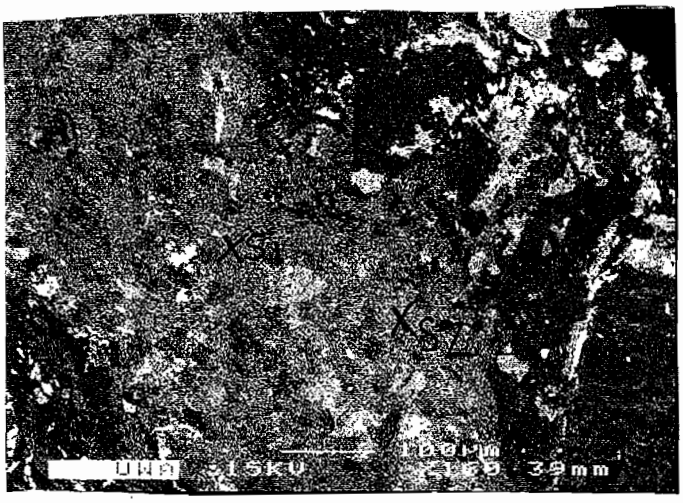

120R - 1094·5 AREA 3

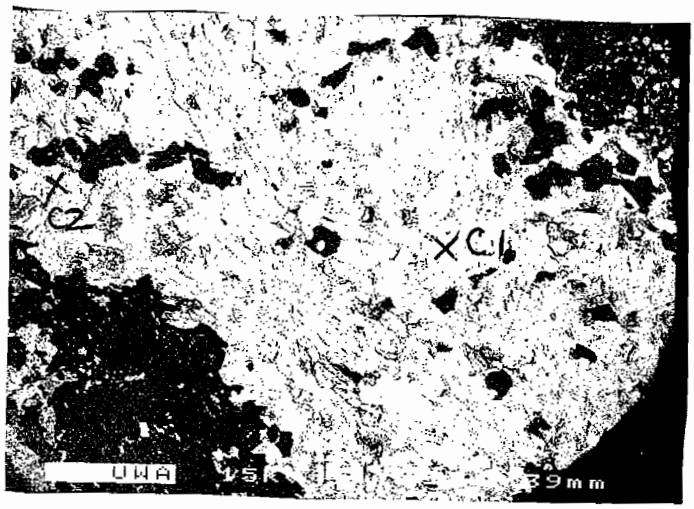

120R - 1094·5 AREA 4

120R 1094·5 AREA 5

Sample number: 96-120R-1083 Rock and thin section description

Location: Drill hole 120R, 1083.7 m; north end Rosebery mine

Hand specimen and summary: Middle part of Hangingwall Unit 3a pumice breccia mass flow unit. Plagioclase»qtz phenocrysts enclosed by non-welded pumice clasts and glass shards. Weak-moderate q-ser-carb altered. Disseminated Sp. Alteration comprises mosaics of fine grained feld>qtz»ser-carb, and lesser discontinuous bands rich in ser»chl, all enclosing moderately ser»carb altered feld phenocrysts. The rock has minor fine qtz>carb veinlets.

Mineral percentages in thin section:

plagioclase	?45%	)__	70%
quartz	?25%	)	
sericite	15%		
carbonate	7%		
chlorite	3%		
biotite	1%		
clinozoisite	1%		
sphene-leucox	1%		
opaques (sp)	1%		
allanite	<1%		
zircon	trace		

Primary textures: Plagioclase phenocrysts (15-20%) » 2 % subhedral (subrounded, embayed) qtz phenocrysts, enclosed by moderately preserved, non-welded, round-vesicle and tube-vesicle pumice and glass shards. One large 15% 1mm feld=qtz porphyritic rhyolite lithic clast, and one 10% 1mm feld-porphyritic rhyolite/dacite clast with abundant disseminated sulphide alteration.

Tectonic fabrics: One moderate foliation expressed by orientation of matrix sericite, beard pressure shadow growths on phenocrysts, and folding, elongation and partial transposition of pumice texture. Qtz crystals have undulose extinction and weak-moderate subgrain development.

Alteration, veins: 1-2% ²0.25mm moderately wavy, folded qtz>carb»chl-ser veinlets; folded by S2-F2 and have internal S2 foliation, but overprint S2 deformed opaques (sphalerite).

Pumice porosity and bubble walls are replaced by random- to interpenetrating-twinned, coarse grained plagioclase (probably albite?), in turn extensively, variably replaced by fine grained plag±qtz mosaics, and lesser diffuse discontinuous bands (?pseudofiamme) of ser»chl. Feldspar phenocrysts moderately-strongly, incompletely replaced by ser»carb-clinoz and locally biot (less intense replacement than in 120R-1). Biot appears unfoliated and may replace sericite. Many feldspar phenocrysts have relict plagioclase rims (replacing pumice), comprising homogeneous non-twinned feld, extensively replaced/recrystallized to twinned plagioclase (?albite). Feld phenocrysts have fine internal fractures filled by secondary feldspar of same type and in optical continuity with rim feldspar. Secondary plagioclase of rims is also generally in optical continuity with phenocryst plag. Quartz phenocrysts do not have secondary feld rims.

Carbonate is clean, almost clear (?Fe/Mn-poor; paler than most carb in 96-120R-1).

Opaques are mainly irregular dissemination/impregnation of streaky (foliated) sphalerite. Streaky foliated habit oriented parallel to S2 foliation; indicates Sp is pre- to early-S2. An abundant high relief accessory alteration mineral occurs scattered irregularly throughout: allanite, clinozoisite, titaniferous sphene? There is some definite allanite with brown alteration halo.

Interpretation/important relationships: Qtz veinlets are syn-tectonic (syn-S2) and post-date deformed sphalerite. Sphalerite is disseminated rather than vein related, and appears pre-S2. Fine grained feld±qtz and ser»chl alterations post-date feld replacement of pumice. Earliest preserved feld replacement of

pumice is untwinned optically continuous feld; this replaced/recrystallized to twinned coarse grained plag (albite), then in turn changes to fine grained plag±qtz mosaics. Carbonate scattered throughout, and also occurs in veinlets.
Ser»carb alteration has replaced feld phenocrysts more intensely than matrix feldspar, and has not replaced feld in the fractures within the phenocrysts; this suggests a compositional control and that phenocryst feldspar is different composition to matrix secondary (alteration) feldspar.

Mineral Probe Results:

Carbonates

Sample	Area	Description
120R-1083.7	A3 C1	coarse carbonate in diffuse, foliated vein
120R-1083.7	A3 C2	coarse carbonate in diffuse, foliated vein
120R-1083.7	A2 C1	coarse carbonate patch in matrix
120R-1083.7	A2 C2	coarse carbonate patch in matrix
120R-1083.7	A2 C3	coarse carbonate patch in matrix

Area	FeCO3	MnCO3	MgCO3	CaCO3	Carb total
A3 C1	0.76	3.32	0	99.23	103.31
A3 C2	0.9	3.26	0	97.53	101.69
A2 C1	0.71	2.12	0	98.62	101.45
A2 C2	1.11	3.18	0	95.23	99.52
A2 C3	0.34	1.8	0	99.12	101.26

White Micas

Sample	Area	Description
120R-1083.7	A1 S1	sericite alteration of feldspar phenocryst
120R-1083.7	A1 S2	sericite alteration of feldspar phenocryst
120R-1083.7	A3 S1	sericite in diffuse foliated vein
120R-1083.7	A3 S2	sericite in diffuse foliated vein
120R-1094.5	A1 S2	matrix sericite

Area	SiO2	TiO2	Al2O3	Cr2O3	Fe2O3	FeO	MnO	MgO	CaO	Na2O	K2O	Cl	Oxide total
A1 S1	48.2	0	31.12	0	0	2.61	0	1.26	0	0	11.4	0	94.59
A1 S2	48.36	0.22	29.31	0	0	3.63	0	1.81	0	0.32	11.01	0	94.66
A3 S1	48.61	0.27	29.07	0	0	3.54	0	1.86	0	0	11.17	0	94.52
A3 S2	48.35	0.15	29.26	0	0	2.94	0	1.89	0	0	11.38	0	93.97
A1 S2	34.03	0.8	17.15	1.66	0	12.35	0.84	0.52	12.42	0.31	0	0	80.08

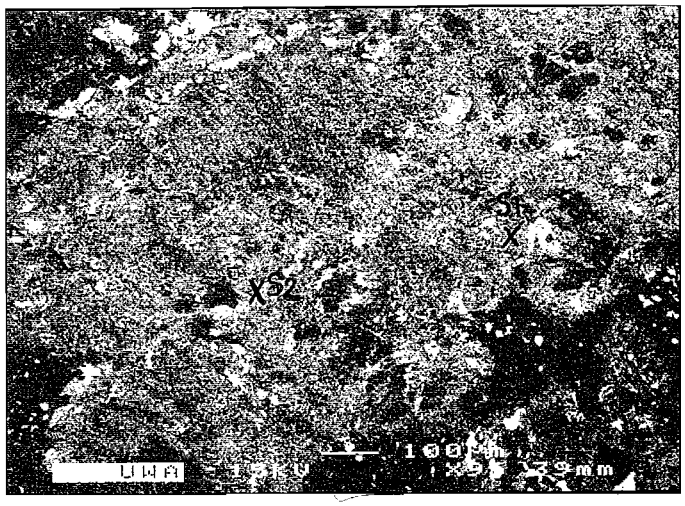

120R - 1083·7 AREA 1

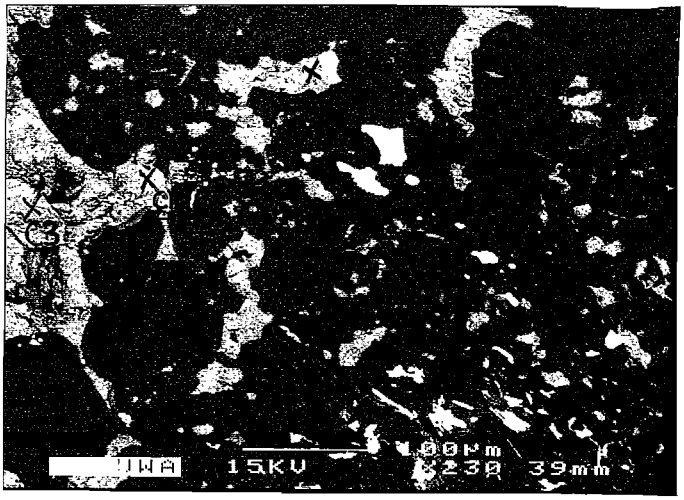

120R - 1083·7 AREA 2

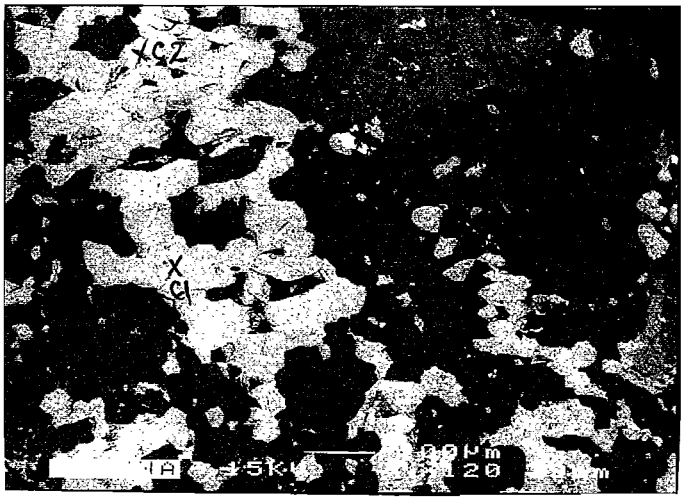

120R - 1083·7 AREA 3

Sample number: 96-120R-1100 Rock and thin section description

Location: Drill hole 120R, 1100.3 m; north end Rosebery mine

Hand specimen and summary: Lower crystal-lithic-rich part of Hangingwall Unit 3a pumice breccia mass flow unit. Intense carb-qtz alteration comprising veins and irregular patches (impregnations). Plagioclase»qtz phenocrysts and lithic clasts are well preserved and enclosed by extensively carb-replaced, originally pumice-rich "matrix". Alteration assemblages have strong S2 foliation.

Mineral percentages in thin section:

plagioclase	?35%	)__	65%
quartz	?30%	)	
carbonate	25%		
sericite	7%		
chlorite	1-2%		
sphene-leucox	2%		
opaques (sp)	1%		

Primary textures: 40% Feld»qtz crystal-rich and lithic-rich pumice breccia similar to 96-120R-3. Feldspar phenocrysts are multiple-twinned plag » simple-twinned Kspar. Primary feldspars well preserved, but pumiceous matrix texture very poorly preserved due to replacement by carbonate and strong foliation. Two ser>chl-rich lenses are strongly foliated fiamme, or pseudofiamme of ser-chl-altered and foliated pumice.

Tectonic fabrics: One strong foliation expressed by orientation of carb, coarse grained qtz, ser-chl, and elongation and partial transposition of matrix ?perlite texture in the lithics. Qtz crystals locally have undulose extinction, but subgrain development is minor. The fiamme-like lenses are strongly S2 foliated and oriented mainly parallel to S2, but locally diverge from S2 orientation, and in these areas are crenulated by S2.

Alteration, veins: Very abundant (40-50%) coarse grained veins, up to several mm wide, both of qtz»carb and carb»qtz. Carb is very pale brown to clear, and twinned (?Fe/Mn-poor ?calcite-dolomite). The carbonate is common in carb-rich veins and as irregular carb-rich patches. Most carb crystals show strong preferred orientation parallel to S2, and consequently are inferred to have grown synchronous with S2 . The irregular carb alteration patches occur preferentially in the pumiceous matrix, which is extensively obliterated by the carb. Interestingly, plag phenocrysts are only weakly ser-carb altered; more weakly altered than the samples further up-hole. Qtz in the q veins is moderately deformed and recrystallized to smaller aggregates of grains with strong preferred orientation parallel to S2. Chl is intergrown with ser, and the greatest concentration of both ser and chl is in the fiamme-like lenses. Sphene ± clinozoisite is abundant in one of these lenses, and is also disseminated through most of the rock, except the qtz-rich veins.

Many feldspar phenocrysts preserve thin relict rims, and internal fracture-fill veinlets, of untwinned secondary feldspar. The part of the matrix that is not extensively replaced by carbonate, comprises a fine grained mosaic of feld-qtz with lesser carb and ser.

Interpretation/important relationships: The strong S2 fabric in the carb and qtz alteration and veins, indicates growth of these minerals during S2 development. The qtz and carb alteration must therefore be pre- or syn-S2. The fiamme-like lenses are probably S1-parallel fiamme that are strongly transposed into the S2 foliation.

Mineral Probe Results

Carbonates

Sample	Area	Description
120R-1100.3	A4 C1	coarse grained carbonate in matrix
120R-1100.3	A4 C2	coarse grained carbonate in matrix
120R-1100.3	A2 C1	coarse grained carbonate patch in matrix
120R-1100.3	A2 C2	coarse grained carbonate patch in matrix
120R-1100.3	A1 C1	coarse grained, foliated carbonate in vein
120R-1100.3	A1 C2	coarse grained, foliated carbonate in vein

Area	FeCO3	MnCO3	MgCO3	CaCO3	Carb total
A4 C1	0.37	1.46	0	99.46	101.29
A4 C2	0.39	1.28	0	100.25	101.91
A2 C1	0.32	1.25	0	99.59	101.16
A2 C2	0.58	1.98	0	98.3	100.86
A1 C1	0.35	1.86	0.42	101.66	104.29
A1 C2	0.37	1.7	0	101.51	103.58

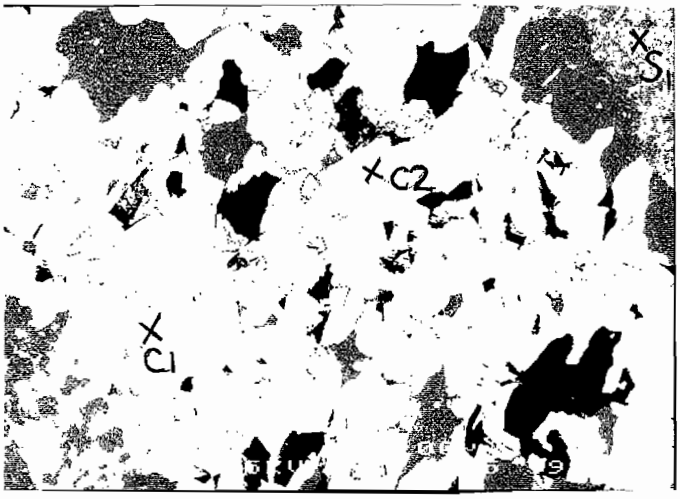

120R - 1100·3 AREA1

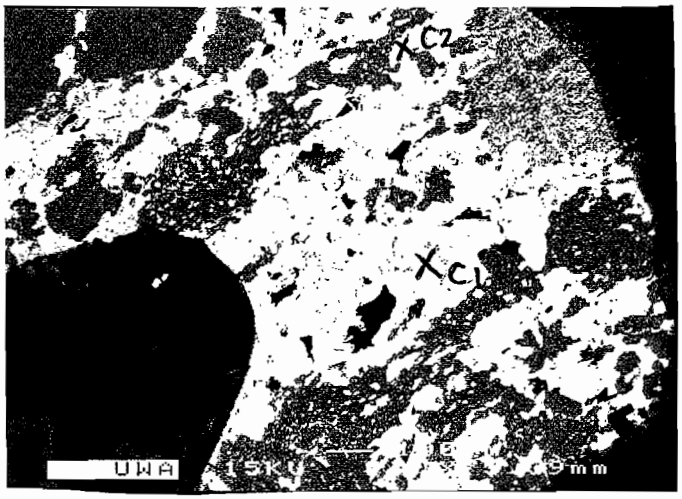

120R - 1100·3 AREA2

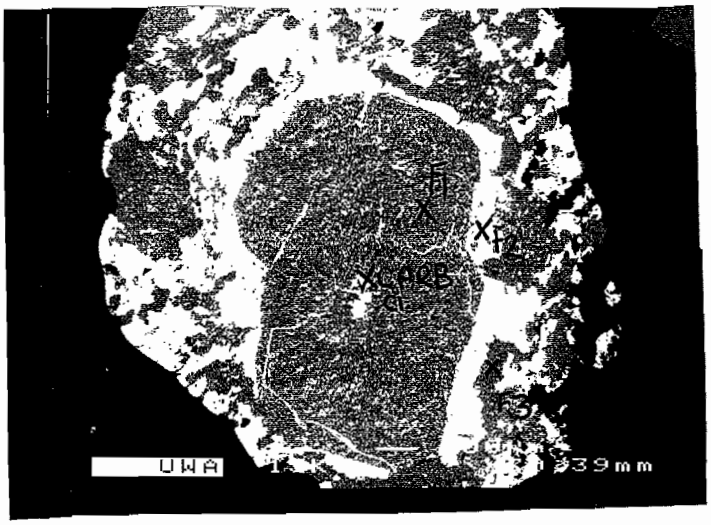

120R- 1100·3 AREA 3

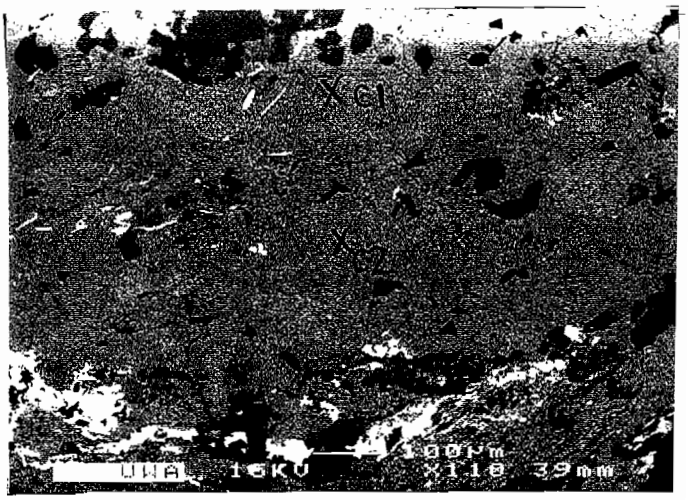

120R-1100·3 AREA 4

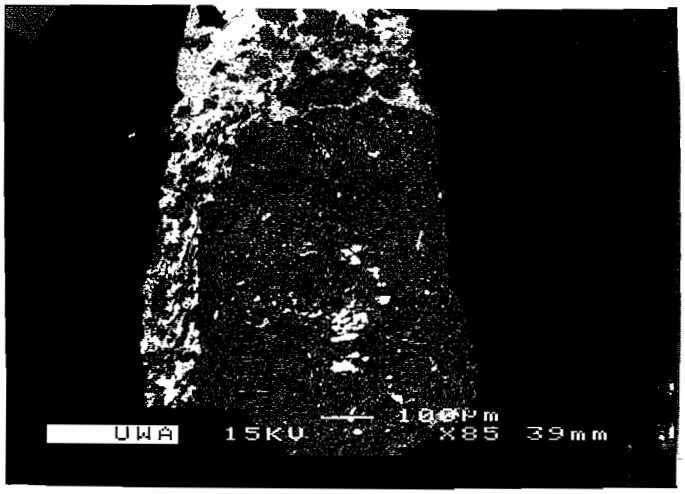

120R- 1100·3 AREA5

120R-1100·3 AREA 6

Sample number: 96-120R-1115 Rock and thin section description

Location: Drill hole 120R, 1115.9 m; north end Rosebery mine

Hand specimen and summary: Upper pumice shred-rich, feld>qtz crystal-poor part of Hangingwall Unit 2a (= ?Unit 2b) pumice breccia mass flow unit. Weak q-ser>chl alteration. Minor biotite alteration. Moderate-strong S2 cleavage.

Mineral percentages in thin section:

plagioclase	?55%	)__	80%
quartz	?25%	)	
sericite	10%		
chlorite	4%		
sphene-leucox	3-4%		
biotite	2%		
carbonate	1%		
opaques (sp)	²1%		
zircon	trace		

The mineral interpreted as sphene-leucoxene is common in many of the Rosebery thin sections. It is interpreted to be sphene extensively altered to leucoxene (very fine grained, cloudy). The mineral is non- to weakly-pleochroic pale to medium brown; high relief (similar to zircon and higher than clinozoisite); moderately high birefringence (bright yellow, green, red); occurs as irregular blocky to granular aggregates; poor cleavage, but internal thick black fractures and commonly also very fine granular ?fracture texture.

Primary textures: 7-10% 0.7mm feld (plag + ?Kspar) and 2% 0.5mm qtz crystals scattered in moderately-strongly foliated pumice matrix. The pumiceous matrix is probably a mat of close-packed, small, round-vesicle and tube-vesicle pumice clasts. Boundaries between clasts indistinct. Where best preserved, the pumice texture comprises plag replacement of both the bubble walls and the vesicles, and a fine trail of ser>chl along the boundary between the walls and vesicles. This grades rapidly to more sericitic areas in which sericite has grown out from these boundaries, partially replacing and obscuring the pumice structure.

Tectonic fabrics: Moderate to strong S2 foliation expressed by orientation of ser, chl, and elongation and extensive transposition of pumice texture. Qtz crystals have undulose extinction and minor subgrain development. Some feld crystals are pulled apart along the S2 cleavage. There is a weak crenulation cleavage oblique to S2, expressed by folding of the S2 mica foliation.

Alteration, veins: Pumice mainly altered to fine grained plag±qtz»ser mosaics, enclosing subordinate relics of coarser grained plag mosaics. Ser mainly occurs in the pumiceous matrix as diffuse streaks and disseminations. A smaller proportion of the ser occurs as alteration of feld phenocrysts, where it is intergrown and probably overprinted (partially replaced) by biot. Chl occurs with ser in the pumice. Ser and chl are clearly foliated parallel to S2, but biot appears relatively unfoliated. Carb is very minor, and very pale brown to clear (?Fe/Mn-poor ?calcite-dolomite).

Minor very thin, weakly folded, late syn-tectonic q veinlets with very minor sulphide.

Interpretation/important relationships: good example of foliated, fine pumice breccia.

Mineral Probe Results

Mica

Sample	Area	Description
120R-1115.9	A3 S2	matrix sericite
120R-1115.9	A3 S3	matrix sericite

Area	SiO2	TiO2	Al2O3	Cr2O3	Fe2O3	FeO	MnO	MgO	CaO	Na2O	K2O	Cl	Oxide total
A3 S2	52.35	0.19	27.51	0	0	3.05	0	1.12	0.1	1.93	8.97	0	95.22
A3 S3	49.6	0.17	28.38	0	0	3.19	0	1.32	0	0	10.84	0	93.5

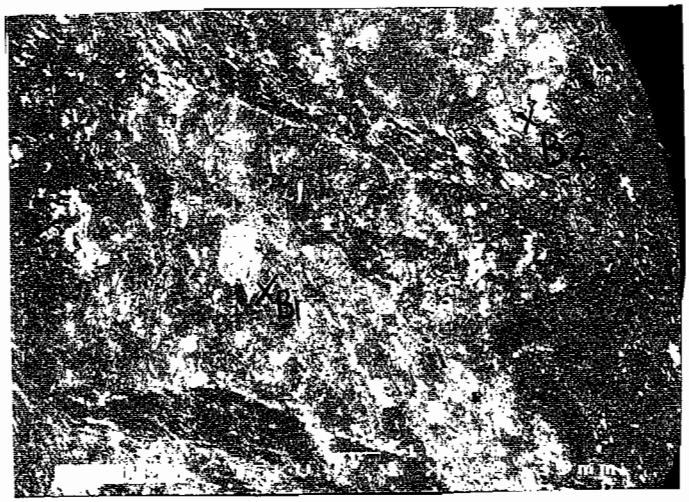

120 R - 1115·9 - AREA 1

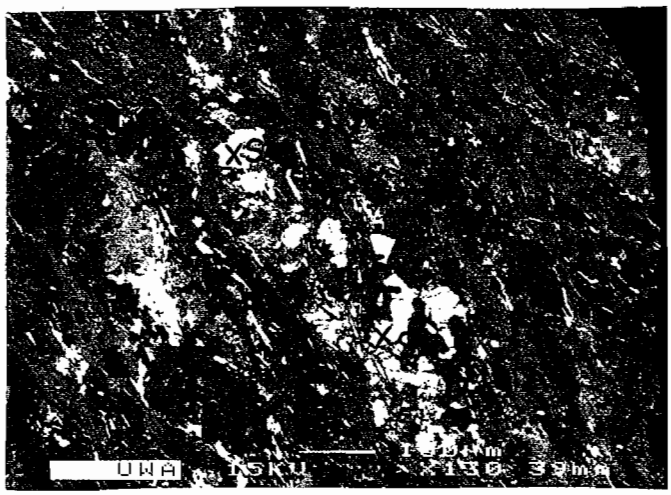

120R - 1115·9 AREA 2

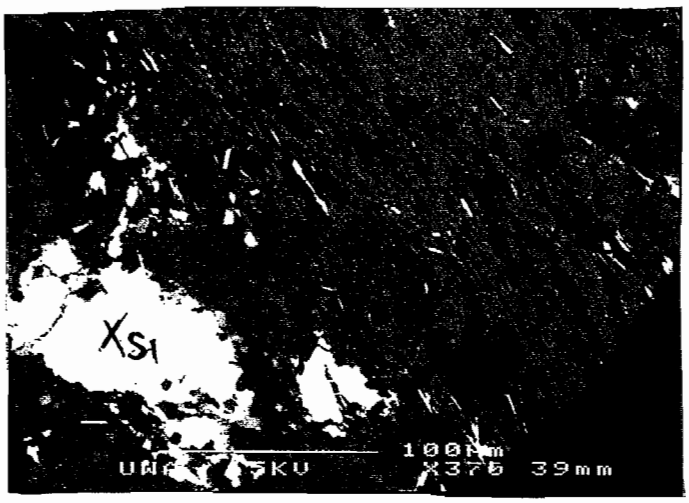

120R - 1115·9 AREA 3

Sample number: 96-120R-1147 Rock and thin section description

Location: Drill hole 120R, 1147.8 m; north end Rosebery mine

Hand specimen and summary: Middle, moderately feld>qtz crystal-rich part of Hangingwall Unit 2a pumice breccia mass flow unit. Moderate ser>carb>chl alteration of phenocrysts and ser alteration of matrix. Moderate S2 cleavage.

Mineral percentages in thin section:

plagioclase	?38%	)__	55%
quartz	?17%	)	
sericite	26%		
carbonate	12%		
chlorite	6%		
sphene-leucox	4%		
opaques (sp-py)	2%		

Primary textures: 40% crystals, comprising 30% 1.5mm (average) feld and 10% 1mm qtz, in moderately-strongly foliated pumice matrix. Most feld crystals appear to be plag; Kspar may or may not be present. Crystals include subhedral unbroken and angular broken shapes, but fragmentation of crystals mainly in situ tectonic. Matrix to crystals is foliated, fine grained and sericitic, with rare faintly preserved pumice texture. 20% of the rock comprises larger lenses of fine grained sericite containing a few subhedral feld and qtz crystals; these lenses probably represent deformed altered pumice clasts and pumice fiamme.

Tectonic fabrics: One moderate pervasive foliation expressed by orientation of ser, sphene-leucoxene, and beard growths on phenocrysts. Qtz crystals have undulose extinction and minor subgrain development. Many phenocrysts are in situ fractured, but not appreciably dismembered.

Alteration, veins: Feld phenocrysts strongly carb³ser»chl altered. Pumiceous matrix to phenocrysts moderately-strongly altered to ser-very minor chl-trace carb, and very fine grained feld-qtz mosaics. Carbonate is clear (?Fe/Mn-poor ?calcite-dolomite). Chl appears poorly foliated compared to ser. Irregular grains/patches of murky-cloudy sphene-leucoxene is abundant in the matrix as disseminations and deformed ?S1 trains.

Minor (1%) very thin (0.05-0.1 mm), moderately folded qtz veinlets, oriented at high angle to foliation.

Interpretation/important relationships: Ser strongly deformed and therefore probably pre ± syn-foliation in age. Chl and carb mainly occur within feld phenocrysts, consequently relation to foliation uncertain. Occurrence of some chl-carb within extensional syn-foliation fractures indicates at least some chl-carb growth during deformation.

Mineral Probe Results

Carbonates

Sample	Area	Description
120R-1147	A1 C1	carbonate patch within altered feldspar
120R-1147	A1 C2	carbonate patch within altered feldspar
120R-1147	A2 C1	carbonate patch within altered feldspar
120R-1147	A2 C2	carbonate patch within altered feldspar

Area	FeCO3	MnCO3	MgCO3	CaCO3	Carb total
A1 C1	1.34	3	0	96.39	100.73
A1 C2	1.52	2.8	0	95.84	100.16
A2 C1	0.79	2.09	0	99.41	102.29
A2 C2	1.29	2.93	0.36	97.14	101.72

White Micas

Sample	Area	Description
120R-1147	A3 S2	sericite rich matrix patch
120R-1147	A3 S3	sericite rich matrix patch

Area	SiO2	TiO2	Al2O3	Cr2O3	Fe2O3	FeO	MnO	MgO	CaO	Na2O	K2O	Cl	Oxide total
A3 S2	65.85	0.2	21.16	0	0	1.7	0	0.85	0	0	7.53	0	97.29
A3 S3	62.59	0.25	23.34	0	0	1.68	0	0.86	0	0	8.42	0	97.14

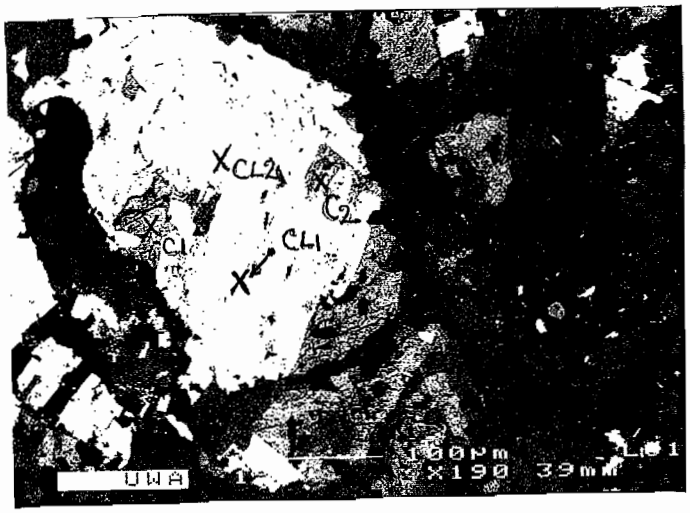

120R-1147·8 - AREA1

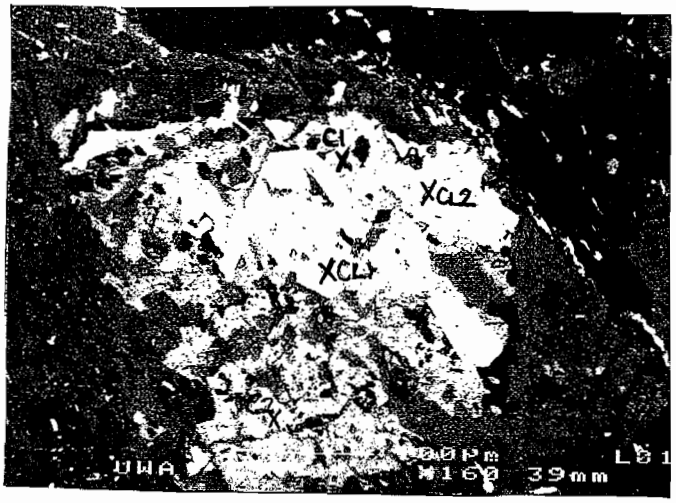

120R - 1147·8 AREA 2

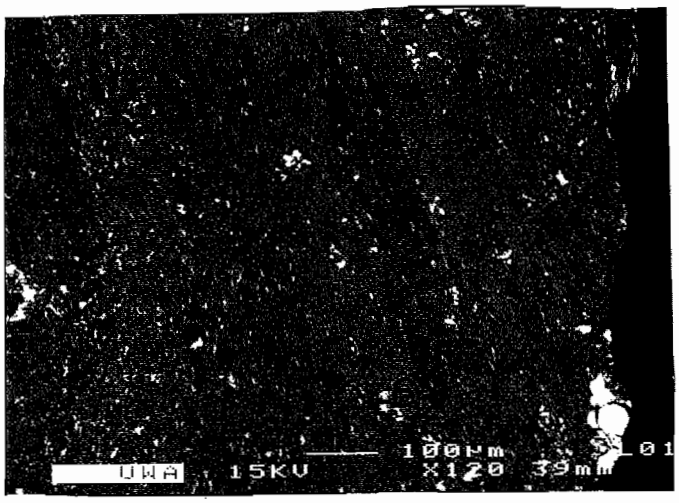

120R - 1147·8 AREA 3

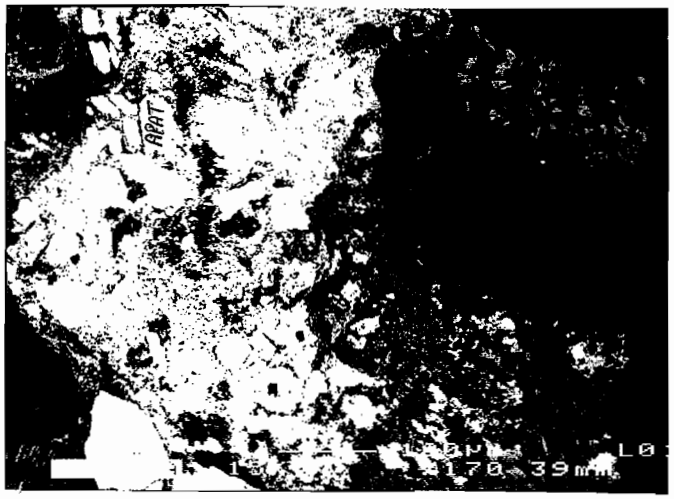

120R - 1147·8 AREA 4

Sample number: 96-120R-1169 Rock and thin section description

Location: Drill hole 120R, 1169.7 m; north end Rosebery mine

Hand specimen and summary: Lower, feld>qtz crystal-rich part of Hangingwall Unit 2a pumice breccia mass flow unit. Weak-moderate ser-carb>chl alteration, mainly of matrix to phenocrysts. Strong S2 foliation.

Mineral percentages in thin section:

plagioclase	?45%	)__	65%
quartz	?20%	)	
sericite	20%		
carbonate	7%		
chlorite	4%		
sphene-leucox	1-2%		
opaques (py)	2%		
zircon	trace		

Primary textures: 40% crystals/phenocrysts, comprising 33% 1.5mm (average) feld and 7% 1mm qtz, in strongly foliated matrix. Feld crystals are multiple twinned plag = untwinned to simple twinned ?Kspar. Matrix to crystals is foliated, fine grained and sericitic, with rare faintly preserved pumice texture. 20% of the rock comprises larger lenses of fine grained sericite containing a few feld and qtz phenocryst; these lenses probably represent deformed altered pumice clasts and pumice fiamme.

Tectonic fabrics: One strong pervasive foliation-lineation expressed by orientation of ser, sphene-leucoxene, beard growths on phenocrysts, and extensive dismembering of phenocrysts. Qtz crystals have undulose extinction and minor subgrain development. Most phenocrysts are in situ fractured and dismembered.

Alteration, veins: Feld phenocrysts are only weakly ser-carb altered, but have very fine brown dusting, which could be the dark grey ?carbon dusting seen in hand specimen; and the feld phenos also have somewhat quartzose appearance in cross polars, which may reflect partial silicification. Matrix to phenocrysts moderately-strongly altered to fine grained ser³feld-qtz-minor sphene-leucoxene-trace ?carbon. Chl is foliated and mainly occurs in beard growths/pressure shaddows and extensional fractures in tectonically dismembered phenocrysts. Carb occurs mainly as irregular patches/impregnation of the matrix, and extensively in beard growths/pressure shaddows and extensional fractures in tectonically dismembered phenocrysts. The carb is commonly foliated, and has only faint brownish tinge (?Fe/Mn-poor ?calcite-dolomite). Sphene-leucoxene and opaques (sulphide) occur together in spaced, foliated, anastomosing trails that could be deformed S1 stylolitic foliation; and sphene-leucoxene also is more abundant than elsewhere in the carbonate-rich pressure shadows and veins, i.e. there is an association between carbonate and sphene abundance. Zircons are relatively common in these trails also.

Rare (<1%) very thin (0.05-0.1 mm), moderately folded qtz ± carb veinlets, oriented at high angle to foliation.

Interpretation/important relationships: Chl and carb grew (in pressure shadows) during S2 foliation development. Ser is pre- to syn-S2 foliation.

Mineral Probe Results

Carbonates

Sample	Area	Description
120R-1169	A1-C2	carbonate grain within feldspar
120R-1169	A3 C1	granular carbonate in pressure shadow of feldspar
120R-1169	A3 C2	granular carbonate in pressure shadow of feldspar
120R-1169	A3 C3	granular carbonate in pressure shadow of feldspar
120R-1169	A3 C4	granular carbonate in pressure shadow of feldspar
120R-1169	A3 C5	granular carbonate in pressure shadow of feldspar

Area	FeCO3	MnCO3	MgCO3	CaCO3	Carb total
A1-C2	1.6	2.41	0	97.98	101.99
A3 C1	1.42	1.93	0.4	100.85	104.6
A3 C2	2.42	2.19	0.61	95.96	101.17
A3 C3	1.97	2.33	0.46	96.09	100.85
A3 C4	1.58	2.12	0.38	98.44	102.52
A3 C5	1.84	2.06	0.33	99.96	104.19

White Micas

Sample	Area	Description
120R-1169	A2-SER1	foliated sericite in matrix
120R-1169	A2 M2	foliated sericite in matrix
120R-1169	A2 M3	foliated sericite in matrix
120R-1169	A4 S1	elongate sericite altered domain
120R-1169	A4 S2	elongate sericite altered domain
120R-1169	A4 S3	elongate sericite altered domain

Area	SiO2	TiO2	Al2O3	Cr2O3	Fe2O3	FeO	MnO	MgO	CaO	Na2O	K2O	Cl	Oxide total
A2-SER1	47.79	0.3	32.01	0	0	1.69	0	1.1	0	0	11.36	0	94.25
A2 M2	47.92	0.5	32.69	0	0	1.88	0	1.26	0	0	11.25	0	95.5
A2 M3	47.94	0.45	32.48	0	0	1.53	0	1.16	0	0	11.29	0	94.85
A4 S1	47.96	0.31	30.79	0	0	3.07	0	1.37	0	0	10.55	0	94.05
A4 S2	47.29	0.44	32.93	0	0	1.58	0	1.11	0	0	11.26	0	94.61
A4 S3	47.47	0.27	32.27	0	0	1.94	0	1.28	0	0	11.33	0	94.56

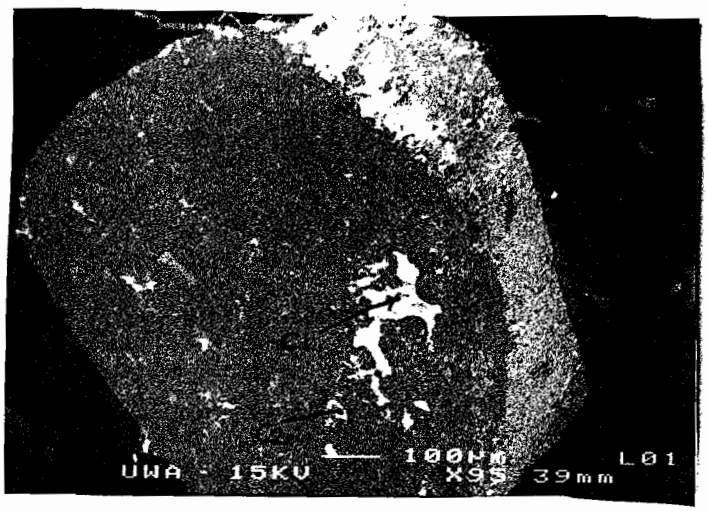

120R-1169.7 - AREA 1

120R-1169.7 - AREA 2

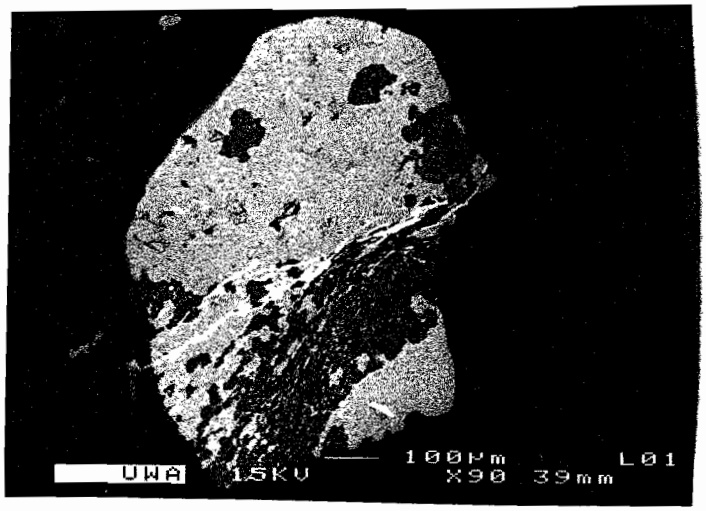

120R-1169.7 - AREA 3

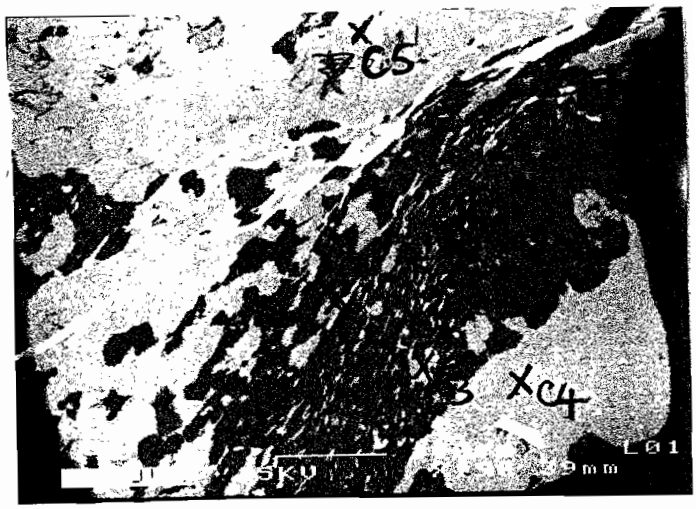

120R-1169.7 - AREA 4

120R-1169.7 - AREA 5

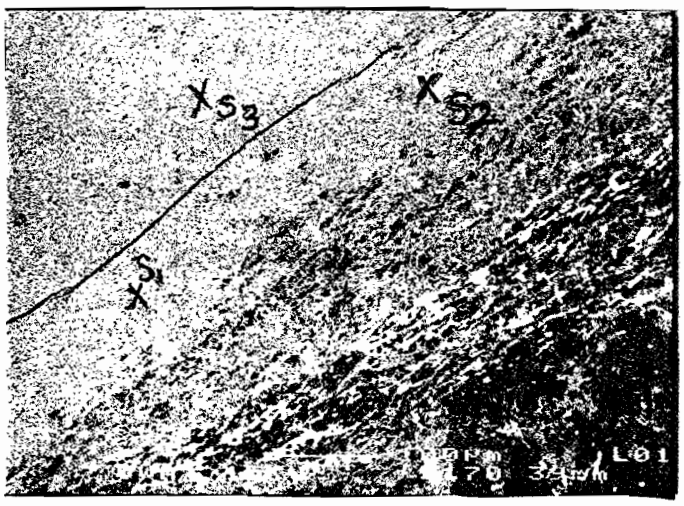

120R-1169.7 - AREA 6

Sample number: 96-120R-1184 Rock and thin section description

Location: Drill hole 120R, 1184.0 m; north end Rosebery mine

Hand specimen and summary: Upper part of upper of two black slate units; Unit 1 of hangingwall succession. Fine parallel syn-tectonic qtz-carb veining. Strong S2 foliation.

Mineral percentages in thin section:

sericite	50%			
plagioclase		?10%	)__	35%
quartz		?25%	)	
carbonate		7%		
graphite/carbon		5%		
sphene-leucox		3%		
opaques (pyrh-py)	2-3%			

Primary textures: Rare: local relict primary lamination at high angle to cleavage; comprises 0.5-1mm bands of coarser grained qtz-feld-opaques-sphene-leucoxene.

Tectonic fabrics: One strong pervasive slatey cleavage = S2. Very locally there is a faint S1 or early S2 crenulated by the main cleavage (even in the margin of veins). There is no distinct bedding-parallel S1 foliation. The qtz-carb veins are boudinaged (veins have strong pinch and swell morphology) and locally foliated by S2. The cleavage is slightly oblique to the veins, and has a moderately anastomosing style. The veins are planar, whereas the faint primary lamination is folded (by F2-S2).

Alteration, veins: 25% of the rock comprises thin (²2mm, average 0.3mm), parallel, qtz³carb»ser-sulphide veinlets. Qtz in the veins is mainly fine grained anhedral mosaics, recrystallized from original larger qtz grains. Sulphides occur equally as very fine grained dissemination within the slate and as coarser blebs within the veins. Most or all of the carb appears to be in the veins. The carbonate is white calcitic in handspecimen, and pale non- to very weakly pleochroic in plane polarised light in thin section.

Interpretation/important relationships: Most likely the qtz-carb veins developed early during the S2-F2 deformation, and were themselves deformed by S2.

Mineral Probe Results

Carbonates

Sample	Area	depth	Description
120R-1184.0	A2 C1	1184	carbonate within quartz vein
120R-1184.0	A1 C1	1184	vein carbonate
120R-1184.0	A1 C2	1184	vein carbonate
120R-1184.0	A3 C1	1184	vein carbonate
120R-1184.0	A3 C2	1184	vein carbonate

Area	FeCO3	MnCO3	MgCO3	CaCO3	NiCO3	SiO2	Al2O3	Carb total
A2 C1	1.81	1.26	1.23	96.93	0	0	0	101.23
A1 C1	1.92	1.15	1.25	95.41	0	0	0	99.73
A1 C2	2.11	1.2	1.53	96.3	0	0	0	101.14
A3 C1	2.47	1.38	1.9	95.8	0	0	0	101.55
A3 C2	1.81	1.1	1.53	96.57	0	0	0	101

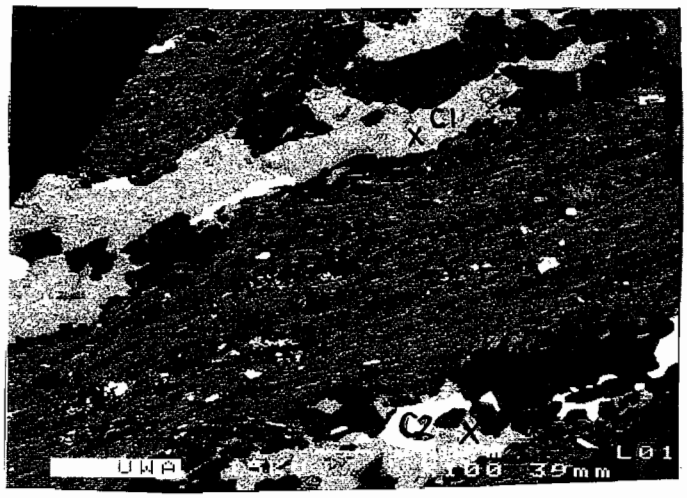

120R-1184.0 AREA 1

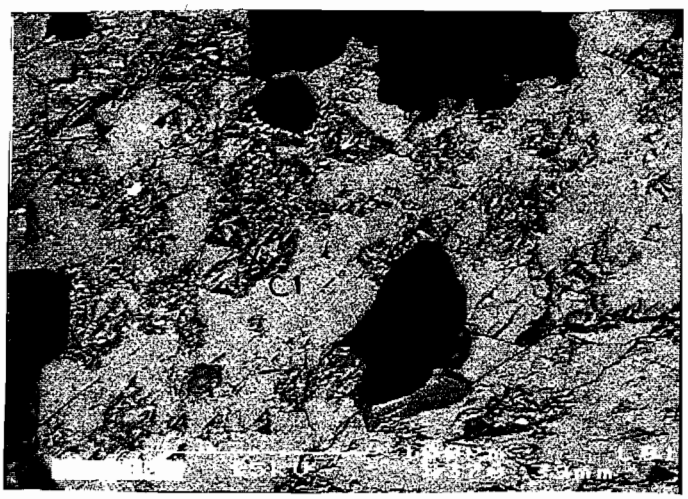

120R-1184.0 AREA 2

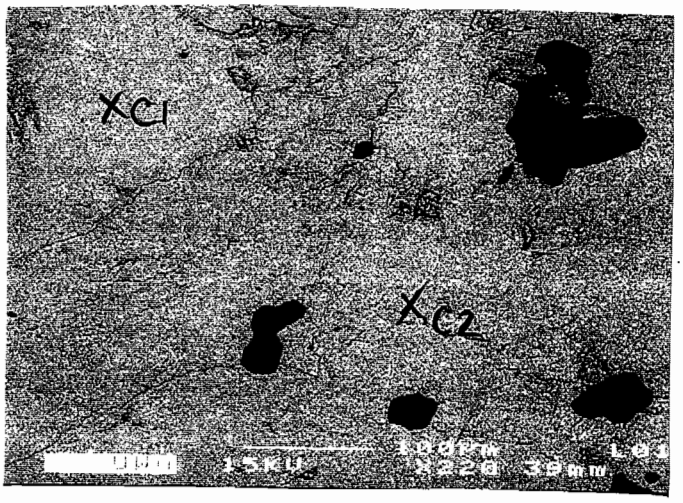

120R-1184.0 AREA 3

Sample number: 96-120R-1229 Rock and thin section description

Location: Drill hole 120R, 1229.3 m; north end Rosebery mine

Hand specimen and summary: Lower part of upper of two black slate units; Unit 1 of hangingwall succession. Fine parallel syn-tectonic qtz-carb veining. Strong S2 foliation.

Mineral percentages in thin section:

sericite	35%		
plagioclase	?5%	)__	40%
quartz	?35%	)	
carbonate	10%		
graphite/carbon	10%		
sphene-leucox	2%		
opaques (pyrh-py-sp)	2%		

Primary textures: Rare: local relict primary lamination at high angle to cleavage; comprises 0.5-1mm bands of coarser grained qtz-feld-opaques-sphene-leucoxene.

Tectonic fabrics: One strong pervasive slatey cleavage = S2. Locally there is a faint but distinct S1 foliation parallel to bedding (primary lamination). The qtz-carb veins are boudinaged (veins have strong pinch and swell morphology) and foliated by S2. The cleavage is slightly oblique to the veins, and has a moderately anastomosing style. The veins are planar, whereas the faint primary lamination is folded (by F2-S2).

Alteration, veins: Similar to 96-120R-1184, but more veinlets and more carb, and there is a subordinate synchronous qtz-carb vein set oblique to the main set. 35% of the rock comprises thin (²5mm, average 0.4mm), parallel, qtz>carb»ser-sulphide veinlets and carb>qtz»ser-sulphide veinlets. Qtz in the veins is mainly fine grained anhedral mosaics, recrystallized from original larger qtz grains. Almost all sulphides occur as coarse euhedral crystals and blebs within the veins. Most or all of the carb appears to be in the veins. The carbonate is white calcitic in handspecimen, and pale non- to very weakly pleochroic in plane polarised light in thin section.

Interpretation/important relationships: Most likely the qtz-carb veins developed early during the S2-F2 deformation, and were themselves deformed by S2.

Mineral Probe Results

Carbonates

Sample	Area	depth	Description
120R-1229.3	A1 C1	1229.3	coarse carbonate in vein
120R-1229.3	A1 C2	1229.3	coarse carbonate in vein
120R-1229.3	A2 C1	1229.3	fine carbonate in vein
120R-1229.3	A2 C2	1229.3	fine carbonate in vein

Area	FeCO3	MnCO3	MgCO3	CaCO3	NiCO3	SiO2	Al2O3	Carb total
A1 C1	1.87	0.99	1.67	93.71	0	0	0	98.24
A1 C2	1.42	0.7	1.42	95.91	0	0	0	99.45
A2 C1	0.98	0.6	0.77	96.37	0	0	0	98.73
A2 C2	0.65	0.34	0.27	96.09	0	0	0	97.34

Sample number: 96-120R-1237 Rock and thin section description

Location: Drill hole 120R, 1237.2 m; north end Rosebery mine

Hand specimen and summary: Upper part of upper interval of TSV (host rocks), between black slate units. Very strong carb>ser>chl alteration, mainly of matrix to phenocrysts. Strong S2 foliation.

Mineral percentages in thin section:

carbonate	40%
plagioclase	30%
sericite	15%
quartz	?7%
chlorite	3%
sphene-leucox	1-2%
opaques (py-pyrrh)	3%

Primary textures: The rock has the relict primary texture of a moderate to well sorted, feld crystal-lithic sandstone. Crystals: 60-70% of rock originally; average 1.2mm; all plagioclase, commonly with concentric zoning (this zoning much more prominent than in hangingwall sequence). Lithics: 7% of rock; all same textural and compositional type; probably andesitic; <5% small phenocrysts (²1mm) of feld»ilmenite/magnetite; fine granular feld-microlitic to micropoikilitic devitrified, feldpar-rich groundmass, with 2-5% fine dusting of opaques (?mag, ilmen, sphene, py) and ²10% very fine chl laths; similar to lithics in the Rosebery-Hercules footwall pumice breccia.

Tectonic fabrics: One strong pervasive foliation-lineation expressed by orientation of carb, ser, chl, and beard growths on phenocrysts. Cross-cutting carb>qtz veins are less deformed.

Alteration, veins: Very strong carb>ser alteration comprising: Feld crystals moderately to strongly ser³carb altered. Lithics have only weak ser-chl-carb alteration. Matrix and local larger patches (i.e. including feld crystals) have intense carb>ser>chl replacement. This cut by younger coarse grained carb»qtz veins with little or no foliation (much less than the alteration they cut). The carb is commonly foliated (occurs as elongate grains parallel to the foliation), and has only faint brownish tinge/dustgin (?Fe/Mn-poor ?calcite-dolomite). Sphene-leucoxene and opaques (sulphide) occur disseminated throughout, and in spaced, foliated, anastomosing stylolitic trails.

Interpretation/important relationships: Groundmass carb grew and/or recrystallized during S2 foliation development. Cross-cutting carb>qtz veins are younger than groundmass carb>ser alteration.

Mineral Probe Results

Carbonates

Sample	Area	depth	Description
120R-1237	R4 C1	1237	coarse vein carbonate
120R-1237	R4 C2	1237	coarse vein carbonate
120R-1237	A2 C2	1237	foliated matrix carbonate
120R-1237	A2 C3	1237	foliated matrix carbonate
120R-1237	A1 C1	1237	

Area	FeCO3	MnCO3	MgCO3	CaCO3	NiCO3	SiO2	Al2O3	Carb total
R4 C1	0.5	0.5	0.86	96.23	0	0	0	98.09
R4 C2	0.37	0.45	0	97.05	0	0	0	97.88
A2 C2	0	0.53	0	101.16	0	0	0	101.69
A2 C3	0.42	0	0.27	101.26	0	0	0	101.95
A1 C1	0	0.23	0	101.28	0	0	0	101.51

White Micas

Sample	Depth	Area	Description
120R-1237	1237	A3 S1	sericite in elongate ?pumice clast
120R-1237	1237	A3 S2	sericite in elongate ?pumice clast
120R-1237	1237	A3 S3	sericite in elongate ?pumice clast

Area	SiO2	TiO2	Al2O3	Cr2O3	Fe2O3	FeO	MnO	MgO	CaO	Na2O	K2O	Cl	Oxide total
A3 S1	45.75	0.21	35.09	0	0	0.15	0	0.42	0	2.3	7.18	0	91.1
A3 S2	45.41	0.18	34.92	0	0	0.28	0	0.73	0	1.82	8.12	0	91.46
A3 S3	45.51	0	34.76	0	0	0.2	0	0.63	0.12	1.36	8.49	0	91.07

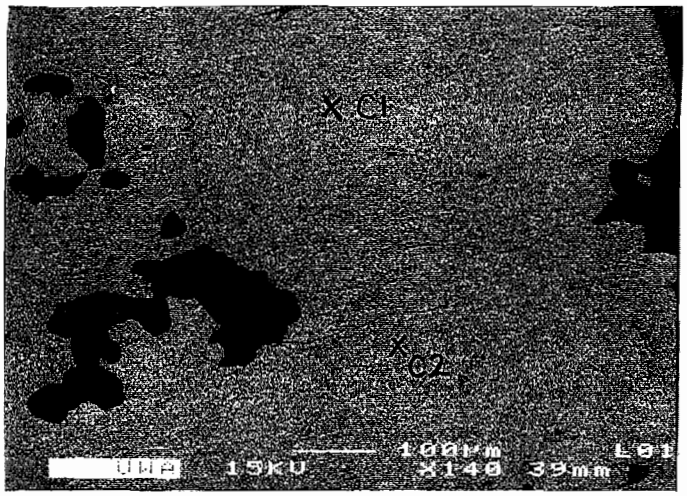

120R 1229·3 AREA 1

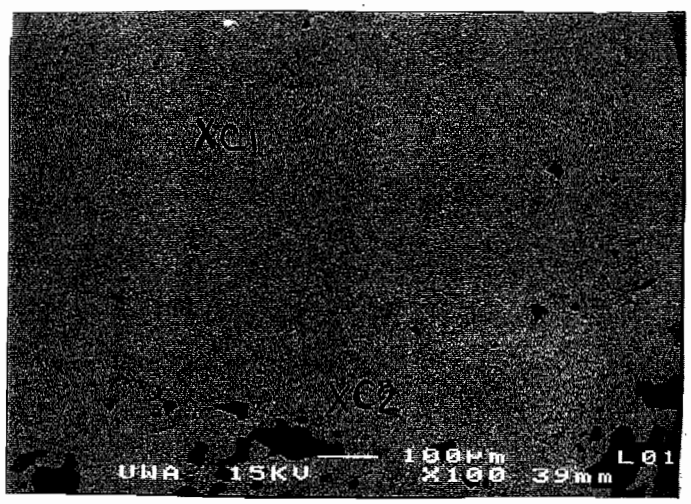

120R 1229·3 AREA 2

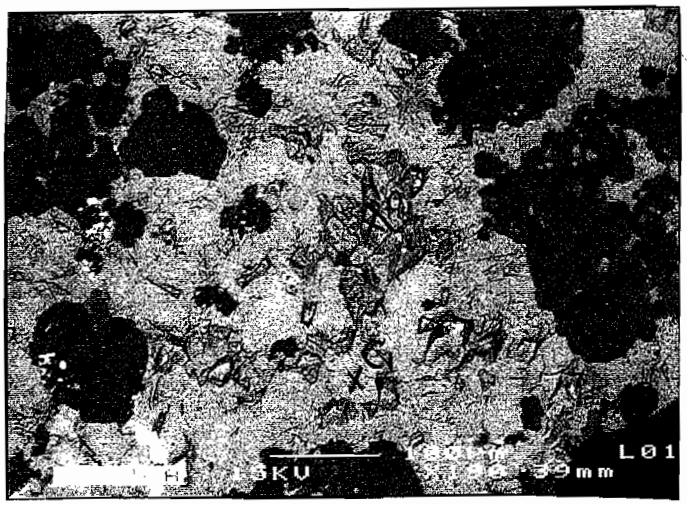

120R - 1237.2 - AREA 1

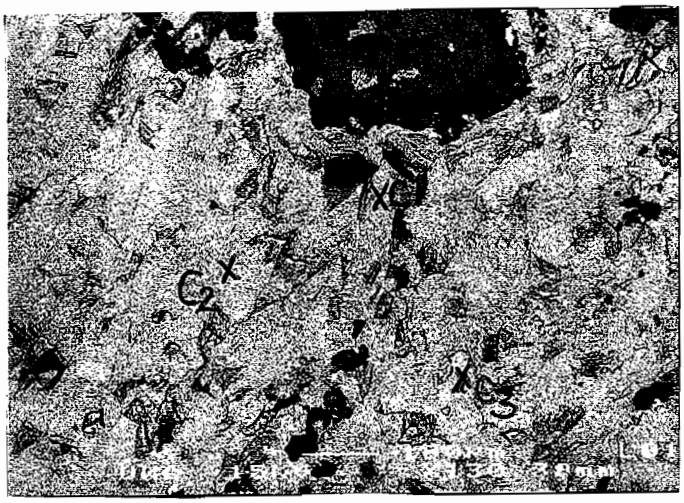

120R - 1237.2 - AREA 2

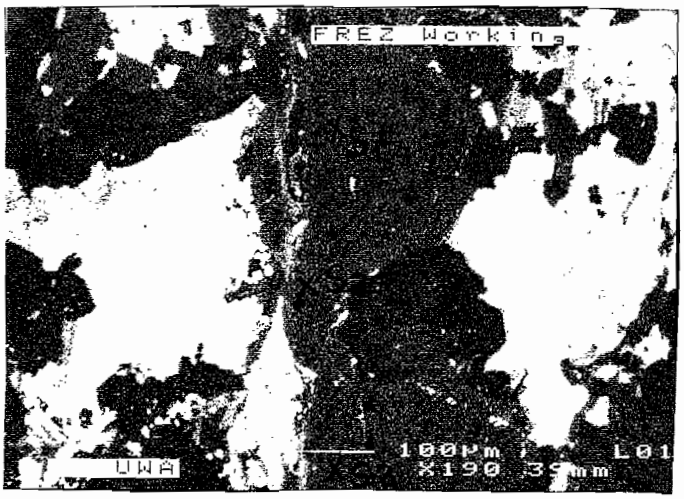

120R - 1237.2 - AREA 3

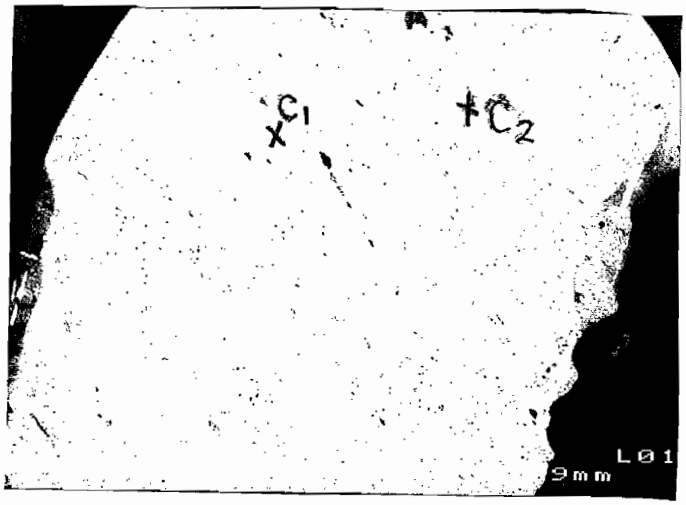

120R - 1237.2 - AREA 4

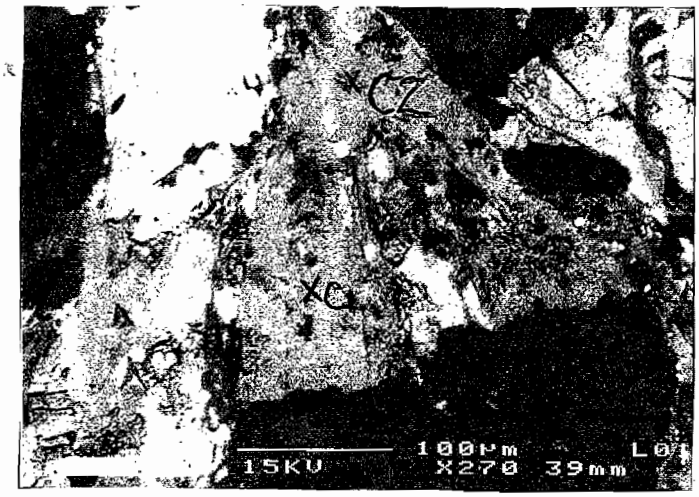

120R - 1237.2 - AREA 5

Sample number: 96-120R-1241 Rock and thin section description

Location: Drill hole 120R, 1241.8 m; north end Rosebery mine

Hand specimen and summary: Lower part of upper interval of TSV (host rocks), between black slate units. Strong ser>qtz>py alteration. Strong S2 foliation.

Mineral percentages in thin section:

plagioclase	?20%	)__	40%
quartz	?20%	)	
sericite	35%		
chlorite	5%		
opaques (py)	5%		
carbonate	4%		
sphene-leucox	3%		
apatite	1%		

Primary textures: The rock has the relict primary texture of a moderate to well sorted, medium grained, crystal-lithic sandstone. Crystals form approximately 30% of rock; average 0.8mm; all inferred to be feld (ser replaced), except 1% ²0.5mm subhedral to broken angular qtz crystals. Lithic clasts are very abundant (10% of rock) and are all the same textural and compositional type: fine grained microlitic to micropoikilitic andesite clasts the same as in 96-120R-1237. Notably some of the lithics are moderately to well rounded.

Tectonic fabrics: A strong pervasive foliation-lineation is expressed by orientation of altered feld crystals and lithic clasts, ser, chl, and beard growths on phenocrysts. This foliation overprints, and is axial planar to micro-folds in, a spaced, dark, stylolitic S1 foliation expressed by concentration of sphene, apatite and fine opaques. In one part of this S1 foliation there is a large white mica grain oriented parallel to the S1 foliation, and crenulated by the main S2 foliation (very top of thin section).

Alteration, veins: Strong ser>qtz>py alteration comprising: intense ser-minor carb replacement of feld crystals, moderate alteration of matrix to qtz±feld>ser composition, and weak to moderate ser-chl-carb alteration of lithics. Sphene, apatite and opaques are abundant. Opaques appear to be mainly fine grained euhedral pyrite. Sphene-leucoxene and opaques (sulphide) occur disseminated throughout, but are especially abundant in spaced, foliated, stylolitic S1 trails. Carb is minor and occurs mainly with ser in the feld crystals.

Interpretation/important relationships: Good evidence for an S1 foliation with concentration of sphene, apatite, opaques, and with some pre-S2 micas. The S1 is strongly foliated and crenulated by S2.

Mineral Probe Results

Carbonates

Sample	Area	depth	Description
120R-1241	A3 C1	1241	carbonate altered feldspar
120R-1241	A1 C1	1241	coarse carbonate in carb-pyrite vein
120R-1241	A1 C2	1241	coarse carbonate in carb-pyrite vein
120R-1241	M082	1241	coarse carbonate in carb-pyrite vein

Area	FeCO3	MnCO3	MgCO3	CaCO3	NiCO3	SiO2	Al2O3	Carb total
A3 C1	0.81	0.5	0.48	95.73	0.33	0	0	97.85
A1 C1	0.84	0.92	0	100.53	0	0	0	102.29
A1 C2	1.65	0.7	0.84	95.1	0	0	0	98.28
M082	1.13	0.31	0.48	96.84	0	0	0	98.75

White Micas

Sample	Depth	Area	Description
120R-1241	1241	A2 S1	sericite in strongly altered feldspar
120R-1241	1241	A2 S2	sericite in strongly altered feldspar
120R-1241	1241	A3 S1	altered feldspar crystal
120R-1241	1241	A3 S2	altered feldspar crystal

Area	SiO2	TiO2	Al2O3	Cr2O3	Fe2O3	FeO	MnO	MgO	CaO	Na2O	K2O	Cl	Oxide total
A2 S1	46.08	0	33.92	0	0	0.26	0	0.78	0	0.87	9.07	0	90.98
A2 S2	45.57	0.19	33.91	0	0	0.29	0	0.75	0	0.81	9.16	0	90.68
A3 S1	45.68	0.23	34.01	0	0	0.34	0	0.7	0	0.83	9.18	0	90.97
A3 S2	39.13	0.15	33.67	0	0	6.82	0	4.99	0.17	4.11	1.87	0	90.91

120R-1241 - AREA 1

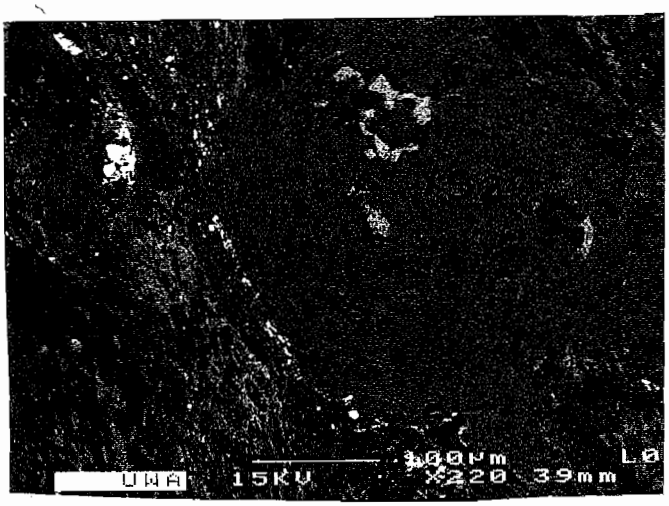

120R - 1241 AREA 2

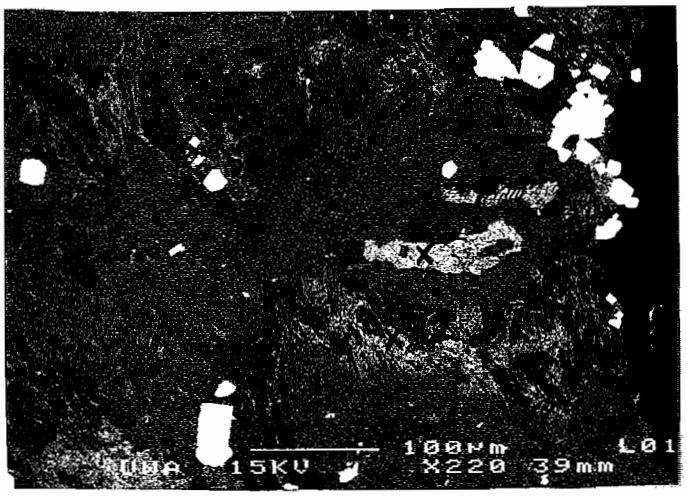

120R - 1241 AREA 3

Sample number: 96-120R-1256 Rock and thin section description

Location: Drill hole 120R, 1256.0 m; north end Rosebery mine

Hand specimen and summary: Lower black slate unit, between upper and lower members of TSV. Fine parallel syn-tectonic qtz-carb-sulphide veining. Strong S2 foliation.

Mineral percentages in thin section:

sericite	30%	
plagioclase	?5%	)__ 50%
quartz	?45%	)
carbonate	5%	
graphite/carbon	8%	
sphene-leucox	2%	
opaques (pyrh-py-sp)	4%	

Primary textures: Rare: local relict primary lamination at high angle to cleavage; comprises 0.5-1mm bands of coarser grained qtz-feld-opaques-sphene-leucoxene.

Tectonic fabrics: One strong pervasive slatey cleavage = S2. Locally there is a faint S1 foliation, crenulated by S2. The qtz-carb veins are boudinaged (veins have strong pinch and swell morphology) and foliated by S2. The cleavage is slightly oblique to the main set of veinlets, and has a moderately anastomosing style. The veins subparallel to S2 are planar, whereas the high angle veins and faint primary lamination are folded (by F2-S2).

Alteration, veins: Similar to 96-120R-1184. 25% of the rock comprises thin (?5mm, average 0.4mm), subparallel, qtz>carb>sulphide veinlets. Qtz-carb veinlets subparallel to the foliation » veinlets at high angle to foliation. Veinlets are mainly qtz>carb, and sulphides are most abundant in the veins dominated by qtz, or sections of veins dominated by qtz. The parallel veins cut across (post-date) the high angle veins. The parallel veins are mainly granular with moderate relict recrystallized qtz-carb foliation. The high angle veins have strong qtz fibre growth parallel to S2. Almost all sulphides occur as coarse euhedral crystals and blebs within the veins. Most or all of the carb appears to be in the veins. The carbonate is white calcitic in handspecimen, and pale non- to very weakly pleochroic in plane polarised light in thin section.

Interpretation/important relationships: The qtz-carb veins appear to have developed early during the S2-F2 deformation, and were themselves deformed by S2.

Mineral Probe Results

Carbonates

Sample	Area	depth	Description
120R-1256.0	A2 C1	1256	coarse qtz - carbonate vein
120R-1256.0	A2 C2	1256	coarse qtz - carbonate vein
120R-1256.0	A1 C1	1256	recrystallised foliated vein carbonate
120R-1256.0	A1 C2	1256	recrystallised foliated vein carbonate

Area	FeCO3	MnCO3	MgCO3	CaCO3	NiCO3	SiO2	Al2O3	Carb total
A2 C1	0.45	0.81	1	97.84	0	0	0	100.1
A2 C2	0.69	1	1.15	96.28	0	0	0	99.13
A1 C1	0.42	0.92	0.54	98.17	0	0	0	100.06
A1 C2	0.68	1.05	0.86	96.76	0	0	0	99.35

120R-1256 AREA 1

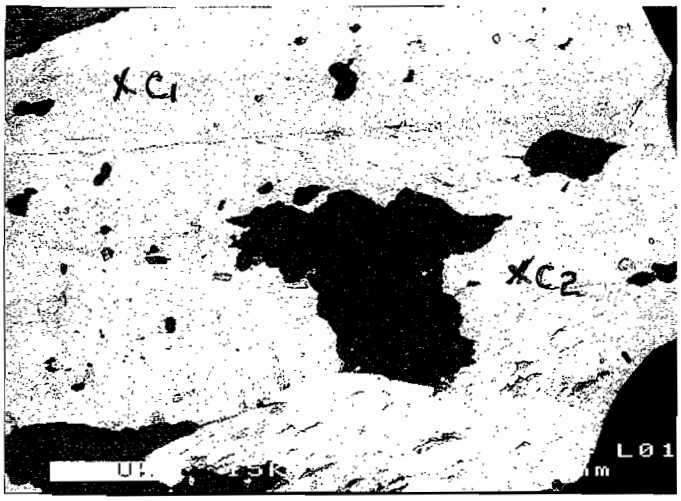

120R-1256 AREA 2

Sample number: 96-120R-1265 Rock and thin section description

Location: Drill hole 120R, 1265.5 m; north end Rosebery mine

Hand specimen and summary: Middle interval of TSV (host rocks), between the lower black slate unit and the qtz-feld-biot-porphyritic rhyolite sill. Diffuse stratified, medium-coarse grained, crystal-lithic sandstone. Boundary between strong carb>ser and weak ser-qtz alteration. Moderate S2 foliation, and prominent weak S1 stylolitic foliation.

Mineral percentages in thin section:

plagioclase	45%	)__ 65%
quartz	?20%	)
carbonate	15%	
sericite	15%	
sphene-leucox	5%	
opaques (py-pyrrh)	1%	

Primary textures: The rock has the relict primary texture of a well sorted, medium grained, crystal-lithic sandstone. Crystals: 35% of rock originally; average 0.5mm, mainly broken angular, plagioclase » qtz (1-2%); many plagioclase crystals have concentric zoning (this zoning much more prominent than in hangingwall sequence). Lithic clasts form 15% of the rock, and comprise two textural types of aproximately equal abundance: (1) fine grained, feld microlitic to micropoikilitic andesite, the same as lithics in 96-120R-1237, -1241 (<5% small phenocrysts (²1mm) of feld»ilmenite/magnetite; fine granular feld-microlitic to micropoikilitic devitrified, feldpar-rich groundmass, with 2-5% fine dusting of opaques (?mag, ilmen, sphene, py) and ²10% very fine chl laths); (2) massive clasts with fine grained anhedral qtz mosaic texture. The latter type could be a silicified equivalent of the fine grained andesitic clasts. Rest of rock is probably deformed, altered pumice clasts.

Tectonic fabrics: There is one moderate intensity, pervasive foliation-lineation expressed by orientation of ser, carb, beard growths on phenocrysts, and orientation of elongate feld phenocrysts. There is also a spaced, dark, S1 stylolitic foliation composed of a concentration of sphene-leucoxene along wavy anastomosing trails subparallel to, but generally slightly oblique to, the pervasive S2 foliation. S2 is axial planar to local microfolds in the S1 sphene-leucoxene trails. The S1 sphene-leucoxene trails probably correspond to the faint lamination seen in hand specimen. Minor cross-cutting carb>qtz-py veins are moderately folded about S2.

Alteration, veins: There is a rapid gradational boundary in the thin section between strong carb>ser alteration at one end of the thin section, and weak ser-qtz at the other end. The carb>ser alteration comprises 30% foliated carb»ser in the matrix to the feld crystals and lithic clasts. The ser-qtz alteration comprises 10% ser in a fine grained feld-qtz matrix. Feld crystals/phenocrysts are only very weakly ser-carb altered in the weak ser-qtz alteration, and are only slightly more (weakly) ser-carb altered in the strong carb>ser altered zone. Sphene-leucoxene is very abundant and mainly occurs as spaced, anastomosing, stylolitic S1 trails. Minor carb»qtz-py veinlets occur at a high angle to S2. Carb has only faint brownish tinge/dusting (?Fe/Mn-poor ?calcite-dolomite).

Interpretation/important relationships: Ser and carb were both present during S2 deformation. Timing relationship between ser and carb uncertain, but it appears that carb overprints ser.

Mineral Probe Results

Carbonates

Sample	Area	depth	Description
120R-1265	A2 C1	1265	coarse S2 vein carbonate
120R-1265	A2 C2	1265	coarse S2 vein carbonate
120R-1265	A1 C1	1265	foliated matrix carbonate
120R-1265	A1 C2	1265	foliated matrix carbonate
120R-1265	A1 C3	1265	foliated matrix carbonate

Area	FeCO3	MnCO3	MgCO3	CaCO3	NiCO3	SiO2	Al2O3	Carb total
A2 C1	0.61	0.73	0.33	103.07	0	0	0	104.74
A2 C2	0	0.24	0	103.07	0	0	0	103.31
A1 C1	0.44	0.34	0	100.14	0	0	0	100.91
A1 C2	0.6	0.63	0.31	102.51	0	0	0	104.05
A1 C3	0.37	0.53	0	101.21	0	0	0	102.12

White Micas

Sample	Depth	Area	Description
120R-1265	1265	A3 S2	sericite in elongate ?pumice clast

Area	SiO2	TiO2	Al2O3	Cr2O3	Fe2O3	FeO	MnO	MgO	CaO	Na2O	K2O	Cl	Oxide total
A3 S2	47.13	0.19	36.64	0	0	0.33	0	0.44	0.11	2.36	7.61	0	94.81

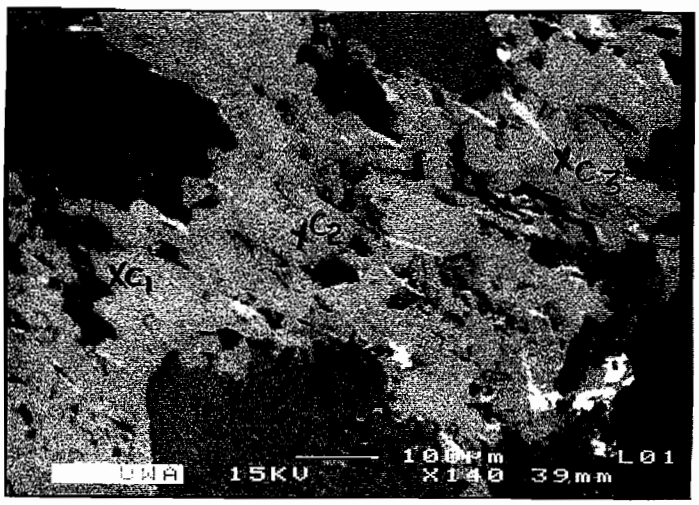

120R - 1265.5 AREA 1

120R - 1265.5 AREA 2

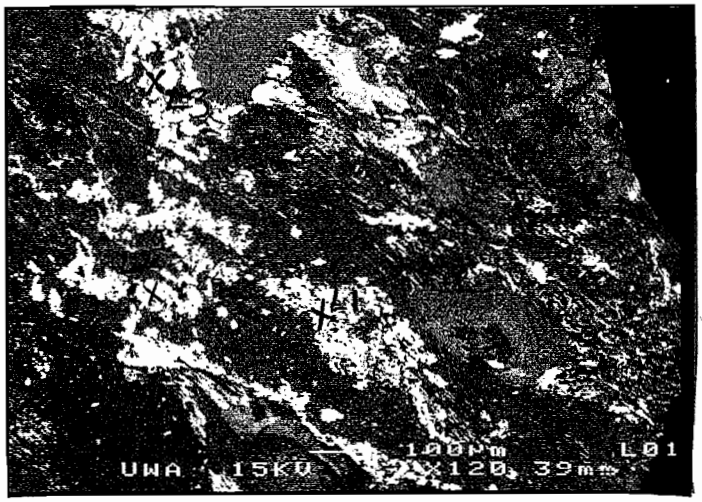

120R - 1265.5 AREA 4

Sample number: 96-120R-1291 Rock and thin section description

Location: Drill hole 120R, 1291.8 m; north end Rosebery mine

Hand specimen and summary: Top of feld-qtz-biot porphyritic rhyolite sill within TSV (host rocks). Groundmass strongly altered to ser; biot phenocrysts altered to sphene-leucoxene-chl-qtz, and there is a lot of sphene-leucoxene scattered through the groundmass. Moderate S2 foliation.

Mineral percentages in thin section:

sericite	45%	
plagioclase	?28%	)__ 43%
quartz	?15%	)
carbonate	3%	
sphene-leucox	5%	
chlorite	2%	
opaques (py-pyrrh)	2%	
zircon	trace	

Primary textures: Coarsely feld>qtz>biot porphyritic rhyolite. Phenocrysts 35% average 2mm, including 10% qtz and 2-3% biot. Phenocrysts mainly unbroken; qtz subhedral, subrounded, embayed, and with thin rim of fine grained qtz±feld mosaic interpreted as recrystallized spherulitic rim. This rim only occurs on qtz phenocrysts, not on feld and biot. Groundmass comprises faintly flow banded groundmass with 10% scattered, small recrystallized spherulites set in altered sericitic, originally glassy groundmass. Feld phenocrysts all or mainly plagioclase, many with concentric zoning. There are a few 2-3mm clasts/inclusions of rhyolite porphyry with a much more feld-microporphyritic matrix texture, i.e. more crystalline. Biot phenocrysts are cream coloured in hand specimen due to intense alteration to disseminations and ribbons of fine-grained sphene-leucoxene (25% of biot phenocrysts) alternating with ribbons of chl and qtz.

Tectonic fabrics: There is one weak-moderate intensity, pervasive foliation-lineation (S2-L2) expressed mainly by orientation of matrix ser.

Alteration, veins: The originally glassy groundmass is very strongly replaced by ser. However, the small spherulites in the groundmass and the feld phenocrysts are only weakly ser-carb altered. Carb is relatively clear or has only faint brownish tinge/dusting (?Fe/Mn-poor ?calcite-dolomite). Sphene-leucoxene is very abundant and occurs both as irregular spots and blebs of granular sphene-leucoxene>opaques (?sulphides) scattered through the groundmass, and as an alteration of biot phenocrysts.

Interpretation/important relationships: Biot phenocrysts alter to fine grained granular sphene-leucoxene, alternating with ribbons of qtz and chl, and there is abundant sphene-leucoxene in the groundmass. The groundmass has been intensely replaced by ser, but the rest of the rock is only weakly altered, suggesting that the overall alteration intensity is only moderate, and is related to the glassy composition of the groundmass. The top of the rhyolite sill here is interpreted as coherent (from thin section and drill core logging) and peperitic (from drill core logging). There appears to be no sedimented clastic facies of the same composition as the rhyolite sill sitting on top of the rhyolite sill.

Mineral Probe Results

Carbonates

Sample	Area	depth	Description
120R-1291.8	A2 C1	1291.8	carbonate grains within plag phenocryst
120R-1291.8	A2 C2	1291.8	carbonate grains within plag phenocryst

Area	FeCO3	MnCO3	MgCO3	CaCO3	NiCO3	SiO2	Al2O3	Carb total
A2 C1	0.44	0.92	0.5	97.98	0	0	0	99.84
A2 C2	0.42	0.83	0.59	97.12	0	0	0	98.95

White Micas

Sample	Depth	Area	Description
120R-1291.8	1291.8	A3 S1	moderately coarse groundmass sericite
120R-1291.8	1291.8	A3 S2	moderately coarse groundmass sericite
120R-1291.8	1291.8	A3 S3	moderately coarse groundmass sericite

Area	SiO2	TiO2	Al2O3	Cr2O3	Fe2O3	FeO	MnO	MgO	CaO	Na2O	K2O	Cl	Oxide total
A3 S1	46.03	0	33.73	0	0	0.26	0	1.08	0	0.57	10.5	0	92.17
A3 S2	46.21	0.2	33.81	0	0	0.18	0	1.14	0	0.54	10.36	0	92.44
A3 S3	46.63	0	33.39	0	0	0.18	0	1.04	0	0.45	10.43	0	92.12

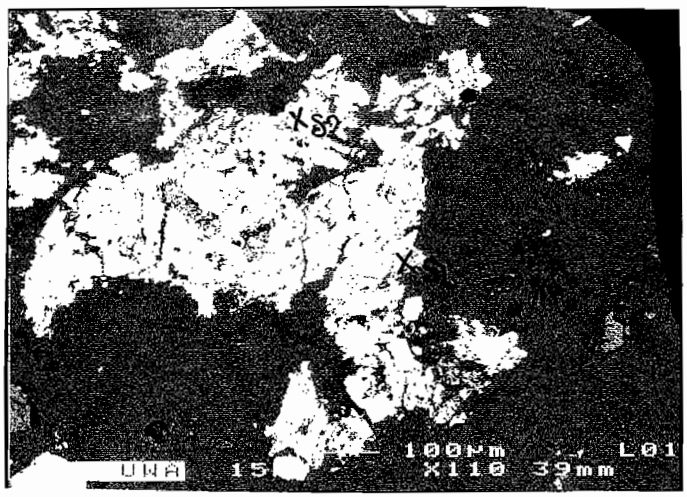

120R - 1291.8 AREA 1

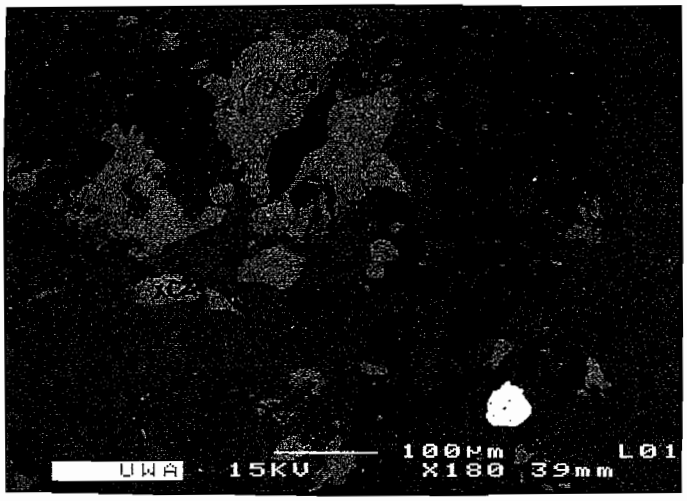

120R - 1291.8 AREA 2

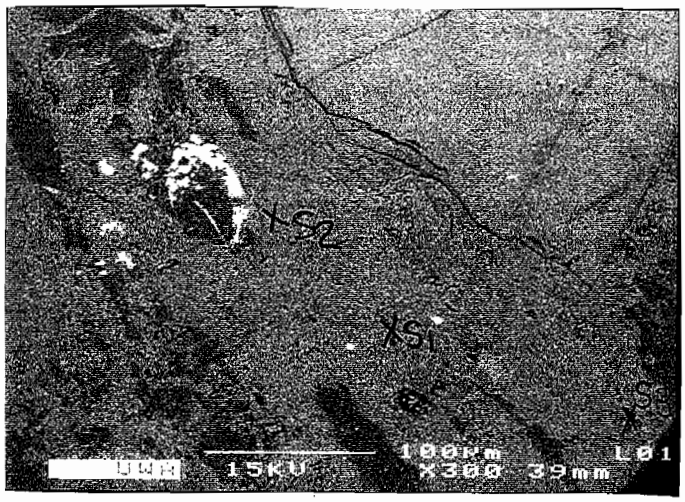

120R - 1291.8 AREA 3

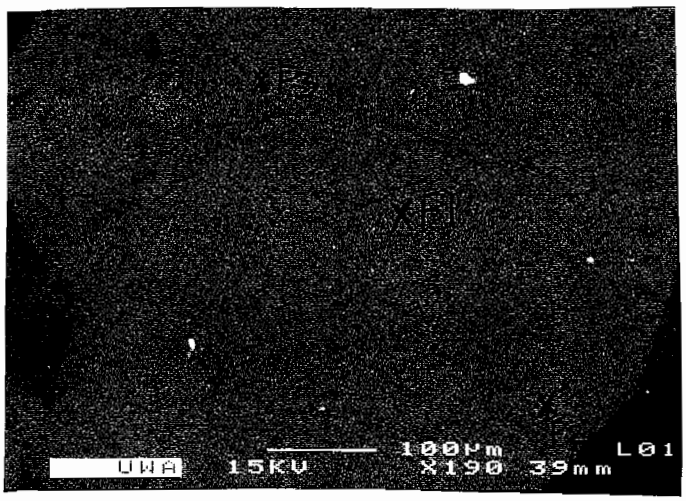

120R - 1291.8 AREA 4

120R - 1291.8 AREA 5

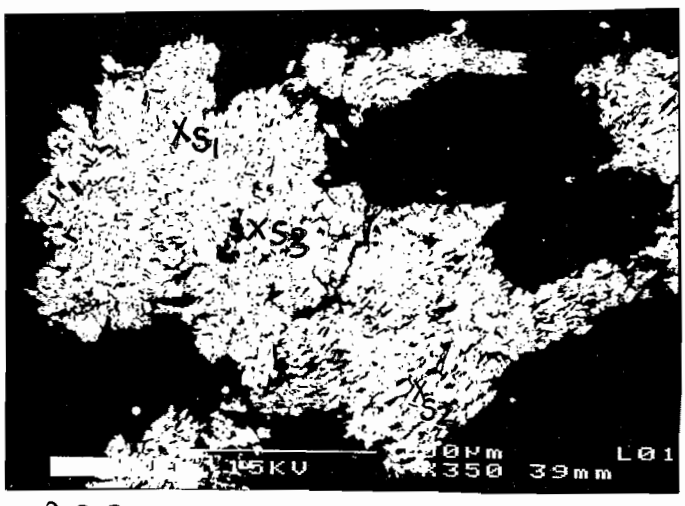

120R - 1291.8 AREA 6

Sample number: 96-120R-1315 Rock and thin section description

Location: Drill hole 120R, 1315.4 m; north end Rosebery mine

Hand specimen and summary: Middle of feld-qtz-biot porphyritic rhyolite sill within TSV (host rocks). Strongly spherulitic groundmass. Weak ser-qtz and biot alteration. Moderate S2 foliation.

Mineral percentages in thin section:

plagioclase	?35%	)__ 65%
quartz	?30%	)
sericite	20%	
biot	4%	
carbonate	3%	
sphene-leucox	3%	
chlorite	1%	
opaques (py-pyrrh)	1%	
zircon	<1%	(relatively abundant)

Primary textures: Primary textures well preserved. Coarsely feld>qtz>biot porphyritic rhyolite. Phenocrysts 30% average 2.5mm, comprising 20% feld, 8% qtz and 2% biot. Phenocrysts mainly unbroken; feld euhedral and comprises multiple twinned plag » some potential Kspar. Qtz phenos subhedral, subrounded, embayed, and with thin rim of fine grained qtz±feld mosaic interpreted as recrystallized spherulitic rim. This rim only occurs on qtz phenocrysts, not on feld and biot. Groundmass strongly spherulitic (much more than 96-120R-14), and comprises abundant small recrystallized spherulites (rounded aggregates of coarse grained quartz±feld) set in a fine grained qtz-feld>ser matrix. Only a few feld phenocrysts preserve faint concentric zoning. There is a 5mm clast/inclusion of feld-opaques-rich porphyry with a feld-microporphyritic matrix texture, i.e. more crystalline. Zircons relatively abundant, and mainly occur in small ser>biot lenses interpreted to be altered biot phenocrysts.

Tectonic fabrics: There is one moderate intensity, pervasive foliation-lineation (S2-L2) expressed by orientation of matrix ser, biot and chl, and elongation of spherulites. There appears to be weak development of an anastomosing S1 stylolitic foliation expressed by concentration of sphene-leucoxene, opaques and biot.

Alteration, veins: Weak ser-qtz and biot alteration. Biot, chl and ser are intergrown, and are alteration products of each other. Biot mainly occurs in pressure shadows/beard growths of phenocrysts and groundmass structures. 3% of the rock comprises 1mm lenses of foliated ser>biot³sphene-opaques, with up to 3% euhedral and subhedral zircons. These lenses interpreted to be deformed, altered biot phenocrysts. There are no strongly sphene-leucoxene altered biot phenocrysts like in 96-120R-14. Feld phenocrysts only very weakly altered by ser-carb. Groundmass has weak ser-biot alteration. Sphene-leucoxene occurs disseminated throughout, but has elevated concentration in the weak S1 stylolitic foliation.

Interpretation/important relationships: Biot, ser and chl are most commonly all foliated, and consequently grew during S2 deformation. Biot mainly occurs in pressure shadows/beard growths of phenocrysts and groundmass structures, consequently must have grown during S2 cleavage development. However, the timing relation of biot, ser and chl is uncertain. Chlorite mainly appears to alter from biot. Many examples of intergrown ser and biot do not give clear timing relations. However, at a few places relatively unfoliated biot overprints/replaces strongly foliated ser, so is interpreted to be younger. A weak S1 foliation appears to be present, and indicates S1 even developed (weakly) in competant rocks such as this massive rhyolite sill. Biot phenocrysts show ser>biot-opaques alteration rather than the intense sphene-leucoxene replacement in 96-120R-14; the biot phenocrysts contain abundant zircons.

Mineral Probe Results

Carbonates

Sample	Area	depth	Description
120R-1315	A3 C1	1315	early foliated qtz - carb veinlet
120R-1315	A3 C2	1315	early foliated qtz - carb veinlet

Area	FeCO3	MnCO3	MgCO3	CaCO3	NiCO3	SiO2	Al2O3	Carb total
A3 C1	0.95	2.32	0	99.12	0	0	0	102.39
A3 C2	1.19	2.54	0.31	99.05	0	0	0	103.1

White Micas

Sample	Depth	Area	Description
120R-1315	1315	A2 S1	mod coarse matrix sericite

Area	SiO2	TiO2	Al2O3	Cr2O3	Fe2O3	FeO	MnO	MgO	CaO	Na2O	K2O	Cl	Oxide total
A2 S1	46.37	0.34	28.17	0	0	6.76	0	1.38	0	0	11.07	0	94.09

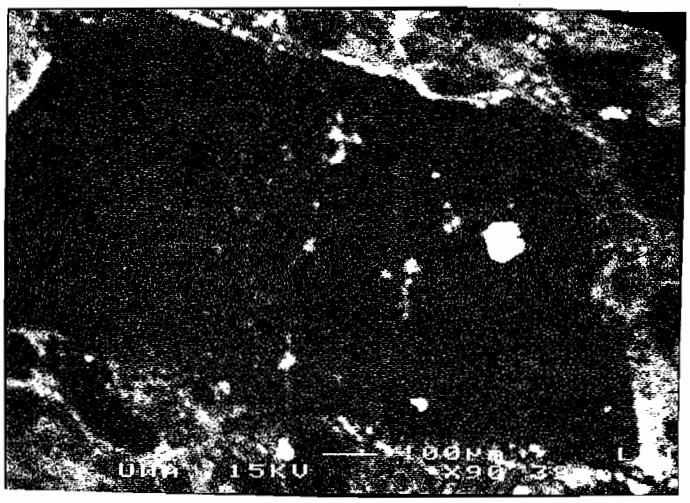

120R - 1315.4 AREA 1

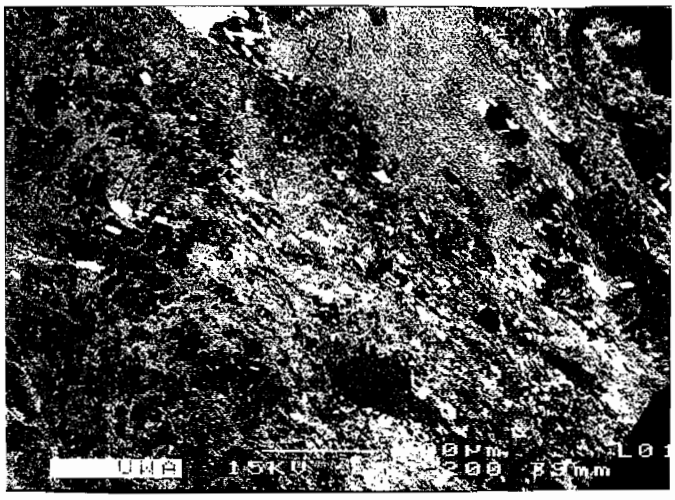

120R - 1315.4 AREA 2

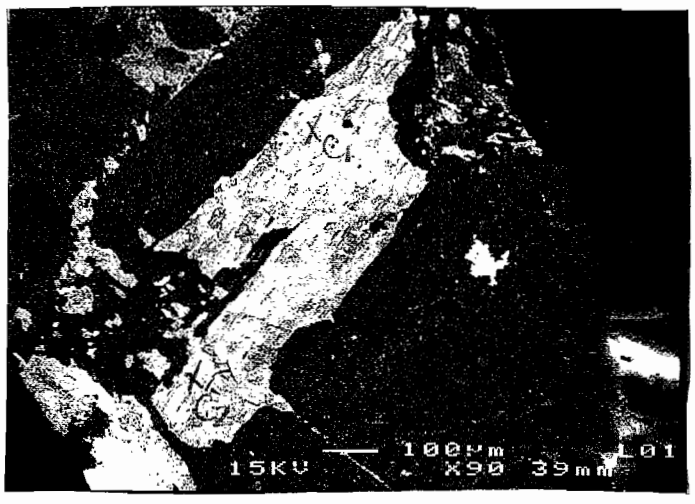

120R - 1315.4 AREA 3

Sample number: 96-120R-1353 Rock and thin section description

Location: Drill hole 120R, 1353.8 m; north end Rosebery mine

Hand specimen and summary: Base of feld-qtz-biot porphyritic rhyolite sill within TSV (host rocks). Weak-moderate qtz-ser alteration. Moderate S2 foliation.

Mineral percentages in thin section:

sericite	35%	
plagioclase	?30%	)__ 55%
quartz	?25%	)
carbonate	5%	
sphene-leucox	2%	
opaques (py-pyrrh)	1%	
brown laths	<1%	(pale brown, very high birefr, mod-high relief)
zircon	trace	

Primary textures: Primary textures moderately to well preserved. Coarsely feld>qtz>biot porphyritic rhyolite. Phenocrysts 25-30% average 2.5mm, comprising 20% feld, 7% qtz and 2% biot. Phenocrysts mainly unbroken; feld euhedral and comprises multiple twinned plag. Qtz phenos subhedral, subrounded, embayed, and with thin rim of fine grained qtz±feld mosaic interpreted as recrystallized spherulitic rim. Groundmass moderately spherulitic (less than 96-120R-15), and comprises abundant small recrystallized spherulites (rounded aggregates of coarse grained quartz±feld) set in a fine grained ser-qtz-feld matrix. Some feld phenocrysts preserve faint concentric zoning. There are clasts/inclusions of feld-rich porphyry with a feld-microporphyritic matrix texture, i.e. more crystalline texture. Zircons relatively abundant, and mainly occur in small ser lenses interpreted to be altered biot phenocrysts. Some of the leucoxene (1% of rock) is alteration of equant, massive to skeletal magnetite/ilmenite micro-phenocrysts.

Tectonic fabrics: There is one moderate intensity, pervasive foliation-lineation (S2-L2) expressed by orientation of matrix ser, beard growths on phenocrysts, and elongation of spherulites. There is also weak development of an anastomosing S1 stylolitic foliation expressed by concentration of sphene-leucoxene and opaques. S1 clearly micro-folded and overprinted by S2.

Alteration, veins: Weak-moderate qtz-ser alteration. Groundmass has moderate qtz-ser alteration, and the more altered parts have diffuse patches and veins of more coarsely crystalline anhedral qtz-rich mosaics = silicification. Sphene-leucoxene occurs disseminated throughout, but has elevated concentration in the weak S1 stylolitic foliation. Carb mainly occurs in the pressure shadows of phenocrysts, as an alteration of feld phenocrysts, and as a minor component of the diffuse granular silicification veins and patches. The carb is clear to very pale brown dusted (probably low Fe-Mn calcite/dolomite?). 3% of the rock comprises 1mm lenses of foliated ser>sphene-opaques, with up to 2% euhedral and subhedral zircons. These lenses interpreted to be deformed, altered biot phenocrysts. Feld phenocrysts only weakly altered by carb>ser, and may also be slightly silicified.

Interpretation/important relationships: The qtz-rich veins and patches are more diffuse bounded and more deformed than those in samples from higher in the hole, and they are interpreted to be pre-S2. Carb occurs in pressure shadows/beard growths of phenocrysts and groundmass structures, consequently must have in part grown during S2 cleavage development. A weak S1 foliation is present, and indicates S1 even developed (weakly) in competant rocks such as this massive rhyolite sill. Biot phenocrysts show ser>sphene-leucoxene-opaques alteration; the biot phenocrysts contain zircons.

Mineral Probe Results

Carbonates

Sample	Area	depth	Description
120R-1353.8	A1 C1	1353.8	carbonate patch in feldspar pressure shadow
120R-1353.8	A1 C2	1353.8	carbonate patch in feldspar pressure shadow
120R-1353.8	A2 C1	1353.8	carbonate within plag phenocryst
120R-1353.8	A2 C2	1353.8	carbonate within plag phenocryst
120R-1353.8	A3 C1	1353.8	matrix carbonate
120R-1353.8	A3 C2	1353.8	matrix carbonate

Area	FeCO3	MnCO3	MgCO3	CaCO3	NiCO3	SiO2	Al2O3	Carb total
A1 C1	0.79	6.64	0.56	91.82	0	0	0	99.82
A1 C2	2.03	9.06	1.44	86.59	0	0	0	99.12
A2 C1	1.6	8.1	1.05	88.18	0	0	0	98.92
A2 C2	0.97	6.06	0.56	91.18	0	0	0	98.77
A3 C1	1.53	7.79	0.86	89.34	0	0	0	99.52
A3 C2	1.82	8.8	1.42	86.27	0	0	0	98.31

White Micas

Sample	Depth	Area	Description
120R-1353.8	1353.8	A2 S1	
120R-1353.8	1353.8	A3 S1	matrix sericite
120R-1353.8	1353.8	A3 S2	matrix sericite
120R-1353.8	1353.8	A4 S1	matrix sericite
120R-1353.8	1353.8	A4 S2	matrix sericite

Area	SiO2	TiO2	Al2O3	Cr2O3	Fe2O3	FeO	MnO	MgO	CaO	Na2O	K2O	Cl	Oxide total
A2 S1	46.54	0.94	29.87	0	0	2.02	0	1.52	0	0.22	10.65	0	91.76
A3 S1	46.97	0.63	29.58	0	0	2.28	0	1.85	0	0	10.86	0	92.17
A3 S2	46.42	0.83	29.55	0	0	1.88	0	1.56	0	0	10.94	0	91.18
A4 S1	82.96	0	8.54	0	0	0.43	0	0.28	0	1.13	2.55	0	95.89
A4 S2	45.85	0.91	29.92	0	0	1.97	0	1.48	0	0	10.95	0	91.08

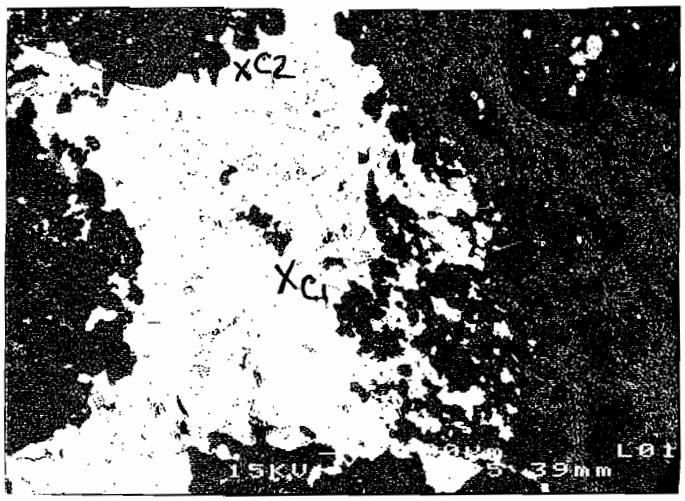

120R-1353.8 AREA 1

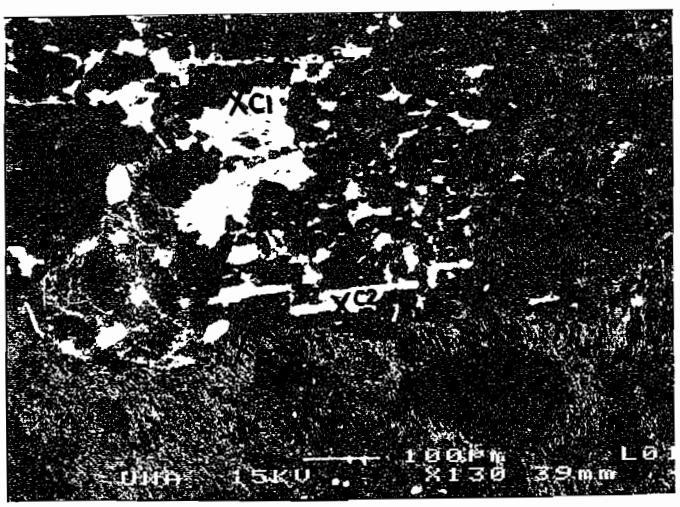

120R-1353.8 AREA 2

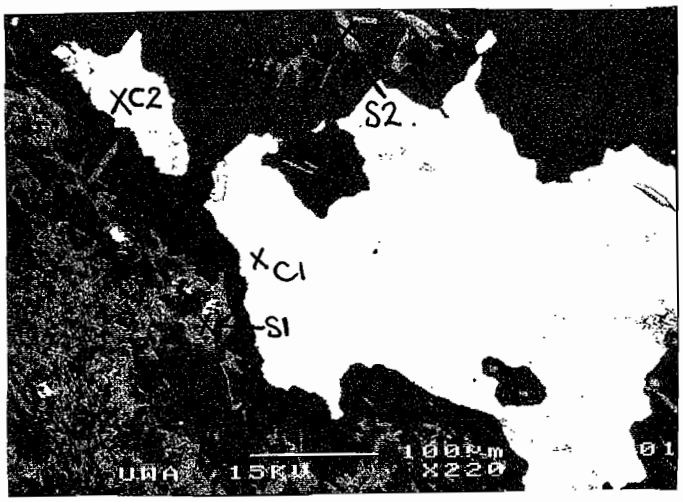

120R-1353.8 AREA 3

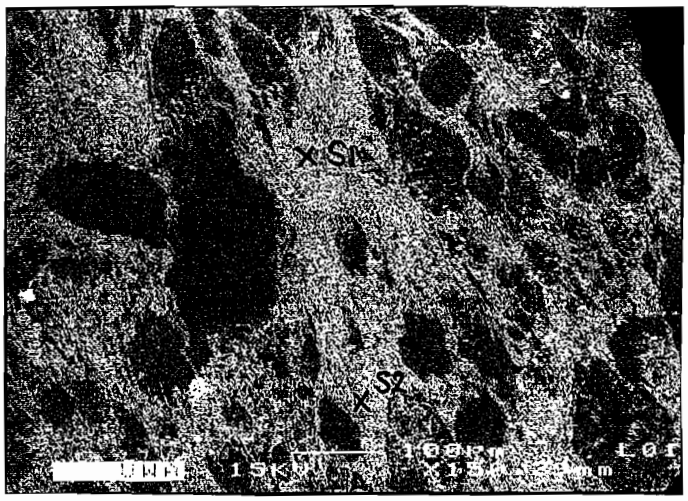

120R-1353.8 AREA 4

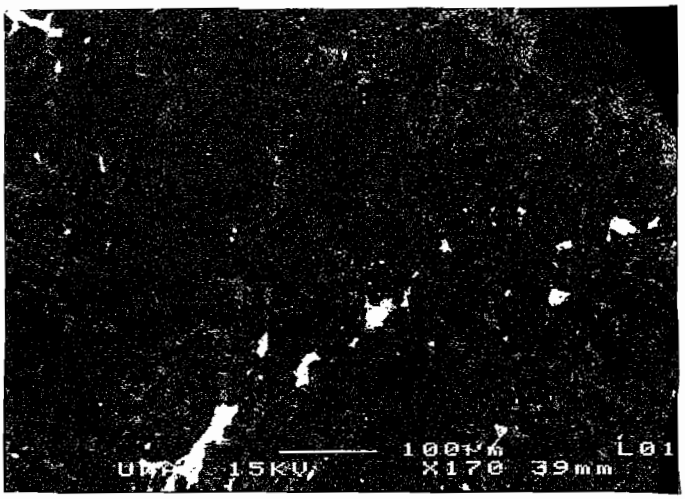

120R-1353.8 AREA 5

Sample number: 96-120R-1357 Rock and thin section description

Location: Drill hole 120R, 1357.4 m; north end Rosebery mine

Hand specimen and summary: Top of spotty carbonate zone in top of footwall feldspar-phyric pumice breccia, above K lens mineralization. Intense carbonate>ser alteration. Moderate S2 foliation.

Mineral percentages in thin section:

carbonate	80%
sericite	11%
quartz	3%
opaques: py	5%
sp	<1%
sphene-leucox	1%

Primary textures: Primary textures obliterated except for faint, poorly preserved, probable round-vesicle pumice texture within a few of the earlier carbonate spheroids.

Tectonic fabrics: There is one moderate intensity, pervasive foliation-lineation (S2-L2) expressed by orientation of matrix ser, and beard growths on some carbonate spheroids. There is also weak development of an anastomosing S1 stylolitic foliation expressed by concentration of sphene-leucoxene and opaques. S1 clearly overprinted by S2.

Alteration, veins: Intense carbonate>sericite alteration, comprising three distinct types:

(1) Moderately deformed (S2), close-packed to moderately dispersed (matrix-supported), carbonate spheroids, with interstitial foliated (by S2) sericite and trails of py>sphene-leucoxene. The latter are subparallel to, and foliated by S2, and could be deformed S1-parallel bands. The carb spheroids are fractured, moderately dismembered and weakly foliated in response to S2 deformation. Fractures and interstices are filled with sericite. Extinction pattern of the deformed carbonate spheroids varies from radial to radial-mosaic to irregular mosaic extinction, and gradations between these styles occur. Most of the pyrite occurs in these domains as thin stringers with sphene-leucoxene and sericite.

(2) Two, 1-1.5 cm wide lenses (or veins) of massive intergrown spheroidal carbonate. These are pre-S2 (local beard growths), but are only weakly deformed. They preserve superb radial cross extinction. Most of the sphalerite and a minor part of the pyrite occurs in these domains as irregular anhedral blebs within carbonate.

(3) Veins or patches of very coarse grained carbonate with simple/normal extinction, and local abundant inclusions of small carbonate rhombs, qtz grains and sericite. These indicate the large carbonate grains grew over earlier formed grains. Growth could be pre- and/or syn-S2.

Most carbonate in all domains is dusty pale brown with pale carbonate-brown birefringence (only minor areas of bright colours in centre of some spheroids), and is probably Mn-Fe-bearing ?rhodocrositic carbonate.

Interpretation/important relationships: The gradations between radial, mosaic and simple/normal carbonate extinction suggest that they represent the various stages of increasing recrystallization (partly or mainly due to deformation) of originally fine-grained concretionary carbonate with radial extinction. The radial extinction probably reflects an original radial spherulitic growth pattern (formed during concretionary growth). The deformed carbonates, which contain most of the sulphide mineralization are pre-S2 in timing, and probably pre- to syn-S1.

Mineral Probe Results

Carbonates

Sample	Area	depth	Description
120R-1357.4	A1 C1	1357.4	coarse recrystallised vein carbonate
120R-1357.4	A1 C2	1357.4	coarse recrystallised vein carbonate
120R-1357.4	A3 C1	1357.4	early coarse carbonate vein
120R-1357.4	A3 C2	1357.4	early coarse carbonate vein
120R-1357.4	A2 C1	1357.4	recrystallised carbonate spheroid
120R-1357.4	A2 C2	1357.4	recrystallised carbonate spheroid

Area	FeCO3	MnCO3	MgCO3	CaCO3	NiCO3	SiO2	Al2O3	Carb total
A1 C1	7.69	33.97	6.65	47.93	0	0	0	96.24
A1 C2	7.5	33.66	6.42	49.07	0	0	0	96.65
A3 C1	7.66	33.74	6.84	48.73	0	0	0	96.97
A3 C2	7.53	34.64	7.4	47.52	0	0	0	97.09
A2 C1	6.98	34.2	7.3	48.37	0	0	0	96.85
A2 C2	6.31	35.74	6.19	49.91	0	0	0	98.14

White Micas

Sample	Depth	Area	Description
120R-1357.4	1357.4	A2 S1	sericite within deformed carbonate spheroid
120R-1357.4	1357.4	A2 S2	sericite within deformed carbonate spheroid

Area	SiO2	TiO2	Al2O3	Cr2O3	Fe2O3	FeO	MnO	MgO	CaO	Na2O	K2O	Cl	Oxide total
A2 S1	45.67	0.71	28.5	0	0	2.33	0	2.09	0	0	10.91	0	90.21
A2 S2	45.8	0.55	28.87	0	0	2.43	0	1.99	0	0	10.81	0	90.45

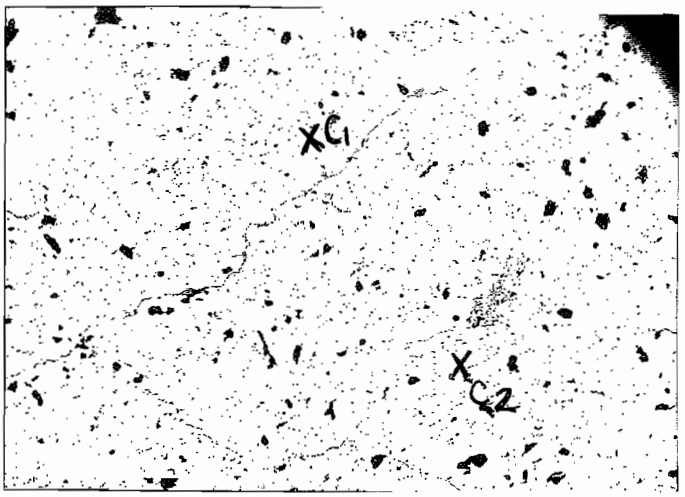

120R - 1357.4 AREA 1

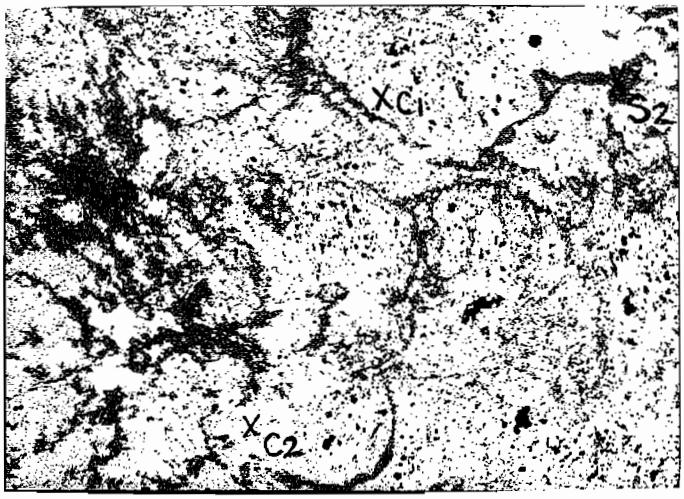

120R - 1357.4 AREA 2

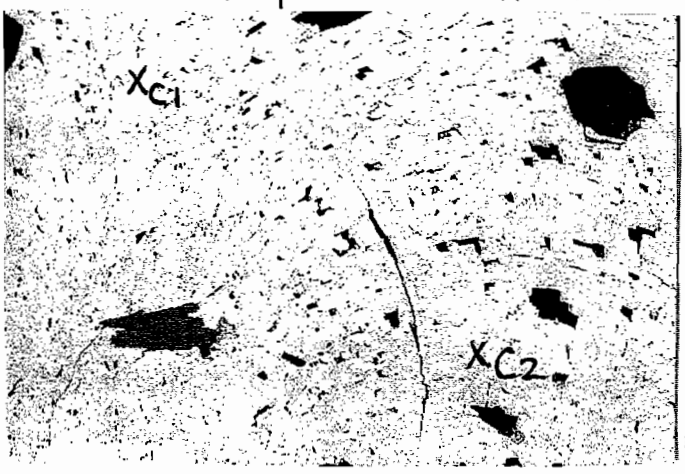

120R - 1357.4 AREA 3

Sample number: 96-120R-1361 a, b Rock and thin section description

Location: Drill hole 120R, 1361.4 m; north end Rosebery mine

Hand specimen and summary: Middle of spotty carbonate zone in top of footwall feldspar-phyric pumice breccia, just above K lens mineralization. Intense carbonate-ser alteration. Strong S2 foliation.

Mineral percentages in thin section:

carbonate	45%
sericite	44%
quartz	7%
opaques: py	3%
sphene-leucox	?1%

Primary textures: Primary undeformed glass shard textures are faintly preserved in some of the carbonate spheroids, but nowhere near as well as in sample 120R-1364. Care must be taken to distinguish relict primary shard and pumice textures from the arcuate-subradial and concentric fractures caused during deformation of the spheroids.

Tectonic fabrics: There is one strong, pervasive foliation-lineation (S2-L2) expressed by orientation of matrix ser, and beard growths on carbonate spheroids. There is also weak development of an anastomosing S1 stylolitic foliation expressed by concentration of opaques. Carbonate spheroids are commonly fractured, dismembered and stretched in the S2-L2 fabric. Fractures are filled by sericite or new carbonate. The carbonate behaved as extremely competant bodies during deformation, in contrast to the readily foliated sericite.

Alteration, veins: Mainly intense carbonate-sericite alteration, comprising the following types in order of decreasing abundance:

(1) Variably tectonically dismembered, moderately dispersed (matrix-supported), carbonate spheroids, set in foliated (S2) sericite matrix. Many of the spheroids have superbly preserved, very fine concentric rings (shells) of varying carbonate colour and dustyness. These are fine concretionary growth rings (shells). Extinction pattern of the deformed carbonate spheroids varies from radial to radial-mosaic extinction, and gradations between these styles occur. Carbonate spheroids are dusty pale brown with pale carbonate-brown birefringence (only minor areas of bright colours in centre of some spheroids). They are probably Mn-Fe-bearing ?rhodocrositic carbonate. Pyrite occurs as diffuse stringers subparallel to, and foliated by S2, and could be deformed S1-parallel bands.

(2) The domains described above are cut by deformed, pre-S2 or syn-S2, quartz-carbonate veins. Quartz in the veins has undulose extinction and the vein margins are foliated (S2). Carbonate in the veins occurs as a complex intergrowth of arcuate-spheroidal carbonate with striking sub-radial arcuate extinction pattern. Locally, where more strongly deformed (S2 foliated), the vein carbonate comprises foliated irregular mosaics without radial-arcuate extinction. The vein carbonate is paler brown, less dusted, than the adjacent spheroidal carbonate, indicating a probable difference in composition. Locally one vein preserves growth structure of alternating quartz and carbonate, oriented perpendicular to the vein margins.

Interpretation/important relationships: The deformation style of the carbonate spheroids indicates they are cleary pre-S2 in timing. The very fine concentric layering of the spheroids indicates very early, concretionary growth in a very low stress environment. They must have grown during early diagenesis. The radial extinction probably reflects an original radial and concentric spherulitic growth pattern (formed during concretionary growth). The carbonate-quartz veins appear to be early, pre-S2 (or very early S2) veins, and indicate that sub-spheroidal carbonate growth also occurred in (early) veins, and was recrystallized to irregular mosaics by subsequent deformation.

Mineral Probe Results

Carbonates

Sample	Area	depth	Description
120R-1361.4A	A1 C1	1361.4	interlocking carb within early qtz-carb vein
120R-1361.4A	A1 C2	1361.4	interlocking carb within early qtz-carb vein
120R-1361.4A	A2 C1	1361.4	concentric layered carbonate spheroid
120R-1361.4A	A2 C2	1361.4	concentric layered carbonate spheroid
120R-1361.4A	A2 C3	1361.4	concentric layered carbonate spheroid
120R-1361.4A	A2 C4	1361.4	concentric layered carbonate spheroid
120R-1361.4A	A2 C5	1361.4	concentric layered carbonate spheroid
120R-1361.4A	A2 C6	1361.4	concentric layered carbonate spheroid
120R-1361.4B	A1 C1	1361.4	recrystallised (late S2) carb within foliated vein
120R-1361.4B	A1 C2	1361.4	recrystallised (late S2) carb within foliated vein
120R-1361.4B	A1 C3	1361.4	recrystallised (late S2) carb within foliated vein
120R-1361.4B	A1 C4	1361.4	recrystallised (late S2) carb within foliated vein
120R-1361.4B	A1 C5	1361.4	recrystallised (late S2) carb within foliated vein
120R-1361.4B	A1 C6	1361.4	recrystallised (late S2) carb within foliated vein
120R-1361.4B	A2 C1	1361.4	concentric layered carbonate spheroid
120R-1361.4B	A2 C2	1361.4	concentric layered carbonate spheroid
120R-1361.4B	A2 C3	1361.4	concentric layered carbonate spheroid
120R-1361.4B	A2 C4	1361.4	concentric layered carbonate spheroid
120R-1361.4B	A2 C5	1361.4	concentric layered carbonate spheroid

Area	FeCO3	MnCO3	MgCO3	CaCO3	NiCO3	SiO2	Al2O3	Carb total
A1 C1	5.68	39.01	5.52	46.55	0	0	0	96.76
A1 C2	4.74	40.71	5.29	45.98	0	0	0	96.72
A2 C1	11.61	7.73	25.89	54.32	0.29	0	0	99.83
A2 C2	7.37	87.14	1.46	2.32	0	0	0	98.3
A2 C3	11.87	6.56	24.55	55.39	0	0	0	98.37
A2 C4	8.95	16.33	22.33	50.57	0	0	0	98.18
A2 C5	10.79	8.52	25.38	53.76	0	0	0	98.46
A2 C6	6.86	88.81	1	2.05	0	0	0	98.72
A1 C1	6.71	88.39	1.97	4.03	0	0	0	101.1
A1 C2	22.39	57.88	11.65	10.62	0	0	0	102.54
A1 C3	27.18	55.81	13.59	6.73	0.35	0	0	103.66
A1 C4	8.05	84.05	3.91	5.03	0	0	0	101.04
A1 C5	9.73	35.15	10.25	46.64	0	0	0	101.77
A1 C6	10.42	36.55	8.28	46.14	0	0	0	101.39
A2 C1	8.23	87.43	2.28	3.57	0	0	0	101.51
A2 C2	7.73	86.73	2.91	4.69	0	0	0	102.06
A2 C3	8.05	88.6	2.63	2.28	0	0	0	101.57
A2 C4	2.45	45.51	5.92	47.02	0	0	0	100.89
A2 C5	2.61	74.16	11.86	12.44	0	0	0	101.07

White Micas

Sample	Depth	Area	Description
120R-1361.4B	1361.4	A3 S1	sericite matrix to carbonate spheroids
120R-1361.4B	1361.4	A3 S2	sericite matrix to carbonate spheroids

Area	SiO2	TiO2	Al2O3	Cr2O3	Fe2O3	FeO	MnO	MgO	CaO	Na2O	K2O	Cl	Oxide total
A3 S1	47.84	0.81	30.96	0	0	1.37	0	2.13	0	0	11.3	0	94.41
A3 S2	46.82	0.76	29.77	0	0	1.48	0	2.07	0	0	11	0	91.9

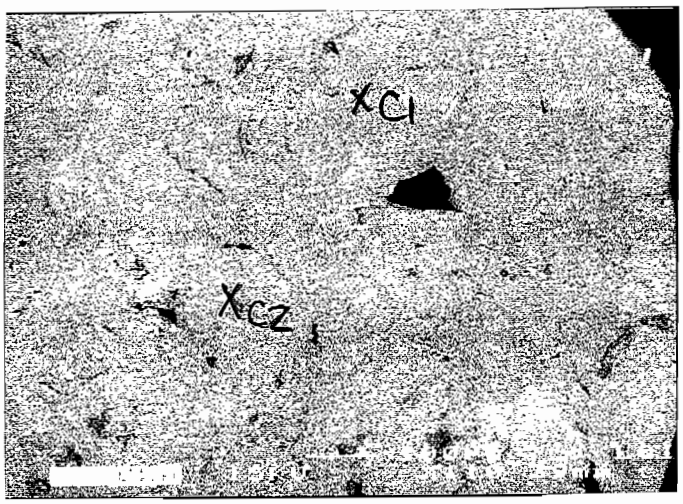

120R-1361.4 A AREA 1

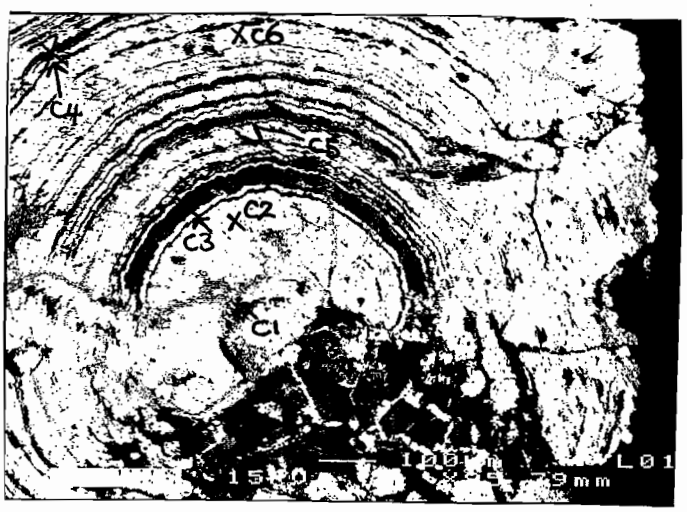

120R-1361.4 A AREA 2

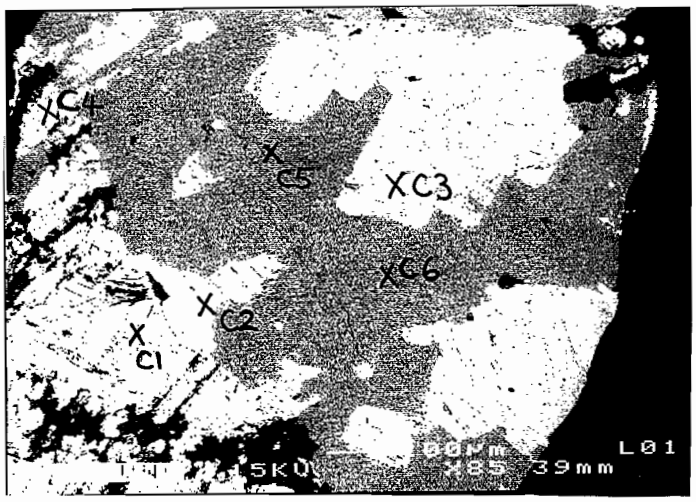

120R-1361.4B AREA 1

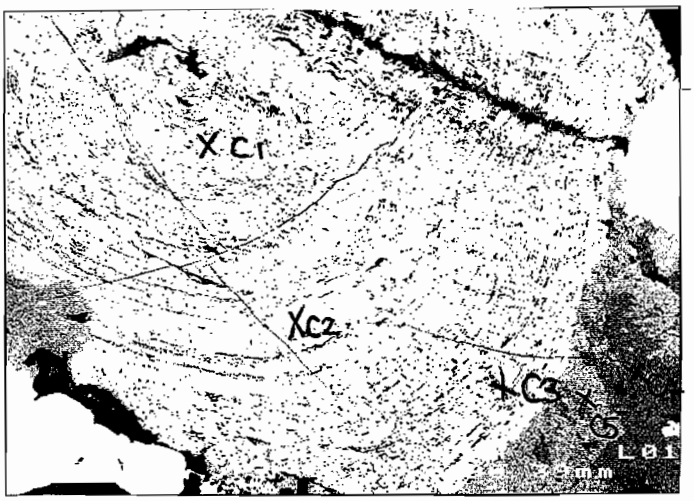

120R-1361.4B AREA 2

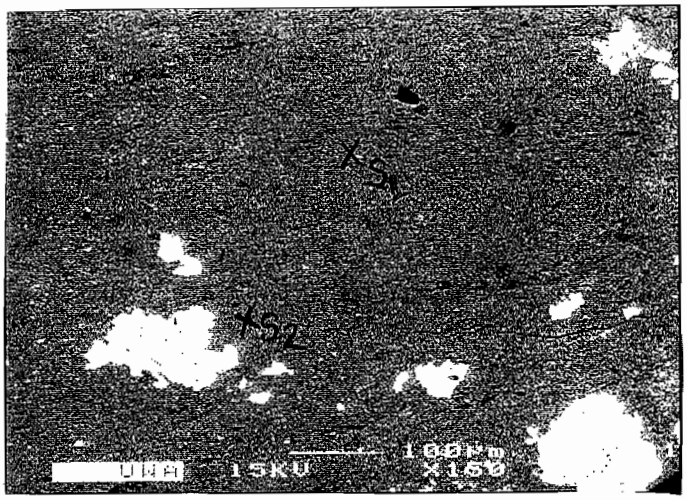

120R-1361.4B AREA 3

Sample number: 96-120R-1364 a, b Rock and thin section description

Location: Drill hole 120R, 1364.4 m; north end Rosebery mine

Hand specimen and summary: Lower part of spotty carbonate zone in top of footwall feldspar-phyric pumice breccia, just above K lens mineralization. Intense carbonate-ser alteration. Strong S2 foliation.

Mineral percentages in thin section:

carbonate	60%
sericite	30%
quartz	4%
opaques: py>sp	5%
sphene-leucox	1%

Primary textures: Completely undeformed glass shard and pumice textures are extremely well preserved in some of the carbonate spheroids. No primary textures are preserved outside the spheroids. These relict textures indicate that the primary character of the rock was a massive, uncompacted, vitric pyroclastic deposit with small bubble-wall glass shards > round-vesicle pumice clasts > tube pumice. The shards and pumice are preserved by fine sericite alteration of their rims/surfaces. The cores of some thicker shards and pumice walls, and the fine vitric dust between the shards and pumices, and within the vesicles of the pumice, are replaced by massive to faintly concentric banded carbonate. Some thick shards are nearly completely replaced by sericite; locally with faint axiolitic texture (growth perpendicular to shard surfaces). Locally, the concentric growth bands and fibre orientations of the carbonate spheroids are influenced by the shape of round-vesicle shards, whereas in other examples the concentric carbonate growth bands and radial fibre orientations continue in orientation regardless of the dispersed shards. Some larger carbonate spheroids enclose large euhedral sericite>feld-quartz altered feldspar phenocrysts.

Tectonic fabrics: There is one strong, pervasive foliation-lineation (S2-L2) expressed by orientation of matrix sericite, and beard growths on carbonate spheroids. There is also a weak foliation at a high angle to S2, expressed as an alignment of small carbonate spheroids and the sericite septa between the spheroids. This foliation could be S1. Carbonate spheroids are commonly fractured, dismembered and stretched in the S2-L2 fabric. Fractures are filled by sericite or new carbonate. The carbonate behaved as extremely competant bodies during deformation, in contrast to the readily foliated sericite.

Alteration, veins: Close-packed to dispersed, large (1-3 mm) carbonate spheroids, with spherulitic texture comprising faint to moderately strong concentric layering and faint radial-fibrous texture. The large spheroids are set in a finer matrix of carbonate and foliated sericite. The spheroids have radial to radial-mosaic extinction. The carbonate of the "matrix" varies in texture, and includes:

(1) Close-packed to dispersed, small (0.2-0.8 mm), lozenge-shaped carbonate grains with internal concentric layering. The carbonate grains are separated by foliated sericite.

(2) Close-packed to dispersed, small (0.25 mm), spheroidal carbonate grains with internal concentric layering.

(3) Close-packed to dispersed, small (0.25 mm), rhombic carbonate grains with internal concentric layering.

Carbonate spheroids and matrix carbonate are pink-cream coloured in hand specimen and dusty pale brown with pale carbonate-brown birefringence in thin section (only minor areas of bright colours in centre of some spheroids). They are probably Mn-Fe-bearing ?rhodocrositic carbonate. Pyrite occurs as diffuse stringers subparallel to S2. Carbonate veins are minor, and are composed of paler carbonate as in sample 120R-18.

Interpretation/important relationships: The deformation style of the carbonate spheroids indicates they are pre-S2 in timing. The fine concentric layering of the spheroids indicates very early, concretionary growth in a very low stress environment. They must have grown during early diagenesis. The radial extinction probably reflects an original radial and concentric growth pattern (formed during concretionary growth). The amazingly well preserved glass shard and pumice textures, confined to within carbonate spheroids also indicate that the spheroids grew prior to any compaction of the strata and prior to S1 foliation. Carbonate spheroid growth was preceded by clay/phyllosilicate alteration of the surfaces of the glass shards and pumice. The shard-rich, relatively pumice poor character of the rock suggests it could be part of the fine, graded top of a coarser pumice breccia bed.

Mineral Probe Results

Carbonates

Sample	Area	depth	Description
120R-1364A	A1 C1	1364.4	carbonate spheroid enclosing feldspar phenocryst
120R-1364A	A1 C2	1364.4	carbonate spheroid enclosing feldspar phenocryst
120R-1364A	A1 C3	1364.4	carbonate spheroid enclosing feldspar phenocryst
120R-1364A	A2 C1	1364.4	carbonate spheroids
120R-1364A	A2 C2	1364.4	carbonate spheroids
120R-1364A	A2 C3	1364.4	carbonate spheroids
120R-1364.4B	A3 C1	1364.4	carbonate in altered plagioclase phenocryst
120R-1364.4B	A4 C1	1364.4	carbonate in early carb-qtz vein
120R-1364.4B	A4 C2	1364.4	carbonate in early carb-qtz vein
120R-1364.4B	A6 C1	1364.4	carbonate grain
120R-1364.4B	A7 C1	1364.4	carbonate in early carb-qtz vein
120R-1364.4B	A7 C2	1364.4	carbonate in early carb-qtz vein
120R-1364.4B	A7 C3	1364.4	carbonate in early carb-qtz vein
120R-1364.4B	A8 C1	1364.4	partially recrystallised carbonate spheroid
120R-1364.4B	A8 C2	1364.4	partially recrystallised carbonate spheroid

Area	FeCO3	MnCO3	MgCO3	CaCO3	NiCO3	SiO2	Al2O3	Carb total
A1 C1	6.95	90.61	2.68	2.48	0	0	0	102.72
A1 C2	2.84	94.09	1.3	4.09	0	0	0	102.31
A1 C3	5.05	90.33	5.04	1.07	0	0	0	101.49
A2 C1	6.74	87.61	3.45	3.62	0	0	0	101.43
A2 C2	5.26	89.68	4.45	2.39	0	0	0	101.79
A2 C3	7.02	87.32	4.16	3.46	0	0	0	101.96
A3 C1	0.92	95.99	2.11	0.73	0.48	0	0	100.22
A4 C1	3.89	44.26	4.93	47.75	0	0	0	100.83
A4 C2	2.77	40.9	4.1	52.41	0	0	0	100.19
A6 C1	5.08	91.24	3.76	1.73	0	0	0	101.81
A7 C1	2.81	41.78	4.35	52.1	0	0	0	101.04
A7 C2	12.77	69.55	8.03	10	0	0	0	100.35
A7 C3	2.86	44.83	3.81	48.77	0	0	0	100.25
A8 C1	1.39	89.88	1.57	6.66	0	0	0	99.49
A8 C2	4.73	91.27	2.47	2.87	0	0	0	101.34

White Micas

Sample	Depth	Area	Description
120R-1364.4B	1364.4	A1 S1	sericite matrix to carbonate spheroids
120R-1364.4B	1364.4	A1 S2	sericite matrix to carbonate spheroids
120R-1364.4B	1364.4	A2 S2	sericite of glass shard within carb spheroid
120R-1364.4B	1364.4	A2 S2	sericite of glass shard within carb spheroid
120R-1364.4B	1364.4	A3 S1	ser altered plag within carb spheroid
120R-1364.4B	1364.4	A4 S1	sericite near carbonate - qtz vein
120R-1364.4B	1364.4	A4 S2	sericite near carbonate - qtz vein
120R-1364.4B	1364.4	A4 S3	sericite near carbonate - qtz vein
120R-1364.4B	1364.4	A4 S4	sericite near carbonate - qtz vein
120R-1364.4B	1364.4	A5 S1	sericite matrix to carbonate spheroids
120R-1364.4B	1364.4	A5 S2	sericite matrix to carbonate spheroids
120R-1364.4B	1364.4	A6 S1	matrix
120R-1364.4B	1364.4	A6 S2	matrix
120R-1364.4B	1364.4	A7 S1	repeat of A4

Area	SiO2	TiO2	Al2O3	Cr2O3	Fe2O3	FeO	MnO	MgO	CaO	Na2O	K2O	Cl	Oxide total
A1 S1	48.51	0.63	30.43	0	0	1.24	0	2.26	0	0	11.2	0	94.27
A1 S2	48.01	0.72	30.67	0	0	1.36	0	2.13	0	0	11.27	0	94.16
A2 S2	48.39	0.79	31.09	0	0	1.2	0.19	2.09	0	0	11.05	0	94.8
A2 S2	47.53	0.77	30.39	0	0	1.39	0.85	2.15	0	0	10.96	0	94.04
A3 S1	48.13	0.64	30.18	0	0	1.43	0	2.31	0	0	11.16	0	93.85
A4 S1	47.72	0.84	30.59	0	0	1.26	0	2.22	0	0	11.05	0	93.68
A4 S2	47.94	1.02	30.83	0	0	1.36	0	2.25	0	0	11.2	0	94.6
A4 S3	48.07	0.54	29.93	0	0	1.7	0	2.19	0	0	11.54	0	93.97
A4 S4	48.17	0.78	30.36	0	0	1.29	0	2.41	0	0	11.19	0	94.2
A5 S1	48.18	0.92	30.52	0	0	1.09	0	2.08	0	0	11.13	0	93.92
A5 S2	47.97	0.8	30.85	0	0	1.42	0	2.16	0	0	11.1	0	94.3
A6 S1	47.82	0.74	30.36	0	0	1.32	0.14	2.17	0	0	11.15	0	93.7
A6 S2	47.83	0.71	30.4	0	0	1.17	0.15	2.23	0	0	11.04	0	93.53
A7 S1	48.42	0.87	30.81	0	0	1.3	0	2.17	0	0	11.2	0	94.77

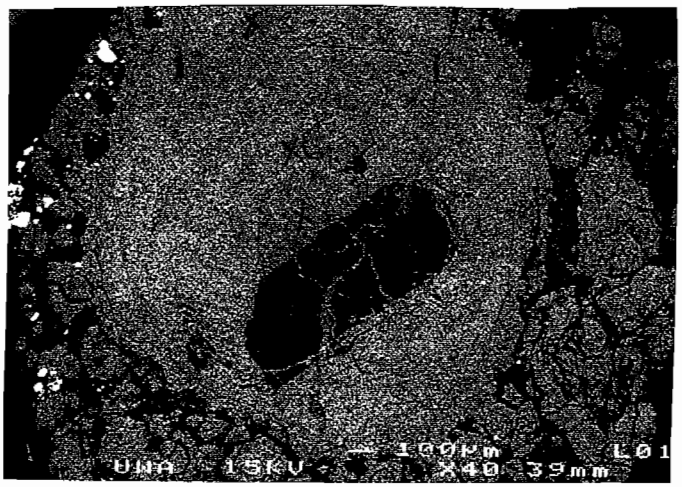

120R - 1364a AREA 1

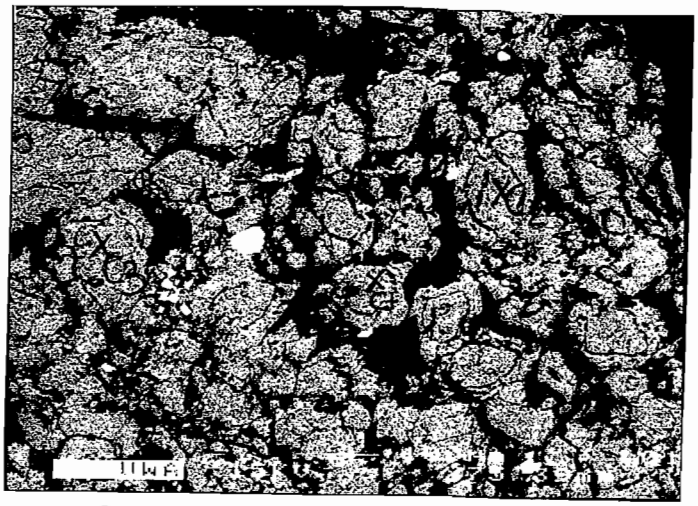

120R - 1364a AREA 2

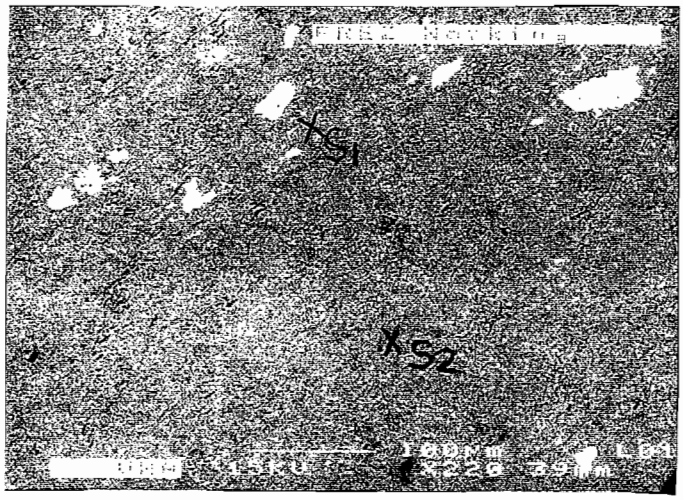

120R - 1364b AREA 1

120R - 1364b AREA 2

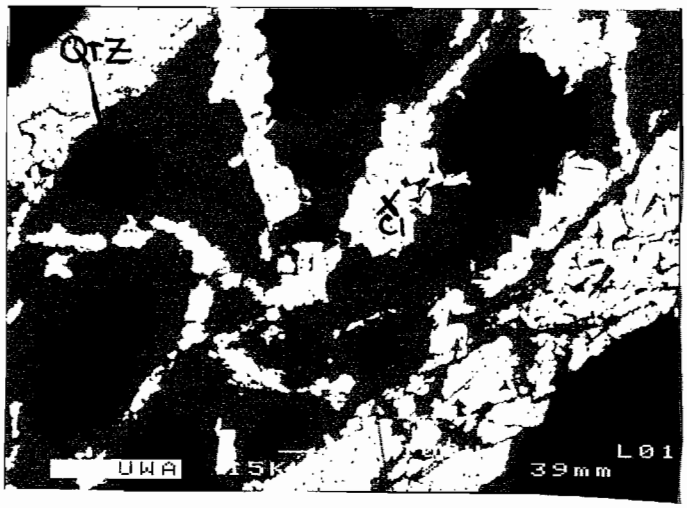

120R - 1364b AREA 3

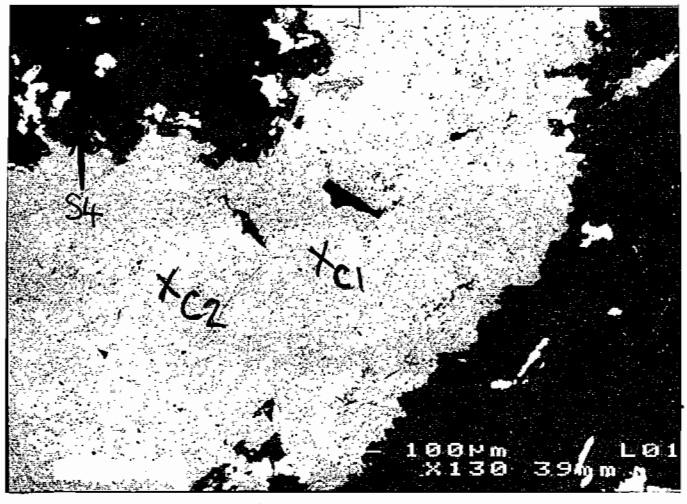

120R - 1364b AREA 4

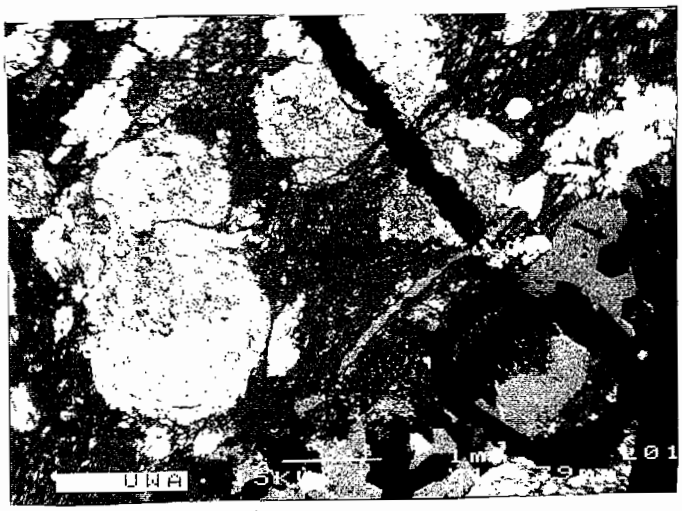

120R-1364b AREA 5

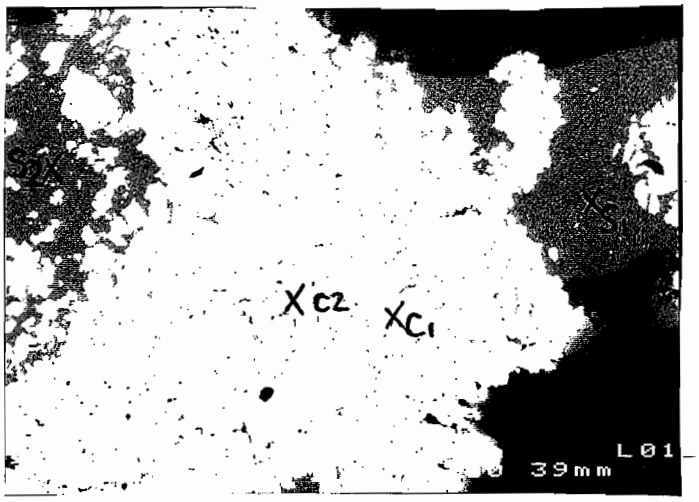

120R-1364b AREA 6

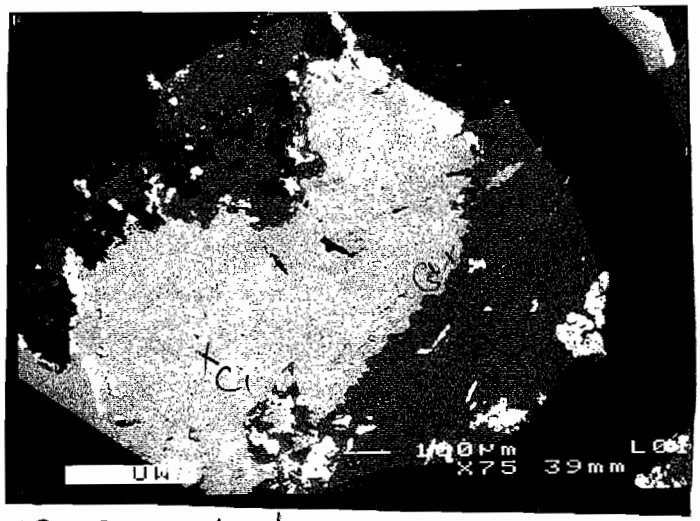

120R-1364b AREA 7

120R-1364b AREA 8

Sample number: 96-120R-1365 a, b Rock and thin section description

Location: Drill hole 120R, 1365.4 m; north end Rosebery mine

Hand specimen and summary: Lower part of spotty carbonate zone in top of footwall feldspar-phyric pumice breccia, just above K lens mineralization. Intense carbonate>ser alteration with carbonate veining. Strong S2 foliation.

Mineral percentages in thin section:

carbonate	68%
sericite	20%
coarse muscovite	2%
chlorite	1%
quartz	5%
opaques: py>sp	3%
sphene-leucox	1%

Primary textures: 1365a has a multiple generation, coarse grained, carbonate vein cutting fine grained, intensely carbonate-sericite altered, pumice breccia. The latter has probable faint relict round vesicle pumice texture locally preserved in the less deformed carbonate patches. Sample 1365b has no definite primary textures.

Tectonic fabrics: Outside the veins there is one strong, pervasive foliation-lineation (S2-L2) expressed by orientation of matrix sericite, and pull-apart texture in the more competent carbonate. The latter comprises tectonically dismembered carbonate with foliated fine sericite in the fractures between carbonate fragments.

Alteration, veins: Sample 1365b is massive carbonate comprising 1-10 mm irregular patches of coarse-grained carbonate (with tiny sericite inclusions), surrounded by a partly amoeboid, partly spotty textured, finer grained mass of carbonate with some interstitial sericite. Sample 1365a is a similar rock, but cut by later generation carbonate veins. Two types of veins occur: (1) massive to curdled textured carbonate with curvi-radial extinction, with no strong tectonic fabric, locally overprinted by later banded carbonate > quartz, (2) banded carbonate > quartz; banding perpendicular to vein margins and looks similar in texture to syn-tectonic fibre veins; carbonate foliated parallel to cleavage, which is at high angle to banding. Both vein types have selvedges/margins and discontinuous bands within the veins (along the vein-perpendicular carbonate banding) of coarse-grained, undeformed/weakly deformed fan-shaped chlorite and white-tan pleochroic mica intergrowths and sphalerite > pyrite and irregular, inclusion-rich, deformed quartz, crudely banded parallel to the carbonate veining.

Interpretation/important relationships: The carbonate-fine sericite alteration is strongly deformed and consequently probably pre- (to early) cleavage in timing, and is overprinted by ?pre-cleavage curvi-radial extinction carbonate veins, which are in turn overprinted by banded syn-tectonic carbonate and quartz. These veins in 1365a have late overgrowths and replacements of green and tan coarse micas and sulphides. The green and tan micas clearly replace each other, but which came first is ambiguous. These micas also clearly same timing as the sphalerite-pyrite within the veins, and this timing is late in the syn-tectonic veins (after deformed carbonate). This suggests the coarse mica-sphalerite assemblage is late tectonic ?remobilized mineralization. In sample 1365b there are multiple cross-cutting white syn-tectonic carbonate veinlets that post-date the pervasive browner dusty carbonate alteration, and these veins have subordinate tan and green mica intergrowths commonly associated with sp-py. Most of the sulphides in these 2 samples are associated with the late veins.

Mineral Probe Results

Carbonates

Sample	Area	depth	Description
120R-1365.4A	A1 C1	1365.4	carbonate within deformed carbonate vein
120R-1365.4A	A1 C2	1365.4	carbonate within deformed carbonate vein
120R-1365.4A	A2 C1	1365.4	vein carbonate
120R-1365.4A	A2 C2	1365.4	vein carbonate
120R-1365.4A	A6 C1	1365.4	vein carbonate
120R-1365.4A	A6 C2	1365.4	vein carbonate
120R-1365.4B	A1 C1	1365.4	carbonate aggregate ? replacing feldspar
120R-1365.4B	A1 C2	1365.4	carbonate aggregate ? replacing feldspar
120R-1365.4B	A2 C1	1365.4	coarse dusty brown carbonate
120R-1365.4B	A2 C2	1365.4	coarse dusty brown carbonate
120R-1365.4B	A3 C1	1365.4	irregular vein carbonate aggregates
120R-1365.4B	A3 C2	1365.4	irregular vein carbonate aggregates
120R-1365.4B	A4 C1	1365.4	dusty brown matrix carbonate
120R-1365.4B	A4 C2	1365.4	dusty brown matrix carbonate
120R-1365.4B	A5 C2	1365.4	syn tectonic carbonate vein
120R-1365.4B	A5 C2	1365.4	syn tectonic carbonate vein
120R-1365.4B	A5 C3	1365.4	matrix carbonate near vein

Area	FeCO3	MnCO3	MgCO3	CaCO3	NiCO3	SiO2	Al2O3	Carb total
A1 C1	6	39.45	7.72	46.71	0	0	0	99.88
A1 C2	5.39	38.67	7.21	49.05	0	0	0	100.32
A2 C1	3.95	44.81	4.7	47.21	0	0	0	100.68
A2 C2	4.05	43.12	4.62	49.43	0	0	0	101.22
A6 C1	3.56	41.25	3.83	52.07	0	0	0	100.7
A6 C2	3.4	40.56	3.93	52.18	0.35	0	0	100.42
A1 C1	5.39	26.67	16.56	51.93	0	0	0	100.54
A1 C2	4.87	27.33	15.41	53.32	0	0	0	100.93
A2 C1	3.31	27.36	16.48	53.92	0	0	0	101.07
A2 C2	2.84	26.1	17.61	53.98	0	0	0	100.52
A3 C1	7.82	35.4	6.63	49.91	0	0	0	99.76
A3 C2	7.02	31.49	5.44	55.98	0	0	0	99.92
A4 C1	4.18	26.39	15.75	54.03	0	0	0	100.34
A4 C2	2.42	24.79	19.53	52.78	0	0	0	99.52
A5 C2	9.66	36.82	7.84	45.91	0	0	0	100.24
A5 C2	10.26	36.39	8.05	46.95	0	0	0	101.64
A5 C3	3.97	27.44	16.9	52.94	0	0	0	101.25

White Micas

Sample	Depth	Area	Description
120R-1365.4B	1365.4	A4 S1	sericite in matrix carbonate aggregate

Area	SiO2	TiO2	Al2O3	Cr2O3	Fe2O3	FeO	MnO	MgO	CaO	Na2O	K2O	Cl	Oxide total
A4 S1	49.43	0.43	29.32	0	0	2.28	0.15	2.81	0.14	0	11.11	0	95.67

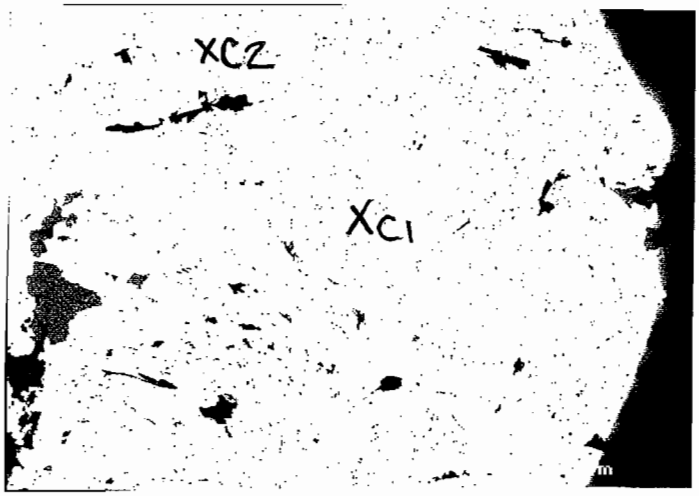

120R - 1365.4 A AREA 1

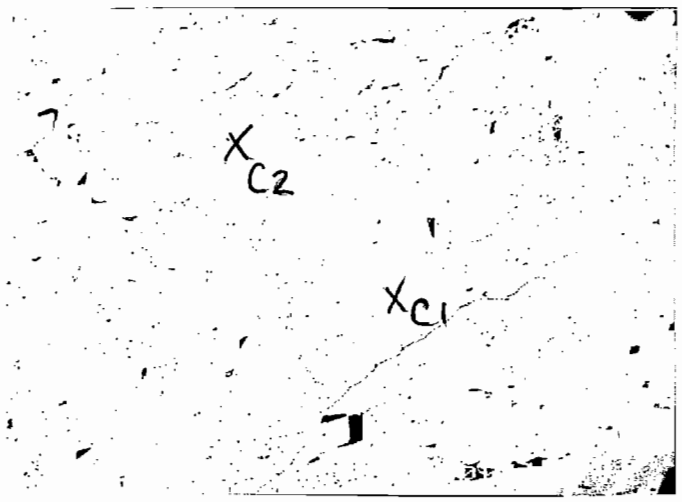

120R - 1365.4 A AREA 2

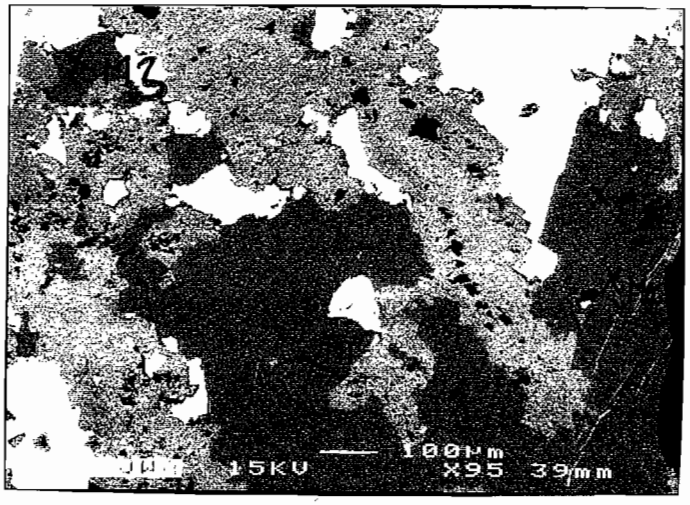

120R - 1365.4 A AREA 3

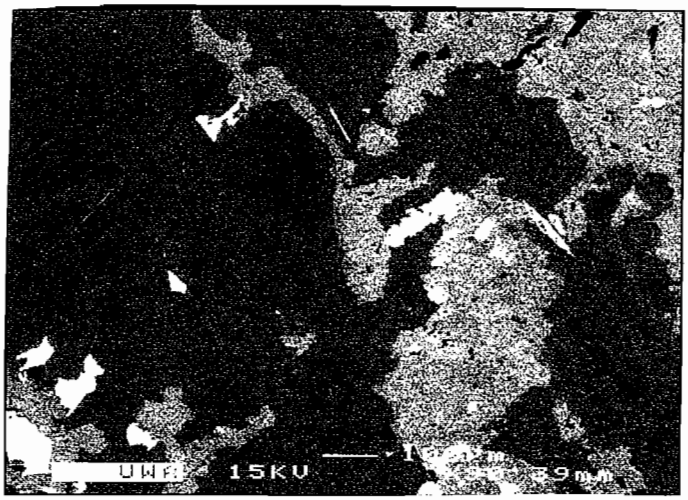

120R - 1365.4 A AREA 4

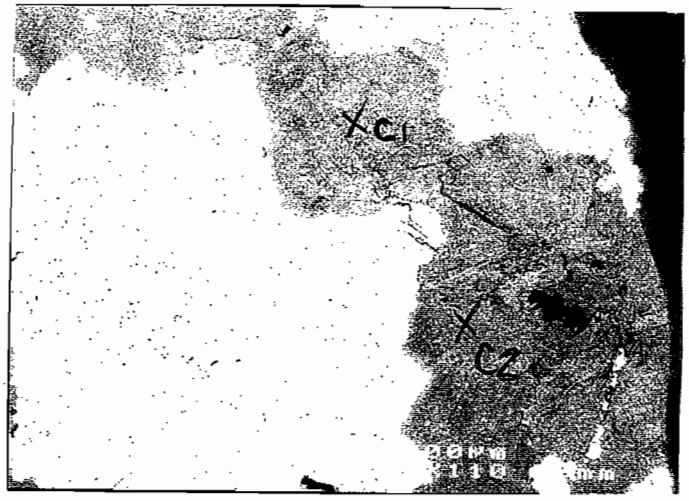

120R - 1365.4 A AREA 5

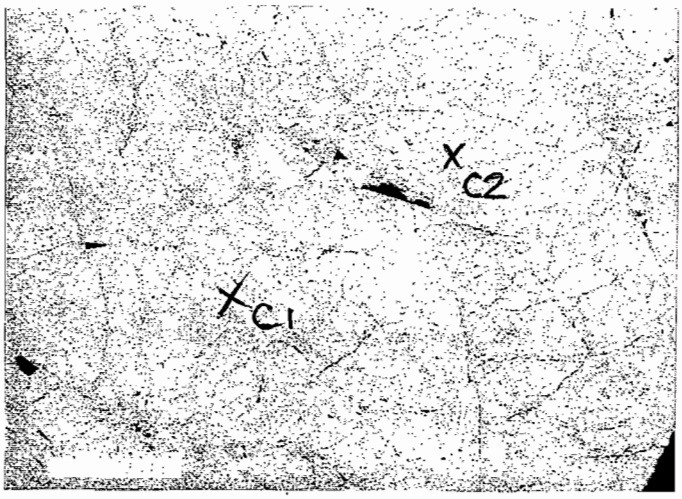

120R - 1365.4 A AREA 6

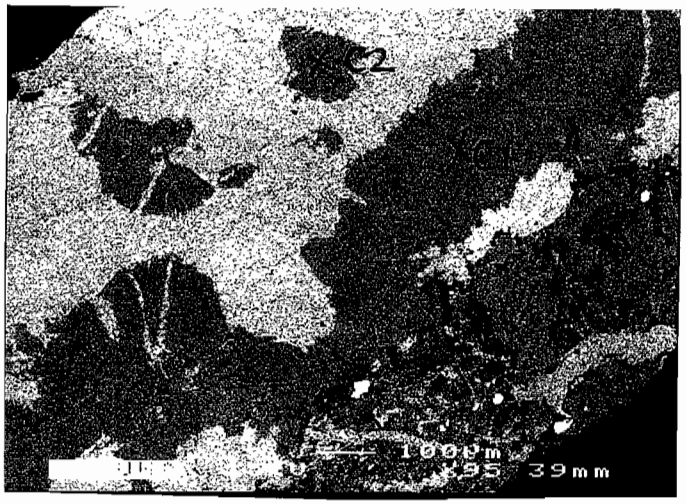

120R - 1365.4A AREA 7

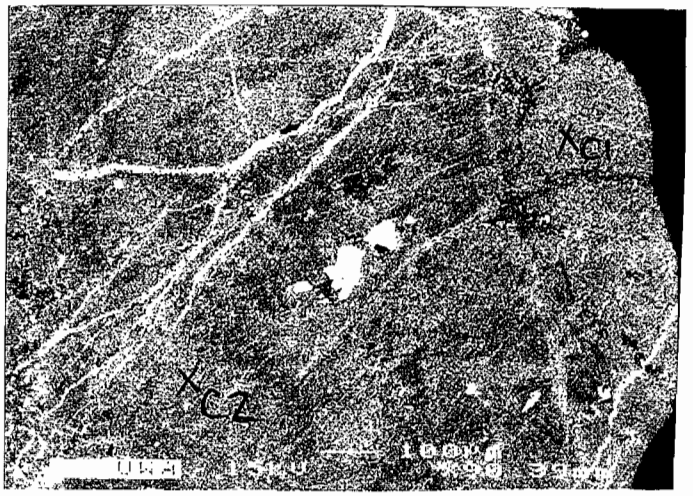

120R - 1365.4B AREA 1

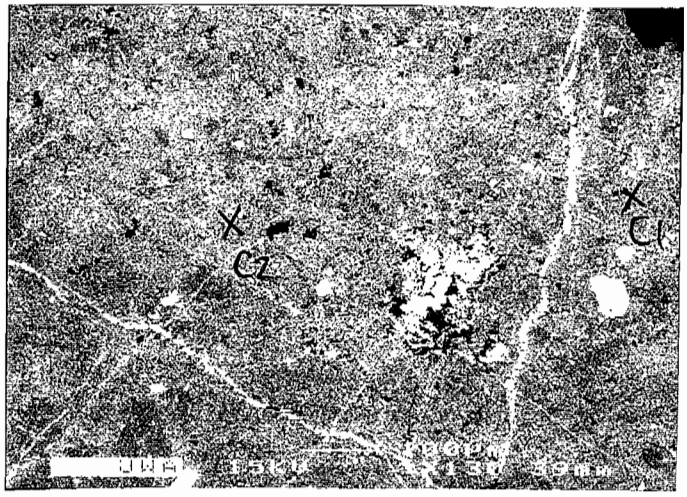

120R - 1365.4B AREA 2

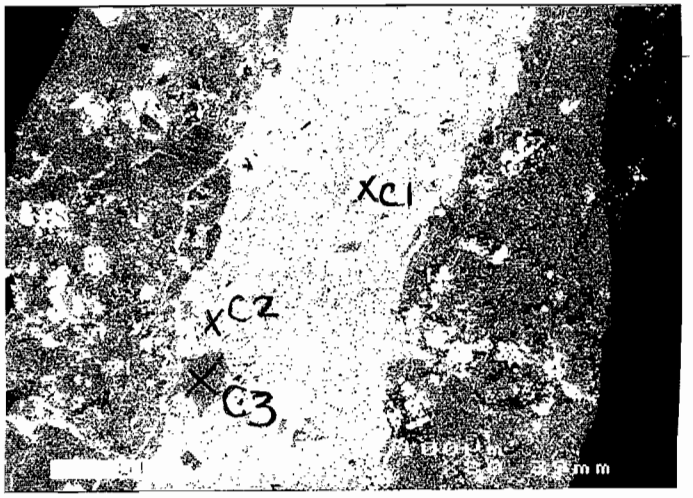

120R - 1365.4B AREA 3

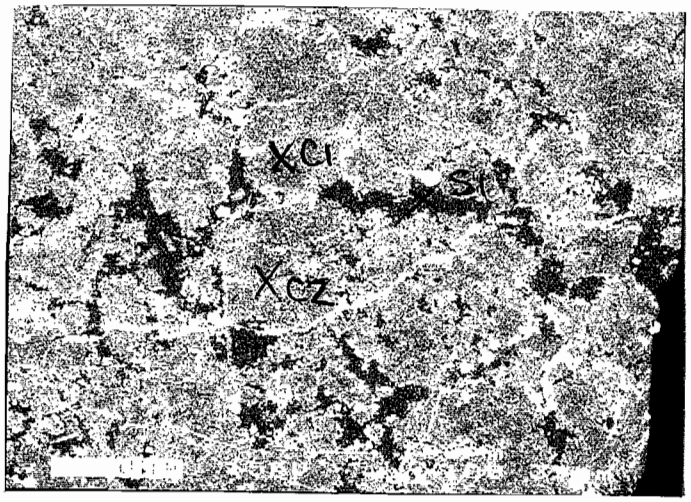

120R - 1365.4B AREA 4

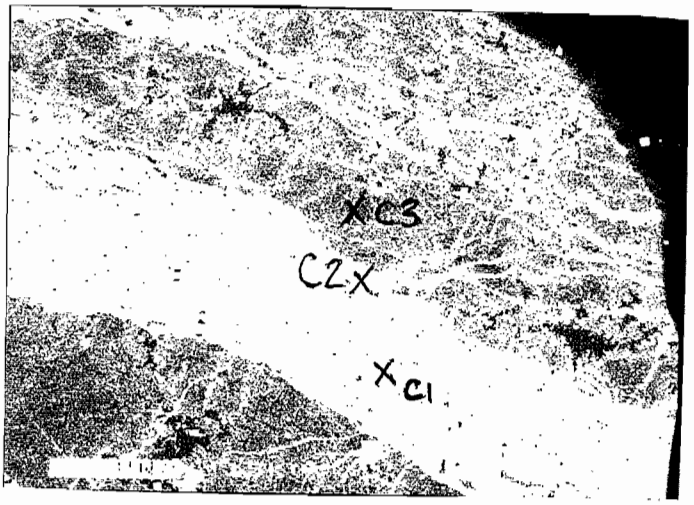

120R - 1365.4B AREA 5

Sample number: 96-120R-1366 Rock and thin section description

Location: Drill hole 120R, 1366.0 m; north end Rosebery mine

Hand specimen and summary: Semi-massive sphalerite-rich sulphide with many mica schist inclusions, from top of K ore lens.

Mineral percentages in thin section:

sulphides	40%
white mica	40%
quartz	15%
carbonate	3%
sphene-leucox	2% (3-4% of the white mica schist)

Primary textures: Some mica schist aggregates have sub-polygonal feldspar phenocryst-like shapes and could be pseudomorphs after feldspar.

Tectonic fabrics: Pools of sphalerite are unfoliated and cut across S2 / S3 crenulation cleavage in adjacent mica schist wall rock and inclusions. The mica schist has two distinct foliations. The S1 is best preserved in fine sericite areas, where it is crenulated by the main cleavage of the sample (S2 or S3). Coarse white mica is less deformed than the sericite and has grown along S1, the crenulation cleavage, and grows as undeformed fans between crenulation cleavage planes. The sulphides have flowed during deformation, whereas the sericite altered wall rocks have been cleaved, folded and partially plastically deformed during flowage of the sulphides.

Alteration, veins: Distinctive texture of pools of medium brown, translucent sphalerite enclosing small interconnected spots of anhedral to subhedral pyrite, anhedral galena and patches of quartz, pale grey carbonate and white mica schist. Sphalerite in these pools is unfoliated but inclusions of schist are strongly foliated and plastically deformed after S2. The carbonate patches are slightly dusty white in plane polars and a medium to dark grey colour in cross polars, and they have corroded irregular shapes and have abundant small inclusions.

Interpretation/important relationships: The sulphides have flowed and recrystallized during deformation. The present sulphide texture relates to S2 - S3 deformation, which is syn- to post-crenulation cleavage. During flowage the sulphide has transported inclusions of wall rock mica schist. Texture of the carbonate inclusions in the sulphide suggest they are an earlier generation than the sulphide.

Mineral Probe Results

Carbonates

Sample	Area	depth	Description
120R 1366.0	A2 C1	1366	carbonate surrounded by sphalerite
120R 1366.0	A2 C2	1366	carbonate surrounded by sphalerite
120R 1366.0	A2 C3	1366	carbonate surrounded by sphalerite
120R 1366.0	A2 C4	1366	carbonate surrounded by sphalerite
120R 1366.0	A3 C1	1366	carbonate surrounded by sphalerite
120R 1366.0	A3 C2	1366	carbonate surrounded by sphalerite
120R 1366.0	A4 C1	1366	carbonate surrounded by sphalerite
120R 1366.0	A4 C2	1366	carbonate surrounded by sphalerite

Area	FeCO3	MnCO3	MgCO3	CaCO3	NiCO3	SiO2	Al2O3	Carb total
A2 C1	24.61	71.23	4.56	2.5	0	0	0	102.9
A2 C2	23.76	70.16	4.68	3.37	0	0	0	101.98
A2 C3	35.68	51.19	12.9	2.78	0	0	0	102.56
A2 C4	29.34	54.08	13.86	5.39	0	0	0	102.67
A3 C1	25.68	71.15	4.01	1.09	0	0	0	101.93
A3 C2	30.86	54.64	13.15	4.07	0	0	0	102.72
A4 C1	24.71	65.71	7	5.8	0	0	0	103.22
A4 C2	28.31	55.63	13.32	5.41	0	0	0	102.67

White Micas

Sample	Depth	Area	Description
120R 1366.0	1366	A1 S1	coarse white mica associated with ZnS
120R 1366.0	1366	A1 S2	coarse white mica associated with ZnS
120R 1366.0	1366	A5 S1	large zone of sericite
120R 1366.0	1366	A5 S2	large zone of sericite

Area	SiO2	TiO2	Al2O3	Cr2O3	Fe2O3	FeO	MnO	MgO	CaO	Na2O	K2O	Cl	Oxide total
A1 S1	47.42	0.49	31.27	0	0	1.82	0	1.81	0	0	11.4	0	94.21
A1 S2	47.37	0.4	30.67	0	0	1.97	0	1.78	0	0	11.24	0	93.43
A5 S1	47.89	0.27	31.6	0	0	1.77	0	1.54	0	0	11.29	0	94.36
A5 S2	47.74	0.28	31.55	0	0	1.61	0	1.52	0	0	11.3	0	94

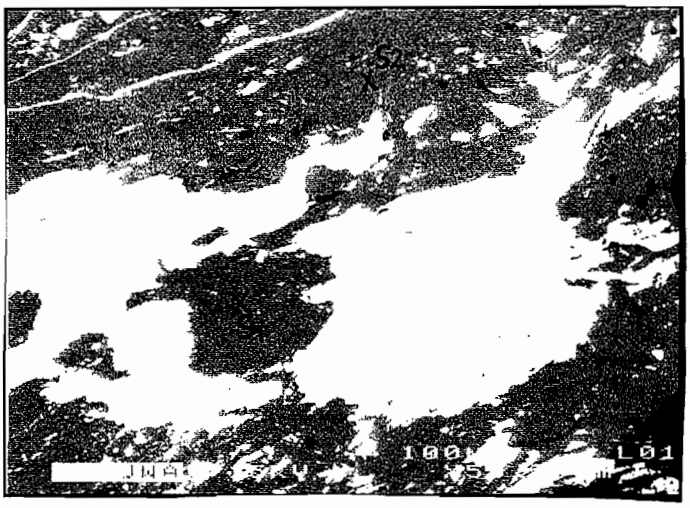

120R - 1366.0 AREA 1

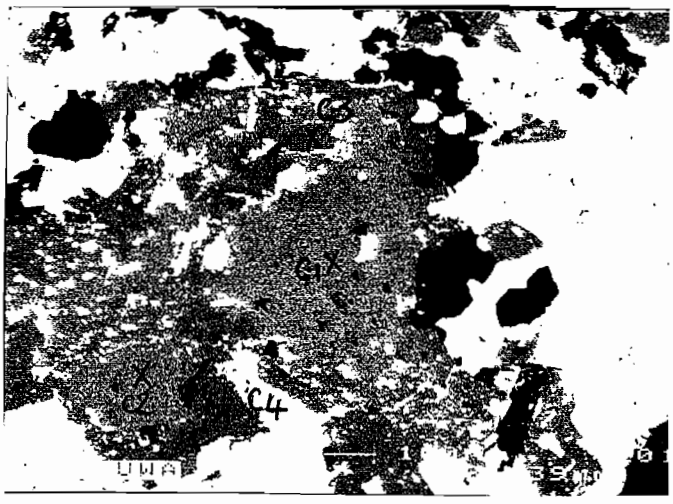

120R - 1366.0 AREA 2

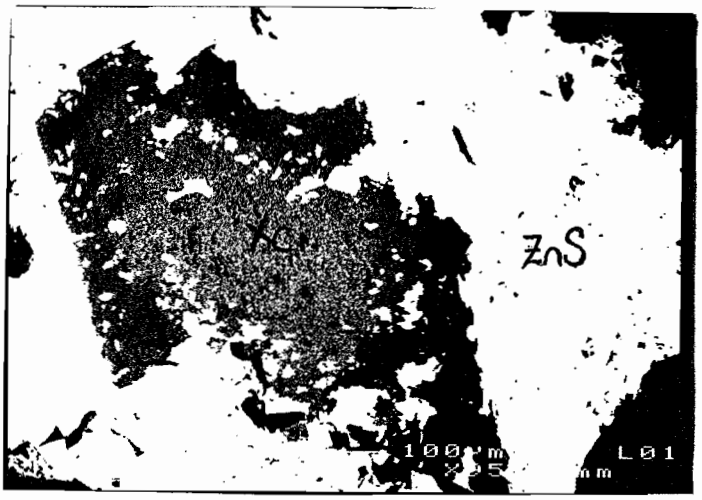

120 R - 1366.0 AREA 3

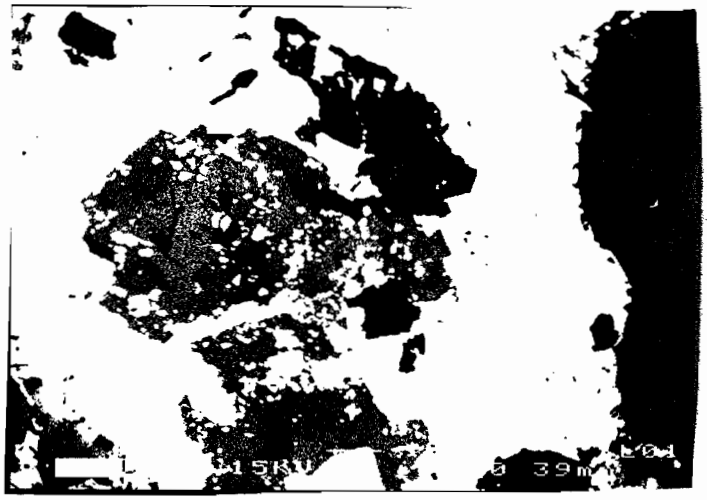

120 R - 1366.0 AREA 4

120 R - 1366.0 AREA 5

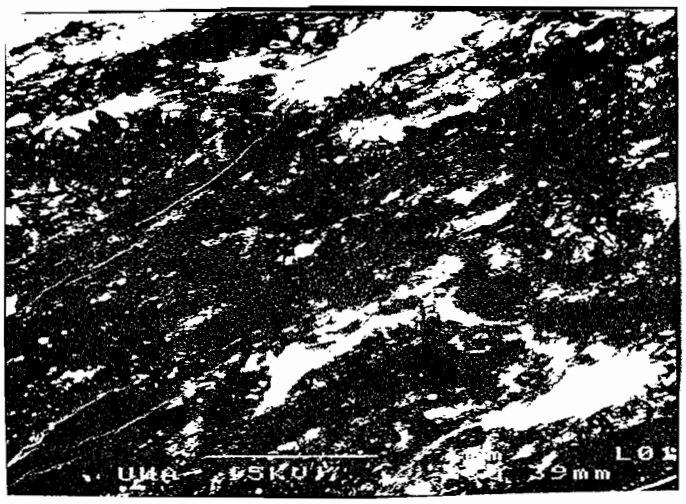

120R - 1366.0 AREA 5

Sample number: 96-120R-1399 Rock and thin section description

Location: Drill hole 120R, 1399.5 m; north end Rosebery mine

Hand specimen and summary: Buff-cream-grey, moderate sericite-quartz-carbonate altered pumice breccia in the footwall below K ore lens.

Mineral percentages in thin section:

quartz	50%
sericite	35%
feldspar	minor
chlorite	2%
carbonate	7%
sphene-leucox	3-4%
sulphides	2% (mainly pyrite)
zircon	trace

Primary textures: Poorly preserved, but slightly better than sample 1386. Tube pumice textures locally very faintly preserved, but strongly foliated. Feldspar phenocryst pseudomorphs visible, replaced by irregular coarse-grained blobs of quartz-carbonate > sericite-chlorite.

Tectonic fabrics: Two distinct foliations: a moderate-weak mica foliation especially within the more sericitic domains and a strong S2 cleavage within all domains. The foliations are at an acute angle and could both be components of a shear foliation. Pyrite occurs as small euhedral grains disseminated throughout and has large quartz-rich pressure shadow beard growths parallel to the main strong cleavage. The abundant veins are folded and cleaved. Consequently, they probably formed early in, or before, the main cleavage (S2) deformation. Quartz veinlets cut the altered phenocrysts.

Alteration, veins: Pervasive, moderate, fine-grained quartz-sericite alteration. Feldspar phenocrysts completely replaced by irregular coarse-grained blobs of quartz-carbonate > sericite-chlorite. Abundant (5%) quartz-rich veinlets occur mainly at high angle to main cleavage. Chlorite occurs both in the deformed ?syntectonic veins and as minor component of the replaced feldspar phenocrysts. Chlorite and sphalerite are more abundant in some of the veins than in the wall rock. One thin quartz±feldspar vein has an abundant high relief mineral that appears less dusty than the normal sphene-leucoxene aggregates. What is it?

Interpretation/important relationships: This is first sample below ore with appreciable carbonate. Compared to samples between here and ore, this one has more sericite, carbonate, and less quartz and chlorite. Sample shows strong feldspar destruction and replacement by quartz-caarbonate instead of just quartz as in higher footwall. Chlorite appears at least in part related to the early ?syn-tectonic quartz veinlets. Composition of chlorite probably different to sample 1386 because here is pleochroic pale to medium green, not green to tan. Sphene most abundant in end of thin section with least amount of carbonate. Disseminated pyrite probably pre-cleavage as strongly deformed, and most of the quartz veins must have formed early during deformation as they are also deformed. Could some of them be pre-tectonic?

Mineral Probe Results

Carbonates

Sample	Area	depth	Description
120R-1399.5	A2 C1	1399.5	coarse carbonate probably replacing feldspar
120R-1399.5	A2 C2	1399.5	coarse carbonate probably replacing feldspar
120R-1399.5	A3 C1	1399.5	coarse carbonate probably replacing feldspar
120R-1399.5	A3 C2	1399.5	coarse carbonate probably replacing feldspar

Area	FeCO3	MnCO3	MgCO3	CaCO3	NiCO3	SiO2	Al2O3	Carb total
A2 C1	10.23	28.3	13.51	48.53	0	0	0	100.57
A2 C2	11.08	26.54	14.28	48.78	0	0	0	100.68
A3 C1	9.45	29	10.73	50.94	0	0	0	100.12
A3 C2	11.74	21.79	16.48	50.8	0	0	0	100.81

White Micas

Sample	Depth	Area	Description
120R-1399.5	1399.5	A3 S1	sericite in carbonate altered matrix
120R-1399.5	1399.5	A4 S1	matrix
120R-1399.5	1399.5	A5 S1	sericite in altered feldspar domain
120R-1399.5	1399.5	A7 S1	matrix sericite
120R-1399.5	1399.5	A7 S2	matrix sericite

Area	SiO2	TiO2	Al2O3	Cr2O3	Fe2O3	FeO	MnO	MgO	CaO	Na2O	K2O	Cl	Oxide total
A3 S1	47.72	0.46	28.48	0	0	3.79	0	3.01	0	0	11.05	0	94.51
A4 S1	48.54	0.51	29.06	0	0	2.97	0	2.41	0	0	11.23	0	94.72
A5 S1	49.09	0.38	28.36	0	0	2.87	0	2.57	0	0	11.45	0	94.72
A7 S1	48.73	0.4	28.47	0	0	2.93	0	2.35	0	0	11.46	0	94.34
A7 S2	48.25	0.46	28.83	0	0	2.78	0	2.17	0	0	11.61	0	94.1

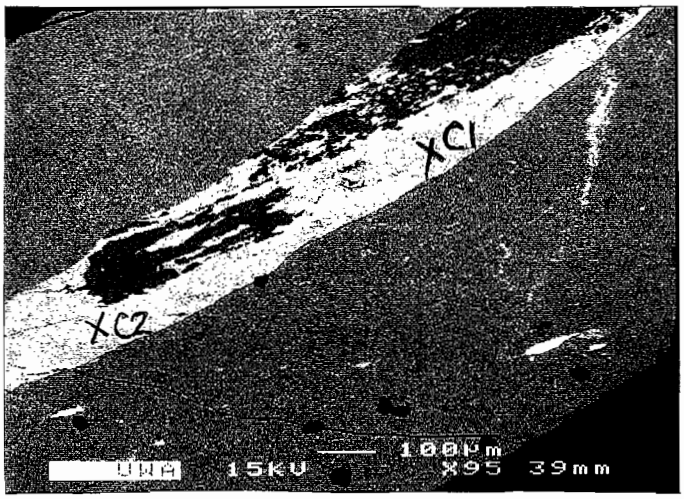

120R-1399.5 AREA 1

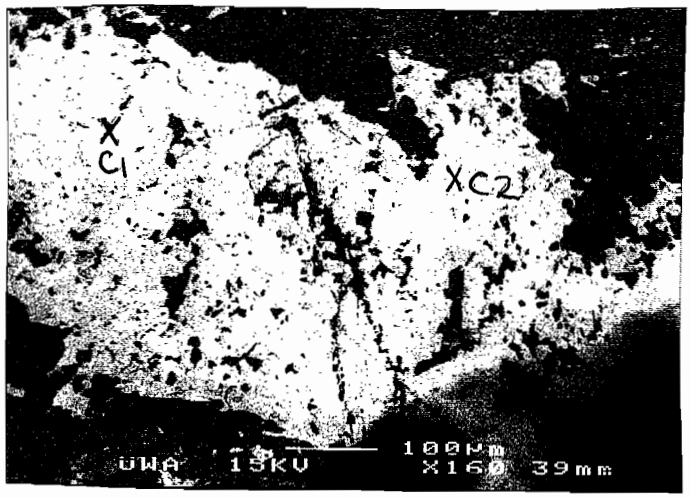

120R-1399.5 AREA 2

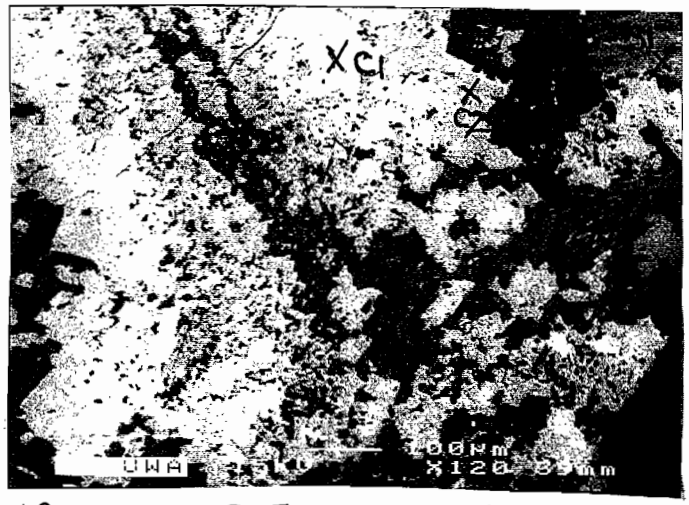

120R-1399.5 AREA 3

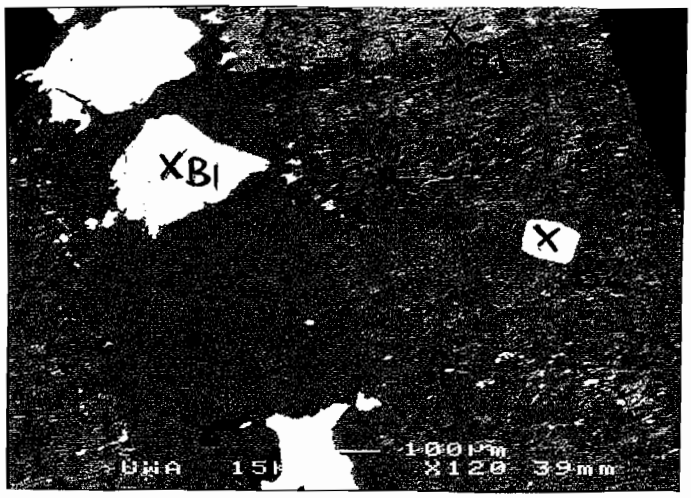

120R-1399.5 AREA 4

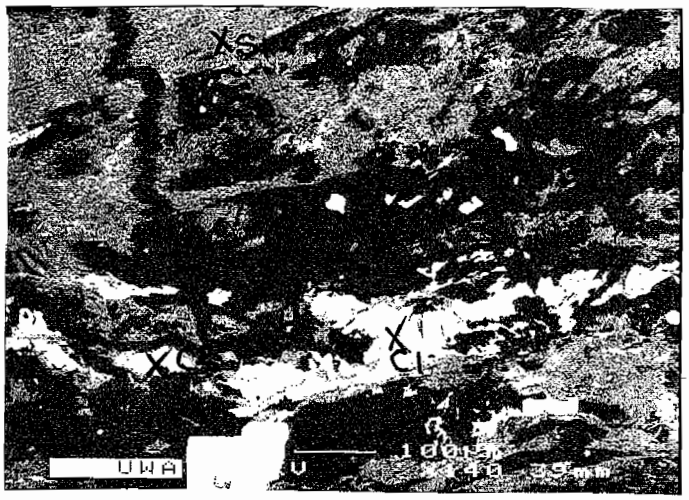

120R-1399.5 AREA 5

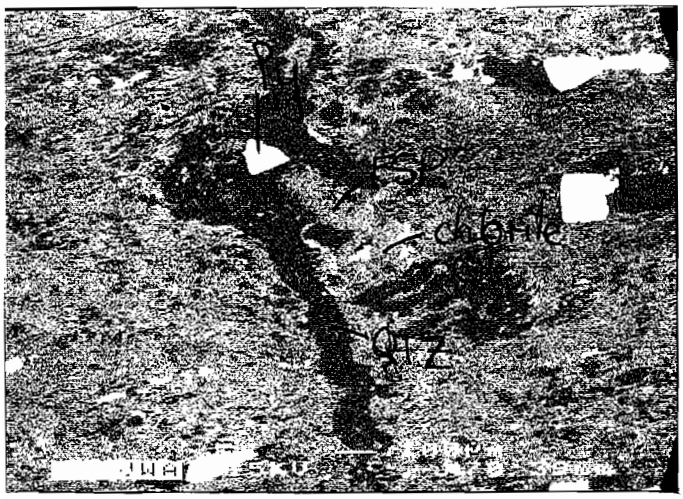

120R-1399.5 AREA 6

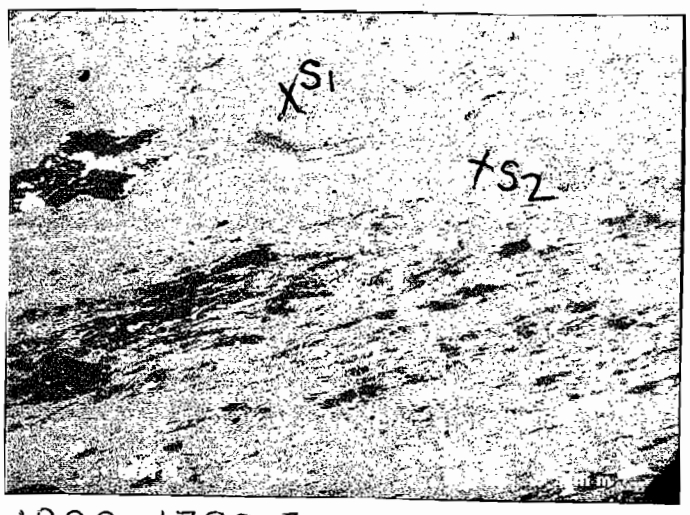

120R-1399.5 AREA 7

Sample number: 96-120R-1421 Rock and thin section description

Location: Drill hole 120R, 1421.8 m; north end Rosebery mine

Hand specimen and summary: Buff-cream-grey, weak sericite-carbonate altered pumice breccia in the footwall below K ore lens.

Mineral percentages in thin section:

sericite	45%
quartz	28%
plagioclase	15%
carbonate	5%
?clinozoisite	4%
sphene-leucox	3%
sulphides	<1% (pyrite)
zircon	trace

Primary textures: 15-20% 2mm, moderately-strongly foliated, feldspar porphyritic texture well preserved. Phenocrysts are scattered in a fine-grained, strongly foliated, sericitic matrix with almost no relict primary texture. The original pumice textures obliterated by pervasive sericite and the strong foliation that resulted because of the sericitic composition.

Tectonic fabrics: Strong foliation of matrix. Feldspar phenocrysts are extended in the foliation-lineation, commonly dismembered/pulled apart along the lineation, and have strong beard growths of quartz-sericite-?clinozoisite.

Alteration, veins: Major alteration change to sample 1399. Feldspar phenocrysts much less altered (only 5-25% of feldspar phenocryst is replaced, the remainder is fairly clean plagioclase), and pumice enclosing the phenocrysts is more sericite less quartz altered. The plagioclase phenocrysts are partly replaced by carbonate>sericite>?clinozoisite. Minor quartz veinlets are strongly deformed.

Interpretation/important relationships: This is first sample below ore with remnant phenocryst feldspar. Compared to samples between here and ore, this one has more sericite, feldspar and less carbonate, quartz and chlorite. No evidence of secondary feldspar growth around feldspar phenocrysts, but its possible it did exist and has been obliterated by the strong sericite alteration and cleavage.

Mineral Probe Results

Carbonates

Sample	Area	depth	Description
120R-1421.8	A1 C1	1421.8	carbonate alteration in feldspar phenocryst
120R-1421.8	A1 C2	1421.8	carbonate alteration in feldspar phenocryst
120R-1421.8	A5 C1	1421.8	carbonate alteration in feldspar phenocryst
120R-1421.8	A5 C2	1421.8	carbonate alteration in feldspar phenocryst

Area	FeCO3	MnCO3	MgCO3	CaCO3	NiCO3	SiO2	Al2O3	Carb total
A1 C1	27.92	3.52	18.36	52.37	0	0	0	102.17
A1 C2	30.07	3.92	16.02	52.26	0	0	0	102.27
A5 C1	18.95	3.24	23.73	56.05	0	0	0	101.97
A5 C2	20.53	2.98	24.26	53.78	0	0	0	101.55

White Micas

Sample	Depth	Area	Description
120R-1421.8	1421.8	A1 S1	matrix sericite
120R-1421.8	1421.8	A2 S1	matrix sericite
120R-1421.8	1421.8	A3 S1	intense sericite alteration
120R-1421.8	1421.8	A3 S2	intense sericite alteration
120R-1421.8	1421.8	A3 S3	intense sericite alteration
120R-1421.8	1421.8	A4 S1	intense sericite alteration
120R-1421.8	1421.8	A4 S2	intense sericite alteration
120R-1421.8	1421.8	A5 S1	matrix to carb altered feldspar

Area	SiO2	TiO2	Al2O3	Cr2O3	Fe2O3	FeO	MnO	MgO	CaO	Na2O	K2O	Cl	Oxide total
A1 S1	51.29	0.48	27.05	0	0	3.57	0	2.15	0	0	10.98	0	95.52
A2 S1	48.65	0.59	28.18	0	0	3.49	0	2.5	0	0	11.47	0	94.88
A3 S1	53.5	0.47	25.78	0	0	3.18	0	2.24	0	0	10.4	0	95.57
A3 S2	51.66	0.59	26.99	0	0	3.1	0	2.34	0	0	11.09	0	95.77
A3 S3	49.84	0.62	27.64	0	0	3.42	0	2.47	0	0	11.04	0	95.03
A4 S1	49.7	0.58	28.31	0	0	3.39	0	2.53	0	0	11.64	0	96.15
A4 S2	52.27	0.69	26.35	0	0	3.39	0	2.35	0	0	10.82	0	95.87
A5 S1	49.2	0.77	28.08	0	0	3.46	0	2.54	0.11	0	11.26	0	95.42

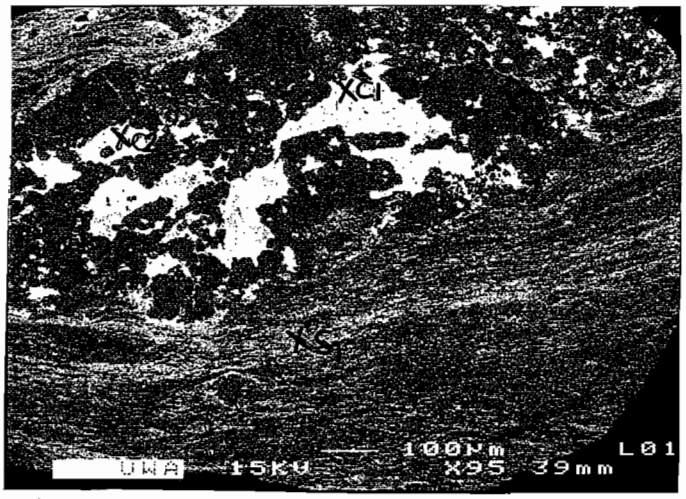

120R-1421.8 AREA 1

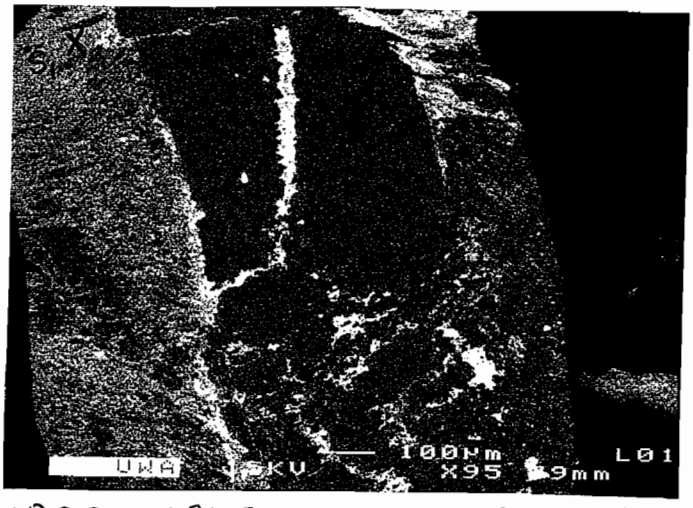

120R-1421.8 AREA 2

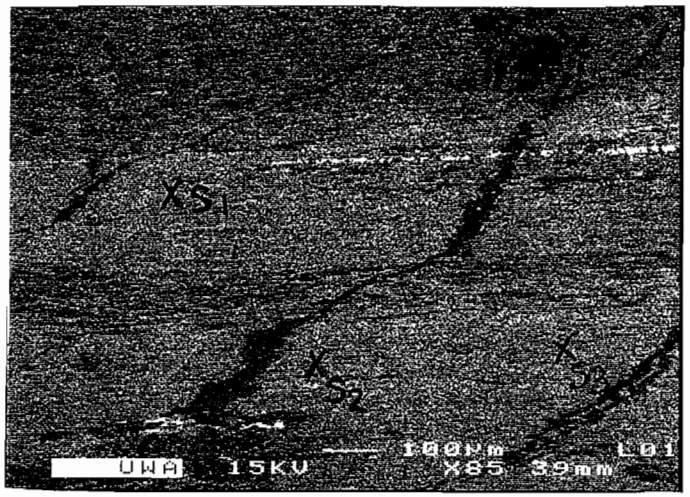

120R-1421.8 AREA 3

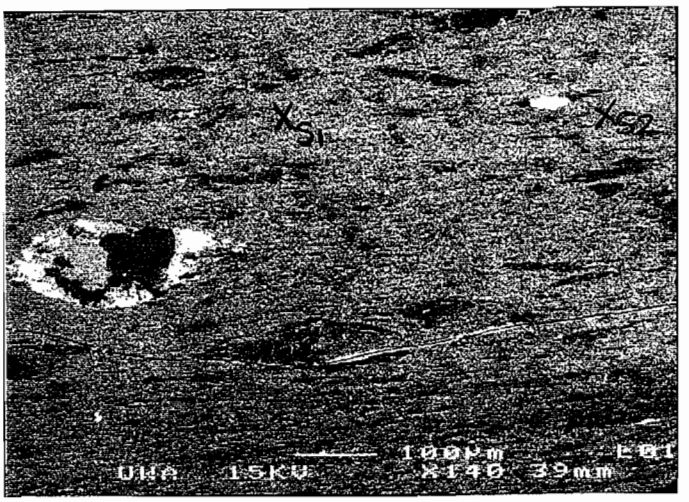

120R-1421.8 AREA 4

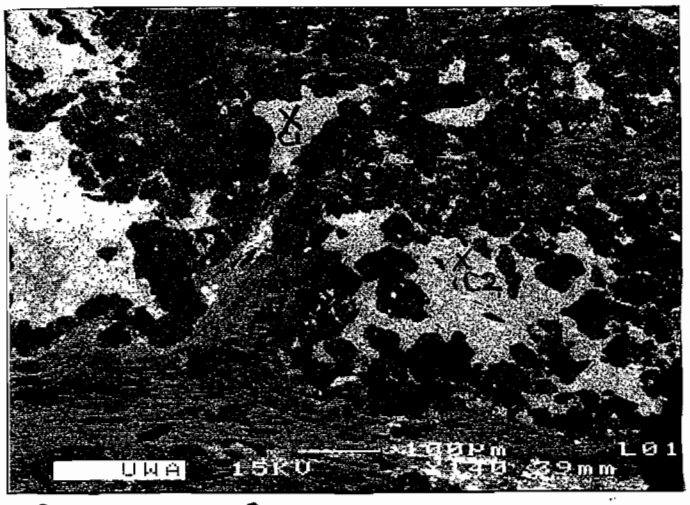

120R-1421.8 AREA 5

Sample number: 96-120R-1436 Rock and thin section description

Location: Drill hole 120R, 1436.2 m; north end Rosebery mine

Hand specimen and summary: Arsenopyrite-carbonate vein within buff-cream-grey, weak sericite-carbonate altered pumice breccia in the footwall below K ore lens.

Mineral percentages in thin section:

sericite	35%
quartz	35%
chlorite	7%
plagioclase	5%
carbonate	6%
sphene±clinozoisite	5%
sulphides	5% (arsenopyrite)
tourmaline	2%
zircon	trace

Primary textures: 15-20% 2mm, moderately-strongly foliated, feldspar porphyritic texture well preserved, but the phenocrysts are completely replaced by sericite-chlorite>carbonate-sphene±clinozoisite. Fine-grained, strongly foliated, sericite-quartz matrix with almost no relict primary texture. The original pumice textures obliterated by pervasive sericite and the strong foliation that resulted because of the sericitic composition.

Tectonic fabrics: Strong foliation of sericite-quartz matrix. Feldspar phenocrysts are slightly extended in the foliation-lineation. The chlorite-carbonate-arsenopyrite vein is undeformed, and chlorite in the wall rock pumice breccia is undeformed.

Alteration, veins: The wall rock (pumice breccia) has moderate quartz-sericite±carbonate alteration overprinted by chlorite-sphene(±clinozoisite)-carbonate alteration mainly as alteration of the feldspar phenocrysts. There is more sphene and much more chlorite than in next sample higher in footwall. Phenocrysts are completely replaced by chlorite-sericite>carbonate-sphene±clinozoisite. The chlorite looks the same as in the thick vein. The prominent vein is composed of chlorite-carbonate>?albite-arsenopyrite>tourmaline. The chlorite is the distinctive bright green to pale yellow-tan pleochroic fan-radiating chlorite. In cross polars the chlorite has bue-grey and green colours with a patchwork to radiating texture.

Interpretation/important relationships: This sample shows that the green to yellow tan, fan-radiating chlorite is associated with post-cleavage, probably granite-related, veining and that this chlorite also occurs in alteration selvedges around the veins.

Mineral Probe Results

Carbonates

Sample	Area	depth	Description
120R-1436.2	A1 C1	1436.2	carbonate alteration in feldspar phenocryst
120R-1436.2	A1 C2	1436.2	carbonate alteration in feldspar phenocryst
120R-1436.2	A2 C2	1436.2	vein carbonate
120R-1436.2	A3 C1	1436.2	vein carbonate
120R-1436.2	A3 C2	1436.2	vein carbonate
120R-1436.2	A4 C1	1436.2	vein carbonate
120R-1436.2	A4 C2	1436.2	vein carbonate

Area	FeCO3	MnCO3	MgCO3	CaCO3	NiCO3	SiO2	Al2O3	Carb total
A1 C1	35.95	58.6	4.68	3.98	0	0	0	103.21
A1 C2	29.13	64.07	3.74	4.48	0	0	0	101.43
A2 C2	62.49	4.57	10.89	0	0	0	0	77.95
A3 C1	18.94	70.49	2.78	9.48	0	0	0	101.68
A3 C2	19.6	69.64	2.63	10.23	0	0	0	102.1
A4 C1	27.32	62.68	5.27	6.43	0	0	0	101.7
A4 C2	32.5	60.83	4.52	4.59	0	0	0	102.44

White Micas

Sample	Depth	Area	Description
120R-1436.2	1436.2	A1 S1	sericite carbonate alteration of feldspar
120R-1436.2	1436.2	A1 S2	matrix to altered feldspar
120R-1436.2	1436.2	A6 S1	sericite near chlorite alteration outside vein
120R-1436.2	1436.2	A6 S2	sericite near chlorite alteration outside vein

Area	SiO2	TiO2	Al2O3	Cr2O3	Fe2O3	FeO	MnO	MgO	CaO	Na2O	K2O	Cl	Oxide total
A1 S1	47.75	0	30.62	0	0	5.1	0	1.55	0	0	10.08	0	95.1
A1 S2	49.3	0	30.59	0	0	2.2	0	1.5	0	0	10.75	0	94.34
A6 S1	48.33	0.47	28.46	0	0	3.44	0	2.24	0	0	11.43	0	94.37
A6 S2	49.24	0	30.78	0	0	2.3	0	1.58	0	0	11.25	0	95.15

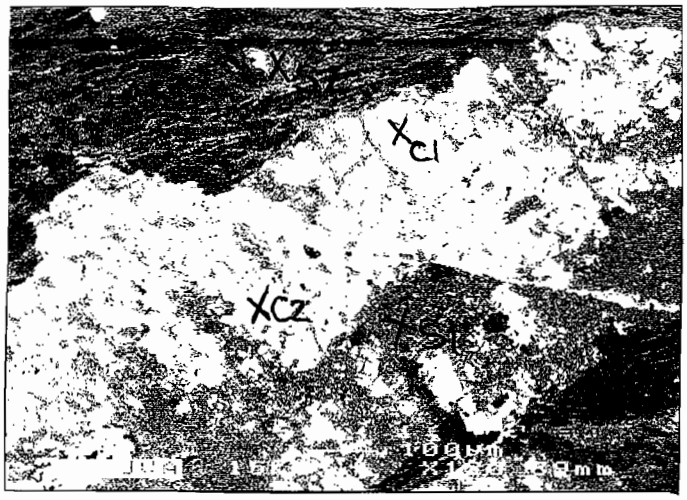

120R-1436.2 AREA 1

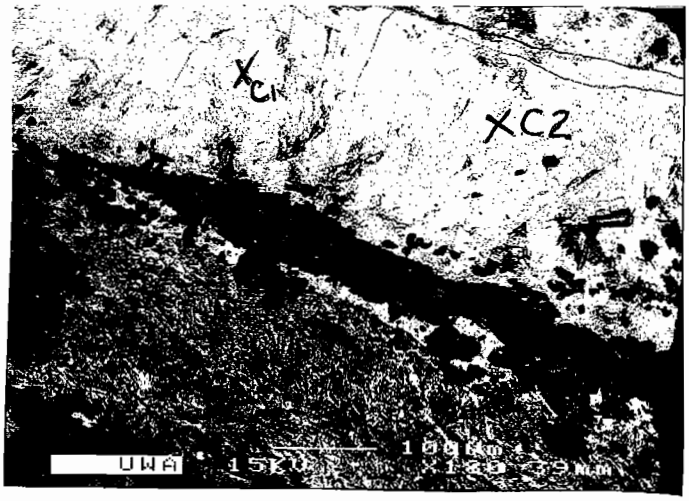

120R-1436.2 AREA 2

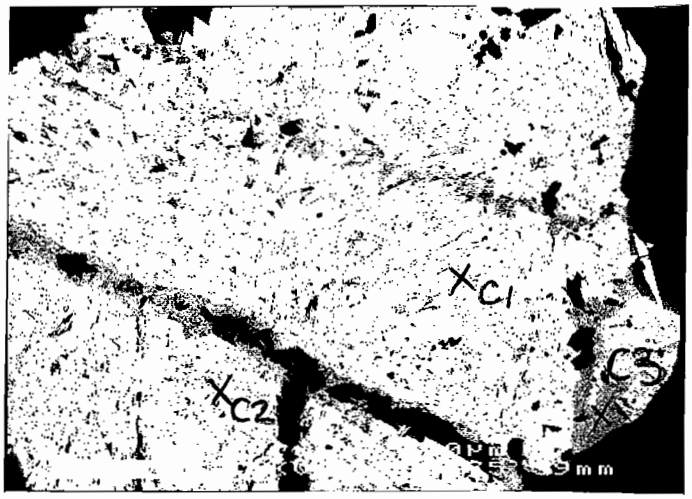

120R-1436.2 AREA 3

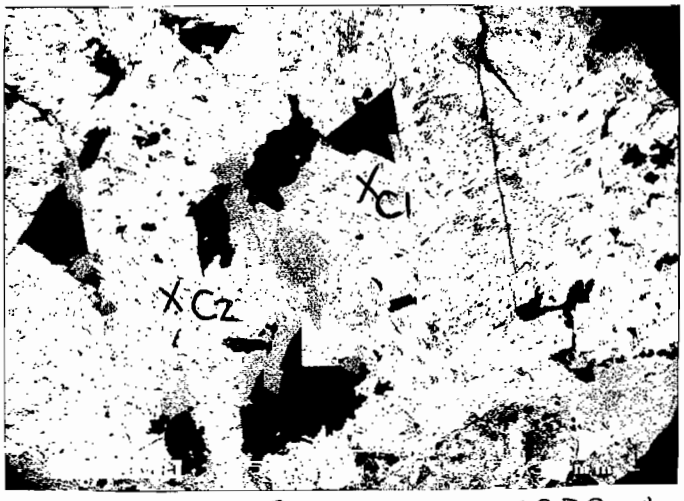

120R-1436.2 AREA 4

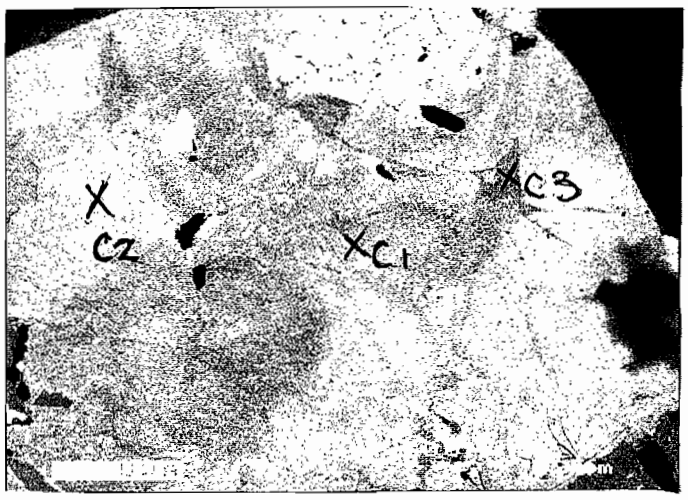

120R-1436.2 AREA 5

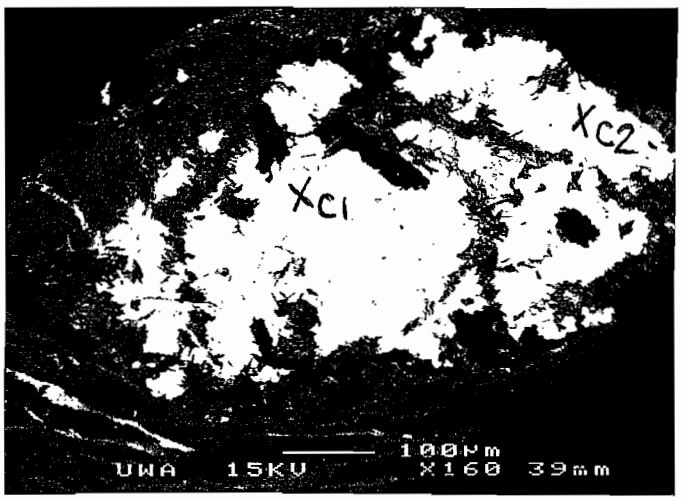

120R-1436.2 AREA 6

Sample number: 96-120R-1440 Rock and thin section description

Location: Drill hole 120R, 1440.5 m; north end Rosebery mine

Hand specimen and summary: weakly sericite-quartz»chlorite altered pumice breccia in the footwall below K ore lens.

Mineral percentages in thin section:

fg qtz-feld groundmass	63%
plagioclase phenos	15%
sericite	15%
carbonate	2%
sphene-leucox	3%
chlorite	1%
biotite	1%
sulphides	rare (pyrite)
zircon	trace

Primary textures: Well preserved tube pumice breccia texture and 15-20% 2mm feldspar porphyritic texture. Phenocrysts relatively unaltered. Tube pumice texture comprises fine grained sericite along vesicle walls and rest of pumice replaced by fine-grained feldspar-quartz mosaics, with relics of a coarser grained feldspar precurser. Spaced moderately sericitic bands occur and are pseudo-fiamme foliation rather than fiamme (see below).

Tectonic fabrics: Moderate foliation of matrix pumice texture, sericite in matrix, and weak development of beard growths on feldspar phenocrysts. Sericite and opaques concentrated along spaced, stylolitic S1 foliation bands, in turn overprinted by main pervasive cleavage.

Alteration, veins: Pervasive secondary feldspar alteration (see above), overprinted by weak quartz-sericite-minor carbonate and very minor chlorite. Phenocrysts have only very minor sericite-carbonate alteration. The phenocrysts are relatively clear feldspar with slightly faint or mottled extinction, which may suggest they have been altered to secondary feldspar.

Interpretation/important relationships: This rock has pervasive, strong diagenetic alteration that is not texturally destructive, and no obvious hydrothermal alteration associated with mineralization. The sericitic bands clearly overprint the secondary feldspar alteration of the pumice. They are not fiamme, because there is clear evidence that they partially replace uncollapsed, feldspar altered pumice breccia. The sericite bands are syn-S1 ± syn-S2 in timing.

Mineral Probe Results

Carbonates

Sample	Area	depth	Description
120R-1440.5	A3 C1	1440.5	carbonate alteration within feldspar
120R-1440.5	A5 C1	1440.5	carbonate patches on feldspar phenocryst
120R-1440.5	A5 C2	1440.5	carbonate patches on feldspar phenocryst

Area	FeCO3	MnCO3	MgCO3	CaCO3	NiCO3	SiO2	Al2O3	Carb total
A3 C1	1.65	2.8	0.75	94.02	0	0	0	99.22
A5 C1	1.05	2.54	0.33	97.09	0	0	0	101.01
A5 C2	2.06	3.08	0.92	96.71	0	0	0	102.77

Micas

Sample	Depth	Area	Description
120R-1440.5	1440.5	A2 S1	sericite in altered feldspar fracture
120R-1440.5	1440.5	A5 S1	matrix sericite near altered feldspar phenocryst

Area	SiO2	TiO2	Al2O3	Cr2O3	Fe2O3	FeO	MnO	MgO	CaO	Na2O	K2O	Cl	Oxide total
A2 S1	47.46	0.56	28.07	0	0	4.77	0	2.09	0	0	11.51	0	94.46
A5 S1	48.26	0.83	28.19	0	0	4.91	0	2.15	0	0	11.4	0	95.74

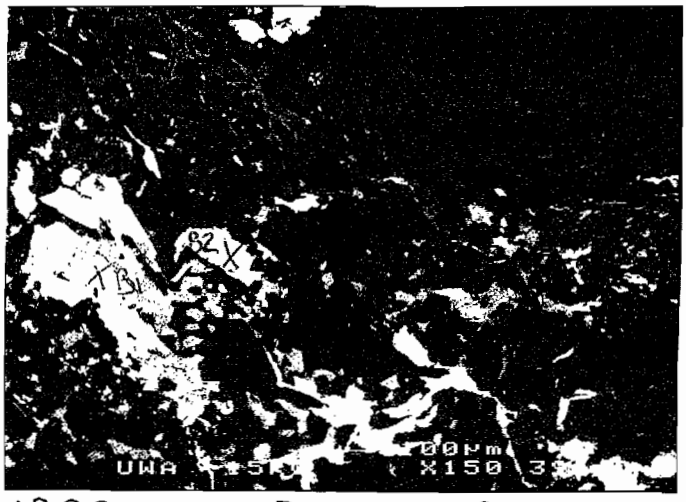

120R - 1440.5 AREA 1

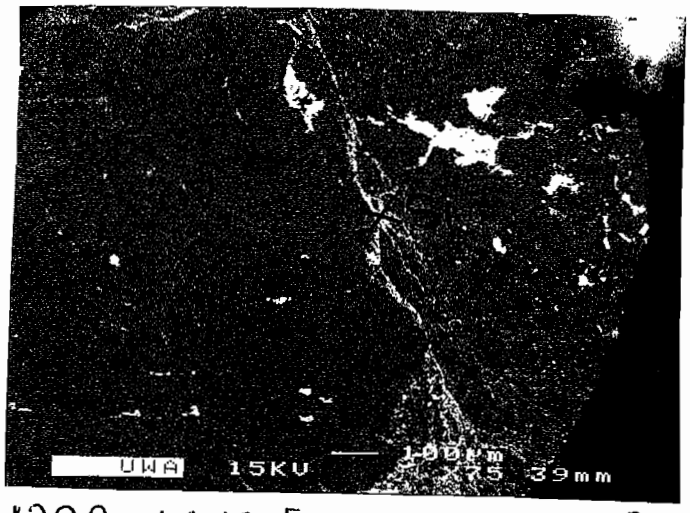

120R - 1440.5 AREA 2

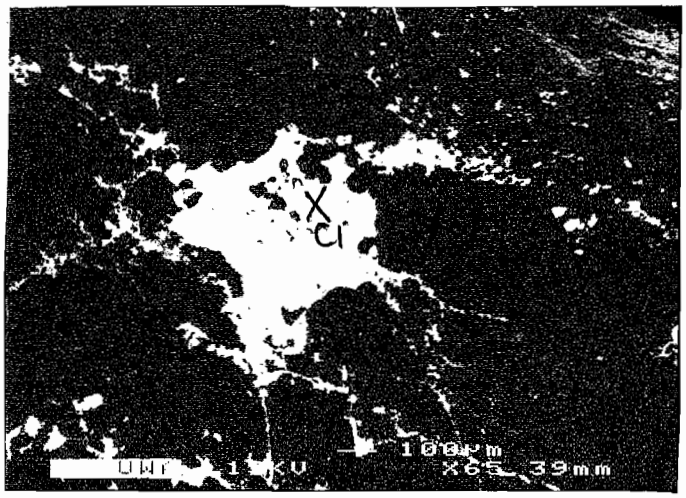

120R - 1440.5 AREA 3

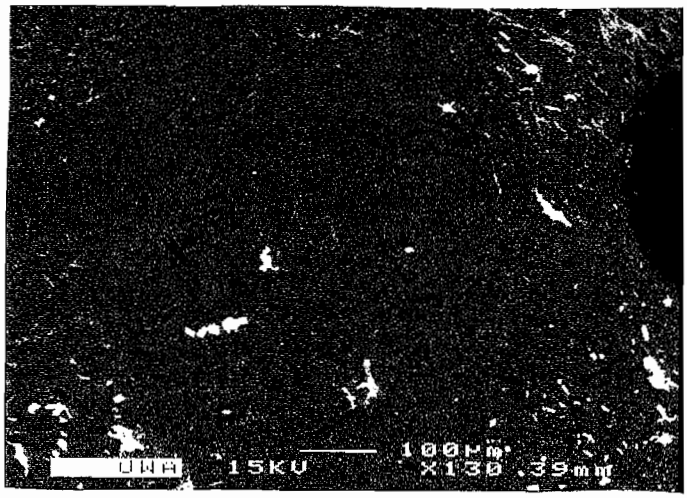

120R - 1440.5 AREA 4

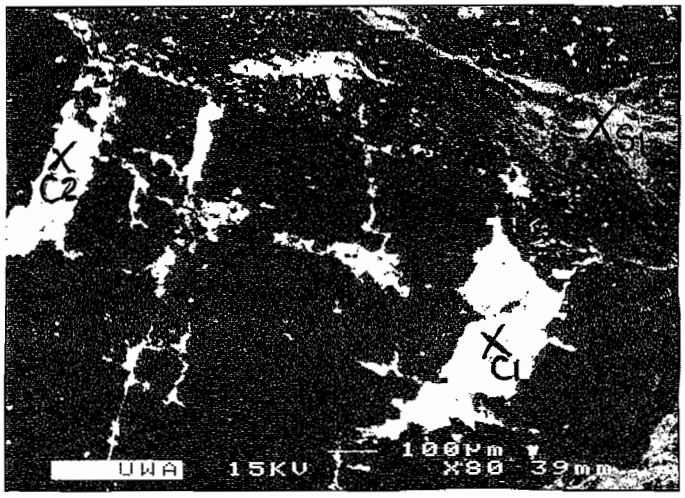

120R - 1440.5 AREA 5

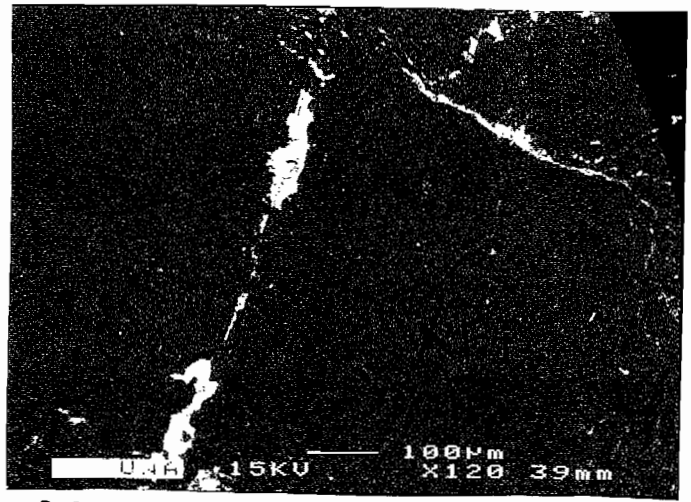

120R - 1440.5 AREA 6